

Geotechnical, Geological and Earthquake Engineering

Atila Ansal *Editor*

Perspectives on European Earthquake Engineering and Seismology

Volume 2



Springer Open

Perspectives on European Earthquake Engineering and Seismology

GEOTECHNICAL, GEOLOGICAL AND
EARTHQUAKE ENGINEERING

Volume 39

Series Editor

Atilla Ansal, School of Engineering, Özyeğin University, Istanbul, Turkey

Editorial Advisory Board

Julian Bommer, Imperial College London, U.K.

Jonathan D. Bray, University of California, Berkeley, U.S.A.

Kyriazis Pitilakis, Aristotle University of Thessaloniki, Greece

Susumu Yasuda, Tokyo Denki University, Japan

More information about this series at <http://www.springer.com/series/6011>

Atila Ansal
Editor

Perspectives on European Earthquake Engineering and Seismology

Volume 2

 Springer Open

ISTANBUL PROJECT
COORDINATION UNIT
IPKB 

Editor
Atilla Ansal
School of Engineering
Özyeğin University
Istanbul, Turkey

ISSN 1573-6059 ISSN 1872-4671 (electronic)
Geotechnical, Geological and Earthquake Engineering
ISBN 978-3-319-16963-7 ISBN 978-3-319-16964-4 (eBook)
DOI 10.1007/978-3-319-16964-4

Library of Congress Control Number: 2014946618

Springer Cham Heidelberg New York Dordrecht London

© The Editor(s) and if applicable the Author(s) 2015. The book is published with open access at <http://link.springer.com>

Open Access This book is distributed under the terms of the Creative Commons Attribution Noncommercial License which permits any noncommercial use, distribution, and reproduction in any medium, provided the original author(s) and source are credited.

All commercial rights are reserved by the Publisher, whether the whole or part of the material is concerned, specifically the rights of translation, reprinting, re-use of illustrations, recitation, broadcasting, reproduction on microfilms or in any other way, and storage in data banks. Duplication of this publication or parts thereof is permitted only under the provisions of the Copyright Law of the Publisher's location, in its current version, and permission for commercial use must always be obtained from Springer. Permissions for commercial use may be obtained through RightsLink at the Copyright Clearance Center. Violations are liable to prosecution under the respective Copyright Law.

The use of general descriptive names, registered names, trademarks, service marks, etc. in this publication does not imply, even in the absence of a specific statement, that such names are exempt from the relevant protective laws and regulations and therefore free for general use.

While the advice and information in this book are believed to be true and accurate at the date of publication, neither the authors nor the editors nor the publisher can accept any legal responsibility for any errors or omissions that may be made. The publisher makes no warranty, express or implied, with respect to the material contained herein.

Printed on acid-free paper

Springer International Publishing AG Switzerland is part of Springer Science+Business Media (www.springer.com)

Preface

The collection of chapter contributions compiled in this second volume of *Perspectives on European Earthquake Engineering and Seismology* is composed out of 4 keynote and 15 theme lectures presented during the Second European Conference on Earthquake Engineering and Seismology (2ECEES) held in Istanbul, Turkey, from August 24 to 29, 2014. Since the Conference was a joint event of European Association of Earthquake Engineering (EAEE) and the European Seismological Commission (ESC), the chapter contributions cover the major topics of earthquake engineering and seismology along with priority issues of global importance.

On the occasion of the 50th anniversary of the establishment of the European Association of Earthquake Engineering, and for the first time in the book series “Geotechnical, Geological, and Earthquake Engineering”, we are publishing an Open Access book that can be downloaded freely by anybody interested in these topics. We believe that this option adopted by the Advisory Committee of 2ECEES, will enable a wide distribution and readability of the contributions presented by very prominent researchers in Europe.

The chapters in this second volume are composed of four keynote lectures, first of which is given by Shamita Das, the recipient of the first Inge Lehmann Lecture Award. Her lecture is entitled “*Supershear Earthquake Ruptures – Theory, Methods, Laboratory Experiments and Fault Superhighways: An Update*”. The other three keynote lectures are “*Civil Protection Achievements and Critical Issues in Seismology and Earthquake Engineering Research*” by Mauro Dolce and Daniela Di Bucci, “*Earthquake risk assessment: Certitudes, Fallacies, Uncertainties and the Quest for Soundness*” by Kyriazis Pitilakis and “*Variability and Uncertainty in Empirical Ground-Motion Prediction for Probabilistic Hazard and Risk Analyses*” by Peter J. Stafford.

The next nine chapters are the EAEE Theme Lectures: “*Seismic Code Developments for Steel and Composite Structures*” by Ahmed Y. Elghazouli; “*Seismic Analysis and Design of Foundation Soil-Structure Interaction*” by Alain Pecker; “*Performance-Based Seismic Design and Assessment of Bridges*” by Andreas Kappos; “*An Algorithm to Justify the Design of Single Story Precast Structures*”

by H.F. Karadoğan, I.E. Bal, E. Yüksel, S. Z. Yüce, Y.Durgun, and C. Soydan; “*Developments in Seismic Design of Tall Buildings: Preliminary Design of Coupled Core Wall Systems*” by M. Nuray Aydınoğlu and Eren Vuran; “*Seismic Response of Underground Lifeline Systems*” by Selçuk Toprak, Engin Nacaroğlu, and A. Cem Koç; “*Seismic Performance of Historical Masonry Structures Through Pushover and Nonlinear Dynamic Analyses*” by Sergio Lagomarsino and Serena Cattari; “*Developments in Ground Motion Predictive Models and Accelerometric Data Archiving in the Broader European Region*” by Sinan Akkar and Özkan Kale; and “*Towards the ‘Ultimate Earthquake-Proof’ Building: Development of an Integrated Low-Damage System*” by Stefano Pampanin.

The remaining six chapters are the ESC Theme Lectures “*Archive of Historical Earthquake Data for the European-Mediterranean Area*” by Andrea Rovida and Mario Locati; “*A Review and Some New Issues on the Theory of the HV Technique for Ambient Vibrations*” by Enrico Lunedei and Peter Malischewsky; “*Macroseismic Intervention Group: the Necessary Field Observation*” by Christophe Sira; “*Bridging the Gap Between Nonlinear Seismology as Reality and Earthquake Engineering*” by Gheorghe Marmureanu, Carmen-Ortanza Cioflan, Alexandru Marmureanu, Constantin Ionescu, and Elena-Florinela Manea; “*The Influence of Earthquake Magnitude on Hazard Related to Induced Seismicity*” by Benjamin Edwards; and “*On the Origin of Mega-Thrust Earthquakes*” by Kuvvet Atakan.

The Editor and the Advisory Committee of the Second European Conference on Earthquake Engineering and Seismology appreciate the support given by the Istanbul Governorship, Istanbul Project Coordination Unit, for the publication of the *Perspectives on European Earthquake Engineering and Seismology* volumes as Open Access books.

Istanbul, Turkey

A. Ansal

Contents

1	Supershear Earthquake Ruptures – Theory, Methods, Laboratory Experiments and Fault Superhighways: An Update	1
	Shamita Das	
2	Civil Protection Achievements and Critical Issues in Seismology and Earthquake Engineering Research	21
	Mauro Dolce and Daniela Di Bucci	
3	Earthquake Risk Assessment: Certitudes, Fallacies, Uncertainties and the Quest for Soundness	59
	Kyriazis Pitilakis	
4	Variability and Uncertainty in Empirical Ground-Motion Prediction for Probabilistic Hazard and Risk Analyses	97
	Peter J. Stafford	
5	Seismic Code Developments for Steel and Composite Structures	129
	Ahmed Y. Elghazouli	
6	Seismic Analyses and Design of Foundation Soil Structure Interaction	153
	Alain Pecker	
7	Performance-Based Seismic Design and Assessment of Bridges	163
	Andreas J. Kappos	
8	An Algorithm to Justify the Design of Single Story Precast Structures	207
	H.F. Karadoğan, I.E. Bal, E. Yüksel, S. Ziya Yüce, Y. Durgun, and C. Soydan	

9	Developments in Seismic Design of Tall Buildings: Preliminary Design of Coupled Core Wall Systems	227
	M. Nuray Aydınoğlu and Eren Vuran	
10	Seismic Response of Underground Lifeline Systems	245
	Selçuk Toprak, Engin Nacaroğlu, and A. Cem Koç	
11	Seismic Performance of Historical Masonry Structures Through Pushover and Nonlinear Dynamic Analyses	265
	Sergio Lagomarsino and Serena Cattari	
12	Developments in Ground Motion Predictive Models and Accelerometric Data Archiving in the Broader European Region	293
	Sinan Akkar and Özkan Kale	
13	Towards the “Ultimate Earthquake-Proof” Building: Development of an Integrated Low-Damage System	321
	Stefano Pampanin	
14	Archive of Historical Earthquake Data for the European-Mediterranean Area	359
	Andrea Rovida and Mario Locati	
15	A Review and Some New Issues on the Theory of the H/V Technique for Ambient Vibrations	371
	Enrico Lunedei and Peter Malischewsky	
16	Macroseismic Intervention Group: The Necessary Field Observation	395
	Christophe Sira	
17	Bridging the Gap Between Nonlinear Seismology as Reality and Earthquake Engineering	409
	Gheorghe Marmureanu, Carmen Ortanza Cioflan, Alexandru Marmureanu, Constantin Ionescu, and Elena Florinela Manea	
18	The Influence of Earthquake Magnitude on Hazard Related to Induced Seismicity	429
	Benjamin Edwards	
19	On the Origin of Mega-thrust Earthquakes	443
	Kuvvet Atakan	

Chapter 1

Supershear Earthquake Ruptures – Theory, Methods, Laboratory Experiments and Fault Superhighways: An Update

Shamita Das

Abstract The occurrence of earthquakes propagating at speeds not only exceeding the shear wave speed of the medium (~ 3 km/s in the Earth’s crust), but even reaching compressional wave speeds of nearly 6 km/s is now well established. In this paper, the history of development of ideas since the early 1970s is given first. The topic is then discussed from the point of view of theoretical modelling. A brief description of a method for analysing seismic waveform records to obtain earthquake rupture speed information is given. Examples of earthquakes known to have propagated at supershear speed are listed. Laboratory experiments in which such speeds have been measured, both in rocks as well as on man-made materials, are discussed. Finally, faults worldwide which have the potential to propagate for long distances ($>$ about 100 km) at supershear speeds are identified (“fault superhighways”).

1.1 Introduction

Seismologists now know that one of the important parameters controlling earthquake damage is the fault rupture speed, and changes in this rupture speed (Madariaga 1977, 1983). The changes in rupture speed generate high-frequency damaging waves. Thus, the knowledge of how this rupture speed changes during earthquakes and its maximum possible value are essential for reliable earthquake hazard assessment. But how high this rupture speed can be has been understood only relatively recently. In the 1950–1960s, it was believed that earthquake ruptures could only reach the Rayleigh wave speed. This was based partly on very idealized models of fracture mechanics, originating from results on tensile crack propagation velocities which cannot exceed the Rayleigh wave speed and which were simply

S. Das (✉)

Department of Earth Sciences, University of Oxford, Oxford OX1 3AN, UK

e-mail: das@earth.ox.ac.uk

© The Author(s) 2015

A. Ansal (ed.), *Perspectives on European Earthquake Engineering and Seismology*, Geotechnical, Geological and Earthquake Engineering 39, DOI 10.1007/978-3-319-16964-4_1

transferred to shear cracks. But more importantly, seismologists estimated the average rupture speed for several earthquakes by studying the directivity effects and spectra of seismic waves. The first was for the 1952 Ms ~7.6 Kern County, California earthquake. Benioff (1955) concluded that “the progression speed is in the neighborhood of speed of Rayleigh waves” using body wave studies. Similar conclusions were reached for several great earthquakes, including the 1960 great Chile earthquake (Press et al. 1961), the 1957 Mongolian earthquake (Ben-Menahem and Toksöz 1962), the 1958 Alaska earthquake (Brune 1961, 1962; Ben-Menahem and Toksöz 1963a) and the 1952 Kamchatka earthquake (Ben-Menahem and Toksöz 1963b) by studying directivity effects and/or spectra of very long wave length surface waves.

In the early 1970s, Wu et al. (1972) conducted laboratory experiments on plastic polymer, under very low normal stresses, and found supershear rupture speeds. This was considered unrealistic for real earthquakes, both the material and the low normal stress, and the results were ignored. Soon after, BurrIDGE (1973) demonstrated that faults with friction but without cohesion across the fault faces could exceed the shear wave speed and even reach the compressional wave speed of the medium. But since such faults are unrealistic for actual earthquakes, the results were again not taken seriously. In the mid- to late 1970s the idea that for in-plane shear faults with cohesion, terminal speeds exceeding not only the Rayleigh wave speed but even being as high as the compressional-wave speed was possible finally started being accepted, based on the work of Hamano (1974), Andrews (1976), Das (1976), and Das and Aki (1977). Once the theoretical result was established, scientists interpreting observations became more inclined to believe results showing supershear fault rupture speeds, and at the same time the data quality and the increase in the number of broadband seismometers worldwide, required to obtain detailed information on fault rupture started becoming available. Thus, the theory spurred the search for supershear earthquake ruptures.

The first earthquake for which supershear wave rupture speed was inferred was the 1979 Imperial Valley, California earthquake which had a moment-magnitude (M_w) of 6.5, studied by Archuleta (1984), and by Spudich and Cranswick (1984) using strong motion accelerograms. But since the distance for which the earthquake propagated at the high speed was not long, the idea was still not accepted universally. And then for nearly 25 years there were no further developments, perhaps because earthquakes which attain supershear speeds are rare, and none are known to have occurred. This provided ammunition to those who resisted the idea of super-sonic earthquake rupture speeds being possible.

Then, in the late 1990 to early 2000s, there were two major developments. Firstly, a group at Caltech, led by Rosakis, measured earthquake speeds in the laboratory, not only exceeding the shear wave speed (Rosakis et al. 1999; Xia et al. 2004) but even reaching the compressional wave speed (Xia et al. 2005). Secondly, several earthquakes with supershear wave rupture speeds actually occurred, with one even reaching the compressional wave speed. The first of these was the strike-slip earthquake of 1999 with M_w 7.6 in Izmit, Turkey (Bouchon et al. 2000, 2001), with a total rupture length of ~150 km, and with the

length of the section rupturing at supershear speeds being about 45 km. This study was based on two components of near-fault accelerograms recorded at one station (SKR). Then two larger supershear earthquakes occurred, namely, the 2001 Mw 7.8 Kunlun, Tibet earthquake (Bouchon and Vallée 2003; Antolik et al. 2004; Robinson et al. 2006b; Vallée et al. 2008; Walker and Shearer 2009), and the 2002 Mw 7.9 Denali, Alaska earthquake (Dunham and Archuleta 2004; Ellsworth et al. 2004; Frankel 2004; Ozacar and Beck 2004; Walker and Shearer 2009). Both were very long, narrow intra-plate strike-slip earthquakes, with significantly long sections of the faults propagating at supershear speeds. At last, clear evidence of supershear rupture speeds was available. Moreover, by analysing body wave seismograms very carefully, Robinson et al. (2006b) showed that not only did the rupture speed exceed the shear wave speed of the medium; it reached the compressional wave speed, which is about 70 % higher than the shear wave speed in crustal rocks.

Once convincing examples of supershear rupture speeds started to be found, theoretical calculations were carried out (Bernard and Baumont 2005; Dunham and Bhat 2008) and these suggested that the resulting ground shaking can be much higher for such rapid ruptures, due to the generation of Mach wave fronts. Such wave fronts, analogous to the “sonic boom” from supersonic jets, are characteristics and their amplitudes decrease much more slowly with distance than usual spherical waves do. Of course, much work still remains to be done in this area. Figure 1.1 shows a schematic illustrating that formulae from acoustics cannot be directly transferred to seismology. The reason is that many regions of the fault area are simultaneously moving at these high speeds, each point generating a Mach cone,

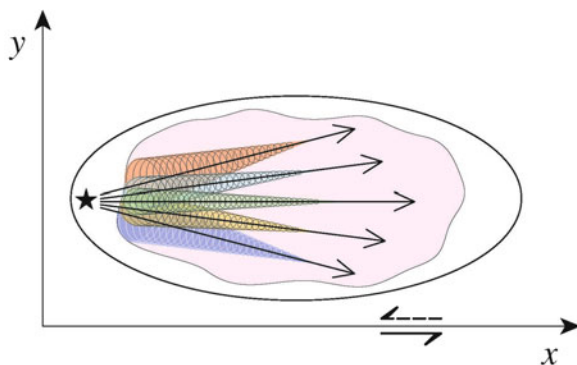


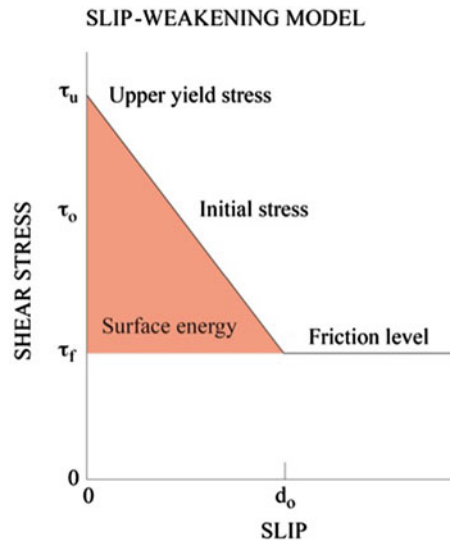
Fig. 1.1 Schematic representation of the leading edges of the multiple S-wave Mach cones generated by a planar fault spreading out in many directions, along the *black arrows*, from the hypocenter (*star*). The *pink shaded* region is the region of supershear rupture. The *thick black arrows* show the direction of the applied tectonic stress across the x - y plane. Supershear speeds cannot be reached in the y -direction (that is, by the Mode III or the anti-plane shear mode). The higher the rupture speed, the narrower each cone would be. Dunham and Bhat (2008) showed that additional Rayleigh wave Mach fronts would be generated along the Earth’s surface during supershear earthquake ruptures

and resulting in a the Mach surface. Moreover, different parts of the fault could move at different supershear speeds, again introducing complexity into the shape and amplitudes of the Mach surface. Finally, accounting for the heterogeneity of the medium surrounding the fault through which these Mach fronts propagate would further modify the Mach surface. There could be special situations where the individual Mach fronts comprising the Mach surface could interfere to even lower, rather than raise, the resulting ground shaking. Such studies would be of great interest to the earthquake engineering community.

1.2 Theory

Since damaging high-frequency waves are generated when faults change speed (Madariaga 1977, 1983), the details of how faults start from rest and move at increasing speeds is very important. Though in-plane shear faults (primarily strike-slip earthquakes) can not only exceed the shear wave speed of the medium, but can even reach the compressional wave speed, steady-state (constant speed) calculations on singular cracks (with infinite stress at the fault edges) had shown that speeds between the Rayleigh and shear wave speeds were not possible, due to the fact that in such a case there is negative energy flux into the fault edge from the surrounding medium, that is, such a fault would not absorb elastic strain-energy but generate it (Broberg 1989, 1994, 1999). Theoretical studies by Andrews (1976) and Burridge et al. (1979) using the non-singular slip-weakening model (Fig. 1.2), introduced by Ida (1972) suggested that even for such 2-D in-plane faults which start from rest and accelerate to some terminal velocity, such a forbidden zone does exist.

Fig. 1.2 The linear “slip-weakening model”, relating the fault slip to the stress at the edge of the fault. The region between 0 to d_0 is called the “break-down” zone, where the earthquake stress release occurs. Cruz-Atienza and Olsen (2010) estimated d_0 to be ~ 2 m for the 1999 Izmit, Turkey and 2002 Denali, Alaska earthquakes



Recent work of Bizzari and Das (2012) showed that for the 3-D mixed in-plane and anti-plane shear mode fault, propagating under this slip-weakening law, the rupture front actually does pass smoothly through this forbidden zone, but very fast. The width of the cohesive zone initially decreases, then increases as the rupture exceeds the shear wave speed and finally again decreases as the rupture accelerates to a speed of $\sim 90\%$ of the compressional wave speed. The penetration of the ‘forbidden zone’ has very recently also been confirmed for the 2-D in-plane shear fault for the same linear slip-weakening model by Liu et al. (2014). To reiterate, this is important as this smooth transition from sub- to super- shear wave speeds would reduce damage.

1.3 Seismic Data Analysis

The inverse problem of earthquake source mechanics consists of analysing seismograms to obtain the details of the earthquake rupture process. This problem is known to be unstable (Kostrov 1975; Olson and Apsel 1982; Kostrov and Das 1988; Das and Kostrov 1990) and requires additional constraints to stabilize it. In order to demonstrate the basic ideas involved, we follow the formulation of Das and Kostrov (1990, 1994) here.

By modifying the representation theorem (e.g., equation (3.2) of Aki and Richards (1980, 2002); equation (3.2.18) of Kostrov and Das (1988)), the displacement at a seismic station can be written as the convolution of the components of the slip rate on the fault with a step-function response of the medium. Note that the usual formulation convolves the slip with the delta function response of the medium, but since moving the time derivative from one term of the convolution to the other does not change the value of the integral, Das and Kostrov’s formulation uses the slip rate on the fault convolved with a singular term but with a weaker integrable singularity, making the problem mathematically more tractable and more stable. The convolution extends over the fault area and the time over which the fault slips. Full details can be found in Das and Kostrov (1990, 1994). The resulting integral equation is of the first kind and known to be unstable. Thus, these authors stabilized the equations by adding physically-based additional constraints, the most important of this being that the slip-rate on the fault is non-negative, called the “no-backslip constraint”. Numerical modelling of ruptures show that this is very likely for large earthquakes. To solve the integral equation numerically, it must be discretized. For this, the fault area is divided into a number of rectangular cells and the slip-rate is approximated within each cell by linear functions in time and along strike and by a constant along dip. The time at the source is discretized by choosing a fixed time step, and assuming that the slip rate during the time step varies linearly with time. The Heaviside kernel is then integrated over each cell analytically, and the integrals over the fault area and over time are replaced by sums. The optimal size of the spatial cells and the time steps should be determined

by some synthetic tests, as discussed, for example by Das and Suhadolc (1996), Das et al. (1996), and Sarao et al. (1998) for inversions using strong ground motion data and by Henry et al. (2000, 2002) for teleseismic data inversions. The fault area and the total source duration are not assigned a priori but determined as part of the inversion process. An initial fault area is assigned based on the aftershock area and then refined. An initial value of the finite source duration is estimated, based on the fault size and a range of average rupture speeds, and it cannot be longer than the longest record used. The integral equation then takes the form of a system of linear equations $\mathbf{A} \mathbf{x} \approx \mathbf{b}$, where \mathbf{A} is the kernel matrix obtained by integrating it over each cell, each column of \mathbf{A} corresponding to different cells and time instants of the source duration, ordered in the same way as the vector of observed seismograms \mathbf{b} , and \mathbf{x} is vector of unknown slip rates on the different cells on the fault at different source time-steps. The no back-slip constraint then becomes $\mathbf{x} \geq 0$. In order to reduce the number of unknowns, a very weak causality condition could be introduced, for example, x 's beyond the first compressional wave from the hypocenter could be set to 0. If desired, the seismic moment could be required to be equal to that obtained say, from the centroid-moment tensor (CMT) solution. With the high-quality of broadband data now available, this constraint is not necessary and it is found that when stations are well distributed in azimuth around the earthquake, the seismic moment obtained by the solution is close to the CMT moment. In addition, Das and Kostrov (1990, 1994) permitted the entire fault behind the rupture front to slip, if the data required it, unlike studies where slipping is confined only to the vicinity of the rupture front. If there is slippage well behind the main rupture front in some earthquake, then this method would find it whereas others would not. Such a case was found by Robinson et al. (2006a) for the 2001 Mw 8.4 Peru earthquake.

Thus, the inverse problem is the solution of the linear system of equations under one or more constraints, in which the number of equations m is equal to the total number of samples taken from all the records involved and the number of unknowns n is equal to the number of spatial cells times on the fault times the number of time steps at the source. Taking $m > n$, the linear system is over determined and a solution \mathbf{x} which provides a best fit to the observations is obtained. It is well known that the matrix \mathbf{A} is often ill-conditioned which implies that the linear system admits more than one solution, equally well fitting the observations. The introduction of the constraints reduces the set of permissible (feasible) solutions. Even when a unique solution does exist, there may be many other solutions that almost satisfy the equations. Since the data used in geophysical applications often contain experimental noise and the models used are themselves approximations to reality, solutions almost satisfying the data are also of great interest.

Finally, for the system of equations together with the constraints to comprise a complete mathematical problem, the exact form of what the "best fit" to observations means has to be stated. For this problem, we have to minimize the vector of residuals, $\mathbf{r} = \mathbf{b} - \mathbf{A} \mathbf{x}$, and some norm of the vector \mathbf{r} must be adopted. One may choose to minimize minimize the ℓ_1 , the ℓ_2 or the ℓ_∞ norm (see Tarantola 1987 for a discussion of different norms), all three being equivalent in the sense that they tend

to zero simultaneously. Das and Kostrov (1990, 1994) used the linear programming method to solve the linear system and minimized the ℓ_1 norm subject to the positivity constraint, using programs modified from Press et al. (1986). In various studies, they have evaluated the other two norms of the solution to investigate how they behave, and find that when the data is fitted well, the other two norms are also small. A method with many similarities to that of Das and Kostrov (1990, 1994) was developed by Hartzell and Heaton (1983). Hartzell et al. (1991) also carried out a comprehensive study comparing the results of using different norms in the inversion. Parker (1994) has discussed the positivity constraint in detail.

In order to confirm that the solution obtained is reliable Das and Kostrov (1994), introduced additional levels of optimization. For example, if a region with high or low slip was found, fitting the data by lowering or raising the slip in that region was attempted to see if the data was still well fitted. If it did not, then the features were considered robust. If high rupture speed was found in some portion of the fault, its robustness was treated similarly. All features interpreted geophysically can be tested in this way. Some examples can be found in Das and Kostrov (1994), Henry et al. (2000), Henry and Das (2002), Robinson et al. (2006a, b).

1.4 A Case Study of a Supershear Earthquake

1.4.1 *The 2001 Mw 7.8 Kunlun, Tibet Earthquake*

This >400 km long earthquake was, at the time of its occurrence, the longest known strike-slip earthquake, on land or underwater, since the 1906 California earthquake. The earthquake occurred on a left-lateral fault, propagating unilaterally from west to east, on one of the great strike-slip faults of Tibet, along which some of the northward motion of the Indian plate under Tibet is accommodated by lateral extrusion of the Tibetan crust. It produced surface ruptures, reported from field observations, with displacements as high as 7–8 m (Xu et al. 2002), [initially even larger values were estimated by Lin et al. (2002) but these were later revised down], this large value being supported by interferometric synthetic aperture radar (InSAR) measurements (Lasserre et al. 2005), as well as the seismic body wave studies referred to below. Bouchon and Vallée (2003) used mainly Love waves from regional seismograms to show that the average rupture speed was ~ 3.9 km/s, exceeding the shear wave speed of the crustal rocks, and P-wave body wave studies confirmed this (Antolik et al. 2004; Ozacar and Beck 2004). More detailed analysis of SH body wave seismograms, using the inversion method of Kostrov and Das (1990, 1994), showed that the rupture speed on the Kunlun fault during this earthquake was highly variable and the rupture process consisted of three stages (Robinson et al. 2006b). First, the rupture accelerated from rest to an average speed of 3.3 km/s over a distance of 120 km. The rupture then propagated for another 150 km at an apparent rupture speed exceeding the P wave speed, the

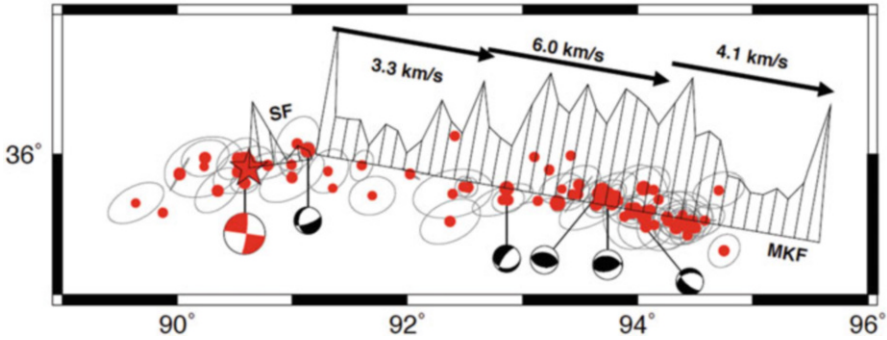


Fig. 1.3 Schematic showing the final slip distribution for the 2001 Kunlun, Tibet earthquake, with the average rupture speeds in 3 segments marked. Relocated aftershocks for the 6 month period following the earthquake (Robinson et al. 2006a, b) are shown as *red dots*, with the symbol size scaling with earthquake magnitude. The maximum slip is ~ 6.95 m. The centroid-moment tensor solution for the main shock (*star* denotes the epicenter, its cmt is in *red*) and those available for the larger aftershocks (cmts in *black*) are shown. The longitude (E) and latitude (N) are marked. The impressive lack of aftershocks, both in number and in size, for such a large earthquake was shown by Robinson et al. (2006b)

longest known segment propagating at such a high speed for any earthquake fault (Fig. 1.3). Finally, the fault bifurcated and bent, the rupture front slowed down, and came to a stop at another sharper bend, as shown in Robinson et al. (2006b). The region of the highest rupture velocity coincided with the region of highest fault slip, highest fault slip rate, highest stress drop (stress drop is what drives the earthquake rupture), the longest fault slipping duration and had the greatest concentration of aftershocks. The location of the region of the large displacement has been independently confirmed from satellite measurements (Lasserre et al. 2005). The fault width (in the depth direction) for this earthquake is variable, being no more than 10 km in most places and about 20 km in the region of highest slip.

Field observations, made several months later, showed a ~ 25 km wide region to the south of the fault in the region of supershear rupture speed, with many off-fault open (tensile) cracks. These open cracks are confined only to the off-fault section of high speed portion of the fault, and were not seen off-fault of the lower rupture speed portions of the fault, though those regions were also visited by the scientists (Bhat et al. 2007). Theoretical results show that as the rupture moves from sub- to super- shear speeds, large normal stresses develop in the off-fault regions close to the fault, as the Mach front passes through. Das (2007) has suggested that observations of such off-fault open cracks could be used as an independent diagnostic tool for identifying the occurrence of supershear rupture and it would be useful to search for and document them in the field for large strike-slip earthquakes.

The special faulting characteristics (Bouchon et al. 2010) and the special pattern of aftershocks for this and other supershear earthquakes (Bouchon and Karabulut 2008) has been recently been noted.

1.5 Conditions Necessary for Supershear Rupture

A striking observation for the 2001 Kunlun earthquake is that the portion of the fault where rupture propagated at supershear speeds is very long and very straight. Bouchon et al. (2001) showed that for the 1999 Izmit, Turkey earthquake fault the supershear eastern segment of the fault was very straight and very simple, with no changes in fault strike, say, jogs, bends, step-overs, branching etc. Examination of the 2002 Denali, Alaska earthquake fault shows the portion of the fault identified by Walker and Shearer (2009) as having supershear rupture speeds is also long and straight. The Kunlun earthquake showed that a change in fault strike direction slows the fault down, and a large variation in strike stops the earthquake (Robinson et al. 2006b). Based on these, we can say that necessary (though not sufficient) conditions for supershear rupture to continue for significant distances are: (i) The strike-slip fault must be very straight (ii) The longer the straight section, the more likely is supershear speed, provided: (a) fault friction is low (b) no other impediments or barriers exist on the fault. Of course, very locally short sections could reach supershear speeds, but the resulting Mach fronts would be small and local, and thus less damaging. It is the sustained supershear wave speed over long distances that would create large Mach fronts.

1.6 Laboratory Experiments

Important support, and an essential tool in the understanding of supershear rupture speeds in earthquakes, comes from laboratory experiments on fracture. As mentioned in the introduction, the first time supershear rupture speeds were ever mentioned with respect to earthquakes was the experiment of Wu et al. (1972). The pioneering work led by Rosakis at Caltech, starting in the late 1990s, finally convinced scientists that such earthquake rupture speeds were possible. Though these experiments were carried out on man-made material (Homalite), and the rupture and wave fronts were photographed, they revolutionised our way of thinking. More recently, Passelègue et al. (2013) at the École Normale Supérieure in Paris obtained supershear rupture speeds in laboratory experiments on rock samples (Westerly granite). The rupture front position was obtained by analysis of acoustic high-frequency recordings on a multistation array. This is clearly very close to the situation in seismology, where the rupture details are obtained by seismogram (time-series) analysis, as discussed earlier. However, in the real Earth, the earthquake ruptures propagate through material at higher temperatures and pressures than those in these experiments. Future plans by the Paris group includes upgrading their equipment to first studying the samples at higher pressures, and then moving on to higher temperatures as well, a more technologically challenging problem.

1.7 Potential Supershear Earthquake Hazards

Earthquakes start from rest and need to propagate for some distance to reach their maximum speed (Kostrov 1966). Once the maximum speed is reached, the earthquake could continue at this speed, provided the fault is straight, and no other barriers exist on it, as mentioned above. Faults with many large changes in strike, or large step-overs, would thus be less likely to reach very high rupture speeds as this would cause rupture on such faults to repeatedly slow down, before speeding up again, if the next segment is long enough. The distance necessary for ruptures to propagate in order to attain supershear speeds is called the transition distance and is currently still a topic of vigorous research and depends on many physical parameters of the fault, such as the fault strength to stress-drop ratio, the critical fault length required to reach supershear speeds, etc. (Andrews 1976; Dunham 2007; Bizzari and Das 2012; Liu et al. 2014).

Motivated by the observation that the rare earthquakes which propagated for significant distances at supershear speeds occurred on very long straight segments of faults, we examined every known major active strike-slip fault system on land worldwide and identified those with long (>100 km) straight portions capable not only of sustained supershear rupture speeds but having the potential to reach compressional wave speeds over significant distances, and call them “*fault superhighways*”. Detailed criteria for each fault chosen to be considered a superhighway are discussed in Robinson et al. (2010), including when a fault segment is considered to be straight. Every fault selected, except one portion of the Red River fault and the Dead Sea Fault has had earthquakes of magnitude >7 on it in the last 150 years. These superhighways, listed in Table 1.3, include portions of the 1,000 km long Red River fault in China and Vietnam passing through Hanoi, the 1,050 km long San Andreas fault in California passing close to Los Angeles, Santa Barbara and San Francisco, the 1,100 km long Chaman fault system in Pakistan north of Karachi, the 700 km long Sagaing fault connecting the first and second cities of Burma (Rangoon and Mandalay), the 1,600 km Great Sumatra fault, and the 1,000 km Dead Sea fault. Of the 11 faults classified as ‘superhighways’, 9 are in Asia and 2 in North America, with 7 located near areas of very dense population. Based on the population distribution within 50 km of each fault superhighway, obtained from the United Nations database for the Year 2005 (Gridded Population of the World 2007), we find that more than 60 million people today have increased seismic hazards due to such faults. The main aim of this work was to identify those sections of faults where additional studies should be targeted for better understanding of earthquake hazard for these regions. Figure 1.4 shows the world map, with the locations of the superhighways marked, and the world population density.

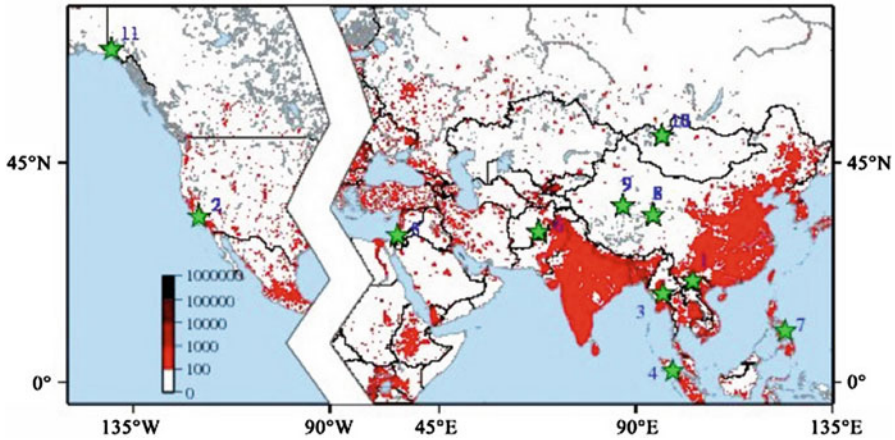


Fig. 1.4 Location of earthquake superhighways worldwide, shown as *green stars*, numbered as in Table 1.3. The world population (Gridded Population of the World 2007), in inhabitants per $30' \times 30'$, is coloured as per the key. The zigzag band has no superhighways in it

1.7.1 The Red River Fault, Vietnam/China

Since we consider this to be the most dangerous fault in the world (Robinson et al. 2010), as well as one less well studied compare to some other faults, particularly the San Andreas fault, it is discussed here in detail, in order to encourage more detailed studies there. The Red River fault runs for about 1,000 km, through one of the most densely populated regions of the world, from the south-eastern part of Tibet through Yunnan and North Vietnam to the South China Sea. Controversy exists regarding total geological offsets, timing of initiation and depth of the Red River fault. Many authors propose that it was a long-lasting plate boundary (between Indochina and South China ‘blocks’) initiated ~ 35 Ma ago, accommodating between 500 and 1,050 km of left-lateral offset, and extending down into the mantle. Many others propose that it is only a crustal scale fault, ~ 29 – 22 Myold. Although mylonites along the metamorphic complexes show ubiquitous left-lateral shear fabrics, geodetic data confirm that recent motion has been right-lateral. Seismic sections across the Red River delta in the Gulf of Tonkin clearly suggest that at least offshore of Vietnam the fault is no longer active.

Although the Red River fault system is highly complex, Robinson et al. (2010) were able to identify three sections of it as having potential for supershear rupture (Fig. 1.5). In Vietnam, the Red River fault branches into numerous strands as it runs through the thick sediments of the Red River delta near Hanoi. Although there is no known record of recent major earthquakes on the main Red River fault in Vietnam (Utsu 2002), two sub-parallel strands of this fault near Hanoi appear remarkably straight, hence we identify two ~ 250 km sections here as being superhighways. The consequences of a long supershear rupture in this area would be catastrophic. A second, 280 km long, segment is identified in the Chuxiong Basin section of the

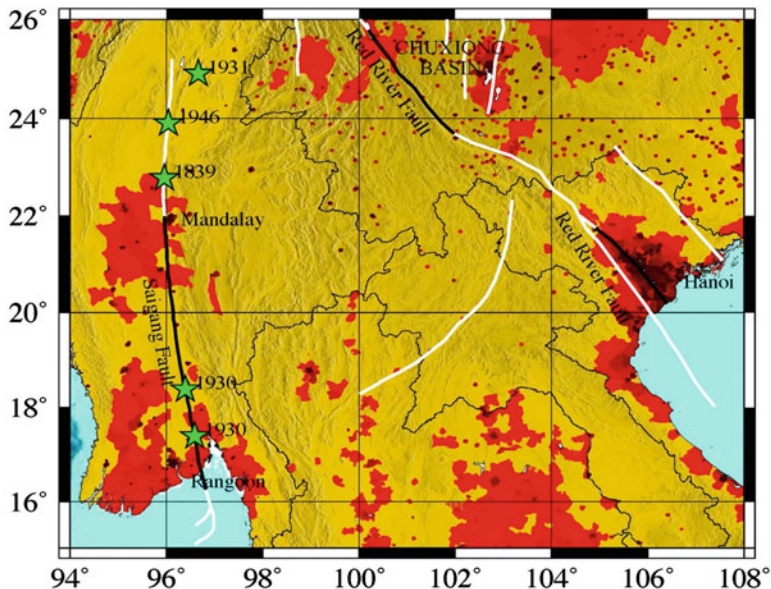


Fig. 1.5 Map of southeastern China, Vietnam and Myanmar showing the 700 km superhighway of the 1,000 km long Sagaing fault, Myanmar, and the 280 and 250 km superhighways of the 800 km Red River (Honghe) fault. Known faults (Yeats et al. 1997) are shown as white lines, with superhighways shown in black. The world population (Gridded Population of the World) (in inhabitants per $30' \times 30'$) is shown, according to the colour key shown in Fig. 1.4, with populations less than 100 people per $30' \times 30'$ shown as transparent, overlain on a digital elevation map of the region. Locations of known large earthquakes on these faults (Table 1.3) are marked

fault, where it appears to be straight and simple. This area has a long history of documented significant earthquakes on nearby faults (Yeats et al. 1997; Fig. 8.12 of Yeats 2012).

1.7.2 The Sagaing Fault, Burma

The second-most dangerous superhighway in Table 1.3 is the San Andreas fault in California but since it has been very heavily discussed in the literature we do not discuss it here. Instead, we discuss the third-most dangerous superhighway. This 1,100 km long right-lateral strike-slip fault in Myanmar (Burma) forms the present-day eastern plate boundary of India (Fig. 1.5). Estimates of long-term geological offsets along the fault range from 100 to 150 km to ~450 km, motion along the Sagaing Fault probably initiating ~22 Ma. The Sagaing fault is very continuous between Mandalay and Rangoon, with the central 700 km from (17 to 23°N) being “remarkably linear” (Vigny et al. 2003). It is the longest, continuous linear strike-slip fault identified globally. North of 23°N, the fault begins to curve slightly but it

is still possible that supershear rupture could proceed for a considerable distance. We have identified about 700 km of this fault as having the potential for sustained supershear rupture (Fig. 1.5). There were large earthquakes on the fault in 1931, 1946, 1839, 1929, and two in 1930 (Yeats et al. 1997). With the cities of Rangoon (Yangon) (population exceeding five million) and Mandalay (population approaching one million) at, respectively, the southern and northern ends of this straight portion, supershear earthquakes propagating either northwards or southwards could focus energy on these cities. In addition, the highly populated off-fault regions would have increased vulnerability due to the passing Mach fronts, thereby exacerbating the hazard.

1.8 Discussion

Tables 1.1 and 1.2 show that it is only in the last 2 years that we have found the first example of two under-water earthquakes reaching supershear speeds, showing that this is even rarer for marine earthquakes than ones on continents. Very recently, a deep earthquake at ~650 km depth has been inferred to have had supershear speed (Zhan et al. 2014).

Sometimes earthquakes in very different parts of the world in very different tectonic regimes have remarkable similarities. Das (2007) has compared the 2001 Tibet earthquake and the 1906 California earthquake, the repeat of which would be a far greater disaster, certainly in financial terms, than the 2004 Sumatra-Andaman earthquake and tsunami! They are both vertical strike-slip faults, have similar M_w , fault length and width, and hence similar average slip and average stress drop. The right-lateral 1906 earthquake rupture started south of San Francisco, and propagated bilaterally, both to the northwest and to the southeast. Geodetic measurements showed that the largest displacements were on the segment to the north of San Francisco, which is in agreement with results obtained by inversion of the very few available seismograms. It has recently been suggested that this northern segment may have reached supershear rupture speeds (Song et al. 2008). The fact that the high fault displacement region is where the fault is very straight, would provide additional support to this, if the 1906 and the 2001 earthquakes behaved similarly. Unfortunately, due to heavy rains and rapid rebuilding following the 1906 earthquake, no information is available on whether or not off-fault cracks appeared in this region. The cold desert climate of Tibet had preserved the off-fault open cracks from the 2001 earthquake, un-eroded during the winter months, till the scientists visited in the following spring. Similar considerations deserve to be made for other great strike-slip faults around the world, for example, along the Himalayan-Alpine seismic belt, New Zealand, Venezuela, and others, some of which are discussed next.

Table 1.1 Recent large strike-slip earthquakes without supershear rupture speed

Date	Location	Mw	Fault length (km)	On land or underwater	References
1989	Macquarie Ridge	8.0	200	Underwater	Das (1992, 1993))
1998	Antarctic Ocean	8.1	140, 60 ^a	''	Henry et al. (2000)
2000	Wharton Basin	7.8	80	''	Robinson et al. (2001)
2004	Tasman Sea	8.1	160, 100 ^a		Robinson (2011)

^aTwo sub-events

Table 1.2 Strike-slip earthquakes known to have reached supershear rupture speeds

Year	Mw	Location	Supershear segment length (km)	Type of data used to study the quake	Land or sea	Reference
1979	6.5	Imperial Valley, California	35	Strong ground motion	Land	Archuleta (1984), Spudich and Crowsick (1984)
1999	7.6	Izmit, Turkey	45	''	''	Bouchon et al. (2002)
1999	7.2	Duzce, Turkey	40	''	''	Bouchon et al. (2001)
2001	7.8	Kunlun, Tibet	>400	Teleseismic	''	Robinson et al. (2006a, b)
2002	7.9	Denali, Alaska	340	''	''	Walker and Shearer (2009)
2012	8.6	N. Sumatra	200, 400, 400	''	Sea	Wang et al. (2012)
2013	7.5	Craig, Alaska	100	''	''	Yue et al. (2013)

1.9 Future Necessary Investigations

There are several other faults with shorter straight segments, which may or may not be long enough to reach supershear speeds. Although we do not identify them as fault superhighways, they merit mention. Of these, the 1,400 km long North Anatolian fault in Turkey is the most particularly note-worthy, since supershear (though not near-compressional wave speed) rupture has actually been inferred to have occurred on it (Bouchon et al. 2001). The fault is characterized by periods of quiescence (of about 75–150 years) followed by a rapid succession of earthquakes, the most famous of these is the “unzipping” of the fault starting in 1939. For the most part the surface expression of the fault is complex, with many segments and en-echelon faults. It seems that large earthquakes (e.g., 1939, 1943, 1944) are able to rupture multiple segments of these faults but it is unlikely that in jumping from one segment to another, they will be able to sustain rupture velocities in excess of

the shear wave velocity. The longest “straight, continuous” portion of the North Anatolian Fault lies in the rupture area of the 1939 Erzincan earthquake, to the west of its epicenter, just prior to a sharp bend of the fault trace to the south (Yeats et al. 1997). This portion of fault is approximately 80 km long. Additionally, this branch which continues in the direction of Ankara (the Sungurlu fault zone) appears to be very straight. However, the Sungurlu fault zone is characterized by very low seismicity and is difficult to map due to its segmentation. Thus it is unlikely that supershear rupture speeds could be maintained on this fault for a significant distance. Since the North Anatolian fault runs close to Ankara and Istanbul, it is a candidate for further very detailed in-depth studies.

Another noteworthy fault is the Wairarapa fault in New Zealand, which is reported to have the largest measured coseismic strike-slip offset worldwide during the 1855 earthquake, with an average offset of ~16 m (Rodgers and Little 2006), but this high displacement is estimated over only 16 km of its length. Although a ~120 km long fault scarp was produced in the 1855 earthquake, the Wairarapa fault is complex for much of its length as a series of splay faults branch off it. One straight, continuous, portion of the fault is seen in the Southern Wairarapa valley, but this is only ~40 km long. Thus it is less likely that this fault could sustain supershear rupture over a considerable distance.

It is interesting to note that since the mid-1970s, when very accurate magnitudes of earthquakes became available, no strike-slip earthquake on land appears to have $M_w > 7.9$ (two earthquakes in Mongolia in 1905 are supposed to have been > 8 , but the magnitudes of such old earthquakes are not reliably known), even some with rupture lengths > 400 km. Yet they can produce surprisingly large damage. Perhaps this could be explained by the multiple shock waves, carrying large ground velocities and accelerations, generated by supershear ruptures. A good example is the 1812 Caracas, Venezuela earthquake, described by John Milne (see Milne and Lee 1939), which devastated the city with more than 10,000 killed in 1 min. The earthquake is believed to be of magnitude about 7.5, and to have occurred on the Bocono fault, which is ~125 km away (Perez et al. 1997), but there is no known local geological feature, such as a sedimentary basin, to amplify the motion. So one could suggest either that the fault propagated further towards Caracas than previously believed, or reached supershear rupture speeds, or both.

1.10 Conclusions

Table 1.3 is ordered by the number of people expected to be affected by a fault superhighway, and the list would look very different if it was listed in financial terms. In addition, faults in less populated areas could then become much more important. The 2011 Christchurch, New Zealand earthquake with a M_w of only 6.1 led to the second largest insurance claim in history (Financial Times, London, March 28, 2012). Even though no supershear rupture was involved in this, it shows that financial losses depend on very different circumstances than simply the number

Table 1.3 Earthquake fault superhighways

	Fault system and location	Total length (km)	Segment lengths ^a (km)	Affected population (millions) ^b	Size and dates of past earthquakes ^c
1	Red River, Vietnam/China	1,000	280, 230, 290	25.7	7.7 (1733), 8.0 (1833)
2	San Andreas, California	1,050	160, 230	13.1	7.9 (1857), 7.9 (1906)
3	Sagaing, Burma	1,000	700	9.1	N.D. (1839), 7.3 (1930), 7.3 (1930), 7.6 (1931), 7.5 (1936), 7.4 (1946),
4	Great Sumatra	1,600	100, 160, 220, 200	6.7	7.7 (1892), 7.6 (1909), 7.5 (1933), 7.4 (1943), 7.6 (1943)
5	Dead Sea, Jordan/Israel	1,000	100, 125	5.2	N.D. (1068), N.D. (1170), N.D. (1202)
6	Chaman/Herat, Pakistan/Afghanistan	1,100	170, 320, 210	2.5	N.D. (1892)
7	Luzon, Philippines	1,600	130	2.1	7.8 (1990)
8	Kunlun, Tibet	1,600	270, 130, 180, 100	0.15	7.5 (1937), 7.8 (2001)
9	Altyn Tagh, Tibet	1,200	100, 100, 150	0.062	7.6 (1932)
10	Bulnay, Mongolia	300	100, 200	0.020	7.8, 8.2 (1905)
11	Denali, Alaska	1,400	130	Negligible	7.8 (2002)

^aLengths of straight segments, identified as superhighways, listed from south to north

^bCurrent population, in millions, within 50 km of the superhighways, this being the region expected to be most damaged by earthquakes propagating along the superhighways

^cMagnitude of old earthquakes are surface wave magnitude or moment-magnitude, as available; N.D. if unknown

of people affected. Another interesting example is the 2002 Denali, Alaska fault, which intersects the Trans-Alaska pipeline. Due to extreme care in the original construction (Pers. Comm., Lloyd Cluff), it was not damaged, but the environmental catastrophe for an oil spill in the pristine national park would have had indirect financial consequences, the most important being the possible prevention of it being ever allowed to re-open again. In many places of low population density, Governments may consider placing power plants (nuclear or otherwise), and such installations need to be built keeping in mind the possibility of supershear rupture on nearby faults. Clearly, many other major strike-slip faults worldwide, not classed as a superhighway yet, deserve much closer inspection with very detailed studies to fully assess their potential to reach supershear rupture speeds.

Acknowledgements I would like to thank two distinguished colleagues, Raul Madariaga and Michel Bouchon, for reading the manuscript and providing many useful comments, which improved and clarified it.

Open Access This chapter is distributed under the terms of the Creative Commons Attribution Noncommercial License, which permits any noncommercial use, distribution, and reproduction in any medium, provided the original author(s) and source are credited.

References

- Aki K, Richards P (1989) Quantitative seismology: theory and methods. WH Freeman and Company, San Francisco
- Aki K, Richards P (2002) Quantitative seismology: theory and methods. University Science, Sausalito
- Antolik M, Abercrombie RE, Ekström G (2004) The 14 November 2001 Kokoxili (Kunlunshan), Tibet, earthquake: rupture transfer through a large extensional step-over. *Bull Seismol Soc Am* 94:1173–1194
- Andrews DJ (1976) Rupture velocity of plane strain shear cracks. *J Geophys Res* 81:5679–5687
- Archuleta R (1984) Faulting model for the 1979 Imperial Valley earthquake. *J Geophys Res* 89:4559–4585
- Benioff H (1952) Mechanism and strain characteristics of the White Wolf fault as indicated by the aftershock sequence, Earthquakes in Kern County, California during 1952. *Bull Calif Div Mines Geology* 171:199–202
- Ben-Menahem A, Toksöz MN (1962) Source mechanism from spectra of long-period seismic surface waves 1. The Mongolian earthquake of December 4, 1957. *J Geophys Res* 67:1943–1955
- Ben-Menahem A, Toksöz MN (1963a) Source mechanism from spectrums of long-period surface waves: 2. The Kamchatka earthquake of November 4, 1952. *J Geophys Res* 68:5207–5222
- Ben-Menahem A, Toksöz MN (1963b) Source mechanism from spectrums of long-period seismic surface waves. *Bull Seismol Soc Am* 53:905–919
- Bernard P, Baumont D (2005) Shear Mach wave characterization for kinematic fault rupture models with constant supershear rupture velocity. *Geophys J Int* 162:431–447
- Bhat HS, Dmowska R, King GCP, Klinger Y, Rice JR (2007) Off-fault damage patterns due to supershear ruptures with application to the 2001 Mw 8.1 Kokoxili (Kunlun) Tibet earthquake. *J Geophys Res* 112:B06301
- Bizzari A, Das S (2012) Mechanics of 3-D shear cracks between Rayleigh and shear wave speeds. *Earth Planet Sci Lett* 357–358:397–404
- Bouchon M, Toksöz MN, Karabulut H, Bouin MP, Dietrich M, Aktar M, Edie M (2002) Space and time evolution of rupture and faulting during the 1999 Izmit (Turkey) earthquake. *Bull Seismol Soc Am* 92:256–266
- Bouchon M, Vallée M (2003) Observation of long supershear rupture during the magnitude 8.1 Kunlunshan earthquake. *Science* 301:824–826
- Bouchon M et al (2010) Faulting characteristics of supershear earthquakes. *Tectonophysics* 493:244–253
- Bouchon M, Karabulut H (2008) The aftershock signature of supershear earthquakes. *Science* 320:1323–1325
- Bouchon M, Bouin MP, Karabulut H, Toksöz MN, Dietrich M, Rosakis AJ (2001) How fast is rupture during an earthquake? New insights from the 1999 Turkey earthquakes. *Geophys Res Lett* 28:2723–2726

- Bouchon M, Toksoz MN, Karabulut H, Bouin MP, Dietrich M, Aktar M, Edie M (2000) Seismic imaging of the Izmit rupture inferred from the near-fault recordings. *Geophys Res Lett* 27:3013–3016
- Broberg KB (1989) The near-tip field at high crack velocities. *Int J Fract* 39:1–13
- Broberg KB (1994) Intersonic bilateral slip. *Geophys J Int* 119:706–714
- Broberg KB (1999) *Cracks and fracture*. Academic, New York
- Brune JN (1961) Radiation pattern of Rayleigh waves from the Southeast Alaska earthquake of July 10, 1958. *Publ Dom Observ* 24:1
- Brune JN (1962) Correction of initial phase measurements for the Southeast Alaska earthquake of July 10, 1958, and for certain nuclear explosions. *J Geophys Res* 67:3463
- Burridge R (1973) Admissible speeds for plane-strain self-similar shear crack with friction but lacking cohesion. *Geophys J Roy Astron Soc* 35:439–455
- Burridge R, Conn G, Freund LB (1979) The stability of a rapid Mode II shear crack with finite cohesive traction. *J Geophys Res* 84:2210–2222
- Cruz-Atienza VM, Olsen KB (2010) Supershear Mach-waves expose the fault breakdown slip. *Tectonophysics* 493:285–296
- Das S (2007) The need to study speed. *Science* 317:889–890
- Das S (1992) Reactivation of an oceanic fracture by the Macquarie Ridge earthquake of 1989. *Nature* 357:150–153
- Das S (1993) The Macquarie Ridge earthquake of 1989. *Geophys J Int* 115:778–798
- Das S (1976) A numerical study of rupture propagation and earthquake source mechanism DSc thesis, Massachusetts Institute of Technology, Cambridge
- Das S, Aki K (1977) A numerical study of two-dimensional rupture propagation. *Geophys J Roy Astron Soc* 50:643–668
- Das S, Kostrov BV (1994) Diversity of solutions of the problem of earthquake faulting inversion: application to SH waves for the great 1989 Macquarie Ridge earthquake. *Phys Earth Planet Int* 85:293–318
- Das S, Kostrov BV (1990) Inversion for slip rate history and distribution on fault with stabilizing constraints – the 1986 Andreanof Islands earthquake. *J Geophys Res* 95:6899–6913
- Das S, Suhadolc P (1996) On the inverse problem for earthquake rupture. The Haskell-type source model. *J Geophys Res* 101:5725–5738
- Das S, Suhadolc P, Kostrov BV (1996) Realistic inversions to obtain gross properties of the earthquake faulting process. *Tectonophysics* 261:165–177. Special issue entitled *Seismic Source Parameters: from Microearthquakes to Large Events*, ed. C. Trifu
- Dunham EM (2007) Conditions governing the occurrence of supershear ruptures under slip-weakening friction. *J Geophys Res* 112:B07302
- Dunham EM, Archuleta RJ (2004) Evidence for a supershear transient during the 2002 Denali fault earthquake. *Bull Seismol Soc Am* 94:S256–S268
- Dunham EM, Bhat HS (2008) Attenuation of radiated ground motion and stresses from three-dimensional supershear ruptures. *J Geophys Res* 113:B08319
- Ellsworth WL, Celebi M, Evans JR, Jensen EG, Kayen R, Metz MC, Nyman DJ, Roddick JW, Spudich P, Stephens CD (2004) Nearfield ground motion of the 2002 Denali Fault, Alaska, earthquake recorded at Pump Station 10. *Earthq Spectra* 20:597–615
- Frankel A (2004) Rupture process of the M7.9 Denali fault, Alaska, earthquake: subevents, directivity, and scaling of high-frequency ground motion. *Bull Seismol Soc Am* 94:S234–S255
- Gridded Population of the World, version 3 (GPWv3) (2007) Center for International Earth Science Information Network (CIESIN), Columbia University; and Centro Internacional de Agricultura Tropical (CIAT). 2005, Palisades. Available at <http://sedac.ciesin.columbia.edu/gpw>
- Hamano Y (1974) Dependence of rupture time history on the heterogeneous distribution of stress and strength on the fault, (abstract). *Transact Am Geophys Union* 55:352

- Hartzell SH, Heaton TH (1983) Inversion of strong ground motion and teleseismic waveform data for the fault rupture history of the 1979 Imperial Valley, California, earthquake. *Bull Seismol Soc Am* 73:1553–1583
- Hartzell SH, Stewart GS, Mendoza C (1991) Comparison of L_1 and L_2 norms in a teleseismic waveform inversion for the slip history of the Loma Prieta, California, earthquake. *Bull Seismol Soc Am* 81:1518–1539
- Ida Y (1972) Cohesive force across the tip of a longitudinal-shear crack and Griffith's specific surface energy. *J Geophys Res* 77:3796–3805
- Henry C, Das S (2002) The Mw 8.2 February 17, 1996 Biak, Indonesia earthquake: rupture history, aftershocks and fault plane properties. *J Geophys Res* 107:2312
- Henry C, Das S, Woodhouse JH (2000) The great March 25, 1998 Antarctic Plate earthquake: moment tensor and rupture history. *J Geophys Res* 105:16097–16119
- Kostrov BV (1975) Mechanics of the tectonic earthquake focus (in Russian). Nauka, Moscow
- Kostrov BV (1966) Unsteady propagation of longitudinal shear cracks. *J Appl Math Mech* 30:1241–1248
- Kostrov BV, Das S (1988) Principles of earthquake source mechanics. Cambridge University Press, New York
- Lin A, Fu B, Guo J, Zeng Q, Dang G, He W, Zhao Y (2002) Co-seismic strike-slip and rupture length produced by the 2001 Ms 8.1 Central Kunlun earthquake. *Science* 296:2015–2016
- Liu C, Bizzari A, Das S (2014) Progression of spontaneous in-plane shear faults from sub-Rayleigh up to compressional wave rupture speeds. *J Geophys Res Solid Earth* 119 (11):8331–8345
- Lasserre C, Peltzer G, Cramp F, Klinger Y, Van der Woerd J, Tapponnier P (2005) Coseismic deformation of the 2001 Mw = 7.8 Kokoxili earthquake in Tibet, measured by synthetic aperture radar interferometry. *J Geophys Res* 110:B12408
- Madariaga R (1983) High-frequency radiation from dynamic earthquake fault models. *Ann Geophys* 1:17–23
- Madariaga R (1977) High-frequency radiation from crack (stress drop) models of earthquake faulting. *Geophys J Roy Astron Soc* 51:625–651
- Milne J, Lee AW (1939) Earthquakes and other earth movements. K Paul, Trench, Trubner and Co., London
- Olson AH, Apsel RJ (1982) Finite faults and inverse theory with applications to the 1979 Imperial Valley earthquake. *Bull Seismol Soc Am* 72:1969–2001
- Ozacar AA, Beck SL (2004) The 2002 Denali fault and 2001 Kunlun fault earthquakes: complex rupture processes of two large strike-slip events. *Bull Seismol Soc Am* 94:S278–S292
- Parker RL (1994) Geophysical inverse theory. Princeton University Press, Princeton
- Passelègue FX, Schubnel A, Nielsen S, Bhat HS, Madariaga R (2013) From sub-Rayleigh to supershear ruptures during stick-slip experiments on crustal rock. *Science* 340 (6137):1208–1211
- Perez OJ, Sanz C, Lagos G (1997) Microseismicity, tectonics and seismic potential in southern Caribbean and northern Venezuela. *J Seismol* 1:15–28
- Press F, Ben-Menahem A, Toksöz MN (1961) Experimental determination of earthquake fault length and rupture velocity. *J Geophys Res* 66:3471–3485
- Press WH, Flannery BP, Teukolsky SA, Vetterling WT (1986) Numerical recipes: the art of scientific computing. Cambridge University Press, New York
- Robinson DP, Das S, Searle MP (2010) Earthquake fault superhighways. *Tectonophysics* 493:236–243
- Robinson DP (2011) A rare great earthquake on an oceanic fossil fracture zone. *Geophys J Int* 186:1121–1134
- Robinson DP, Das S, Watts AB (2006a) Earthquake rupture stalled by subducting fracture zone. *Science* 312:1203–1205
- Robinson DP, Brough C, Das S (2006b) The Mw 7.8 Kunlunshan earthquake: extreme rupture speed variability and effect of fault geometry. *J Geophys Res* 111:B08303

- Robinson DP, Henry C, Das S, Woodhouse JH (2001) Simultaneous rupture along two conjugate planes of the Wharton Basin earthquake. *Science* 292:1145–1148
- Rodgers DW, Little TA (2006) World's largest coseismic strike-slip offset: the 1855 rupture of the Wairarapa Fault, New Zealand, and implications for displacement/length scaling of continental earth-quakes. *J Geophys Res* 111:B12408
- Rosakis AJ, Samudrala O, Coker D (1999) Cracks faster than the shear wave speed. *Science* 284:1337–1340
- Sarao A, Das S, Suhadolc P (1998) A comprehensive study of the effect of non-uniform station distribution on the inversion for seismic moment release history and distribution for a Haskell-type rupture model. *J Seismol* 2:1–25
- Spudich P, Cranswick E (1984) Direct observation of rupture propagation during the 1979 Imperial Valley earthquake using a short baseline accelerometer array. *Bull Seismol Soc Am* 74:2083–2114
- Song SG, Beroza GC, Segall P (2008) A unified source model for the 1906 San Francisco earthquake. *Bull Seismol Soc Am* 98:823–831
- Tarantola A (1987) Inverse problem theory. Methods for data fitting and model parameter estimation. Elsevier, New York
- Utsu T (2002) A list of deadly earthquakes in the world (1500–2000). In: Lee WHK, Kanamori H, Jennings PC, Kisslinger C (eds) *International handbook of earthquake and engineering seismology part A*. Academic, New York, p 691
- Vallée M, Landès M, Shapiro NM, Klinger Y (2008) The 14 November 2001 Kokoxili (Tibet) earthquake: High-frequency seismic radiation originating from the transitions between sub-Rayleigh and supershear rupture velocity regimes". *J Geophys Res* 113:B07305
- Vigny C, Socquet A, Rangin Chamot-Rooke N, Pubellier M, Bouin M-N, Bertrand G, Becker M (2003) Present-day crustal deformation around Sagaing fault, Myanmar. *J Geophys Res* 108:2533
- Walker KT, Shearer PM (2009) Illuminating the near-sonic rupture velocities of the intracontinental Kokoxili Mw 7.8 and Denali fault Mw 7.9 strike-slip earthquakes with global P wave back projection imaging. *J Geophys Res* 114:B02304
- Wang D, Mori J, Uchide T (2012) Supershear rupture on multiple faults for the Mw 8.6 off Northern Sumatra, Indonesia earthquake. *Geophys Res Lett* 39:L21307
- Wu FT, Thomson KC, Kuenzler H (1972) Stick-slip propagation velocity and seismic source mechanism. *Bull Seismol Soc Am* 62:1621–1628
- Xia K, Rosakis AJ, Kanamori H (2004) Laboratory earthquakes: the sub-Rayleigh-to-supershear transition. *Science* 303:1859–1861
- Xia K, Rosakis AJ, Kanamori H, Rice JR (2005) Laboratory earthquakes along inhomogeneous faults: directionality and supershear. *Science* 308:681–684
- Xu X, Chen W, Ma W, Yu G, Chen G (2002) Surface rupture of the Kunlunshan earthquake (Ms 8.1), northern Tibet plateau, China. *Seismol Res Lett* 73:884–892
- Yeats RS, Sieh K, Allen CR (1997) *The geology of earthquakes*. Oxford University Press, New York
- Yeats R (2012) *Active faults of the world*. Cambridge University Press, New York
- Yue H, Lay T, Freymuller JT, Ding K, Rivera L, Ruppert NA, Koper KD (2013) Supershear rupture of the 5 January 2013 Craig, Alaska (Mw 7.5) earthquake. *J Geophys Res* 118:5903–5919
- Zhan Z, Helmberger DV, Kanamori H, Shearer PM (2014) Supershear rupture in a Mw 6.7 aftershock of the 2013 Sea of Okhotsk earthquake. *Science* 345:204–207

Chapter 2

Civil Protection Achievements and Critical Issues in Seismology and Earthquake Engineering Research

Mauro Dolce and Daniela Di Bucci

Abstract A great complexity characterizes the relationships between science and civil protection. Science attains advances that can allow civil protection organizations to make decisions and undertake actions more and more effectively. Provided that these advances are consolidated and shared by a large part of the scientific community, civil protection has to take them into account in its operational procedures and in its decision-making processes, and it has to do this while growing side by side with the scientific knowledge, avoiding any late pursuit.

The aim of the paper is to outline the general framework and the boundary conditions, to describe the overall model of such relationships and the current state-of-the-art, focusing on the major results achieved in Italy and on the many criticalities, with special regards to research on seismic risk.

Among the boundary conditions, the question of the different roles and responsibilities in the decision-making process will be addressed, dealing in particular with the contribution of scientists and decision-makers, among the others, in the risk management. In this frame, the different kinds of contributions that civil protection receives from the scientific community will be treated. Some of them are directly planned, asked and funded by civil protection. Some contributions come instead from research that the scientific community develops in other frameworks. All of them represent an added value from which civil protection wants to take advantage, but only after a necessary endorsement by a large part of the scientific community and an indispensable adaptation to civil protection utilization. This is fundamental in order to avoid that any decision and any consequent action, which could in principle affect the life and property of many citizens, be undertaken on the basis of non-consolidated and/or minor and/or not shared scientific achievements.

M. Dolce (✉) • D. Di Bucci

Department of Civil Protection, Presidency of the Council of Ministers, Rome, Italy
e-mail: mauro.dolce@protezionecivile.it; daniela.dibucci@protezionecivile.it

© The Author(s) 2015

A. Ansal (ed.), *Perspectives on European Earthquake Engineering and Seismology*, Geotechnical, Geological and Earthquake Engineering 39, DOI 10.1007/978-3-319-16964-4_2

2.1 Introduction

In the last decade, within their activities at the Italian Department of Civil Protection (DPC), the authors had the opportunity to contribute to develop the relationships between the “Civil Protection” and the “Scientific Community”, especially in the field of seismic and seismo-induced risks.

During these years, the DPC has faced difficult circumstances, not only in emergency situations, which have required strong and continuous interactions with the scientific community. As it can be easily understood in theory, but much less easily in practice, the civil protection approach to seismic risk problems is strongly different from the research approach, although important synergies could arise from a cooperation and a reciprocal understanding. From the DPC point of view, there are many good reasons for a close connection between civil protection and research, e.g.: the opportunity to reach a scientific consensus on evaluations that imply wide uncertainties; a better management of the resource allocation for risk mitigation; the possibility to make precise and rapid analyses for fast and effective emergency actions; the optimization of resources and actions for the emergency overcoming. There are of course positive implications also for the scientific community, such as, for instance: a clear finalization of the research activities; wider investigation perspectives, too often strictly focused on the achievement of specific academic advancements; the ethical value of a research that has direct and positive social implications (Dolce 2008).

Creating a fruitful connection between the two parts implies a continuous and dynamic adaptation to the different ways of thinking about how to solve problems. This involves different fields: the language first of all, including the reciprocal and outward communication, then the timing for the response, the budget available, the right balance among the different stakeholders, the scientific consensus on the most significant achievements and, ultimately, the responsibilities.

A great complexity generally characterizes the relationships between science and civil protection. As will be shown in the following sections, science attains advances that can allow civil protection organizations to make decisions and undertake actions more and more effectively. Provided that these advances are consolidated and shared by a large part of the scientific community, civil protection has to take them into account in its operational procedures and in its decision-making processes, and it has to do this while growing side by side with the scientific knowledge, avoiding any late pursuit.

Such a complexity is summarized in the scheme of Fig. 2.1, which also represents the backbone of this paper. The aim of the work here presented, indeed, is to outline the framework and the boundary conditions, to show the overall model of such relationships and to describe the current state-of-the-art, focusing on the major results achieved in Italy and on the many criticalities that still remain to be solved.

Among the boundary conditions, the question of the different roles and responsibilities in the decision-making process will be addressed, dealing in particular

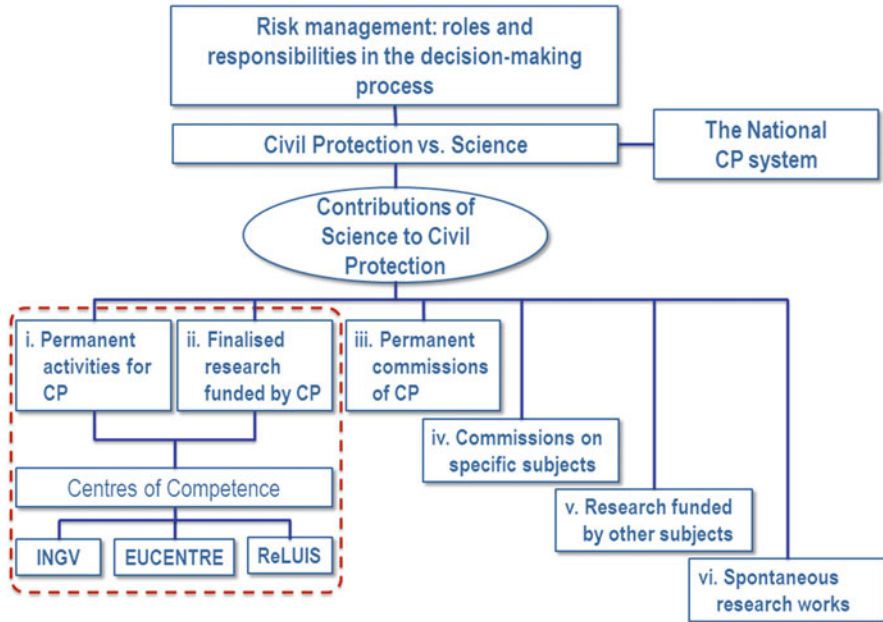


Fig. 2.1 Chart of the relationships between civil protection and science

with the contribution of scientists and decision-makers, among the others, in the risk management. In this frame, and given the specific organization of the civil protection system in Italy, which is the cradle of the experience here presented, the different kinds of contributions that civil protection receives from the scientific community will then be treated. The collection of these contributions follows different paths. Some of them are directly planned, asked and funded by civil protection, although with a different commitment for the scientific institutions or commissions involved, which especially regards their activity field and the related duration through times (points i to iv in Fig. 2.1). Some contributions come instead from research that the scientific community develops in other frameworks: European projects, Regional funds, etc. (points v to vi in Fig. 2.1). All of them represent an added value from which civil protection wants to take advantage for sure, but only after a necessary endorsement by a large part of the scientific community and an indispensable adaptation to civil protection utilization. This is fundamental in order to avoid that any decision and any consequent action, which could in principle affect the life and property of many citizens, be undertaken on the basis of non-consolidated and/or minor and/or not shared scientific achievements.

Table 2.1 Points of view of scientists and decision-makers

Scientists	Decision-makers
Frequently model events that occurred in the past in order to understand their dynamics	Need well-tested models, which are able to describe events possibly occurring in the future
Follow a scientific approach to the risks that is often probabilistic, and always affected by uncertainties	In most cases are asked to make decisions that necessarily require a yes or no answer
Need a relatively long time for their work, in order to acquire more data trying to reduce uncertainties, preferring to wait rather than to be wrong	Are generally asked to give an immediate response, often balancing low occurrence probabilities versus envisaged catastrophic consequences
Exert the “art of doubt”	Need solutions
Estimate the costs to carry out their best research	Manage a pre-defined (often limited) budget

2.2 Roles and Responsibilities in the Decision-Making Process

2.2.1 *Scientists and Decision-Makers in the Risk Management*

Scientists and decision-makers are often considered as two counterparts which dynamically interact in the decision-making process. As a matter of fact, within the civil protection system, they represent two different points of view that have to be continuously reconciled (Dolce and Di Bucci 2014), as summarized in Table 2.1.

A further complexity is noticeable, especially in civil protection activities, i.e., the roles and the responsibilities of decision-makers at the different levels of the decisional process. One should discriminate between political decision-makers (PDMs) and technical decision-makers (TDMs). Moreover, PDMs operate in relation to either general risk management policies or specific scenarios. Indeed, a further and more subtle distinction could be made (Bretton 2014) between politicians and policy makers. Nevertheless, for the sake of simplicity, only three categories, i.e., scientists, PDMs, and TDMs, will be referred hereinafter as the three main actors in the decisional chain.

There is no doubt that in many cases it can be hard to totally separate the contribution of each of them, since some feedback and interactions are often necessary. However, in every step of an ideal decision-making process, each of these actors should play a primary role, as summarized in Table 2.2.

These sophisticated links and interactions can obviously cause distortions in the roles to be played, and thus in the responsibilities to be taken. This can further happen if the participants in the decisional process do not, or cannot, accomplish their tasks or if, for various reasons, they go beyond the limits of their role.

Scientists, for instance, could either:

- not provide fully quantitative evaluations;
- miss to supply scientific support in cost–benefit analyses;
- give undue advice concerning civil protection actions.

Table 2.2 Steps of an ideal decision-making process, and role virtually played by the different participants

Step	Description	Scientists	PDMs	TDMs
1	definition of the acceptable level of risk according to established policy (i.e., in a probabilistic framework, of the acceptable probability of occurrence of quantitatively estimated consequences for lives and property)	x	X	
2	allocation of proper budget for risk mitigation		X	x
3	quantitative evaluation of the risk (considering hazard, vulnerability, and exposure)	X		x
4	identification of specific actions capable of reducing the risk to the acceptable level			X
5	cost-benefit evaluation of the possible risk-mitigating actions	X		x
6	adoption of the most suitable technical solution, according to points 1, 4, and 5	x	x	X
7	implementation of risk-mitigating actions			X

PDMs political decision-makers, *TDMs* technical decision-makers, *X* primary role, *x* occasional support

PDMs could:

- decide not to establish the acceptable risk levels for the community they represent;
- prefer to state that a “zero” risk solution must be pursued, which is in fact a non-decision;
- not allocate an adequate budget for risk mitigation.

TDMs could tend (or could be forced, in emergency conditions) to make and implement decisions they are not in charge for, because of the lack of:

- scientific quantitative evaluations;
- acceptable risk statements (or impossibility to get them);
- budget.

A number of examples of individuals usurping or infringing on roles not assigned to them in the decisional process is reported by Dolce and Di Bucci (2014).

2.2.2 Other Actors in the Decision Process

Other actors, besides scientists and decision makers, play an important role in the risk cycle management; among them mass media, judiciary, and citizens deserve to be especially mentioned, because their behaviours can strongly affect the decision-making process.

Table 2.3 Pros and cons for civil protection in the mass media behaviour

Pros	Cons
Spreading knowledge about risks and their reduction in order to increase people's awareness on risks	Distortion of information due to incompetence or to commercial or political purposes
Disseminating best practices on behaviours to be adopted both in ordinary and in emergency conditions	Accreditation of non-scientific ideas and non-expert opinions
Spreading civil protection alerts	Spreading false alarms

Dealing with the communication of civil protection matters to the public through the media, it is worth mentioning Franco Gabrielli, the Head of the Italian Department of Civil Protection since 2010. He well summarized the complexity of this issue when he affirmed that “We have the duty of communicating with citizens, but we are voiceless and invisible if we don't pass through the «cultural mediation» of the information channels and their managers. Maybe we have neither analysed deeply enough the consequences of such mediation, nor we have learned well enough to avoid traps and to take the possible advantages” (Gabrielli 2013).

As a matter of fact, the importance of mass media (newspapers, radio, television, as well as web and social networks) is quickly increasing in any field and, therefore, also in risk management. There is a great need for an effective collaboration between civil protection TDMs and the media. It can determine the advantages summarized in the left-hand-side of Table 2.3 and, in the meanwhile, could reduce some of the problems reported in the right-hand-side of the same table, mostly induced by the need that media have to increase their audience for commercial purposes, or to support some political orientations.

Two points, well established since long time by the theories of mass communication, have to be carefully taken into account in the civil protection activities. The first one deals with the “cause and effect” of communication, stating that “some kinds of communication, on some kinds of issues, brought to the attention of some kinds of people, under some kinds of conditions, have some kinds of effects” (Berelson 1948). The second one was expressed by Wilbur Schramm in 1954: “It is misleading to think of the communication process as starting somewhere and ending somewhere. It is really endless. We are little switchboard centres handling and rerouting the great endless current of information . . .” (Schramm 1954).

These two statements clearly demonstrate how impossible is to establish a direct and unique link between the original message and the effects on the audience's mind due to the complex process leading to those effects. It is of paramount importance to account for this complexity in the communication of civil protection issues, if definite effects are expected or wanted.

Concerning the judiciary, the question is multifaceted, also depending on the legal framework of each country. In general, the magistrates' action is strictly related to the roles and specific responsibilities of the various actors in risk management. After the 2009 L'Aquila earthquake and the following legal

controversies (original documents, along with comments, can be found in the following blogs: <http://processoaquila.wordpress.com/>, <http://terremotiegradirischi.com/> and <http://eagris2014.com/>), a lively discussion has been opened worldwide on this theme, that has been addressed in international conferences and workshops (e.g., AGU Fall Meeting 2012; Gasparini 2013, in the Goldschmidt Conference; 2nd ECEES – Special Session “Communication of risk and uncertainty to the general public”; workshop “Who evaluates, who decides, who judges”, 2011 —http://www.protezionecivile.gov.it/resources/cms/documents/locandina_incontro_di_studio.pdf; workshop “Civil protection in the society of risk: procedures, guarantees, responsibilities”, 2013 —<http://www.cimafoundation.org/convegno-nazionale-2013/>), as well as in books and peer reviewed papers (e.g., DPC and CIMA Ed. 2013, 2014; Alexander 2014a, b; Gabrielli and Di Bucci 2014; Mucciarelli 2014). Due to the importance at international level of this issue, the Global Science Forum of the Organisation for Economic Co-operation and Development (OECD) promoted an activity, involving senior science policy officials of the OECD member countries in a study of “the quality of scientific policy advice for governments and consequences on the role and responsibility of scientists” (<http://www.oecd.org/sti/sci-tech/oecdglobalscienceforum.htm>).

The experience currently made in Italy, referred to many different kinds of risks, can be summarized by quoting the words of the Head of the Italian Department of Civil Protection: “. . . a significant increase of the judiciary actions after a disaster has occurred, to find the guilt in the behaviour of the catastrophe management actors. The investigation area is enlarged to the phase of prevision and of ‘prevision information management’ . . .” (Gabrielli 2013).

In this perspective, it can be easily understood that decisions of the judiciary can significantly affect the behaviour of the civil protection individual stakeholders and then of the system, as pointed out in the proceedings of one of the workshops mentioned above (DPC and CIMA 2013). Some passages in these proceedings provide the opinion of some judges and experts of criminal law on the bias that can affect the legal interpretation and the possible consequences of a punishing approach (i.e., an approach which looks only for a guilty party after a catastrophic event) on the decision-making process. For instance, Renato Bricchetti, president of the Court of Lecco, states: “I realize . . . that most of the people feel the need to find a responsible, I don’t want to say a scapegoat, but to know who has to be blamed for what happened. And the mass media world amplifies this demand for justice”. Moreover, Francesco D’Alessandro, Professor of Criminal Law at the Università Cattolica of Milan, addresses the “Accusatory approach to the error: a scheme of analysis for which, in case of errors or incidents, the main effort is made to find who is the possible responsible for the event that occurred, in order to punish him. Whereas those elements of the organization that may have contributed to the adoption of a behaviour characterized by negligence, imprudence, incompetence, are left in the background.” He also affirms that: “As a consequence, even if you punish a specific person, the risk conditions and the possibility to commit the same error again still continue to persist.” Finally, D’Alessandro depicts the devastating

effects of this approach on the risk mitigation: “The accusatory approach . . . induces a feeling of fear in the operators of the possible punishment . . . and this keeps them from reporting on the near misses, thus impeding learning by the organization. This phenomenon . . . is characterized by a progressive, regular adoption of behaviours that are not aimed at better managing the risk, but rather at attempting to minimize the possibility to be personally involved in a future legal controversy.”

Dealing with the role played by citizens in a fully developed civil protection system, it has to be underlined that this role is fundamental both in ordinary and in emergency conditions.

On the one hand, in ordinary conditions, citizens should reduce as much as they can the risks threatening their lives and property, by:

- asking for and/or contributing to create adequately safe conditions at their places of work, study, and entertainment;
- verifying that civil protection authorities have prepared in advance the preventive measures that must be adopted in case of catastrophic events, especially civil protection plans, of which citizens are primary users;
- being more aware of the risks which they are exposed to, and having an adequate civil protection culture, which would allow them to adopt the aforementioned precautionary measures and induce political representatives to carry out risk-prevention policies through both their vote and their active involvement in the local political activities.

On the other hand, in case (or in the imminence, when possible) of an event, citizens can undertake different actions, depending on the kind of risk and on the related forecasting probabilities:

- in the immediate aftermath of an event (or in case of an alert), they should follow and implement the civil protection plans (if available) and the correct behaviours learned;
- in case of very low occurrence probabilities, they should adopt individual behaviours, more or less cautious, calibrated on their own estimate of the risk acceptability.

Finally, citizens can provide support to the civil protection system also by being part of volunteers organizations.

2.3 Civil Protection and Science

Two main aspects of the relationships between civil protection and science are relevant from the civil protection point of view:

- scientific advances can allow for more effective civil protection decisions and actions concerning the entire risk cycle;

- civil protection has to suitably re-shape its activities and operational procedures to include the scientific advances, as soon as they become available and robust.

In order to fully understand the problems and the possible solutions in the civil protection – science relationships, it is essential to explain what “having procedures” means for a civil protection system, and to provide an overview of the possible scientific products for civil protection use and of the organization of the Italian civil protection system.

2.3.1 Civil Protection Procedures

Civil protection operates following pre-defined procedures, which are needed on the one hand to improve its efficiency in decision-making and to rapidly undertake actions during a crisis or an emergency and, on the other hand, to make roles and responsibilities clear. As the procedures are defined quite rigidly and involve many actors, modifying them is often “uncomfortable”, especially on the basis of those new scientific advancements that increase the uncertainties or do not quantify them.

The progressive updating of the procedures is made even more complex by the fact that civil protection organizations are different in different countries. A technical-scientific product/tool/study that is suitable for one country or for a given civil protection system can therefore turn out to be inadequate for another one. As a matter of fact, each civil protection organization has its own procedures, that are derived from the distillation of practical experiences and successive adjustments. These procedures are somehow “digested” by the civil protection personnel and officials, by the civil protection system and, sometimes, by media and population, thus creating complex interrelationships which are hard and sometimes dangerous to change abruptly.

Changing procedures is an inescapable fact, that however can be much more difficult and slow than making scientific advances and improving scientific tools.

2.3.2 Scientific Products for Civil Protection

Scientific products, i.e., any scientific result, tool or finding, for their intrinsic nature do not usually derive from an overall view of the reality, but they tend to emphasize some aspects, while neglecting or oversimplifying some others. Therefore, often research findings can turn out to be unreliable for practical applications, and sometimes falsely precise or tackling only part of a problem, whereas they leave unsolved other important parts. To minimize this contingency, research activities finalized to civil protection aims should proceed in close cooperation with civil protection stakeholders in defining objectives and products to achieve, as well as in validating results and/or tools.

Generally speaking, science can, more or less effectively, contribute to civil protection in the following two ways:

1. with specific scientific products, explicitly requested (and generally funded) by civil protection and subjected to a wide consensus of the scientific community; the scientific results provided, although responding to the civil protection needs, can be still not suitably shaped for a direct or immediate translation into civil protection procedures and actions, needing further adaptation and a pre-operational stage before their full operational utilization.
2. with scientific products made freely available by the scientific community, which typically pertain to one of the following three categories:
 - (i) many different findings on the same subject; as expected in these cases, in which the scientific community is still developing a theme and a conclusive result is still far from being reached, they can be (and often are) inconsistent or conflicting among them;
 - (ii) totally new products “standing out from the crowd”; they are proposed by the authors as innovative/revolutionary/fundamental, and are often conveyed to the public through media, claiming their great usefulness for risk mitigation. In this way, these products can benefit from the favour of a large public that, however, has not the needed expertise to evaluate the quality of their scientific content;
 - (iii) totally new and often scientifically valuable products; in any case they need to be adapted, if actually possible, to civil protection operability.

A more in-depth and articulated analysis of the different scientific products proposed for civil protection use is shown in section 4.

2.3.3 The Italian National Civil Protection System

In Italy, civil protection is not just a single self-contained organization but a system, called National Service of Civil Protection (SNPC), which operates following the idea that the civil protection is not an administration or an authority, but rather a function that involves the entire society. Several individuals and organizations contribute with their own activities and competences to attain the general risk mitigation objectives of SNPC.

The coordination of this complex system is entrusted to the National Department of Civil Protection, which acts on behalf of the Prime Minister. The SNPC’s mandate is the safeguarding of human life and health, property, national heritage, human settlements and environment from all natural or manmade disasters.

All the ministries, with their national operational structures, including Fire Brigades, Police, Army, Navy, Air Force, Carabinieri, State Forest Corps and Financial Police, as well as Prefectures, Regional and local civil protection organizations, contribute to SNPC actions. Public and private companies of highways,

roads and railways, electricity and telecommunication, as well as volunteers associations and individual citizens, are part of the system. The volunteers associations can have both general aims of assistance to the population, and specific aims related to particular technical/professional skills (for instance, architects, engineers, geologists, medical doctors, etc.). Finally, an important strength of SNPC is represented by the full involvement of the scientific community, which enables timely translation of up-to-date scientific knowledge into operability and decision making.

All the kinds of natural and manmade risks are dealt with by the SNPC, including seismic, hydrogeological, flood, volcanic, forest fire, industrial and nuclear, technological, transports, supply networks and environmental risks. Different kinds of engagement are envisaged, at different territorial levels, according to the local, regional or national level of the emergency to be faced and, more in general, to the civil protection activities to be carried out in ordinary conditions.

2.4 How Science Contributes to Civil Protection

Science can provide different kinds of contributions to civil protection. They can be distinguished and classified according to the type of relationship between the scientific contributors and the civil protection organizations. The main kinds of contributions can be categorized as follows:

- (i) well-structured scientific activities, permanently performed by scientific institutions on behalf of civil protection organizations, which usually endow them;
- (ii) finalized research activities carried out by scientific institutions, funded by civil protection organizations to provide results and products for general or specific purposes of civil protection;
- (iii) advices regularly provided by permanent commissions or permanent consultants of civil protection organizations;
- (iv) advices on specific topics, provided by temporary commissions *ad hoc* established by civil protection organizations;
- (v) research activities developed in other frameworks and funded by other subjects (European projects, Regional funds, etc.), that achieve results of interest for civil protection organizations, especially when these latter are involved as end-users;
- (vi) free-standing research works, producing results of potential interest for civil protection without any involvement of civil protection organizations.

Hereinafter, the above different kinds of scientific contributions are described and discussed in the light of the experience made by the DPC, devoting a special concern to the criticalities observed.

2.4.1 *Permanent (i) and Finalized Research Activities (ii) for Civil Protection – The Competence Centres*

In Italy, there is a long-lasting tradition of interactions between civil protection and scientific community on earthquake research topics. A first important link was developed after the 1976 Friuli earthquake and continued until 2002, with projects funded by the DPC and coordinated by the National Research Council that gave a strong impulse to this research field, involving the whole scientific community. An even stronger integration between civil protection and research was then promoted in 2004, with a new organization of the relationships between the DPC and the scientific community, on behalf of which the “Competence Centres” play a primary role.

The Competence Centres (CC) of the DPC are scientific institutions which provide services, information, data, elaborations, technical and scientific contributions for specific topics, to share the best practices in risk assessment and management. These centres are singled out by a decree of the Head of DPC. The activities carried out by the CC are funded by DPC through annual agreements, according to general multi-year understandings that establish the main lines of activities to be carried out in the reference period.

The interrelationships between DPC and CC are in many cases multifaceted, and their management needs therefore a unified view. With this aim, for each CC which deals with the seismic risk a DPC-CC joint committee has been established. This committee, made of an equal number of DPC and CC components (typically 3–4 representatives per part), manages practically the relationships between the DPC and the CC. Ultimately, the job of the joint committee, consists of acting as a sort of hinge, a functional linkage between the two worlds of civil protection and seismic risk science. This role, as much interesting as uncomfortable, guarantees consistency in the management of all the activities concerned. In addition to the committee components, DPC representatives assure the correct finalization for civil protection application of each activity/project developed by a CC and of the final products, directly interacting with the CC scientific managers of the activity/project. DPC representatives in charge and CC scientific managers report to their directors and to the DPC-CC joint committee on the regular development of the activities, on the possible needs that could arise and on the relevant decisions to be taken, according to the scheme shown in Fig. 2.2.

The three main CC for the seismic risk are:

- INGV – the National Institute of Geophysics and Volcanology;
- ReLUIS – the National Network of University Laboratories of Earthquake Engineering;
- EUCENTRE – the European Centre for Training and Research in Earthquake Engineering.

INGV provides DPC with scientific advices and products related to seismological (as well as volcanological, not addressed in the present work) issues, while

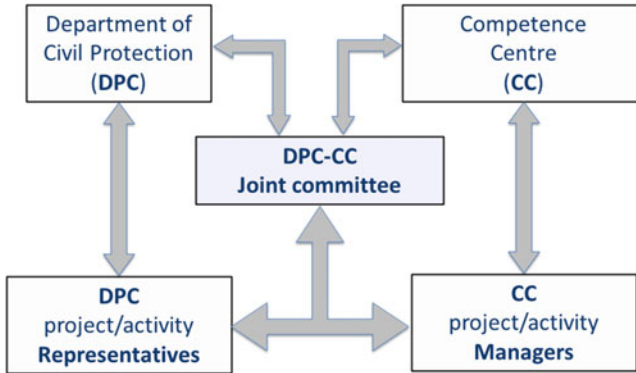


Fig. 2.2 Scheme of the relationships management between the Italian Department of Civil Protection and a Competence Centre

EUCENTRE and ReLUIS operate in the field of earthquake engineering. All of them represent the reference scientific system on seismic risk for DPC, and provides the most advanced scientific knowledge in Seismology and Earthquake Engineering. Moreover, these CC have the capability to produce considerable progress and organisation of the scientific information and to promote a strong finalisation of research towards products for civil protection purposes (Dolce 2008).

2.4.1.1 INGV

A 10 year agreement between DPC and INGV (<http://www.ingv.it/en/>) was signed in 2012, for the period 2012–2021. It envisages three types of activities, that are described hereinafter with regards to earthquakes.

A-type: operational service activities.

Several different activities pertain to this type:

- seismic monitoring and 24/7 surveillance, through the National Earthquake Centre (INGV-CNT),
- implementation and maintenance of data bases useful for civil protection purposes,
- preparedness and management of technical-scientific activities during the emergencies,
- divulgation and training activities in coordination with DPC.

B-type: development of operational service activities.

On the one hand, this type concerns the actions to be undertaken by DPC and INGV in order to improve and develop the activities mentioned in the above A-type description. On the other hand, it deals with the pre-operational, and

then operational, implementation of research achievements (C-type below) for civil protection. This occurs when validated scientific outcomes derived from C-type activities, or from other INGV research, have to be transformed into products that can be submitted to civil protection pre-operational, experimental testing. In case of positive outcome, the scientific product/tool/study can then become part of a fully operational service among the A-type activities.

C-type: finalized research activities.

They consist of seismological-geological projects funded by DPC that involve the entire scientific community.

Some examples of the above three types of activities are described in the following paragraphs.

“A-Type” Activities

According to a national law (D. Lgs. 381/99), INGV has in charge the seismic (and volcanic) monitoring and surveillance of the Italian territory. It manages and maintains the velocimetric National Seismic Network (more than 300 stations), whose data are collected and elaborated at the INGV-CNT, providing DPC with quasi-real-time information on location and magnitude of Italian earthquakes, with the capability to detect $M > 2$ earthquakes all over the Italian territory (Sardinia excluded, in relation to the negligible seismicity of this region) and $M > 1$ in many of the most hazardous regions (see Fig. 2.3).

Among the INGV A-type activities, the implementation and maintenance of data bases that are important for their civil protection applications deserve to be mentioned. For instance:

- DISS – The Database of Individual Seismogenic Sources (<http://diss.rm.ingv.it/diss/>; Basili et al. 2008; DISS Working Group 2010; Fig. 2.4) is, according to <http://diss.rm.ingv.it/diss/UserManual-Intro.html>, a “georeferenced repository of tectonic, fault and paleoseismological information; it includes individual, composite and debated seismogenic sources. Individual and composite seismogenic sources are two alternative seismic source models to choose from. They are tested against independent geophysical data to ensure the users about their level of reliability”. Each record in the Database is backed by a Commentary, a selection of Pictures and a list of References, as well as fault scarp or fold axis data when available (usually structural features with documented Late Pleistocene – Holocene activity). The Database can be accessed through a web browser or displayed on Google Earth. DISS was adopted as the reference catalogue of Italian seismogenic sources by the EU SHARE Project (see below).

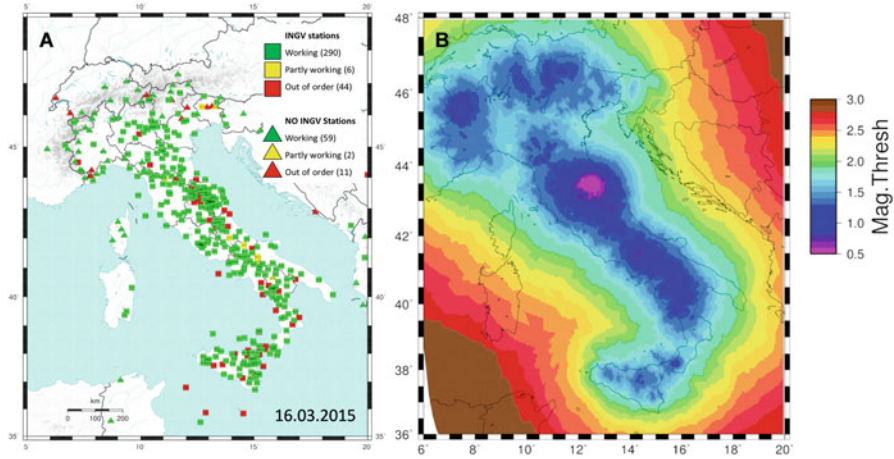


Fig. 2.3 (a) Distribution of the Italian seismic network operated by INGV; and (b) example of magnitude detection threshold on march 16, 2015 (Data provided by INGV to DPC)



Fig. 2.4 DISS website (<http://diss.rm.ingv.it/diss/>; Basili et al. 2008; DISS Working Group 2010)

- ISIDe – The Italian Seismological Instrumental and parametric Data-basE (<http://iside.rm.ingv.it/iside/standard/index.jsp>; Fig. 2.5a) provides verified information on the current seismicity as soon as it is available, once reviewed by the seismologists working at the INGV-CNT, along with the updated information of past instrumental seismicity contained in the Italian Seismic Bulletin (Mele and Ripotati 2007).

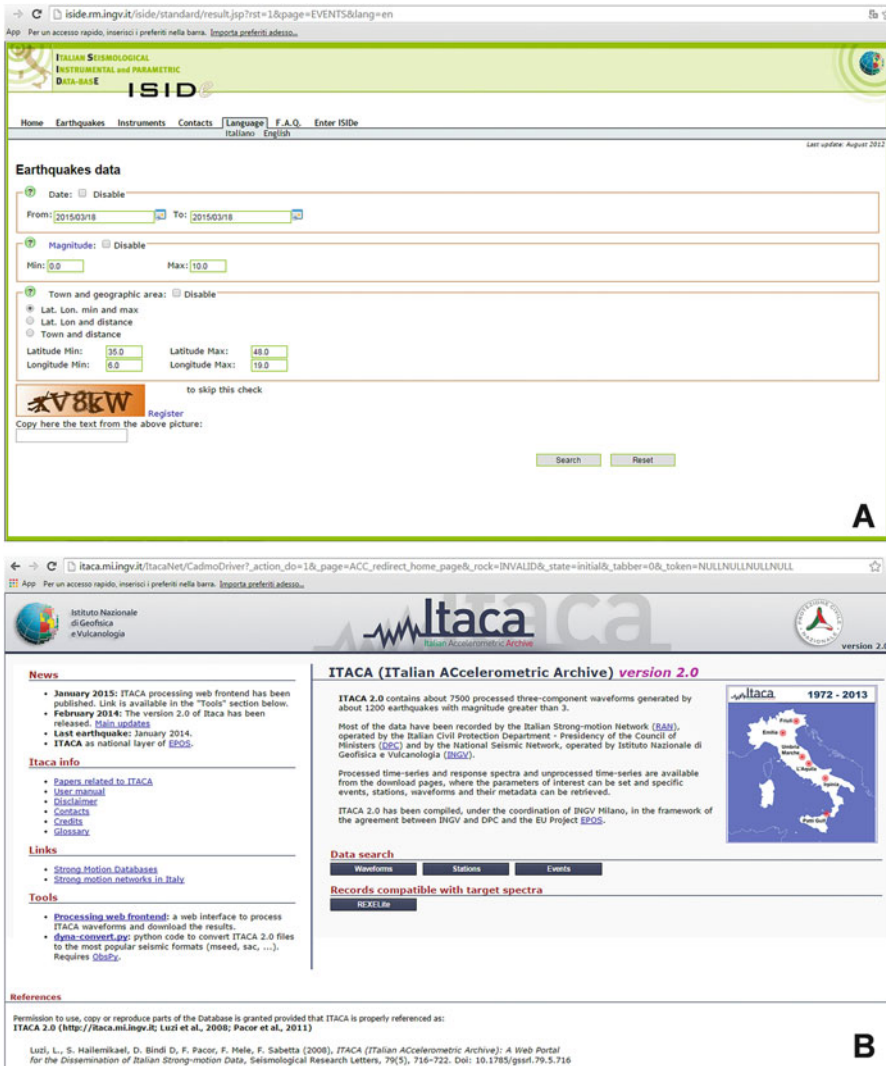


Fig. 2.5 Websites of the data bases (a) ISIDE, and (b) ITACA

- ITACA – The ITalian ACcelerometric Archive (<http://itaca.mi.ingv.it>; Fig. 2.5b) contains about 7,500 processed three-component waveforms, generated by about 1,200 earthquakes with magnitude greater than 3. Most of the data have been recorded by the Italian Strong-motion Network (<http://www.protezionecivile.gov.it/jcms/it/ran.wp>), operated by DPC, and also by the National Seismic Network, operated by INGV (<http://itaca.mi.ingv.it/>; Luzi et al. 2008; Pacor et al. 2011). Processed time-series and response spectra, as well as unprocessed

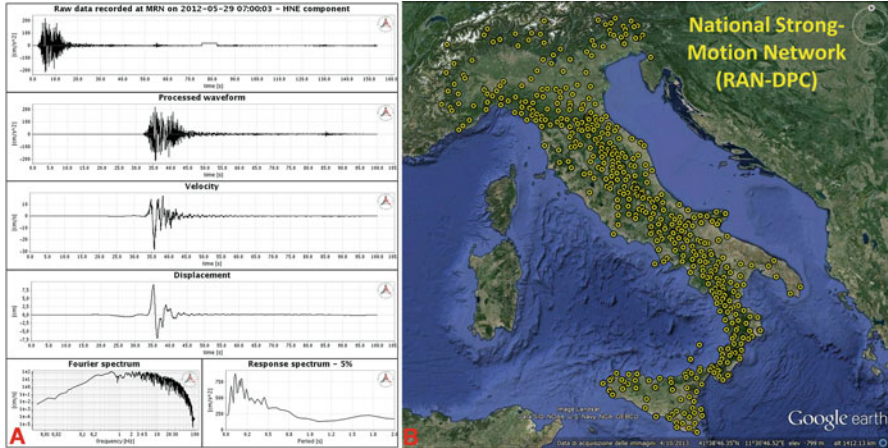


Fig. 2.6 (a) waveforms extracted from ITACA database, and (b) geographical distribution of the National Strong-Motion Network (RAN-DPC)

time-series, are available from the download pages, where the parameters of interest can be set and specific events, stations, waveforms and related metadata can be retrieved (Fig. 2.6).

“B-Type” Activities

Apart from the actions aimed at improving and developing the operational service activities (A-type), among the pre-operational and operational implementation of research achievements for civil protection, there are some activities recently implemented that deserve to be mentioned.

CPS – Centre of Seismic Hazard

The Centre of Seismic Hazard (INGV-CPS) was established in 2013 (<http://ingvcp.wordpress.com/chi-siamo/>), promoted and co-funded by DPC. It operates, in the current experimental phase, working on three different time scales of seismic hazard: long-term, mid-term and short-term, for different possible applications.

For the long-term seismic hazard the time-window is typically of 50 years, assuming the basic hypothesis of time-independence for the earthquake occurrence. Within this framework, the CPS aims at updating the seismic hazard model of Italy and the relevant maps according to the most recent advances in the international state-of-the-art and using the most updated information that contributes to the hazard assessment of the Italian territory.

For the mid-term seismic hazard the time-window is typically of years to tens of years, assuming some time-dependence hypothesis to model the earthquake

occurrence. In this case, the activities are aimed at producing and comparing time-dependent hazard models and maps, and defining a consensus-model or an ensemble-model that can be useful to set up risk mitigation strategies for the near future.

For the short-term seismic hazard (also known in the international literature as Operational Earthquake Forecasting, OEF), that is modelled using time-dependent processes, the time-window is typically days to months. About its possible outcomes, Jordan et al. (2014) explain: “We cannot yet predict large earthquakes in the short term with much reliability and skill, but the strong clustering exhibited in seismic sequences tells us that earthquake probabilities are not constant in time; . . . OEF must provide a complete description of the seismic hazard—ground-motion exceedance probabilities as well as short-term rupture probabilities—in concert with the long-term forecasts of probabilistic seismic-hazard analysis (PSHA)”.

The CPS activities are carried out by a dedicated working group, which uses a new technological infrastructure for (i) the computation of the seismic hazard, by integrating the most recent data and different models, (ii) the management of the available data bases, and (iii) the representation of the hazard estimation, even using web applications. Moreover, IT tools are developed to facilitate the preparation, implementation and comparison of hazard models, according to standard formats and common procedures, in order to make fast checks of the sensitivity of the estimations. Synergies with some international activities, like the *Collaboratory for the Study of Earthquake Predictability*, CSEP (<http://www.cseptesting.org/>), and the *Global Earthquake Model*, GEM (<http://www.globalquakemodel.org/>), as well as with the Italian seismic hazard community, are pursued.

CAT – Tsunami Alert Centre

The Tsunami Alert Centre (INGV-CAT) was established in 2013 in order to contribute to the Italian Tsunami Alert System (see Fig. 2.7). A Memorandum of Understanding was then signed on January 16th, 2014, between DPC and INGV.

This centre operates within the activities promoted by the Intergovernmental Coordination Group for the Tsunami Early Warning and Mitigation System in the North-Eastern Atlantic, the Mediterranean and connected seas (ICG/NEAMTWS). This group was formally established by the Intergovernmental Oceanographic Commission of UNESCO (IOC-UNESCO) through the Resolution IOC-XXIII-14.

The Italian Tsunami Alert System deals with earthquake-induced tsunamis and encompasses different functions: the event detection; the alert transmission to the potentially involved areas and, more in general, to the entire civil protection system; the preparedness to the operational response by drawing up the tsunami civil protection plans at different scales; the citizens’ formation about the correct behaviour in the case of event. These functions are carried out by different subjects which operate in close coordination. In particular, three public administrations are involved in this task: DPC, INGV and ISPRA (Italian Institute for Environmental Protection and Research) with the following roles:

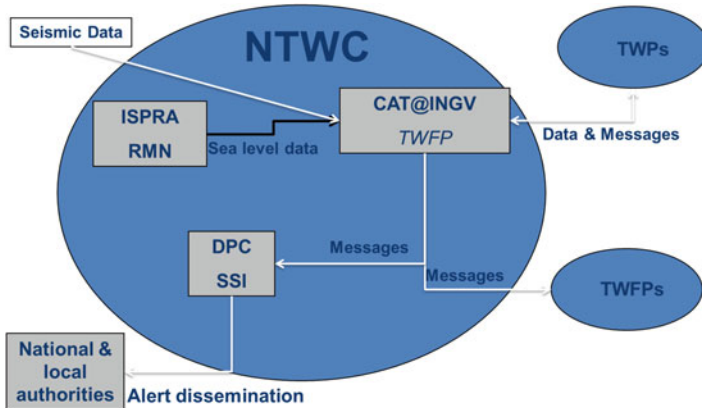


Fig. 2.7 The Italian Tsunami Warning System (Michellini A, personal communication 2014)

- DPC has the role of Tsunami National Contact (TNC);
- INGV has the role of National Tsunami Warning Centre (NTWC); at national scale, this corresponds to the INGV-CAT, which is part of the INGV-CNT;
- the Director of the INGV-CNT has the role of National Tsunami Warning Focal Point (NTWFP);
- ISPRA guarantees the sea level monitoring and surveillance, ensuring the transmission to the INGV-CAT of the data acquired by its National Mareographic Network (RMN). From August 2013, ISPRA sends to CAT@INGV sea level measurements recorded *in real time*.

Since October 1st, 2014, the INGV-CAT has assumed the role of Candidate Tsunami Watch Provider (CTWP) for the IOC/UNESCO member states in the Mediterranean. Moreover, a DPC officer is currently in charge of the IGC/NEAMTWS Vice-Chair.

The INGV-CAT will operate within the INGV earthquake operational room, also with the mission to organize the scientific and technological competences which deal, for instance, with the physics and the modelling of the seismogenic and tsunami sources, the tsunami hazard, the real-time seismology, the related computer-science applications. The strong connection with the INGV earthquake operational room will allow the INGV-CAT to take advantage from the INGV experience on seismic monitoring activities.

At present, the entire Italian Tsunami Alert System is undergoing a pre-operational testing phase, which involves the operational structures of the National Service of Civil Protection and representatives of the Regional authorities.

“C-Type” Activities

DPC promotes a series of seismological projects that are organized in a research program developed to achieve objectives of specific interest for civil protection in the field of earthquakes. They are funded by DPC and managed by INGV in the frame of a 10 year agreement between DPC and INGV (2012–2021; <http://istituto.ingv.it/l-ingv/progetti/progetti-finanziati-dal-dipartimento-di-protezione-civile-1/Progetti%20DPC-INGV%20Convenzione%20C>). These projects also involve many universities and other research institutes, and in general are carried out with the contribution of the national and international scientific community.

The ongoing research program is organized in three main projects, which are presently coming to an end.

- Project S1 – Base-knowledge improvement for assessing the seismogenic potential of Italy.

This project is structured into three parts. Two of them address the activities related to geographical areas of interest (Po Plain, Sannio-Matese to the Calabria-Lucania border), whereas the third one concerns the activities which may have a specific interest as special case studies or application of innovative techniques. The project has been structured in sub-projects and tasks. All sub-projects address regional-scale issues and specific targets within a region, with one exception, aimed at promoting the optimization of techniques which are used for earthquake geology and seismic monitoring.

- Project S2 – Constraining observations into seismic hazard

This project aims at comparing and ranking different hazard models, according to open-shared and widely agreed validation rules, in order to select the best “local” hazard assessment. The goal is to validate the hazard maps on instrumental observations, combining expected shakings at bedrock with site-specific information gathered at local scale.

- Project S3 – Short term earthquake forecasting

The basic aim of this project is the full exploitation of the huge amount of data collected, with special care to the potential detection of possible large scale/short term (weeks to months) transient strain field variations, that could be related to incoming earthquakes. Two are the study areas of major concern (Po plain and Southern Apennines). In particular, due the larger amount of information available for the Po Plain (GPS, InSAR, piezometric data, etc.) most of activities is focused on this area.

The total funding for the current, 2 years seismological topics was 2 M€, 60 % of which have been devoted to the participation of universities and other scientific institutions, while 40 % are for the research units of INGV. Several tens of research units are involved in this program.

2.4.1.2 ReLUIIS

DPC and ReLUIIS (<http://www.reluis.it/>) signed a 5 years agreement for the 2014–2018 period. The object of the agreement is related to two main groups of activities carried out for DPC in the field of earthquake engineering, namely the technical-scientific support and divulgation, and the development of knowledge. More in detail, ReLUIIS supports DPC in:

- post-earthquake technical emergency management;
- training and divulgation activities in earthquake engineering and seismic risk (teachers' availability, high-level course organization, meetings and seminars, technical-scientific divulgation, conferences);
- training of professionals on the post-earthquake evaluations;
- campaigns of divulgation and spreading of the civil protection culture.

For what concerns the development of knowledge, themes of civil protection interest are developed according to the following lines of activity:

- finalized research programs on earthquake engineering and seismic risk mitigation;
- coordination with the DPC, CC and with other technical-scientific subjects;
- implementation, revision and publication of manuals, guidelines, pre-normative documents;
- assistance for drafting/revising technical norms.

The finalized research programs are in a continuity line with the previous projects, that started in 2005 (Manfredi and Dolce 2009). For the 2014–2016 period, they are organized according to the following general lines:

- (i) General Themes, relevant to design, safety verifications and vulnerability assessment of buildings and constructions (e.g., R/C and masonry buildings, bridges, tanks, geotechnical works, dams, etc.);
- (ii) Territorial Themes, aimed at improving the knowledge of the types of buildings and of their actual territorial distribution, in order to set up tools for the improvement of the vulnerability and risk assessment at national/local scale;
- (iii) Special Projects on specific topics (e.g. distribution networks and utilities, provisional interventions, etc.) that are not dealt with in the General Themes, or on across-the-board themes (e.g., near-source effects on structures, treatment of uncertainties in the safety assessment of existing buildings).

Territorial Themes deserve a special attention from the civil protection point of view. Seismic risk evaluations at the national scale are currently based on the data derived from the national population census, which includes only some rough data on buildings (age, number of stories, type of structural material, i.e., R/C or masonry). A new approach has been set up, aimed at improving such evaluation for what concerns the vulnerability and exposure components on a territorial basis, trying to extract as much information as possible from the knowledge of local

experts (i.e., professionals and local administration officials) on the building characteristics. This approach takes profit of the network organization of ReLUIS, that involves more than 40 universities all over Italy. It is based on the identification of the common structural and non-structural features of buildings pertaining to each district of a given municipality, characterized by a good homogeneity in terms of age and main characteristics of the building stock (Zuccaro et al. 2014).

2.4.1.3 EUCENTRE

DPC and EUCENTRE (<http://www.eucentre.it/>) signed an agreement for the 2014–2016 period. Also in this case, as for ReLUIS, the object of the agreement is related to the two main groups of earthquake engineering activities carried out for DPC, i.e., the technical-scientific support and divulgation, and the development of knowledge. In detail, EUCENTRE supports DPC in:

- training and divulgation;
- experimental laboratory testing on structural models, sub-assemblages and elements;
- management of seismic data banks;
- planning, preparing and managing technical-scientific activities in emergency.

Of particular interest is the management of seismic data banks, due to the implemented capability of making risk and scenario evaluations. This management is organized in the following lines of activities (see Fig. 2.8):

- Tool for System Integration (S.3.0 in Fig. 2.8)
- Seismic risk of the Italian dwelling buildings
- Seismic risk of the Italian schools (S.3.2 in Fig. 2.8)
- Management system of the post-event dwelling needs
- Seismic Risk of the Italian road system
- Seismic Risk of the Italian sea harbours (S.3.5 in Fig. 2.8)
- Seismic Risk of the Italian earth dams (S.3.6 in Fig. 2.8)
- Seismic Risk of the Italian airports
- Data base of past earthquake damage to buildings
- Seismic vulnerability of the Italian tunnels
- WebGIS for private buildings upgrade funded by the State with Law n. 77/2009, Art. 11

The activities devoted to the development of knowledge are related to the two following themes: (1) Maps of seismic design actions at uniform risk, and (2) Fragility curves and probability of damage state attainment of buildings designed according to national codes. This latter theme encompasses the seismic safety of masonry buildings (including the limited knowledge of the structure and of the uncertainty sources, the improvement of procedures of analysis and verification of structures, and the fragility curves of masonry buildings), the Displacement Based

Implementation/management of seismic data banks

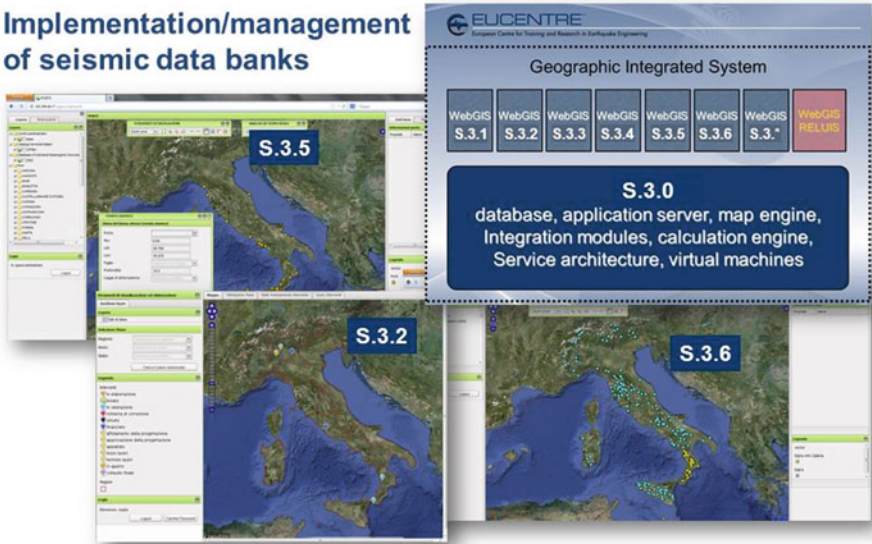


Fig. 2.8 Examples of WEB-GIS applications by EUCENTRE

Design in low hazard zones and relevant software implementation DBDsoft, and the Fragility curves of precast building structures.

2.4.2 *Permanent Commissions – The Major Risks Commission*

The National Commission for forecasting and prevention of Major Risks is the highest-level, connecting structure between the Italian civil protection system and the scientific community. It is an independent scientific consultation body of DPC, but it is not part of the Department itself. The Commission was established by Law n. 225/1992. Its organization and functions have been re-defined in 2011 (DPCM 7 October 2011).

The Major Risks Commission provides advice on technical-scientific matters, both autonomously and on request of the Head of the Department of Civil Protection, and may provide recommendations on how to improve capabilities for evaluation, forecasting and prevention of the various risks.

The Commission is structured in a Presidency Office and five sectors relevant to:

- seismic risk,
- volcanic risk,
- weather-hydrogeological, hydraulic and landslide risk,

- chemical, nuclear and industrial and transport risk,
- environmental and fire risk.

Each sector has a coordinator and ten to twelve members coming from the whole scientific community, including experts from the CC.

The term of the office is 5 years. The Commission meets separately for each risk sector, or in joint sessions for the analysis of inter-disciplinary matters. It usually meets once a year in plenary session and normally gathers in the DPC premises. In order to get further scientific contributions, the President can invite also external experts without voting right.

As far as the formal communications of the Commission are concerned, according to the current rules the results of each meeting have to be summarized in minutes that are released to the Head of the Department of Civil Protection. In case of specific communication needs, the same results can be further summarized in a public statement, which represents the only official way to provide the opinions of the Commission to the public.

2.4.3 Commissions on Specific Subjects

In the recent past, DPC turned to the advice of high-level international panels of scientists to deal with specific and delicate questions of civil protection interest. Two cases related to seismic risk are summarized in this section.

2.4.3.1 ICEF – International Commission on Earthquake Forecasting

The International Commission on Earthquake Forecasting was charged by DPC on May 20th, 2009, after the April 6th, 2009, L’Aquila earthquake, to report on the current state of knowledge of short-term prediction and forecasting of tectonic earthquakes and to indicate guidelines for utilization of possible forerunners of large earthquakes to drive civil protection actions. The Commission worked during 4 months to firstly draft an Executive Summary, that was released on October 2nd, 2009. The final ICEF Report, including state-of-art, evaluations and findings, was then completed and published on August 2011 (Jordan et al. 2011).

The Commission was composed of ten members from nine countries, namely: T. H. Jordan, Chair – USA, Y.-T. Chen – China, P. Gasparini, Secretary – Italy, R. Madariaga – France, I. Main – United Kingdom, W. Marzocchi – Italy, G. Papadopoulos – Greece, G. Sobolev – Russia, K. Yamaoka – Japan, J. Zschau – Germany.

The final ICEF report is organized into five sections, as follows.

- I. Introduction: describes the charge to the Commission, the L’Aquila earthquake context, and the Commission’s activities.

- II. Science of Earthquake Forecasting and Prediction: summarizes the state of knowledge in earthquake forecasting and prediction and discusses methods for testing and validating forecasting models.
- III. Status of Operational Earthquake Forecasting: reports on how governmental agencies in China, Greece, Italy, Japan, Russia and United States use operational forecasting for earthquake risk management.
- IV. Key Findings and Recommendations: states the Commission's key findings and makes specific recommendation on policies and actions that can be taken by DPC to improve earthquake forecasting and its utilization in Italy.
- V. Roadmap for Implementation: summarizes the DPC actions needed to implement the main recommendations in Italy.

Among the recommendations, it is worth to mention the following ones:

Recommendation A: DPC should continue to track the scientific evolution of probabilistic earthquake forecasting and deploy the infrastructure and expertise needed to utilize probabilistic information for operational purposes.

Recommendation D: DPC should continue its directed research program on development of time-independent and time-dependent forecasting models with the objective of improving long-term seismic hazard maps that are operationally oriented.

Recommendation G2: Quantitative and transparent protocols should be established for decision-making that include mitigation actions with different impacts that would be implemented if certain thresholds in earthquake probability are exceeded.

Although the activities of the CC, especially of INGV, were already in line with such recommendations, they have been somewhat re-addressed, according to them. In the meanwhile, DPC is rethinking about the delicate management of seismic sequences, in the light of the recent scientific advancements suggested by the ICEF Commission. In fact, managing seismic sequences from a civil protection point of view is a very complex question, due to the variety of situations and to the difficulties in structuring well defined procedures.

Main aspects are:

- the very low probabilities of a strong event during swarms and their communication to authorities and to citizens (and then to media). This information competes with different kinds of predictions made available to the public, as well known since the seventies: "In the 1976 . . . I warned that the next 10 years were going to be difficult ones for us, with many 'messy' predictions to deal with as we gradually developed a prediction capability. Certainly this has proved to be the case, with many of the most difficult situations arising from predictions by amateurs or self-proclaimed scientists who nevertheless gained public credibility through the news media" (Allen 1982). Although it is well known that the strengthening of constructions remains by far the more effective way to mitigate seismic risk, there is still a strong request for predictions or any action that can

alleviate worries and fears of citizens caused by shakes during a seismic sequence;

- the relatively high probabilities of strong aftershocks following a major event, especially for what concerns the management of civil protection activities after a big earthquake, like search and rescue, population assistance, damage assessment, safety countermeasures, etc.

These points have to do with the short-term seismic hazard, and DPC is carefully evaluating the possibility of using the related information, availing of INGV-CPS evaluations. An in-depth analysis is going on among and within different DPC sectors (Technical, Emergency, Communication, Press), also involving the Major Risks Commission for what concerns the accuracy of the evaluation methods and other scientific issues. Some of the questions that are more strictly related to civil protection issues are relevant to the communication to the large public and the media (about: delivering simplified or complete probabilistic information, either regularly or just in case of swarms or major events; evaluating how this kind of communication could encourage private and public owners to undertake the structural strengthening of their buildings, rather than discourage them; communicating risk/loss forecast rather than just hazard; educating public, media and administrators to make good use of short-term hazard information), to the civil protection actions that can be effectively carried out, especially related to the knowledge of the high probabilities of strong aftershocks, and to the tasks and responsibilities of information providers and of civil protection organizations.

2.4.3.2 ICHESE – International Commission on Hydrocarbon Exploration and Seismicity in the Emilia Region

The need for an international commission to deal with ‘Hydrocarbon Exploration and Seismicity in the Emilia Region’ was expressed by the President of the Emilia Romagna Region after the 2012 Emilia earthquakes. Members of the commission were five scientists, namely Peter Styles, Chair – UK, Paolo Gasparini, Secretary – Italy, Ernst Huenges – Germany, Stanislaw Lasocki – Poland, Paolo Scandone – Italy, and a representative of the Ministry of Economic Development – Franco Terlizese.

On February 2014, the Commission released a final report answering the following questions, on the basis of the technical-scientific knowledge available at the moment:

1. *Is it possible that the seismic crisis in Emilia has been triggered by the recent research activities at the Rivara site, particularly in the case of invasive research activities, such as deep drilling, fluids injections, etc.?*
2. *Is it possible that the Emilia seismic crisis has been triggered by activities for the exploitation and utilization of reservoirs carried out in recent times in the close neighbourhood of the seismic sequence of 2012?*

While the answer to the first question was trivial, once verified that there had been no field research activities at the Rivara site, the answer to the second question was articulated as follows:

- The study does not indicate that there is evidence which can associate the Emilia 2012 seismic activity to the operation activities in Spilamberto, Recovato, Minerbio and Casaglia fields,
- it cannot be ruled out that the activities carried out in the Mirandola License area have had a triggering effect,
- In any case, the whole Apennine orogen under the Po Plain is seismically active and therefore it is essential that the production activity are accompanied by appropriate actions, which will help to manage the seismic risk associated with these activities.

Apart from the specific findings, the importance of the Commission stands in having addressed the induced/triggered seismicity issue in Italy, a research field still to be thoroughly explored in this country. As it can be easily understood, however, not only is this topic of scientific interest, but it has also an impact on the hydrocarbon E&P and the gas storage activities, due to the increased awareness of national policy makers, local authorities and population (see, for a review of the current activities on induced/triggered seismicity in Italy, D'Ambrogi et al. 2014).

2.4.4 Research Funded by Other Subjects

In the past, international research projects were little finalized to products for civil protection use, and the stakeholders' role, although somehow considered, was not enough emphasized. Looking at the research funding policy currently undertaken by the European Union, a more active role is expected from the stakeholders (e.g., Horizon 2020, Work Programme 2014–15, 14. Secure societies; http://ec.europa.eu/research/participants/data/ref/h2020/wp/2014_2015/main/h2020-wp1415-security_en.pdf) and, among them, from civil protection organizations, as partners or end-user advisors. Some good cases of EU-funded research projects, finalised to the achievement of results potentially useful for civil protection can be mentioned, however, also for the previous EU Seventh Framework Program. Three examples are here discussed, to show how important is the continuous interaction between scientific community and civil protection stakeholders to achieve results that can be exploited immediately or prospectively in practical situations, and how long is the road to get a good assimilation of scientific products or results within civil protection procedures.

A different case, not dealt in detail, is represented by the GEM Programme and promoted by the Global Science Forum (OECD). This is a global collaborative effort in which science is applied to develop high-quality resources for transparent assessment of earthquake risk and to facilitate their application for risk management around the globe (<http://www.globalquakemodel.org/>). DPC supported the establishment of GEM in Pavia and currently funds the programme, representing Italy in the Governing Board.

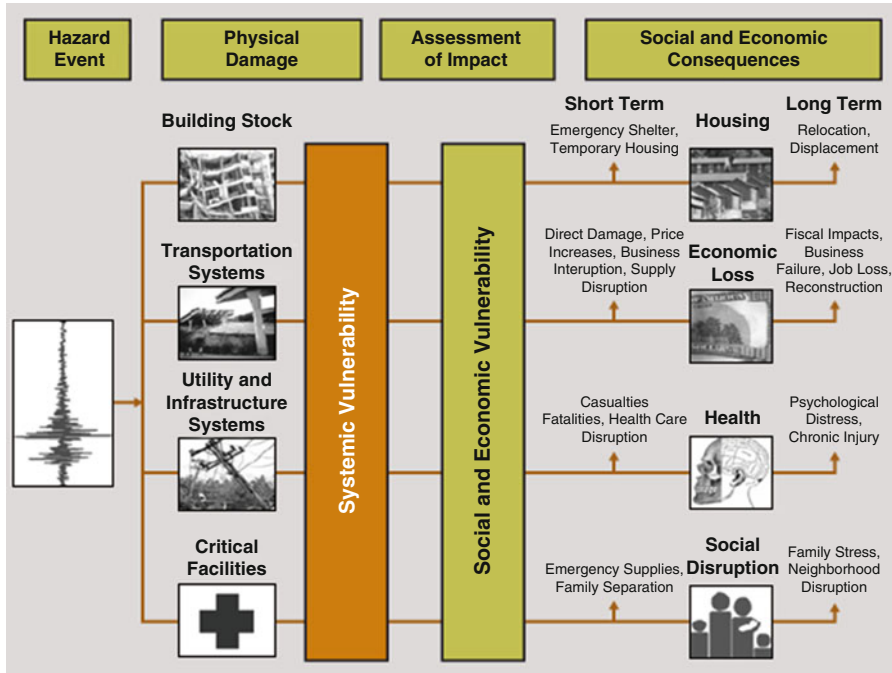


Fig. 2.9 General graphic layout of the concept and goals of SYNER-G (<http://www.vce.at/SYNER-G/files/project/proj-overview.html>)

2.4.4.1 SYNER-G

Syner-G is a EU project developed within the Seventh Framework Programme, Theme 6: Environment, and focused on the systemic seismic vulnerability and risk analysis of buildings, lifelines and infrastructures. It started on November 2009, with a 3 years duration (Pitilakis et al. 2014a, b). Eleven partners from eight European countries and three from outside Europe (namely USA, Japan and Turkey) participated to the project, that was coordinated by the Aristotle University of Thessaloniki (Greece) (Fig. 2.9).

The main goals of Syner-G were (see <http://www.vce.at/SYNER-G/files/project/proj-overview.html>):

- to elaborate, in the European context, appropriate fragility relationships for the vulnerability analysis and loss estimation of all elements at risk,
- to develop social and economic vulnerability relationships for quantifying the impact of earthquakes,
- to develop a unified methodology and tools for systemic vulnerability assessment, accounting for all components exposed to seismic hazard, considering interdependencies within a system unit and between systems,

- to validate the methodology and the proposed fragility functions in selected sites (at urban scale) and systems, and to implement them in an appropriate open source and unrestricted access software tool.

DPC acted as an end-user of this project, providing data and expertise; moreover, one of the authors of the present paper was part of the advisory board. The comments made in the end-user final report, summarized below, provide an overview of the possible interactions and criticalities of this kind of projects with civil protection organizations. Among the positive aspects:

- the analysis of the systemic vulnerability and risk is a very complex task;
- considerable steps ahead have been made, in Syner-G, both in questions not dealt with before or in topics that have been better finalized during the project;
- brilliant solutions have been proposed for the problems dealt with and sophisticated models have been utilized;
- of great value is the coordination with other projects, especially with GEM.

It was however emphasized that:

- large gaps still exist between many scientific approaches and practical decision-makers' actions;
- the use of very sophisticated approaches and models has often required to neglect some important factors affecting the real behaviour of some systems;
- when dealing with a specific civil protection issue, all important affecting factors should be listed, not disregarding any of them, and their influence evaluated, even though roughly;
- a thorough and clear representation of results is critical for a correct understanding by end-users;
- models and results calibration should be referred to events at different scale, due to the considerable differences in the system response and in the actions to be undertaken;
- cases of induced technological risks should be considered as well, since nowadays the presence of dangerous technological situations is widespread in the partner countries.

2.4.4.2 REAKT

REAKT – Strategies and tools for Real time Earthquake risK reducTION (<http://www.reaktproject.eu/>) as well is a EU project developed within the Seventh Framework Programme, Theme 6: Environment. It started on September 2011, with a 3 years duration. Twenty-three partners from nine European countries and six from the rest of the world (namely Jamaica, Japan, Taiwan, Trinidad and Tobago, Turkey, USA) participated to the project, that was coordinated by AMRA (Italy; <http://www.amracenter.com/en/>). Many different types of stakeholders acted as end-users of the Project, among which the Italian DPC, represented

by the authors of this paper. DPC has actively cooperated, by putting at disposal data and working on application examples.

Among the main objectives of REAKT, one of them deserves specific attention for the scopes of the present paper, namely: “the definition of a detailed methodology to support optimal decision making associated with earthquake early warning systems (EEWS), with operational earthquake forecasting (OEF) and with real-time vulnerability and loss assessment, in order to facilitate the end-users’ selection of risk reduction countermeasures”.

Much in detail, the attention is here focused on the EEWS and, specifically, on the content of the first version of the “Final Report for Feasibility Study on the Implementation of Hybrid EEW Approaches on Stations of RAN” (Picozzi et al. 2014). Actually, during the project, an in-depth study on the possibility of exploiting for EEW purposes the National Strong-Motion Network RAN was carried out. It is worth to notice that within the project, consistently with the purpose of the related task, the attention was exclusively focused on the most challenging scientific aspects, on which an excellent and exhaustive research work has been carried out. Summarising, the main outcomes of this work are related to the reliability of the real-time magnitude computation and to the evaluation of the lead time, i.e., the time needed for the assessment of the magnitude of the impending earthquake and for the arrival of this information to the site where some mitigating action has to be undertaken before strong shear waves arrive. Such evaluation is referred to the performances and the geographical distribution of the RAN network (see Fig. 2.6b), and to the performances of the algorithm PRESto (Satriano et al. 2010) for the fast evaluation of the earthquake parameters. The knowledge of the lead time allows an evaluation of the so-called blind and safe zones to be made, where the “blind zone” is the area around the epicentre where the information arrives after the strong shake starts, while the “safe zone” is the surrounding area where the information arrives before and where the shake is still strong enough for the real-time mitigating action to be really useful.

However, neither other technological and scientific requirements that must be fulfilled have been analysed, nor other components necessary to make a complete EEW system useful to mitigate risk have been considered, many of which dealing with civil protection actions. This case appears useful, therefore, to show the different points of view of science and civil protection and to emphasize again how important is to consider all the main factors affecting a given problem – in this case the feasibility and effectiveness of an EEWS – and to evaluate, even roughly, their influence. At this aim, some of the comments made by DPC to the first draft of the final report (Picozzi et al. 2014) are summarized below. The main aspects dealt with are about the effectiveness of EEW systems for real-time risk mitigation. This latter requires at least that:

- efficiency of all the scientific components is guaranteed,
- efficiency of all the technological components is guaranteed,
- targets and mitigation actions to be carried out are defined,
- time needed for the actions is added to the (scientific) lead time,

Scientific vs. Operational Safe Zone

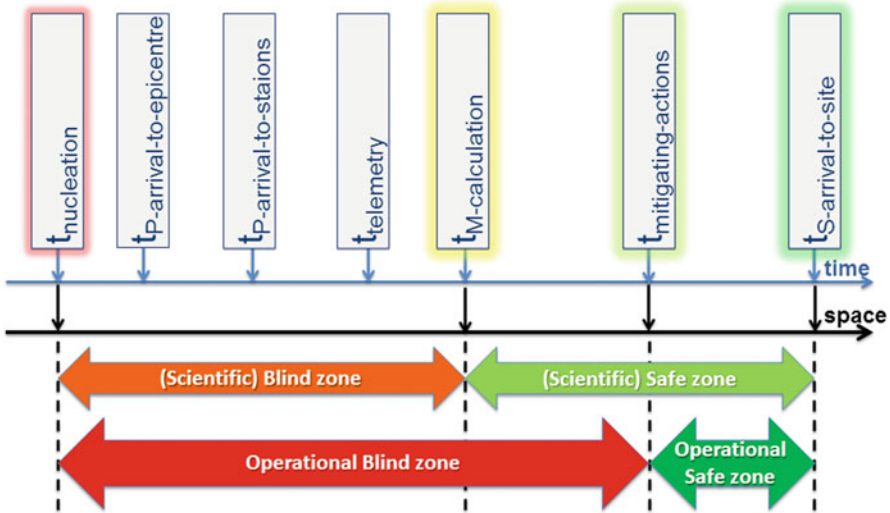


Fig. 2.10 Different definitions of blind and safe zone from the scientific and the operational (civil protection) points of view

- end-users (including population) are educated and trained to receive messages and act consequently and efficiently,
- costs and benefits of the actions are evaluated,
- infrastructures required for automatic actions are efficient,
- downtime is avoided in the links among elements of the EEW chain,
- responsibilities related to false and missed alarms and legal framework are well defined.

A very important point, which is strictly related to the capability of an EEWs to really mitigate risk in real time, is how to identify the so-called “blind zone”, where no real-time mitigating action can be carried out, as the information about the impending earthquake arrives too late; and, consequently, how to identify the “safe zone”, where potentially some mitigating action can be made (see Fig. 2.10). Actually, defining this latter as a “safe” zone solely on the basis of the above mentioned scientific evaluations can be misleading, because the identification of a “safe” zone should also account for the time needed to undertake a specific “real-time” mitigation action that, obviously, requires from some seconds to some tens of seconds (Goltz 2002). When including also this time interval in the calculation of the “blind zone” radius, a considerable increase occurs, from 30–35 km to some 50–60 km. Unfortunately, this reduces considerably the effectiveness of the EEWs for Italian earthquakes, which are historically characterized by magnitudes that rarely exceeded 7.0. Dealing with these values, the EEW applicability in the severely damaged zones around the epicentral area is totally excluded, whereas

the zones of its potential utilization actually correspond to areas where the felt intensity implies no or negligible structural damage.

From a communication perspective, it has to be noticed that spreading a purely scientific information that, though correct, neglects a comprehensive analysis including civil protection issues could determine in the stakeholders and in the general public undue expectations, beyond the actual EEW potential capabilities in Italy, if it is based on a regional approach.

2.4.4.3 SHARE

SHARE – Seismic Hazard Harmonization in Europe (<http://www.share-eu.org/>) is a Collaborative Project in the Cooperation programme of the EU Seventh Framework Programme. “SHARE’s main objective is to provide a community-based seismic hazard model for the Euro-Mediterranean region with update mechanisms. The project aims at establishing new standards in Probabilistic Seismic Hazard Assessment (PSHA) practice by a close cooperation of leading European geologists, seismologists and engineers. . . . SHARE produced more than 60 time-independent European Seismic Hazard Maps, spanning spectral ordinates from 0 (PGA) to 10 s and exceedance probabilities ranging from 10^{-1} to 10^{-4} yearly probability”.

Eighteen scientific partners from thirteen countries contributed to the project, which started on September 2011, with a 3 years duration. No stakeholder acted as end-user. The most renowned product of SHARE is the 475 years return period PGA map of Europe, shown in Fig. 2.11, which reproduces the poster of the project, entitled “European Seismic Hazard Map”.

In Italy, the official set of seismic hazard maps is a product of a DPC-INGV project released in 2004 (<http://esse1-gis.mi.ingv.it/>). These maps were enforced in 2006 (OPCM 3519/2006) and they were included in the current Italian seismic code in 2008 (DM 14 January 2008).

If one compares the two corresponding (475 years return period) PGA hazard maps, as shown in Fig. 2.12, considerable differences in PGA can be observed, with systematically greater values in the SHARE map. Such differences are typically in the order of +0.10 g (up to 0.15–0.20 g, locally), resulting in percentage differences reaching 50 % even in high hazard areas (Meletti et al. 2013). Based on this comparison, one could infer that not only is the national official map set “wrong”, assuming the most recent being the “right” one, but also highly non-conservative. Therefore, severe doubts about the correctness of the Italian official hazard and classification maps could arise, along with general problems of communication with the general public and the media.

From an engineering viewpoint, on the contrary, spectral accelerations are the only ones that enter into the design procedures and are, therefore, much more important than PGA for seismic risk mitigation. From this perspective, if one looks at the hazard maps in terms of spectral accelerations corresponding to $T=0.5$ s vibration period, differences of only ± 0.05 g are typically detected (Meletti et al. 2013). Being of opposite signs, these differences highlight that the

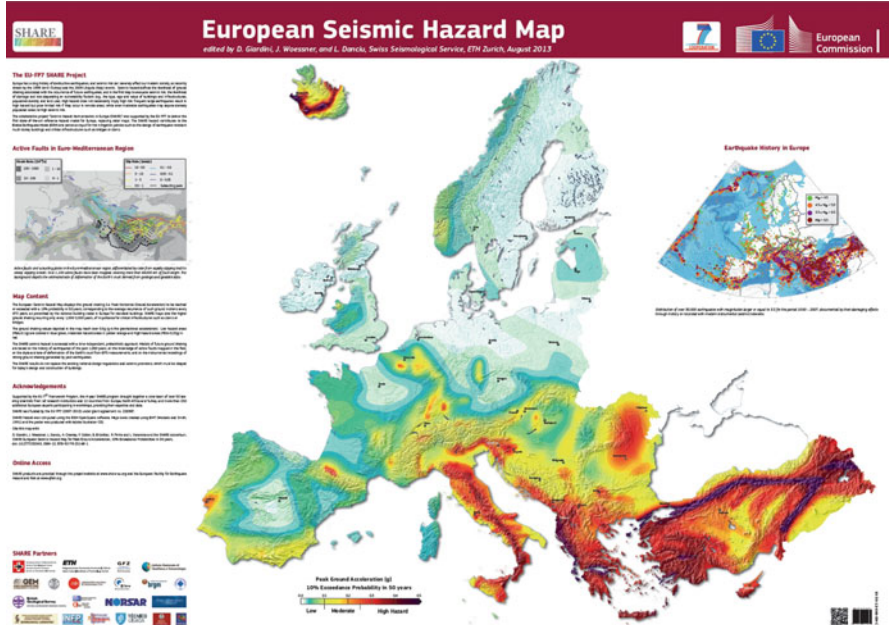


Fig. 2.11 Poster of the SHARE project, which reproduces the 475 return period PGA map of Europe (http://www.share-eu.org/sites/default/files/SHARE_Brochure_public.web_.pdf)

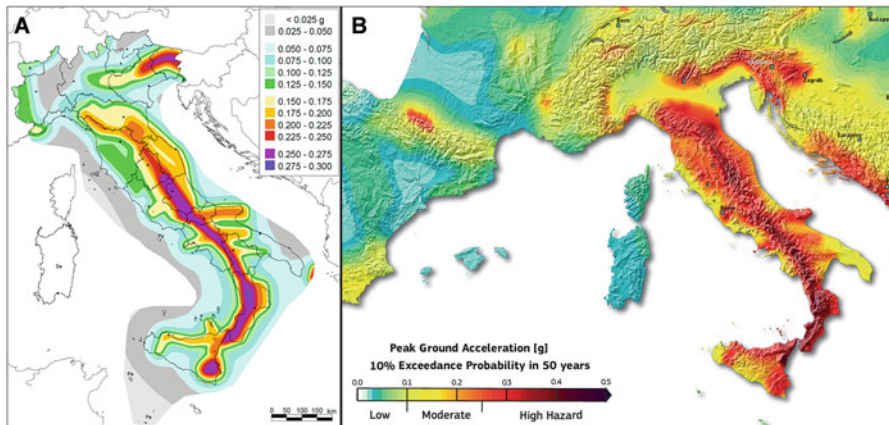


Fig. 2.12 Official (seismic code) PGA hazard map of Italy (a) vs. SHARE PGA hazard map (b) for the same area, referred to 10 % probability in 50 years (Maps are taken, respectively, from: http://zonesismiche.mi.ingv.it/mappa_ps_apr04/italia.html, and http://www.share-eu.org/sites/default/files/SHARE_Brochure_public.web_.pdf)

Italian official hazard model is not under-conservative, differently from what the PGA maps would induce to believe, and are instead acceptable from an engineering point of view.

2.4.5 Free Research Works

As anticipated in section 3, there is also a large amount of scientific studies and published papers that are independently produced by the scientific community, and sometimes by inventors and amateurs, that could have repercussions on civil protection activities. They are in many cases related to:

- drafting new hazard maps,
- making earthquake predictions (short- and medium-term),
- discovering new active faults (especially in built environments),
- inventing instruments that try to make a sort of earthquake early warning,
- conceiving new structural devices or building techniques,
- inventing antiseismic indoor shelters, like antiseismic boxes, rooms, cellules, beds, etc.

There is a very large number of examples that could be mentioned here, but anyone reading this paper can focalize on his own experience about some of the above situations raising almost daily.

Without discussing the scientific value, sometimes high, of these products made freely available, it is quite clear that their integration in the civil protection procedures or decisional processes cannot be immediate. As a matter of fact, intrinsic in the research activity is the scientific debate on the new findings. Therefore, before a new scientific product can be taken into consideration for civil protection purposes, not only it has to be published on peer reviewed journals, but it has also to be widely and publicly discussed and somehow “accepted” by a large part of the scientific community (also assuming that a 100 % consensus is practically impossible to reach). After this pre-requisite is fulfilled, these scientific results need to be envisaged in the civil protection decisional chain (including a cost-benefit analysis), and in most cases they need to be adapted and calibrated to civil protection operability. Finally, a testing phase follows, aimed at verifying if their use, ultimately, brings advantage in the achievement of the system goals. All these steps stand to reason that civil protection decisions and actions have a strong and direct impact on the society, and thus they have to be undertaken on well-grounded premises.

As one can imagine, this integration process takes time, and therefore it can suffer from some shortcuts followed for instance by individual scientists, who promote the immediate use of their results through the mass media and the political authorities, at both national and local level. No matter if the new findings are the outcome of valuable research or not, when civil protection is improperly urged to promptly acknowledge or adopt some specific new findings and take any useful

action to mitigate risk based on them, this will cause a damage to the entire system. This problem can be overcome only by increasing the awareness that scientists, media, PDMs and TDMs, all of them compose the same puzzle, and cooperation, interchange, correct communication are the only way to attain the shared goal of a more effective civil protection when working for risk mitigation.

2.5 Conclusion

The relationships between science and civil protection, as shown in this paper, are very complex, but they can imply important synergies if correctly addressed. On the one hand, scientific advances can allow for more effective civil protection decisions and actions, although critical issues can arise for the civil protection system, that has to suitably shape its activities and operational procedures according to these advances. On the other hand, the scientific community can benefit from the enlargement of the investigation perspectives, the clear finalisation of the applied research activities and their positive social implications.

In the past decades the main benefits from civil protection-science interaction in Italy were a general growth of interest on Seismology and Earthquake Engineering and a general increase of the amount and of the scientific quality of research in these fields. But there were also a still inadequate finalisation of the products and some inconsistencies of the results not solved within and among the research groups (i.e., lack of consensus).

Progresses recently achieved, consequent to a re-organization effort that started in 2004, encompass:

- better structured scientific activities, finalised to civil protection purposes;
- an improved coordination among research units for the achievement of civil protection objectives;
- the realization of products of ready use (e.g.: tools for hazard analysis, databases in GIS environment, guidelines);
- a substantial increase of experimental investigations, data exchanging and comparisons within large groups, as well as the achievement of a consensus on results, strictly intended for decisional purposes;
- a renewed cooperation in the divulgation activities aimed at increasing risk awareness in the population;
- better structured advisory activities of permanent and special commissions.

While important progresses are registered, a further improvement in the cooperation can be still pursued, and many problems also remain in case of non-structured interactions between civil protection and scientific community.

For all the above reasons, a smart interface between civil protection and scientific community continues to be necessary (Di Bucci and Dolce 2011), in order to identify suitable objectives for the research funded by DPC, able to respond to civil protection needs and consistent with the state-of-the-art at international level.

After the 2009 L'Aquila and 2012 Emilia earthquakes, the scientific partners have provided a considerable contribution to the National Service of Civil Protection in Italy, not only with regard to the technical management of the emergency but also the divulgation campaigns for the population under the DPC coordination. However, an even more structured involvement of the CC is envisaged, even in the emergency phase.

The authors strongly believe in the need and the opportunity that the two worlds, scientific community and civil protection, carry on cooperating and developing an interaction capability, focusing on those needs that are a priority for the society and implementing highly synergic relationships, which favour an optimized use of the limited resources available. Some positive examples come from the Italian experience and have been described along with some of the tackled difficulties. They deal with many different themes and are intended to show the multiplicity and diversity of issues that have to be considered in a day-by-day work of interconnection between civil protection and scientific community. These examples can help to get a more in-depth mutual understanding between these two worlds and provide some suggestions and ideas for the audience, national and international, which forms the seismic risk world.

Acknowledgments The Authors are responsible for the contents of this work, which do not necessarily reflect the position and official policy of the Italian Department of Civil Protection.

Open Access This chapter is distributed under the terms of the Creative Commons Attribution Noncommercial License, which permits any noncommercial use, distribution, and reproduction in any medium, provided the original author(s) and source are credited.

References

- AGU Fall Meeting (2012) Lessons learned from the L'Aquila earthquake verdicts press conference. <http://www.youtube.com/watch?v=xNK5nmDFgy8>
- Alexander DE (2014a) Communicating earthquake risk to the public: the trial of the "L'Aquila Seven". *Nat Hazards*. doi:10.1007/s11069-014-1062-2
- Alexander DE (2014b) Reply to a comment by Franco Gabrielli and Daniela Di Bucci: "Communicating earthquake risk to the public: the trial of the 'L'Aquila Seven'". *Nat Hazards*. doi:10.1007/s11069-014-1323-0
- Allen CR (1982) Earthquake prediction—1982 overview. *Bull Seismol Soc Am* 72(6B):S331–S335
- Basili R, Valensise G, Vannoli P, Burrato P, Fracassi U, Mariano S, Tiberti MM, Boschi E (2008) The Database of Individual Seismogenic Sources (DISS), version 3: summarizing 20 years of research on Italy's earthquake geology. *Tectonophysics*. <http://dx.doi.org/10.1016/j.tecto.2007.04.014>
- Berelson B (1948) Communication and public opinion. In: Schramm W (ed) *Communication in modern society*. University of Illinois Press, Urbana
- Bretton R (2014) The role of science within the rule of law. "Science, uncertainty and decision making in the mitigation of natural risks", Workshop of Cost Action IS1304 "Expert Judgment Network: Bridging the Gap Between Scientific Uncertainty and Evidence-Based Decision Making". Rome, 8-9-10 Oct 2014. Oral presentation

- D'Ambrogio C, Di Bucci D, Dolce D, Donda F, Ferri F, Improta L, Mucciarelli M, Panei L, Scrocca D, Stabile TA, Vittori E (2014) Tavolo di Lavoro interistituzionale ISPRA. Rapporto sullo stato delle conoscenze riguardo alle possibili relazioni tra attività antropiche e sismicità indotta/innescata in Italia. ISPRA. <http://www.isprambiente.gov.it/it/news/rapporto-sullo-stato-delle-conoscenze-riguardo-alle-possibili-relazioni-tra-attivita-antropiche-e-sismicita-indotta-innescata-in-italia>. 27 June 2014
- Di Bucci D, Dolce M (2011) Research projects in seismology funded by the Italian Department of Civil Protection. DVD e Volume degli atti della "First Sino Italian Conference on: Advanced Methodologies and Technologies in Geophysics, Geodynamics and Seismic Hazard Assessment". Pechino, 29–30 Marzo 2010, pp 43–45
- Dipartimento della Protezione Civile and Fondazione CIMA (DPC and CIMA) (eds) (2013) Protezione Civile e responsabilità nella società del rischio. Chi valuta, chi decide, chi giudica (Civil protection and responsibilities in the risk society. Who evaluates, who decides, who judges). ETS Editor, p 152
- Dipartimento della Protezione Civile and Fondazione CIMA (DPC and CIMA) (eds) (2014) La Protezione Civile nella società del rischio. Procedure, Garanzie, Responsabilità (Civil protection in the risk society. Procedures, guarantees, responsibilities) ETS Editor, p 92
- DISS Working Group (2010) Database of Individual Seismogenic Sources (DISS), Version 3.1.1: a compilation of potential sources for earthquakes larger than M 5.5 in Italy and surrounding areas. <http://diss.rm.ingv.it/diss/>, © INGV 2010 – Istituto Nazionale di Geofisica e Vulcanologia – All rights reserved; doi:10.6092/INGV.IT-DISS3.1.1
- Dolce M (2008) Civil protection vs. earthquake engineering and seismological research, Proceeding of 14th world conference on earthquake engineering, Oct 2008, Beijing, Keynote speech
- Dolce M, Di Bucci D (2014) Risk management: roles and responsibilities in the decision-making process. In: Peppoloni S, Wyss M (eds) Geoethics: ethical challenges and case studies in earth science. Section IV: Communication with the public, officials and the media, Chapter 18. Elsevier. Publication Date: 21 Nov 2014 | ISBN-10: 0127999353 | ISBN-13: 978-0127999357 | Edition: 1
- Gabrielli F (2013) Preface in: Dipartimento della Protezione Civile and Fondazione CIMA (DPC and CIMA) (eds), 2013. Protezione Civile e responsabilità nella società del rischio. Chi valuta, chi decide, chi giudica (Civil protection and responsibilities in the risk society. Who evaluates, who decides, who judges). ETS Editor, pp 3–10
- Gabrielli F, Di Bucci D (2014) Comment on "communicating earthquake risk to the public: the trial of the 'L'Aquila Seven'" by David E. Alexander. *Nat Hazards*. doi:10.1007/s11069-014-1322-1. Published online: 19.07.2014
- Gasparini P (2013) Natural hazards and scientific advice: interactions among scientists, decision makers and the public. Plenary Lecture, 2013 Goldschmidt Conference (Florence, Italy). *Mineral Mag* 77(5):1146
- Goltz JD (2002) Introducing earthquake early warning in California: a summary of social science and public policy issues, technical report, Governor's Off. of Emergency Serv., Pasadena
- HORIZON 2020, Work Programme 2014–2015. 14. Secure societies – protecting freedom and security of Europe and its citizens. European Commission Decision C (2014) 4995 of 22 July 2014. http://ec.europa.eu/research/participants/data/ref/h2020/wp/2014_2015/main/h2020-wp1415-security_en.pdf
- Jordan T, Chen Y, Gasparini P, Madariaga R, Main I, Marzocchi W, Papadopoulos G, Sobolev G, Yamaoka K, Zschau J (2011) Operational earthquake forecasting. State of knowledge and guidelines for utilization. *Ann Geophys* 54(4). doi:10.4401/ag-5350
- Jordan TH, Marzocchi W, Michael AJ, Gerstenberger MC (2014) Operational earthquake forecasting can enhance earthquake preparedness. *Seismol Res Lett* 85(5):955–959
- Luzi L, Hailemichael S, Bindi DD, Pacor F, Mele F, Sabetta F (2008) ITACA (ITalian ACcelerometric Archive): a web portal for the dissemination of Italian strong-motion data. *Seismol Res Lett* 79(5):716–722. doi:10.1785/gssrl.79.5.716

- Manfredi G, Dolce M (eds) (2009) The state of the art of earthquake engineering research in Italy: the ReLUIIS-DPC 2005–2008 Project, Doppiavoce, Napoli. <http://www.reluis.it/CD/ReLUIIS-DPC/ReLUIIS-DPC.htm>
- Mele F, Riposati D (2007) ISIDE, Italian Seismological Instrumental and parametric Data-basE. NGT5 2007
- Meletti C, Rovida A, D’Amico V, Stucchi M (2013) Seismic hazard models for the Italian area: “MPS04-S1” and “SHARE”, Progettazione Sismica – Vol. 5, N. 1, Anno 2014. doi:[10.7414/PS.5.1.15-25](https://doi.org/10.7414/PS.5.1.15-25) – <http://dx.medra.org/10.7414/PS.5.1.15-25>
- Mucciarelli M (2014) Some comments on the first degree sentence of the “L’Aquila trial”. In: Peppoloni S, Wyss M (eds) *Geoethics: ethical challenges and case studies in earth science*. Elsevier. Publication Date: 21 Nov 2014 | ISBN-10: 0127999353 | ISBN-13: 978–0127999357 | Edition: 1
- Pacor F, Paolucci R, Luzi L, Sabetta F, Spinelli A, Gorini A, Marcucci S, Nicoletti M, Filippi L, Dolce M (2011) Overview of the Italian strong motion database ITACA 1.0. *Bull Earthq Eng* 9 (6):1723–1739. doi:[10.1007/s10518-011-9327-6](https://doi.org/10.1007/s10518-011-9327-6), Springer Ltd, Dordrecht, The Netherlands
- Picozzi M, Zollo A, Brondi P, Colombelli S, Elia L, Martino C (2014) Exploring the feasibility of a nation-wide earthquake early warning system in Italy, First draft of the final report for the REAKT Project
- Pitilakis K, Crowley E, Kaynia A (eds) (2014a) SYNER-G: typology definition and fragility functions for physical elements at seismic risk, vol 27, Geotechnical, geological and earthquake engineering. Springer Science + Business Media, Dordrecht. ISBN 978-94-007-7872-6
- Pitilakis K, Franchin P, Khazai B, Wenzel H (eds) (2014b) SYNER-G: systemic seismic vulnerability and risk assessment of complex urban, utility, lifeline systems and critical facilities, vol 31, Geotechnical, geological and earthquake engineering. Springer Science + Business Media, Dordrecht. ISBN 978-94-017-8835-9
- Satriano C, Elia L, Martino C, Lancieri M, Zollo A, Iannaccone G (2010) PRESTo, the earthquake early warning system for southern Italy: concepts, capabilities and future perspectives. *Soil Dyn Earthq Eng*. doi:[10.1016/j.soildyn.2010.06.008](https://doi.org/10.1016/j.soildyn.2010.06.008)
- Schramm W (1954) How communication works. In: Schramm W (ed) *The process and effects of mass communication*. University of Illinois Press, Urbana
- Zuccaro G, De Gregorio D, Dolce M, Speranza E, Moroni C (2014) Manuale per la compilazione della scheda di 1° livello per la caratterizzazione tipologico-strutturale dei comparti urbani costituiti da edifici ordinari (Manual for the compilation of the 1st level form to characterize urban districts with respect to the structural types of ordinary building), preliminary draft. ReLUIIS

Chapter 3

Earthquake Risk Assessment: Certitudes, Fallacies, Uncertainties and the Quest for Soundness

Kyriazis Pitilakis

Abstract This paper addresses, from engineering point of view, issues in seismic risk assessment. It is more a discussion on the current practice, emphasizing on the multiple uncertainties and weaknesses of the existing methods and approaches, which make the final loss assessment a highly ambiguous problem. The paper is a modest effort to demonstrate that, despite the important progress made the last two decades or so, the common formulation of hazard/risk based on the sequential analyses of source (M, hypocenter), propagation (for one or few IM) and consequences (losses) has probably reached its limits. It contains so many uncertainties affecting seriously the final result, and the way that different communities involved, modellers and end users are approaching the problem is so scattered, that the seismological and engineering community should probably re-think a new or an alternative paradigm.

3.1 Introduction

Seismic hazard and risk assessments are nowadays rather established sciences, in particular in the probabilistic formulation of hazard. Long-term hazard/risk assessments are the base for the definition of long-term actions for risk mitigation. However, several recent events raised questions about the reliability of such methods. The occurrence of relatively “unexpected” levels of hazard and loss (e.g., Emilia, Christchurch, Tohoku) and the continuous increase of hazard with time, basically due to the increase of seismic data, and the increase of exposure, make loss assessment a highly ambiguous problem.

Existing models present important discrepancies. Sometimes such discrepancies are only apparent, since we do not always compare two “compatible” values. There

K. Pitilakis (✉)

Department of Civil Engineering, Aristotle University of Thessaloniki,
Thessaloniki 54124, Greece
e-mail: kpitilak@civil.auth.gr

© The Author(s) 2015

A. Ansal (ed.), *Perspectives on European Earthquake Engineering and Seismology*,
Geotechnical, Geological and Earthquake Engineering 39,
DOI 10.1007/978-3-319-16964-4_3

are several reasons for this. In general, it is usually statistically impossible to falsify one model only with one (or too few) datum. Whatever the value of probability for such an event is, a probability (interpreted as “expected annual frequency”) value greater than zero means that the occurrence of the event is possible, and we cannot know how much unlucky we have been. If the probability is interpreted as “degree of belief”, is instead in principle not testable. In addition, the assessments are often based on “average” values, knowing that the standard deviations are high. This is common practice, but this also means that such assessments should be compared to the average over multiple events, instead of one single specific event. However, we almost never have enough data to test long-term assessments. This is probably the main reason why different alternative models exist.

Another important reason why significant discrepancies are expected is the fact that we do know that many sources of uncertainties do exist in the whole chain from hazard to risk assessment. However, are we propagating accurately all the known uncertainties? Are we modelling the whole variability? The answer is that often it is difficult to define “credible” limits and constraints to the natural variability (aleatory uncertainty). One of the consequences is that the “reasonable” assessments are often based on “conservative” assumptions. However, conservative choices usually imply subjectivity and statistical biases, and such biases are, at best, only partially controlled. In engineering practice this is often the rule, but can this be generalized? And if yes, how can it be achieved? Epistemic uncertainty usually offers a solution to this point in order to constrain the limits of “subjective” and “reasonable” choices in the absence of rigorous rules. In this case, epistemic uncertainties are intended as the variability of results among different (but acceptable) models. But, are we really capable of effectively accounting for and propagating epistemic uncertainties? In modelling epistemic uncertainties, different alternative models are combined together, often arbitrarily, assuming that one true model exists and, judging this possibility, assigning a weight to each model based on the consensus on its assumptions. Here, two questions are raised. First, is the consensus a good metric? Are there any alternatives? How many? Second, does a “true” model exist? Can a model be only “partially” true, as different models are covering different “ranges” of applicability? To judge the “reliability” of one model, we should analyze its coherence with a “target behaviour” that we want to analyze, which is a-priori unknown and more important it is evolving with time. The model itself is a simplification of the reality, based on the definition of the main degrees of freedom that control such “target behaviour”.

In the definition of “target behaviour” and, consequently, in the selection of the appropriate “degrees of freedom”, several key questions remain open. First, are we capable of completely defining what the target of the hazard/risk assessments is? What is “reasonable”? For example, we tend to use the same approach at different spatiotemporal levels, which is probably wrong. Is the consideration of a “changing or moving target” acceptable by the community? Furthermore, do we really explore all the possible degrees of freedom to be accounted for? And if yes, are we able to do it accurately considering the eternal luck of good and well-focused data? Are we missing something? For example, in modelling fragility, several degrees of freedom are missing or over-simplified (e.g., aging effects, poor modelling including the

absence of soil-structure interaction), while recent results show that this “degree of freedom” may play a relevant role to assess the actual vulnerability of a structure. More in general, the common formulation of hazard/risk is based on the sequential analyses of source (M , hypocenter), propagation (for one or few intensity measures) and consequences (impact/losses). Is this approach effective, or is it just an easy way to tackle the complexity of the nature, since it keeps the different disciplines (like geology, geophysics and structural engineering) separated? Regarding “existing models”, several attempts are ongoing to better constrain the analyses of epistemic uncertainties like critical re-analysis of the assessment of all the principal factors of hazard/risk analysis or proposal of alternative modelling approaches (e.g., Bayesian procedures instead of logic trees). All these follow the conventional path to go. Is this enough? Wouldn't it be better to start criticizing the whole model? Do we need a change of the paradigm? Or maybe better, can we think of alternative paradigms? The general tendency is to complicate existent models, in order to obtain new results, which we should admit are sometimes better correlated with specific observations or example cases. Is this enough? Have we really deeply thought that in this way we may build “new” science over not consolidated roots? Maybe it is time to re-think these roots, in order to evaluate their stability in space, time and reliability.

The paper that follows is a modest effort to argue on these issues, unfortunately without offering any idea of the new paradigm.

3.2 Modelling, Models and Modellers

3.2.1 Epistemology of Models

Seismic hazard and risk assessments are made with models. The biggest problem of models is the fact that they are made by humans who have a limited knowledge of the problem and tend to shape or use their models in ways that mirror their own notion of which a desirable outcome would be. On the other hand, models are generally addressed to end users with different level of knowledge and perception of the uncertainties involved. Figure 3.1 gives a good picture of the way that different communities perceive “certainty”. It is called the “certainty trough”.

In the certainty trough diagram, users are presented as either under-critical or over-critical, in contrast to producers, who have detailed understanding of the technology's strengths and weaknesses. Model producers or modellers are a-priori aware of the uncertainties involved in their model. At least they should be. For end-users communities the situation is different. Experienced over-critical users are generally in better position to evaluate the accuracy of the model and its uncertainties, while the alienated under-critical users have the tendency to follow the “believe the brochures” concept. When this second category of end-users uses a model, the uncertainties are generally increased.

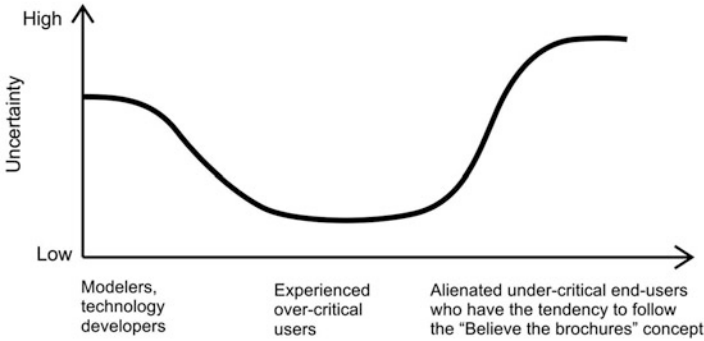


Fig. 3.1 The certainty trough (after MacKenzie 1990)

The present discussion focuses on the models and modellers and less on the end-users; however, the criticism will be more from the side of the end users.

All models are imperfect. Identifying model errors is difficult in the case of simulations of complex and poorly understood systems, particularly when the simulations extend to hundreds or thousands of years. Model uncertainties are a function of a multiplicity of factors (degrees of freedom). Among the most important are limited availability and quality of empirical-recorded data, the imperfect understanding of the processes being modelled and, finally, the poor modelling capacities. In the absence of well-constrained data, modellers often gauge any given model's accuracy by comparing it with other models. However, the different models are generally based on the same set of data, equations and assumptions, so that agreement among them may indicate very little about their realism.

A good model is based on a wise balance of observation and measurement of accessible phenomena with informed judgment "theory", and not in inconvenience. Modellers should be honestly aware of the uncertainties involved in their models and of how the end users could make use of them. They should take the models "seriously but not literally", avoiding mixing up "qualitative realism" with "quantitative realism". However, modellers typically identify the problem as users' misuse of their model output, suggesting that the latter interpret the results too uncritically.

3.2.2 Data: Blessing or Curse

It is widely accepted that science, technology, and knowledge in general, are progressing with the accumulation of observation and data. However, it is equally true that without proper judgment, solid theoretical background and focus, an accumulation of data may fade out the problem and drive the scientist-modeller to a wrong direction. The question is how much aware of that is the modeller.

Une accumulation de faits n'est pas plus une science qu'un tas de pierres n'est une maison.
Jules Henri Poincare

Historically the accumulation of seismic and strong motion data resulted in higher seismic hazard when seismic design motion is targeted. Typical example is the increase of the design Peak Ground Acceleration (PGA) value in Greece since 1956 and the even further increase recently proposed in SHARE (Giardini et al. 2013).

Data are used to propose models, for example Ground Motion Prediction Equations (GMPEs), or improve existing ones. There is a profound belief that more data lead to better models and deeper knowledge. This is not always true. The majority of recording stations worldwide are not located after proper selection of the site and in most cases the knowledge of the parameters affecting the recorded ground motion is poor and limited. Rather simple statistics and averaging, often of heterogeneous data, is usually the way to produce “a model” but not “the model”, which should describe the truth. A typical example is the research on the “sigma” on GMPEs. Important research efforts have been dedicated during the last two decades to improve “sigma” but in general it refuses to be improved, except for few cases of very well constrained conditions. Sometimes less data of excellent quality and well constrained in terms of all involved parameters, lead to better solutions and models. This is true in both engineering seismology and earthquake engineering. An abundant mass of poorly constrained and mindless produced data is actually a curse and probably it will strangle an honest and brave modeller. Unfortunately, this is often the case when one considers the whole chain from seismic hazard to risk assessment.

3.2.3 Modeller: Sisyphus or Prometheus

A successful parameterization requires understanding of the phenomena being parameterized, but such understanding is often lacking. For example, the influence of seismic rupture and wave propagation patterns in complex media are poorly known and poorly modelled.

When confronted with limited understanding of how the seismic pattern is, and engineering structures or human behaviours are, modellers seek to make their models comply with the expected earthquake generation, spatial distribution of ground motion and structural response. The adjustments may “save appearances” without integrating precise understanding of the causal relationships the models are intended to simulate.

Huge research in seismic risk consists of modifying a subset of variables in models developed elsewhere. This complicates clear-cut distinctions between users and producers of models. And even more important: there is no in depth criticism on the paradigm used (basic concepts). Practically no scientist single-handedly

develops a complex risk model from bottom-up. He is closer to Sisyphus while sometimes he believes to be Prometheus.

Modellers are sometimes identified with their own models and become invested in their projections, which in turn can reduce sensitivity to their inaccuracy. Users are perhaps in the best position to identify model inaccuracies.

Model producers are not always willing or they are not always able to recognize weaknesses in their own models, contrary to what it is suggested by the certainty trough. They spend a lot of time working on something, and they are really trying to do their best at simulating what happens in the real world. It is easy to get caught up in it and start to believe that what happens in the model must be what happens in the real world. And often that is not true. The danger is that the modeller begins to lose some objectivity on the response of the model and starts to believe that the model really works like the real world and then he begins to take too seriously its response to a change in forcing.

Modellers often “trust” their models and sometimes they have some degree of “genuine confidence, maybe over-confidence” in their quantitative projections. It is not simply a “calculating seduction” but a “sincere act of faith”!

3.2.4 Models: Truth or Heuristic Machines

Models should be perceived as “heuristic” and not as “truth machines”. Unfortunately, very often modellers – keen to preserve the authority of their models – deliberately present and encourage interpretations of models as “truth machines” when speaking to external audiences and end users. They “oversell” their products because of potential funding considerations. Highest level of objectivity about a given technology should be found among those who produced it, and this is not always achieved.

3.3 Risk, Uncertainties and Decision-Making

Risk is uncertain by definition. The distinction between uncertainty and risk remains of fundamental importance today. The scientific and engineering communities do not unanimously accept the origins of the concept of uncertainty in risk studies. However, it is permanently criticized and subsequently it evolved into dominant models of decision making upon which the dominant risk-based theories of seismic risk assessment and policy-making were subsequently built.

The challenge is really important. Everything in our real world is formed and is working with risk and uncertainty. Multiple conventions deserve great attention as we seek to understand the preferences and strategies of economic and political actors. Within this chaotic and complicate world, risk assessment and policy-making is a real challenge.

Usually uncertainties (or variability) are classified in two categories: aleatory variability and epistemic uncertainty. *Aleatory variability* is the natural-intrinsic randomness in a phenomenon and a process. It is a result of our simplified modelling of a complex process parameterized by probability density functions. *Epistemic uncertainty* is considered as the scientific uncertainty in the simplified model of the process and is characterized by alternative models. Usually it is related to the lack of knowledge or the necessity to use simplified models to simulate the nature or the elements at risk.

Uncertainty is also related to the perception of the model developer or the user. Often these two distinctive terms of uncertainties are familiar to the model developers but not to the users for whom there is only one uncertainty seen in a scale “low” to “high”. A model developer probably believes that the two terms provide an unambiguous terminology. However this is not the case for the community of users. In most cases they cannot even understand it. So, they are often forced to “believe” the scientists, who have or should have the “authority” of the “truth”. At least the modellers should know better the limits of their model and the uncertainties involved and communicate them to the end-users.

A common practice to anticipate the epistemic uncertainty is through the use of the “logic tree” approach. Using this approach to overcome the lack of knowledge and the imperfection of the modelling is strongly based on subjectivity, regarding the credibility of each model, which is not a rigorous scientific method. It may be seen as a compromising method to smooth “fighting” among models and modellers. Moreover, a typical error is to put aleatory variability on some of the branches of the logic tree. The logic tree branches should be mainly relevant to the source characterization, the GMPE used and furthermore to the fragility curves used for the different structural typologies.

An important problem is then raised up. Is using many alternative models for each specific site and project a wrong or a wise approach? The question in its simplicity seems stupid and the answer obvious, but this is not true because more data usually lead to larger uncertainties.

For example, in a poorly known fault with few data and only one hazard study, there will be a single model and consequently 100 % credibility. In a very well known and studied fault, with many data, there will be probably several good or “acceptable” models and the user should be forced to attribute much lower credibility to each one of them, which leads to the absurd situation for the poorly known fault to have lower uncertainty than well known faults!

Over time additional hazard models are developed, but our estimates of the epistemic uncertainty have increased, not decreased, as additional data have been collected and new models have been developed!

Fragility curves on the other hand are based on simplified models (usually equivalent SDOF systems), which are an oversimplification of the real world and it is not known whether this oversimplification is on the conservative side. In any case, the scatter among different models is so high (Pitilakis et al. 2014a) that a logic tree approach should be recommended to treat the epistemic uncertainties related to the selection of the fragility curves. No such approach has been used so

far. Moreover these curves, normally produced for simplified structures, are used to estimate physical damages and implicitly the associated losses for a whole city with a very heterogeneous fabric and typology of buildings. Then aleatory and epistemic uncertainties are merged.

At the end of the game there is always a pending question: How can we really differentiate the two sources of uncertainty?

Realizing the importance of all different sources of uncertainties characterizing each step of the long process from seismic hazard to risk assessment, including all possible consequences and impact, beyond physical damages, it is understood how difficult it is to derive a reliable global model covering the whole chain from hazard to risk. For the moment, scientists, engineers and policy makers are fighting with rather simple weapons, using simple paradigms. It is time to re-think the whole process merging their capacities and talents.

3.4 Taxonomy of Elements at Risk

The key assumption in the vulnerability assessment of buildings, infrastructures and lifelines is that structures and components of systems, having similar structural characteristics, and being in similar geotechnical conditions (e.g., a bridge of a given typology), are expected to perform in the same way for a given seismic excitation. Within this context, damage is directly related to the structural properties of the elements at risk. The hazard should be also related to the structure under study. Taxonomy and typology are thus fundamental descriptors of a system that are derived from the inventory of each element and system. Geometry, material properties, morphological features, age, seismic design level, anchorage of the equipment, soil conditions, and foundation details are among usual typology descriptors/parameters. Reinforced concrete (RC) buildings, masonry buildings, monuments, bridges, pipelines (gas, fuel, water, waste water), tunnels, road embankments, harbour facilities, road and railway networks, have their own specific set of typologies and different taxonomy.

The elements at risk are commonly categorized as populations, communities, built environment, natural environment, economic activities and services, which are under the threat of disaster in a given area (Alexander 2000). The main elements at risk, the damages of which affect the losses of all other elements, are the multiple components of the built environment with all kinds of structures and infrastructures. They are classified into four main categories: buildings, utility networks, transportation infrastructures and critical facilities. In each category, there are (or should be) several sets of fragility curves, that have been developed considering the taxonomy of each element and their typological characteristics. In that sense there are numerous typologies for reinforced concrete or masonry buildings, numerous typologies for bridges and numerous typologies for all other elements at risk of all systems exposed to seismic hazard.

The knowledge of the inventory of a specific structure in a region and the capability to create classes of structural types (for example with respect to material, geometry, design code level) are among the main challenges when carrying out a general seismic risk assessment for example at a city scale, where it is practically impossible to perform this assessment at building level. It is absolutely necessary to classify buildings, and other elements at risk, in “as much as possible” homogenous classes presenting more-or-less similar response characteristics to ground shaking. Thus, the derivation of appropriate fragility curves for any type of structure depends entirely on the creation of a reasonable taxonomy that is able to classify the different kinds of structures and infrastructures in any system exposed to seismic hazard.

The development of a homogenous taxonomy for all engineering elements at risk exposed to seismic hazard and the recommendation of adequate fragility functions for each one, considering also the European context, achieved in SYNER-G project (Pitilakis et al. 2014a), is a significant contribution to the reduction of seismic risk in Europe and worldwide.

3.5 Intensity Measures

A main issue related to the construction and use of fragility curves is the selection of appropriate earthquake Intensity Measures (IM) that characterize the strong ground motion and best correlate with the response of each element at risk, for example, building, pier bridge or pipeline. Several intensity measures of ground motion have been proposed, each one describing different characteristics of the motion, some of which may be more adverse for the structure or system under consideration. The use of a particular IM in seismic risk analysis should be guided by the extent to which the measure corresponds to damage to the components of a system or the system of systems. Optimum intensity measures are defined in terms of practicality, effectiveness, efficiency, sufficiency, robustness and computability (Cornell et al. 2002; Mackie and Stojadinovic 2003, 2005).

Practicality refers to the recognition that the IM has some direct correlation to known engineering quantities and that it “makes engineering sense” (Mackie and Stojadinovic 2005; Mehanny 2009). The practicality of an IM may be verified analytically via quantification of the dependence of the structural response on the physical properties of the IM such as energy, response of fundamental and higher modes, etc. It may also be verified numerically by the interpretation of the structure’s response under non-linear analysis using existing time histories.

Sufficiency describes the extent to which the IM is statistically independent of ground motion characteristics such as magnitude and distance (Padgett et al. 2008). A sufficient IM is the one that renders the structural demand measure conditionally independent of the earthquake scenario. This term is more complex and is often at odds with the need for computability of the IM. Sufficiency may be quantified via statistical analysis of the response of a structure for a given set of records.

The *effectiveness* of an IM is determined by its ability to evaluate its relation with an engineering demand parameter (EDP) in closed form (Mackie and Stojadinovic 2003), so that the mean annual frequency of a given decision variable exceeding a given limiting value (Mehanny 2009) can be determined analytically.

The most widely used quantitative measure from which an optimal IM can be obtained is *efficiency*. This refers to the total variability of an engineering demand parameter (EDP) for a given IM (Mackie and Stojadinovic 2003, 2005).

Robustness describes the efficiency trends of an IM-EDP pair across different structures, and therefore different fundamental period ranges (Mackie and Stojadinovic 2005; Mehanny 2009).

In general and in practice, IMs are grouped in two general classes: empirical intensity measures and instrumental intensity measures. With regards to the empirical IMs, different macroseismic intensity scales could be used to identify the observed effects of ground shaking over a limited area. In the instrumental IMs, which are by far more accurate and representative of the seismic intensity characteristics, the severity of ground shaking can be expressed as an analytical value measured by an instrument or computed by analysis of recorded accelerograms.

The selection of the intensity parameter is also related to the approach that is followed for the derivation of fragility curves and the typology of element at risk. The identification of the proper IM is determined from different constraints, which are first of all related to the adopted hazard model, but also to the element at risk under consideration and the availability of data and fragility functions for all different exposed assets.

Empirical fragility functions are usually expressed in terms of the macroseismic intensity defined according to different scales, namely EMS, MCS and MM. Analytical or hybrid fragility functions are, on the contrary, related to instrumental IMs, which are related to parameters of the ground motion (PGA, PGV, PGD) or of the structural response of an elastic SDOF system (spectral acceleration S_a or spectral displacement S_d for a given value of the period of vibration T). Sometimes integral IMs, which consider a specific integration of a motion parameter can be useful, for example Arias Intensity I_A or a spectral value like the Housner Intensity I_H . When the vulnerability of elements due to ground failure is examined (i.e., liquefaction, fault rupture, landslides) permanent ground deformation (PGD) is the most appropriate IM.

The selection of the most adequate and realistic IMs for every asset under consideration is still debated and a source of major uncertainties.

3.6 Fragility Curves and Vulnerability

The vulnerability of a structure is described in all engineering-relevant approaches using vulnerability and/or fragility functions. There are a number of definitions of vulnerability and fragility functions; one of these describes vulnerability functions as the probability of losses (such as social or economic losses) given a level of

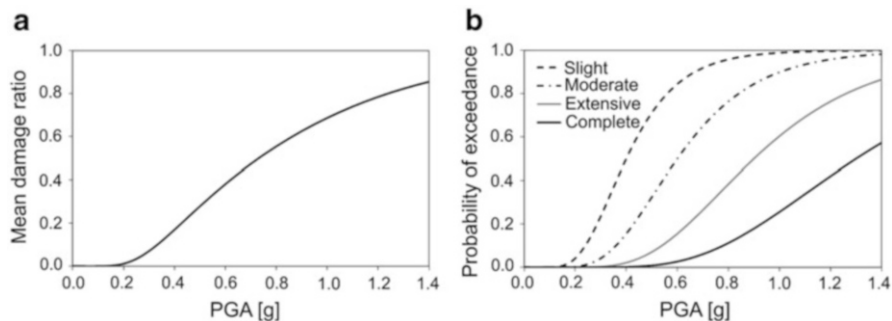


Fig. 3.2 Examples of (a) vulnerability function and (b) fragility function

ground shaking, whereas fragility functions provide the probability of exceeding different limit states (such as physical damage or injury levels) given a level of ground shaking. Figure 3.2 shows examples of vulnerability and fragility functions. The former relates the level of ground shaking with the mean damage ratio (e.g., ratio of cost of repair to cost of replacement) and the latter relates the level of ground motion with the probability of exceeding the limit states. Vulnerability functions can be derived from fragility functions using consequence functions, which describe the probability of loss, conditional on the damage state.

Fragility curves constitute one of the key elements of seismic risk assessment and at the same time an important source of uncertainties. They relate the seismic intensity to the probability of reaching or exceeding a level of damage (e.g., minor, moderate, extensive, collapse) for the elements at risk. The level of shaking can be quantified using different earthquake intensity parameters, including peak ground acceleration/velocity/displacement, spectral acceleration, spectral velocity or spectral displacement. They are often described by a lognormal probability distribution function as in Eq. 3.1 although it is noted that this distribution may not always be the best fit.

$$P_f(ds \geq ds_i | IM) = \Phi \left[\frac{1}{\beta_{tot}} \cdot \ln \left(\frac{IM}{IM_{mi}} \right) \right] \quad (3.1)$$

where $P_f(\cdot)$ denotes the probability of being at or exceeding a particular damage state, ds_i , for a given seismic intensity level defined by the earthquake intensity measure, IM (e.g., peak ground acceleration, PGA), Φ is the standard cumulative probability function, IM_{mi} is the median threshold value of the earthquake intensity measure IM required to cause the i_{th} damage state and β_{tot} is the total standard deviation. Therefore, the development of fragility curves according to Eq. 3.1 requires the definition of two parameters, IM_{mi} and β_{tot} .

There are several methods available in the literature to derive fragility functions for different elements exposed to seismic hazard and in particular to transient ground motion and permanent ground deformations due to ground failure. Conventionally, these methods are classified into four categories: *empirical*, *expert*

elicitation, analytical and hybrid. All these approaches have their strengths and weaknesses. However, analytical methods, when properly validated with large-scale experimental data and observations from recent strong earthquakes, have become more popular in recent years. The main reason is the considerable improvement of computational tools, methods and skills, which allows comprehensive parametric studies covering many possible typologies to be undertaken. Another equally important reason is the better control of several of the associated uncertainties.

The two most popular methods to derive fragility (or vulnerability) curves for buildings and pier bridges are the capacity spectrum method (CSM) (ATC-40 and FEMA273/356) with its alternatives (e.g., Fajfar 1999), and the incremental dynamic analysis (IDA) (Vamvatsikos and Cornell 2002). Both have contributed significantly and marked the substantial progress observed the last two decades; however they are still simplifications of the physical problem and present several limitations and weaknesses. The former (CSM) is approximate in nature and is based on static loading, which ignores the higher modes of vibration and the frequency content of the ground motion. A thorough discussion on the pushover approach may be found in Krawinkler and Miranda (2004).

The latter (IDA) is now gaining in popularity because among other advantages it offers the possibility to select the most relevant to the structural response Engineering Demand Parameters (EDP) (inter-story drifts, component inelastic deformations, floor accelerations, hysteretic energy dissipation etc.). IDA is commonly used in probabilistic seismic assessment frameworks to produce estimates of the dynamic collapse capacity of global structural systems. With the IDA procedure the coupled soil-foundation-structure system is subjected to a suite of multiply scaled real ground motion records whose intensities are “ideally?” selected to cover the whole range from elasticity to global dynamic instability. The result is a set of curves (IDA curves) that show the EDP plotted against the IM used to control the increment of the ground motion amplitudes. Fragility curves for different damage states can be estimated through statistical analysis of the IDA results (pairs of EDP and IM) derived for a sufficiently large number of ground motions (normally 15–30). Among the weaknesses of the approach is the fact that scaling of the real records changes the amplitude of the IMs but keeps the frequency content the same throughout the inelastic IDA procedure. In summary both approaches introduce several important uncertainties, both aleatory and epistemic.

Among the most important latest developments in the field of fragility curves is the recent publication “SYNER-G: Typology Definition and Fragility Functions for Physical Elements at Seismic Risk”, Pitilakis K, Crowley H, Kaynia A (Eds) (2014a).

Several uncertainties are introduced in the process of constructing a set of fragility curves of a specific element at risk. They are associated to the parameters describing the fragility curves, the methodology applied, as well as to the selected damage states and the performance indicators (PI) of the element at risk. The uncertainties may again be categorized as aleatory and epistemic. However, in

this case epistemic uncertainties are probably more pronounced, especially when analytical methods are used to derive the fragility curves.

In general, the uncertainty of the fragility parameters is estimated through the standard deviation, β_{tot} that describes the total variability associated with each fragility curve. Three primary sources of uncertainty are usually considered, namely the definition of damage states, β_{DS} , the response and resistance (capacity) of the element, β_{C} , and the earthquake input motion (demand), β_{D} . Damage state definition uncertainties are due to the fact that the thresholds of the damage indexes or parameters used to define damage states are not known. Capacity uncertainty reflects the variability of the properties of the structure as well as the fact that the modelling procedures are not perfect. Demand uncertainty reflects the fact that IM is not exactly sufficient, so different records of ground motion with equal IM may have different effects on the same structure (Selva et al. 2013). The total variability is modelled by the combination of the three contributors assuming that they are stochastically independent and log-normally distributed random variables, which is not always true.

Paolo Emilio Pinto (2014) in Ptilakis et al. (2014a) provides the general framework of the treatment of uncertainties in the derivation of the fragility functions. Further discussion on this issue is made in the last section of this paper.

3.7 Risk Assessment

3.7.1 *Probabilistic, Deterministic and the Quest of Reasonable*

In principle, the problem of seismic risk assessment and safety is probabilistic and several sources of uncertainties are involved. However, a full probabilistic approach is not applied throughout the whole process. For the seismic hazard the approach is usually probabilistic, at least partially. Deterministic approach, which is more appreciated by engineers, is also used. Structures are traditionally analyzed in a deterministic way with input motions estimated probabilistically. PSHA ground motion characteristics, determined for a selected return period (e.g., 500 or 1,000 years), are traditionally used as input for the deterministic analysis of a structure (e.g., seismic codes). On the other hand, fragility curves by definition represent the conditional probability of the failure of a structure or equipment at a given level of ground motion intensity measure, while seismic capacity of structures and components is usually estimated deterministically. Finally, damages and losses are estimated in a probabilistic way, mainly, if not exclusively, because of PSHA and fragility curves used. So in the whole process of risk assessment, probabilistic and deterministic approaches are used indifferently without knowing exactly what the impact of that is and how the involved uncertainties are treated and propagated.

In the hazard assessment the main debate is whether deterministic or probabilistic approach is more adequate and provides more reasonable results for engineering applications and in particular for the evaluation of the design ground motion. In the deterministic hazard approach, individual earthquake scenarios (i.e., M_w and location) are developed for each relevant seismic source and a specified ground motion probability level is selected (by tradition, it is usually either 0 or 1 standard deviation above the median). Given the magnitude, distance, and number of standard deviations, the ground motion is then computed for each earthquake scenario using one or several ground motion models (GMPEs) that are based on empirical data (records). Finally, the largest ground motion from any of the considered scenarios is used for the design.

Actually with this approach single values of the parameters (M_w , R , and ground motion parameters with a number of standard deviations) are estimated for each selected scenario. However, the final result regarding the ground shaking is probabilistic in the sense that the ground motion has a probability being exceeded given that the scenario earthquake occurred.

In the probabilistic approach all possible and relevant deterministic earthquake scenarios (e.g., all possible M_w and location combinations of physically possible earthquakes) are considered, as well as all possible ground motion probability levels with a range of the number of standard deviations above or below the median. The scenarios from the deterministic analyses are all included in the full set of scenarios from the probabilistic analysis. For each earthquake scenario, the ground motions are computed for each possible value of the number of standard deviations above or below the median ground motion. So the probabilistic analysis can be considered as a large number of deterministic analyses and the chance of failure is addressed by estimating the probability of exceeding the design ground motion.

The point where the two approaches are coinciding is practically the choice of the standard deviations. The deterministic approach traditionally uses at most one standard deviation above the median for the ground motion, but in the probabilistic approach, larger values of the number of standard deviations above the median ground motion are considered. As a result, the worst-case ground motions will be much larger than the 84th percentile deterministic ground motions.

Considering that in both deterministic and probabilistic approaches the design ground motions, (and in particular the largest ones), are controlled by the number of the standard deviations above the median, which usually are different in the two approaches, how can the design motion or the worst case scenario be estimated in a rigorous way?

If now we enter in the game the selection of standard deviations in all other stages of the risk assessment process, namely in the estimation of site effects, the ground motion variability, the fragility and capacity curves, without mentioning the necessary hypothesis regarding the intensity measures, performance indicators and damage states to be used, it is realized that the final result is highly uncertain.

At the end of the game the quest of soundness is still illusionary and what is reasonable is based on past experience and economic constraints considering engineering judgment and political decision. In other words we come back to the

modeler's "authority" and the loneliness and sometime desolation of the end-user in the decision making procedure.

3.7.2 *Spatial Correlation*

Ground motion variability and spatial correlation could be attributed to several reasons, i.e., fault rupture mechanism, complex geological features, local site conditions, azimuth and directivity effects, basin and topographic effects and induced phenomena like liquefaction and landslides. In practice most of these reasons are often poorly known and poorly modelled, introducing important uncertainties. The occurrence of earthquake scenarios (magnitude and location) and the occurrence of earthquake shaking at a site are related but they are not the same. Whether probabilistic or deterministic scenario is used, the ground motion at a site should be estimated considering the variability of ground motion. However in practice, and in particular in PSHA, this is not treated in a rigorous way, which leads to a systematic underestimation of the hazard (Bommer and Abrahamson 2006). PSHA should always consider ground motion variability otherwise in most cases it is incorrect (Abrahamson 2006).

With the present level of know-how for a single earthquake scenario representing the source and the magnitude of a single event, the estimation of the spatial variation of ground motion field is probably easier and in any case better controlled. In a PSHA, which considers many sources and magnitude scenarios to effectively sample the variability of seismogenic sources, the presently available models to account for spatial variability are more complicated and often lead to an underestimation of the ground motion at a given site, simply because all possible sources and magnitudes are considered in the analysis.

In conclusion it should not be forgotten that seismic hazard is not a tool to estimate a magnitude and a location but to evaluate the design motion for a specific structure at a given site. To achieve this goal more research efforts should be focused on better modelling of the spatial variability of ground motion considering all possible sources for that, knowing that there are a lot of uncertainties hidden in this game.

3.7.3 *Site Effects*

The important role of site effects in seismic hazard and risk assessment is now well accepted. Their modelling has been also improved in the last two decades.

In Eurocode 8 (CEN 2004) the influence of local site conditions is reflected with the shape of the PGA-normalized response spectra and the so-called "soil factor" S , which represents ground motion amplification with respect to outcrop conditions. As far as soil categorization is concerned, the main parameter used is $V_{s,30}$, i.e., the

Table 3.1 Improved soil factors for EC8 soil classes (Pitilakis et al. 2012)

Soil class	Type 2 ($M_s \leq 5.5$)		Type 1 ($M_s > 5.5$)	
	Improved	EC8	Improved	EC8
B	1.40	1.35	1.30	1.20
C	2.10	1.50	1.70	1.15
D	1.80 ^a	1.80	1.35 ^a	1.35
E	1.60 ^a	1.60	1.40 ^a	1.40

^aSite specific ground response analysis required

time-based average value of shear wave velocity in the upper 30 m of the soil profile, first proposed by Borchardt and Glassmoyer (1992). $V_{s,30}$ has the advantage that it can be obtained easily and at relatively low cost, since the depth of 30 m is a typical depth of geotechnical investigations and sampling borings, and has definitely provided engineers with a quantitative parameter for site classification. The main and important weakness is that the single knowledge of the V_s profile at the upper 30 m cannot quantify properly the effects of the real impedance contrast, which is one of the main sources of the soil amplification, as for example in case of shallow (i.e., 15–20 m) loose soils on rock or deep soil profiles with variable stiffness and contrast. Quantifying site effects with the simple use of $V_{s,30}$ introduces important uncertainties in the estimated IM.

Pitilakis et al. (2012) used an extended strong motion database compiled in the framework of SHARE project (Giardini et al. 2013) to validate the spectral shapes proposed in EC8 and to estimate improved soil amplification factors for the existent soil classes of Eurocode 8 for a potential use in an EC8 update (Table 3.1). The soil factors were estimated using a logic tree approach to account for the epistemic uncertainties. The major differences in S factor values were found for soil category C. For soil classes D and E, due to the insufficient datasets, the S factors of EC8 remain unchanged with a prompt for site-specific ground response analyses.

In order to further improve design spectra and soil factors Pitilakis et al. (2013) proposed a new soil classification system that includes soil type, stratigraphy, thickness, stiffness and fundamental period of soil deposit (T_0) and average shear wave velocity of the entire soil deposit ($V_{s,av}$). They compiled an important subset of the SHARE database, containing records from sites, which dispose a well-documented soil profile concerning dynamic properties and depth up to the “seismic” bedrock ($V_s > 800$ m/s). The soil classes of the new classification scheme are illustrated in comparison to EC8 soil classes in Fig. 3.3.

The proposed normalized acceleration response spectra were evaluated by fitting the general spectral equations of EC8 closer to the 84th percentile, in order to account as much as possible for the uncertainties associated with the nature of the problem. Figure 3.4 is a representative plot, illustrating the median, 16th and 84th percentiles, and the proposed design normalized acceleration spectra for soil sub-class C1. It is obvious that the selection of a different percentile would affect dramatically the proposed spectra and consequently the

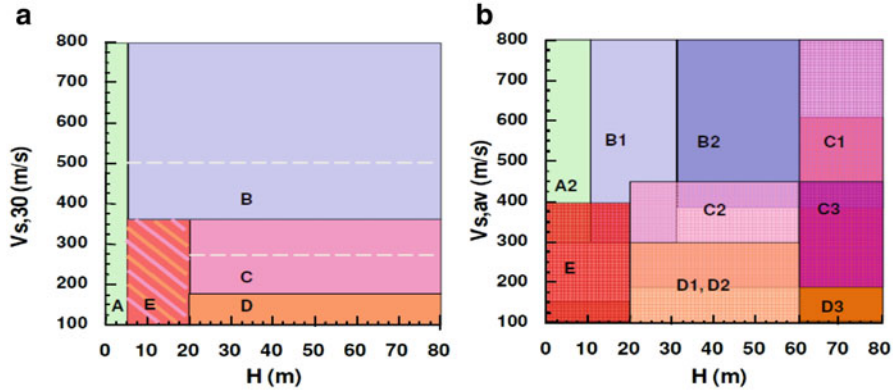


Fig. 3.3 Simplified illustration of ground types according to (a) EC8 and (b) the new classification scheme of Pitalakis et al. (2013)

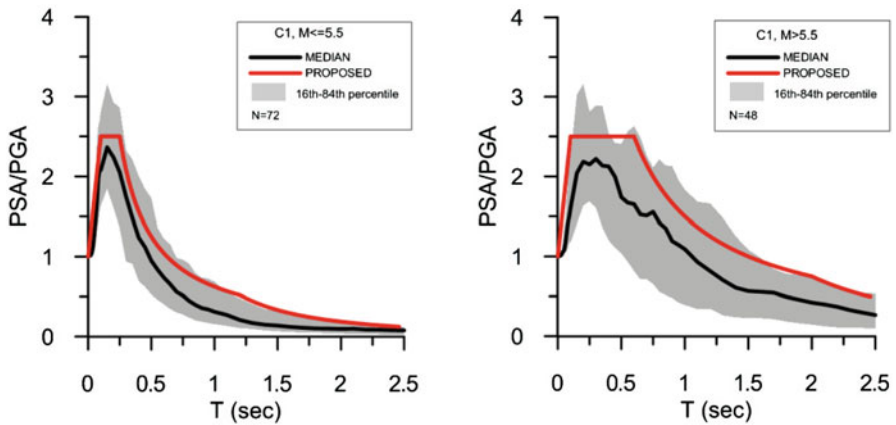


Fig. 3.4 Normalized elastic acceleration response spectra for soil class C1 of the classification system of Pitalakis et al. (2013) for Type 2 seismicity (left) and Type 1 seismicity (right). Red lines represent the proposed spectra. The range of the 16th to 84th percentile is illustrated as a gray area

demand spectra, the performance points and the damages. While there is no rigorous argument why the median should be chosen, 84th percentile or close to this sounds more reasonable.

The proposed new elastic acceleration response spectra, normalized to the design ground acceleration at rock-site conditions PGA_{rock} , are illustrated in Fig. 3.5. Dividing the elastic response spectrum of each soil class with the corresponding response spectrum for rock, period-dependent amplification factors can be estimated.

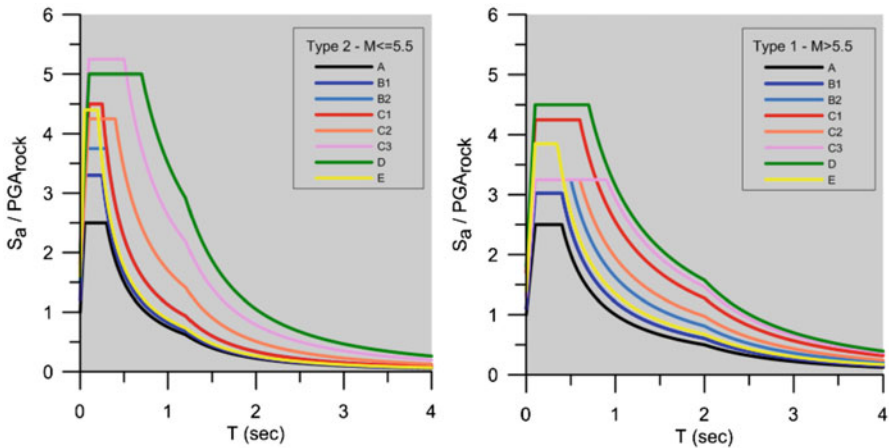


Fig. 3.5 Type 2 (*left*) and Type 1 (*right*) elastic acceleration response spectra for the classification system of Pitilakis et al. (2013)

3.7.4 Time Dependent Risk Assessment

Nature and earthquakes are unpredictable both in short and long term especially in case of extreme or “rare” events. Traditionally seismic hazard is estimated as time independent, which is probably not true. We all know that after a strong earthquake it is rather unlikely that another strong earthquake will happen in short time on the same fault. Exceptions like the sequence of Christchurch earthquakes in New Zealand or more recently in Cephalonia Island in Greece are rather exceptions that prove the general rule, if there is any.

Exposure is certainly varying with time, normally increasing. The vulnerability is also varying with time, increasing or decreasing (for example after mitigation countermeasures or post earthquake retrofitting have been undertaken). On the other hand aging effects and material degradation with time increase the vulnerability (Pitilakis et al. 2014b). Consequently the risk cannot be time independent. Figure 3.6 sketches the whole process.

For the time being time dependent seismic hazard and risk assessment are in a very premature stage. However, even if in the near future rigorous models should be developed, the question still remains: is it realistic to imagine that time dependent hazard could be ever introduced in engineering practice and seismic codes? If it ever happens, it will have a profound political, societal and economic impact.

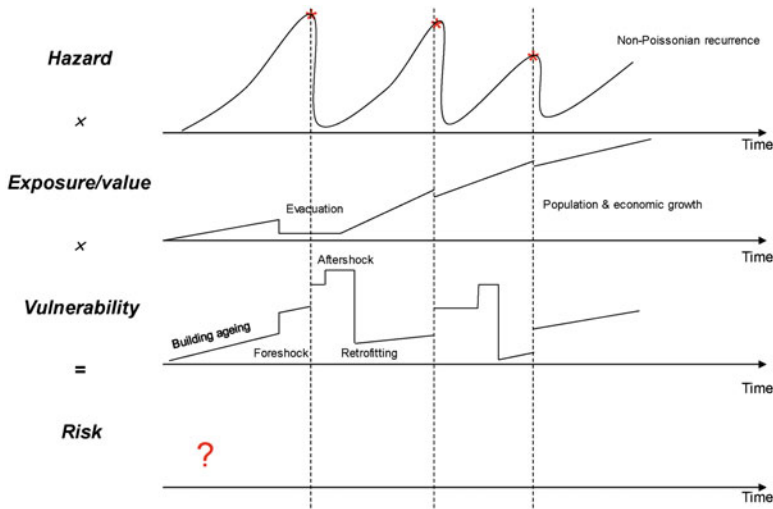


Fig. 3.6 Schematic illustration of time dependent seismic hazard, exposure, vulnerability and risk (After J. Douglas et al. in REAKT)

3.7.5 Performance Indicators and Resilience

In seismic risk assessment, the performance levels of a structure, for example a RC building belonging to a specific class, can be defined through damage thresholds called *limit states*. A limit state defines the boundary between two different damage conditions often referred to as *damage states*. Different damage criteria have been proposed depending on the typologies of elements at risk and the approach used for the derivation of fragility curves. The most common way to define earthquake consequences is a classification in terms of the following damage states: no damage; slight/minor; moderate; extensive; complete.

This qualitative approach requires an agreement on the meaning and the content of each damage state. The number of damage states is variable and is related to the functionality of the components and/or the repair duration and cost. In this way the total losses of the system (economic and functional) can be estimated.

Traditionally physical damages are related to the expected serviceability level of the component (i.e., fully or partially operational or inoperative) and the corresponding functionality (e.g., power availability for electric power substations, number of available traffic lanes for roads, flow or pressure level for water system). These correlations provide quantitative measures of the component’s performance, and can be applied for the definition of specific Performance Indicators (PIs). Therefore, the comparison of a demand with a capacity quantity, or the consequence of a mitigation action, or the accumulated consequences of all damages (the “impact”) can be evaluated. The restoration cost, when provided, is given as the percentage of the replacement cost. Downtime days to identify the elastic or the collapse limits are also purely qualitative and cannot be generalized for any

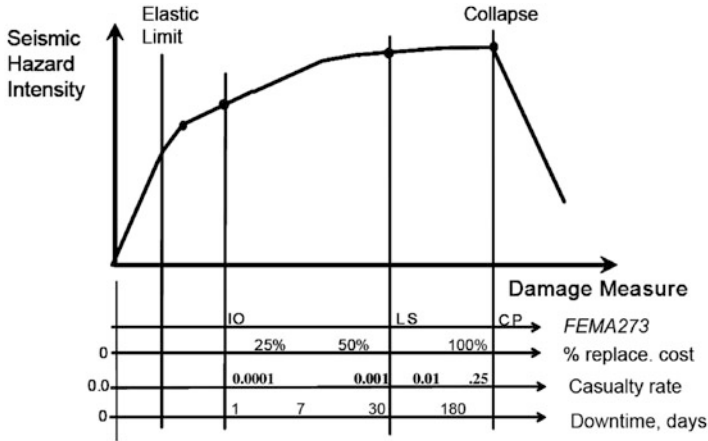


Fig. 3.7 Conceptual relationship between seismic hazard intensity and structural performance (From Krawinkler and Miranda (2004), courtesy W. Holmes, G. Deierlein)

structure type. These thresholds are qualitative and are given as general outline (Fig. 3.7). The user could modify them accordingly, considering the particular conditions of the structure, the network or component under study. The selection of any value of these thresholds inevitably introduces uncertainties, which are affecting the target performance and finally the estimation of damages and losses.

Methods for deriving fragility curves generally model the damage on a discrete damage scale. In empirical procedures, the scale is used in reconnaissance efforts to produce post-earthquake damage statistics and is rather subjective. In analytical procedures the scale is related to limit state mechanical properties that are described by appropriate indices, such as for example displacement capacity (e.g., inter-story drift) in the case of buildings or pier bridges. For other elements at risk the definition of the performance levels or limit states may be more vague and follow other criteria related, for example in the case of pipelines, to the limit strength characteristics of the material used in each typology.

The definition and consequently the selection of the damage thresholds, i.e., limit states, are among the main sources of uncertainties because they rely on rather subjective criteria. A considerable effort has been made in SYNER-G (Pitilakis et al. 2014a) to homogenize the criteria as much as possible.

Measuring seismic performance (risk) through economic losses and downtime (and business interruption), introduces the idea of measuring risk through a new more general concept: the resilience.

Resilience referring to a single element at risk or a system subjected to natural and/or manmade hazards usually goes towards its capability to recover its functionality after the occurrence of a disruptive event. It is affected by attributes of the system, namely robustness (for example residual functionality right after the disruptive event), rapidity (recovery rate), resourcefulness and redundancy (Fig. 3.8).

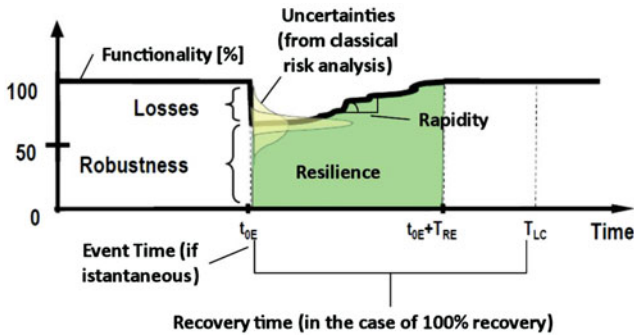


Fig. 3.8 Schematic representation of seismic resilience concept (Bruneau et al. 2003)

It is also obvious that resilience has very strong societal, economic and political components, which amplify the uncertainties.

Accepting the resilience to measure and quantify performance indicators and implicitly fragility and vulnerability, means that we introduce a new complicated world of uncertainties, in particular when from the resilience of a single asset e.g., a building, we integrate the risk in a whole city, with all its infrastructures, utility systems and economic activities.

3.7.6 Margin of Confidence or Conservatism?

The use of medians is traditionally considered as a reasonably conservative approach. Increased margin of confidence, i.e., 84th percentiles, is often viewed as over-conservatism. Conservatism and confidence are not actually reflecting the same thing in a probabilistic process. Figures 3.9 and 3.10 illustrate in a schematic example the estimated damages when using the median or median ± 1 standard deviation (depending on which one is the more “conservative” or reasonable) in all steps of the assessment process of damages, from the estimation of UHS for rock and the soil amplification factors to the capacity curve and the fragility curves. The substantial differences observed in the estimated damages cannot be attributed to an increased margin of confidence or conservatism. Considering all relevant uncertainties, all assumptions are equally possible or at least “reasonable”. Who can really define in a scientifically rigorous way the threshold between conservatism and reasonable? Confidence is a highly subjective term varying among different end-users and model producers.

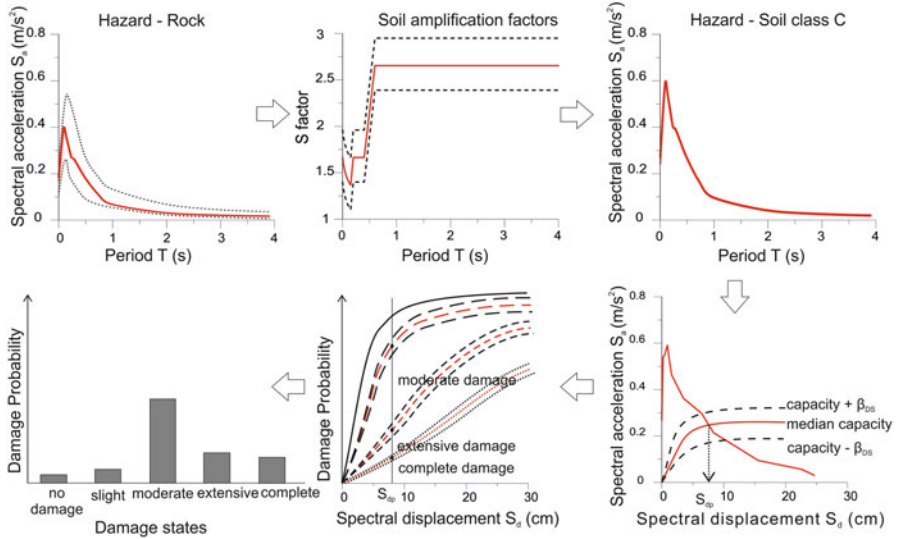


Fig. 3.9 Schematic example of estimated damages when using the median for UHS for rock, soil amplification factors, capacity curve and fragility curves

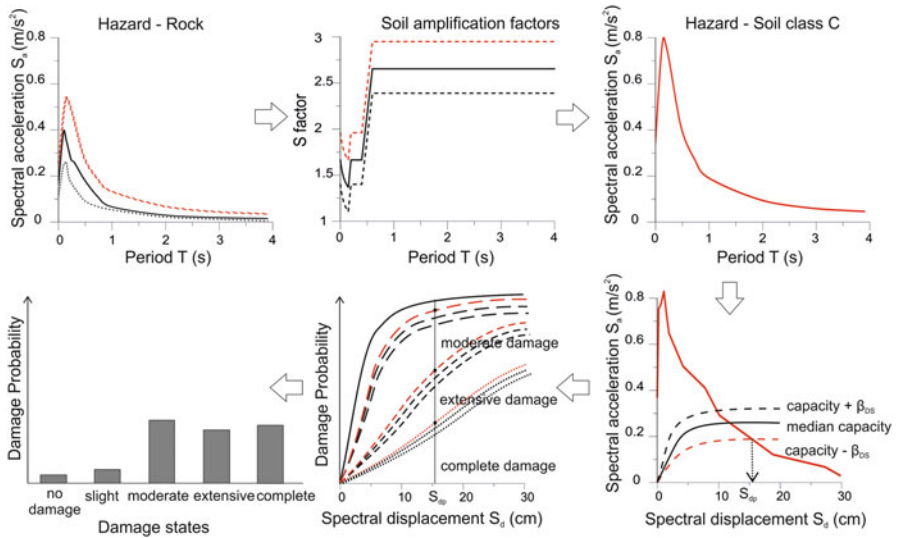


Fig. 3.10 Schematic example of estimated damages when using the median ± 1 standard deviation (depending on which one is the more “conservative” or reasonable) for UHS for rock, soil amplification factors, capacity curve and fragility curves

3.8 Damage Assessment: Subjectivity and Ineffectiveness in the Quest of the Reasonable

To further highlight the inevitable scatter in the current risk assessment of physical assets we use as example the seismic risk assessment and the damages of building stock in an urban area and in particular the city of Thessaloniki, Greece. Thessaloniki is the second largest city in Greece with about one million inhabitants. It has a long seismic history of devastating earthquakes, with the most recent one occurring in 1978 ($M_w = 6.5$, $R = 25$ km). Since then a lot of studies have been performed in the city to estimate the seismic hazard and to assess the seismic risk. Due to the very good knowledge of the different parameters, the city has been selected as pilot case study in several major research projects of the European Union ([SYNER-G](#), [SHARE](#), [RISK-UE](#), [LessLoss](#) etc.)

3.8.1 Background Information and Data

The study area considered in the present application (Fig. 3.11) covers the central municipality of Thessaloniki. With a total population of 380,000 inhabitants and about 28,000 buildings of different typologies (mainly reinforced concrete), it is divided in 20 sub-city districts (SCD) (<http://www.urbanaudit.org>). Soil conditions are very well known (e.g., Anastasiadis et al. 2001). Figures 3.12 and 3.13 illustrate the classification of the study area based on the classification schemes of EC8 and Pitilakis et al. (2013) respectively. The probabilistic seismic hazard (PSHA) is estimated applying SHARE methodology (Giardini et al. 2013), with its rigorous treatment of aleatory and epistemic uncertainties. The PSHA with a 10 % probability of exceedance in 50 years and the associated UHS have been estimated for outcrop conditions. The estimated rock UHS has been then properly modified to account for soil conditions applying adequate period-dependent amplification factors. Three different amplification factors have been used: the current EC8 factors (Hazard 1), the improved ones (Pitilakis et al. 2012) (Hazard 2) and the new ones based on a more detailed soil classification scheme (Pitilakis et al. 2013) (Hazard 3) (see Sect. 3.7.3). Figure 3.14 presents the computed UHS for soil type C (or C1 according to the new classification scheme). Vulnerability is expressed through appropriate fragility curves for each building typology (Pitilakis et al. 2014a). Damages and associated probability of a building of a specific typology to exceed a specific damage state have been calculated with the Capacity Spectrum Method (Freeman 1998; Fajfar and Gaspersic 1996).

The detailed building inventory for the city of Thessaloniki, which includes information about material, code level, number of storeys, structural type and volume for each building, allows a rigorous classification in different typologies according to SYNER-G classification and based on a Building Typologies Matrix representing practically all common RC building types in Greece (Kappos

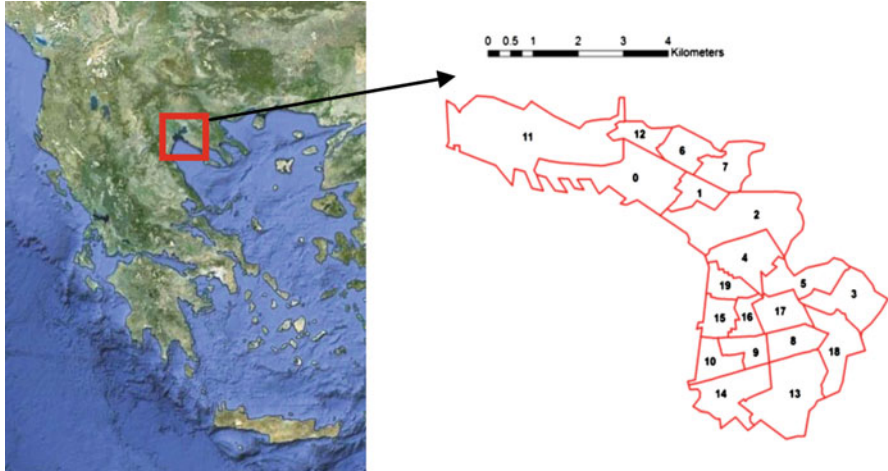
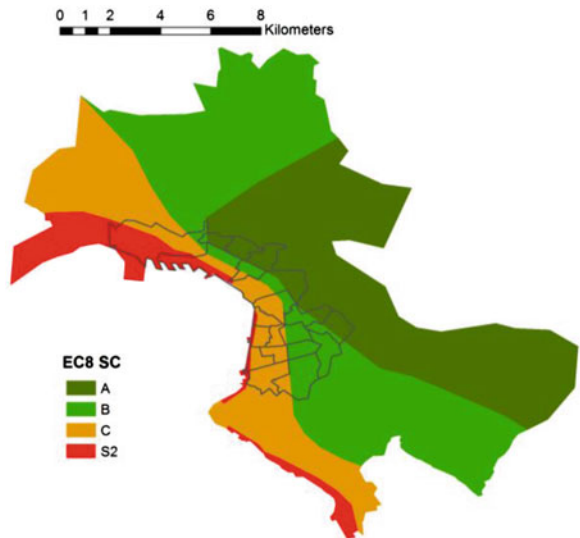


Fig. 3.11 Municipality of Thessaloniki. Study area; *red lines* illustrate Urban Audit Sub-City Districts (SCDs) boundaries

Fig. 3.12 Map of EC8 soil classes (based on $V_{s,30}$) for Thessaloniki



et al. 2006). The building inventory comprises 2,893 building blocks with 27,738 buildings, the majority of which (25,639) are reinforced concrete (RC) buildings. The buildings are classified based on their structural system, height and level of seismic design (Fig. 3.15). Regarding the structural system, both frames and frame-with-shear walls (dual) systems are included, with a further distinction based on the configuration of the infill walls. Regarding the height, three subclasses are considered (low-, medium- and high-rise). Finally, as far as the level of seismic design is concerned, four different levels are considered:

Fig. 3.13 Map of the soil classes according to the new soil classification scheme proposed by Pitilakis et al. (2013) for Thessaloniki

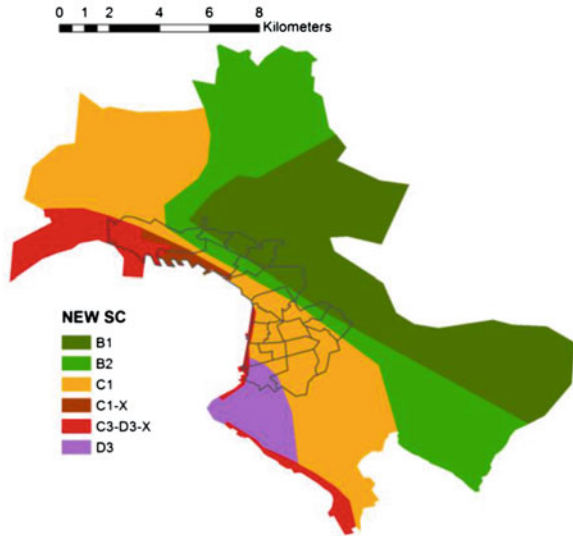
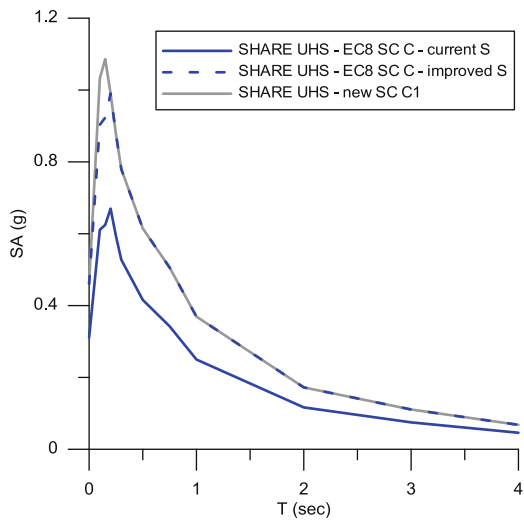


Fig. 3.14 SHARE rock UHS for Thessaloniki amplified with the current EC8 soil amplification factor for soil class C (CEN 2004), the improved EC8 soil amplification factor for soil class C (Pitilakis et al. 2012) and the soil amplification factors for soil class C1 of the classification system of Pitilakis et al. (2013). All spectra refer to a mean return period $T = 475$ years



- No code (or pre-code): R/C buildings with very low level of seismic design and poor quality of detailing of critical elements.
- Low code: R/C buildings with low level of seismic design.
- Medium code: R/C buildings with medium level of seismic design (roughly corresponding to post-1980 seismic code and reasonable seismic detailing of R/C members).

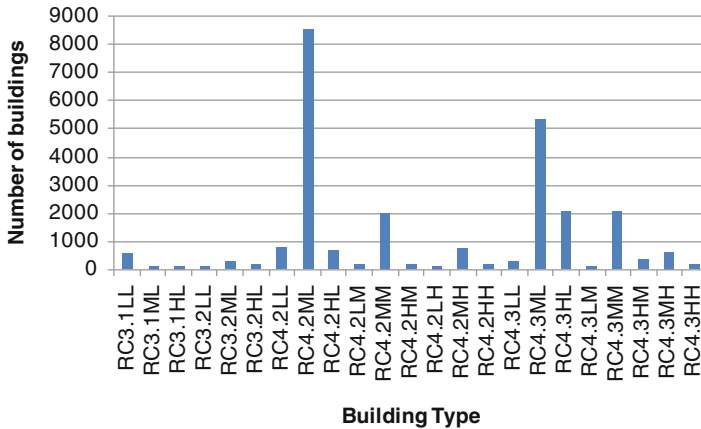


Fig. 3.15 Classification of the RC buildings of the study area (Kappos et al. 2006). The first letter of each building type refers to the height of the building (*L* low, *M* medium, *H* high), while the second letter refers to the seismic code level of the building (*N* no, *L* low, *M* medium, *H* high)

- High code: R/C buildings with enhanced level of seismic design and ductile seismic detailing of R/C members according to the new Greek Seismic Code (similar to Eurocode 8).

The fragility functions used (in terms of spectral displacement S_d) were derived through classical inelastic pushover analysis. Bilinear pushover curves were constructed for each building type, so that each curve is defined by its yield and ultimate capacity. Then they were transformed into capacity curves (expressing spectral acceleration versus spectral displacement). Fragility curves were finally derived from the corresponding capacity curves, by expressing the damage states in terms of displacements along the capacity curves (See Sect. 3.6 and in D’Ayala et al. 2012).

Each fragility curve is defined by a median value of spectral displacement and a standard deviation. Although the standard deviation of the curves is not constant, for the present application a standard deviation equal to 0.4 was assigned to all fragility curves, due to a limitation of the model used to perform the risk analyses. This hypothesis will be further discussed later in this section.

Five damage states were used in terms of S_d : DS1 (slight), DS2 (moderate), DS3 (substantial to heavy), DS4 (very heavy) and DS5 (collapse) (Table 3.2). According to this classification a spectral displacement of 2 cm or even lower can bring ordinary RC structures in the moderate (DS2) damage state, which is certainly a conservative assumption and in fact is penalizing, among other things, seismic risk assessment.

The physical damages of the buildings have been estimated using the open-source software Earthquake Risk Model (EQRM <http://sourceforge.net/projects/eqrm>, Robinson et al. 2005), developed by Geoscience Australia. The software is based on the HAZUS methodology (FEMA and NIBS 1999; FEMA 2003) and has

Table 3.2 Damage states and spectral displacement thresholds (D’Ayala et al. 2012)

Damage state	Bare frames	Infilled frames with $S_{du,bare} \geq 1.1S_{du}$	Bare dual	Infilled dual-infill walls failure
	Infilled frames with $S_{du,bare} < 1.1S_{du}$		Infilled dual – shear wall drop strength	
DS1	$0.7S_{dy}$		$0.7S_{dy}$	
DS2	$S_{dy} + 0.05 (S_{du} - S_{dy})$		$S_{dy} + 0.05 (S_{du} - S_{dy})$	
DS3	$S_{dy} + (1/3) (S_{du} - S_{dy})$	$S_{dy} + (1/2) (S_{du} - S_{dy})$	$S_{dy} + (1/2) (S_{du} - S_{dy})$	$0.9S_{du}$
DS4	$S_{dy} + (2/3) (S_{du} - S_{dy})$	S_{du}	S_{du}	$S_{du,bare}$
DS5	S_{du}	$S_{du,bare}$	$1.3S_{du}$	$1.3S_{du,bare}$

S_{dy} spectral displacement for yield capacity

S_{du} spectral displacement for ultimate capacity

been properly modified so that it can be used for any region of the world (Crowley et al. 2010). The method is based on the Capacity Spectrum Method. The so called “performance points”, after properly adjusted to account for the elastic and hysteretic damping of each structure, have been overlaid with the relevant fragility curves in order to compute the damage probability in each of the different damage states and for each building type.

The method relies on two main parameters: The demand spectra (properly modified to account for the inelastic behaviour of the structure), which are driven from the hazard analysis, and the capacity curve. The latter is not user-defined and it is automatically estimated by the code using the building parameters supplied by the user. The capacity curve is defined by two points: the yield point (S_{dy}, S_{ay}) and the ultimate point (S_{du}, S_{dy}) and is composed of three parts: a straight line to the yield point (representing elastic response of the building), a curved part from the yield point to the ultimate point expressed by an exponential function and a horizontal line starting from the ultimate point (Fig. 3.16). The yield point and ultimate point are defined in terms of the building parameters (Robinson et al. 2005) introducing inevitably several extra uncertainties, especially in case of existing buildings, designed and constructed several decades ago. In overall the following data are necessary to implement the Capacity Spectrum Method in EQRM: height of the building, natural elastic period, design strength coefficient, fraction of building weight participating in the first mode, fraction of the effective building height to building displacement, over-strength factors, ductility factor and damping degradation factors for each building or building class. All these introduce several uncertainties, which are difficult to be quantified in a rigorous way mainly because the uncertainties are mostly related to the difference between any real RC structure belonging in a certain typology and the idealized model.

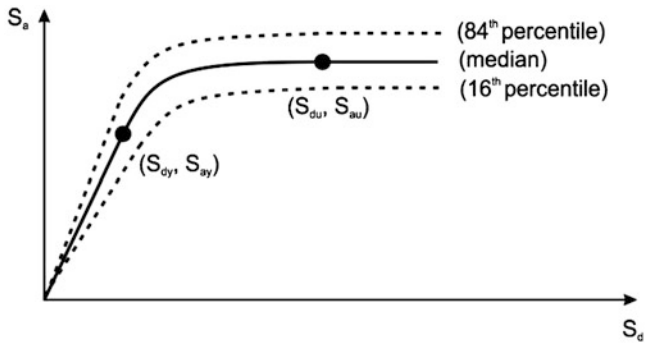


Fig. 3.16 Typical capacity curve in EQR software, defined by the yield point (S_{dy}, S_{ay}) and the ultimate point (S_{du}, S_{du}) (Modified after Robinson et al. (2005))

3.8.2 Physical Damages and Losses

For each building type in each building block, the probabilities for slight, moderate, extensive and complete damage were calculated. These probabilities were then multiplied with the total floor area of the buildings of the specific building block that are classified to the specific building type in order to estimate for this building type the floor area, which will suffer each damage state. Repeating this for all building blocks which belong to the same sub-city district (SCD) and for all building types, the total floor area of each building type that will suffer each damage state in the specific SCD can be calculated (Fig. 3.17). The total percentages of damaged floor area per damage state for all SCD and for the three hazard analyses illustrated in the previous figures are given in Table 3.3.

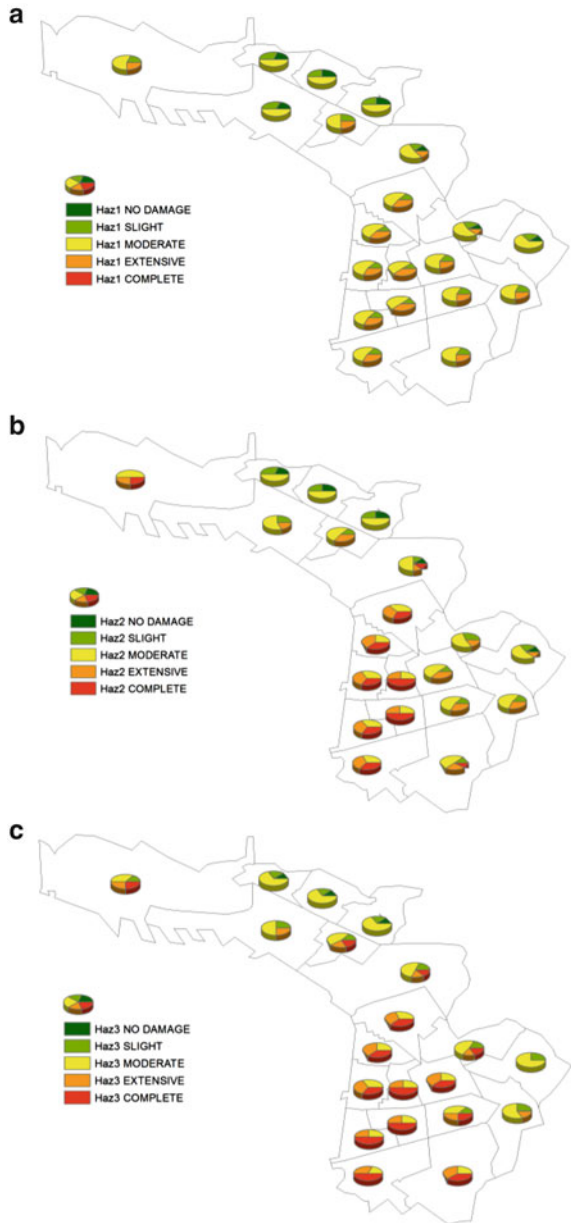
The economic losses were estimated through the mean damage ratio (MDR) (Table 3.4), multiplying then this value with an estimated replacement cost of 1,000 €/m² (Table 3.5).

3.8.3 Discussing the Differences

The observed differences in the damage assessment and losses are primarily attributed to the numerous uncertainties associated to the hazard models, to the way the uncertainties are treated and to the number of standard deviations accepted in each step of the analysis. Higher site amplification factors associated for example to median value plus one standard deviation, result in increasing building damages and consequently economic losses. The way inelastic demand spectra are estimated and the difference between computed UHS and a real earthquake records may also affect the final result (Fig. 3.18).

Despite the important influence of the hazard parameters, there are several other sources of uncertainties related mainly to the methods used. The effect of some of

Fig. 3.17 Thessaloniki. Seismic risk per Sub-City District for a mean return period of 475 years in terms of the percentage of damaged floor area per damage state for (a) Hazard 1, (b) Hazard 2 and (c) Hazard 3



the most influencing parameters involved in the methodological chain of risk assessment will be further discussed for the most common building type (RC4.2ML) located in SCD 16. In particular the effect of the following parameters will be discussed:

Table 3.3 Percentages of damaged floor area per damage state for hazard cases 1–3, for a mean return period of 475 years

	Hazard 1 (%)	Hazard 2 (%)	Hazard 3 (%)
No	7.4	6.4	4.3
Slight [D1]	17.6	12.9	11.1
Moderate [D2]	54.4	43.9	42.2
Extensive [D3]	18.9	22.4	20.3
Complete [D5]	1.7	14.4	22.1

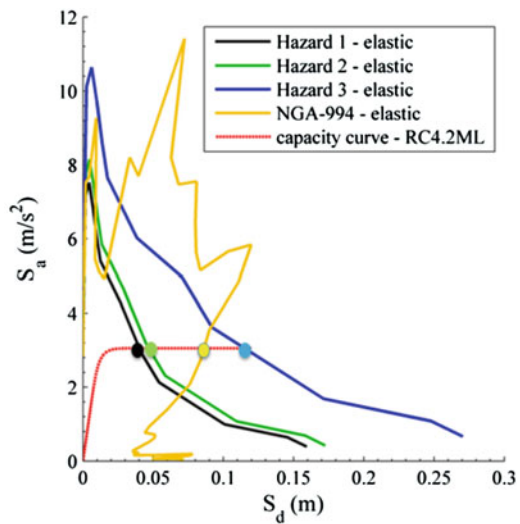
Table 3.4 Mean damage ratios for hazard cases 1–3, for a mean return period of 475 years

	Hazard 1 (%)	Hazard 2 (%)	Hazard 3 (%)
MDR	7.94	18.28	23.87

Table 3.5 Economic losses for hazard cases 1–3, for a mean return period of 475 years, assuming an average replacement cost equal to 1,000 €/m² (in billions €)

	Hazard 1	Hazard 2	Hazard 3
Economic losses	2.7	6.2	8.1

Fig. 3.18 Estimation of the performance points: demand spectra (elastic) for Hazard 1, Hazard 2 and Hazard 3, and for a real record (Northridge, 1994); mean capacity curve of the most frequent building classes (RC4.2ML) and resulted performance points



- Selection of the reduction factors for the inelastic demand spectra.
- Effect of the duration of shaking.
- Methodology for estimation of performance (EQRM versus N2).
- Uncertainties in the fragility curves.

Reduction factors of the inelastic demand spectra

One of the main debated issues of CSM is the estimation of the inelastic demand spectrum for the estimation of the final performance of the structure. When buildings are subjected to ground shaking they do not remain elastic and dissipate hysteretic energy. Hence, the elastic demand curve should be appropriately reduced in order to incorporate the inelastic energy dissipation. Reduction of spectral values to account for the hysteretic damping associated with the inelastic behaviour of structures may be carried out using different techniques like the ATC-40 methodology, or inelastic design spectra and equivalent elastic over-damped spectra.

In the present study the ATC-40 methodology (ATC 1996) has been used combined with HAZUS methodology (FEMA and NIBS 1999; FEMA 2003). More specifically, damping-based spectral reduction factors were used assuming different reduction factors associated to different periods of the ground motion. According to this pioneer method the effective structural damping is the sum of the elastic damping and the hysteretic one. The hysteretic damping B_h is a function of the yield and ultimate points of the capacity curve (Eq. 3.2).

$$B_h = 63.5 \cdot \kappa \cdot \left(\frac{A_{yi}}{A_u} - \frac{D_{yi}}{D_u} \right) \quad (3.2)$$

k is a degradation factor that defines the effective amount of hysteretic damping as a function of earthquake duration and energy-absorption capacity of the structure during cyclic earthquake load. This factor depends on the duration of the ground shaking while it is also a measure of the effectiveness of the hysteresis loops. When k factor is equal to unity, the hysteresis loops are full and stable. On the other hand when k factor is equal to 0.3 the hysteretic behaviour of the building is poor and the loop area is substantially reduced. It is evident that for a real structure the selection of the value of k is based on limited information, and hence practically introduces several uncontrollable uncertainties. In the present study a k factor equal to 0.333 is applied assuming moderate duration and poor hysteretic behaviour according to ATC-40 (ATC 1996).

Except from Newmark and Hall (1982) damping based spectral reduction factors, in the literature there are several other strength or spectral reduction factors one can use in order to estimate inelastic strength demands from elastic strength demands (Miranda and Bertero 1994). To illustrate the effect of the selection of different methods we compared the herein used inelastic displacement performance according to HAZUS (assuming k factor equal to 0.333 and 1), with other methods, namely those proposed by Newmark and Hall (1982) (as a function of ductility), Krawinkler and Nassar (1992), Vidic et al. (1994) and Miranda and Bertero (1994).

Applying the above methods for one building type (e.g., RC4.2ML) subjected to Hazard 3 (new soil classification and soil amplification factors according to Pitilakis et al. 2013), it is observed (Table 3.6) that the method used herein gives the highest displacements compared to all other methodologies (Fig. 3.19), a fact which further explains the over-predicted damages (Table 3.6).

Table 3.6 Inelastic displacement demand computed with different methods and total physical damages for SCD16 and Hazard 3, for a mean return period of 475 years in terms of the percentage of damage per damage state using various methodologies for the reduction of the elastic spectrum

	d _{pp} (cm)	DS1 (%)	DS2 (%)	DS3 (%)	DS4 (%)	DS5 (%)
ATC-40_Hazus, k = 0.33 (Hazus_k = 0.333)	8.0	0.00	0.00	0.94	35.99	63.08
ATC-40_Hazus, k = 1 (Hazus_k = 1)	4.2	0.00	0.04	22.85	66.98	10.13
Newmark and Hall (1982) (NH)	2.5	0.02	1.90	68.95	28.60	0.53
Krawinkler and Nassar (1992) (KN)	2.2	0.10	5.01	78.54	16.21	0.14
Vidic et al. (1994) (VD)	2.2	0.06	3.83	76.86	19.06	0.20
Miranda and Bertero (1994) (MB)	1.8	0.31	9.99	81.14	8.53	0.04

Duration of shaking

The effect of the duration of shaking is introduced through the k factor. It is supposed that the shorter the duration is, the higher the damping value should be. Applying this approach to the study case it is found that the effective damping for short earthquake duration is equal to 45 % while the effective damping for moderate earthquake duration is equal to 25 %. The differences are too high to underestimate the importance of the rigorous selection of this single parameter. Figure 3.20 presents the damages for SCD16 in terms of the percentage of damage per damage state considering short, moderate or long duration of the ground shaking.

EQRم versus N2 method (Fajfar 1999)

There are various methodologies that can be used for the vulnerability assessment and thus for building damage estimation (e.g., Capacity Spectrum Method, N2 Method). CSM (ATC-40 1996) that is also utilized in EQRم, evaluates the seismic performance of structures by comparing structural capacity with seismic demand curves. The key to this method is the reduction of 5 %-damped elastic response spectra of the ground motion to take into account the inelastic behaviour of the structure under consideration using appropriate damping based reduction factors. This is the main difference of EQRم methodology compared to “N2” method (Fajfar 1999, 2000), in which the inelastic demand spectrum is obtained from code-based elastic design spectra using ductility based reduction factors. The computed damages in SCD16 for Hazard 3 using EQRم and N2 methodology are depicted in Fig. 3.21. It is needless to comment on the differences.

Uncertainties in the Fragility Curves

Figure 3.22 shows the influence of beta (β) factor of the fragility curves. EQRم considers that beta factor is equal to 0.4. However the selection of a different, equally logical value, results in a very different damage level.

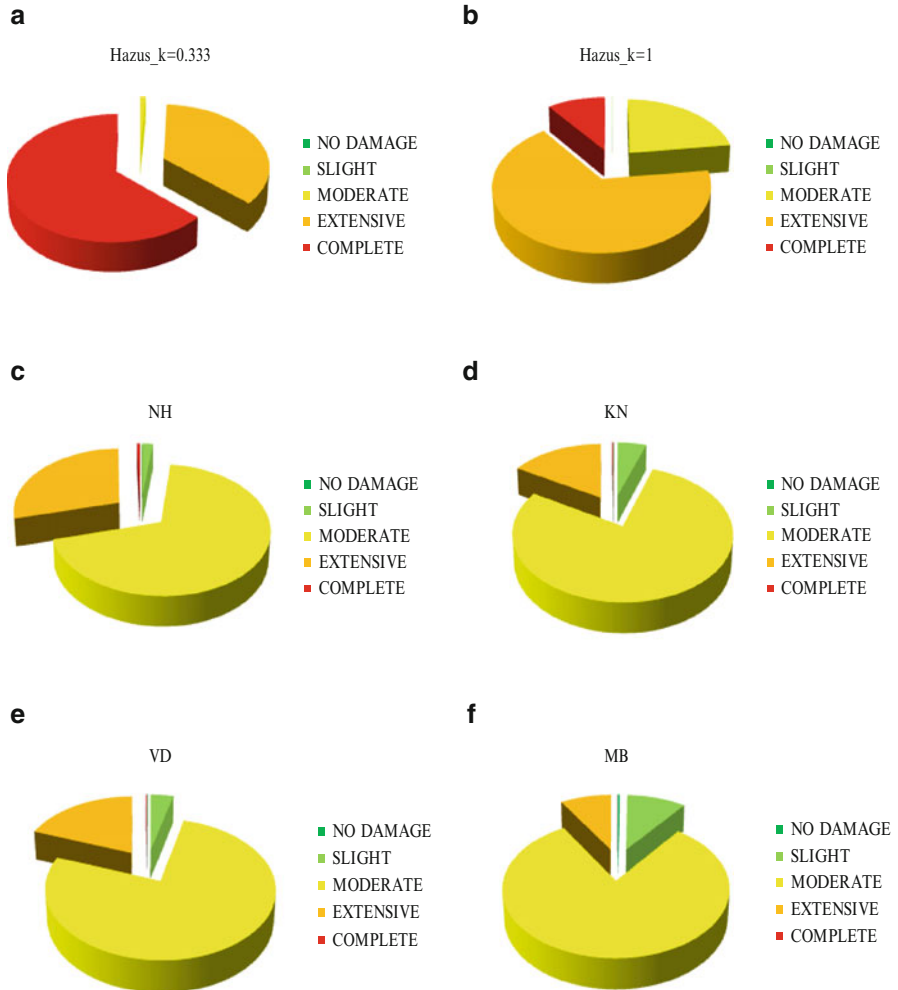


Fig. 3.19 Seismic risk (physical damages) in SCD16 for Hazard 3 and mean return period of 475 years in terms of the percentage of damage per damage state using (a) ATC-40 methodology combined with Hazus for $k = 0.333$ (b) ATC-40 methodology combined with Hazus for $k = 1$ (c) Newmark and Hall (1982) (d) Krawinkler and Nassar (1992) (e) Vidic et al. (1994) and (f) Miranda and Bertero (1994)

3.9 Conclusive Remarks

The main conclusion that one could make from this short and fragmented discussion is that we need a re-thinking of the whole analysis chain from hazard assessment to consequences and loss assessment. The uncertainties involved in every step of the process are too important, affecting the final result. Probably it is time to change the paradigm because so far we just use the same ideas and models trying to

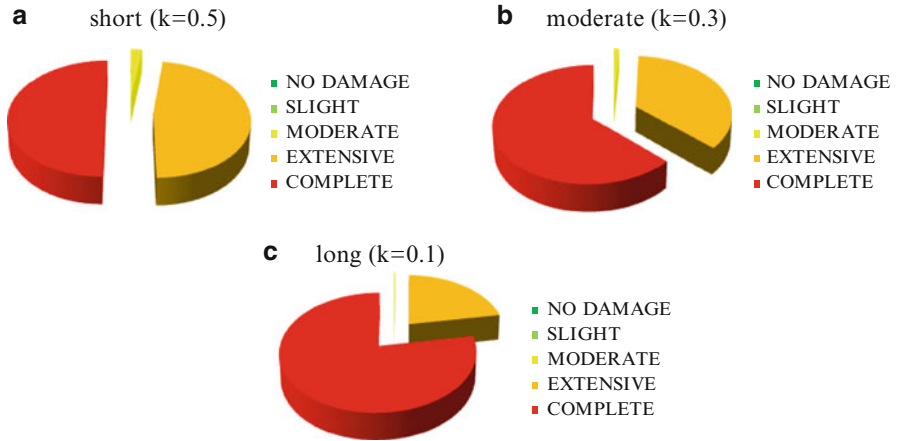


Fig. 3.20 Computed damages for SCD16 for Hazard 3 and mean return period of 475 years in terms of the percentage of damage per damage state considering (a) short (b) moderate and (c) long duration of the ground shaking

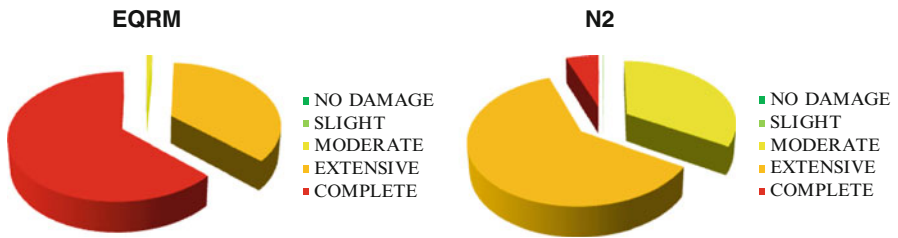


Fig. 3.21 Computed damages in SCD16 for Hazard 3 and mean return period of 475 years in terms of the percentage of damage per damage using EQRm and N2 methodology

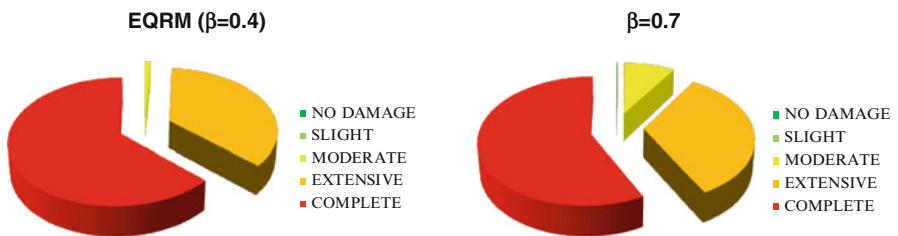


Fig. 3.22 Seismic risk for SCD16 for Hazard 3 and mean return period of 475 years in terms of the percentage of damage per damage state using EQRm with different β factor

improve them (often making them very complex), not always satisfactorily. Considering the starting point of the various models and approaches and the huge efforts made so far, the progress globally is rather modest. More important is that in many cases the uncertainties are increased, not decreased, a fact that has a serious

implication to the reliability and efficiency of the models regarding the assessment of the physical damages in particular in large scale e.g., city scale. Alienated end-users are more apt to serious mistakes and wrong decisions; wrong in the sense of extreme conservatism, high cost or unacceptable safety margins. It should be admitted, however, that our know-how has increased considerably and hence there is the necessary scientific maturity for a qualitative rebound towards a new global paradigm reducing partial and global uncertainties.

Acknowledgments Special acknowledgment to Dr Jacopo Selva, Dr Sotiris Argyroudou and Professor Theodoros Chatzigogos for several breakthrough discussions we had on the nature and the practical treatment of uncertainties. Also to Dr Zafeiria Roumelioti, Dr Stavroula Fotopoulou and my PhD students Evi Riga, Anna Karatzetzou and Sotiria Karapetrou for helping me in preparing this lecture and paper.

Open Access This chapter is distributed under the terms of the Creative Commons Attribution Noncommercial License, which permits any noncommercial use, distribution, and reproduction in any medium, provided the original author(s) and source are credited.

References

- Abrahamson NA (2006) Seismic hazard assessment: problems with current practice and future developments. Proceedings of First European Conference on Earthquake Engineering and Seismology, Geneva, September 2006, p 17
- Alexander D (2000) Confronting catastrophe: new perspectives on natural disasters. Oxford University Press, New York, p 282
- Anastasiadis A, Raptakis D, Pitilakis K (2001) Thessaloniki's detailed microzoning: subsurface structure as basis for site response analysis. *Pure Appl Geophys* 158:2597–2633
- ATC-40 (1996) Seismic evaluation and retrofit of concrete buildings. Applied Technology Council, Redwood City
- Bommer JJ, Abrahamson N (2006) Review article “Why do modern probabilistic seismic hazard analyses often lead to increased hazard estimates?”. *Bull Seismol Soc Am* 96:1967–1977. doi:[10.1785/0120070018](https://doi.org/10.1785/0120070018)
- Borcherdt RD, Glassmoyer G (1992) On the characteristics of local geology and their influence on ground motions generated by the Loma Prieta earthquake in the San Francisco Bay region, California. *Bull Seismol Soc Am* 82:603–641
- Bruneau M, Chang S, Eguchi R, Lee G, O'Rourke T, Reinhorn A, Shinozuka M, Tierney K, Wallace W, Von Winterfeldt D (2003) A framework to quantitatively assess and enhance the seismic resilience of communities. *EERI Spectra J* 19(4):733–752
- CEN (European Committee for Standardization) (2004) Eurocode 8: Design of structures for earthquake resistance, Part 1: General rules, seismic actions and rules for buildings. EN 1998–1:2004. European Committee for Standardization, Brussels
- Cornell CA, Jalayer F, Hamburger RO, Foutch DA (2002) Probabilistic basis for 2000 SAC/FEMA steel moment frame guidelines. *J Struct Eng* 128(4):26–533
- Crowley H, Colombi M, Crempien J, Erduran E, Lopez M, Liu H, Mayfield M, Milanese (2010) GEM1 Seismic Risk Report Part 1, GEM Technical Report, Pavia, Italy 2010–5
- D'Ayala D, Kappos A, Crowley H, Antoniadis P, Colombi M, Kishali E, Panagopoulos G, Silva V (2012) Providing building vulnerability data and analytical fragility functions for PAGER, Final Technical Report, Oakland, California

- Fajfar P (1999) Capacity spectrum method based on inelastic demand spectra. *Earthq Eng Struct Dyn* 28(9):979–993
- Fajfar P (2000) A nonlinear analysis method for performance-based seismic design. *Earthq Spectra* 16(3):573–592
- Fajfar P, Gaspercic P (1996) The N2 method for the seismic damage analysis for RC buildings. *Earthq Eng Struct Dyn* 25:23–67
- FEMA, NIBS (1999) HAZUS99 User and technical manuals. Federal Emergency Management Agency Report: HAZUS 1999, Washington DC
- FEMA (2003) HAZUS-MH Technical Manual. Federal Emergency Management Agency, Washington, DC
- FEMA 273 (1996) NEHRP guidelines for the seismic rehabilitation of buildings — ballot version. U.S. Federal Emergency Management Agency, Washington, DC
- FEMA 356 (2000) Prestandard and commentary for the seismic rehabilitation of buildings. U.S. Federal Emergency Management Agency, Washington, DC
- Freeman SA (1998) The capacity spectrum method as a tool for seismic design. In: Proceedings of the 11th European Conference on Earthquake Engineering, Paris
- Giardini D, Woessner J, Danciu L, Crowley H, Cotton F, Gruenthal G, Pinho R, Valensise G, Akkar S, Arvidsson R, Basili R, Cameelbeck T, Campos-Costa A, Douglas J, Demircioglu MB, Erdik M, Fonseca J, Glavatovic B, Lindholm C, Makropoulos K, Meletti F, Musson R, Pitilakis K, Sesetyan K, Stromeyer D, Stucchi M, Rovida A (2013) Seismic Hazard Harmonization in Europe (SHARE): Online Data Resource. doi:[10.12686/SED-00000001-SHARE](https://doi.org/10.12686/SED-00000001-SHARE)
- Kappos AJ, Panagopoulos G, Penelis G (2006) A hybrid method for the vulnerability assessment of R/C and URM buildings. *Bull Earthq Eng* 4(4):391–413
- Krawinkler H, Miranda E (2004) Performance-based earthquake engineering. In: Bozorgnia Y, Bertero VV (eds) *Earthquake engineering: from engineering seismology to performance-based engineering*, chapter 9. CRC Press, Boca Raton, pp 9.1–9.59
- Krawinkler H, Nassar AA (1992) Seismic design based on ductility and cumulative damage demands and capacities. In: Fajfar P, Krawinkler H (eds) *Nonlinear seismic analysis and design of 170 reinforced concrete buildings*. Elsevier Applied Science, New York, pp 23–40
- LessLoss (2007) Risk mitigation for earthquakes and landslides, Research Project, European Commission, GOCE-CT-2003-505448
- MacKenzie D (1990) *Inventing accuracy: a historical sociology of nuclear missile guidance*. MIT Press, Cambridge
- Mackie K, Stojadinovic B (2003) Seismic demands for performance-based design of bridges, PEER Report 2003/16. Pacific Earthquake Engineering Research Center, University of California, Berkeley
- Mackie K, Stojadinovic B (2005) Fragility basis for California highway overpass bridge seismic decision making. Pacific Earthquake Engineering Research Center, University of California, Berkeley
- Mehanny SSF (2009) A broad-range power-law form scalar-based seismic intensity measure. *Eng Struct* 31:1354–1368
- Miranda E, Bertero V (1994) Evaluation of strength reduction factors for earthquake-resistant design. *Earthq Spectra* 10(2):357–379
- Newmark NM, Hall WJ (1982) *Earthquake spectra and design*. Earthquake Engineering Research Institute, EERI, Berkeley
- Padgett JE, Nielson BG, DesRoches R (2008) Selection of optimal intensity measures in probabilistic seismic demand models of highway bridge portfolios. *Earthq Eng Struct Dyn* 37:711–725
- Pinto PE (2014) Modeling and propagation of uncertainties. In: Pitilakis K, Crowley H, Kaynia A (eds) *SYNER-G: typology definition and fragility functions for physical elements at seismic risk*, vol 27, Geotechnical, geological and earthquake engineering. Springer, Dordrecht. ISBN 978-94-007-7872-6

- Pitilakis K, Riga E, Anastasiadis A (2012) Design spectra and amplification factors for Eurocode 8. *Bull Earthq Eng* 10:1377–1400. doi:10.1007/s10518-012-9367-6
- Pitilakis K, Riga E, Anastasiadis A (2013) New code site classification, amplification factors and normalized response spectra based on a worldwide ground-motion database. *Bull Earthq Eng* 11(4):925–966. doi:10.1007/s10518-013-9429-4
- Pitilakis K, Crowley H, Kaynia A (eds) (2014a) SYNER-G: typology definition and fragility functions for physical elements at seismic risk, vol 27, Geotechnical, geological and earthquake engineering. Springer, Dordrecht. ISBN 978-94-007-7872-6
- Pitilakis K, Karapetrou ST, Fotopoulou SD (2014b) Consideration of aging and SSI effects on seismic vulnerability assessment of RC buildings. *Bull Earthq Eng*. doi:10.1007/s10518-013-9575-8
- REAKT (2014) Strategies and tools for real time earthquake and risk reduction. Research Project, European Commission, Theme: ENV.2011.1.3.1-1, Grant agreement: 282862. <http://www.reaktproject.eu>
- RISK-UE (2004) An advanced approach to earthquake risk scenarios with applications to different European towns. Research Project, European Commission, DG XII2001-2004, CEC: EVK4-CT-2000-00014
- Robinson D, Fulford G, Dhu T (2005) EQRM: Geoscience Australia's earthquake risk model technical manual Version 3.0. Geoscience Australia Record 2005/01
- Selva J, Argyroudis S, Pitilakis K (2013) Impact on loss/risk assessments of inter-model variability in vulnerability analysis. *Nat Hazards* 67(2):723–746. doi:10.1007/s11069-013-0616-z
- SHARE (2013) Seismic Hazard Harmonization in Europe. Research Project, European Commission, ENV.2008.1.3.1.1, Grant agreement: 226769. www.share-eu.org
- SYNER-G (2013) Systemic seismic vulnerability and risk analysis for buildings, lifeline networks and infrastructures safety gain. Research Project, European Commission, ENV-2009-1-244061
- Vamvatsikos D, Cornell CA (2002) Incremental dynamic analysis. *Earthq Eng Struct Dyn* 31:491–514
- Vidic T, Fajfar P, Fischinger M (1994) Consistent inelastic design spectra: strength and displacement. *Earthq Eng Struct Dyn* 23:507–521

Chapter 4

Variability and Uncertainty in Empirical Ground-Motion Prediction for Probabilistic Hazard and Risk Analyses

Peter J. Stafford

Abstract The terms aleatory variability and epistemic uncertainty mean different things to people who routinely use them within the fields of seismic hazard and risk analysis. This state is not helped by the repetition of loosely framed generic definitions that actually inaccurate. The present paper takes a closer look at the components of total uncertainty that contribute to ground-motion modelling in hazard and risk applications. The sources and nature of uncertainty are discussed and it is shown that the common approach to deciding what should be included within hazard and risk integrals and what should be pushed into logic tree formulations warrants reconsideration. In addition, it is shown that current approaches to the generation of random fields of ground motions for spatial risk analyses are incorrect and a more appropriate framework is presented.

4.1 Introduction

Over the past few decades a very large number of empirical ground-motion models have been developed for use in seismic hazard and risk applications throughout the world, and these contributions to engineering seismology collectively represent a significant body of literature. However, if one were to peruse this literature it would, perhaps, not be obvious what the actual purpose of a ground-motion model is. A typical journal article presenting a new ground-motion model starts with a brief introduction, proceeds to outlining the dataset that was used, presents the functional form that is used for the regression analysis along with the results of this analysis, shows some residual plots and comparisons with existing models and then wraps up with some conclusions. In a small number of cases this pattern is broken by the authors giving some attention to the representation of the standard deviation of the model. Generally speaking, the emphasis is very much upon the development and

P.J. Stafford (✉)

Department of Civil & Environmental Engineering, Imperial College London, London, UK
e-mail: p.stafford@imperial.ac.uk

© The Author(s) 2015

A. Ansal (ed.), *Perspectives on European Earthquake Engineering and Seismology*,
Geotechnical, Geological and Earthquake Engineering 39,
DOI 10.1007/978-3-319-16964-4_4

97

behaviour of the median predictions of these models and the treatment of the standard deviation (and its various components) is very minimal in comparison. If it is reasonable to suspect that this partitioning of effort in presenting the model reflects the degree of effort that went into developing the model then there are two important problems with this approach: (1) the parameters of the model for the median predictions are intrinsically linked to the parameters that represent the standard deviation – they cannot be decoupled; and (2) it is well known from applications of ground-motion models in hazard and risk applications that the standard deviation exerts at least as much influence as the median predictions for return periods of greatest interest.

The objective of the present article is to work against this trend by focussing almost entirely upon the uncertainty associated with ground-motion predictions. Note that what is actually meant by ‘uncertainty’ will be discussed in detail in subsequent sections, but the scope includes the commonly referred to components of aleatory variability and epistemic uncertainty. Furthermore, the important considerations that exist when one moves from seismic hazard analysis into seismic risk analysis will also be discussed.

As noted in the title of the article, the focus herein is upon empirical ground-motion models and discussion of the uncertainties associated with stochastic simulation-based models, or seismological models is not within the present scope. That said, some of the concepts that are dealt with herein are equally applicable to ground-motion models in a more general sense.

While at places in the article reference will be made to peak ground acceleration or spectral acceleration, the issues discussed here are not limited to these intensity measures. For the particular examples that are presented, although the extent of various effects will be tied to the choice of intensity measure, the emphasis is upon the underlying concept rather than the numerical results.

4.2 Objective of Ground-Motion Prediction

In both hazard and risk applications the objective is usually to determine how frequently a particular state is exceeded. For hazard, this state is commonly a level of an intensity measure at a site, while for risk applications the state could be related to a level demand on a structure, a level of damage induced by this demand, or the cost of this damage and its repair, among others. In order to arrive at estimates of these rates (or frequencies) of exceedance it is not currently possible to work with empirical data related to the state of interest as a result of insufficient empirical constraint. For example, if one wished to compute an estimate of the annual rate at which a level of peak ground acceleration is exceeded at a site then an option in an ideal world would be to assume that the seismogenic process is stationary and that what has happened in the past is representative of what might happen in the future. On this basis, counting the number of times the state was exceeded and dividing this by the temporal length of the observation period would provide an estimate of the

exceedance rate. Unfortunately, there is not a location on the planet for which this approach would yield reliable estimates for return periods of common interest.

To circumvent the above problem hazard and risk analyses break down the process of estimating rates of ground-motions into two steps: (1) estimate the rates of occurrence of particular earthquake events; and (2) estimate the rate of exceedance of a particular state of ground motion *given* this particular earthquake event. The important point to make here is that within hazard and risk applications the role of an empirical ground-motion model is to enable this second step in which the rate of exceedance of a particular ground-motion level is computed *for a given earthquake scenario*. The manner in which these earthquake scenarios are (or can be) characterised has a strong impact upon how the ground-motion models can be developed. For example, if the scenario can only be characterised by the magnitude of the event and its distance from the site then it is only meaningful to develop the ground-motion model as a function of these variables.

To make this point more clear, consider the discrete representation of the standard hazard integral for a site influenced by a single seismic source:

$$\lambda_{Y>y^*} = \nu \sum_{k=1}^K \sum_{j=1}^J P[Y > y^* | m_j, r_k] P[M = m_j, R = r_k] \quad (4.1)$$

where, Y is a random variable representing the ground-motion measure of interest, y^* is a particular value of this measure, ν is the annual rate of occurrence of earthquakes that have magnitudes greater than some minimum value of interest, and M and R generically represent magnitude and distance, respectively. If we factor out the constant parameter ν , then we have an equation in terms of probabilities and we can see that the objective is to find:

$$\begin{aligned} P[Y > y^*] &= \frac{\lambda_{Y>y^*}}{\nu} = \sum_{k=1}^K \sum_{j=1}^J P[Y > y^* | m_j, r_k] P[M = m_j, R = r_k] \\ &= \int_{y^*}^{\infty} f_Y(y) dy = \iint \int_{y^*}^{\infty} f_{Y|m,r}(y|m,r) f_{M,R}(m,r) dm dr \end{aligned} \quad (4.2)$$

When we discuss the uncertainty associated with ground-motion models it is important to keep this embedding framework in mind. The framework shows that the role of a ground-motion model is to define the distribution $f_{Y|m,r}(y|m,r)$ of levels of motion that can occur for a given earthquake scenario, defined in this case by m and r . The uncertainty that is ultimately of interest to us relates to the estimate of $P[Y > y^*]$ and this depends upon the uncertainty in the ground-motion prediction as well as the uncertainty in the definition of the scenario itself.

For seismic hazard analysis, the ground-motion model alone is sufficient to provide the univariate distribution of the intensity measure for a given earthquake scenario. However, for seismic risk applications, a typical ground-motion model may need to be coupled with a model for spatial, and potentially spectral,

correlations in order to define a multivariate conditional distribution of motions at multiple locations (and response periods) over a region.

At a given site, both in hazard and risk applications, the conditional distribution of ground-motions (assuming spectral acceleration as the intensity measure) given a scenario is assumed to be lognormal and is defined as:

$$\ln Sa \sim N(\mu_{\ln Sa}, \sigma_{\ln Sa}^2) \quad (4.3)$$

where the moments of the distribution are specific to the scenario in question, *i.e.*, $\mu_{\ln Sa} \equiv \mu_{\ln Sa}(m, r, \dots)$ and $\sigma_{\ln Sa} \equiv \sigma_{\ln Sa}(m, r, \dots)$. The probability of exceeding a given level of motion for a scenario is therefore defined using the cumulative standard normal distribution $\Phi(z)$:

$$P[Sa > Sa^* | m, r, \dots] = 1 - \Phi\left[\frac{\ln Sa^* - \mu_{\ln Sa}}{\sigma_{\ln Sa}}\right] \quad (4.4)$$

The logarithmic mean $\mu_{\ln Sa}$ and standard deviation $\sigma_{\ln Sa}$ for a scenario would differ for hazard and risk analyses as in the former case one deals with the marginal distribution of the motions conditioned upon the given the scenario while in the latter case one works with the conditional distribution of the motions, conditioned upon both the given scenario and the presence of a particular *event term* for the scenario. That is, in portfolio risk analysis one works at the level of inter-event variability and intra-event variability while for hazard analysis one uses the total variability.

An empirical ground-motion model must provide values of both the logarithmic mean $\mu_{\ln Sa}$ and the standard deviation $\sigma_{\ln Sa}$ in order to enable the probability calculations to be made and these values must be defined in terms of the predictor variables M and R , among potentially others. Both components of the distribution directly influence the computed probabilities, but can exert greater or lesser influence upon the probability depending upon the particular value of $\ln Sa^*$.

4.3 Impact of Bias in Seismic Hazard and Risk

Equation (4.4) is useful to enable one to understand how the effects of bias in ground-motion models would influence the contributions to hazard and risk estimates. The computation of probabilities of exceedance is central to both cases. Imagine that we assume that any given ground-motion model is biased for a particular scenario in that the predicted median spectral accelerations differ from an unknown true value by a factor γ_μ and that the estimate of the aleatory variability also differs from the true value by a factor of γ_σ . To understand the impact of these biases upon the probability computations we can express Eq. (4.4) with explicit

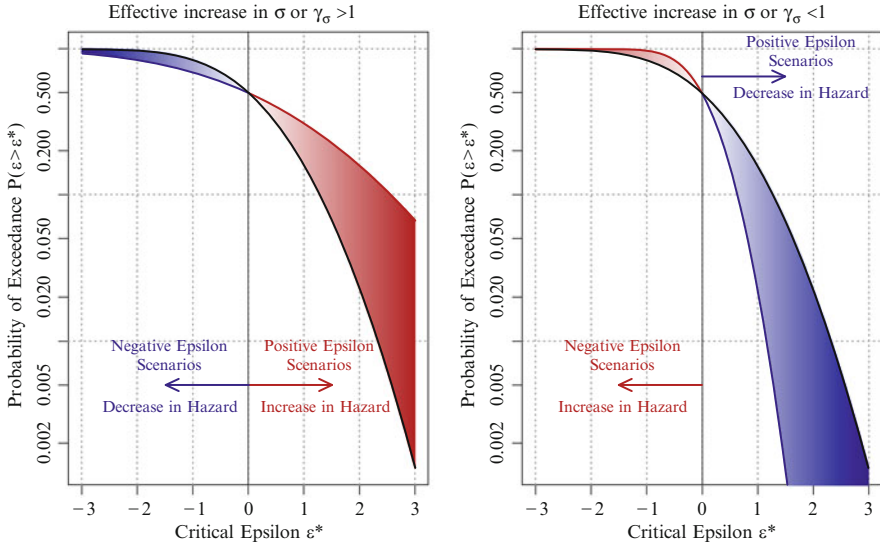


Fig. 4.1 Illustration of the effect that a bias in the logarithmic standard deviation has upon the computation of probabilities of exceedance. The *left* panel corresponds to $\gamma_\sigma = 2$ while the *right* panel shows $\gamma_\sigma = 1/2$

inclusion of these bias factors as in Eq. (4.5). Now we recognise that the probability that we compute is an estimate and denote this as \hat{P} .

$$\hat{P} [Sa > Sa^* | m, r, \dots] = 1 - \Phi \left[\frac{\ln Sa^* - \ln \gamma_\mu - \mu_{\ln Sa}}{\gamma_\sigma \sigma_{\ln Sa}} \right] \quad (4.5)$$

This situation is actually much closer to reality than Eq. (4.4). For many scenarios predictions of motions will be biased by some unknown degree and it is important to understand how sensitive our results are to these potential biases. The influence of the potential bias in the logarithmic standard deviation is shown in Fig. 4.1. The case shown here corresponds to an exaggerated example in which the bias factor is either $\gamma_\sigma = 2$ or $\gamma_\sigma = 1/2$.

What sort of bias could one expect to be reasonable for a given ground-motion model? This is a very difficult question to answer in any definitive way, but one way to get a feel for this is to compare the predictions of both median logarithmic motions and logarithmic standard deviations for two generations of modern ground-motion models. In particular, the very recent release of the models from the second phase of the PEER NGA project (NGA West 2) provides one with the ability to compare the predictions from the NGA West 1 and NGA West 2 studies.

Figures 4.2 and 4.3 show these estimates of the possible extent of bias for the ground-motion models of Campbell and Bozorgnia (2008, 2014) and Chiou and Youngs (2008, 2014). It should be noted that the point here is not that these models are necessarily biased, but that it is reasonable to assume that the 2014 versions are

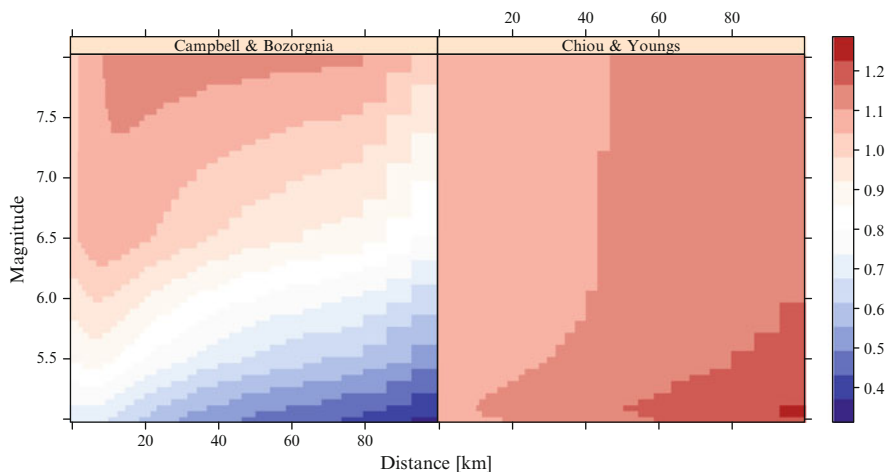


Fig. 4.2 Example *bias factors* computed as the ratios between predictions of two generations of models from the same developers. The *left* panel shows ratios between the medians, $Sa(T = 0.01s)$, of Campbell and Bozorgnia (2014, 2008) – 2014:2008, while the *right* panel is for Chiou and Youngs (2014, 2008) – 2014:2008

less biased than their 2008 counterparts. Therefore, the typical extent of bias that has existed through the use of the 2008 NGA models over the past few years can be characterised through plots like those shown in Figs. 4.2 and 4.3. However, in order to see how these differences in predicted moments translate into differences in hazard estimates the following section develops hazard results for a simple academic example.

4.3.1 Probabilistic Seismic Hazard Analysis

A probabilistic seismic hazard analysis is conducted using the ground-motion models of Campbell and Bozorgnia (2008, 2014) as well as those of Chiou and Youngs (2008, 2014). The computations are conducted for a hypothetical case of a site located in the centre of a circular source. The seismicity is described by a doubly-bounded exponential distribution with a b -value of unity and minimum and maximum magnitudes of 5 and 8 respectively. The maximum distance considered in the hazard integrations is 100 km. For this exercise, the depths to the top of the ruptures for events of all magnitudes are assumed to be the same and it is also assumed that the strike is perpendicular to the line between the site and the closest point on the ruptures. All ruptures are assumed to be for strike-slip events and the site itself is characterised by an average shear-wave velocity over the uppermost 30 m of 350 m/s. Note that these assumptions are equivalent to ignoring finite source dimensions and working with a point-source representation. For the

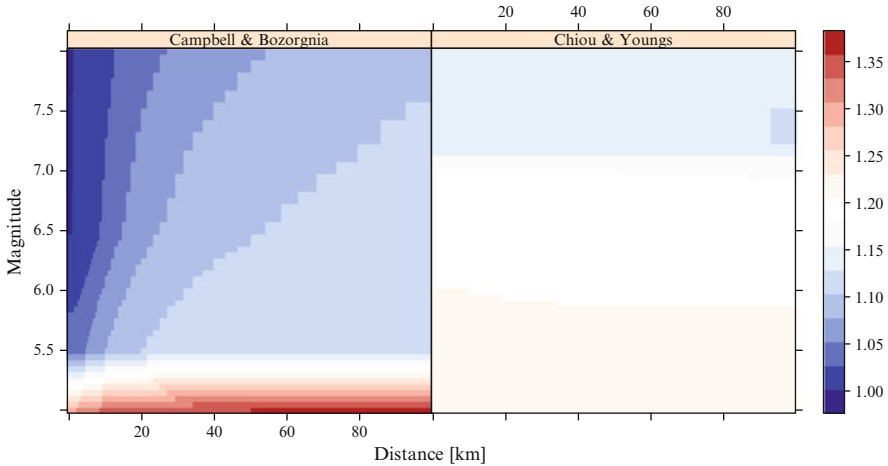


Fig. 4.3 Example *bias factors* for the logarithmic standard deviations. The *left* panel shows ratios between the $\sigma_{\ln Sa}$ predictions of Campbell and Bozorgnia (2014, 2008) – 2014:2008, while the *right* panel shows the ratios for Chiou and Youngs (2014, 2008) – 2014:2008. The standard deviations are for a period of 0.01 s

purposes of this exercise, this departure from a more realistic representation does not influence the point that is being made.

Hazard curves for spectral acceleration at a response period of 0.01 s are computed through the use of the standard hazard integral in Eq. (4.6).

$$\lambda_{Y>y^*} = \sum_{i=1} \nu_i \iint P[Y > y^* | m, r] f_{M,R}(m, r) dm dr \tag{4.6}$$

For this particular exercise we have just one source ($i = 1$) and will also appreciate that ν_i simply scales the hazard curve linearly and so using $\nu_1 = 1$ enables us to convert the annual rates of exceedance $\lambda_{Y>y^*}$ directly into annual probabilities of exceedance.

Hazard curves computed according to this equation are shown in Fig. 4.4. The curves show that for long return periods the hazard curves predicted by both models of Campbell and Bozorgnia are very similar while at short return periods there are significant differences between the two versions of their model. From consideration of Figs. 4.2 and 4.3 we can see that the biggest differences between the two versions of the Campbell and Bozorgnia model for the scenarios of relevance to this exercise ($T = 0.01$ seconds and $V_{S,30} = 350$ m/s) are at small magnitudes between roughly $M_w 5.0$ and $M_w 5.5$ where the new model predicts significantly smaller median motions but also has a much larger standard deviation for these scenarios. As will be shown shortly, both of these effects lead to a reduction in the hazard estimates for these short return periods.

In contrast, the two versions of the Chiou and Youngs model compare favourably for the short return periods but then exhibit significant differences as

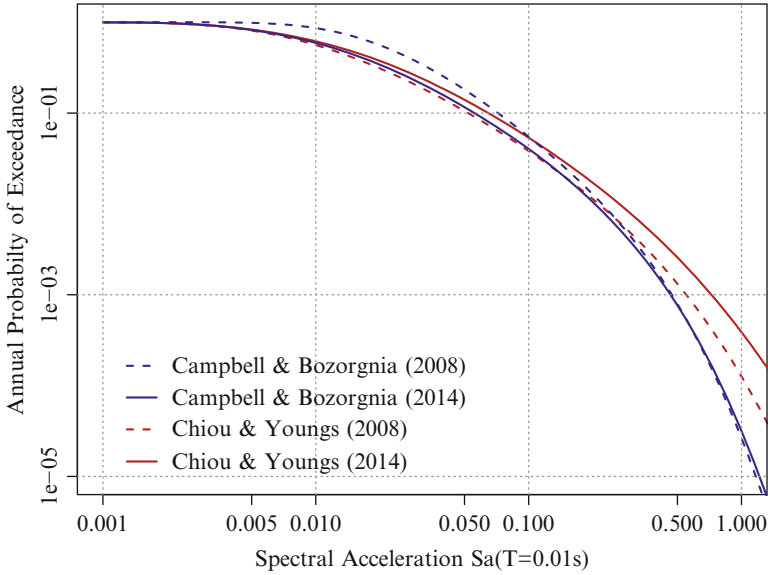


Fig. 4.4 Hazard curves computed for the ground-motion models of Campbell and Bozorgnia (2008, 2014) and Chiou and Youngs (2008, 2014)

one moves to longer return periods. Again making use of Figs. 4.2 and 4.3 we can see that the latest version of their model provides a relatively consistent, yet mild ($\gamma_\mu \approx 1.0 - 1.1$), increase in motions over the full magnitude-distance space considered here and that we have a 15–20 % increase in the standard deviation over this full magnitude-distance space. Again, from the developments that follow, we should expect to observe the differences between the hazard curves at these longer return periods.

We have just seen how *bias factors* for the logarithmic mean γ_μ and logarithmic standard deviation γ_σ can influence the computation of estimates of the probability of exceedance for a given scenario. The hazard integral in Eq. (4.6) is simply a weighted sum over all relevant scenarios as can be seen from the approximation (that this ceases to be an approximation in the limit as $\Delta m, \Delta r \rightarrow 0$):

$$\lambda_{Y>y^*} \approx \sum_{i=1} v_i \sum_j \sum_k P[Y > y^* | m_j, r_k] f_{M,R}(m_j, r_k) \Delta m \Delta r \quad (4.7)$$

If we now accept that when using a ground-motion model we will only obtain an estimate of the annual rate of exceedance we can write:

$$\hat{\lambda}_{Y>y^*} \approx \sum_{i=1} v_i \sum_j \sum_k \hat{P}[Y > y^* | m_j, r_k] f_{M,R}(m_j, r_k) \Delta m \Delta r \quad (4.8)$$

where now this expression is a function of the bias factors for both the logarithmic

motions for every scenario. One can consider the effects of systematic bias from the ground motion model expressed through factors modifying the conditional mean and standard deviation for a scenario. The biases in this case hold equally for all scenarios (although this can be relaxed). At least for the standard deviation, this assumption is not bad given the distributions shown in Fig. 4.3.

Therefore, for each considered combination of m_j and r_k we can define our estimate of the probability of exceeding y^* from Eq. (4.5). Note that the bias in the median ground motion is represented by a factor γ_μ multiplying the median motion $\hat{S}a = \gamma_\mu Sa$. This translates to an additive contribution to the logarithmic mean leading to $\mu_{\ln Sa} + \ln \gamma_\mu$ representing the biased median motion.

To understand how such systematic biases could influence hazard estimates we can compute the partial derivatives with respect to these bias factors, considering one source of bias at a time.

$$\frac{\partial \hat{\lambda}}{\partial \gamma_\mu} \approx \sum_{i=1} \nu_i \sum_j \sum_k \frac{\partial}{\partial \gamma_\mu} \left[1 - \Phi \left(\frac{\ln y^* - \ln \gamma_\mu - \mu}{\sigma} \right) \right] f_{M,R}(m_j, r_k) \Delta m \Delta r \quad (4.9)$$

and

$$\frac{\partial \hat{\lambda}}{\partial \gamma_\sigma} \approx \sum_{i=1} \nu_i \sum_j \sum_k \frac{\partial}{\partial \gamma_\sigma} \left[1 - \Phi \left(\frac{\ln y^* - \mu}{\gamma_\sigma \sigma} \right) \right] f_{M,R}(m_j, r_k) \Delta m \Delta r \quad (4.10)$$

which can be shown to be equivalent to:

$$\frac{\partial \hat{\lambda}}{\partial \gamma_\mu} = \sum_{i=1} \nu_i \iint \frac{1}{\gamma_\mu \sigma \sqrt{2\pi}} \exp \left[-\frac{(\ln \gamma_\mu + \mu - \ln y^*)^2}{2\sigma^2} \right] f_{M,R}(m, r) dm dr \quad (4.11)$$

and

$$\frac{\partial \hat{\lambda}}{\partial \gamma_\sigma} = \sum_{i=1} \nu_i \iint \frac{\ln y^* - \mu}{\gamma_\sigma^2 \sigma \sqrt{2\pi}} \exp \left[-\frac{(\mu - \ln y^*)^2}{2\gamma_\sigma^2 \sigma^2} \right] f_{M,R}(m, r) dm dr \quad (4.12)$$

When these expressions are evaluated for the hypothetical scenario that we have considered we obtain partial derivatives as shown in Fig. 4.5. The curves in this figure show that the sensitivity of the hazard curve to changes in the mean predictions for the scenarios is most significant when there is relatively weak influence from the standard deviation. That is, when the hazard curve is dominated by contributions with epsilon values near zero then biases in the mean predictions matter most strongly.

The scaling of the partial derivatives with respect to the bias in the standard deviation is more interesting, and reflects the schematic result previously shown in Fig. 4.1. We see that we have positive gradients for the larger spectral accelerations

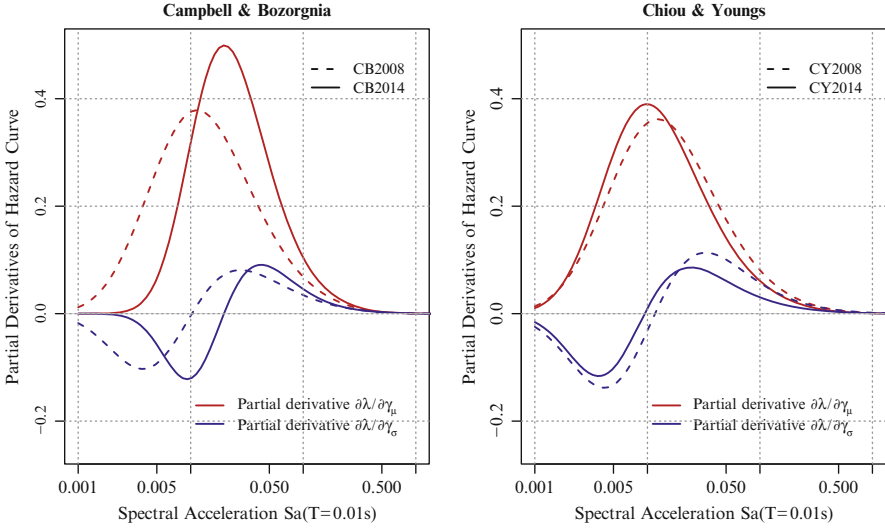


Fig. 4.5 Partial derivatives of the hazard curves with respect to the bias factors γ_μ and γ_σ

while we have negative gradients for weak motions. These ranges effectively represent the positive and negative epsilon ranges that were shown explicitly in the previous section. However, in this case we must recognise that when considering the derivative of the hazard curve that we have many different contributions for epsilon values corresponding to a given target level of the intensity measure y^* and that the curves shown in Fig. 4.5 reflect a weighted average of the individual curves that have the form shown in Fig. 4.1.

The utility of the partial derivative curves shown in Fig. 4.5 is that they enable one to appreciate over which range of intensity measures (and hence return periods) changes to either the median motion or logarithmic standard deviation will have the greatest impact upon the shape of the hazard curves. Note that with respect to the typical hazard curves shown in Fig. 4.4, these derivatives should be considered as being in some sense *orthogonal* to the hazard curves. That is, they are not representing the slope of the hazard curve (which is closely related to the annual rate of occurrence of a given level of ground-motion), but rather saying that for any given level of motion, how sensitive is the annual rate of exceedance to a change in the logarithmic mean and standard deviation. It is clear from Fig. 4.4 that a change in the standard deviation itself has a strong impact upon the actual nature of the hazard curve at long return periods, whereas the sensitivity indicated in Fig. 4.5 is low for the corresponding large motions. However, it should be born in mind that these partial derivatives are $\partial \hat{\lambda} / \partial \gamma_i$ rather than, say, $\partial \ln \hat{\lambda} / \partial \gamma_i$ and that the apparently low sensitivity implied by Fig. 4.6 should be viewed in terms of the fact that small changes $\Delta \hat{\lambda}$ are actually very significant when the value of $\hat{\lambda}$ itself is very small over this range.

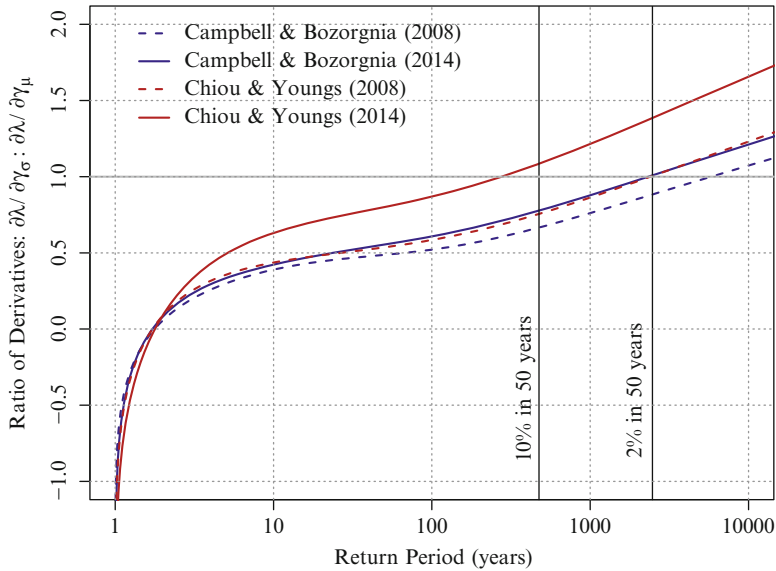


Fig. 4.6 Ratios of the partial derivatives with respect to the logarithmic standard deviation and mean. Vertical lines are shown to indicate the commonly encountered 475 and 2,475 year return periods

Another way of making use of these partial derivatives is to compare the relative sensitivity of the hazard curve to changes in the logarithmic mean and standard deviation. This relative sensitivity can be computed by taking the ratio of the partial derivatives with respect to both the standard deviation and the mean and then seeing the range of return periods (or target levels of the intensity measure) for which one or the other partial derivative dominates. Ratios of this type are computed for this hypothetical scenario and are shown in Fig. 4.6. When ratios greater than one are encountered the implication is that the hazard curves are more sensitive to changes in the standard deviation than they are to changes in the mean. As can be seen from Fig. 4.6, this situation arises as the return period increases. However, for the example shown here (which is fairly typical of active crustal regions in terms of the magnitude-frequency distribution assumed) the influence of the standard deviation tends to be at least as important as the median, if not dominant, at return periods of typical engineering interest (on the order of 475 years or longer).

The example just presented has highlighted that ground-motion models must provide estimates of both the logarithmic mean and standard deviation for any given scenario, and that in many cases the ability to estimate the standard deviation is at least as important as the estimate of the mean. Historically, however, the development of ground-motion models has focussed overwhelmingly upon the scaling of median predictions, with many people (including some ground-motion model developers) still viewing the standard deviation as being some form of error in the prediction of the median rather than being an important parameter of the

ground-motion distribution that is being predicted. The results presented for this example here show that ground-motion model developers should shift the balance of attention more towards the estimation of the standard deviation than what has historically occurred.

4.3.2 Probabilistic Seismic Risk Analysis

When one moves to seismic risk analyses the treatment of the aleatory variability can differ significantly. In the case that a risk analysis is performed for a single structure the considerations of the previous section remain valid. However, for portfolio risk assessment it becomes important to account for the various correlations that exist with ground-motion fields for a given earthquake scenario. These correlations are required for developing the conditional ground-motion fields that correspond to a multivariate normal distribution.

The multivariate normal distribution represents the conditional random field of relative ground-motion levels (quantified through normalised intra-event residuals) conditioned upon the occurrence of an earthquake and the fact that this event will generate seismic waves with a source strength that may vary from the expected strength. The result of this source deviation is that all locations that register this ground-motion will have originally had this particular level of source strength. This event-to-event variation that systematically influences all sites is represented in ground-motion models by the inter-event variability, while the conditional variation of motions at a given site is given by the intra-event variability.

For portfolio risk analysis it is therefore important to decompose the total aleatory variability in ground-motions into a component that reflects the source strength (the inter-event variability) and a component that reflects the site-specific aleatory variability (the intra-event variability). It should also be noted in passing that this is not strictly equivalent to the variance decomposition that is performed using mixed effects models in regression analysis.

When one considers ground-motion models that have been developed over recent years it is possible to appreciate that some significant changes have occurred to the value of the total aleatory variability that is used in hazard analysis, but also to the decomposition of this total into the inter-event and intra-event components. For portfolio risk analysis, this decomposition matters. To demonstrate why this is the case, Fig. 4.7 compares conditional ground-motion fields that have been simulated for the 2011 Christchurch Earthquake in New Zealand. In each case shown, the inter-event variability is assumed to be a particular fraction of the total variability and this fraction is allowed to range from 0 to 100 %. As one moves from a low to a high fraction it is clear that the within event spatial variation of the ground-motions reduces.

For portfolio risk assessment, these differences in the spatial variation are important as the extreme levels of loss correspond to cases in which spatial regions of high-intensity ground-motion couple with regions of high vulnerability and

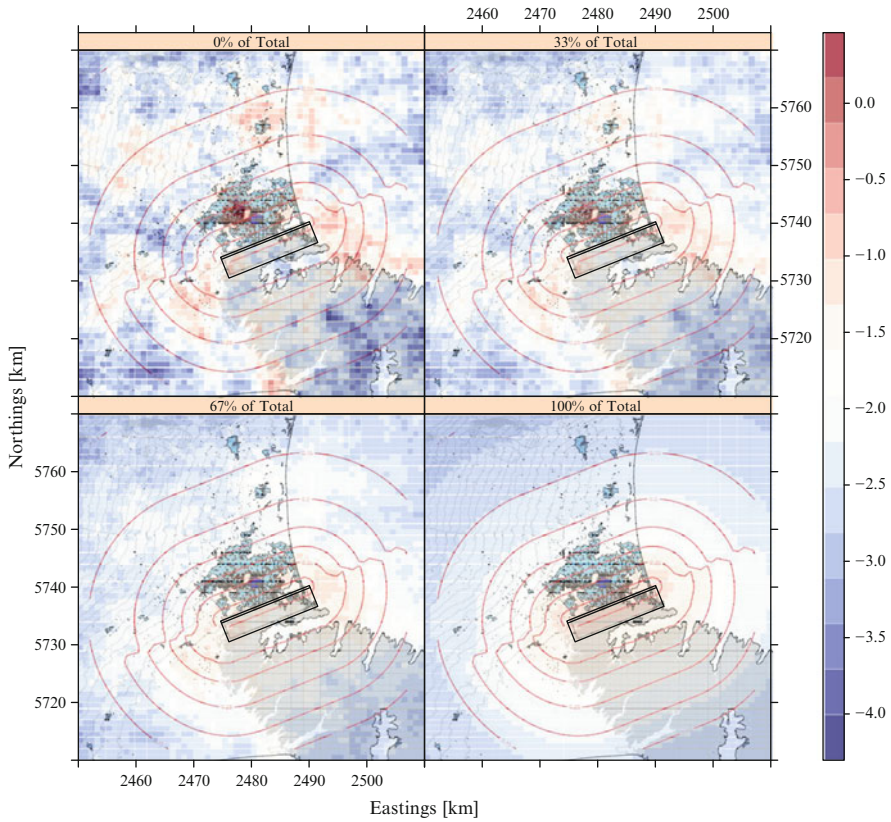


Fig. 4.7 Impact upon the nature of ground-motion fields generated assuming that the inter-event variability is a given fraction of the total aleatory variability. The ground-motion fields shown are possible fields consistent with a repeat of the Christchurch earthquake

exposure. The upper left panel of Fig. 4.7 shows a clear example of this where a patch of high intensity is located in a region of high exposure.

In addition to ensuring that the total aleatory variability is well-estimated, it is therefore also very important (for portfolio risk analysis) to ensure that the partitioning of the total variability between inter- and intra-event components is done correctly.

4.4 Components of Uncertainty

The overall uncertainty in ground-motion prediction is often decomposed into components of Aleatory Variability and Epistemic Uncertainty. In the vast majority of applications *only* these two components are considered and they are defined in

such as way that the aleatory variability is supposed to represent inherent randomness in nature while epistemic uncertainties represent contributions resulting from our lack of knowledge. The distinction is made for more than semantic reasons and the way that each of these components is treated within hazard and risk analysis differ. Using probabilistic seismic hazard analysis as an example, the aleatory variability is directly accounted for within the *hazard integral* while epistemic uncertainty is *accounted for* or *captured* through the use of logic trees.

However, when one constructs a logic tree the approach is to consider alternative hypotheses regarding a particular effect, or component, within the analysis. Each alternative is then assigned a weight that has been interpreted differently by various researchers and practitioners, but is ultimately treated as a probability. No alternative hypotheses are considered for effects that we do not know to be relevant. That is, the representation of epistemic uncertainty in a logic tree only reflects our uncertainty regarding the components of the model that we think are relevant. If we happen to be missing an important physical effect then we will never think to include it within our tree and this degree of ignorance is never reflected in our estimate of epistemic uncertainty.

It is therefore clear that there is a component of the overall uncertainty in our analyses that is not currently accounted for. This component is referred to as *Ontological Uncertainty* (Elms 2004) and represents the unknown unknowns from the famous quote of Donald Rumsfeld.

These generic components of uncertainty are shown schematically in Fig. 4.8. The actual numbers that are shown in this figure are entirely fictitious and the objective is not to define this partitioning. Rather, the purpose of this figure is to illustrate the following:

- What we currently refer to as being aleatory variability is not all aleatory variability and instead contains a significant component of epistemic uncertainty (which is why it reduces from the present to the near future)
- The fact that ontological uncertainty exists means that we cannot assign a numerical value to epistemic uncertainty
- The passage of time allows certain components to be reduced

In the fields of seismic hazard and risk it is common for criticism to be made of projects due to the improper handling of aleatory variability and epistemic uncertainty by the analysts. However, the distinction between these components is not always clear and this is at least in part a result of loose definitions of the terms as well as a lack of understanding about the underlying motivation for the decomposition.

As discussed at length by Der Kiureghian and Ditlevsen (2009), what is aleatory or epistemic can depend upon the type of analysis that is being conducted. The important point that Der Kiureghian and Ditlevsen (2009) stress is that the categorisation of an uncertainty as either aleatory or epistemic is largely at the discretion of the analyst and depends upon what is being modelled. The uncertainties themselves are generally not properties of the parameter in question.

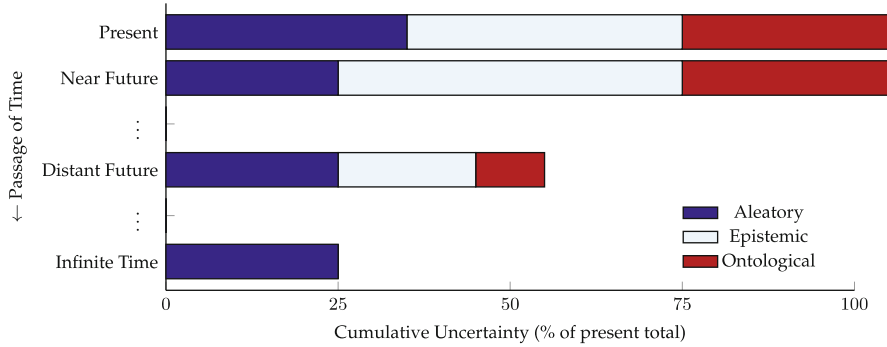


Fig. 4.8 Components of the total uncertainty in ground motion prediction, and their evolution in time. The percentage values shown are entirely fictitious

4.4.1 Nature of Uncertainty

Following the more complete discussion provided by Der Kiureghian and Ditlevsen (2009), consider the physical process that results in the generation of a ground motion y for a particular scenario. The underlying basic variables that parameterise this physical process can be written as \mathbf{X} .

Now consider a perfect deterministic ground-motion model (*i.e.*, one that makes predictions with no error) that provides a mathematical description of the physical link between these basic variables and the observed motion. In the case that we knew the exact values of all basic variables for a given scenario we would write such a model as:

$$y = g(\mathbf{x}, \theta_g) \quad (4.13)$$

where, here θ_g are the parameters or coefficients of the model. Note that the above model must account for all relevant physical effects related to the generation of y . In practice, we cannot come close to accounting for all relevant effects and so rather than working with the full set \mathbf{X} , we instead work with a reduced set \mathbf{X}_k (representing the known random variables) and accept that the effect of the unknown basic variables \mathbf{X}_u will manifest as differences between our now approximate model \hat{g} and the observations. Furthermore, as we are working with an observed value of y (which we assume to be known without error) we also need to recognise that we will have an associated observed instance of \mathbf{X}_k that is not perfectly known \mathbf{x}_k . Our formulation is then written as:

$$y = \hat{g}(\hat{\mathbf{x}}_k, \hat{\theta}_g) + \varepsilon \quad (4.14)$$

What is important to note here is that the residual error ε is the result of three distinct components:

- The effect of unobserved, or not considered, variables \mathbf{X}_u
- The imperfection of our mathematical model, both in terms of its functional form and the estimation of its parameters $\hat{\theta}_g$
- The uncertainties associated with estimated known variables $\hat{\mathbf{x}}_k$

The imperfection referred to in the second point above means that the residual error ε does not necessarily have a zero mean (as is the case for regression analysis). The reason being that the application of imperfect physics does not mean that our simplified model will be unbiased – both when applied to an entire ground-motion database, but especially when applied to a particular scenario. Therefore, it could be possible to break down the errors in prediction into components representing bias, $\Delta(\hat{\mathbf{x}}, \hat{\theta}_g)$, and variability, ε' :

$$\varepsilon \rightarrow \Delta(\hat{\mathbf{x}}, \hat{\theta}_g) + \varepsilon' \quad (4.15)$$

In the context seismic hazard and risk analysis, one would ordinarily regard the variability represented by ε as being aleatory variability and interpret this as being inherent randomness in ground motions arising from the physical process of ground-motion generation. However, based upon the formulation just presented one must ask whether any actual inherent randomness exists, or whether we are just seeing the influence of the unexplained parameters \mathbf{x}_u . That is, should our starting point have been:

$$y = g(\mathbf{x}, \theta_g) + \varepsilon_A \quad (4.16)$$

where here the ε_A represents intrinsic randomness associated with ground motions.

When one considers this problem one must first think about what type of randomness we are dealing with. Usually when people define aleatory variability they make an analogy with the rolling of a die, but often they are unwittingly referring to one particular type of randomness. There are broadly three classes of randomness:

- **Apparent Randomness:** This is the result of viewing a complex deterministic process from a simplified viewpoint.
- **Chaotic Randomness:** This randomness arises from nonlinear systems that evolve from a particular state in a manner that depends very strongly upon that state. Responses obtained from very slightly different starting conditions can be markedly different from each other, and our inability to perfectly characterise a particular state means that the system response is unpredictable.
- **Inherent Randomness:** This randomness is an intrinsic part of reality. Quantum mechanics arguably provides the most pertinent example of inherent randomness.

Note that there is also a subtle distinction that can be made between systems that are deterministic, yet unpredictable, and systems that possess genuine randomness.

In addition, some (including historically Einstein) argue that systems that possess ‘genuine randomness’ are actually driven by deterministic processes and variables that we simply are not aware of. In this case, these systems would be subsumed within the one or more of the other categories of apparent or chaotic randomness. However, at least within the context of quantum mechanics, Bell’s theorem demonstrates that the randomness that is observed at such scales is in fact inherent randomness and not the result of apparent randomness.

For ground-motion modelling, what is generally referred to as aleatory variability is at least a combination of both apparent randomness and chaotic randomness and could possibly also include an element of inherent randomness – but there is no hard evidence for this at this point. The important implication of this point is that the component associated with apparent randomness is actually an epistemic uncertainty that can be reduced through the use of more sophisticated models. The following two sections provide examples of apparent and chaotic randomness.

4.4.2 Apparent Randomness – Simplified Models

Imagine momentarily that it is reasonable to assume that ground-motions arise from deterministic processes but that we are unable to model all of these processes. We are therefore required to work with simplified models when making predictions. To demonstrate how this results in apparent variability consider a series of simplified models for the prediction of peak ground acceleration (here denoted by y) as a function of moment magnitude \mathbf{M} and rupture distance R :

Model 0

$$\ln y = \beta_0 + \beta_1 \mathbf{M} \quad (4.17)$$

Model 1

$$\ln y = \beta_0 + \beta_1 \mathbf{M} + \beta_2 \ln \sqrt{R^2 + \beta_3^2} \quad (4.18)$$

Model 2

$$\ln y = \beta_0 + \beta_1 \mathbf{M} + \beta_2 \ln \sqrt{R^2 + \beta_3^2} + \beta_4 \ln V_{S,30} \quad (4.19)$$

Model 3

$$\begin{aligned} \ln y = & \beta_0 + \beta_1 \mathbf{M} + \beta_{1a} (\mathbf{M} - 6.5)^2 + [\beta_2 + \beta_{2a} (\mathbf{M} - 6.5)] \ln \sqrt{R^2 + \beta_3^2} \\ & + \beta_4 \ln V_{S,30} \end{aligned} \quad (4.20)$$

Model 4

$$\ln y = \beta_0 + \beta_1 \mathbf{M} + \beta_{1a} (\mathbf{M} - 6.5)^2 + [\beta_2 + \beta_{2a} (\mathbf{M} - 6.5)] \ln \sqrt{R^2 + \beta_3^2} + \beta_4 \ln V_{S,30} + \beta_5 F_{nm} + \beta_6 F_{rv} \quad (4.21)$$

Models 5 and 6

$$\ln y = \beta_0 + \beta_1 \mathbf{M} + \beta_{1a} (\mathbf{M} - 6.5)^2 + [\beta_2 + \beta_{2a} (\mathbf{M} - 6.5)] \ln \sqrt{R^2 + \beta_3^2} + \beta_4 \ln V_{S,30} + \beta_5 F_{nm} + \beta_6 F_{rv} + \beta_7 F_{as} \quad (4.22)$$

where we see that the first of these models is overly simplified, but that by the time we reach Models 5 and 6, we are accounting for the main features of modern models. The difference between Models 5 and 6 is not in the functional form, but in how the coefficients are estimated. Models 1–5 use standard mixed effects regression with one random effect for event effects. However, Model 6 includes this random effect, but also distinguishes between these random effects depending upon whether we have mainshocks or aftershocks and also partitions the intra-event variance into components for mainshocks and aftershocks. The dataset consists of 2,406 records from the NGA database.

Figure 4.9 shows estimates of apparent randomness for each of these models, assuming that Model 6 is ‘correct’. That is, the figure shows the difference between the total standard deviation of Model i and Model 6 and because we assume the latter model is correct, this difference in variance can be attributed to apparent randomness. The figure shows that the inclusion of distance scaling and distinguishing between mainshocks and aftershocks has a very large impact, but that other additions in complexity provide a limited reduction in apparent randomness. The important point here is that this apparent randomness is actually epistemic uncertainty – not aleatory as is commonly assumed.

4.4.3 Chaotic Randomness – Bouc-Wen Example

Chaotic randomness is likely to be a less-familiar concept than apparent randomness given that the latter is far more aligned with our normal definition of epistemic uncertainty. To explain chaotic randomness in the limited space available here is a genuine challenge, but I will attempt this through the use of an example based heavily upon the work of Li and Meng (2007). The example concerns the response of a nonlinear oscillator and is not specifically a ground-motion example. However, this type of model has been used previously for characterising the effects of nonlinear site response. I consider the nonlinear Bouc-Wen single-degree-of-freedom system characterised by the following equation:

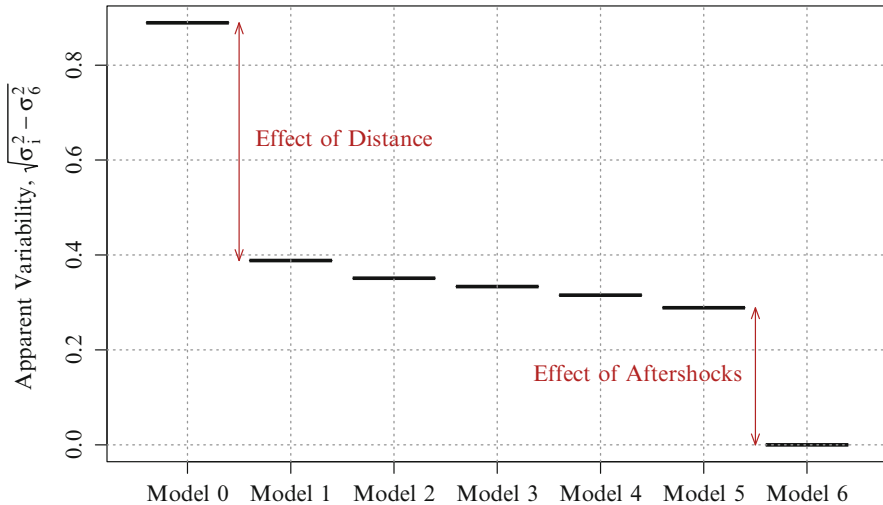


Fig. 4.9 Variation of apparent randomness associated with models of increasing complexity

$$\ddot{u} + 2\zeta\omega_0\dot{u} + \alpha\omega_0^2u + (1 - \alpha)\omega_0^2z = B \sin(\Omega t) \tag{4.23}$$

where the nonlinear hysteretic response is defined by:

$$\dot{z} = A\dot{u} - \gamma|\dot{u}|z|z|^{n-1} - \beta\dot{u}|z|^n \tag{4.24}$$

This model is extremely flexible and can be parameterised so that it can be applied in many cases of practical interest, but in the examples that follow we will assume that we have a system that exhibits hardening when responding in a nonlinear manner (see Fig. 4.10).

Now, if we subject this system to a harmonic excitation we can observe a response at relatively low amplitudes that resembles that in Fig. 4.11. Here we show the displacement response, the velocity response, the trajectory of the response in the phase space ($u - \dot{u}$ space) and the nonlinear restoring force. In all cases the line colour shifts from light blue, through light grey and towards a dark red as time passes. In all panels we can see the influence of the initial transient response before the system settles down to a steady-state. In particular, we can see that we reach a limit-cycle in the phase space in the lower left panel.

For Fig. 4.11 the harmonic amplitude is $B = 5$ and we would find that if we were to repeat the analysis for a loading with an amplitude slightly different to this value that our response characteristics would also only be slightly different. For systems in this low excitation regime we have predictable behaviour in that the effect of small changes to the amplitude can be anticipated.

However, consider now a plot of the maximum absolute displacement and maximum absolute velocity against the harmonic amplitude shown in Fig. 4.12. Note that the response values shown in this figure correspond to what are essentially

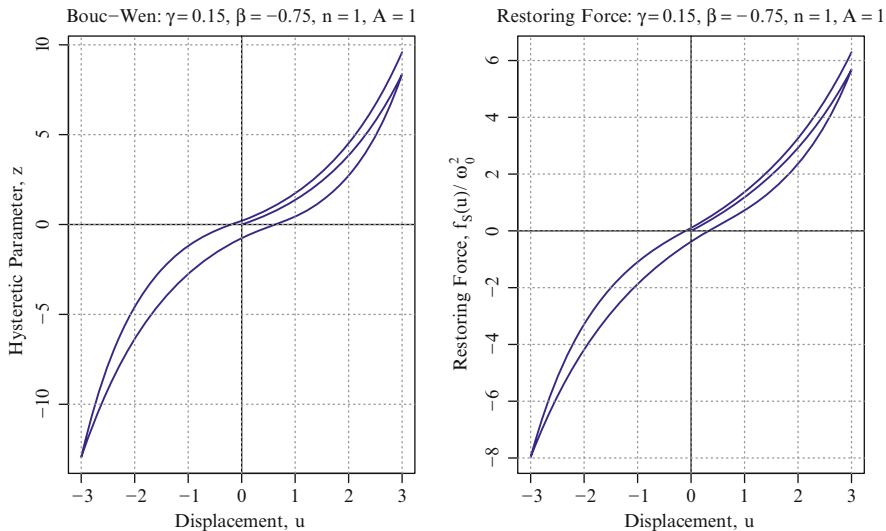


Fig. 4.10 Dependence of the hysteretic parameter z (left), and the normalised restoring force $f_S(u, \dot{u}, z)$ (right) on the displacement for the example system considered

steady-state conditions. For this sort of system we expect that the transient terms will decay according to $\exp(-\zeta\omega_0 t)$ and for these examples we have set $\zeta = 0.05$ and $\omega_0 = 1.0$ and we only look at the system response after 200 s have passed in order to compute the maximum displacement and velocity shown in Fig. 4.12. We would expect that the transient terms would have decayed to less than 0.5×10^{-5} of their initial amplitudes at the times of interest.

Figure 4.12 shows some potentially surprising behaviour for those not familiar with nonlinear dynamics and chaos. We can see that for low harmonic amplitudes we have a relatively smoothly varying maximum response and that system response is essentially predictable here. However, this is not to say that the response does not become more complex. For example, consider the upper row of Fig. 4.13 that shows the response for $B = 15$. Here we can see that the system tends towards some stable state and that we have a stable limit-cycle in the phase space. However, it has a degree of periodicity that corresponds to a loading/unloading phase for negative restoring forces.

This complexity continues to increase as the harmonic amplitude increases as can be seen in the middle row of Fig. 4.13 where we again have stable steady-state response, but also have another periodic component of unloading/reloading for both positive and negative restoring forces. While these figures show increased complexity as we move along the harmonic amplitude axis of Fig. 4.12, the system response remains stable and predictable in that we know that small changes in the value of B continues to map into small qualitative and quantitative changes to the response. However, Fig. 4.12 shows that once the harmonic amplitude reaches values of roughly $B = 53$ we suddenly have a qualitatively different behaviour. The

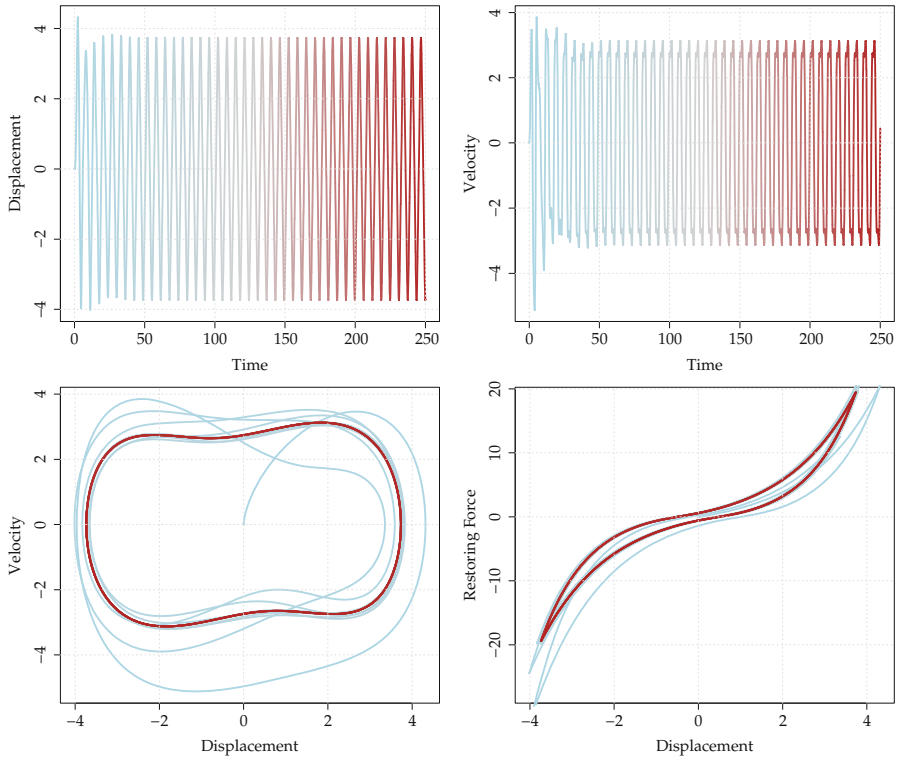


Fig. 4.11 Response of the nonlinear system for a harmonic amplitude of $B = 5$. *Upper left* panel shows the displacement time-history; *upper right* panels shows the velocity time history; *lower right* panel shows the response trajectory in phase space; and *lower right* panel shows the hysteretic response

system response now becomes extremely sensitive to the particular value of the amplitude that we consider. The reason for this can be seen in the bottom row of Fig. 4.13 in which it is clear that we never reach a stable steady state. What is remarkable in this regime is that we can observe drastically different responses for very small changes in amplitude of the forcing function. For example, when we move from $B = 65.0$ to $B = 65.1$ we have transition back into a situation in which we have a stable limit cycle (even if it is a complex cycle).

This lesson here is that for highly nonlinear processes there exist response regimes where the particular response trajectory and system state depends very strongly upon a prior state of the system. There are almost certainly aspects of the ground-motion generation process that can be described in this manner. Although these can be deterministic processes, as it is impossible to accurately define the state of the system the best we can do is to characterise the observed chaotic randomness. Note that although this is technically epistemic uncertainty, we have no choice but to treat this as aleatory variability as it is genuinely irreducible.

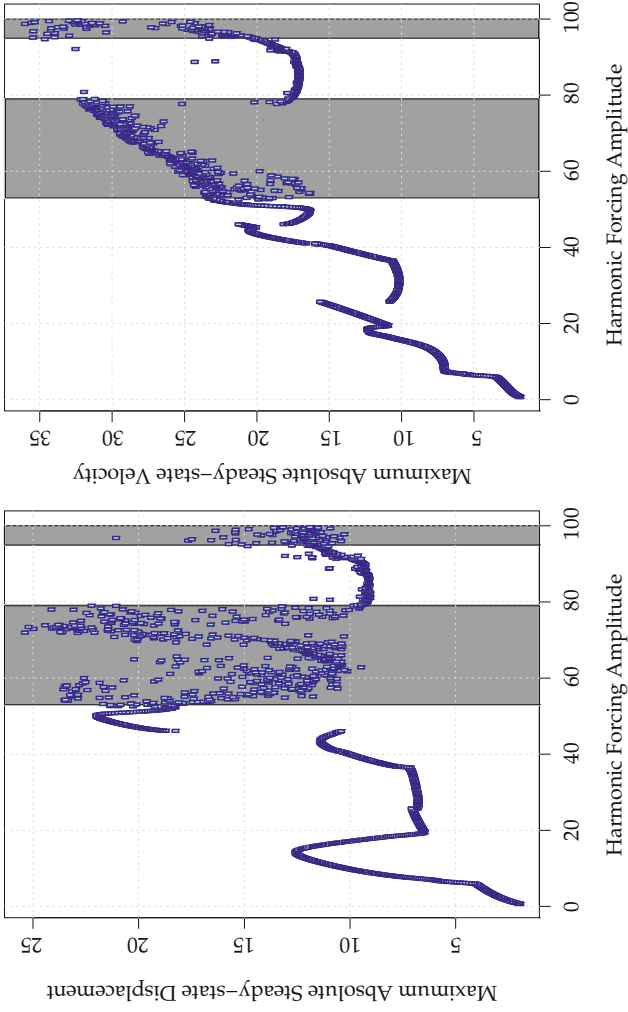


Fig. 4.12 Maximum absolute steady-state displacement (*left*) and velocity (*right*) response against the harmonic forcing amplitude B

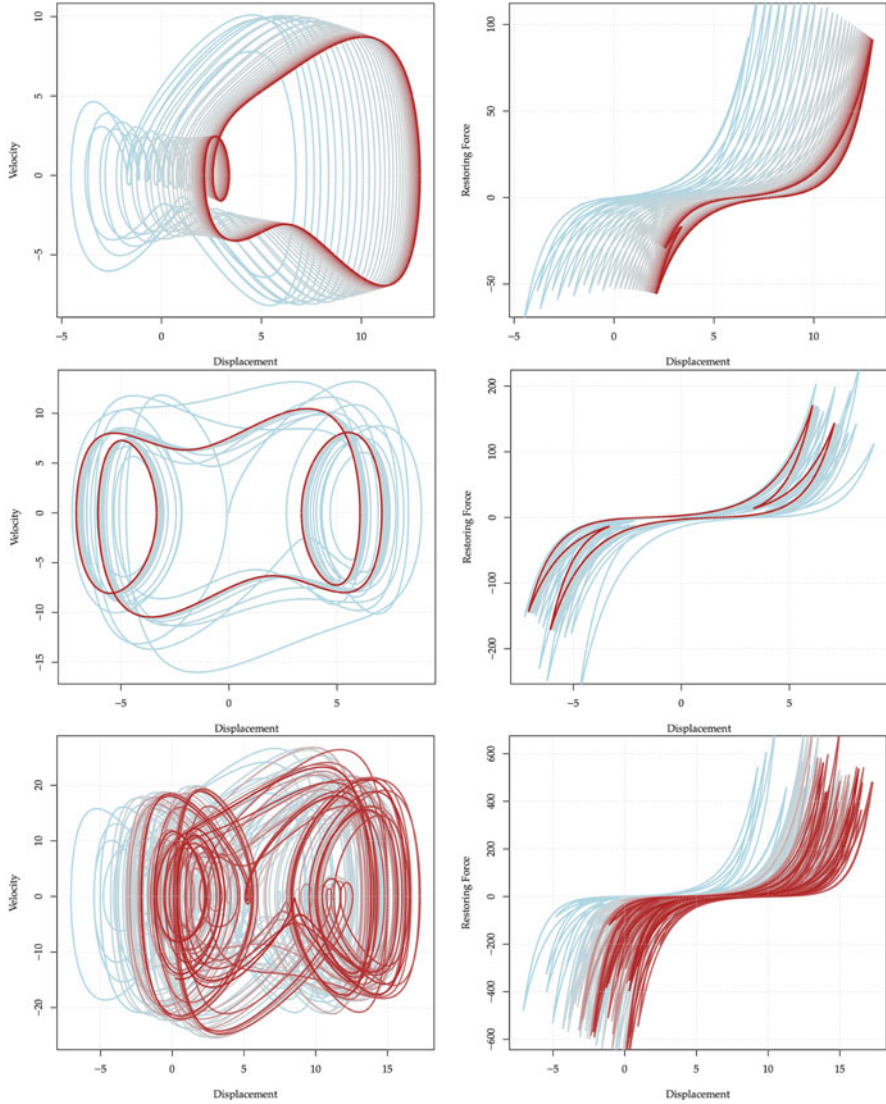


Fig. 4.13 Response of the nonlinear system for a harmonic amplitude of $B = 15$ (top), $B = 35$ (middle), and $B = 65$ (bottom). Panels on the left show the response trajectory in phase space; and panels on the right show the hysteretic response

4.4.4 Randomness Represented by Ground-Motion Models

The standard deviation that is obtained during the development of a ground-motion model definitely contains elements of epistemic uncertainty that can be regarded as apparent randomness, epistemic uncertainty that is the result of imperfect metadata,

and variability that arises from the ergodic assumption. It is also almost certain that the standard deviation reflects a degree of chaotic randomness and possibly also includes some genuine randomness and it is only these components that are actually, or practically, irreducible. Therefore, it is clear that the standard deviation of a ground-motion model does not reflect aleatory variability as it is commonly defined – as being ‘inherent variability’.

If the practical implications of making the distinction between aleatory and epistemic are to dictate what goes into the hazard integral and what goes into the logic tree then one might take the stance that of these contributors to the standard deviation just listed we should look to remove the effects of the ergodic assumption (which is attempted in practice), we should minimise the effects of metadata uncertainty (which is not done in practice), and we should increase the sophistication of our models so that the apparent randomness is reduced (which some would argue has been happening in recent years, *vis-à-vis* the NGA projects).

An example of the influence of metadata uncertainty can be seen in the upper left panel of Fig. 4.14 in which the variation in model predictions is shown when uncertainties in magnitude and shear-wave velocity are considered in the regression analysis. The boxplots in this figure show the standard deviations of the predictions for each record in the NGA dataset when used in a regression analysis with Models 1–6 that were previously presented. The uncertainty that is shown here should be regarded as a lower bound to the actual uncertainty associated with meta-data for real ground-motion models. The estimates of this variable uncertainty are obtained by sampling values of magnitude and average shear-wave velocity for each event and site assuming a (truncated) normal and lognormal distribution respectively. This simulation process enables a hypothetical dataset to be constructed upon which a regression analysis is performed. The points shown in the figure then represent the standard deviation of median predictions from each developed regression model.

Figure 4.14 also shows how an increase in model complexity is accompanied by an increase in parametric uncertainty for the models presented previously. It should be noted that these estimates of parametric uncertainty are also likely to be near lower bounds given that the functional forms used for this exercise are relatively simple and that the dataset is relatively large (consisting of 2,406 records from the NGA database). The upper right panel of Fig. 4.14 shows this increasing parametric uncertainty for the dataset used to develop the models, but the lower panel shows the magnitude dependence of this parametric uncertainty when predictions are made for earthquake scenarios that are not necessarily covered by the empirical data. In this particular case, the magnitude dependence is shown when motions are computed for a distance of just 1 km and a shear-wave velocity of 316 m/s is used. It can be appreciated from this lower panel that the parametric uncertainty is a function of both the model complexity but also of the particular functional form adopted. The parametric uncertainty here is estimated by computing the covariance matrix of the regression coefficients and then sampling from the multivariate normal distribution implied by this covariance matrix. The simulated coefficients

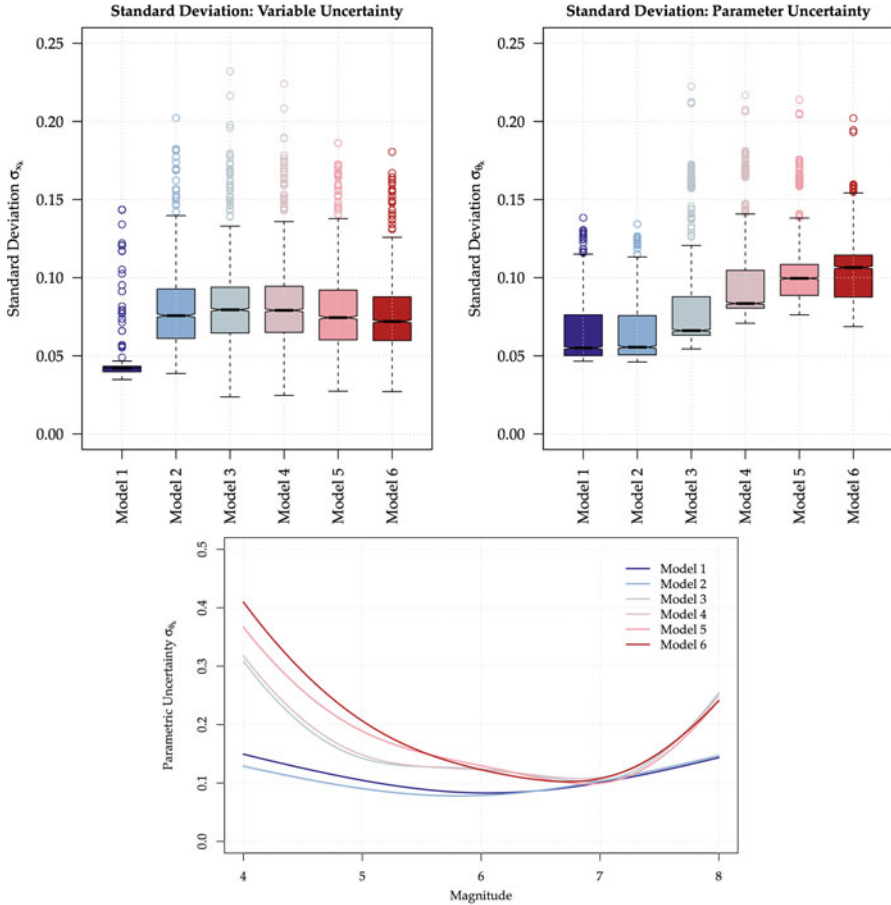


Fig. 4.14 Influence of meta-data uncertainty (*upper left*), increase in parametric uncertainty with increasing complexity of models (*upper right*), and the dependence of parametric uncertainty upon magnitude (*bottom*)

are then used to generate predictions for each recording and the points shown in this panel represent the standard deviation of these predictions for every record.

Rather than finally looking to increase the complexity of the functional forms that are used for ground-motion predictions, herein I propose that we look at this problem in a different light and refer back to Eq. (4.2) in which we say explicitly that what matters for hazard and risk is the overall estimate of ground-motion exceedance and that this is the result of two components (not just the ground-motion model). We should forget about trying to push the concept that only aleatory variability should go into the hazard integral and rather take the viewpoint that our *optimal model* (which is a model of the ground motion *distribution* – not median predictions) should go into the hazard integral and that our uncertainties should then be reflected in the logic tree. The reason why we should forget about only pushing

aleatory variability into the hazard integral is that from a quantitative ground-motion perspective we are still not close to understanding what is actually aleatory and irreducible.

The proposed alternative of defining an *optimal model* is stated in the light of minimising the uncertainty in the estimate of the probability of exceedance of ground-motions. This uncertainty comes from two components: (1) our ability to accurately define the probability of occurrence of earthquake scenarios; and (2) our ability to make robust predictions of the conditional ground-motion distribution. Therefore, while a more complex model will act to reduce the apparent variability, if this same model requires the specification of a number of independent variables that are poorly constrained in practice then the overall uncertainty will be large. In such cases, one can obtain a lower level of overall uncertainty in the prediction of ground-motion exceedance by using a less complex ground-motion model. A practical example of this trade-off is related to the requirement to define the depth distribution of earthquake events. For most hazard analyses this depth distribution is poorly constrained and the inclusion of depth-dependent terms in ground-motion models only provides a very small decrease in the apparent variability.

Figure 4.15 presents a schematic illustration of the trade-offs between apparent randomness (the epistemic uncertainty that is often regarded as aleatory variability) and parametric uncertainty (the epistemic uncertainty that is usually ignored) that exist just on the ground-motion modelling side. The upper left panel of this figure shows, as we have seen previously, that the apparent randomness decreases as we increase the complexity of our model. However, the panel also shows that this reduction saturates once we reach the point where we have chaotic randomness, inherent randomness, or a combination of these irreducible components. The upper right panel, on the other hand, shows that as this model complexity increases we also observe an increase in parametric uncertainty. The optimal model must balance these two contributors to the overall uncertainty as shown in the lower left panel. On this basis, one can identify an optimal model when only ground-motion modelling is considered. When hazard or risk is considered then the parametric uncertainty shown here should reflect both the uncertainty in the model parameters (governed by functional form complexity, and data constraints) and the uncertainty associated with the characterisation of the scenario (*i.e.*, the independent variables) and its likelihood.

The bottom right panel of Fig. 4.15 shows how one can justify an increased complexity in the functional form when the parametric uncertainty is reduced, as in this case the optimal complexity shifts to the right. To my knowledge, these sorts of considerations have never been explicitly made during the development of more complex ground-motion models. Although, in some ways, the quantitative inspection of residual trends and of parameter p -values is an indirect way of assessing if increased complexity is justified by the data.

Recent years have seen the increased use of external constraint during ground-motion model development. In particular, numerical simulations are now commonly undertaken in order to constrain nonlinear site response scaling, large

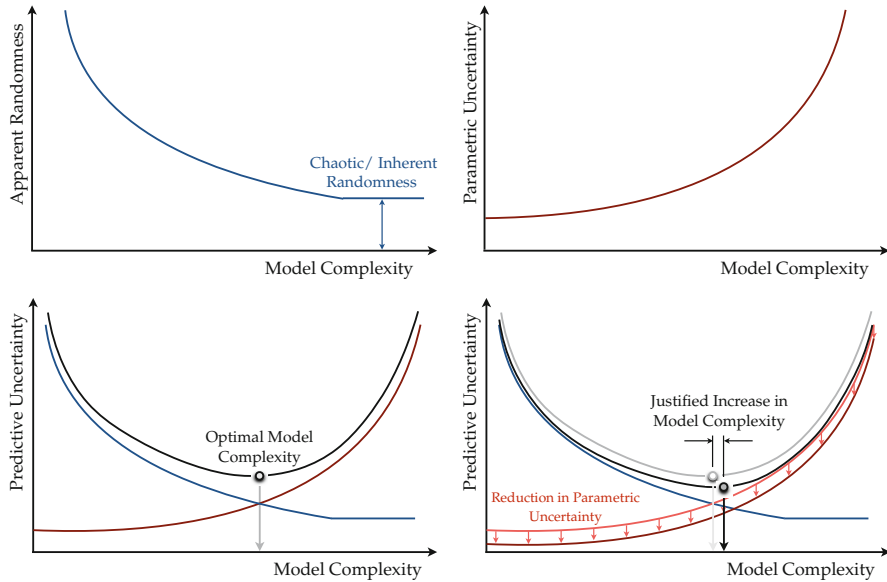


Fig. 4.15 Schematic illustration of the trade-off that exists between the reduction in apparent randomness (*upper left*) and the increase in parametric uncertainty (*upper right*). The optimal model in this context balances the two components (*lower left*) and an increase in complexity is justified when parametric uncertainty is reduced (*lower right*)

magnitude scaling, and near field effects. Some of the most recent models that have been presented have very elaborate functional forms and the model developers have justified this additional complexity on the basis of the added functional complexity being externally constrained. In the context of Fig. 4.15, the implication is that the model developers are suggesting that the red curves do not behave in this manner, but rather that they saturate at some point as all of the increasing complexity does not contribute to parametric uncertainty. On one hand, the model developers are correct in that the application of external constraints does not increase the estimate of the parametric uncertainty *from the regression analysis on the free parameters*. However, on the other hand, in order to properly characterise the parametric uncertainty the uncertainty associated with the models used to provide the external constraint must also be accounted for. In reality this additional parametric uncertainty is actually larger than what would be obtained from a regression analysis because the numerical models used for these constraints are normally very complex and involve a large number of poorly constrained parameters. Therefore, it is not clear that the added complexity provided through the use of external constraints is actually justified.

4.5 Discrete Random Fields for Spatial Risk Analysis

The coverage thus far has been primarily focussed upon issues that arise most commonly within hazard analysis, but that are also relevant to risk analysis. However, in this final section the attention is turned squarely to a particular issue associated with the generation of ground-motion fields for use in earthquake loss estimation for spatially-distributed portfolios. This presentation is based upon the work of Vanmarcke (1983) and has only previously been employed by Stafford (2012).

The normal approach that is taken when performing risk analyses over large spatial regions is to subdivide the region of interest into geographic cells (often based upon geopolitical boundaries, such as districts, or postcodes). The generation of ground-motion fields is then made by sampling from a multivariate normal distribution that reflects the joint intra-event variability of epsilon values across a finite number of sites equal to the number of geographic cells. The multivariate normal distribution for epsilon values is correctly assumed to have a zero mean vector, but the covariance matrix of the epsilon values is computed using a combination of the point-to-point distances between the centroids of the cells (weighted geographically, or by exposure) and a model for spatial correlation between two points (such as that of Jayaram and Baker 2009). The problem with this approach is that the spatial discretisation of the ground-motion field has been ignored. The correct way to deal with this problem is to discretise the random field to account for the nature of the field over each geographic cell and to define a covariance matrix for the average ground-motions over the cells. This average level of ground-motion over the cell is a far more meaningful value to pass into fragility curves than a single point estimate.

Fortunately, the approach for discretisation of a two-dimensional random field is well established (Vanmarcke 1983). The continuous field is denoted by $\ln y(\mathbf{x})$ where y is the ground motion and \mathbf{x} now denotes a spatial position. The logarithmic motion at a point can be represented as a linear function of the random variable $\varepsilon(\mathbf{x})$. Hence, the expected value of the ground motion field at a given point is defined by Eq. (4.25), where $\mu_{\ln y}$ is the median ground motion, and η is an event term.

$$E[\ln y(\mathbf{x})] = \mu_{\ln y} + \eta + E[\varepsilon(\mathbf{x})] \quad (4.25)$$

Therefore, in order to analyse the random field of ground motions, attention need only be given to the random field of epsilon values. Once this field is defined it may be linearly transformed into a representation of the random field of spectral ordinates.

In order to generate ground-motion fields that account for the spatial discretisation, under the assumption of joint normality, we require three components:

- An expression for the average mean logarithmic motion over a geographic cell
- An expression for the variance of motions over a geographic cell
- An expression for the correlation of average motions from cell-to-cell

For the following demonstration, assume that the overall region for which we are conducting the risk analysis is discretised into a regular grid aligned with the N-S and E-W directions. This grid has a spacing (or dimension) in the E-W direction of D_1 and a spacing in the N-S direction of D_2 . Note that while the presentation that follows concerns this regular grid, Vanmarcke (1983) shows how to extend this treatment to irregularly shaped regions (useful for regions defined by postcodes or suburbs, *etc.*).

Within each grid cell one may define the local average of the field by integrating the field and dividing by the area of the cell ($A = D_1 D_2$).

$$\ln y_A = \frac{1}{A} \int_A \ln y(\mathbf{x}) d\mathbf{x} \quad (4.26)$$

Now, whereas the variance of the ground motions for a single point in the field, given an event term, is equal to σ^2 , the variance of the local average $\ln y_A$ must be reduced as a result of the averaging. Vanmarcke (1983) shows that this reduction can be expressed as in Eq. (4.27).

$$\sigma_A^2 = \gamma(D_1, D_2) \sigma^2 \quad \rightarrow \quad \gamma(D_1, D_2) = \frac{1}{D_1 D_2} \int_{-D_2}^{D_2} \int_{-D_1}^{D_1} \left(1 - \frac{|\delta_1|}{D_1}\right) \left(1 - \frac{|\delta_2|}{D_2}\right) \rho(\delta_1, \delta_2) d\delta_1 d\delta_2 \quad (4.27)$$

In Eq. (4.27), the correlation between two *points* within the region is denoted by $\rho(\delta_1, \delta_2)$, in which δ_1 and δ_2 are orthogonal co-ordinates defining the relative positions of two points within a cell. In practice, this function is normally defined as in Eq. (4.28) in which b is a function of response period.

$$\rho(\delta_1, \delta_2) = \exp\left(-\frac{3\sqrt{\delta_1^2 + \delta_2^2}}{b}\right) \quad (4.28)$$

The reduction in variance associated with the averaging of the random field is demonstrated in Fig. 4.16 in which values of $\gamma(D_1, D_2)$ are shown for varying values of the cell dimension and three different values of the range parameter b . For this example the cells are assumed to be square.

With the expressions for the spatial average and the reduced variance now given, the final ingredient that is required is the expression for the correlation between the average motions over two cells (rather than between two points). This is provided in Eq. (4.29), with the meaning of the distances D_{1k} and D_{2l} shown in Fig. 4.17.

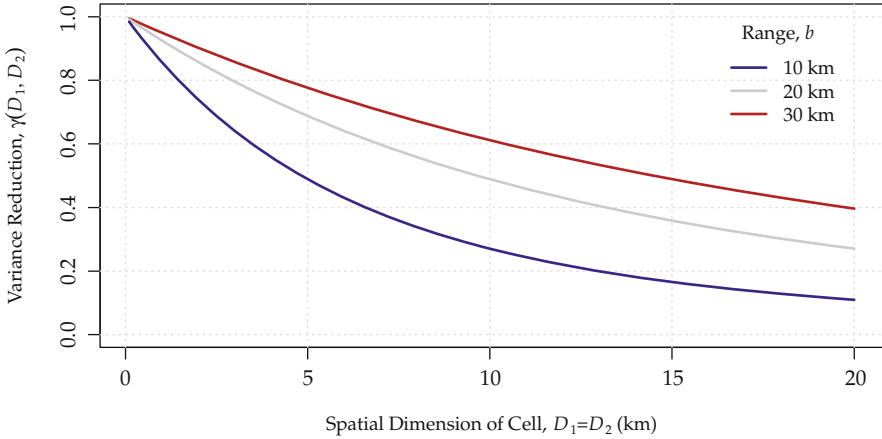


Fig. 4.16 Variance function for a regular square grid

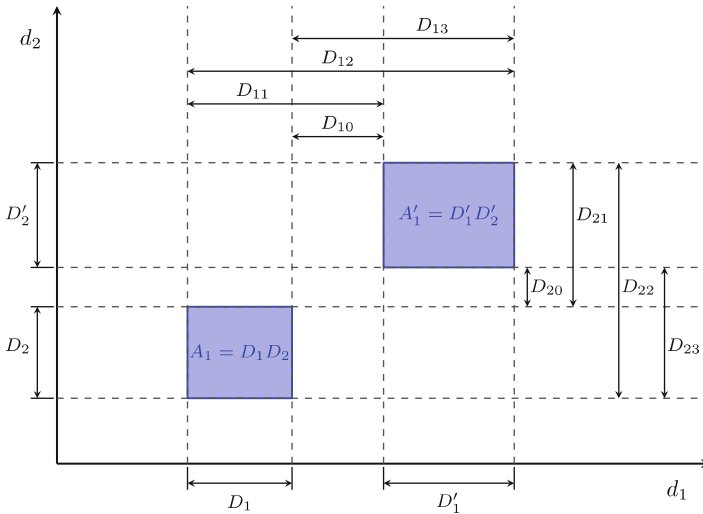


Fig. 4.17 Definition of geometry used in Eq. (4.29) (Redrawn from Vanmarcke (1983))

$$\rho(\ln y_{A_1}, \ln y_{A_2}) = \frac{\sigma^2}{4A_1 A_2 \sigma_{A_1} \sigma_{A_2}} \sum_{k=0}^3 \sum_{l=0}^3 (-1)^k (-1)^l (D_{1k} D_{2l})^2 \gamma(D_{1k}, D_{2l}) \quad (4.29)$$

The correlations that are generated using this approach are shown in Fig. 4.18 both in terms of the correlation against separation distance of the cell centroids and in terms of the correlation against the separation measured in numbers of cells. Figure 4.18 shows that the correlation values can be significantly higher than the corresponding point-estimate values (which lie close to the case for the smallest

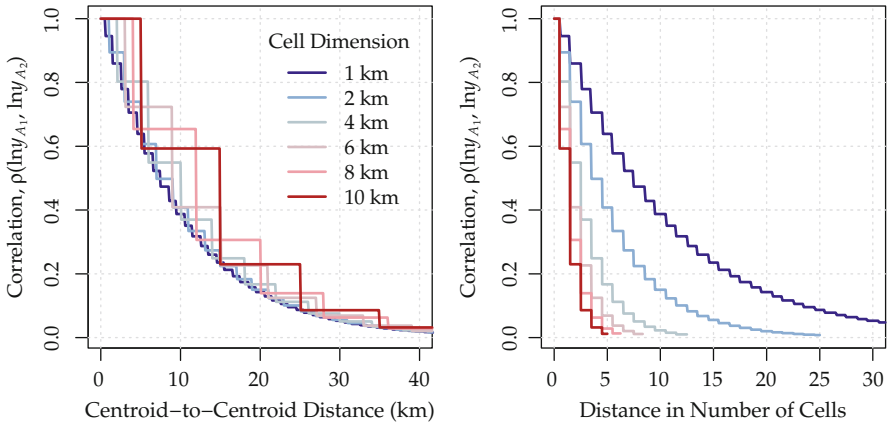


Fig. 4.18 Example correlations computed using Eq. (4.29) for square cells of differing dimension

dimension shown). However, the actual covariances do not differ as significantly due to the fact that these higher correlations must be combined with the reduced variances.

4.6 Conclusions

Empirical ground-motion modelling is in a relatively mature state, but the historical emphasis has been biased towards median predictions with the result that the characterisation of ground-motion variability has been somewhat neglected. This paper emphasises the importance of the variance of the ground-motion distribution and quantifies the sensitivity of hazard results to this variance. The partitioning of total uncertainty in ground-motion modelling among the components of aleatory and epistemic uncertainty is also revisited and a proposal is made to relax the definitions that are often blindly advocated, but not properly understood. A new approach for selecting an optimal model complexity is proposed. Finally, a new framework for generating correlated discrete random fields is presented.

Open Access This chapter is distributed under the terms of the Creative Commons Attribution Noncommercial License, which permits any noncommercial use, distribution, and reproduction in any medium, provided the original author(s) and source are credited.

References

- Campbell KW, Bozorgnia Y (2008) NGA ground motion model for the geometric mean horizontal component of PGA, PGV, PGD and 5 %-damped linear-elastic response spectra for periods ranging from 0.01 to 10.0 s. *Earthq Spectra* 24:139–171
- Campbell KW, Bozorgnia Y (2014) NGA-West2 ground motion model for the average horizontal components of PGA, PGV, and 5%-damped linear acceleration response spectra. *Earthq Spectra*. <http://dx.doi.org/10.1193/062913EQS175M>
- Chiou BSJ, Youngs RR (2008) An NGA model for the average horizontal component of peak ground motion and response spectra. *Earthq Spectra* 24:173–215
- Chiou BSJ, Youngs RR (2014) Update of the Chiou and Youngs NGA model for the average horizontal component of peak ground motion and response spectra. *Earthq Spectra*. <http://dx.doi.org/10.1193/072813EQS219M>
- Der Kiureghian A, Ditlevsen O (2009) Aleatory or epistemic? Does it matter? *Struct Saf* 31:105–112
- Elms DG (2004) Structural safety – issues and progress. *Prog Struct Eng Mat* 6:116–126
- Jayaram N, Baker JW (2009) Correlation model for spatially distributed ground-motion intensities. *Earthq Eng Struct D* 38:1687–1708
- Li H, Meng G (2007) Nonlinear dynamics of a SDOF oscillator with Bouc-Wen hysteresis. *Chaos Soliton Fract* 34:337–343
- Stafford PJ (2012) Evaluation of the structural performance in the immediate aftermath of an earthquake: a case study of the 2011 Christchurch earthquake. *Int J Forensic Eng* 1(1):58–77
- Vanmarcke E (1983) *Random fields, analysis and synthesis*. The MIT Press, Cambridge, MA

Chapter 5

Seismic Code Developments for Steel and Composite Structures

Ahmed Y. Elghazouli

Abstract As with other codified guidance, seismic design requirements undergo a process of continuous evolution and development. This process is usually guided by improved understanding of structural behaviour based on new research findings, coupled with the need to address issues identified from the practical application of code procedures in real engineering projects. Developments in design guidance however need to balance detailed technical advancements with the desire to maintain a level of practical stability and simplicity in codified rules. As a result, design procedures inevitably incorporate various simplifications and idealisations which can in some cases have adverse implications on the expected seismic performance and hence on the rationale and reliability of the design approaches. With a view to identifying the needs for future seismic code developments, this paper focuses on assessing the underlying approaches and main procedures adopted in the seismic design of steel and composite framed structures, with emphasis on the current European seismic design code, Eurocode 8. Codified requirements in terms of force reduction factors, ductility considerations, capacity design verifications, and connection design procedures, are examined. Various requirements that differ notably from other international seismic codes, particularly those incorporated in North American provisions, are also pointed out. The paper highlights various issues related to the seismic design of steel and composite frames that can result in uneconomical or impractical solutions, and outlines several specific seismic code development needs.

5.1 Introduction

Steel and composite steel/concrete structures may be designed based on EC8 (Eurocode 8 2005) according to either non-dissipative or dissipative behaviour. The former is normally limited to areas of low seismicity or to structures of special

A.Y. Elghazouli (✉)

Department of Civil and Environmental Engineering, Imperial College London, London, UK
e-mail: a.elghazouli@imperial.ac.uk

© The Author(s) 2015

A. Ansal (ed.), *Perspectives on European Earthquake Engineering and Seismology*,
Geotechnical, Geological and Earthquake Engineering 39,
DOI 10.1007/978-3-319-16964-4_5

129

use and importance, although it could also be applied for higher seismicity areas if vibration reduction or isolation devices are incorporated. Otherwise, the code aims to achieve economical design by employing dissipative behaviour which, apart from for special irregular or complex structures, is usually performed by assigning a structural behaviour factor to reduce the code-specified forces resulting from idealised elastic response spectra. This is carried out in conjunction with the capacity design concept which requires an appropriate determination of the capacity of the structure based on a pre-defined plastic mechanism, coupled with the provision of sufficient ductility in plastic zones and adequate over-strength factors for other regions.

This paper examines the dissipative seismic design provisions for steel and composite framed structures, which are mainly covered in Part 1 (general rules, seismic actions and rules for buildings) of Eurocode 8 (2005). General provisions in other sections of EC8 Part 1 are also referred to where relevant. Additionally, where pertinent, reference is made to US procedures for the seismic design of steel and composite structures (ASCE7 2010; AISC341 2010). The assessment focuses on the behaviour factors, ductility considerations, capacity design rules and connection design requirements stipulated in EC8. Particular issues that warrant clarification or further developments are highlighted and discussed.

5.2 Behaviour Factors

EC8 focuses essentially on three main structural steel frame systems, namely moment resisting, concentrically braced and eccentrically braced frames. Other systems such as hybrid and dual configurations are referred to in EC8, but limited information is provided. It should also be noted that additional configurations such as those incorporating buckling restrained braces, truss moment frames or special plate shear walls, which are covered in recent US provisions, are not directly addressed in the current version of EC8.

The behaviour factors are typically recommended by codes of practice based on background research involving extensive analytical and experimental investigations. The reference behaviour factors (q) stipulated in EC8 for steel-framed structures are summarised in Table 5.1. These are upper values of q allowed for each system, provided that regularity criteria and capacity design requirements are met. For each system, the dissipative zones are specified in the code (e.g. beam ends, diagonals, link zones in moment, concentrically braced and eccentrically braced frames, respectively). The multiplier α_u/α_1 depends on the failure/first plasticity resistance ratio of the structure, and can be obtained from push-over analysis (but should not exceed 1.6). Alternatively, default code values can be used to determine q (as given in parenthesis in Table 5.1).

Table 5.1 Behaviour factors in European and US Provisions

European Provisions	Ductility class	q	q_d
Non-dissipative	DCL	1.5	1.5
Moment frames	DCM	4.0	4.0
	DCH	$5 \alpha_u/\alpha_1$ (5.5–6.5)	$5 \alpha_u/\alpha_1$ (5.5–6.5)
Concentric braced	DCM	4.0	4.0
	DCH	4.0	4.0
V-braced	DCM	2.0	2.0
	DCH	2.5	2.5
Eccentrically braced	DCM	4.0	4.0
	DCH	$5 \alpha_u/\alpha_1$ (6.0)	$5 \alpha_u/\alpha_1$ (6.0)
Dual moment-concentric braced	DCM	4.0	4.0
	DCH	$4 \alpha_u/\alpha_1$ (4.8)	$4 \alpha_u/\alpha_1$ (4.8)
US Provisions	Frame type	R	C_d
Non-dissipative	Non-seismic detailing	3.0	3.0
Moment frames (steel)	OMF	3.5	3.0
	IMF	4.5	4.0
	SMF	8.0	5.5
Moment frames (composite)	C-OMF	3.0	2.5
	C-IMF	5.0	4.5
	C-SMF	8.0	5.5
	C-PRMF	6.0	5.5
Concentric braced (steel)	OSCBF	5.0	4.5
	SSCBF	6.0	5.0
Concentric braced (composite)	C-OCBF	3.0	3.0
	C-SCBF	5.0	4.5
Eccentrically braced	EBF(MC ^a)	8.0	4.0
	EBF(non-MC ^a)	7.0	4.0
Eccentrically braced (composite)	C-EBF	8.0	4.0
Dual moment-braced	Various detailed systems	4.0–8.0	3.0–6.5

^aMC refers to moment beam-to-column connections away from the links

The same upper limits of the reference behaviour factors specified in EC8 for steel framed structures are also employed for composite structures. This applies to composite moment resisting frames, composite concentrically braced frames and composite eccentrically braced frames. However, a number of additional composite structural systems are also specified, namely: steel or composite frames with connected infill concrete panels, reinforced concrete walls with embedded vertical steel members acting as boundary/edge elements, steel or composite coupling beams in conjunction with reinforced concrete or composite steel/concrete walls, and composite steel plate shear walls. These additional systems are beyond the scope of the discussions in this paper which focuses on typical frame configurations.

Although a direct comparison between codes can only be reliable if it involves the full design procedure, the reference q factors in EC8 appear generally lower than R values in US provisions for similar frame configurations as depicted in Table 5.1. It is also important to note that the same force-based behaviour factors (q) are typically proposed as displacement amplification factors (q_d) in EC8. This is not the case in US provisions where specific seismic drift amplification factors (C_d) are suggested; these values appear to be generally lower than the corresponding R factors for most frame types. Recent research studies on inelastic seismic drift demands in moment frames (Kumar et al. 2013; Elghazouli et al. 2014) suggest that the EC8 approach is generally over-conservative compared to the US provisions in most cases, and improved prediction methods which account for earthquake characteristics are proposed.

It is also noteworthy that US provisions include the use of a ‘system over-strength’ parameter (Ω_o , typically 2.0–3.0) as opposed to determining the level of over-strength within the capacity design procedures in the case of EC8. Other notable differences include the relatively low q assigned to V-braced frames in EC8, in contrast with the US provisions which adopt the same R values used for conventional concentric bracing. To this end, there seems to be a need to improve the guidance provided in EC8 on behaviour factors, particularly for braced and dual frames, and to extend it to other forms such as ‘zipper’ and ‘buckling restrained’ configurations.

5.3 Local Ductility

EC8 explicitly stipulates three ductility classes, namely DCL, DCM and DCH referring to low, medium and high dissipative structural behaviour, respectively. For DCL, global elastic analysis can be adopted alongside non-seismic detailing. The recommended reference ‘ q ’ factor for DCL is 1.5–2.0. In contrast, structures in DCM and DCH need to satisfy specific requirements primarily related to ensuring sufficient ductility in the main dissipative zones. The application of a behaviour factor larger than 1.5–2.0 must be coupled with sufficient local ductility within the critical dissipative zones. For buildings which are not seismically isolated or incorporating effective dissipation devices, design to DCL is only recommended for low seismicity areas. It should be noted however that this recommendation can create difficulties in practice (ECCS 2013), particularly for special or complex structures. Although suggesting the use of DCM or DCH for moderate and high seismicity often offers an efficient approach to providing ductility reserve against uncertainties in seismic action, achieving a similar level of reliability could be envisaged through the provision of appropriate levels of over-strength, possibly coupled with simple inherent ductility provisions where necessary.

5.3.1 Steel Sections

For steel elements in compression or bending, local ductility is ensured in EC8 by restricting the width-to-thickness (c/t or b/t) ratios within the section to avoid local buckling and hence reduce the susceptibility to low cycle fatigue and fracture. The classification used in EC3 (Eurocode 3 2005) is adopted but with restrictions related to the value of the q factor (DCM: Class 1, 2, 3 for $1.5 < q \leq 2.0$, or Class 1, 2 for $2.0 < q \leq 4$; DCH: Class 1 for $q > 4$).

Comparison between width-to-thickness limits in EC8 and AISC reveals some notable differences (Elghazouli 2010). Figure 5.1, compares the ‘seismically-compact’ limits (λ_{ps}) in AISC with Class 1 width-to-thickness requirements in EC3/EC8. Whilst the limits for flange outstands in compression are virtually identical, there are significant differences for circular (CHS) and rectangular (RHS) hollow sections, which are commonly used for bracing and column members. For both CHS and RHS, the limits of λ_{ps} are significantly more stringent than Class 1, with the limit being nearly double in the case of RHS. Although the q factors for framed systems are generally lower than R factors in most cases, the differences in cross-section limits in the two codes are significantly more severe. This suggests that tubular members satisfying the requirements of EC8 are likely to be more vulnerable to local buckling and ensuing fracture in comparison with those designed to AISC. There seems to be a need for further assessment of the adequacy of various EC3 section classes in satisfying the cyclic demands imposed under realistic seismic conditions.

5.3.2 Composite Sections

EC8 refers to three general design concepts for composite steel/concrete structures: (i) *Concept a*: low-dissipative structural behaviour – which refers to DCL in the same manner as in steel structures; (ii) *Concept b*: dissipative structural behaviour with composite dissipative zones for which DCM and DCH design can be adopted with additional rules to satisfy ductility and capacity design requirements; *Concept c*: dissipative structural behaviour with steel dissipative zones, and therefore specific measures are stipulated to prevent the contribution of concrete under seismic conditions; in this case, critical zones are designed as steel, although other ‘non-seismic’ design situations may consider composite action to Eurocode 4 (2004).

For dissipative composite zones (i.e. *Concept b*), the beneficial presence of the concrete parts in delaying local buckling of the steel components is accounted for by relaxing the width-to-thickness ratio as indicated in Table 5.2 which is adapted from EC8. In the table, partially encased elements refer to sections in which concrete is placed between the flanges of I or H sections, whilst fully encased elements are those in which all the steel section is covered with concrete. The cross-section limit c/t_f refers to the slenderness of the flange outstand of length c and

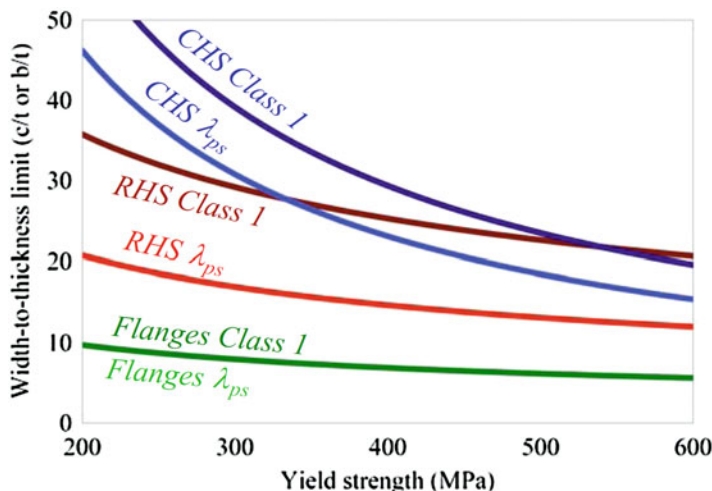


Fig. 5.1 Comparison of width-to-thickness requirements for high ductility

Table 5.2 Cross-section limits for composite sections in EC8

Ductility classes	Partially or fully encased sections	Concrete filled rectangular sections	Concrete filled circular sections
DCM ($q \leq 1.5-2.0$)	$c/t_f \leq 20 \sqrt{235/f_y}$	$h/t \leq 52 \sqrt{235/f_y}$	$d/t \leq 90 (235/f_y)$
DCM ($1.5-2.0 \leq q \leq 4.0$)	$c/t_f \leq 14 \sqrt{235/f_y}$	$h/t \leq 38 \sqrt{235/f_y}$	$d/t \leq 85 (235/f_y)$
DCM ($q > 4.0$)	$c/t_f \leq 9 \sqrt{235/f_y}$	$h/t \leq 24 \sqrt{235/f_y}$	$d/t \leq 80 (235/f_y)$

thickness t_f . The limits in hollow rectangular steel sections filled with concrete are represented in terms of h/t , which is the ratio between the maximum external dimension h and the tube thickness t . Similarly, for filled circular sections, d/t is the ratio between the external diameter d and the tube thickness t . As in the case of steel sections, notable differences also exist between the limits in EC8 for composite sections when compared with equivalent US provisions. Also, it should be noted that the limits in Table 5.2 for partially encased sections (Elghazouli and Treadway 2008) may be relaxed even further if special additional details are provided to delay or inhibit local buckling as indicated in Fig. 5.2 (Elghazouli 2009).

For beams connected to slabs, a number of requirements are stipulated in EC8 in order to ensure satisfactory performance as dissipative composite elements (i.e. for *Concept b*). These requirements comprise several criteria including those related to the degree of shear connection, ductility of the cross-section and effective width assumed for the slab. As in other codes, EC8 aims to ensure ductile behaviour in composite sections by limiting the maximum compressive strain that can be imposed on concrete in the sagging moment regions of the dissipative zones. This

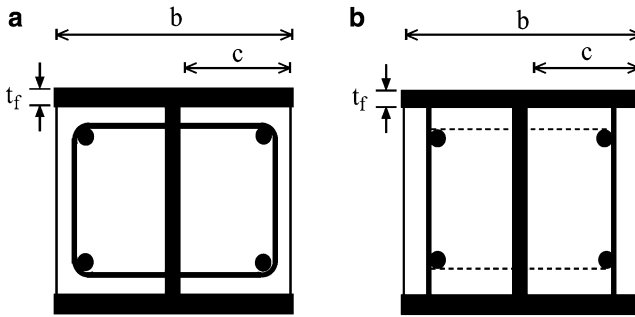


Fig. 5.2 Partially encased composite sections: (a) conventional, (b) with welded bars

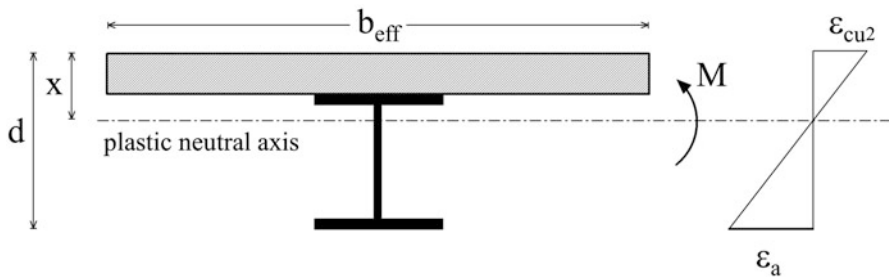


Fig. 5.3 Ductility and effective width of composite beam sections

is achieved by limiting the maximum ratio of x/d , as shown in Fig. 5.3. Limiting ratios are provided as a function of the ductility class (DCM or DCH) and yield strength of steel (f_y). Close observation suggests that these limits are derived based on assumed values for ϵ_{cu2} of 0.25 % and ϵ_a of $q \times \epsilon_y$, where ϵ_y is the yield strain of steel.

For dissipative zones of composite beams within moment frames, EC8 requires the inclusion of ‘seismic bars’ in the slab at the beam-to-column connection region. The objective is to incorporate ductile reinforcement detailing to ensure favourable dissipative behaviour in the composite beams. The detailed rules are given in Annex C of Part 1 and include reference to possible mechanisms of force transfer in the beam-to-column connection region of the slab. The provisions are largely based on background European research involving detailed analytical and experimental studies (Plumier et al. 1998). It should be noted that Annex C of the code only applies to frames with rigid connections in which the plastic hinges form in the beams; the provisions in the annex are not intended, and have not been validated, for cases with partial strength beam-to-column connections.

Another important consideration related to composite beams is the extent of the effective width b_{eff} assumed for the slab, as indicated also in Fig. 5.3. EC8 includes two tables for determining the effective width. These values are based on the condition that the slab reinforcement is detailed according to the provisions of Annex C since the same background studies (Plumier et al. 1998; Doneux and

Plumier 1999) were used for this purpose. The first table gives values for negative (hogging) and positive (sagging) moments for use in establishing the second moment of area for elastic analysis. These values vary from zero to 10 % of the beam span depending on the location (interior or exterior column), the direction of moment (negative or positive) and existence of transverse beams (present or not present). On the other hand, the second table in the code provides values for use in the evaluation of the plastic moment resistance. The values in this case are as high as twice those suggested for elastic analysis. They vary from zero to 20 % of the beam span depending on the location (interior or exterior column), the sign of moment (negative or positive), existence of transverse beams (present or not present), condition of seismic reinforcement, and in some cases on the width and depth of the column cross-section. Clearly, design cases other than the seismic situation would require the adoption of the effective width values stipulated in EC4. Therefore, the designer may be faced with a number of values to consider for various scenarios. Nevertheless, since the sensitivity of the results to these variations may not be significant (depending on the design check at hand), some pragmatism in using these provisions appears to be warranted. Detailed research studies (Castro et al. 2007) indicate that the effective width is mostly related to the full slab width, although it also depends on a number of other parameters such as the slab thickness, beam span and boundary conditions.

5.4 Capacity Design Requirements

5.4.1 Moment Frames

As in other seismic codes, EC8 aims to satisfy the ‘weak beam/strong column’ concept in moment frames, with plastic hinges allowed at the base of the frame, at the top floor of multi-storey frames and for single-storey frames. To obtain ductile plastic hinges in the beams, checks are made that the full plastic moment resistance and rotation are not reduced by coexisting compression and shear forces. To satisfy capacity design, columns should be verified for the most unfavourable combination of bending moments M_{Ed} and axial forces N_{Ed} (obtained from $M_{Ed} = M_{Ed,G} + 1.1\gamma_{ov}\Omega M_{Ed,E}$, and similarly for axial loads), where Ω is the minimum over-strength in the connected beams ($\Omega_i = M_{pl,Rd}/M_{Ed,i}$). The parameters $M_{Ed,G}$ and $M_{Ed,E}$ are the bending moments in the seismic design situation due to the gravity loads and lateral earthquake forces, respectively, as shown in Fig. 5.4 (Elghazouli 2009).

The beam over-strength parameter ($\Omega = M_{pl,Rd}/M_{Ed}$) as adopted in EC8 involves a major approximation as it does not account accurately for the influence of gravity loads on the behaviour (Elghazouli 2010). This issue becomes particularly pronounced in gravity-dominated frames (i.e. with large beam spans) or in low-rise configurations (since the initial column sizes are relatively small), in which the

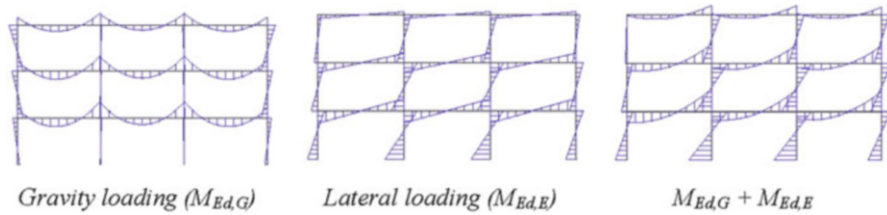


Fig. 5.4 Moment action under gravity and lateral components in the seismic situation

beam over-strength may be significantly underestimated. The extent of the problem depends on the unclear interpretation of the code and whether Ω is used in isolation or in combination with an additional capacity design criterion based on a limiting ratio of 1.3 on the column-to-beam capacity. It is also important to note that whilst codes aim to achieve a ‘weak-beam/strong-column’ behaviour, some column hinging is often unavoidable. In the inelastic range, points of contra-flexure in members change and consequently the distribution of moments vary considerably from idealised conditions assumed in design. The benefit of meeting code requirements is to obtain relatively strong columns such that beam rather than column yielding dominates over several stories, hence achieving adequate overall performance.

The above-noted issue becomes more significant in composite moment frames where relatively large spans are typical. Detailed studies on composite frames (Elghazouli et al. 2008) indicate that design to EC8 can result in significant column hinging. Full beam hinging is also significantly hampered by the difference between the sagging and hogging moment capacities in composite sections. Another uncertainty in composite moment frames is related to the effective slab width as discussed before. Whilst US provisions employ the same approaches used in non-seismic design, EC8 suggests more involved procedures for seismic design in which this width varies depending on the direction of moment, location of beam, and whether the check is for resistance or capacity design. This adds to the complexity of the design and can have a notable influence on capacity design procedures. To this end, it is important to note that the dissipative zones at the beam ends of composite moment frames can be considered as steel-only sections in EC8 (i.e. following *Concept c*). To achieve this, the slab needs to be ‘totally disconnected’ from the steel members in a circular zone with a diameter of at least $2b_{eff}$ around the columns, with b_{eff} determined on the basis of the larger effective width of the connected beams. This ‘total disconnection’ also implies that there is no contact between the slab and the sides of any vertical element such as the columns, shear connectors, connecting plates, corrugated flange, etc.

The above consideration, of disregarding the composite action and designing for steel-only dissipative zones, can be convenient in practical design. Clearly, two EI values for the beams need to be accounted for in the analysis: composite in the middle and steel at the ends. The beams are composite in the middle, hence providing enhanced stiffness and capacity under gravity loading conditions. On the other hand, in the seismic situation, the use of steel dissipative zones avoids the

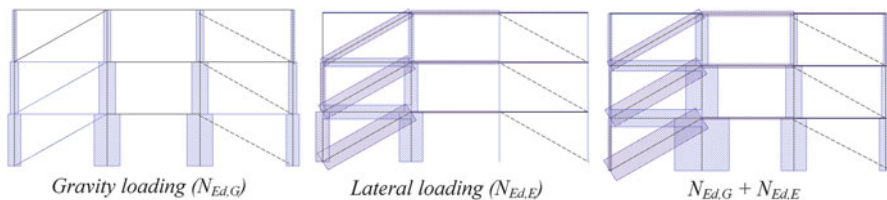


Fig. 5.5 Axial action under gravity and lateral components in the seismic situation

need for detailed considerations in the slab, including those related to seismic rebars, effective width and ductility criteria associated with composite dissipative sections. This consideration also implies that the connections would be designed on the plastic capacity of the steel beams only. Additionally, the columns need to be capacity designed for the plastic resistance of steel instead of composite beam sections, which avoids over-sizing of the column members.

5.4.2 Braced Frames

Whilst for moment frames, the dissipative zones may be steel or composite, the dissipative zones in braced frames are typically only allowed to be in steel according to EC8. In other words, the diagonal braces in concentrically braced frames, and the bending/shear links in eccentrically braced frames, should typically be designed and detailed such that they behave as steel dissipative zones. This limitation is adopted in the code as a consequence of the uncertainty associated with determining the actual capacity and ductility properties of composite steel/concrete elements in these configurations. As a result, the design of composite braced frames follows very closely those specified for steel, an issue which merits further assessment and development.

Capacity design of concentrically braced frames in EC8 is based on ensuring yielding of the diagonals before yielding or buckling of the beams or columns and before failure of the connections. Due to buckling of the compression braces, tension braces are considered to be the main ductile members, except in V and inverted-V configurations. According to EC8, columns and beams should be capacity designed for the seismic combination actions. The design resistance of the beam or column under consideration $N_{Ed}(M_{Ed})$ is determined (i.e. $N_{Ed}(M_{Ed}) \geq N_{Ed,G} + 1.1\gamma_{ov}\Omega N_{Ed,E}$) with due account of the interaction with the bending moment M_{Ed} , where $N_{Ed,G}$ and $N_{Ed,E}$, are the axial loads due to gravity and lateral actions, respectively, in the seismic design situation, as illustrated in Fig. 5.5 (Elghazouli 2009); Ω is the minimum value of axial brace over-strength over all the diagonals of the frame and γ_{ov} is the material over-strength. However, Ω of each diagonal should not differ from the minimum value by more than 25 % in order to ensure reasonable distribution of ductility. It is worth noting that unlike in moment frames, gravity

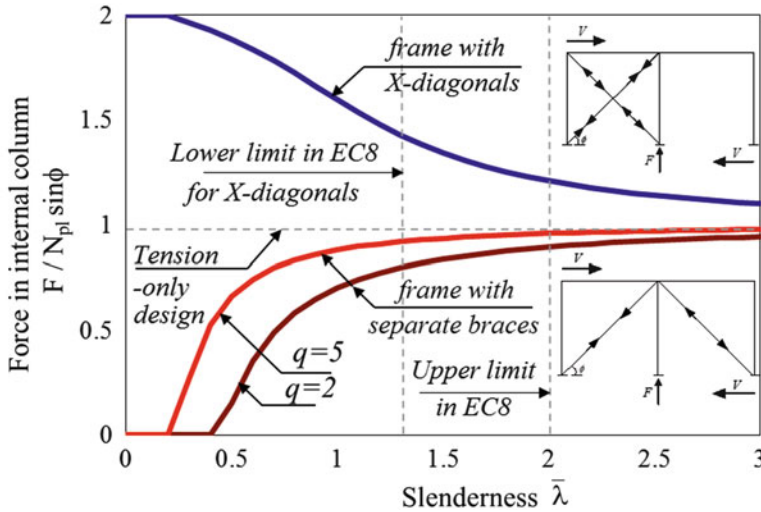


Fig. 5.6 Forces developing in columns of concentrically braced frames

loading does not normally have an influence on the accuracy of Ω . It should also be noted that the 25 % limit can result in difficulties in practical design; it can be shown (Elghazouli 2010) that this limit can be relaxed or even removed if measures related to column continuity and stiffness are incorporated in design.

As mentioned previously, US provisions (AISC341 2010) for braced frames differ from those in EC8 in terms of the R factors recommended as well as cross-section limits for some section types. However, the most significant difference is related to the treatment of the brace buckling in compression which may lead to notably dissimilar seismic behaviour depending mainly on the slenderness of the braces. This has been examined in detail in recent studies (Elghazouli 2010), and has significant implications on the frame over-strength as well as on the applied forces and ductility demand imposed on various frame components.

As expected, in the design of the diagonal members in concentrically braced frames, the non-dimensional slenderness $\bar{\lambda}$ used in EC3 plays an important role in the behaviour (Elghazouli 2003). In earlier versions of EC8, an upper limit of 1.5 was proposed to prevent elastic buckling. However, further modifications have been made in subsequent versions of EC8 and the upper limit has been revised to a value of 2.0 which results in a more efficient design. On the other hand, in frames with X-diagonal braces, EC8 stipulates that $\bar{\lambda}$ should be between 1.3 and 2.0. The lower limit is specified in order to avoid overloading columns in the pre-buckling stage of diagonals. Satisfying this lower limit can however result in significant difficulties in practical design (Elghazouli 2009). It would be more practical to avoid placing such limits, yet ensure that forces applied on components other than the braces are based on equilibrium at the joints, with due account of the relevant actions in compression. Figure 5.6 illustrates, for example, the compression force F (normalised by $N_{pl} \sin\phi$) developing in a column of X and decoupled brace

configurations (Elghazouli 2010), where N_{pl} is the axial plastic capacity of the brace cross-section and ϕ is the brace angle. These actions can be based on the initial buckling resistance (N_b) or the post-buckling reserve capacity (N_{pb}) depending on the frame configuration and design situation. Based on available experimental results (Goggins et al. 2005; Elghazouli et al. 2005), a realistic prediction of N_{pb} can be proposed (Elghazouli 2010) accounting for brace slenderness as well as expected levels of ductility.

5.4.3 Material Considerations

In addition to conforming to the requirements of EC3 and EC4, EC8 stipulates further criteria related to structural steel, connection components, and reinforcement types as well as lower and upper bounds for concrete strength, amongst others. A key consideration is determining a realistic value for the over-strength of steel material (γ_{ov}) for use in capacity design checks. A number of conditions are given in EC8 (Elghazouli 2009), but the suggested default value of 1.25 is typically adopted in practice. It is however recognised (ECCS 2013) that the level of over-strength varies significantly depending on the type and grade of steel, with the over-strength expected to be more pronounced in lower grades. As a consequence, US codes (AISC341 2010) adopt factors varying between 1.1 and 1.6, depending on the type and grade of steel. Some National Annexes to EC8 also already suggest a deviation from the recommended value of 1.25 as a function of the steel grade. Another solution would be to produce seismic steel grades with specified upper bound strength, as adopted in Japan, although this may not be practical for European manufacturers. Overall, there seems to be a need for more reliable guidance in EC8 on the levels and sources of over-strength that should be adopted in practice. Another area that requires clarification and development in EC3 and EC8 is related to the steel material toughness for application in seismic design (ECCS 2013), although this has been addressed in the National Annexes of several European countries. Specific guidance appears to be needed particularly in relation to reference temperatures and strain rates that would be appropriate to employ in seismic design situations.

5.5 Lateral Over-Strength

An important factor influencing seismic response is the over-strength exhibited by the structure. There are several sources that can introduce over-strength, such as material effects caused by a higher yield stress compared to the characteristic value as discussed in the previous section, or size effects due to the selection of members from standard lists, as in those used for steel sections. Additional factors include contribution of non-structural elements, or increase in member sizes due to other

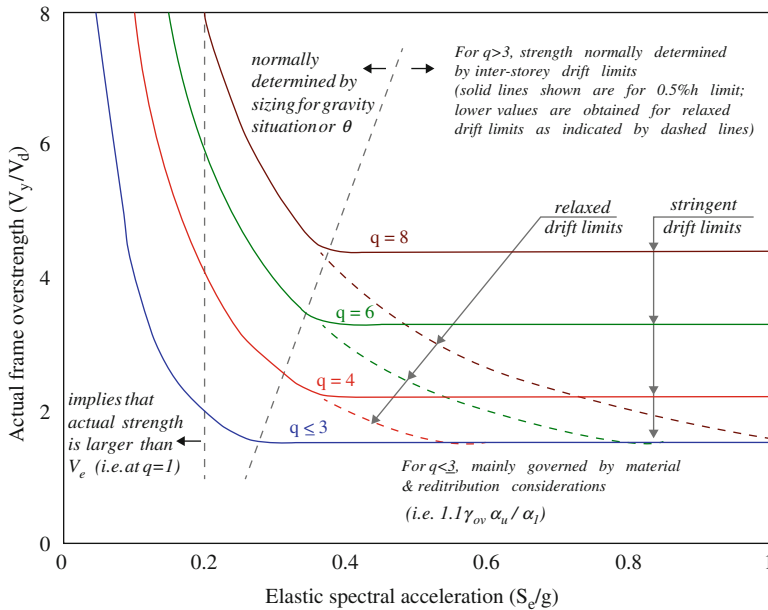


Fig. 5.7 Expected levels of lateral over-strength in moment frames

load cases or architectural considerations. Most notably, over-strength is often a direct consequence of the application of drift related requirements or inherent idealisations and simplifications within the design approaches and procedures.

5.5.1 Stability and Drift Implications

It can be shown that, in comparison with North American and other international provisions, drift-related requirements in EC8 are significantly more stringent (Elghazouli 2010). This is particularly pronounced in case of the stability coefficient θ , which is a criterion that warrants further detailed consideration. As a consequence of the stern drift and stability requirements and the relative sensitivity of framed structures, particularly moment frames, to these effects, they can often govern the design leading to considerable over-strength, especially if a large behaviour factor is assumed. This over-strength (represented as the ratio of the actual base shear V_y to the design value V_d) is also a function of the normalised elastic spectral acceleration (S_a/g) and gravity design, as illustrated in Fig. 5.7 (Elghazouli 2010).

Whereas the presence of over-strength reduces the ductility demand in dissipative zones, it also affects forces imposed on frame and foundation elements. A rational application of capacity design necessitates a realistic assessment of lateral

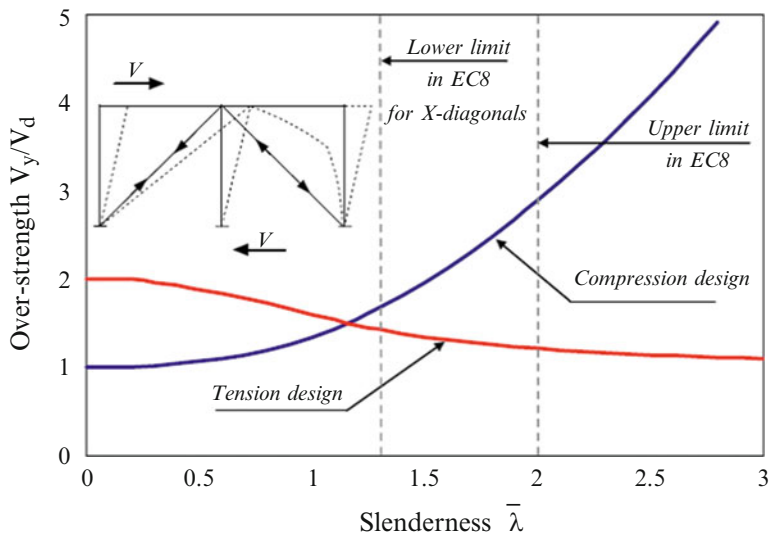


Fig. 5.8 Lateral frame over-strength arising from tension and compression design

capacity after the satisfaction of all provisions, followed by a re-evaluation of global over-strength and the required ‘ q ’. Although high ‘ q ’ factors are allowed for moment frames, in recognition of their ductility and energy dissipation capabilities, it should be noted that such a choice is often unnecessary and could lead to undesirable effects.

5.5.2 Influence of Design Idealisations

As noted above, simplifications in the design procedure can result directly in considerable levels of structural over-strength. A most significant source of over-strength in concentrically braced frames arises from the simplification associated with the treatment of brace buckling in compression. To enable the use of linear elastic analysis tools, commonly employed in design practice, two different approaches are normally adopted in design methods. Whereas several codes, such as US provisions (AISC341 2010), base the design strength on the brace buckling capacity in compression (with a few exceptions), European provisions are largely based on the brace plastic capacity in tension (except for V and inverted-V configurations).

Whilst both the tension and compression based approaches lead to frame over-strength, they have directly opposite trends with the respect to the brace slenderness (Elghazouli 2003), as illustrated in Fig. 5.8. The over-strength arising from the tension-based idealisation is insignificant for relatively slender braces but approaches a factor of two for relatively stocky braces. In contrast, the over-

strength arising from the compression design is insignificant for stocky members but increases steadily with the slenderness ratio. As noted previously, it is important to quantify the level of over-strength in a frame and assess the actual forces sustained by the braces in compression. Depending on the specific design situation and frame configuration, it may be necessary to estimate either the maximum or minimum forces attained in compression members in a more realistic manner as opposed to the idealised approaches currently adopted in seismic codes.

5.6 Connection Design

5.6.1 *Steel Moment Connections*

Steel moment frames have traditionally been designed with rigid full-strength connections, usually of fully-welded or hybrid welded/bolted configuration. Typical design provisions ensured that connections are provided with sufficient over-strength such that dissipative zones occur mainly in the beams. However, the reliability of commonly-used forms of full-strength beam-to-column connection has come under question following poor performance in large seismic events, particularly in Northridge and Kobe earthquakes (SAC 1995). The extent and repetitive nature of damage observed in several types of welded and hybrid connections have directed considerable research effort not only to repair methods for existing structures but also to alternative connection configurations to be incorporated in new designs.

Observed seismic damage to welded and hybrid connections was attributed to several factors including defects associated with weld and steel materials, welding procedures, stress concentration, high rotational demands, scale effects, as well as the possible influence of strain levels and rates (FEMA 2000). In addition to the concerted effort dedicated to improving seismic design regulations for new construction, several proposals have been forwarded for the upgrading of existing connections. As shown schematically in Fig. 5.9 (Elghazouli 2009), this may be carried out by strengthening of the connection through haunches, cover or side plates, or other means. Alternatively, it can be achieved by weakening of the beam by trimming the flanges (i.e. reduced beam section ‘RBS’ or ‘dog-bone’ connections), perforating the flanges, or by reducing stress concentrations through slots in beam webs, enlarged access holes, etc. In general, the design can be based on either prequalified connections or on prototype tests. Prequalified connections have been proposed in the US (AISC358 2010), and a similar European activity is currently underway. It should be noted however that most prequalification activities have been focusing on connections to open section columns, with comparatively less attention given to connections to tubular columns (Elghazouli and Packer 2014).

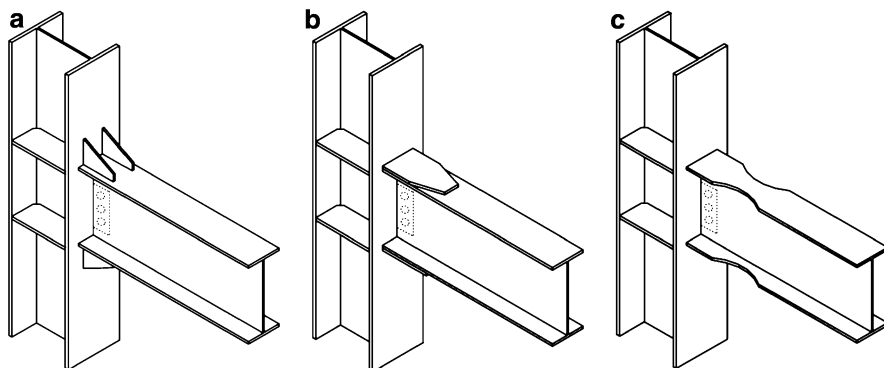


Fig. 5.9 Examples of modified moment beam-to-column connection configurations: (a) with haunches, (b) with cover plates; (c) reduced beam section

Another important aspect of connection behaviour is related to the influence of the column panel zone. This has direct implications on the ductility of dissipative zones as well as on the overall frame performance. Recent research studies (Castro et al. 2008), involved the development of realistic modelling approaches for panel zones within moment frames as well as assessment of current design procedures. One important issue is related to the treatment of the two yield points corresponding to the onset of plasticity in the column web and surrounding components, respectively. Another key design consideration is concerned with balancing the extent of plasticity between the panel zone and the connected beams, an issue which can be significantly affected by the level of gravity applied on the beams. On the one hand, allowing a degree of yielding in the panel reduces the plastic hinge rotations in the beams yet, on the other hand, relatively weak panel zone designs can result in excessive distortional demands which can cause unreliable behaviour of other connection components particularly in the welds. The approaches used in European guidance, through the combined provisions of EC3 or EC4 with EC8, appear to lead to significantly different design in comparison with that adopted in US provisions, an issue which requires further examination and development.

Bolted connections, which can be designed as rigid or semi-rigid, can alleviate many of the drawbacks of welded forms (Elghazouli 2009). However, the guidance for semi-rigid bolted connections varies in detail between US and EC8 procedures. In AISC, partially-restrained (PR) connections are not permitted for intermediate or special moment frames connections. They can only be used in ordinary moment frames, provided the nominal connection strength is not less than 50 % of the plastic moment capacity of the beam, and the stiffness, strength and deformation capacity of the PR moment connections are considered in the design including the effect on overall frame stability. On the other hand, EC8 permits in principle the use of partial strength (i.e. dissipative) connections in primary lateral load-resisting systems provided that: (i) all connections have rotation capacity consistent with global deformations, (ii) members framing into connections are stable at the ultimate limit

state, and (iii) connection deformation is accounted for through nonlinear analysis. Unlike in AISC, there is no limit given in EC8 on the minimum moment ratio, nor on the use with different ductility classes. Dissipative connections should satisfy the rotational demand implied for plastic hinge zones, irrespective of whether the connections are partial or full strength; these are specified as 25 and 35 mrad for DCM and DCH, respectively, which are broadly similar to the demands in IMF and SMF in AISC 341 (total drift of 0.02 and 0.04 rad, for IMF and SMF, respectively).

5.6.2 Composite Moment Connections

As discussed previously, EC8 permits three general design concepts for composite structures (low dissipative behaviour, dissipative composite zones or dissipative steel zones). On the other hand, AISC refers to specific composite systems as indicated in Table 5.1 (e.g. C-OMF, C-IMF, C-SMF). In principle, this classification applies to systems consisting of composite or reinforced concrete columns and structural steel, concrete-encased composite or composite beams. The use of PR connections (C-PRMF) is included, and is applicable to moment frames that consist of structural steel columns and composite beams that are connected with partially restrained (PR) moment connections. Similar to PR steel connections, they should have strengths of at least $0.5M_p$ but additionally should exhibit a rotation capacity of at least 0.02 rad. It should be noted that, as mentioned previously, Annex C in EC8 for the detailing of slabs only applies to frames with rigid connections in which the plastic hinges form in the beams. However, guidance on the detailing of composite joints using partial strength connections are addressed in the commentary of AISC 341 for C-PRMF systems.

The use of composite connections can often simplify some of the challenges associated with traditional steel and concrete construction, such as minimizing field welding and anchorage requirements. Given the many alternative configurations of composite structures and connections, there are few standard details for connections in composite construction. In most composite structures built to date, engineers have designed connections using basic mechanics, equilibrium models (e.g. classical beam-column, truss analogy, strut and tie, etc.), existing standards for steel and concrete construction, test data, and good judgment. As noted above, however, engineers do face inherent complexities and uncertainties when dealing with composite dissipative connections, which can often counterbalance the merits of this type of construction when choosing the structural form. In this context, the ‘total disconnection’ approach permitted in EC8 (i.e. *Concept c*) offers a practical alternative in order to use standard or prequalified steel-only beam-to-column connections. This status can also be achieved using North American codes provided the potential plastic hinge regions are maintained as pure steel members. A similar approach has also been recently used in hybrid flat slab-tubular column connections (Eder et al. 2012), hence enabling the use of flat slabs in conjunction with steel-only dissipative members.

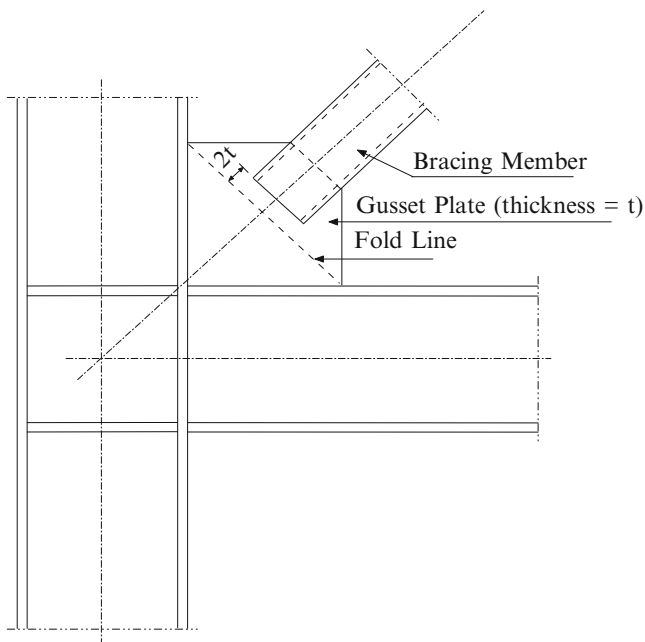


Fig. 5.10 Gusset plate connections in concentrically braced frames

5.6.3 Bracing Connections

Issues related to connection performance and design are clearly not only limited to moment connections, but also extend to other configurations such as connections to bracing members. Many of the failures reported in concentrically braced frames due to strong ground motion have been in the connections. In principle, bracing connections can be designed as rotationally restrained or unrestrained, provided that they can transfer the axial cyclic tension and compression effectively. The in- and out-of-plane behaviour of the connection, and their influence on the beam and column performance, should be carefully considered in all cases. For example, considering gusset plate connections, as shown in Fig. 5.10 (Elghazouli 2009), satisfactory performance can be ensured by allowing the gusset plate to develop plastic rotations. This requires that the free length between the end of the brace and the assumed line of restraint for the gusset can be sufficiently long to permit plastic rotations, yet short enough to preclude the occurrence of plate buckling prior to member buckling. Alternatively, connections with stiffness in two directions, such as crossed gusset plates, can be detailed. The performance of bracing connections, such as those involving gusset plate components, has attracted significant research interest in recent years (e.g. Lehman et al. 2008). Alternative tri-linear and nonlinear fold-line representations have been proposed and validated. A recent European research programme has also examined the performance of alternative

forms of gusset-plate bracing connections and provided recommendations on optimum configurations for use in design (Broderick et al. 2013).

Design examples for bracing-to-gusset plate connections in concentrically and eccentrically braced frames are given in the AISC Seismic Design Manual (2012), in accordance with AISC 341 and ASCE7, and typically require many considerations and design checks. In contrast, as for moment connections, the design of connections between bracing members and beams/columns is only dealt with in a conceptual manner in EC8. Accordingly, designers can adopt details available from the literature, or based on prototype testing.

Designing bracing connections in an efficient and practical manner can be complex and time-consuming, and requires significant expertise (Elghazouli and Packer 2014). This has led to the development of ‘pre-engineered’ proprietary solutions using ‘off-the-shelf’ cast steel connections (Herion et al. 2010). A substantially more compact field-bolted connection is achieved than would otherwise be possible with typical bolted connections using splice plates. Other proprietary connections include yielding ‘fuses’ such as the Yielding Brace System (YBS) (Gray et al. 2014). In this case, dissipation is provided by flexural yielding of parts of the YBS while the bracing member and other frame elements remain essentially elastic. Another ‘off-the-shelf’ solution is also provided through Buckling Restrained Braces which, as noted before, are not currently directly addressed in EC8. It should be noted that AISC358 is limited to prequalified solutions for steel moment connections, and does not prequalify connections for braced frames. At present, ‘pre-engineered’ bracing connections can perhaps be treated in a comparable manner to qualification of custom seismic products which require proof testing. Overall, compared to self-designed connections, proprietary seismic connections could offer improved performance, additional quality assurance, and the potential for savings in cost and construction time.

5.7 Concluding Remarks

This paper highlights various issues related to the seismic design of steel and composite frames that would benefit from further assessment and code development, with particular focus on the provisions of EC8. Since the European seismic code is in general relatively clear in its implementation of the underlying capacity design principles as well as the purpose of the parameters adopted within various procedures, its rules can be readily adapted and modified based on new research findings and improved understanding of seismic behaviour.

Comparison of EC8 provisions with those in AISC in terms of structural configurations and associated behaviour factors highlights a number of issues that are worthy of further development. Several lateral resisting systems that are currently dealt with in AISC are not incorporated in EC8 including steel-truss moment frames, steel-plate walls and buckling-restrained braces. It is anticipated that these will be considered in future revisions of the code. Another notable difference is the

relatively low q assigned to V-braced frames in EC8 compared to AISC, which highlights the need for further assessment of behaviour factors particularly for braced and dual frames in EC8, and to extend it to other forms such as ‘zipper’ and ‘buckling restrained’ configurations. It is also shown that whilst EC8 typically adopts the equal-displacement approach for predicting inelastic drift, US provisions employ specific seismic drift amplification factors. It is however noted that there is a need for seismic codes to adopt improved prediction methods which account for earthquake characteristics.

In terms of local ductility, comparison of the width-to-thickness limits in EC8 and AISC reveals considerable differences, particularly in the case of rectangular and circular tubular members. Since the ductility capacity and susceptibility to fracture are directly related to the occurrence of local buckling, it seems necessary to conduct further assessment of the adequacy of Class 1 sections to satisfy the cyclic demands imposed under prevalent seismic conditions. For composite dissipative sections, the requirements in EC8 for determining the effective width and the detailing in the slab is intricate, and some pragmatism and simplification in its application may be necessary, unless the option of ‘disconnection’ is adopted. It is also noted that allowing DCL or modified-DCL detailing in EC8 for moderate seismicity, with an appropriate reserve capacity, may be desirable particularly for special or complex structures.

It is observed that in EC8 the capacity-design application rules for columns ignore the important influence of gravity loads on the over-strength of beams. This issue becomes particularly pronounced in gravity-dominated frames or in low-rise configurations. The extent of the problem depends on the interpretation of the code and whether Ω is used in isolation or in combination with an additional capacity design criterion based on a limiting ratio of 1.3 on the column-to-beam capacity. The above-noted issue becomes more significant in composite moment frames where relatively large spans are typical. This is also added to the problem of achieving full beam hinging in dissipative composite frames due to the difference between the sagging and hogging moment capacities in composite sections.

In order to mitigate the vulnerability of braced frames to the concentration of inelastic demand within critical storeys, EC8 introduces a 25 % limit on the maximum difference in brace over-strength (Ω_b) within the frame. Detailed studies show that this may not eliminate the problem and can impose additional design effort and difficulties in practical design. Instead, this limit can be significantly relaxed or even removed if measures related to column continuity and stiffness are incorporated in design. Another issue related to concentrically braced frames is the lower slenderness limit of 1.3 imposed in EC8 for X-bracing, in order to limit the compression force in the brace. Satisfying this limit can result in significant difficulties in practical design. It would be more practical to avoid placing such limits, yet ensure that forces applied on components other than the braces are based on equilibrium at the joints, with due account of the relevant actions in compression. Improved procedures that account for brace slenderness as well as expected levels of ductility could be adopted.

For the purpose of capacity design checks, it is important to determine a realistic value for the over-strength of steel material. Unlike AISC, EC8 suggests a default value of 1.25. It is recognised however that the level of over-strength varies significantly depending on the type and grade of steel, with the over-strength expected to be more pronounced in lower grades. There seems to be a need for more reliable guidance in EC8 on the levels and sources of material over-strength that should be adopted in practice. Another area that requires clarification and development in EC3 and EC8 is related to the steel material toughness for application in seismic design. Specific guidance appears to be needed particularly in relation to reference temperatures and strain rates that would be appropriate to employ in seismic design situations.

Apart from over-strength arising from the material, lateral frame over-strength can be a direct result of design idealisations or the application of drift-related criteria. A significant design idealisation in concentrically braced frames is related to the treatment of buckling of the compression braces. Whereas AISC largely bases the design strength on the brace buckling capacity in compression, EC8 adopts the brace plastic capacity in tension with few exceptions. Whilst both simplifications lead to frame over-strength, they have directly opposite trends with respect to the brace slenderness. Depending on the specific design situation and frame configuration, it may be necessary to estimate either the maximum or minimum forces attained in compression members in a more realistic manner as opposed to the idealised approaches currently adopted in seismic codes.

The other key consideration influencing lateral frame over-strength is related to drift criteria. In comparison with other seismic codes, drift and stability requirements in EC8 are significantly more stringent. As a consequence, these checks can often govern the design, leading to considerable over-strength, especially if a high ' q ' is assumed. Whereas the presence of over-strength reduces the ductility demand in dissipative zones, it also affects forces imposed on frame and foundation elements. A rational application of capacity design necessitates a realistic assessment of lateral capacity after the satisfaction of all provisions, followed by a re-evaluation of global over-strength and the required ' q '. Although high ' q ' factors are allowed for various frame types in EC8, such a choice is often unnecessary and undesirable.

In terms of beam-to-column connections, there is clearly a need for a concerted effort to develop European guidance, in conjunction with the principles of EC8, on appropriate connection detailing using representative sections, materials and detailing practices. There is also a need for reviewing the design of column panel zones in moment frames, resulting from the combined application of the rules in EC3 and EC8. In particular, the definition of the yield point as well as the balance of plasticity between the panel and connected beams require further consideration. In general, it seems logical for future activities to promote the development of 'prequalified' or 'pre-engineered' seismic connections that satisfy the requirements of EC8, and to provide supporting design procedures and associated simplified analytical tools. These should not be limited to welded moment connections, but

should extend to bolted rigid and semi-rigid configurations as well as joints of bracing members and link zones in braced frames.

Open Access This chapter is distributed under the terms of the Creative Commons Attribution Noncommercial License, which permits any noncommercial use, distribution, and reproduction in any medium, provided the original author(s) and source are credited.

References

- AISC (2012) Seismic design manual, 2nd edn. American Institute of Steel Construction Inc., AISC, Chicago
- AISC 341 (2010) Seismic provisions for structural steel buildings. ANSI/AISC 341–10 American Institute of Steel Construction Inc., AISC, Chicago
- AISC 358 (2010) Prequalified connections for special and intermediate steel moment frames for seismic applications. ANSI/AISC 358–10, American Institute of Steel Construction Inc., AISC, Chicago
- ASCE7 (2010) ASCE/SEI – ASCE 7–10 – minimum design loads for buildings and other structures. American Society of Civil Engineers/Structural Engineering Institute, Reston
- Broderick BM, Hunt A, Mongabure P, LeMaout A, Goggins JM, Salawdeh, S, O'Reilly G, Beg D, Moze P, Sinur F, Elghazouli AY, and Plumier A (2013) Assessment of the seismic response of concentrically-braced frames. SERIES Concluding Workshop, Earthquake Engineering Research Infrastructures, European Commissions, JRC-Ispra, Italy
- Castro JM, Elghazouli AY, Izzuddin BA (2007) Assessment of effective slab widths in composite beams. *J Constr Steel Res* 63(10):1317–1327
- Castro JM, Davila-Arbona FJ, Elghazouli AY (2008) Seismic design approaches for panel zones in steel moment frames. *J Earthq Eng* 12(S1):34–51
- Doneux C, Plumier A (1999) Distribution of stresses in the slab of composite steel-concrete moment resistant frames submitted to earthquake action. *Stahlbau* 68(6):438–447
- ECCS (2013) Assessment of EC8 provisions for seismic design of steel structures. In: Landolfo R (ed) European convention for constructional steelwork, Brussels
- Eder MA, Vollum RL, Elghazouli AY (2012) Performance of ductile RC flat slab-to-steel column connections under cyclic loading. *Eng Struct* 36(1):239–257
- Elghazouli AY (2003) Seismic design procedures for concentrically braced frames. *Struct Build* 156:381–394
- Elghazouli AY (ed) (2009) Seismic design of buildings to Eurocode 8. Taylor and Francis/Spon Press, London
- Elghazouli AY (2010) Assessment of European seismic design procedures for steel framed structures. *Bull Earthq Eng* 8(1):65–89
- Elghazouli AY, Packer JA (2014) Seismic design solutions for connections to tubular members. *J Steel Constr* 7(2):73–83
- Elghazouli AY, Treadway J (2008) Inelastic behaviour of composite members under combined bending and axial loading. *J Constr Steel Res* 64(9):1008–1019
- Elghazouli AY, Broderick BM, Goggins J, Mouzakis H, Carydis P, Bouwkamp J, Plumier A (2005) Shake table testing of tubular steel bracing members. *Struct Build* 158:229–241
- Elghazouli AY, Castro JM, Izzuddin BA (2008) Seismic performance of composite moment frames. *Eng Struct* 30(7):1802–1819
- Elghazouli AY, Kumar M, Stafford PJ (2014) Prediction and optimisation of seismic drift demands incorporating strong motion frequency content. *Bull Earthq Eng* 12(1):255–276
- Eurocode 3 (2005) Design of steel structures – Part 1.1: General rules and rules for buildings. EN 1993–1: 2005, European Committee for Standardization, CEN, Brussels

- Eurocode 4 (2004) Design of composite steel and concrete structures – Part 1.1: General rules and rules for buildings. EN 1994-1: 2004, European Committee for Standardization, CEN, Brussels
- Eurocode 8 (2005) Design of structures for earthquake resistance – Part 1: General rules, seismic actions and rules for buildings. EN 1998-1: 2004, European Committee for Standardization, Brussels
- FEMA (2000) Federal Emergency Management Agency. Recommended seismic design criteria for new steel moment-frame buildings. Program to reduce earthquake hazards of steel moment-frame structures, FEMA-350, FEMA, Washington, DC
- Goggins JM, Broderick BM, Elghazouli AY, Lucas AS (2005) Experimental cyclic response of cold-formed hollow steel bracing members. *Eng Struct* 27(7):977–989
- Gray MG, Christopoulos C, Packer JA (2014) Cast steel yielding brace system (YBS) for concentrically braced frames: concept development and experimental validations. *J Struct Eng (American Society of Civil Engineers)* 140(4):pp.04013095
- Herion S, de Oliveira JC, Packer JA, Christopoulos C, Gray MG (2010) Castings in tubular structures – the state of the art. *Struct Build (Proceedings of the Institution of Civil Engineers)* 163(SB6):403–415
- Kumar M, Stafford PJ, Elghazouli AY (2013) Influence of ground motion characteristics on drift demands in steel moment frames designed to Eurocode 8. *Eng Struct* 52:502–517
- Lehman DE, Roeder CW, Herman D, Johnson S, Kotulka B (2008) Improved seismic performance of gusset plate connections. *J Struct Eng, ASCE* 134(6):890–901
- Plumier A, Doneux C, Bouwkamp JG, Plumier C (1998) Slab design in connection zones of composite frames. *Proceedings of the 11th ECEE Conference, Paris*
- SAC (1995) Survey and assessment of damage to buildings affected by the Northridge Earthquake of January 17, 1994, SAC95-06, SAC Joint Venture, Sacramento

Chapter 6

Seismic Analyses and Design of Foundation

Soil Structure Interaction

Alain Pecker

Abstract The topic of this paper is to illustrate on a real project one aspect of soil structure interaction for a piled foundation. Kinematic interaction is well recognized as being the cause of the development of significant internal forces in the piles under seismic loading. Another aspect of kinematic interaction which is often overlooked is the modification of the effective foundation input motion. As shown in the paper such an effect may however be of primary importance.

6.1 Introduction

Kinematic interaction is well recognized as being the cause of the development of significant internal forces in the piles under seismic loading. These internal forces are developed as the consequence of the ground displacement induced by the passage of the seismic waves. These displacements are imposed to the piles which may, or may not, follow the soil displacements depending on the bending stiffness of the piles relative to the soil shear stiffness (e.g. Kavvadas and Gazetas 1993). For flexible piles, the internal forces, i.e. pile bending moments and shear forces, can be computed by simply imposing the soil displacements to the pile; for stiff piles a soil structure analysis shall be conducted with proper modelling of the soil-pile interaction. Obviously, kinematic effects are more pronounced when the piles are stiff relative to the surrounding soil and when they cross consecutive layers of sharply different stiffnesses because the soil curvature is very large at such interfaces. This aspect of kinematic interaction is well understood and correctly accounted for in seismic design of piled foundations; for instance the European Seismic code (CEN 2004) requires that kinematic bending moments be computed whenever the two following conditions occur simultaneously:

A. Pecker (✉)

Géodynamique et Structure, Bagnaux, France

Ecole Nationale des Ponts ParisTech, Champs-sur-Marne, France

e-mail: alain.pecker@orange.fr

© The Author(s) 2015

A. Ansal (ed.), *Perspectives on European Earthquake Engineering and Seismology*, Geotechnical, Geological and Earthquake Engineering 39, DOI 10.1007/978-3-319-16964-4_6

153

- The ground profile has an average shear wave velocity smaller than 180 m/s (ground type D) and contains consecutive layers of sharply differing stiffness; consecutive layers of sharply differing stiffness are defined as layers with a ratio for the shear moduli greater than 6.
- The zone is of moderate or high seismicity, i.e. presents a ground surface acceleration larger than 0.1 g, and the category of importance of the structure is higher than normal (importance category III or IV).

There is another aspect of kinematic interaction often overlooked, even in seismic building codes, which is the modification of the effective foundation input motion. For example the European Seismic code (CEN 2004) does not mention it, nor does the ASCE 41-13 standard (2014) which however dedicates several pages to the effect of kinematic interaction for shallow or embedded foundations.

This issue might be critical when substructuring is used and the global soil-structure-interaction problem is solved in several steps. However, when a global model including both the soil and the superstructure is contemplated, kinematic interaction is accounted for in the analysis, provided the global model correctly reflects the physical character of the problem. These aspects are illustrated below on a real bridge project.

6.2 Soil Structure Interaction Modelling

As opposed to spread footings, for which a single method of analysis to determine the forces transmitted by the foundation emerges in practice (based on a substructuring approach and the definition of the foundation stiffness matrix and damping), several modeling techniques are used to model piled foundations for seismic response studies; the most common methods are the simplified beam on Winkler foundation model and the coupled foundation stiffness matrix (substructuring). These two modeling techniques are illustrated in Fig. 6.1 for the global model and in Fig. 6.2 for the substructure model (Lam and Law 2000).

6.2.1 *Global SSI Model for Piled Foundations*

In the global model, piles are represented by beam elements supported by linear or nonlinear, depth-varying, Winkler springs. In the case of earthquake excitation, ground motion would impart different loading at each soil spring and these motions need to be calculated from a separate analysis (site response analysis). Kinematic interaction is therefore correctly accounted for. However, the main drawback of this modeling technique is the large number of degrees of freedom needed to formulate the complete system.

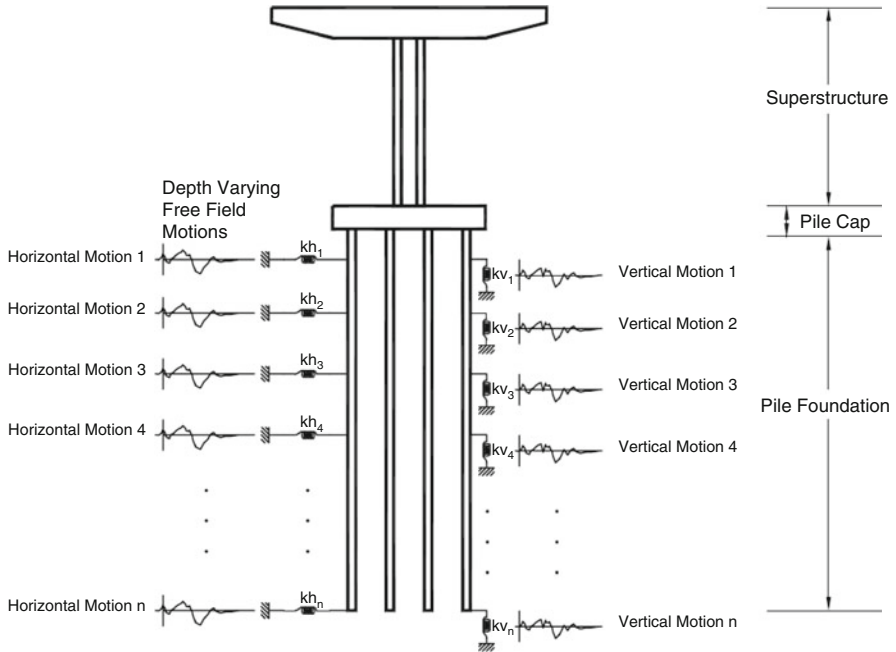


Fig. 6.1 Global pile-structure model

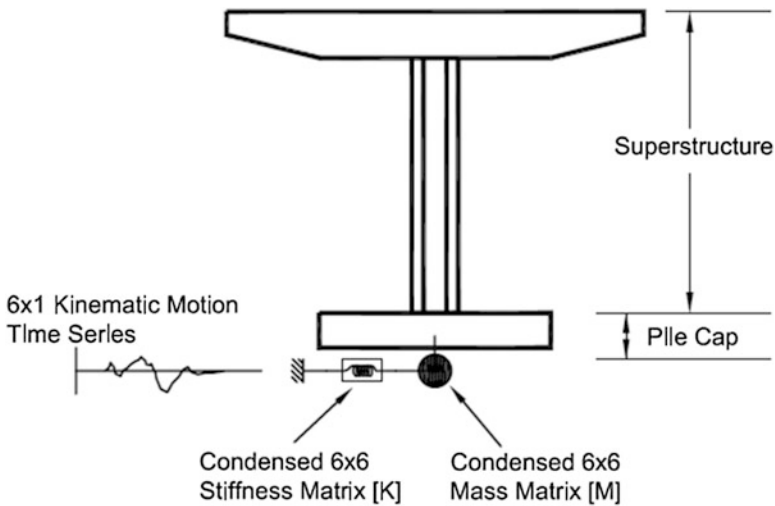


Fig. 6.2 Substructure model

The p-y relation, representing the nonlinear spring stiffness, is generally developed on the basis of a semi-empirical curve, which reflects the nonlinear resistance of the local soil surrounding the pile at specified depths. A number of p-y models

have been proposed by different authors for different soil conditions. The two most commonly used p-y models are those proposed by Matlock et al. (1970) for soft clay and by Reese et al. (1974) for sand. These models are essentially semi-empirical and have been developed on the basis of a limited number of full-scale lateral load tests on piles of small diameters ranging from 0.30 to 0.40 m. To extrapolate the p-y criteria to conditions that are different from the one from which the p-y models were developed requires some judgment and consideration. For instance in Slovenia, values of the spring stiffnesses are derived from the static values, increased by 30 %. Based on some field test results, there are indications that stiffness and ultimate lateral load carrying capacity of a large diameter drilled shaft are larger than the values estimated using the conventional p-y criteria. Pender (1993) suggests that the subgrade modulus used in p-y formulation would increase linearly with pile diameter.

Studies have shown that Matlock and Reese p-y criteria give reasonable pile design solutions. However, the p-y criteria were originally conceived for design against storm wave loading conditions based on observation of monotonic static and cyclic pile load test data. Therefore, Matlock and Reese's static p-y curves can serve to represent the initial monotonic loading path for typical small diameter driven isolated piles. If a complete total system of a bridge is modeled for seismic response study, individual piles and p-y curves can be included in the analytical model.

However, for a large pile group, group effects become important. An example is given in Fig. 6.3 which presents the results of horizontal impedance calculations of the group of piles of half the foundation (22 piles) of one of the pylon of the Vasco da Gama bridge in Lisbon (Pecker 2003); the group efficiency, computed from elastodynamic theory, is of the order of 1/6 at low frequencies and decreases with frequency due to the constructive interference of diffracted waves from adjacent piles. Typically, for large pile groups it is not uncommon to calculate group efficiency in the range 1/3 to 1/6.

Although group effect has been a popular research topic within the geotechnical community, currently there is no common consensus on the design approach to incorporate group effects. Full scale and model tests by a number of authors show that in general, the lateral capacity of a pile in a pile group is less than that of a single isolated pile due to so-called group efficiency. The reduction is more pronounced as the pile spacing is reduced. Other important factors that affect the efficiency and lateral stiffness of the pile are the type and strength of soil, number of piles, type and level of loading. In the past, analyses of group effects were based mostly on elastic halfspace theory due to the absence of costly full-scale pile experiments. In addition to group effect, gapping and potential cyclic degradation have been considered in the recent studies. It has been shown that a concept based on p-multiplier applied on the standard static loading p-y curves works reasonably well to account for pile group and cyclic degradation effects (Brown and Bollman 1996). The p-multiplier is a reduction factor that is applied to the p-term in the p-y curve for a single pile to simulate the behavior of piles in the group.

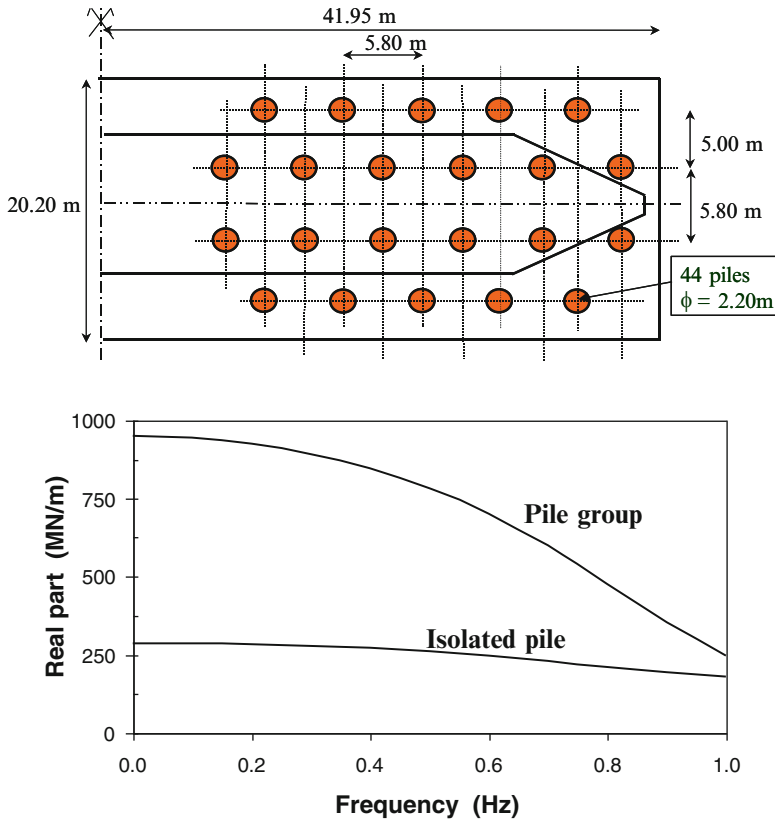


Fig. 6.3 Horizontal pile group impedance for the Vasco da Gama bridge (Pecker 2003)

6.2.2 Substructure Model for Piled Foundations

A direct (or global) interaction analysis in which both the soil and the structure are modelled with finite elements is very time demanding and not well suited for design, especially in 3D. The alternative approach employing a substructure system in which the foundation element is modeled by a condensed foundation stiffness matrix and mass matrix along with equivalent forcing function represented by the kinematic motion, may be more attractive; in addition, it more clearly separates the role of the geotechnical engineer and of the structural engineer. The substructuring approach is based on a linear superposition principle and therefore linear soil behavior is more appropriate. In that case, the condensed stiffness matrix may be obtained either from the beam on Winkler springs model or from continuum impedance solutions (Gazetas 1991). When nonlinear soil behavior is considered, the condensed stiffness matrix is generally evaluated by a pushover analysis of the pile group and linearization at the anticipated displacement amplitude of the pile head.

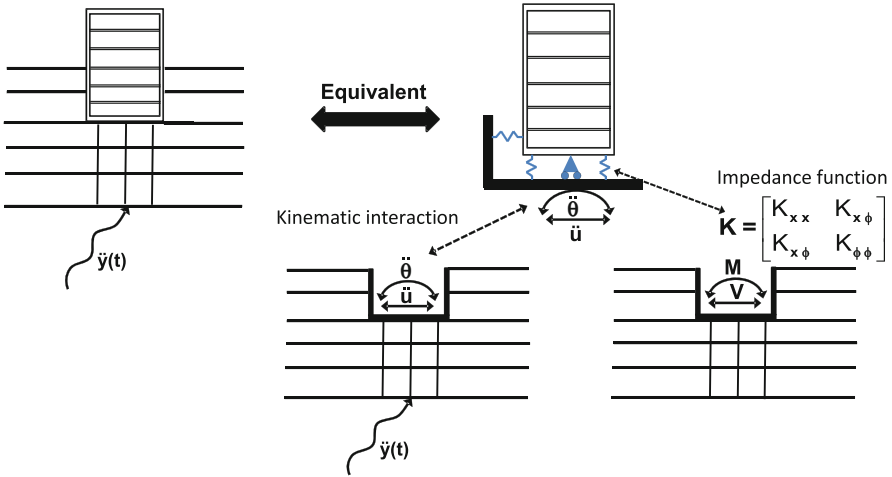


Fig. 6.4 Substructuring approach for soil structure interaction

Substructuring reduces the problem to more amenable stages and does not necessarily require that the whole solution be repeated again if modifications occur in the superstructure. It is of great mathematical convenience and rigor which stem, in linear systems, from the superposition theorem (Kausel et al. 1974). This theorem states that the seismic response of the complete system can be computed in two stages (Fig. 6.4)

- Determination of the kinematic interaction motion, involving the response to base acceleration of a system which differs from the actual system in that the mass of the superstructure is equal to zero;
- Calculation of the inertial interaction effects, referring to the response of the complete soil-structure system to forces associated with base accelerations equal to the accelerations arising from the kinematic interaction.

The second step is further divided into two subtasks:

- computation of the dynamic impedances at the foundation level; the dynamic impedance of a foundation represents the reaction forces acting under the foundation when it is directly loaded by harmonic forces;
- analysis of the dynamic response of the superstructure supported on the dynamic impedances and subjected to the kinematic motion, also called effective foundation input motion.

Although the substructure approach described above is rigorous for the treatment of linear SSI, its practical implementation is subject to several simplifications:

- full linear behavior of the system is assumed; it is well recognized that this assumption is a strong one since nonlinearities occur in the soil and at the soil pile interface. Soil nonlinearities can be partly accounted for, as recommended

in Eurocode 8 – Part 5, by choosing for the calculation of the impedance matrix reduced soil properties, calculated from 1D site response analyses (Idriss and Sun 1992), that reflect the soil nonlinear behavior in the free field. This implicitly assumes that additional nonlinearities taking place at the soil pile interface, along the pile shaft, do not contribute significantly to the overall seismic response.

- kinematic interaction is usually not considered. Very often flexural piles are flexible with respect to the surrounding soil and the soil displacement is not altered by the presence of the pile group. In that case, provided the foundation embedment can be neglected, step 1 is straightforward: the kinematic interaction motion, or foundation effective input motion, is simply the freefield motion. No additional burden is imposed to the analyst since the freefield motion is a given input data.

6.3 Kinematic Interaction Motion

In the remaining of the paper we will focus on the first step of the substructure analysis described above with illustration of two foundations responses of the same bridge.

Foundation 1 is composed of 18 concrete piles, 1,800 mm in diameter, 20 m long, penetrating a 2.50 m thick layer of a residual soil with a shear wave velocity 300 m/s, overlying a 10 m thick weathered layer of the rock formation with a shear wave velocity of 580 m/s; the rock formation is found at 12.50 m below the ground surface. Site response analyses were carried out with the software SHAKE (linear equivalent viscoelastic model) and for seven time histories spectrally matched to the design spectrum; these time histories were input at an outcrop of the rock formation. The foundation response was modeled with the software SASSI-2010; (Ostadan et al. 2010) the model includes the 18 piles, a massless pile cap and the soil layers; the strain compatible properties retrieved from the SHAKE analyses are used for each soil layer and the input motion is represented by the seven ground surface time histories computed in the SHAKE analyses. Figure 6.5 compares the freefield ground surface spectrum to the foundation response spectra calculated at the same elevation. Note that because of the asymmetric pile layout the motion in the X-direction is different from the motion in the Y-direction. As expected since the soil profile is stiffer than the piles in flexure, both the freefield motion and the foundation motions are very close to each other. For that configuration, using the freefield motion for the effective foundation input motion would not be a source of error.

Foundation 2 of the same bridge is composed of 35 large diameter concrete piles (2.5 m), 49 m long, crossing a very soft mud layer, 11 m thick, with a shear wave velocity of the order of 100 m/s; the piles go through a residual soil ($V_S = 250\text{--}400\text{--}m/s$) and reach the competent rock formation at 25 m depth (Fig. 6.6). Freefield and foundation response spectra are compared in Fig. 6.7 The free-field ground response spectrum determined from a site specific response analysis has a smooth shape; the kinematic interaction motion, i.e. the motion of the piled foundation,

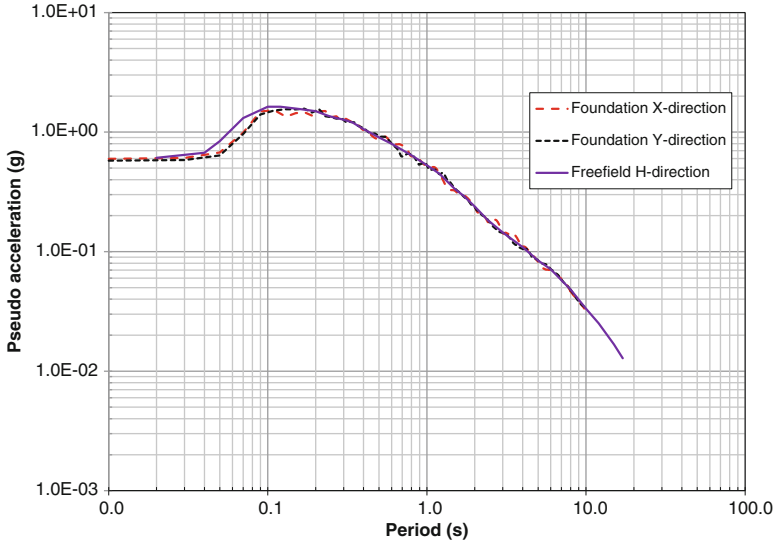


Fig. 6.5 Kinematic interaction motion for “flexible” piled foundation 1

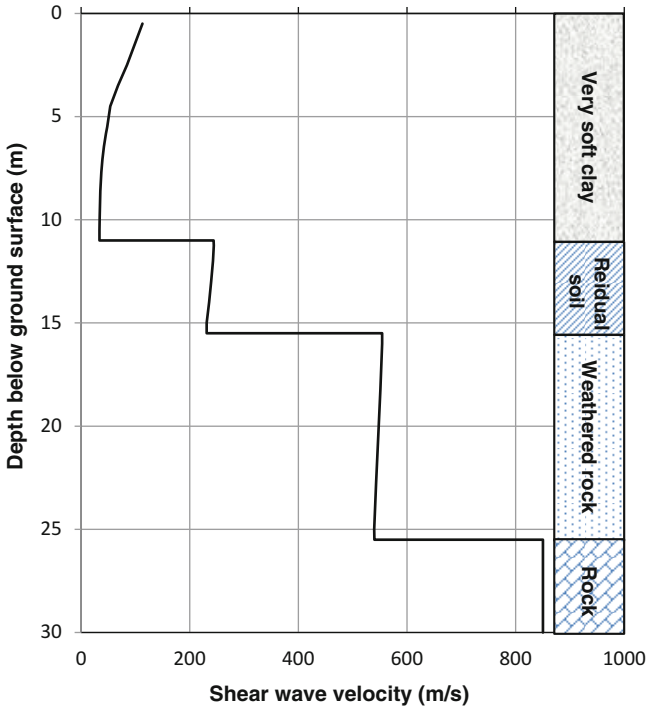


Fig. 6.6 Soil profile at location of foundation 2

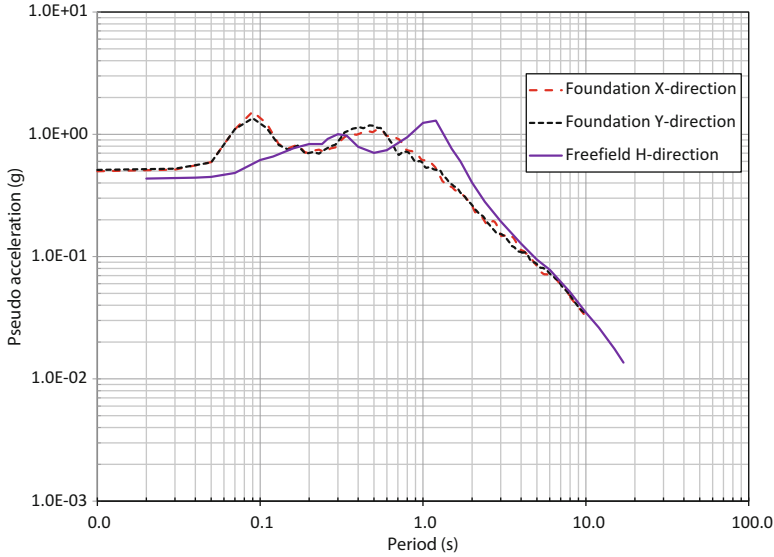


Fig. 6.7 Kinematic interaction motion for “stiff” piled foundation 1

exhibits a marked peak at 0.5 s and a significant deamplification with respect to the free-field motion between 0.8 and 3.0 s. This phenomenon is due to the inability of the piled foundation to follow the ground motion because of the piles stiffnesses.

Obviously, in that case, using the freefield motion for the foundation input motion would be strongly misleading and may produce an unconservative design.

These two examples, drawn from a real project clearly illustrate the need for a careful examination of the relative foundation-soil profile stiffness before deciding whether or not there is a chance that the freefield motion be modified by the foundation. When faced to that latter situation, it is mandatory to correctly evaluate the effective foundation input motion to obtain meaningful results.

6.4 Conclusions

Experience gained from several projects involving piled foundation in a seismic environment shows that the most amenable and versatile approach to soil structure interaction is the substructuring technique. It presents several advantages like a correct treatment of the pile group effect, which is not the case with a global model where the piles are modelled as beams on Winkler foundations, the need for calculating the foundation input motions and foundation impedances only once as long as the foundation is not modified, the reduced size of the structural model, especially for extended structures like bridges, etc... The main drawback of this approach lies in its restriction to linear, or moderately nonlinear, systems. Since it is

attractive, the method is often used with approximations in its implementation and the designer must be fully aware of those shortcuts. In this paper, one such approximation, which consists in taking the freefield motion for the effective foundation input motion, has been illustrated on a real project. It has been shown that significant differences may take place between both motions when the piled foundation cannot be considered flexible with respect to the soil profile. If this situation is faced, rigorous treatment of soil-structure interaction requires that the effective foundation input motion be calculated, an additional step in the design.

Open Access This chapter is distributed under the terms of the Creative Commons Attribution Noncommercial License, which permits any noncommercial use, distribution, and reproduction in any medium, provided the original author(s) and source are credited.

References

- ASCE/SEI 41–13 (2014) Chapter 8: Foundations and geologic site hazards. In: Seismic evaluation and retrofit of existing buildings, vol 52. American Society of Civil Engineers, Reston, pp 1–8
- Brown DA, Bollman HT (1996) Lateral load behavior of pile group in sand. *J Geotech Eng ASCE* 114(11):1261–1276
- CEN (2004) European Standard EN 1998-5: 2004 Eurocode 8: Design of structures for earthquake resistance. Part 5: Foundations, retaining structures, geotechnical aspects. Comité Européen de Normalisation, Brussels
- Gazetas G (1991) Foundation vibrations. In: Fang HY (ed) *Foundation engineering handbook*, 2nd edn. Van Nostrand Reinhold, New York
- Idriss IM, Sun JI (1992) SHAKE 91: a computer program for conducting equivalent linear seismic response analyses of horizontally layered soil deposits. Program modified based on the original SHAKE program published in December 1972 by Schnabel, Lysmer and Seed, Center of Geotechnical Modeling, Department of Civil Engineering, University of California, Davis
- Kausel E, Roesset JM (1974) Soil structure interaction for nuclear containment structures. Proceedings ASCE, power division specialty conference, Boulder
- Kavvasdas M, Gazetas G (1993) Kinematic seismic response and bending of free head piles in layered soils. *Geotechnique* 43(2):207–222
- Lam PI, Law H (2000) Soil structure interaction of bridges for seismic analysis. Technical report MCEER-00-008
- Matlock H (1970) Correlation for design of laterally loaded piles in soft clay. 2nd Annual Offshore Technology Conference. Paper No 1204
- Ostadan F, Nan D (2012) SASSI 2010 – a system for analysis of soil-structure interaction. Geotechnical Engineering Division, Civil Engineering Department, University of California, Berkeley
- Pecker A (2003) Aseismic foundation design process – lessons learned from two major projects: the Vasco da Gama and the Rion-Antirion bridges. Proceedings 5th ACI international conference on seismic bridge design and retrofit for earthquake resistance, La Jolla
- Pender MJ (1993) Aseismic pile foundation design and analysis. *Bull N Z Soc Earthq Eng* 26(1):49–160
- Reese L, Cox W, Koop R (1974) Analysis of laterally load piles in sand. 6th Annual Offshore Technology Conference. Paper No. 2080

Chapter 7

Performance-Based Seismic Design and Assessment of Bridges

Andreas J. Kappos

Abstract Current trends in the seismic design and assessment of bridges are discussed, with emphasis on two procedures that merit some particular attention, displacement-based procedures and deformation-based procedures. The available performance-based methods for bridges are critically reviewed and a number of critical issues are identified, which arise in all procedures. Then two recently proposed methods are presented in some detail, one based on the direct displacement-based design approach, using equivalent elastic analysis and properly reduced displacement spectra, and one based on the deformation-based approach, which involves a type of partially inelastic response-history analysis for a set of ground motions and wherein pier ductility is included as a design parameter, along with displacement criteria. The current trends in seismic assessment of bridges are then summarised and the more rigorous assessment procedure, i.e. nonlinear dynamic response-history analysis, is used to assess the performance of bridges designed to the previously described procedures. Finally some comments are offered on the feasibility of including such methods in the new generation of bridge codes.

7.1 Introduction

Performance-based seismic design (PBD) procedures, in particular displacement-based ones (DBD), are now well-established for buildings (Kappos 2010); however application of these concepts to bridges has been more limited, despite the fact that studies on the so-called ‘direct’ displacement-based design (DDBD) of bridge piers (Kowalsky et al. 1995) or even entire bridges (Calvi and Kingsley 1995) appeared in the mid-1990s. Notwithstanding the now recognised advantages of the DDBD procedure (Priestley et al. 2007), the fact remains that, in its current form, the procedure suffers from two significant disadvantages:

A.J. Kappos (✉)

Civil Engineering Department, City University London, London EC1V 0HB, UK
e-mail: Andreas.Kappos.1@city.ac.uk

© The Author(s) 2015

A. Ansal (ed.), *Perspectives on European Earthquake Engineering and Seismology*, Geotechnical, Geological and Earthquake Engineering 39, DOI 10.1007/978-3-319-16964-4_7

163

- it is applicable to a class of bridges only, i.e. those that can be reasonably approximated by an equivalent single-degree-of-freedom (SDOF) system for calculating seismic demand
- even for this class the procedure is not deemed appropriate for the *final* design of the bridge (whereas it is a powerful tool for its *preliminary* design)

A key source of these disadvantages is the important role that higher modes play in the transverse response of bridges, even of some relatively short ones (Paraskeva and Kappos 2010), which complicates the proper assessment of the displaced shape of the bridge and the target displacement. It is noted that for systems such as multi-span bridges, the DDBD approach requires that the engineer properly define a target displacement profile (duly accounting for inelastic response), rather than just a single target displacement (as in the case of single-column bridges); this usually requires a number of iterations, which inevitably increases the complexity of the procedure.

There is little doubt that the aforementioned disadvantages are the key reason why, even today (about 20 years after they first appeared) DBD/DDBD procedures are not formally adopted by current codes; interestingly, in Appendix I of the SEAOC 1999 Blue Book (Ad Hoc Committee 1999), the first one to provide guidance for DBD of buildings (there are still no guidelines for DBD of bridges), it is explicitly required to carry out a verification of the initial displacement-based design through nonlinear static (pushover) analysis.

In the light of the above, it can be claimed that the current trend in performance-based seismic design of bridges is to make the attractive concept of DBD more suitable for the final design of a sufficiently broad class of bridges, so that it can be deemed suitable for practical application. It is worth recalling here that, as correctly pointed out in one of the first papers on DDBD (Calvi and Kingsley 1995), the concept of the equivalent elastic structure (based on member secant stiffness at target displacement) is feasible and preferable in the preliminary design of the bridge, whereas more sophisticated tools (like nonlinear analysis) are recommended at the final design stage. As will be discussed in more detail in Sect. 7.3, the currently available DDBD procedures work well for the preliminary design of first-mode-dominated bridges in high seismic hazard areas, but present problems in several cases that are common in practice, like bridges with some degree of irregularity, while they are simply not applicable in low and moderate seismic hazard regions.

In Sect. 7.2 a brief overview of available PBD/DBD methods for bridges is critically presented, focussing on the new contributions made by each study, rather than summarising the entire procedures (which are similar in many methods). The key issues involved in developing an appropriate PBD procedure are identified and discussed in the light of the available procedures.

In Sect. 7.3, a PBD procedure is presented based on elastic analysis and the use of the secant stiffness approach and ‘over-damped’ elastic spectra, i.e. the ‘direct displacement based design approach’, pioneered by Priestley and Kowalsky (Priestley et al. 2007; Kowalsky et al. 1995), is extended with a view to making it

applicable to a broad spectrum of bridge systems, including those affected by higher modes, and also introducing additional design criteria not previously used in this method.

In Sect. 7.4 an alternative, more rigorous, method is presented that involves more advanced analysis tools, i.e. response-history analysis (for different levels of ground motion intensity) of bridge models wherein any regions that are expected to yield under the selected seismic actions are modelled as inelastic, whereas the rest of the bridge is modelled as elastic; the initial analysis (relevant to service conditions) is an elastic one. A critical aspect of this (currently under development) procedure is the a-priori definition of the inelastic behaviour of dissipating zones, by exploiting the deformation limits for the specific performance level, which are related to the damage level of the structural members.

Section 7.5 first summarises the current trends worldwide in seismic assessment of bridges and applies the more rigorous assessment procedure, i.e. nonlinear dynamic response-history analysis, to assess the performance of bridges designed to the procedures described in Sects. 7.3 and 7.4. Moreover, comparisons are made between these performance-based designed bridges and similar ones designed to a current international code, namely Eurocode 8.

Finally, in Sect. 7.6, some general conclusions are drawn, regarding the feasibility of using new procedures that aim at a better control of the seismic performance of bridges under different levels of seismic loading.

7.2 Overview of PBD Methods for Bridges

A DDBD procedure was proposed by Kowalsky and his co-workers (Kowalsky 2002; Dwairi and Kowalsky 2006), incorporating basic concepts of the DDBD approach like the target displacement and the displacement profile that should account for inelastic effects, without carrying out an inelastic analysis; the procedure is applicable to multi-degree-of-freedom (MDOF) continuous concrete bridges with flexible or rigid superstructures (decks). A key feature of the method is the EMS (effective mode shape) approach wherein account is taken of higher mode effects by determining the mode shapes of an equivalent elastic model of the bridge based on the column and abutment secant stiffness values at maximum response. A similar version of the method was included in the book by Priestley et al. (2007) on DDBD; this version of the method is simpler than the previously mentioned one (no use of EMS in the design of piers) but also addresses design in the longitudinal direction (which often governs the seismic design of the bridge), and provides some guidance for the treatment of features like the degree of fixity of columns and the effect of higher modes on the superstructure through an EMS approach focusing on forces and moments of the deck only.

Another study (Adhikari et al. 2010) focussed on the difficulties involved in applying DDBD to long-span bridges with tall piers. This study introduced some additional considerations to account for higher mode effects on flexural strength of

plastic hinges in the case of long-span concrete bridges with limited ductile piers. Following the suggestion of Priestley et al. (2007), a response-spectrum analysis (RSA) was used after completion of the DDBD procedure, with two different design spectra (a 5 %-damped design spectrum and a design spectrum with damping value obtained from the DDBD procedure) to determine the design responses (elastic and inelastic, respectively) at critical locations of the bridge as combinations of several modes. The procedure is analogous to what has been called ‘Effective Modal Superposition’ approach by Priestley and his co-workers (Priestley et al. 2007; Alvarez Botero 2004; Ortiz Restrepo 2006) for bridge design. It is worth noting that in the latter, higher mode effects were considered only for determining the design elastic responses (e.g. deck transverse moment, abutment shear force), whereas inelastic responses, such as flexural strengths at plastic hinge locations, were computed directly from the first inelastic mode, considering that mass participation factor for this mode was always more than 80 %.

The DDBD method was further extended by Suarez and Kowalsky (2007, 2010, 2011) who tackled additional issues such as soil-structure interaction of drilled shaft bents, skewed configurations of piers and/or abutments, conditions under which DDBD can be applied using predefined displacement patterns (including the case of expansion joints), and definition of stability-based target displacements that account for $P-\Delta$ effects at the start of the design process. More recently, Kappos et al. (2012a, 2013) have extended the DDBD procedure to properly include higher mode effects and also added additional design criteria (see Sect. 7.3.1).

In an alternative approach, that could qualify as ‘indirect’ displacement-based design of bridges (Bardakis and Fardis 2011), the concept of calculating inelastic rotation demands from elastic analysis, previously used by Fardis and co-workers for buildings, is extended to concrete bridges having deck integral with the piers.

So far, the vast majority of studies performed on this topic do not consider directly higher mode effects, as a result of the inherent limitation of the procedure (due to the equivalent SDOF approach) to structures wherein the fundamental mode dominates the response.

Some key issues involved in the aforementioned methodologies, which can also serve as a basis for classifying them, are identified and discussed in the remainder of this section.

7.2.1 Type of Analysis

The basic options here are elastic analysis and inelastic analysis, in each case either equivalent static or dynamic. Selection of the type of analysis certainly affects the complexity of the procedure and, up to a certain extent, the time and effort required for carrying out the seismic design of the bridge. It is worth pointing out here that all these methods have been used in at least one of the existing procedures, as discussed in the following.

Equivalent static analysis is the method typically used in the DDBD procedure (Priestley et al. 2007), which starts from a target displacement, consistent with a deformation capacity ensured by an appropriate detailing of the structure. Estimating a reasonable value for the yield displacement, the target displacement translates into a displacement ductility demand and a corresponding equivalent damping ratio, which is used to reduce the selected displacement spectra, to account (indirectly) for nonlinear hysteretic behaviour. Entering this response spectrum with the aforementioned target displacement the effective period (secant value at target displacement) of this system is determined; subsequently, the base shear corresponding to the previously defined peak displacement and the secant stiffness calculated from the effective period, is found. From there on, the procedure reduces to a ‘traditional’ equivalent lateral force design of the structure. Some empirical corrections for higher modes are suggested in (Priestley et al. 2007).

Elastic dynamic response spectrum analysis is the reference method of current seismic codes in Europe (CEN 2005), the US (Caltrans 2013), and most of the world. These codes can be deemed as performance-based, although in essence they require verification for one performance objective only. The procedure is well known and will not be described herein. Elastic dynamic analysis is also used in PBD methods wherein inelastic rotation demands are estimated from elastic analysis (Bardakis and Fardis 2011).

There is no complete design method that is based on nonlinear static (pushover) analysis, but several methods used for assessment, e.g. the N2 method, have been applied to bridges (Fischinger et al. 2004) and in principle can be applied for DBD adopting a deformation-calculation based approach, i.e. calculation of the expected maximum displacement for an already designed structural system; detailing is then provided such that the displacement capacity of the bridge and its components exceeds the calculated maximum displacement.

Nonlinear dynamic (response-history) analysis is the most rigorous procedure, but also the most difficult to apply. A method proposed by the author and his co-workers is described later (Sect. 7.4) and combines an initial elastic response-history analysis (for determining the strength of dissipating zones, like pier ends) with two sets of nonlinear analyses (two levels of seismic action) wherein displacements and local ductility demands are checked.

7.2.2 Definition of Seismic Input

The definition of the seismic input depends on the type of analysis used, as well as the design approach adopted, i.e.

- Linear dynamic response spectrum analysis requires a design (pseudo-) acceleration spectrum to derive the pertinent modal forces.
- DDBD procedures estimate the required stiffness of the structure through a design displacement spectrum, and then the corresponding base shear as

described previously (Sect. 7.2.1). It is noted here that the long period range of displacement spectra (beyond about 2 s), which is quite important for DDBD that involves secant stiffnesses at maximum displacement, is not yet reliable enough due to the paucity of digital records of ground motion with frequency content rich in this long-period range.

- Response-history analysis requires a set of input accelerograms (at least 7 if average response quantities are to be used for design) which should be compatible with the design spectrum. The critical issue of properly selecting natural accelerograms that are consistent with the design spectrum falls beyond the scope of this chapter; it is only noted that there are currently sound procedures and the associated software, e.g. (Katsanos and Sextos 2013), for selecting ‘optimum’ sets of seven (or more) accelerograms.

7.2.3 *Stiffness of Dissipating Zones*

Since displacement control is of paramount importance in all PBD procedures, it is crucial that displacements be not underestimated during the design procedure. In the most common type of bridges, having concrete piers, plastic hinges are typically located at the piers, unless a seismic isolation approach is adopted. The stiffness of the yielding piers is clearly paramount in the calculation of bridge displacements and depends on the level of induced inelasticity (secant stiffness decreases with increasing ductility demand). In this respect, DDBD methods adopt the secant stiffness at maximum displacement approach (effective stiffness taken equal to the ratio of strength to target displacement) and this stiffness is a design parameter, found during the process, as described in Sect. 7.2.1.

Practically all other procedures adopt approximate values of the pier stiffness, corresponding to yield conditions (rather than the max displacement), and this stiffness is assumed as known when design seismic actions (e.g. modal forces) are estimated. For the usual case of reinforced concrete piers, these approximate values are either very rough estimates, like the $0.5 EI_g$ (50 % of uncracked section rigidity) adopted by both Eurocode 8–1 (CEN 2004) and AASHTO (2010), or slightly more sophisticated ones taking into account the level of axial loading on the pier (which, in general, is not significantly affected by seismic actions) and/or the reinforcement ratio.

Eurocode 8–2 (the Eurocode for Seismic Design of Bridges) (CEN (Comité Européen de Normalization) 2005) in its (informative) Annex C suggests the following relationship for the effective moment of inertia

$$I_{\text{eff}} = 0.08I_g + I_{\text{cr}} \quad (7.1)$$

where the cracked section inertia can be calculated as the secant value at yield

$$I_{cr} = M_y / (E_c \cdot \varphi_y) \quad (7.2)$$

(M_y is the yield moment and φ_y the yield curvature, E_c the concrete modulus). Obviously, I_{cr} can only be estimated from (7.2) when the pier has been designed, so that both strength and yield curvature can be calculated; hence use of the above is feasible only when iterative elastic analyses, or inelastic analysis are used.

The Caltrans Seismic Design Criteria (2013) is a very recently updated document and hence represents the current practice in earthquake-prone areas of the US; importantly, it does not adopt the DDBD procedures that have been developed several years prior to its publication, although it does place particular emphasis on the calculation of displacement demand and capacity. Regarding stiffness, the same concept as in EC8-2 is retained (secant value at yield), the only exception being that the $0.08 I_g$ term (accounting for tension stiffening effects) is not included in Eq. (7.1). As an alternative, the Caltrans Criteria allow the calculation of effective stiffness as a function of the axial load ratio and the pier reinforcement ratio from graphs provided in (Priestley et al. 1996); this can be directly implemented for carrying out elastic analysis, assuming a reasonable reinforcement ratio and, in principle, analysis should be repeated if the resulting reinforcement is substantially different.

7.2.4 Number of Directly Controlled Design Parameters

Closely related to the issue of pier stiffness, albeit broader, is the issue of the number of directly controlled parameters during the design process. This is arguably the most critical issue, as far as future improvements of seismic design methods for bridges are concerned. Ideally, the designer should both carry out a dimensioning (and reinforcing, in concrete bridges) that satisfies all the selected performance criteria and verify this design by an analysis wherein all member stiffnesses are consistent with the level of inelasticity induced by the seismic actions for which a specific performance objective is verified. This is, clearly, not a realistic design procedure, even if the stiffness and related modelling issues (e.g. gap closures at joints) are overcome by a rather refined nonlinear analysis (accounting for both material and boundary condition nonlinearities). This is, of course, due to the fact that for a reliable nonlinear analysis to be carried out, one needs to know all the details of the bridge, including member dimensions, reinforcement detailing, bearing characteristics, joint widths, and so on. Excluding the case of an epiphany, all these design parameters can at best be guessed at the beginning of the analysis and, as a rule, several iterations will be needed, unless the bridge is overdesigned, rather than designed to meet reasonably closely the selected performance criteria, which would result in an economic design.

In the light of the above, a designer might select to follow the beaten track and use elastic analysis (which is an approximation of the real response of the bridge in

all safety-related verifications) assuming that the period(s) of the structure can be determined beforehand and used to estimate design forces (pseudo-accelerations) that will be used for deriving member action effects (M , V , N) for standard, force-based design. Such a procedure can conveniently account for several factors that affect the seismic response of the bridge, i.e. higher modes, soil-structure interaction, spatial variability of ground motion etc. Nevertheless, satisfaction of the code criteria based on the results of such elastic analyses might well mean simply that the bridge is overdesigned, for instance that smaller piers could have been used without violating any design criteria.

Alternatively, one could select to adopt a DDBD approach, especially during a preliminary design of the bridge (e.g. in the framework of a pre-study), and select as a design parameter the stiffness that has to be assigned to critical members like the piers for the bridge to satisfy the displacement criteria selected as performance indicators. Some of the problems arising from this choice have been discussed in previous sections; it will be added here that target displacements in the DDBD procedure are calculated by empirical procedures, based on assumed inelastic displacement profiles and some calibration studies (Priestley et al. 2007; Kowalsky 2000) that relate pier displacements to material strains (concrete, steel). As a result of the approximations involved, and the fact that material strains and/or local (curvature) ductility requirements are not design parameters, they might end up being different from those envisaged, particularly for bridges with configuration issues.

A tentative conclusion from the above is that a designer should try to strike a balance between the attractive, yet cumbersome if at all feasible, option of directly including several design parameters (member stiffness, displacements, local ductility requirements and/or strain limits), and the more crude approaches like those based on elastic analysis of an assumed as fully known structure, for design forces reduced on the basis of an envisaged global ductility, wherein member forces and displacements are checked at the end of the analysis and if found below the specified limits, the design is assumed to be concluded.

7.2.5 Number of Iterations Required

Last but not least, the practicality of the design procedure also depends on the required number of iterations, in particular the number of required analyses wherein the model of the bridge has to be changed; this, in most cases, requires several sets of analyses run at different times, rather than in a single run, which is the preferred option, especially for practicing engineers. The issue of iterations is closely related to the number of directly controlled design parameters discussed in the previous section. What should be added here is first that for a design approach to be pragmatic the criteria to be satisfied during the iterations should not be excessively strict (e.g. obtaining the target displacement within 1 %), and second that, unfortunately, not all design procedures converge even if the convergence criteria are not

very strict; again this is more the case when higher modes and/or configurations issues are involved (Kappos et al. 2013).

The seismic design procedures described in the next two sections can be deemed as attempts to improve the existing state-of-the-art in PBD of bridges by refining the available procedures; inevitably (in the light of the previous discussions) the proposed improved methods are more cumbersome (to varying degrees) than the existing ones.

7.3 A PBD Procedure Based on Elastic Analysis

For the DDBD method to be applicable to the design for transverse response of bridges with some degree of irregularity, higher mode effects have to be treated as part of the entire design procedure (rather than as a correction of deck shears and moments at the final steps). Hence, in the DDBD method presented in this section the EMS technique (Kowalsky 2002) is included as part of the procedure. A number of idealized bridge configurations were analysed in (Dwairi and Kowalsky 2006) and the results were used for developing guidelines for the selection of displacement patterns (normalized deformed shapes) for continuous bridges with ‘rigid translation’ and ‘flexible symmetric’ deformation patterns. These are useful concepts for preliminary design of bridges, but most actual bridges do not fully comply with these idealizations, e.g. the assumption that all columns have the same longitudinal steel ratio and column diameter, or the assumption that piers are hinged to the soffit of the deck, do not hold for many actual bridges. A procedure is then needed that recognises the fact that design codes require taking into account all the peculiarities of each (real) bridge. It is worth recalling here that bridge design documents that are based on the displacement-based concept, such as the AASHTO Guidelines for Seismic Design (AASHTO 2011), require (among other things) the use of nonlinear analysis procedures as part of the design; this inevitably introduces complexity and increases the design effort, especially since the advanced analysis tools have to be used in a number of iterations if over-conservatism is to be avoided. Hence, the initial stimulus for the method presented herein was this very point, i.e. to identify required extensions and/or modifications of the aforementioned DBD procedure, for it to be applicable to actual bridges wherein the simplifying assumptions made at various stages of the procedure (see next section) do not really hold. A further objective was to obtain some preliminary quantitative data regarding the advantages (or otherwise) of applying the DDBD method, compared to ‘mainstream’ force-based design (FBD), adopted by all current codes.

In view of the aforementioned limitations of DDBD and the fact that bridges are structures wherein higher modes usually play a more critical role than in buildings, the procedure presented herein (Kappos et al. 2013) attempts to refine and extend the procedure for bridges proposed by Dwairi and Kowalsky (2006) by including some additional design criteria and accounting for higher mode effects, not only regarding the proper definition of a target-displacement profile (comprising

non-synchronous displacements, since all significant modes are considered), but also the proper definition of the corresponding peak structural response. The extended procedure, called modal direct displacement-based design, follows the general approach introduced in previous studies of Chopra and Goel (2002) on buildings and Paraskeva et al. (Paraskeva and Kappos 2010; Paraskeva et al. 2006) on bridges, noting that these studies deal with the pushover procedure, rather than with design based on elastic analysis. The efficiency of the presented methodology is then assessed by applying it to an actual bridge, whose different pier heights and the unrestrained transverse displacement at the abutments result in an increased contribution of higher modes. Some additional issues such as the proper consideration of the degree of fixity at the top of the pier and the effect of the deck torsional stiffness are also investigated, and comparisons between the extended and the ‘standard’ DDBD method are made.

7.3.1 Description of the Procedure

The structure of the method is shown in Fig. 7.1 in flow-chart form; the successive steps are described in the following. Several specific aspects of the method (in particular those related to stiffness values) are applicable to concrete (reinforced and/or prestressed) bridges; however, the basic ‘philosophy’ of the method is also applicable to steel and composite bridges.

Step 0 – Definition of initial input parameters. General input parameters are defined including geometry, e.g. column height and diameter (in piers with cylindrical columns), mass properties (e.g. translational mass and mass moment of inertia), and material properties. An initial estimate of the column cross-section is required. As a starting point, the output of the dimensioning of the deck and the piers for the Ultimate and Serviceability Limit States under the pertinent combinations of permanent and transient actions can be used. Then, single or multiple performance levels are set as design objectives, by designating the targeted damage states (‘damage-based’ displacements) for selected seismic hazard levels (expressed in terms of elastic displacement response spectra).

Step 1 – Selection of the displacement pattern. The step prescribed in the ‘standard’ DDBD procedure (Dwairi and Kowalsky 2006) involves the computation of the relative pier-to-deck stiffness (RS) and the determination of whether the bridge has a rigid or a flexible displacement pattern. Given that the procedure presented here is intended for bridges where higher mode contribution should not be ignored, the flexible displacement pattern scenario is adopted, disregarding the relative stiffness parameter. This means that this step is essentially redundant, nevertheless it is deemed advisable to retain it, as it is always useful for the designer to have a proper indication of the relative stiffness of the deck.

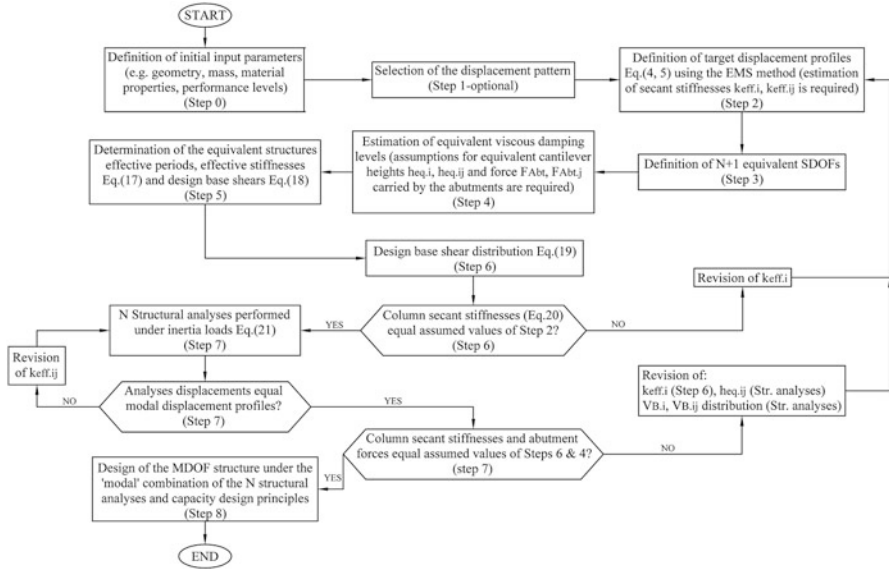


Fig. 7.1 Modal direct displacement-based design of bridges

Step 2 – Definition of target-displacement profiles. The iterative EMS method is followed, according to the following steps:

- (i) *Evaluation of mode shapes (Φ_j):* Due to the unavailability of the member effective properties at the beginning of the process, a first estimation is required. Based on current seismic design practice for bridges it can be assumed that the superstructure, particularly in the common case that it is prestressed, will respond essentially elastically, regarding its flexural stiffness, while for the torsional stiffness of prestressed concrete box girders 20 % of the uncracked value can be assumed, based on the ratios (10 ÷ 30 %) of cracked-to-uncracked torsional stiffness estimated by Katsaras et al. (2009). On the other hand, it is suggested that a secant flexural stiffness based on 10 % the gross section rigidity (EI_g) be used for columns expected to deform inelastically, while 60 % EI_g is suggested for columns that are expected to remain below yield. The reduction in the effective axial and shear stiffness (Priestley et al. 1996) of the column(s) can be considered proportional to the reduction in the effective flexural stiffness. Once the structural properties have been established, the eigenvalue problem can be solved, hence the mode shapes Φ_j can be obtained.
- (ii) *Evaluation of modal participation factors (Γ_j):* The modal participation factors can be computed using standard procedures, i.e. Eq. (7.3), where m represents a diagonal mass matrix and ι is a unit vector.

$$\Gamma_j = \frac{\Phi_j^T \mathbf{m} \mathbf{i}}{\Phi_j^T \mathbf{m} \Phi_j} \quad (7.3)$$

- (iii) *Evaluation of peak modal displacements ($u_{i,j}$):* The peak modal displacements are computed according to Eq. (7.4), where index i represents the DOF associated with a lumped mass, as per the inertial discretization, index j represents the mode number, $\Phi_{i,j}$ is the modal factor of joint i at mode j , and S_{dj} is the spectral displacement for mode j obtained by entering the 5 %-damped design spectra with the period obtained from modal analysis.

$$u_{i,j} = \Gamma_j \Phi_{i,j} S_{dj} \quad (7.4)$$

- (iv) *Evaluation of expected displacement pattern:* The displacement pattern (δ_i) is obtained by an appropriate combination of the peak modal displacements, such as the SRSS combination given by Eq. (7.5); CQC combination is expected to yield better results when the natural frequencies of the participating modes in the response are closely spaced.

$$\delta_i = \sqrt{\sum_j u_{i,j}^2} \quad (7.5)$$

It is noted that a displacement pattern derived from the above procedure accounts for the effect of all significant modes (e.g. those needed to capture around 90 % of the total mass in the transverse direction); therefore, it does not correspond to an actual inelastic deformed shape of the bridge, particularly so in the case of asymmetric systems. To obtain the target displacement profile (Δ_i), the displacement pattern given by Eq. (7.5) is scaled in such a way that none of the member (pier or abutment) displacements exceeds the target displacements obtained based on strain or drift criteria:

$$\Delta_i = \delta_i \frac{\Delta_{D,c}}{\delta_c} \quad (7.6)$$

where $\Delta_{D,c}$ and δ_c are the ‘damage-based’ displacement and the modal value at the location of the critical member, c , whose displacement governs the design, respectively. Prior to applying (7.6) one iteration might be needed to identify the most critical member, when this is not obvious. Then, peak modal displacements ($u_{i,j}$) are scaled to N modal target-displacement profiles ($U_{i,j}$) using the same scaling coefficient as that used to obtain the target-displacement profile in Eq. (7.6):

$$U_{i,j} = u_{i,j} \frac{\Delta_{D,c}}{\delta_c} \quad (7.7)$$

An immediate consequence of the aforementioned procedure is that the combination of the N modal target-displacement profiles ($U_{i,j}$) yields the target-displacement profile (Δ_i); hence, when the SRSS combination rule is used:

$$\Delta_i = \sqrt{\sum_j U_{i,j}^2} \quad (7.8)$$

Step 3 – Definition of $N+1$ equivalent SDOF structures. These idealised structures are established based on equality of the work done by the MDOF bridge and the equivalent SDOF structure (Calvi and Kingsley 1995). Each of the N SDOF structures is related to the corresponding modal target-displacement profile ($U_{i,j}$), whereas the additional SDOF is related to the (final) target-displacement profile (Δ_i). Utilizing Eqs. (7.9) and (7.10), an equivalent system displacement (Δ_{sys} , $U_{sys,j}$), mass (M_{sys} , $M_{sys,j}$), and location (x_{sys} , $x_{sys,j}$) of the SDOF across the MDOF bridge deck is computed for each of the $N+1$ SDOF structures; the ‘location’ of the SDOF system (i.e. of the masses M_{sys} or $M_{sys,j}$) coincides with the point at which the resultant of the modal forces is applied, and is one of the criteria used for checking convergence of the procedure. In Eqs. (7.9) and (7.10), m_i is the mass associated with joint i , and n is the number of joints as per the inertial discretization.

$$U_{sys,j} = \frac{\sum_{i=1}^n m_i U_{i,j}^2}{\sum_{i=1}^n m_i U_{i,j}}, \quad M_{sys(j)} = \frac{\sum_{i=1}^n m_i U_{i,j}}{U_{sys,j}}, \quad x_{sys,j} = \frac{\sum_{i=1}^n (m_i U_{i,j} x_i)}{\sum_{i=1}^n (m_i U_{i,j})} \quad (7.9)$$

$$\Delta_{sys} = \frac{\sum_{i=1}^n m_i \Delta_i^2}{\sum_{i=1}^n m_i \Delta_i}, \quad M_{sys} = \frac{\sum_{i=1}^n m_i \Delta_i}{\Delta_{sys}}, \quad x_{sys} = \frac{\sum_{i=1}^n (m_i \Delta_i x_i)}{\sum_{i=1}^n (m_i \Delta_i)} \quad (7.10)$$

Step 4 – Estimation of equivalent viscous damping levels. Utilizing the target displacement (Δ_i) and the modal target-displacement profiles ($U_{i,j}$), the ductility level is calculated for each member (for each of the $N+1$ profiles), according to Eq. (7.11). Yield curvatures are estimated using Eq. (7.12), where ε_y is the reinforcement yield strain and D is the diameter of a circular section; similar equations are provided for different section shapes (Priestley et al. 1996, 2007).

$$\mu_{\Delta_i} = \Delta_i / \Delta_{yi}, \quad (\text{or } \mu_{\Delta_i} = U_{i,j} / \Delta_{yi,j}) \quad (7.11)$$

$$\varphi_y = 2.25 \varepsilon_y / D \quad (7.12)$$

Figure 7.2 shows the modelling of a pier with a rigid base, whose top is monolithically connected to the deck, whereas possible moment diagrams under transverse loading are also illustrated. A pier moment diagram consists of two

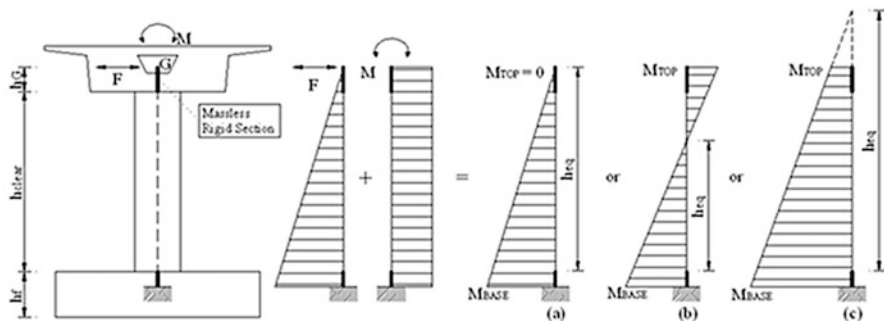


Fig. 7.2 Pier modelling and transverse response accounting for the torsional stiffness of the deck; inflection point: (a) at the top; (b) inside the pier; (c) above the pier

different components; the bending moment derived from the inertial horizontal forces F , acting on the mass centroid (G), and the bending moment induced from the eccentricity of the latter forces with respect to the shear centre, in the usual case wherein the shear centre does not coincide with the mass centroid. The final moment diagram depends on the cracked torsional stiffness of the bridge deck, the superstructure-abutment connection and the pier-superstructure relative stiffness. Likewise it is required to properly account for the degree of fixity at the pier top and hence for the transverse response of the pier regarding its flexural stiffness (k_{pier}) and yield displacement ($\Delta_{y,pier}$), according to Eqs. (7.13) and (7.14a, 7.14b), (referring to case (b) in Fig. 7.2; similar relationships apply to the other cases).

$$x_k = \frac{h_{eq}}{h} = \frac{h_{eq}}{h_{clear} + h_G}, \quad k_{eq} = \frac{3EI}{h_{eq}^3}, \quad k_{pier} = x_k k_{eq} \quad (7.13)$$

$$x_{\Delta y} = \frac{L_{eq}}{L_{eff}} = \frac{h_{eq} + 0.022 f_y d_{bl}}{h_{clear} + h_G + 0.022 f_y d_{bl}} \quad (7.14a)$$

$$\Delta_{y,eq} = \frac{\varphi_y L_{eq}^2}{3}, \quad \Delta_{y,pier} = \frac{1}{x_{\Delta y}} \Delta_{y,eq} \quad (7.14b)$$

In Eqs. (7.13) and (7.14a, 7.14b), $\Delta_{y,eq}$ and k_{eq} are the yield displacement and the flexural stiffness of the equivalent cantilever, E is the elastic modulus of the pier material, I is the moment of inertia of the pier cross-section (modified for cracking effects wherever necessary), d_{bl} is the longitudinal reinforcement bar diameter and $0.022 f_y d_{bl}$ is the strain penetration length (where f_y is the yield stress of the longitudinal reinforcement in MPA). The height of the equivalent cantilever (h_{eq}) cannot be determined at the initial stage of design, therefore either preliminary structural analyses should be performed for each of the $N+1$ equivalent structures under lateral loads compatible with the corresponding profile, or an assumption that the height of the equivalent cantilever equals the height of the pier, be made during the first iteration. The first approach is strongly recommended for the case of

significant higher mode effects, since it reduces the number of iterations required to achieve convergence.

Several relationships (Blandon and Priestley 2005; Guyader and Iwan 2006; Dwairi et al. 2007) between hysteretic damping and ductility have been proposed. The one proposed in (Dwairi et al. 2007) based on Takeda's hysteretic model (Takeda et al. 1970), given by Eq. (7.15), is used herein. Additional elastic viscous damping (ξ_v), up to 5 % should be added to the hysteretic damping in line with the approach proposed by Grant et al. (Grant et al. 2004).

$$\xi_i = \xi_v + \frac{50}{\pi} \left(\frac{\mu_\Delta - 1}{\mu_\Delta} \right) \% \quad (7.15)$$

These damping values need to be combined in some form to obtain system damping for each of the $N+1$ equivalent SDOF structures. A weighted average can be computed, as given by Eq. (7.16), where $W_i/\Sigma W_k$ is a weighting factor, based on the work (W_i) done by each member (Eq. (7.17)), according to (Kowalsky 2002)

$$\xi_{sys} = \sum_{i=1}^n \left(\frac{W_i}{\sum_{k=1}^n W_k} \xi_i \right), \quad \xi_{sys(j)} = \sum_{i=1}^n \left(\frac{W_{i,j}}{\sum_{k=1}^n W_{k,j}} \xi_{i,j} \right) \quad (7.16)$$

$$W_i = V_i \Delta_i, \quad W_{i,j} = V_{i,j} U_{i,j} \quad (7.17)$$

Calculation of the weighting factors presupposes knowledge of member forces (V_i), which are not known at the current step. As a starting point, it can be assumed that the seismic force carried by the abutments is equal to 30 % of the total seismic force carried by the bridge and column shears are inversely proportional to column heights, as illustrated by Eq. (7.18) (Kowalsky 2002), where μ is less than one for elastic columns and equal to one for columns that have yielded. In subsequent iterations, system damping is computed using member forces obtained from structural analysis.

$$W_i = \mu_{\Delta_i} \Delta_i / h_{eq,i}, \quad W_{i,j} = \mu_{\Delta_i} U_{i,j} / h_{eq,i,j} \quad (7.18)$$

Step 5 – Determination of the effective periods of the equivalent structures.

Utilizing the $N+1$ system target displacements (Δ_{sys} , $U_{sys,j}$), levels of system damping (ξ_{sys} , $\xi_{sys,j}$), and elastic response spectra for the chosen seismic demand, the effective periods (T_{eff} , $T_{eff,j}$) of the equivalent structures are determined from the design spectrum (see next section). Once the effective periods have been determined, effective stiffnesses (k_{eff} , $k_{eff,j}$) and design base shears (V_B , $V_{B,j}$) are computed by Eqs. (7.19) and (7.20), respectively.

$$k_{eff} = 4\pi^2 M_{sys}/T_{eff}^2, \quad k_{eff,j} = 4\pi^2 M_{sys,j}/T_{eff,j}^2 \quad (7.19)$$

$$V_B = k_{eff}\Delta_{sys}, \quad V_{B,j} = k_{eff,j}U_{sys,j} \quad (7.20)$$

Step 6 – Verification of design assumptions. Design base shears (V_B , $V_{B,j}$) are distributed in proportion to the inverse of the column height according to Eq. (7.21), which is based on the simplifying assumption that all columns have the same diameter and longitudinal reinforcement ratio, zero post-elastic slope of the force-displacement response, mass small enough, so that inertia forces due to self-weight can be neglected, and the same end-fixity conditions. In Eq. (7.21) μ_i and μ_k are less than one for elastic columns and equal to one for columns that have yielded, and F_{Abr} represents the total force carried by the abutments. R/C member cracked section stiffnesses are computed for each of the $N+1$ profiles, using Eq. (7.22) and are compared with values assumed at Step 2. If the values related to the target-displacement profile (Δ_i) differ significantly, computed secant stiffnesses ($k_{eff,i}$) are utilized in the EMS to obtain revised target-displacement profiles (Δ_i , $U_{i,j}$). Steps 2–6 are repeated by changing column secant stiffnesses until the target profile (Δ_i) stabilises. Although a strict approach requires iteration within Steps 2–6 until all profiles (Δ_i and $U_{i,j}$) stabilise, the implementation of the methodology in the next section indicates that whenever Δ_i stabilises, $U_{i,j}$ also practically stabilise, hence Δ_i can be used as the sole convergence criterion.

$$V_{B,k} = (V_B - F_{Abr}) \frac{\mu_{\Delta,k}}{h_k} / \sum_{i=1}^n \frac{\mu_{\Delta,i}}{h_i}, \quad V_{B,k,j} = (V_{B,j} - F_{Abr,j}) \frac{\mu_{\Delta,kj}}{h_k} / \sum_{i=1}^n \frac{\mu_{\Delta,ij}}{h_i} \quad (7.21)$$

$$k_{eff,i} = V_{B,i}/\Delta_i, \quad k_{eff,ij} = V_{B,ij}/U_{i,j} \quad (7.22)$$

Step 7 – Structural analysis. Once the target-displacement profile (Δ_i) stabilises, base shears ($V_{B,j}$) are distributed as inertia forces to the masses of the MDOF structure in accordance with the modal target-displacement profiles ($U_{i,j}$), given by Eq. (7.23) (Calvi and Kingsley 1995). In this equation $F_{i,j}$ are the bent inertia forces, $V_{B,j}$ are the design base shears, indices i and k refer to joint numbers, and n is the number of joints.

$$F_{k,j} = V_{B,j} (m_k U_{i,j}) / \sum_{i=1}^n (m_i U_{i,j}) \quad (7.23)$$

N structural analyses (as many as the significant modes) are performed on the bridge under the inertia loads, to obtain the ‘modal’ base shear for each column. Secant stiffnesses $k_{eff,ij}$ obtained from the iteration within Step 6, at which stabilisation of Δ_i (hence stabilisation of $U_{i,j}$ as mentioned in Step 6) was observed, should be used in each of the N structural analyses, in order to be consistent with the DDBD philosophy. Afterwards, displacements derived from the N structural analyses are compared with the corresponding profiles $U_{i,j}$. In the case of significantly different displacements, reasonable values for column secant stiffnesses are

assumed and analyses are conducted until convergence is achieved. Once the displacement profiles obtained from structural analyses converge to the assumed modal target-displacement profiles, column secant stiffnesses and abutment forces from each analysis are compared with the values assumed at Step 6, at which stabilisation of $U_{i,j}$ was achieved. It is reminded that during the first loop of iterations the seismic force carried by the abutments is assumed equal to 30 % of the total seismic force carried by the bridge for all the $N+1$ cases. In case of significant discrepancy, the target-displacement profile is revised utilising the EMS method and forces from structural analysis. Steps 2–7 are repeated, until column secant stiffnesses and abutment forces converge.

In order to perform the new loop of iterations and the new EMS in particular, previous loop secant stiffnesses ($k_{eff,i}$) (Step 6) can be assumed as the starting point. Furthermore, revised equivalent cantilever heights are computed according to the results of the N structural analyses, which were previously performed, as far as the modal target-displacement profiles ($U_{i,j}$) are concerned, whereas in the case of the (final) target-displacement profile (Δ_i), proper values of the equivalent cantilever heights can be approximately determined by combining the peak ‘modal’ responses (N structural analyses). Following the same approach, the force carried by the abutments and the base shear distribution for each of the $N+1$ cases required in the subsequent steps are determined from analysis results, instead of utilising Eq. (7.21), which, given the diversity of the column end-fixity conditions, is not accurate enough.

Step 8 – Design of the MDOF structure The MDOF bridge is designed in accordance with capacity design principles (e.g. (CEN 2005; Priestley et al. 1996)) such that the desired failure mechanism is achieved. The response quantities of design interest (displacements, plastic hinge rotations, internal pier forces) are determined by combining the peak ‘modal’ responses (from the N structural analyses), using an appropriate modal combination rule (e.g. SRSS or CQC), and superimposing the pertinent combinations of permanent and transient actions.

7.3.2 Application of the Procedure

The various steps of the PBD method described in Sect. 7.3.1 are applied in the following to an actual concrete bridge (Kappos et al. 2013), whose different pier heights and the unrestrained transverse displacement at the abutments result in an increased contribution of the second mode. The bridge is designed both to the ‘standard’ DDBD procedure proposed by Kowalsky and co-workers (Kowalsky 2002; Dwairi and Kowalsky 2006) and to the more rigorous procedure described in Sect. 7.3.1.

7.3.2.1 Description of Studied Bridge

The selected structure (Overpass T7 in Egnatia Motorway, N. Greece), is quite common in modern motorway construction in Europe. The 3-span structure of total length equal to 99 m (see Fig. 7.3) is characterized by a significant longitudinal slope (approximately 7 %). The deck consists of a 10 m wide prestressed concrete box girder section with a variable geometry across the longitudinal axis of the bridge (see Fig. 7.3). The two piers have a cylindrical cross section, and unequal height (clear column height of 5.94 and 7.93 m), due to the deck’s longitudinal inclination. The deck is monolithically connected to the two piers, while it rests on its abutments through elastomeric bearings; movement in both the longitudinal and the transverse direction is initially allowed at the abutments, but transverse displacements are restrained in the actual bridge whenever the 15 cm gap shown at the bottom of Fig. 7.3 is closed. In applying the proposed design procedure to this bridge, the gap size, as well as the characteristics of the bearings are treated as design parameters. The bridge rests on firm soil and the piers and abutments are supported on surface foundations (footings) of similar configuration.

The T7 Overpass was redesigned (Kappos et al. 2013) using DDBD, both in the form proposed in (Dwairi and Kowalsky 2006), and its modified version presented herein, for two different seismic zones. The Greek Seismic Code (EAK 2000) elastic spectrum (Ministry of Public Works of Greece 2010) for Zone II (PGA of 0.24 g) and III (PGA of 0.36 g) was the basis for seismic design; it corresponded to ground conditions category ‘B’ of the Code, which can be deemed equivalent to subsoil class ‘B’ of older drafts of Eurocode 8 and closer to ground ‘C’ in its final

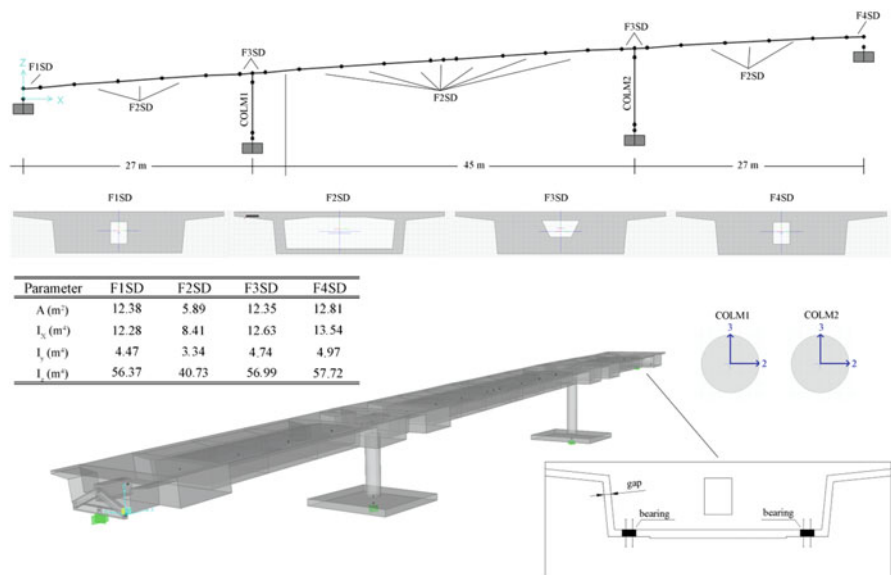


Fig. 7.3 Layout of the bridge configuration and finite element modelling

version (CEN 2004). The bridge was designed as a ductile structure, implying that plastic hinges are expected to form in the piers, while P- Δ effects were taken into consideration. A further parameter that was investigated in applying the DDBD was the effect of the girder torsional stiffness.

In the analyses presented in the following, the focus is on the transverse response of the bridge, as it is well known that this is the most affected by higher modes. Additional analyses in the longitudinal direction were also conducted, however due to space limitations and the fact that longitudinal design was found to be less critical, these analyses are not presented herein. The analysis was carried out using the Ruaumoko 3D software (Carr 2006), whereas SAP2000 (CSI [Computers and Structures Inc.] 2007) was also used for additional verification; the reference finite element model (Fig. 7.3) involved 32 non-prismatic 3D beam-column elements. The elastomeric bearings present at the abutments were modelled using equivalent linear springs ('Link elements' in SAP2000, 'Spring type members' in Ruaumoko) with six DOFs.

Preliminary analyses accounting for soil-structure interaction (SSI) effects, using a foundation compliance matrix, have shown that due to the relatively stiff soil formations underneath the studied bridge, SSI had little effect on the response; hence these effects were subsequently ignored in the design of the bridge.

7.3.2.2 'Standard' Direct Displacement-Based Design (DDBD)

A 'standard' DDBD (Kowalsky 2002; Dwairi and Kowalsky 2006) was first performed, mainly to identify the limitations of the procedure, which arise from its inherent restriction to structures wherein the fundamental mode dominates the response (Calvi and Kingsley 1995). As shown later, the transverse response of the overpass is determined by two dominant modes. A 'damage control' limit state that corresponds to a drift ratio of 3 % was considered; qualitatively, 'damage control' implies that only repairable damage occurs in the columns.

The design displacement spectrum (Fig. 7.4) was derived from the pertinent elastic acceleration response spectrum ($S_d = S_a/\omega^2$). A significant modification was made to the spectrum used for design, i.e. the corner period in S_d was taken equal to 4.0 s, according to the SEAOC (Ad Hoc Committee 1999) recommendations, which is substantially longer than the period values of 2.0 and 2.5 specified by EC8 and the National Annex of Greece, respectively. This modification is not only in line with recent research findings, but also necessary for DDBD to be meaningful (Kappos 2010), in the sense that short corner periods lead to small displacement values in the period range that is common to DDBD (up to the linear branch), which involves secant stiffness values at maximum displacement.

Moreover, the modification to the elastic acceleration spectrum, required to account for ductile response through an increased effective damping ratio, was made using the damping modifier (η) adopted in the final version of EC8 (CEN 2004), i.e. Eq. (7.24) below, where ξ_{s,y_s} is the viscous damping ratio of the structure, expressed as a percentage.

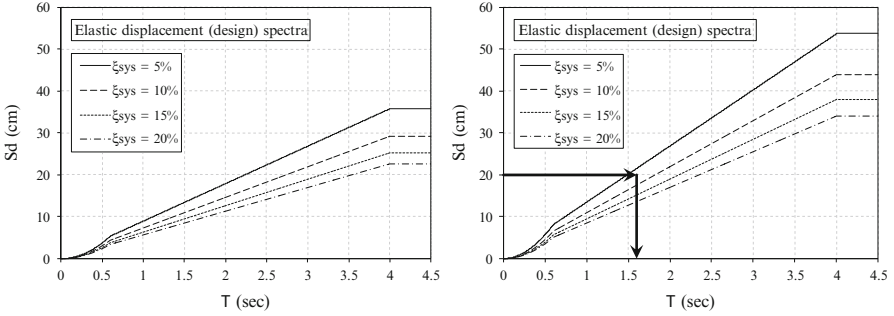


Fig. 7.4 Elastic displacement response spectra for various damping ratios; *left*: Zone II (PGA = 0.24 g), *right*: Zone III (PGA = 0.36 g)

$$\eta = \sqrt{10 / (5 + \xi_{sys})} \quad (7.24)$$

As previously mentioned, the mechanical characteristics of the elastomeric bearings are a design parameter since they affect the displacement capacity of the bridge; hence an initial estimate is required. A rational choice of the elastomer cross-sectional area can be made on the basis of the axial load resulting from service loading, while the total thickness (t_r) of the elastomer should provide the target-displacement profile (see Fig. 7.5) with adequate displacements at the abutments, so that the ‘damage-based’ displacements (Δ_D) of each column, related to the acceptable drift ratio, could be attained, and a reasonable longitudinal reinforcement ratio could be obtained for the columns. The elastomeric bearings selected herein are rectangular in shape (350 mm \times 450 mm) with t_r of 88 mm, horizontal stiffness of 2,506 kN/m and equivalent viscous damping ratio equal to 5 %; two bearings are placed on each abutment, as shown in Fig. 7.3 (bottom-right). The maximum acceptable shear strain ratio (γ_u), from which the ‘damage-based’ displacements of the bearings are derived, is taken equal to 2.0. Introducing the 3 % drift ratios for the columns and accounting for strain penetration effects, the ‘damage-based’ displacements of all members (piers or abutments) were defined as $\Delta_{D,Abt} = 0.176$, $\Delta_{D,Col1} = 0.218$, $\Delta_{D,Col2} = 0.278$ m; a diameter of 2.0 m was initially assumed for the two columns (as in the original design of the bridge).

To obtain the target-displacement profile for the inelastic system, the EMS method (Kowalsky 2002) is used. It is assumed that the prestressed deck will respond essentially elastically, as far as its flexural stiffness is concerned, while its torsional stiffness is set equal to 20 % of the uncracked section torsional stiffness. A secant flexural stiffness equal to 10 % the gross value is applied to the columns (both of them are expected to respond inelastically), while the reduction in the effective axial and shear stiffness is considered to be proportional to the reduction in flexural stiffness. Figure 7.5 illustrates the target-displacement profiles derived from applying the EMS method iteratively; displacement patterns, peak modal displacements and modal mass participation factors for each mode are also

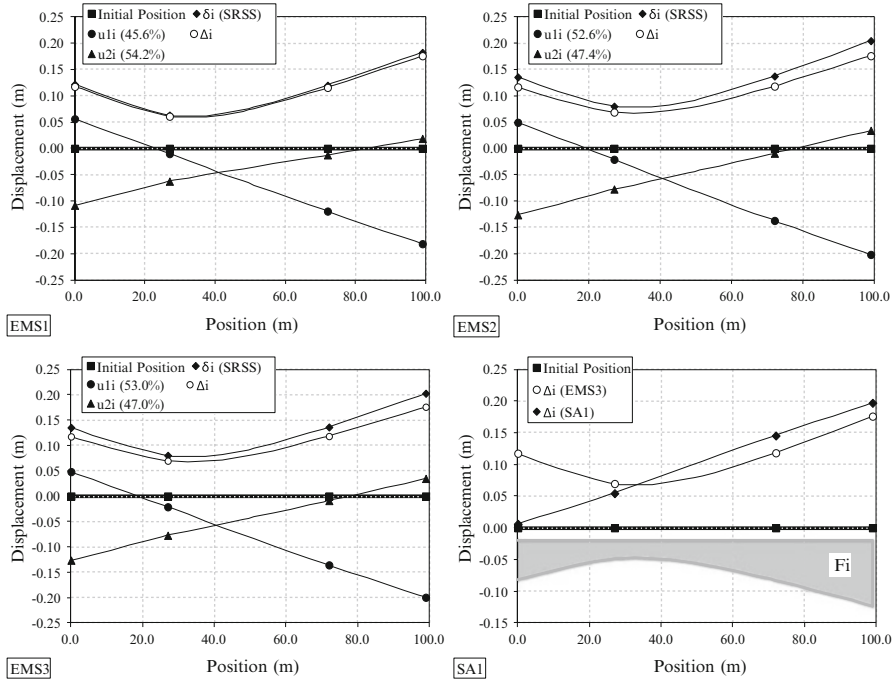


Fig. 7.5 Displacement profiles (EMS): Peak modal displacements $u_{i,j}$, displacement pattern δ_i and target-displacement profiles Δ_i , estimated iteratively from the EMS method. Structural analysis displacement profile (SA1) compared with target-displacement profile (inertia forces (F_i) on the MDOF structure also illustrated)

shown. Convergence was checked with regard to stabilisation of the target-displacement profile or the column secant stiffness from one iteration to the next. Dots on the graphs represent the points of the deck axis passing through its mass centroid, corresponding to the centres of elastomeric bearings and columns.

The next step of the ‘standard’ DDBD method involves structural analysis of the bridge under the inertia loads given by Eq. (7.23), (where, in the ‘standard’ procedure, $U_{i,j}$ corresponds to Δ_i), to obtain the design shear at the base of each column. In Fig. 7.5 (bottom-right) the displacement profile derived from structural analysis Δ_i (SA1), is compared with the target-displacement profile Δ_i (denoted as EMS3). The discrepancy between the two profiles reveals one of the main deficiencies of the ‘standard’ DDBD, i.e. its inability to predict the peak structural response (in terms of displacements and hence internal member forces), on the basis of which design will be carried out.

The target-displacement profile, which generally reflects the ultimate limit state (in terms of displacements) of the structural members, was constructed from the combination of the peak modal displacements (according to the SRSS rule), and then scaled in such a way that none of the member displacements exceeded the ‘damage-based’ design values. By following this procedure, the target-

displacement profile never reflects an actual deformed shape of the structure; instead, it represents a fictitious deformed shape comprised of non-simultaneous displacements, which is deemed to reflect the peak (and non-simultaneous) structural member response. Therefore, in cases (like here) where more than one modes dominate the response, a static structural analysis under a modal combination of seismic lateral forces such as those given by Eq. (7.23) (whose distribution is also shown in Fig. 7.5, bottom-right), cannot, under any circumstances, produce the target-displacement profile. The above discrepancy in the displacement profiles is due neither to errors in the estimation of the equivalent cantilever heights nor to the approximate base shear distribution according to Eq. (7.21) (Kappos et al. 2013).

To be able to compare results from the existing DDBD method with those of the proposed one, the requirement of convergence of the entire profiles was replaced by a lower requirement, namely convergence at the locations of two supporting members only, first the Abutment 2 (that has the largest displacement) and Column 2 (that is the one closest to Abutment 2), and then (as an alternative) the two columns, although neither exhibits the largest design displacement. As shown in Fig. 7.6, several iterations (adjustments of member effective stiffness) using the converged profile from EMS ('Loop 1- Δi (EMS3) in the figure) fail to obtain even a rough match between the EMS displacement profile and that obtained from structural analysis (Δi (SA) in the figure) on the left part of the bridge, while convergence is reached in the area of the left column and the left abutment (Abt2), which are affected by the fundamental mode of the bridge (see also Figs. 7.5 and 7.7). As a result of this, the design of Abutment 1 and Column 1 on the basis of the aforementioned structural analysis is not correct. Similar comments apply in the other case studied, wherein convergence was sought for the two columns.

7.3.2.3 Modal Direct Displacement-Based Design (MDDBD)

The extended (modal) DDBD procedure described in Sect. 7.3.1 was applied to the previous case study; more details than those given herein can be found in (Kappos et al. 2013) and its Appendix available on line.

As in the 'standard' DDBD, a 2.0 m column diameter was assumed as a starting point. However, seismic design for Zone II resulted in column longitudinal reinforcement ratios less than the minimum required by bridge codes. Due to the fact that providing the minimum required ratio would obscure the concepts of DDBD (regarding the target profile, displacement ductilities etc.) and aiming at an optimum design, a 1.5 m column diameter was subsequently used. Preliminary structural analyses were performed for each of the three equivalent SDOF systems ($N + 1$, considering the first 2 modes), under lateral loads compatible with the modal profiles and their SRSS combination, to obtain the equivalent cantilever heights and the uncracked stiffnesses ($K_{g,i}$), according to Eq. (7.13). The assumed characteristics of the elastomeric bearings, the design spectrum and the 'damage-based' displacements were determined as in the 'standard' DDBD.

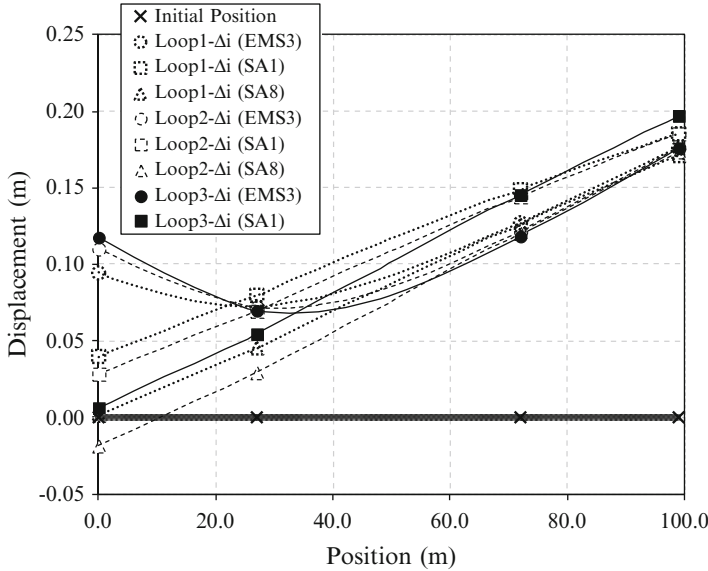


Fig. 7.6 Target-displacement profiles Δ_i (EMS), structural analysis displacement profiles (SA1) based on the secant stiffnesses of EMS and revised structural analysis displacement profiles (SA) that converge to the target-displacement of the critical member (i.e. Abt2) and Col2, derived iteratively from the DDBD methodology

To establish the initial displacement profiles, a modal analysis was conducted where member stiffnesses were set as in the ‘standard’ DDBD. The peak modal displacements ($u_{i,j}$), the displacement pattern (δ_i), the target-displacement profile (Δ_i) and the modal target displacement profiles ($U_{i,j}$) are shown in Fig. 7.7, and it is clear that the abutments are the critical elements. The three equivalent SDOF systems were defined in accordance with Eqs. (7.9) and (7.10).

Once the target-displacement profiles were established, the individual member ductility values (Eqs. (7.11)) were calculated along with the corresponding equivalent viscous damping values (Eq. (7.15)), where elastomeric bearings were assumed to respond elastically ($\xi_{Abt} = 5\%$). Assuming that 30% of the total shear is carried by the abutments (in all 3 cases), the equivalent system damping values were obtained. The effective periods at maximum response were then obtained from the displacement spectra (Fig. 7.4) and then the secant stiffnesses at maximum response were determined. Design base shears were calculated from Eq. (7.20) and member shear forces from Eq. (7.21). As soon as base shears for the SDOF systems are defined, the fraction of the shear carried by the abutments can be recalculated. If the revised fractions of the base shear differ significantly from the assumed values (30%), Steps 4 and 5 are repeated until fractions of x_{Abt} stabilise. It is clear than in the common case of seat-type abutments with bearings the design is simplified on the grounds that the shear carried by the abutment is known from the first iteration. The column secant stiffness values can be recalculated at this point since column

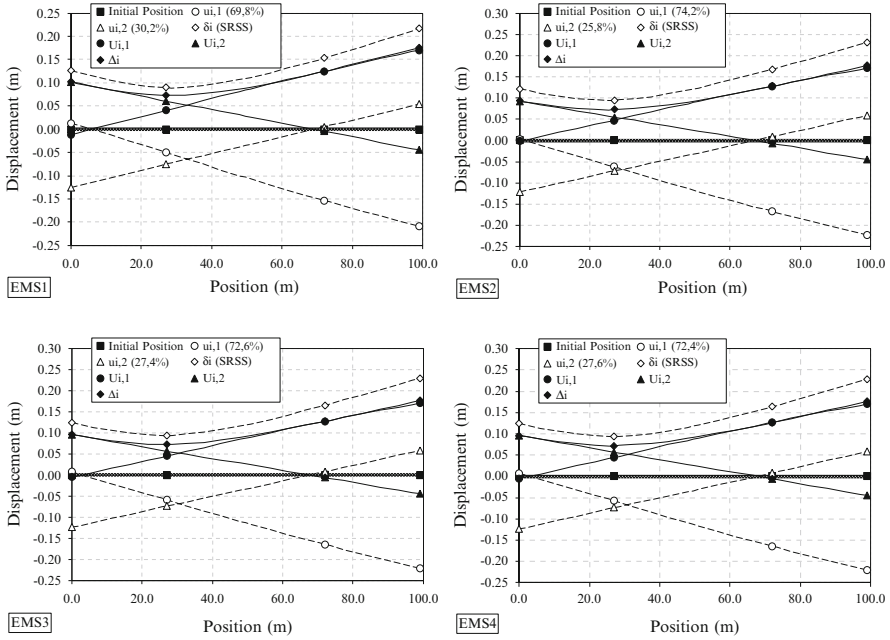


Fig. 7.7 Displacement profiles: Peak modal displacements $u_{i,j}$, displacement pattern δ_i , modal target-displacement profiles $U_{i,j}$ and target-displacement profiles Δ_i , derived iteratively from the EMS method

forces and member displacements are now known. This is then followed by a revised modal analysis with the new secant stiffness properties resulting into new target-displacement profiles (Δ_i, U_{ij}). In total, four iterations were needed until Δ_i stabilised. The finally derived profiles are illustrated in Fig. 7.7. It is evident (from Iterations 3 and 4), that whenever Δ_i stabilises, $U_{i,j}$ also stabilise.

Once the target-displacement profile (Δ_i) converged, two structural analyses of the MDOF structure were performed under the inertia forces of Eq. (7.21), using the secant stiffnesses from the 4th Iteration (Mode 1 and Mode 2). Due to the inconsistency of the derived displacements ($U_{an,ij}$) with the corresponding modal target displacements ($U_{i,j}$), the two analyses were repeated with revised secant stiffnesses until convergence was achieved; U_{i1} and U_{i2} converged after 8 and 5 iterations, respectively. The shear carried by the abutments in the last iteration closely matches the values obtained through EMS (Iteration 4), due to the fact that bearing stiffness is assumed constant, determined from the initial selection of the bearing characteristics. Since the final secant stiffnesses of the columns differed significantly from the assumed ones (Kappos et al. 2013), Steps 1 to 7 were repeated, and new equivalent cantilever heights and column shear distribution were defined from the analysis.

The new loop of iterations attempts to reduce the discrepancy resulting from updating the equivalent cantilever height (which does not change much with respect

to the initially assumed value), and the shear distribution effect according to Eq. (7.21), but not the fraction of the shear carried by the abutments, since this is considered known, as already discussed. It is noted that the $\Delta_{an,i}$ is derived from the SRSS combination of $U_{an,ij}$.

The response quantities of design interest (rotations, internal pier forces) are determined by combining the peak ‘modal’ responses (from the two structural analyses), using the SRSS combination rule, superimposed with the pertinent combinations of permanent and transient actions. P- Δ effects were also taken into account, and it was verified that the stability index satisfied $\theta_{\Delta} \leq 0.20$. Finally, the design procedure yielded a longitudinal steel ratio of 9.8‰ and 12.4‰ for Col₁ and Col₂, respectively. The ratio of Col₁ is just slightly less than the minimum required ratio (1 %), according to the Eurocode.

The procedure was repeated for the case of Zone III (see Fig. 7.4) in which case a 2.0 m column diameter was selected. In this case the design yielded a longitudinal steel ratio of 11.5 and 19.0‰ for Col₁ and Col₂, respectively.

An additional investigation regarding the effect of the box girder torsional stiffness throughout the suggested methodology can be found in (Fischinger et al. 2004). It was found that while a zero torsional stiffness assumption simplifies the design procedure (no iteration for the equivalent cantilever heights is required), it also overestimates the required longitudinal steel ratios (4.2 and 6.2 % for Col₁ and Col₂, respectively) and hence leads to uneconomical design.

7.4 A PBD Procedure Based on Inelastic Analysis

The PBD procedure based on deformation control and involving inelastic response-history analysis, proposed for buildings by Kappos and Stefanidou (2010) is tailored herein to seismic design of bridges. It will be seen that several modifications are required, primarily arising from the fact that the favourable plastic mechanism is different in bridges (energy dissipation takes place in the vertical members, i.e. the piers). Although reference to response-history analysis is made throughout, it should be understood that nonlinear static procedures that duly account for higher mode effects (see Sect. 7.5) can also be used in many cases.

7.4.1 Description of the Procedure

Step 1 – Flexural design of plastic hinge zones based on operability criteria.

The purpose of this step is to establish a basic level of strength in the structure that would ensure that the bridge remains operational during and after an earthquake having a high probability of exceedance (usually taken as 50 % in 50 years). The operability verifications include specific limits for member ductility factors and plastic hinge rotations of critical members (see Step 4) and the corresponding

demands are estimated from *inelastic* analysis of a partially inelastic model of the structure (described in Step 3). Since for any inelastic analysis to be carried out the strength of the yielding zones must be an input parameter, an *initial* elastic analysis is required, which would provide the strength of the members (energy dissipation zones) that will respond inelastically during the operability verification; this analysis constitutes Step 1 and is a vital part of the procedure.

The design of selected dissipation zones, like the pier ends, is carried out using conventional elastic analysis (modal response spectrum, or equivalent static, analysis, depending on the structural system). The strength of these zones is estimated taking into consideration the range within which the inelastic deformations should fall, which corresponds to the degree of damage allowed for the selected performance level (more specifically the allowable rotational ductility factor). The procedure described in the following leads to attaining the permissible values of inelastic deformations (expressed through ductility factors), since the latter are directly related to the reduction of element forces corresponding to elastic behaviour. This is a critical feature, not included in earlier versions of the method (tailored to buildings) that simply included a serviceability check, the result of which typically was that most members either remained elastic or were well below the allowable deformation limits (Kappos and Panagopoulos 2004). The design procedure described herein aims at the development of the selected inelastic deformations in the piers, directly using rotational ductility factor (μ_θ) as a design parameter. It is noted that use of curvature ductility factor (μ_ϕ), plastic hinge rotations and/or strain values for materials is also feasible, although not done here.

To meet the aforementioned goal, element forces and rotations are first obtained from the results of a standard response spectrum (elastic) analysis. Pier stiffness in this case should be estimated on the basis of yield condition in the pier, preferably by taking into account the effects of axial load ratio; the diagrams proposed in (Priestley et al. 1996) and adopted by Caltrans (Bardakis and Fardis 2011) can be used, considering axial load from service loading, and assuming either minimum reinforcement (1 %) or that resulting from design for non-seismic loading (if higher than 1 %); the diagrams of Fig. 7.8.

Design for flexure is carried out in terms of design values of material strength (in R/C piers f_{cd} and f_{yd} for concrete and steel, respectively) using commonly available design aids. On the other hand, operability checks (Step 4) are based on the results of inelastic analysis, for which mean values are commonly adopted (f_{cm} and f_{ym}); furthermore, some members are expected to possess overstrength with respect to the design moments used in their dimensioning, due to detailing requirements, i.e. rounding (upwards) of required reinforcement areas and use of minimum reinforcement specified by codes. For these two reasons, the initial elastic analysis should be carried out for an appropriate fraction ν_o of the earthquake level associated with the operability performance level (e.g. 50 %/50 years). Due to the expected overstrength, the recommended ν_o factor is lower than the ratio of f_{yd}/f_{ym} (equal to 0.79 if the mean yield strength of steel f_{ym} is taken as 10 % higher than the characteristic strength f_{yk}). Furthermore, the ν_o factor should also account for the

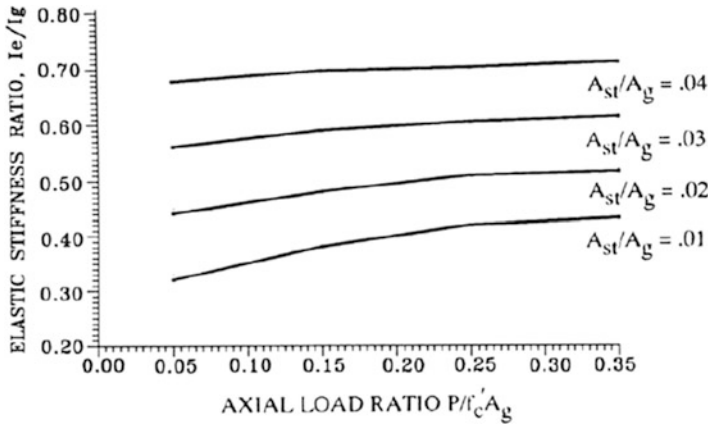
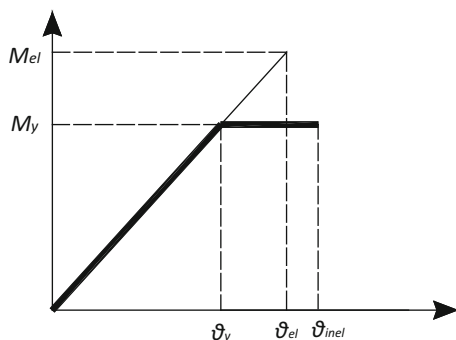


Fig. 7.8 Effective stiffness of cracked reinforced concrete circular sections (Bardakis and Fardis 2011; Priestley et al. 1996)

differences in the moments derived from a response spectrum analysis and those from a series of response history analysis for selected accelerograms (see steps 2 and 4). As an alternative, one could select to use design values of yield moments in the inelastic analysis (a practice not adopted by current codes), in which case a different ν_o factor should be used (note that if $\nu_o = 1$ is selected piers will not yield for the operability earthquake, which is deemed as a very high performance level, typically not justified in economic terms). It is perhaps worth noting that the problem of mixing design and mean values of material strength is by no means specific to the PBD method presented here; modern codes like Eurocode 8 adopt both elastic and inelastic analysis methods and recommend use of design values for strength verifications and of mean values for displacement or deformation verifications.

Subsequently, elastic rotations (θ_{el}) are related to the corresponding inelastic ones (θ_{inel}), using an empirical procedure (like (Kappos et al. 2012a)); use of empirical factors to estimate θ_{inel} is an inherent limitation of the proposed procedure, since otherwise ductility factors cannot be estimated at this stage. Referring to Fig. 7.9, having defined the target rotational ductility factor (μ_θ) and the maximum inelastic rotation, θ_{inel} (this is the *total* chord rotation, not the plastic one), from the θ_{el} found in the elastic analysis, the yield rotation ($\theta_y = \theta_{inel}/\mu_\theta$) is calculated for every pier. For simplicity of the procedure one could assume first that M- θ response is elastic-perfectly plastic (as in Fig. 7.9) and second that the slopes of the elastic and the elastoplastic M- θ diagrams are the same. Then the corresponding yield moment (M_y) can be easily computed, as the intersection of the elastic part of the diagram and the vertical line drawn at θ_y , as shown in Fig. 7.9; this is the moment to be used for the (flexural) design of the pier. A more accurate, and somewhat more involved, procedure is described in the following.

Fig. 7.9 Elastic and elastoplastic $M-\theta$ diagram for piers



Attention should be paid to the fact that an increase in deformation does not come with a proportional decrease in design force, i.e. the slope of the first branch in the elastic and the elastoplastic diagram is generally different (Fig. 7.10). The latter derives from the relation of element moments to rotations ($M-\theta$) that is dependent on the loading history (which is non-proportional). Moments and rotations due to permanent loading (gravity and reduced live loads) are first applied and held constant, and any decrease of the elastic forces (M_{el}) should refer to the seismic loading that is applied after the permanent one. Hence, the yield moment should be

$$M_y = M_g + aM_E \quad (7.25)$$

and since the $M-\theta$ relationship for seismic loading is linear for elastic behaviour, the reduction factor a is the same for moments and rotations. Knowing the moments developing due to permanent loads (M_g), the values of reduced pier forces for design aM_E can then be determined. As the value of the yield rotation θ_y is already known, as well as the elastic rotations due to seismic loading (θ_E), the value of the reduction factor can be estimated from the following relationship (based on the geometry of Fig. 7.10):

$$\alpha = \frac{\theta_y - \theta_g}{\theta_E} \quad (7.26)$$

The differences in the yield moments resulting from the accurate procedure from those from the simplified one are not large (less than 10 % on the average, but in some instances they are higher, especially for the positive M_y).

According to the aforementioned procedure, the reduced design moments are computed for every pier, and they are directly related to the target rotational ductility selected for the operability performance level. The longitudinal reinforcement demand for the piers is calculated using standard flexural design procedures and compared to the minimum requirements according to code provisions. In case the longitudinal reinforcement demands are found to be less than the minimum requirements, reduction of cross sections is in order (reduction of stiffness), otherwise deformations for the considered performance level will be less than

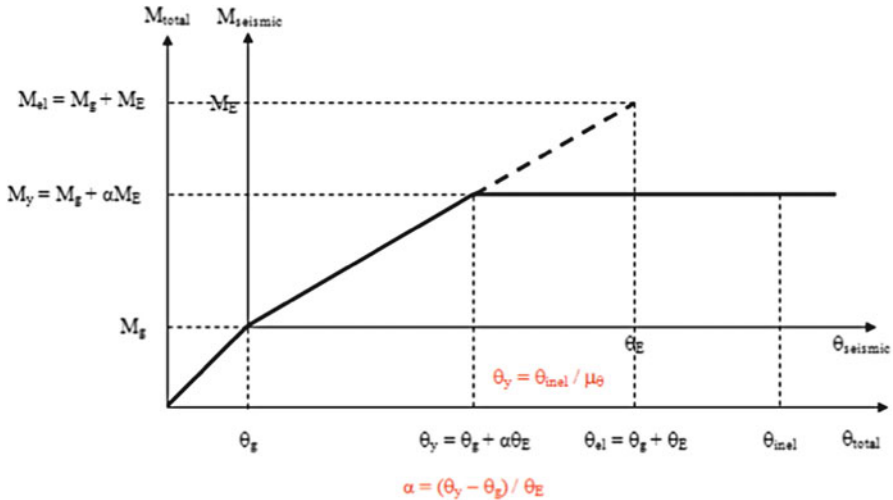


Fig. 7.10 Definition of the correct slope of $M-\theta_{inel}$ diagram and of $\alpha\theta_E$

the allowable ones; clearly, this stage involves striking a balance between economy and performance.

Step 2 – Selection of seismic actions. The response-history analysis necessary for seismic design according to the proposed method requires the definition of appropriately selected input seismic motions (see also Sect. 7.2.2). The accelerogram set used for a 3D analysis should include a pair of components for every seismic motion, provided the vertical component is not important for the design of the bridge (which is not always the case). It is recommended that it be selected based on the results of a seismic hazard analysis (‘deaggregation’ phase, wherein M and R for the site in consideration are determined). Hence the selected input seismic motions should conform to certain criteria concerning magnitude (e.g. $M_s = 6.0-6.5$), and epicentral distance (e.g. $R = 10-25\text{ km}$), and also peak ground acceleration (e.g. $PGA > \sim 0.1\text{ g}$). An additional criterion, not specifically required by Eurocode 8, but important all the same, is the similarity of spectra (those of the selected motions to the target spectrum); software for such multi-criteria selection of the design accelerograms is currently available, e.g. (Katsanos and Sextos 2013).

The earthquake motions used for design, should be properly scaled in order to correspond to the level associated with the limit state examined (‘operationality’ limit state for the design of energy dissipation zones, and ‘life safety’ for the other members). Several scaling procedures have been explored (Kappos et al. 2007) and the one adopted by EC8-Part 2 (Kappos et al. 2013) is suggested, modified with regard to the amount the ordinates of the elastic spectrum are exceeded within the critical range of periods, i.e. 10 % instead of 30 % (which is deemed incompatible with the adopted safety format).

Step 3– Set-up of the partially inelastic model. During this step a partially inelastic model (PIM) of the structure is set up, wherein the columns of the piers (top and bottom if they are monolithically connected to the deck) are modelled as yielding elements, with their strength based on the reinforcement calculated for reduced element moments according to the inelastic deformations allowed for the operationality limit state (step 1). In the same model, the remaining parts of the bridge are modelled as elastic members. Since the dissipating zones have been designed for flexure at step 1, the stiffness of the piers can now be estimated from Eqs. (7.1) and (7.2) using the actual yield curvature and yield moment of the pier ends (mean values, since deformations will be checked at this stage).

Step 4 – Serviceability/operationality verifications. The use of inelastic dynamic response-history analysis in the PIM, involves a set of recorded motions scaled to the intensity corresponding to the operationality level. The verifications include specific limits for maximum drifts and plastic deformations of critical members (i.e. the piers). The limits can be derived on the basis of accepted damage, especially in the context of allowing the bridge to remain operational under this level of seismic action. Several criteria are discussed in (fib 2007) and it is clear that the proposals available in the literature vary substantially, from conservative ones (e.g. (Choi et al. 2004) addressing non-seismically designed columns) to very daring ones (Priestley et al. 1996) intended for modern ductile bridge piers. An appropriate way to define acceptable damage for R/C piers is in terms of strains; for instance, it is clear that the functionality of the bridge will not be impaired if cover concrete does not spall, which typically occurs at strains between 3.5 and 4‰. Such strain values can then be used to derive either displacement limits based on simplifying assumptions for the bending moment in the pier (e.g. (Kowalsky 2002)) or moment – rotation diagrams that are more appropriate for the type of analysis used herein. In the case of bridges (and in contrast to normal buildings) deformation control in the piers does not fully guarantee that the bridge will remain functional (operational); it is equally important to check that bearings (which will be present at least in seat-type abutments) also remain functional. For the usual type of elastomeric bearings this limit could be set to between 50 and 100 mm (Choi et al. 2004), or better, in terms of bearing strain, between 0.5 and 1.0. Moreover, the width of joints (in modern bridges normally located at the abutments, except for very long decks) should be selected such that they remain open under this level of seismic action, to avoid damage at the backwalls.

The purpose of this step, apart from checking the inelastic performance of the structural system, is the verification that the required rotational ductility factor (μ_θ) in the piers is consistent with the values considered during the design. Hence, this step is basically an *assessment* (or verification) of the seismic response of the bridge for the ‘operationality’ level. Since inelastic dynamic analysis is used in order to check the seismic response of the structure for the aforementioned performance level, *mean* values of material strength are considered (f_{cm} and f_{ym} for concrete and steel respectively).

Step 5 – Verifications for the ‘life safety’ or ‘damage limitation’ limit state. The design of members (such as the deck or the abutments) considered elastic in setting up the PIM, is verified on the basis of results of inelastic response-history analyses of the aforementioned model for each of the selected sets of input motions properly scaled to the intensity of the earthquake associated with the ‘life safety’ requirement (probability of exceedance 10 %/50 years, or lower, depending on the importance of the bridge). Equivalently, one can select this as the ‘damage limitation’ limit state discussed in Sect. 7.3.1, i.e. the extent of damage is such that first it can be repaired after the earthquake (closure of the bridge will be required for a certain period) and second there is no noticeable risk to life due to this damage.

This is an important step for buildings (Kappos and Stefanidou 2010) since several critical elements, in particular the columns (except at the base of the ground storey), are designed at this stage. In the case of bridges, it is very likely that the deck and the abutments will have (from non-seismic load combinations) a higher strength than that required on the basis of this analysis. A notable exception is continuity slabs in decks consisting of precast-prestressed beams with cast in situ top slab (a structure quite different from the box girder bridges that are the focus of this chapter). Such slabs will certainly yield under this level of seismic action, but this is perfectly within the design philosophy of such bridges and is also allowed by the codes (Kappos et al. 2013); there is no need for verification of the plastic rotation either, since the shallow sections of R/C slabs can develop very high rotations without rupture. On the contrary, it is essential that bearing deformations be checked at this stage; allowable values are the same as those discussed in the DDBD procedure described in Sect. 7.3.1 (around 2.0, i.e. strains of 200 % in the elastomer).

Step 6– Design for shear. To account for the less ductile nature of this mode of failure, shear forces should be calculated for seismic actions corresponding to the 2 %/50 years earthquake (associated with the ‘collapse prevention’ performance level). However, to simplify the design procedure, design and detailing for shear can be carried out using shear forces calculated from inelastic response-history analysis for the seismic action associated with the ‘life safety’ performance level, and implicitly relate them to those corresponding to the 2 %/50 years earthquake through appropriately selected magnification factors (γ_v). Recommended γ_v factors, accounting mainly for the strain-hardening effect corresponding to higher plastic rotations at this earthquake level, are between 1.15 and 1.20.

Step 7 – Detailing of critical members. Detailing of R/C piers for confinement, anchorages and lap splices, is carried out with due consideration of the expected level of inelasticity. Detailing of piers can be carried out according to the provisions of Chapter 6 of EC8 (Kappos et al. 2013) for ductile members. However, instead of basing the detailing on the default curvature ductilities specified in the Code ($\mu_\phi = 13$ for bridges of ductile behaviour), the actual μ_ϕ estimated for the earthquake associated with the collapse prevention requirement are used in this PBD method. This results in both more rational and, as a rule, more economic, detailing

of the piers. Moreover, it should be verified that bearings do not exceed their ultimate deformability, i.e. a strain in the elastomer of around 5.0.

7.5 Seismic Assessment of Bridges

7.5.1 *Brief Overview of Available Assessment Procedures*

A variety of analytical procedures are currently available for the seismic assessment of structures; the state-of-the-art is quite advanced in the case of buildings for which assessment codes have been developed some time ago, such as Eurocode 8–3 (CEN Techn. Comm. 250/SC8 2005), which however does not cover bridges (this is one of the goals of the evolution of Eurocode 8, that has just started and is expected to last for some years). It has long been recognised that a proper assessment can be carried out only if the post-elastic response of the structure is captured in the analysis, hence revealing the actual plastic mechanism that will develop under a given level of earthquake action. In older and/or poorly designed structures this mechanism can be an unfavourable one, involving concentration of ductility demands in one (or a few) regions; a known example is the case of bridges with significantly unequal heights, wherein a shorter pier is close to the middle of the bridge (such piers yield early on and inelastic deformation tends to concentrate therein).

In the light of the above, leading code-type documents for seismic assessment (of buildings), such as Eurocode 8 – Part 3 (CEN Techn. Comm. 250/SC8 2005) and ASCE 41-06 (ASCE/SEI 2007) recommend and, under specific conditions (such as the presence of irregularities), impose the use of inelastic analysis methods. Both types of inelastic analysis are allowed, but the static (pushover) method is presented in more detail in documents related to seismic assessment, particularly the American ones, such as (ASCE/SEI 2007). Regarding bridges, the most comprehensive document covering assessment is the FHWA Seismic Retrofitting Manual (FHWA 2006). This document includes a number of options for carrying out the analysis of an existing bridge; a total of 4 methods are prescribed, ranging from elastic (static or dynamic) to nonlinear response-history analysis, the applicability of each method depending primarily on the degree of irregularity in the bridge configuration. Interestingly, from a practice perspective, is that there are also options for carrying out a limited assessment of the bridge without any analysis at all, simply by checking the capacity of some critical regions (connections, seat widths) against minimum requirements specified in the Manual. Two options are given for the nonlinear static (pushover) method. The first one ('D1') applies to bridge behaving essentially as SDOF systems (this is the case of straight bridges in their longitudinal directions, when piers are monolithically connected to the deck). All other bridges should be analysed using the second method ('D2'), which combines a response spectrum analysis to assess the displacement demands on

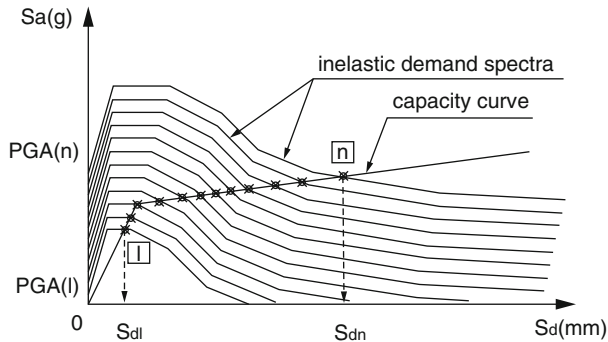


Fig. 7.11 Capacity and demand spectra

the bridge with estimation of capacity through pushover analysis. In both cases the correlation of capacity and demand is made using the capacity spectrum technique (capacity and demand plotted on the same diagram depicting spectral acceleration vs. spectral displacement of an equivalent SDOF system), which has been used for quite some time for buildings following the publication of the ATC-40 Manual (Council 1996). Figure 7.11 shows an example application of this procedure; the demand spectra can be either overdamped elastic spectra as suggested in ATC-40, or proper inelastic spectra as in the figure (Moschonas et al. 2009). It is clear from the figure that the bridge capacity is represented by a single curve, while assessment can be carried out for multiple levels of seismic demand, which is an essential feature of PBD procedures.

The preference of existing codes and guidelines (for both bridges and buildings) for the nonlinear static, as opposed to the nonlinear dynamic, approach should be attributed to the presumption that inelastic static analysis is simpler to apply in practice, which may or may not be true if the limitations of the static method are fully accounted for. More specifically, irregular structural configurations are quite common in both ‘old’ and new bridges, and irregular structures are typically affected by higher modes and/or by changes in their dynamic characteristics in the post-elastic range of their response to seismic actions. Typical examples are long bridges, and also any size bridges with no transverse restraint of the deck over the abutments, wherein consideration of at least the second mode (in the transverse direction of a bridge) is mandatory. Consideration of multiple loading pattern in pushover analysis (as prescribed in CEN Techn. Comm. 250/SC8 2005; ASCE/SEI 2007 and several other codes) is a mixed blessing, in the sense that higher mode effects can still be missed (especially toward the ends of the bridge), whereas basing the final assessment on an ‘envelope’ of the action effects derived from each pattern is very often over-conservative. Therefore, use of inelastic dynamic (response-history) analysis is in many respects an appropriate choice and, with the currently available tools (like those in Carr 2006; CSI [Computers and Structures Inc.] 2007) it is also a feasible one. As an alternative, nonlinear static procedures that properly (albeit approximately) account for higher modes effects can be used. A very

promising procedure is the modal pushover method, originally proposed by Chopra and Goel (2002) for buildings and later extended to bridges by Paraskeva and Kappos (Paraskeva and Kappos 2010; Paraskeva et al. 2006); in this method separate pushover analyses are carried out for various modal force patterns and the results are combined statistically, except for forces in the piers that are derived from the pertinent $M - \theta$ (moment vs. rotation) diagrams.

A broader discussion of the ‘pros’ and ‘cons’ of the aforementioned procedures and the analytical tools for their implementation can be found in a recent book on inelastic methods for the analysis of bridges (Kappos et al. 2012b). By applying the available methods to a number of case studies it was possible to confirm the range of applicability and the feasibility of each method. Table 7.1 presents in matrix form the recommended type of analysis for the assessment of each type of bridge.

A case study of seismic performance assessment is given in the next section; it concerns the bridge designed in Sect. 7.3, which is assessed using inelastic dynamic (response-history) analysis for a set of ground motions; hence, the case-study also serve for furnishing a good idea of the possibilities of current assessment procedures and the parameters that can (and should) be checked in each case. It is noted that rather than using code-prescribed values, assessment is based herein on state-of-the-art methods for estimating the local (plastic rotation) and global (drift) capacity of R/C bridges.

7.5.2 Assessment of the Bridge Designed to the Displacement-Based Procedure

The standard DDBD and the extended MDDBD procedure (Sect. 7.3.2) were assessed using nonlinear response-history analysis (NLRHA) for artificial records closely matching the design spectrum. Two different evaluation approaches were explored as described in the following.

NLRHA was first applied adopting the same assumptions as in the MDDBD. Therefore, yield curvatures and yield moments equal to the design requirements from Step 8 (i.e. SRSS combination of structural analysis results), were used in conjunction with a zero post-elastic slope of the moment-curvature response of the piers. This approach, hereafter referred to as the NLRHA(EI_{des}) case, was deemed necessary for evaluating the efficiency of the proposed MDDBD disengaged from parameters such as material strengths and final detailing of reinforcement. On the other hand, the second evaluation approach, referred to as the NLRHA(EI_{ass}) case, was meant to assess the (M)DDBD design in terms of the expected actual performance of the bridge under the design seismic actions. In particular, the design was deemed as safe if the displacement ductility demand obtained from NLRHA did not exceed the pier displacement ductility assumed in the design. This deterministic assessment requires an accurate and realistic modelling of the inelastic response to obtain the most probable response quantities. To this purpose, moment-curvature

Table 7.1 Recommended types of inelastic analysis (Kappos et al. 2012b)

Type of bridge	Single-mode methods	Multi-mode methods		Nonlinear response history analysis
		Non-adaptive	Adaptive	
<p>Response is governed predominantly by one mode, which does not considerably change:</p> <p>Short bridges on moderate to stiff soil, pinned at the abutments, and not supported by very short columns</p>	X			
<p>The influence of higher modes is limited and their shape does not considerably change when the seismic intensity is increased:</p> <p>Short bridges pinned at the abutments, supported by short side and long central columns</p>	X	X		
<p>Considerable influence of higher modes, that do not significantly changed their shape:</p> <p>Long bridges (or curved) without very short central columns</p>		X	X	
<p>Considerable influence of one or a few number of modes, which significantly change the shape:</p> <p>Short bridges with roller supports at the abutments</p>			X	
<p>Considerable influence of higher modes, which significantly change their shape when the seismic intensity is changed:</p> <p>Short or long bridges supported by very short central and higher side columns</p>				X

analyses based on mean values for material properties and the final detailing of reinforcement, were performed for each pier section utilizing the in-house developed computer program RCCOLA.NET. The assessment in both cases focussed mainly on the target-displacement profiles and on design quantities such as yield displacements, displacement ductilities, stiffnesses, and magnitude of forces developed in critical members of the bridge.

Nonlinear analyses were carried out using Ruaumoko3D (Carr 2006); appropriate nonlinear beam members that in general follow the concept of the one-component model, were introduced in the finite element model (Fig. 7.3) to model the inelastic response of the piers (instead of beam-column members, since there are no changes in axial force that affect the yield moments related to the transverse response of this straight bridge). Herein, the modified Takeda degrading-

stiffness hysteresis rules (Carr 2006), (with parameters $\alpha=0.5$ and $\beta=0$ as assumed for design (Dwairi and Kowalsky 2006) to estimate ξ_i), were adopted.

Since the primary objective of the assessment was the study of the transverse response of the bridge under a seismic excitation which matches as closely as feasible the ‘design excitation’ (i.e. the design spectrum), two sets of NLRHA (EI_{des} , EI_{ass}) were performed for each design case (Zone II, III), using five artificial records, generated using the computer program ASING (Sextos et al. 2003) to fit the elastic design S_a spectra. Response history analyses were performed using the unconditionally stable implicit Newmark constant average acceleration method (Carr 2006), while (after some pilot analyses) Rayleigh damping based on tangent stiffness was selected. The integration time step was set equal to 0.01 s, after trial analyses.

In Fig. 7.12 the target-displacement profiles and the displacement profiles obtained from structural analyses within the DDBD and MDDBD procedures are compared with the displacement envelopes from the NLRHA(EI_{des}) and (EI_{ass}) cases; the deck displacements shown in the figures as the NLRHA case are the average of the maximum displacements recorded in the structure during the five RHAs of each set. It is observed that agreement of the DDBD design profiles with the corresponding response-history results is not satisfactory, since the NLRHA profile is closer to the target-displacement profile Δ_i (derived from EMS and accounting for higher mode effects) instead of the displacement profile obtained from structural analysis, on the basis of which design is carried out. On the other hand, the MDDBD target-displacement profiles are closer to that obtained from NLRHA(EI_{des}), more so in the case of Zone II. The main difference between MDDBD and NLRHA(EI_{des}) is noted towards the abutments of the bridge (critical members in design), with differences diminishing in the area of the piers. These differences should be attributed to the inherent inability of elastic design methodologies that are based on modal analysis (e.g. response spectrum analysis) to capture the modification of the dynamic characteristics of the structure during the successive formation of plastic hinges. The MDDBD procedure attempts to capture the maximum probable response at a given performance level (after the formation of plastic hinges) based on a statistical combination (e.g. SRSS) of the peak ‘modal’ responses.

Additional sets of linear response history analyses (LRHA) for the case ‘(EI_{des})’ were performed to support the above statement. In particular, column stiffnesses were set equal to secant stiffnesses corresponding to maximum displacements obtained from previously run nonlinear analysis (i.e. NLRHA(EI_{des})). The displacement envelopes resulting from these analyses indicate the contribution of the first two modes with similar participation factors as those obtained from the EMS method (Fig. 7.12). The NLRHA(EI_{ass}) case is also given in Fig. 7.12 to underline the divergence (in terms of displacement profiles) arising when pier overstrength, due to the use of mean values for material properties and consideration of strain-hardening of steel reinforcement, is considered.

Similar conclusions are drawn with respect to the other design quantities; yield displacements, displacement ductilities, stiffnesses, ultimate member shears,

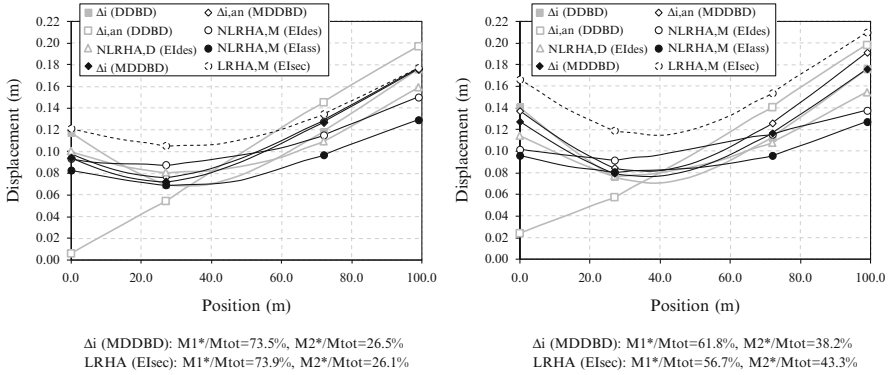


Fig. 7.12 Nonlinear response history maximum displacements for evaluation cases NLRHA (Eldes), (Elass) and linear response history maximum displacements for evaluation case NLRHA(Eldes). *Left*: Zone II; *Right*: Zone III, compared with target-displacements profiles (Δ_i) and displacement profiles obtained from structural analyses ($\Delta_{i,an}$) according to DDBD (D) and Modal DDBD (M)

bearing shear strain and column drift ratios obtained from NLRHA were compared with those estimated at the design stage. Figure 7.13 (supplemented by Table 7.2, as far as the results related to the MDDBD are concerned) illustrates the correlation in the above quantities, for Zone II design. Again, curves shown in the figures as the NLRHA case are the average of the quantities recorded in the structure during the five RHAs, either at the time step each member enters the inelastic range (displacement and shear values at the instant wherein the bending moment at the critical section first reaches the yield bending moment of EI_{des}/EI_{ass} case) or at the time step of maximum response. $V-\Delta$ curves shown as MDDBD were drawn based on the assumptions of the method (i.e. assuming zero post-elastic slope of the shear force vs. displacement response and yield displacement according to Eq. (7.14b)) and the results of structural analyses (SRSS combination). It is clear that, contrary to the DDBD, MDDBD predicts very well (i.e. matches closely the values from the NLRHA(EI_{des}) case) the quantities related to member ultimate response (shear forces, displacements and secant stiffnesses at maximum response), which implies the effectiveness of the equivalent cantilever approach in capturing the degree of fixity at the top of the piers, and the base shear distribution approach according to the results of structural analysis. Differences in the quantities related to pier yield are mainly attributed to the estimation of the yield curvature according to the semi-empirical Eq. (7.14b) and the computation of the equivalent cantilever height according to moment diagrams at maximum response instead of the response at the time of yielding. The resulting underestimation of the equivalent cantilever height contributes to underestimation of yield displacements and overestimation of stiffnesses and shears related to pier yield. It is worth mentioning that DDBD yields similar results with MDDBD as far as Column 2 is concerned (whose design is governed by the first mode), whereas it overestimates the ‘second mode-based’ response of Column 1.

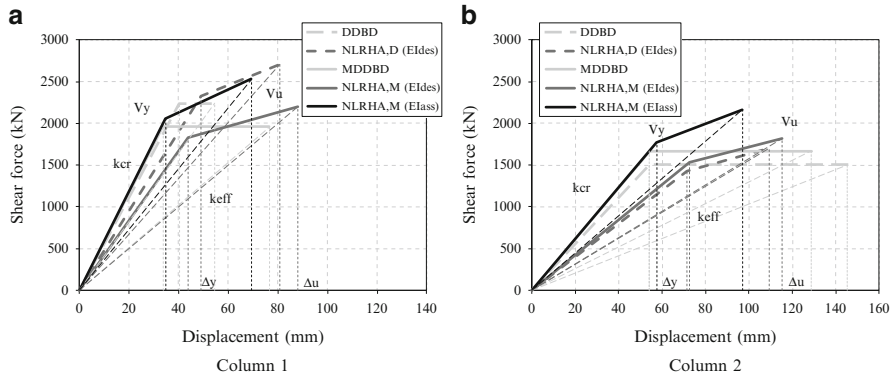


Fig. 7.13 Member shear force vs. displacement curves derived from direct displacement-based design (DDBD), modal direct displacement-based design (MDDBD), and nonlinear response history analyses (NLRHA) for Zone II (PGA = 0.24 g) design

As previously mentioned, the results of the NLRHA(EI_{ass}) case were used to verify the reliability of the proposed design method in terms of ductility demand. Both designs were found to be safe, since required ductilities values for Zones II and III are always lower than the design ductilities (see Table 7.2 for case of Zone II). Figure 7.13 also illustrates the effects of overstrength on the $V-\Delta$ pier response.

A case study presenting the assessment of the same bridge (T7 overpass) designed according to the deformation-based procedure described in Sect. 7.4.1 can be found in (Gkatzogias and Kappos 2014).

7.6 Closing Remarks

It was attempted to provide here an overview and discussion of the various seismic design procedures available for bridges, with emphasis on new proposals for improved design methods (such as the direct displacement-based and deformation-based design procedures presented herein) and whether they could be useful within the frame of a ‘new generation’ of codes. As far as the performance of structures designed to current codes is concerned, the answer is straightforward: Far from being perfect (whatever this might mean in the context of practical design), current codes like Eurocode 8 lead to designing robust bridges with ample margins of safety against collapse, and in this respect they are, indeed, adequate. One can argue that sometimes current codes tend to be over-conservative and/or to result in bridge piers that are difficult to detail on-site, but others could argue that earthquakes keep surprising us, in the sense that ground motions stronger than those recorded in the past keep being recorded, hence the extra safety margins apparently provided by current codes should not be reduced.

Table 7.2 Design quantities for the case depicted in Fig. 7.13

Member case	Abutment 1				Abutment 2				Column 1				Column 2			
	MDDBD	NLRHA (EI _{des})	NLRHA (EI _{ass})	MDDBD	NLRHA (EI _{des})	NLRHA (EI _{ass})	MDDBD	NLRHA (EI _{des})	NLRHA (EI _{ass})	MDDBD	NLRHA (EI _{des})	NLRHA (EI _{ass})	MDDBD	NLRHA (EI _{des})	NLRHA (EI _{ass})	
Δ_y (mm)							34	44	35	54	73	58				
V_y (kN)							1,958.6	1,828.8	2,060.0	1,668.5	1,529.2	1,769.4				
Δ_u (mm)	98	94	83	177	141	129	77	88	69	129	115	97				
V_u (kN)	491.3	469.0	415.2	885.4	707.7	647.6	1,958.6	2,196.2	2,529.2	1,668.5	1,817.8	2,166.4				
K_h (kN/m)	5,011.4	5,011.4	5,011.4	5,011.4	5,011.4	5,011.4										
K_{cr} (kN/m)							58,072.9	41,559.9	59,195.4	30,860.9	21,025.1	30,736.9				
K_{eff} (kN/m)							25,576.3	24,984.6	36,493.2	12,952.7	15,774.0	22,342.8				
μ_Δ							2.27	2.00	1.99	2.38	1.58	1.68				
$\gamma\%$ ($\gamma_u = 2.0$)	1.11	1.06	0.94	2.01	1.60	1.47										
Col drift (%)							1.05	1.21	0.95	1.39	1.24	1.05				
h_{eq} (m)							3.43	3.79	4.43	4.39	5.02	5.61				

The second question, i.e. whether new performance-based design proposals could or should be incorporated in future seismic codes, is more difficult to answer in a definitive way. Based on the (undoubtedly limited) available evidence, it appears that there are two main issues wherein new proposals can 'entice' code developers: better damage control for a number of different earthquake intensities (in particular those lower than the commonly used single design earthquake with 10 %/50 years probability of exceedance), and, of course, economy. As far as damage control is concerned, the writer's opinion is that the direct deformation-control method (Sect. 7.4) is better suited for inclusion in future codes, not only for 'format' reasons (i.e. that it can be incorporated in existing codes by revising them, rather than by, essentially, completely replacing them), but also because, as already pointed out herein, displacement-based methods, even when applied to structural systems for which they were properly calibrated, do not always guarantee that local inelastic deformations will be within the acceptable limits, since checking of these deformations is not part of the procedure. It is clear, nevertheless, that explicitly checking these local deformations requires more refined and costly types of analysis than the simple equivalent static approach put forward by the DDBD developers. In principle, only inelastic analysis can offer a viable alternative here, and for several types of bridges this analysis should be dynamic (response history) rather than static. Moreover, in many cases, analysis should account not only for inelastic member response but also for (nonlinear) soil-structure interaction effects, a crucial issue that has not been addressed here due to space limitations, but very important in the case of bridges. Of course, as one keeps refining the analysis, the latter is made more complex and difficult to apply in a design office context. Seen from a slightly different perspective, the key difference in the interesting new proposals reviewed here is in the level of approximation, since the goal is common in both of them, i.e. control of damage. The direct DBD procedure assumes that the actual bridge can be properly reduced to an SDOF system (or more systems in the MDDBD method described here) based on a reasonable (inelastic) displacement pattern, whereas the direct deformation-based procedure arrives at the inelastic displacement pattern and the associated local deformations through inelastic analysis, albeit of a reduced inelastic model.

Last and not least, the issue of economy has to be addressed, which is arguably the one most difficult to tackle in a comprehensive way. The available evidence is certainly too limited for drawing conclusions of general validity. Moreover, it should be emphasised that the economy of the final design does not depend solely on the way seismic action is defined and the analysis method used (e.g. code-type or PBD), but on several other issues that have not been studied systematically so far. In view of this paucity of comparative studies, the only definitive conclusion regarding the issue of economy is that additional and, especially, more systematic and comprehensive, studies are required to compare the final products resulting from each procedure, wherein these products should be realistic bridges, representative of the current seismic design practice.

Acknowledgements A number of the author's students have made significant contributions to some of the studies summarised herein. The contribution of K. Gkatzogias, PhD student at City University London, is particularly acknowledged.

Open Access This chapter is distributed under the terms of the Creative Commons Attribution Noncommercial License, which permits any noncommercial use, distribution, and reproduction in any medium, provided the original author(s) and source are credited.

References

- AASHTO (2011) Guide specifications for LRFD seismic bridge design. AASHTO, Washington, DC
- AASHTO [American Association of State Highway and Transportation Officials] (2010) LRFD bridge design specifications, 5th edn. AASHTO, Washington, DC
- Adhikari G, Petrini L, Calvi GM (2010) Application of direct displacement based design to long-span bridges. *Bull Earthquake Eng* 8(4):897–919
- Alvarez Botero JC (2004) Displacement-based design of continuous concrete bridges under transverse seismic excitation. M.Sc. dissertation. European school for advanced studies in reduction of seismic risk (Rose School), University of Pavia, Pavia
- Applied Technology Council (1996) ATC-40: seismic evaluation and retrofit of concrete buildings. Rep. SSC 96–01, CSSC-ATC, Redwood City
- ASCE/SEI (2007) Seismic rehabilitation of existing buildings – ASCE standard 41–06. American Society of Civil Engineers, Reston
- Bardakis VG, Fardis MN (2011) A displacement-based seismic design procedure for concrete bridges having deck integral with the piers. *Bull Earthquake Eng* 9:537–560
- Blandon CA, Priestley MJN (2005) Equivalent viscous damping equations for direct displacement-based design. *J Earthquake Engineering* 9:257–278
- Caltrans [California Department of Transportation] (2013) Seismic design criteria ver. 1.7. Caltrans Division of Engineering Services, California, USA
- Calvi GM, Kingsley GR (1995) Displacement-based seismic design of multi-degree-of-freedom bridge structures. *Earthquake Eng Struct Dyn* 24(9):1247–1266
- Carr AJ (2006) Ruaumoko 3D: inelastic dynamic analysis program. University of Canterbury, Christchurch
- CEN (2004) Eurocode 2: design of concrete structures – part 1: general rules and rules for buildings (EN 1992-1-1). CEN, Brussels
- CEN (Comité Européen de Normalization) (2005) Eurocode 8, design of structures for earthquake resistance – part 2: bridges. CEN, Brussels
- CEN Techn. Comm. 250 / SC8 (2005) Eurocode 8: design provisions of structures for earthquake resistance – part 3: assessment and retrofitting of buildings (EN1998-3). CEN, Brussels
- Choi E, DesRoches R, Nielson B (2004) Seismic fragility of typical bridges in moderate seismic zones. *Eng Struct* 26(2):187–199
- Chopra AK, Goel RK (2002) A modal pushover analysis procedure for estimating seismic demands for buildings. *Earthquake Eng Struct Dyn* 31(3):561–582
- CSI [Computers and Structures Inc.] (2007) SAP200: three dimensional static and dynamic finite element analysis and design of structures. Computers and Structures Inc., Berkeley
- Dwairi H, Kowalsky MJ (2006) Implementation of inelastic displacement patterns in direct displacement-based design of continuous bridge structures. *Earthq Spectra* 22(3):631–662
- Dwairi HM, Kowalsky MJ, Nau JM (2007) Equivalent damping in support of direct displacement-based design. *J Earthquake Eng* 11:512–530

- FHWA [Federal Highway Administration] (2006) Seismic retrofitting manual for highway bridges part 1 – bridges (FHWA- HRT-06-032). Turner-Fairbank Highway Research Center, McLean
- fib* (2007) Structural solutions for bridge seismic design and retrofit. *Fib Bull* 39, Lausanne
- Fischinger M, Beg D, Isakovic T, Tomazevic M, Zarnic R (2004) Performance based assessment—from general methodologies to specific implementations. International Workshop on PBSB, Bled, Slovenia, pp 293–308 (published in PEER report 2004-05 (UC Berkeley))
- Gkatzogias KI, Kappos AJ (2014) Performance-based seismic design of concrete bridges. SECED 2015 conference: earthquake risk and engineering towards a Resilient World, Cambridge UK, 9–10 July 2015
- Grant DN, Blandon CA, Priestley MJN (2004) Modeling inelastic response in direct displacement-based design. Report no. ROSE 2004/02, European School of Advanced Studies in Reduction of Seismic Risk, Pavia
- Guyader C, Iwan WD (2006) Determining equivalent linear parameters for use in a capacity spectrum method of analysis. *J Struct Eng* 132(1):59–67
- Kappos AJ (2010) Current trends in the seismic design and assessment of buildings: Ch. 11. In: Garevski M, Ansal A (eds) *Earthquake engineering in Europe, geotechnical, geological, and earthquake engineering*. Springer, Dordrecht
- Kappos AJ, Panagopoulos G (2004) Performance-based seismic design of 3D R/C buildings using inelastic static and dynamic analysis procedures. *ISET J Earthquake Technol Spec* 41 (1):141–158. Issue: Performance-Based Seismic Design (Edited by MJN Priestley)
- Kappos AJ, Stefanidou S (2010) A deformation-based seismic design method for 3D R/C irregular buildings using inelastic dynamic analysis. *Bull Earthquake Eng* 8(4):875–895
- Kappos AJ, Goutzika E, Stefanidou S (2007) An improved performance-based design method for 3d R/C buildings using inelastic analysis. ECCOMAS thematic conference on computational methods in structural dynamics and earthquake engineering, paper no. 1375
- Kappos AJ, Gidaris I, Gkatzogias KI (2012a) Problems associated with direct displacement-based design of concrete bridges with single-column piers, and some suggested improvements. *Bull Earthquake Eng* 10(4):1237–1266
- Kappos AJ, Saïidi M, Aydinoglu N, Isakovic T (2012b) Seismic design and assessment of bridges: inelastic methods of analysis and case studies. Springer, Dordrecht
- Kappos AJ, Gkatzogias KI, Gidaris I (2013) Extension of direct displacement-based design methodology for bridges to account for higher mode effects. *Earthquake Eng Struct Dyn* 42 (4):581–602
- Katsanos EI, Sextos AG (2013) ISSARS: an integrated software environment for structure-specific earthquake ground motion selection. *Adv Eng Softw* 58:70–85
- Katsaras CP, Panagiotakos TB, Koliass B (2009) Effect of torsional stiffness of prestressed concrete box girders and uplift of abutment bearings on seismic performance of bridges. *Bull Earthquake Eng* 7(2):363–375
- Kowalsky MJ (2000) Deformation limit states for circular reinforced concrete bridge columns. *J Struct Eng* 126(8):869–878
- Kowalsky MJ (2002) A displacement-based approach for the seismic design of continuous concrete bridges. *Earthquake Eng Struct Dyn* 31(3):719–747
- Kowalsky MJ, Priestley MJN, MacRae GA (1995) Displacement-based design of RC bridge columns in seismic regions. *Earthquake Eng Struct Dyn* 24(12):1623–1643
- Ministry of Public Works of Greece (2010) Greek seismic code-EAK 2000, Athens, 2000 (amended June, August 2003, March 2010) (in Greek)
- Moschonas IF, Kappos AJ, Panetsos P, Papadopoulos V, Makarios T, Thanopoulos P (2009) Seismic fragility curves for Greek bridges: methodology and case studies. *Bull Earthquake Eng* 7(2):439–468
- Ortiz Restrepo JC (2006) Displacement-based design of continuous concrete bridges under transverse seismic excitation. M.Sc. dissertation. European school for advanced studies in reduction of seismic risk (ROSE School), University of Pavia, Pavia

- Paraskeva T, Kappos AJ (2010) Further development of a multimodal pushover analysis procedure for seismic assessment of bridges. *Earthquake Eng Struct Dyn* 39(2):211–222
- Paraskeva TS, Kappos AJ, Sextos AG (2006) Extension of modal pushover analysis to seismic assessment of bridges. *Earthquake Eng Struct Dyn* 35(11):1269–1293
- Priestley MJN, Seible F, Calvi GM (1996) *Seismic design and retrofit of bridges*. Wiley, New York
- Priestley MJN, Calvi GM, Kowalsky MJ (2007) *Displacement-based seismic design of structures*, 1st edn. IUSS Press, Pavia, 720 pp
- SEAOC Ad Hoc Committee (1999) *Tentative guidelines for performance-based seismic engineering, App. I of: recommended lateral force requirements and commentary*. SEAOC, Sacramento
- Sextos AG, Pitilakis KD, Kappos AJ (2003) Inelastic dynamic analysis of RC bridges accounting for spatial variability of ground motion, site effects and soil-structure interaction phenomena. Part 1: methodology and analytical tools. *Earthquake Eng Struct Dyn*; 32(4):607–627
- Suarez V, Kowalsky MJ (2007) Displacement-based seismic design of drilled shaft bents with soil-structure interaction. *J Earthquake Eng* 11(6):1010–1030
- Suarez VA, Kowalsky MJ (2010) Direct displacement-based design as an alternative method for seismic design of bridges. In: SP-271CD: structural concrete in performance-based seismic design of bridges CD-ROM. ACI, Farmington Hills, Michigan, USA
- Suarez VA, Kowalsky MJ (2011) A stability-based target displacement for direct-displacement-based design of bridge piers. *J Earthquake Eng* 15(5):754–774
- Takeda T, Sozen M, Nielsen N (1970) Reinforced concrete response to simulated earthquakes. *J Struct Div ASCE* 96(12):2557–2573

Chapter 8

An Algorithm to Justify the Design of Single Story Precast Structures

H.F. Karadoğ̃an, I.E. Bal, E. Yüksel, S. Ziya Yüce, Y. Durgun,
and C. Soydan

Abstract An attempt to estimate the displacement demands of precast cantilever columns has been presented here. The purpose of the findings presented is to set up a more reliable design philosophy based on dynamic displacement considerations instead of using acceleration spectrum based design which initiates the action with unclear important assumptions such as the initial stiffness, displacement ductility ratios etc. The sole aim of this chapter is to define a procedure for overcoming the difficulties rising right at the beginning of the traditional design procedure.

For that purpose first 12 groups of earthquake records cover the cases of far field, near field, firm soil, soft soil possibilities for 2/50, 10/50 and 50/50 earthquakes with minimum scale factors are identified associated to the present fundamental period of structure. And they are reselected for each new period of structure during the iterative algorithm presented here and they are used to remove the displacement calculations based on static consideration. Nonlinear time history analysis (NLTHA) are employed within the algorithm presented here which takes into account the strength and stiffness degradations of structural elements and the duration of records which are ignored in the spectrum based design philosophy.

H.F. Karadoğ̃an (✉) • E. Yüksel • Y. Durgun
Faculty of Civil Engineering, Istanbul Technical University (ITU), Istanbul, Turkey
e-mail: karadogan@itu.edu.tr; yukselec@itu.edu.tr; durgunya@itu.edu.tr

I.E. Bal
Earthquake Engineering & Disaster Management Institute, ITU, Istanbul, Turkey
e-mail: iebal@itu.edu.tr

S.Z. Yüce • C. Soydan
Graduate School of Science Engineering and Technology of ITU, Istanbul, Turkey
e-mail: yuceser@itu.edu.tr; cihansoydan@gmail.com

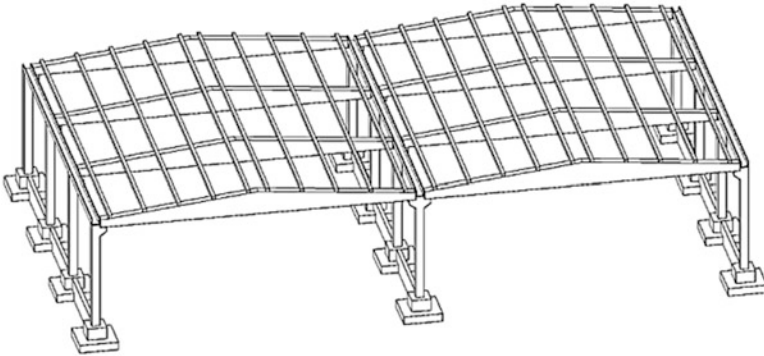


Fig. 8.1 Single story precast frame type structure

8.1 Introduction

Single story precast frame type structures are widely used in the construction of industrial facilities and commercial malls in Turkey. The non-moment resisting *beam-to-column connections* are all wet connections. The lateral strength and stiffness of the structure depend entirely on the cantilevered columns, see Fig. 8.1.

After August 1999 Kocaeli and November 1999 Düzce Earthquakes, site investigations revealed that structural *damage* and *collapse* of one-story precast structures were common especially in uncompleted structures, (Saatcioglu et al. 2001; Ataköy 1999; Sezen et al. 2000; Bruneau 2002; Sezen and Whittaker 2006). Various types of structural damage were frequently observed in one-story precast structures, such as plasticized zones at the base of the columns, axial movement of the roof girders that led to pounding against the supporting columns or falling of the roof girders, (Wood 2003). The post-earthquake observations of one-story precast frame type structures indicate also that

- Lateral stiffness may not be high enough to limit the lateral displacement of column tops which may differ from peripheral columns to center columns simply because of the lack of in-plane rigidity of roofing system, Fig. 8.2a,
- Hence the excessive top rotations of columns and the relative displacement in the plane of roof become perfect reasons to dislocate the long span heavy slender roof beam together with the other two component of earthquake, Fig. 8.2b. They are creating perfect imperfections as well, for out of plane buckling of beams which have very simple insufficient hinge connections to the columns.
- Incompatible column displacement ductility achieved in the field and the lateral load reduction factor used in design, Fig. 8.2c.

In addition to the observations listed above it is also known that, structural alterations done after construction, the effects of nonstructural elements used unconsciously, oversimplified details of connections can be counted among the other important deficiencies of these buildings which causes severe damages.



Fig. 8.2 Observed damages. (a) Out of plane deformations of plane frames; (b) Collapse of a rigid roof beam; (c) Plastic hinge at column base

At the design stage of that type of buildings, the seismic weight coming from the tributary area of columns are determined easily for predicting the earthquake loads. However the *Lateral Displacement Ductility Ratio* which is the main parameter of *Lateral Load Reduction Factor* has to be selected at the beginning of design which is not an easy estimation and has its own uncertainties. Another difficulty is to estimate the lateral rigidity of column which is going to be used to calculate the fundamental period of vibration to go to the spectrum curves. Finally the proposed displacement limits based on static considerations are no longer satisfying the requirements of dynamic displacement calculations.

Those are the factors which are being discussed following experimental and theoretical primary works (Karadoğan 1999; Karadoğan et al. 2006). This Chapter is the scrutinized summary of the findings of the earlier works of the Authors and is aimed to establish a conclusive design algorithm as proposed below.

8.2 Basic Structural Features Observed in the Field and Basic Features of the Current Design Practice

It is probable that all the above mentioned damaged and collapsed buildings they have been neither designed nor manufactured nor mounted properly. From structural engineering point of view the following facts are important to critic the present design practice:

- There exist almost no in-plane rigidity in the roof and in the sides of the examined precast buildings.
- The connections between the long span beams and columns are almost hinged and they are vulnerable to different types of failure modes in addition to shear strength deficiency such as rupture of concrete around the shear studs etc.
- The tributary areas of columns are used to define the earthquake design forces. When this come along the lack of in-plane rigidity of roof then columns in different location with different dynamic characteristics starts to behave independently hence top displacements and top rotations in opposite direction becomes an important issue to keep the long span and heavy roof beam in the required position. Because all kind of imperfection to destabilize the roof beam appears in addition to the inherent tendency towards out of plane buckling.

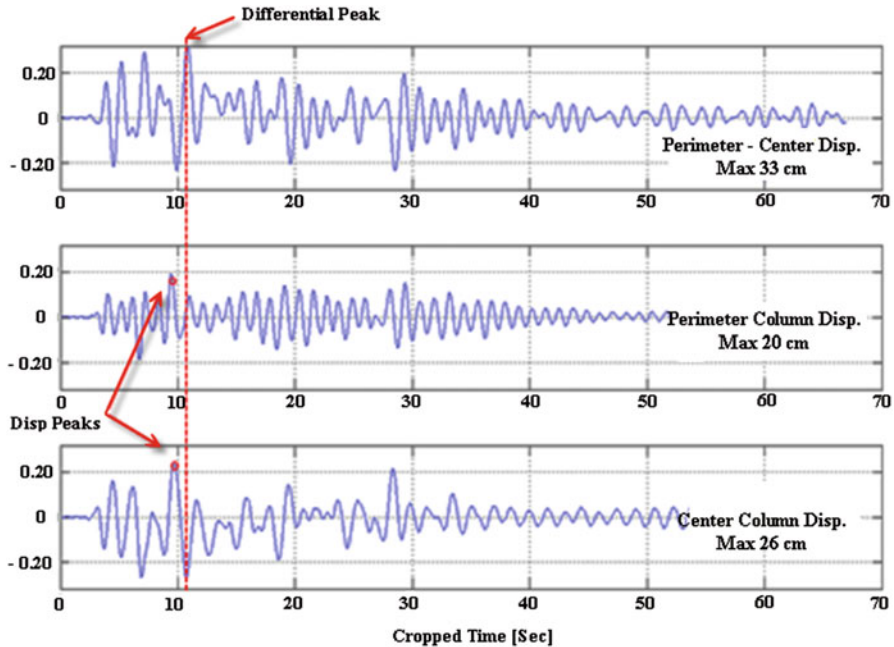


Fig. 8.3 Asynchronized displacement time histories for center and perimeter columns of a single-story precast structure

In local design practice generally un-cracked sections are used to calculate the fundamental period of the structure. Static calculations are required for determination of displacements and a lateral load reduction factors suggested by codes are used to define the design loads.

One of the main issues in precast structures is that the top displacement of center columns in precast single story industrial buildings may not have synchronized seismic oscillations with the perimeter columns despite the fact that they often have the same cross sectional dimensions. The precast industrial structures do not possess in-plane rigidity at roof level in most cases leading thus to lack of load path among the columns resulting individual shaking of each column (Karadoğan et al. 2013). The displacement time-history plots of Column #1, the details of which are given below in the section of *Numerical Analyses*, are presented in Fig. 8.3. The bottom plot in Fig. 8.3 presents that the maximum center column displacement is 26 cm, while the middle column maximum displacement is 20 cm. These two numbers may mislead the engineer to a wrong conclusion that the differential displacement between the perimeter and center columns is just $26 - 20 = 6$ cm. If the top plot with the differential displacement between the two columns in time domain is observed, however, it can be seen that the maximum differential (i.e. asynchronized) displacement reaches up to level of 33 cm. The main reason

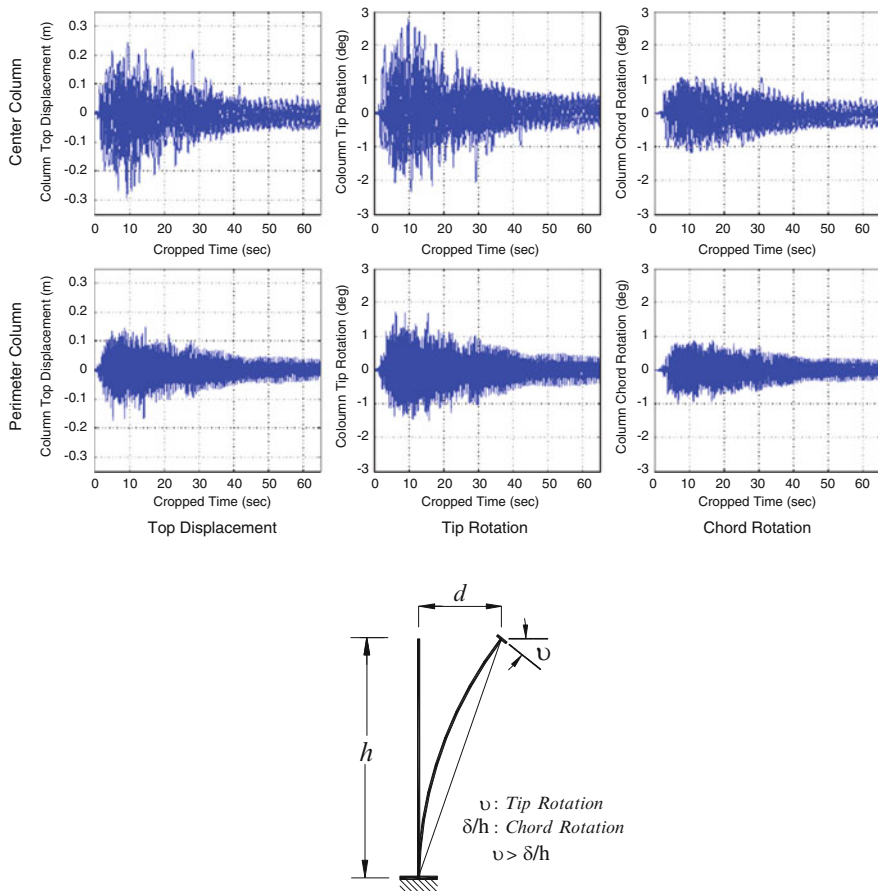


Fig. 8.4 Definition of chord rotation and tip rotations (*top*), comparison of top displacement, tip rotation and chord rotation quantities for an example precast industrial structure (*bottom*)

for that is because the top displacement of each individual column may occur at different time thus the phase difference may cause large asynchronous displacements. In other words, the top displacement of a center and of a perimeter column may have opposite signs.

The top displacement of individual cantilever columns exhibiting opposite signs may lead to instability of the beams which are hinged to the column tops in existing practice. It can be seen in Fig. 8.4 following analyses of perimeter and center columns of a single-story precast structure with 20 code-compatible records that the tip rotation is always higher than the chord rotation (please note that the chord rotation is equal to drift in cantilever systems). In other words, the tip of the column where hinged beams are connected rotates more than the column itself. This is a major parameter neglected in design.

8.3 Why Justification of Code Based Design Procedure Is Needed?

Even if the damaged or collapsed buildings shown in Fig. 8.2 had been designed properly, been manufactured properly and been mounted properly, unless the assumptions done at the beginning of design are not justified at the end, one should have right to keep suspicion about the safety of building.

The basic questions to be kept in mind till the satisfactory design has been reached, are as follows:

- What should be the initial period of the structure on which the fundamental period will be based?
- What should be the displacement ductility factor or lateral load reduction factor on which the design forces will be based?
- To what extent is valid the story drift calculation based on static considerations?

One of the other deficiencies of spectrum based design technique is the length of the record which is not taken into account and the other one is the stiffness and strength deterioration of structure: Unfortunately they are not embedded in the procedure widely used by existing codes.

In order to satisfy the suspicions from which all those questions are arising, an algorithm to justify the design procedures used at the beginning, is presented in the following paragraphs.

8.4 Selection of Partially Code Compatible Records

A simple engineering approach is used here for the selection of records used in nonlinear analyses. The record selection has been done by using the [PEER NGA Database](#) where 7,025 recorded motions were available. An in-house developed software was used to list and download the record automatically and plot the spectra for acceleration at 5 % damping, velocity and displacement.

Twelve bins of records, (http://web.itu.edu.tr/~iebal/Dr_Ihsan_Engin_BAL/SafeCladding_EU_Project), are created where:

1. Earthquake intensity (2/50, 10/50 or 50/50 earthquakes, 3 bins)
2. Far field or near field issue (2 bins)
3. Soil type (firm soil and soft soil, 2 bins)

parameters are checked. Each of these 12 bins have 20 records.

In terms of the selection algorithm, first the acceleration spectrum of the original record is compared to that of the target, in the period window of 0.2–2.0 s. A scale factor is applied to the ordinates. Then the near field vs. far field comparison is made where the distances above 15 km are assumed as far field. Finally a comparison is made in terms of the soil type where the records taken on soil with V_{s30}

higher than 300 m/s are assumed to be recorded on firm soil while records taken on soils with V_{s30} lower than 700 m/s are assumed to be recorded on soft soil. There is certainly an overlap in the soil criteria; this is nevertheless unavoidable if one checks the firm and soft soil borders in the guidelines and codes.

The intensity levels of 2/50, 10/50 and 50/50 are defined to represent 2, 10 and 50 % probabilities of exceedance in 50 years, respectively.

The criteria applied have resulted the number of available records, but it should be mentioned that some each bin does not return the same number of available records. For instance, records which are recorded on soft soil and farm field consist of more than 60 % of the record pool, thus the rest is shared between three different groups which are far field – firm soil, near field – soft soil, and near field – firm soil. As a result, selection criteria have to be loosened in some cases.

The scale factors are set such that average of 20 records does not go below the target spectrum in certain percentages and most of the cases the average spectrum is not allowed to go below the target spectrum at all. Similarly, the average spectrum is not allowed to go above 30 % of the target spectrum in any point within the period window. In order to control the difference of the positive and negative peaks, where positive peaks refer to the peaks above the target spectrum and vice versa, another criterion is also applied to check the individual records. According to this, the individual record is not allowed to go below the target spectrum less than 50 %, or above more than 200–300 % in any of the peaks. This criterion dictates to select rather smooth records with less peaks, however it is a very harsh criterion to be satisfied. The scale factors in overall are not allowed to be below 0.5 and above 2 in any of the selected records so that the energy content can be controlled.

Two more criteria have been applied to control the energy content, one is the PGV and the other is the Arias Intensity. The purpose of the inclusion of these two criteria is to decrease the scatter, i.e. record-to-record variability of the selected records. In order to do so, a record that fits the target spectrum with the least error has been assigned as the best record, and the selected records are not allowed to have PGV or Arias Intensity values above or below certain ratios as compared to those obtained from the best record. The limits for these criteria had be set so high in some of the bins that they were practically not much effective because the number of available records was already low even without these criteria. Generally, the selected records are not allowed to have PGV and Arias intensity values, after scale factors are applied, above 1/0.6–1/0.7 and below 0.6–0.7 of that of the best record.

The selection of records has been done by using acceleration spectra, however similar procedures may and should be produced for velocity and displacement spectra as well.

As an example, acceleration spectra and displacement spectra are given Fig. 8.5. Please note that the differences among the selected records are much higher in displacement spectra when long-period structures are considered, such as the single-story precast structures as presented here.

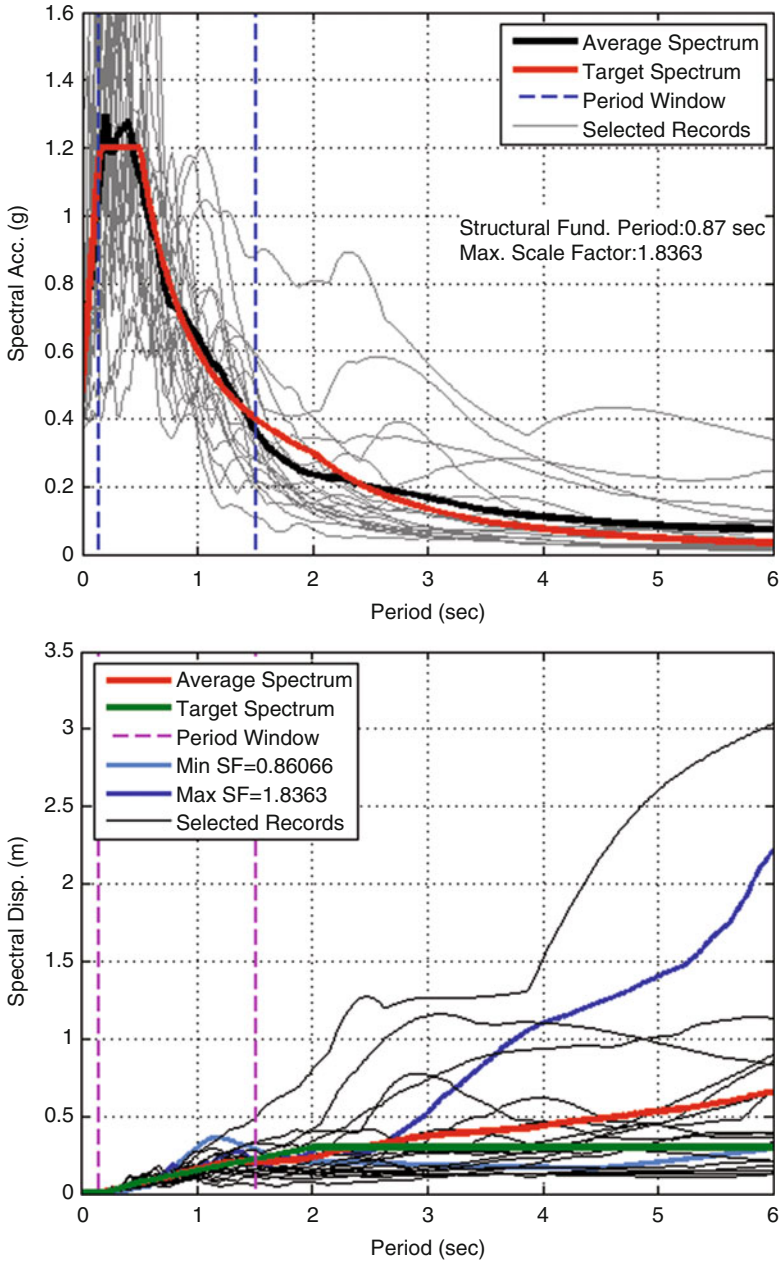


Fig. 8.5 Acceleration spectra and displacement spectra for an example selection

8.5 Proposed Algorithm

The following steps are identified in the proposed algorithm; see the flow chart given in Fig. 8.6 and illustrative description presented in Fig. 8.7:

- It is assumed that the preliminary design of the structure has been completed so that all requirements in the selected seismic code have been satisfied such as strength and displacement limitations etc. There is no need to discuss what should be initial stiffness or what is the most suitable lateral load reduction factor or the displacement equality principal is valid or not.
- Real earthquake records are selected so that the parameters like soil conditions, distance to active faults, and the required intensities such as 2/50–10/50–50/50 are all satisfied with reasonable tolerances and scaling factors are chosen as much as close to unity to make the acceleration curves close to the curve provided by codes in a narrowest window around the fundamental period of the structure. The selected earthquakes should be around 20 and the most meaningful part of the records should be identified to shorten the NLTHA analysis which will be used for all records. The details of this topic is discussed below in another sub section.
- The selected partially code compatible earthquakes are used for linear and non-linear analysis of the structure to check which one of the *displacement or energy equality assumption* is valid for the specific structure under consideration. It is also important to have an idea about what could be the tolerance to accept the validity of one of these equalities.
- Depending on the decision done at the end of last step one can calculate the lateral load reduction factor accordingly using the proper formula given in the flow chart.
- Mean plus one standard deviation of maximum displacement obtained through NLTHA and lateral load reduction factors are calculated.
- Capacity curve of the structure is obtained using any one of the known technique. These curves cannot be only obtained theoretically but also experimentally, empirically, parametrically, they can be in a continuous form or in the bilinear form etc.
- Yielding point and the point corresponds to maximum inelastic displacement found are taken into consideration for defining the *lateral rigidity* and the *achieved displacement ductility* of the structure from where the more realistic lateral load reduction factors will be calculated referring to the same formula used in the previous step.
- It is expected to have almost equal lateral load reduction factors in last two cycles of iterations. If they are not at the close proximity then another step of iteration will be carried out.

In the following paragraphs several definitions and explanations are given and some complementary results of early experimental and theoretical findings for *over strength factor, lateral load reduction factors and capacity curves* are summarized for the sake of having complete information together.

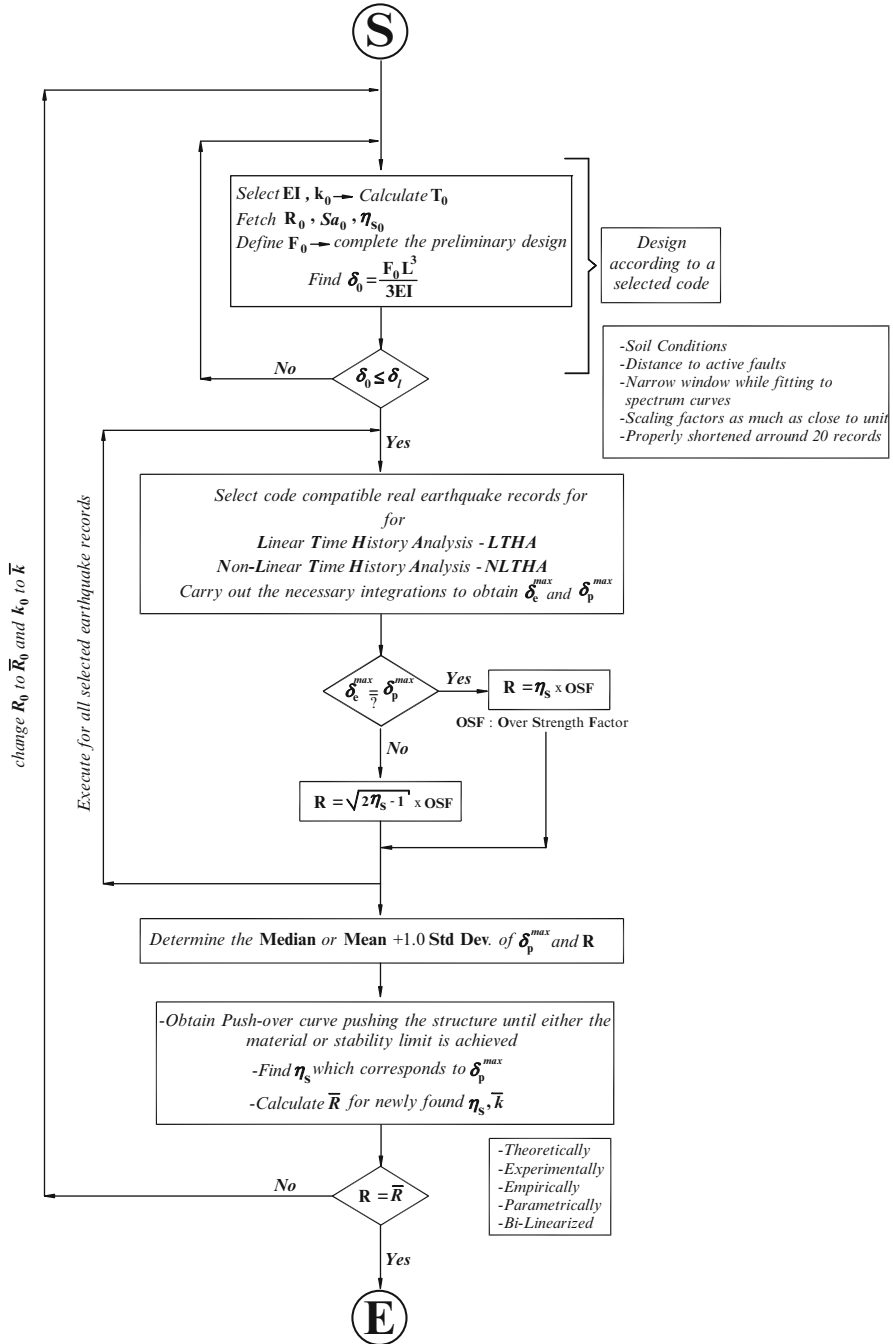


Fig. 8.6 Flow chart of the proposed algorithm

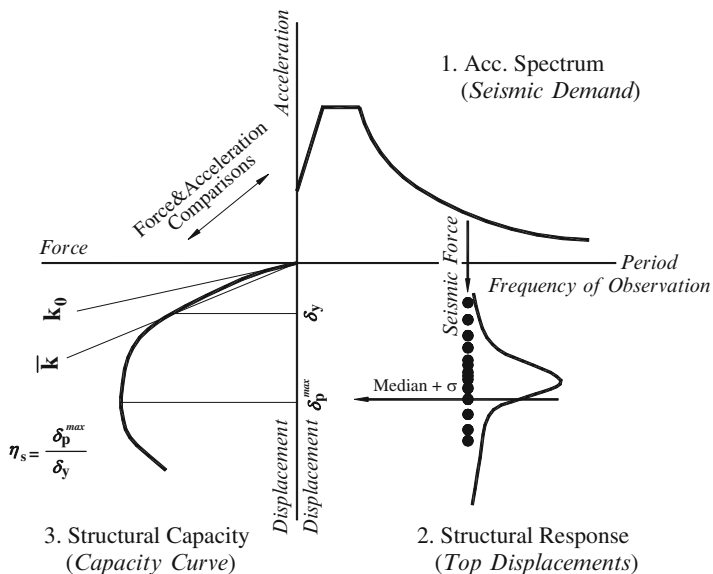


Fig. 8.7 Description of the proposed procedure

8.6 Over Strength and Lateral Load Reduction Factors

For the sake of completeness the early results achieved by reviewing the experimentally obtained and theoretically examined column behavior has been added into this paragraph (Karadoğ an et al. 2006, 2013).

The 4.0 m high column having a cross section of 40 × 40 cm, Fig. 8.8a, subjected to displacement reversals exposed the structural response shown in Fig. 8.8b. The same hysteresis loops have been obtained theoretically and compared in Fig. 8.8c with the experimental results. Then the material coefficients have been reduced from 1.15 to 1.4 to unity for steel and concrete respectively before the similar theoretical works carried out. The envelope of hysteresis curves are compared in Fig. 8.8d.

Similar 12 more tests have completed and similar analyses have been carried out depending on the results obtained and Table 8.1 has been prepared (Karadoğ an et al. 2013). One can found the ultimate loads of the columns when the material coefficient is taken as unity or different than unity, in the first two lines, respectively. The ratio of these two lines give the approximate over-strength factors. It can be concluded that for these type of columns the over-strength factors can be taken as 1.10. If the displacement ductilities obtained from the same tests which are given in the fourth line of Table 8.1 are multiplied by over strength factor the lateral load reduction factors on the fifth line will be achieved.

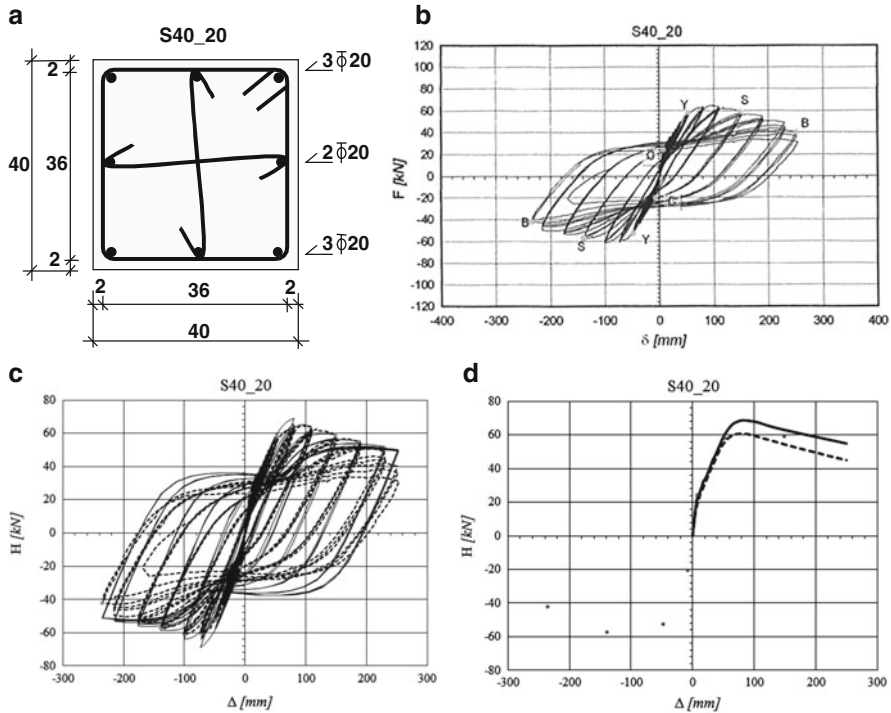


Fig. 8.8 Experimental and analytical evaluation of 40 × 40 cm column (a) Column cross section (b) Typical force-displacement relation (c) Comparison of experimental and analytical results (d) Effect of material coefficient on the envelopes of force-displacement hysteresis

8.7 Capacity Curves

Capacity curves used in the above explained algorithm can be obtained either by means of a theoretical manner or it can be obtained by any one of the known simplified technique. They can be in a continuous form or in bi-linear form.

Sometimes for the same size same quality concrete but for different reinforcement ratios simple ready charts can be utilized for that purpose. An example of a capacity curve for 30 × 30 cm C25 square column obtained experimentally, theoretically and parametrically is presented in Fig. 8.9, as well (Karadoğ an et al. 2006).

8.8 Numerical Examples

The presented algorithm has been used to make clear the following issues;

- To what extent the assumptions made at the beginning of preliminary design are satisfied? Namely, have the strength, the lateral load reduction factor and /or the

Table 8.1 Over strength factors, displacement ductility ratios and possible lateral load reduction factors

	1	2	3	4	5	6	7	8	9	10	11	12	13
Specimen	S30_14	S30_14M	S30_16	S30_18	S30_18Z	S35_1416	S35_18	S35_20	S35_20Z	S40_16	S40_20	S40_20Z	S40_20Z
$P_u (\gamma=1)$	21.30	21.00	29.10	32.60	30.40	33.50	42.50	50.40	48.00	49.30	68.50	88.30	89.76
$P_u (\gamma \neq 1)$	19.00	19.50	25.20	28.60	26.80	29.70	37.70	44.30	42.20	43.70	60.70	77.73	77.40
OSF	1.12	1.08	1.15	1.14	1.13	1.13	1.13	1.14	1.14	1.13	1.13	1.14	1.16
μ	5.30	3.20	5.10	3.70	3.00	5.80	5.50	4.60	3.90	5.20	5.50	3.00	3.40
OSF $\times \mu$	5.94	3.44	5.89	4.22	3.40	6.54	6.20	5.23	4.44	5.87	6.21	3.41	3.94

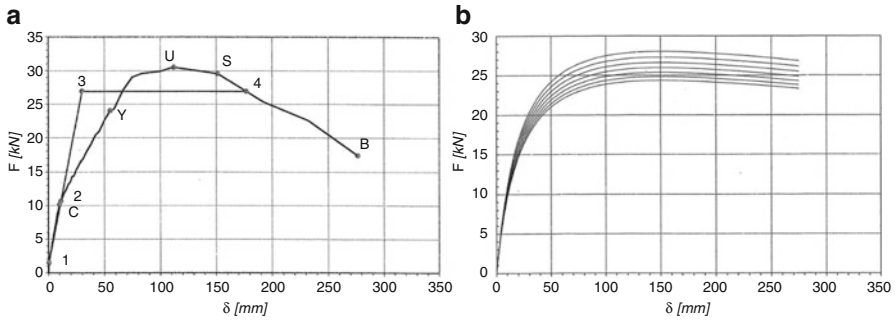


Fig. 8.9 Determination of the column capacity curve (a) Bilinear idealization of capacity curve (b) Effect of longitudinal reinforcement ratio on the capacity curve

displacement ductility assumptions as well as the stiffness values used in design been checked?

- The design is accepted when one or several of parameters are satisfied. What are the tolerance limits for satisfaction of the design criteria?

The initial design parameters and the findings are presented for three columns, Column #1 to #3. The Column #1 is extracted from the benchmark structure of [Safecast FP7 Project](#). Column #2 is one of the prefabricated columns tested at ITU laboratories (Karadoğ an et al. 2006). The Column #3 is extracted from a real structure currently in use in Kocaeli, Turkey.

The algorithm proposed above was run for each of the columns mentioned here. The algorithm has converged in three steps for all columns. The results as well as the key parameters per each analysis step have been presented in Table 8.2.

The results presented in Table 8.2 are based on the assumption that the change of R factor in two consecutive steps will not exceed a tolerance, which is 10 % in this study. This tolerance as well as tolerance limits of other parameters may be adjusted by the user depending on parametric studies and findings.

Comparison of the assumed capacity curve with the pushover and time history analyses results for columns are presented in Figs. 8.10, 8.11, and 8.12.

The results presented in Figs. 8.10, 8.11, and 8.12 are representative of all possible cases in design iterations when the proposed algorithm is used. In the first example, the displacement condition is not satisfied (i.e. the displacement demand of the original column is higher than the displacement capacity of the structure). The strength is not satisfied in the second example. The third example satisfies both conditions but the algorithm was still run in order to see how the design would change. It can be observed in these figures that the column dimensions and/or reinforcement need to be changed in all cases in order to satisfy the design algorithm proposed here.

Please note that the scale factors for some of the records listed in Table 8.3 are higher than 2. These are the cases where the number of available records for the set of criteria used was not high thus the scale factor condition was loosened.

Table 8.2 Progress of the algorithm and the change of key design parameters for the case study columns

Parameter	Unit	Soil type B	Soil type C	Soil type B
		60 × 60 column	40 × 40 column	70 × 70 column
m	tonnes	33	20.4	43.4
K_0	kN/m	2,230	1,946	582.1
T_0	s	0.75	0.64	1.54
$Sa(T = T_0)$	g	0.61	0.95	0.34
R		3	3	3
F_{design}	kN	65.80	63.40	36.70
K_1	kN/m	1,453	829	349
T_1 (yield)	s	0.93	0.98	1.99
$Sa(T = T_1)$	g	0.51	0.66	0.28
R_1		2.26	2.02	1.97
$ (R_1 - R_0)/R_0 $	> 10 %	0.25	0.33	0.34
$F_{design}(m + s)$	kN	73.10	65.40	60.60
K_2	kN/m	1,671	1,129	379
T_1 (yield)	s	0.87	0.84	1.91
$Sa(T = T_1)$	g	0.54	0.76	0.29
R_2		2.43	2.05	2.14
$ (R_2 - R_1)/R_1 $	OK	0.08	0.01	0.09
$F_{design}(m + s)$	kN	71.90	74.20	57.70

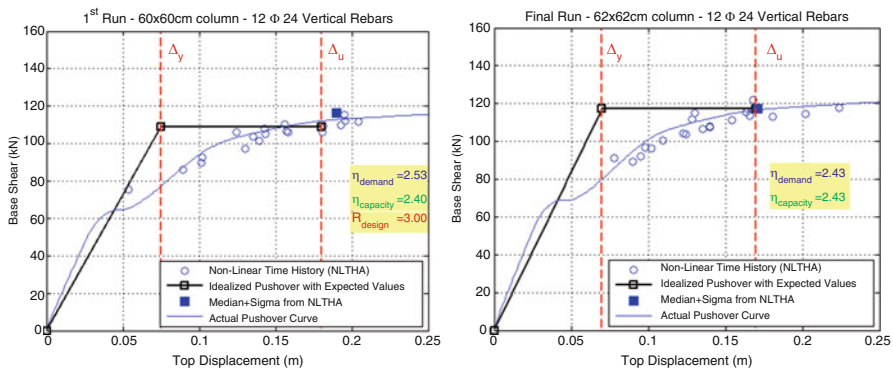


Fig. 8.10 Comparison of the assumed capacity curve with the pushover and time history analyses results for the Column #1

One of the key points of the algorithm proposed here, which is also one of the main motivations of the study, is that the spectral displacement equality (i.e. equal displacement rule) which is the basis of the conventional design is not valid in most of the cases. The analyses show that for the examined three columns, the average plastic displacements calculated by applying selected 20 records on the columns is

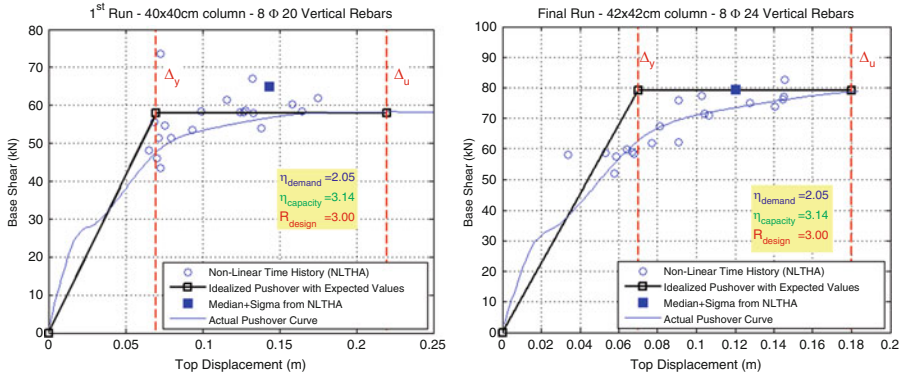


Fig. 8.11 Comparison of the assumed capacity curve with the pushover and time history analyses results for the Column #2

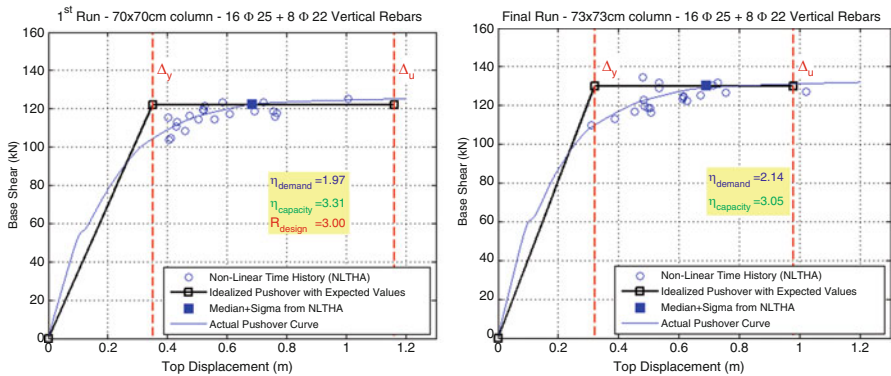


Fig. 8.12 Comparison of the assumed capacity curve with the pushover and time history analyses results for the Column #3

always higher than the spectral displacements found from the displacement spectra of the selected records. In other words, the equal displacement rule certainly does not work for the cases examined.

The displacement equality is the base of the conventional design because the behavior factor, R , is the most important assumption of the conventional design. A graphical description of the terms and the design assumption are presented in Fig. 8.13.

The results shown in Fig. 8.14 indicate a significant disagreement between the spectral and real displacement demands. Please note that the period of the three columns presented in the plot shown in Fig. 8.14, columns of 40×40 , 60×60 and 70×70 , are 0.64 s, 0.75 s and 1.54 s, respectively. As it can be seen in Fig. 8.14, as the period of the system increases, the disagreement becomes even more evident.

Table 8.3 Selected earthquake records and scale factors (SF)

60 × 60 cm column		40 × 40 cm column		70 × 70 cm column	
Record	SF	Record	SF	Record	SF
CHICHI03_TCU129-E	1.25	CHICHI06_TCU078-E	1.31	CHICHI03_TCU122-E	2.42
HECTOR_HEC090	0.98	CHICHI03_TCU129-E	0.99	CHICHI_TCU136-W	2.16
CHICHI_TCU047-N	1.25	CHICHI_CHY046-N	1.58	CHICHI_TCU128-N	1.57
CHICHI_CHY035-N	0.96	BIGBEAR_DHP090	1.44	CHICHI_TCU116-N	1.83
CHICHI_CHY034-W	0.90	MORGAN_G06090	0.97	CHICHI_TCU106-N	1.74
NORTHR_PKC360	0.86	HECTOR_HEC000	1.47	CHICHI_TCU087-N	2.15
NORTHR_STN110	1.03	CHICHI_TCU-E	1.32	CHICHI_TCU063-N	1.35
NORTHR_PEL360	1.28	CHICHI_CHY074-E	1.36	CHICHI_TCU054-N	1.97
LOMAP_G03090	1.22	CHICHI_ALS-E	1.43	CHICHI_TCU039-N	1.85
LOMAP_CYC285	1.04	NORTHR_PKC090	0.91	CHICHI_TCU029-N	1.77
CHICHI_TCU138-N	1.04	NORTHR_MRP090	1.53	CHICHI_CHY029-N	1.73
CHICHI_TCU116-E	1.24	NORTHR_0141-270	1.01	CHICHI_TCU136-N	1.99
CHICHI_TCU063-E	1.26	LANDERS_MVH000	1.45	CHICHI_TCU107-E	1.75
CHICHI_TCU047-E	0.91	LOMAP_SLC270	1.27	CHICHI_TCU082-E	1.96
CHICHI_TCU045-E	1.19	WHITTIER_A-CAS000	1.09	CHICHI_TCU054-E	2.39
CHICHI_CHY024-E	1.28	WESTMORL_PTS225	1.49	CHICHI_TCU039-E	1.72
NORTHR_PKC090	1.04	CORINTH_COR-L	1.33	CHICHI_TCU-E	2.04
NORTHR_LOS000	0.99	VICT_CPE045	0.8	CHICHI_CHY074-E	1.78
LOMAP_STG000	1.04	TABAS_DAY-LN	1.58	CHICHI_ALS-E	1.92
VICT_CPE045	0.93	FRIULI_A-TMZ000	1.45	KOBE_KBU000	1.31

8.9 Conclusions

The following conclusions are drawn:

- Design verification is needed and if necessary redesign step of iterations are carried out.
- It is possible to overcome the inherently existing deficiencies of spectrum based design by the algorithm presented; namely the strength and stiffness degradations and time duration effects can be considered which are not considered in the code specified spectrum analyses. In this technique, at the beginning of design stage, there is no need to make a series of assumptions such as the initial stiffness of the structure, displacement ductility of the structure and lateral load reduction factor which are all effective on the results. It becomes possible to trace the actual behavior of structure during the iteration steps.
- The top displacements obtained by NLTHA which are based on nearly code compatible real earthquake records are generally bigger than code limits and they are practically not equal to the elastic displacements obtained by linear time history analyses. Therefore the widely utilized assumption of *displacement equality* cannot be generalized for the columns analyzed and *equality of*

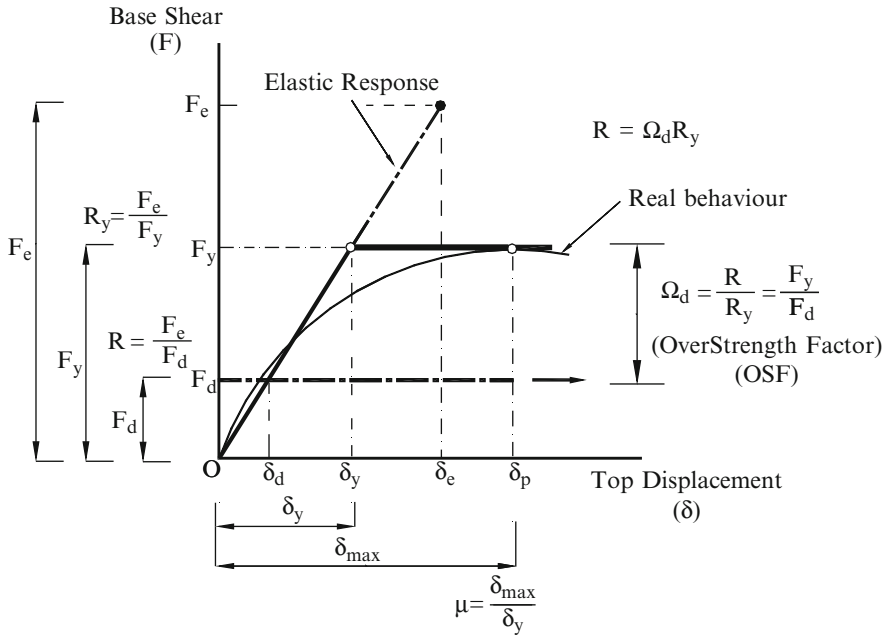
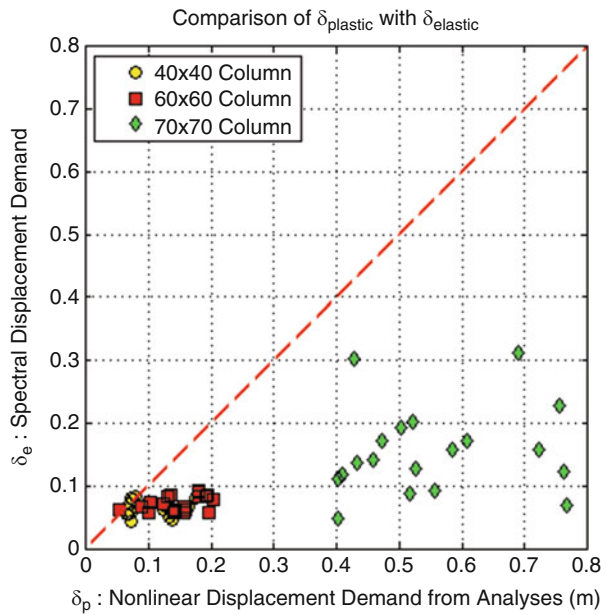


Fig. 8.13 The use of equal displacement rule in design

Fig. 8.14 Comparison of the elastic spectral displacements with the plastic displacement demands obtained from the nonlinear dynamic analyses



velocities or *energies* should be considered wherever is needed. The algorithm presented here is providing a versatile tool for that purpose.

- The proposed procedure can be used not only for single story precast buildings but it can be generalized by minor alterations for the design of bridge columns or piers and for the critical columns of pilot type building structures where all the nonlinear behavior is observed only in one of the generally lower stories.
- The execution time for nonlinear time history analyses needed in the proposed algorithm is not a big issue because of the speed reached by computers but more discussions should be done on the selection of real records and their optimal numbers.
- Several more checks can be added to the flow chart to have more refined one for controlling the sufficiency of sectional ductility needed to provide the required displacement ductility and to check the allowable tip rotations to keep the top beams stable in their original position. The algorithm proposed may be altered to depend on other limits or other parameters based on available research.

Open Access This chapter is distributed under the terms of the Creative Commons Attribution Noncommercial License, which permits any noncommercial use, distribution, and reproduction in any medium, provided the original author(s) and source are credited.

References

- Ataköy H (1999) 17 August Marmara earthquake and the precast structures built by TPCA members. Turkish Precast Concrete Association, Ankara
- Bruneau M (2002) Building damage from the Marmara, Turkey earthquake of August 17, 1999. *J Seismol* 6(3):357–377
- Bal IE Personel Webpage: http://web.itu.edu.tr/~iebal/Dr_Ihsan_Engin_BAL/SafeCladding_EU_Project.html
- Karadoğan F (1999) Prefabricated industrial type structures of Adapazari. In: Irregular structures asymmetric and irregular structures, vol 2. European Association of Earthquake Engineering, Task Group 8, Istanbul
- Karadoğan F, Yüksel E, Yüce S, Taskın K, Saruhan H (2006) Experimental study on the original and retrofitted precast columns. Technical report (in Turkish), Istanbul Technical University
- Karadoğan F, Yüce S, Yüksel E, Bal IE, Hasel FB (2013) Single story precast structures in seismic zones-I. COMPDYN 2013, 4th ECCOMAS thematic conference on computational methods in structural dynamics and earthquake engineering, Kos Island, 12–14 June 2013
- PEER NGA Database. Pacific earthquake engineering research center: NGA database. http://peer.berkeley.edu/peer_ground_motion_database/
- Saatcioglu M, Mitchell D, Tinawi R, Gardner NJ, Gillies AG, Ghobarah A et al (2001) The August 17, 1999, Kocaeli (Turkey) earthquake – damage to structures. *Can J Civ Eng* 28:715–737
- SAFECAS FP7 (2008–2011) Project Performance of innovative mechanical connections in precast building structures under seismic conditions, coordinated by Dr. Antonella Colombo
- Sezen H, Whittaker AS (2006) Seismic performance of industrial facilities affected by the 1999 Turkey earthquake. *J Per Const Fac ASCE* 20(1):28–36

- Sezen H, Elwood KJ, Whitaker AS, Mosalam KM, Wallace JW, Stanton JF (2000) Structural engineering reconnaissance of the August 17, 1999. Kocaeli (Izmit), Turkey. Earthquake rep No 2000/09. Pacific Engineering Research Center. University of California, Berkeley
- Wood SL (2003) Seismic rehabilitation of low-rise precast industrial buildings in Turkey. In: Wasti T, Ozcebe G (eds) Advances in earthquake engineering for urban risk reduction. NATO science series. IV. Earth and environmental sciences, vol 66. Kluwer Academic Publishers, Published by Springer, Dordrecht, pp 167–77

Chapter 9

Developments in Seismic Design of Tall Buildings: Preliminary Design of Coupled Core Wall Systems

M. Nuray Aydınoglu and Eren Vuran

Abstract Performance-based seismic engineering has brought new dimensions to tall building design, leading to a major transformation from the *prescriptive/linear* strength-based approach to the explicit *non-prescriptive/nonlinear* deformation-based design approach. In this context, current tall building seismic design practice is based on a well-established design methodology, which starts with a preliminary design followed by two *performance evaluation* stages. In this methodology, preliminary design represents the critical phase of the tall building design where all structural elements have to be preliminarily proportioned and reinforced for the subsequent performance evaluation stages. However, there are several problems inherent in the existing preliminary design practice. Preliminary design based on linear analysis could lead to unacceptable sizing and reinforcing of the main structural elements of tall buildings. In particular, linear preliminary design procedures applied to coupled core wall systems would most likely lead to an overdesign of coupling beams with inappropriate and heavily congested reinforcement requirements. In addition, linear analysis with reduced seismic loads may result in under-designed wall elements especially in terms of their shear strength. Simple procedures based on first principles have been developed to estimate base overturning moment capacity, total coupling shear capacity and overall ductility demand of the coupled core wall systems, which can be efficiently used in the preliminary seismic design of tall buildings.

M.N. Aydınoglu (✉)

Department of Earthquake Engineering, Kandilli Observatory and Earthquake Research Institute, Boğaziçi University, Çengelköy, Istanbul 34684, Turkey
e-mail: aydinogn@boun.edu.tr

E. Vuran

Balkar Engineering & Consultancy Ltd, Ebulula Cad. 7/A, Levent, Istanbul 34330, Turkey
e-mail: evuran@balkar.com.tr

© The Author(s) 2015

A. Ansal (ed.), *Perspectives on European Earthquake Engineering and Seismology*, Geotechnical, Geological and Earthquake Engineering 39, DOI 10.1007/978-3-319-16964-4_9

227

9.1 Introduction

Tall building seismic design has evolved during the last decade to become a major area of application of performance-based earthquake engineering. This development has opened a new door to structural design engineers who were struggling to overcome the structural restrictions imposed on tall buildings by traditional prescriptive seismic design codes. In a broader sense, performance-based earthquake engineering has brought new dimensions to tall building design, leading to a major transformation from the linear strength-based design to a nonlinear deformation-based design practice. In line with this development, special seismic design recommendations/guidelines and consensus documents for tall buildings based on performance-based design principles have been developed and published in the last decade by several institutions. In this respect starting from 2005, Los Angeles Tall Buildings Structural Design Council has published and continuously updated a series of *consensus documents* (LATBSDC 2005, 2008, 2011, 2013, 2014), reflecting the progress achieved in the state of practice of performance-based seismic design of tall buildings. In 2007 Structural Engineers Association of Northern California – SEAONC Tall Buildings Task Group (2007) published its first recommendations on tall building seismic design, which is adopted in 2008 and later updated by San Francisco Department of Building Inspection (2014). On the other hand Council on Tall Buildings and Urban Habitat published in 2008 its design recommendations prepared by Seismic Working Group (CTBUH 2008). As a parallel development, a draft version of a tall building design code was prepared in 2008 for the Istanbul Metropolitan Municipality by the *Kandilli Observatory and Earthquake Research Institute* (IMM 2008; Aydınoğlu 2011) at the time when tall building construction started booming. In the meantime Pacific Earthquake Engineering Research Center (PEER) conducted a multi-year collaborative effort, called Tall Buildings Initiative (TBI), to develop more comprehensive performance-based seismic design guidelines for tall buildings (PEER/TBI 2010) along with a supporting document on modeling and acceptance criteria for nonlinear response (PEER/ATC 2010).

Current tall building seismic design guidelines/consensus documents (PEER/TBI 2010; SFDBI 2014; LATBSDC 2014) are all based on the same design methodology, starting with a preliminary design followed by two *performance evaluation* stages. In the preliminary design, tall building structural system is preliminarily proportioned and reinforced on the basis of linear analyses and *capacity design principles*. San Francisco practice (SFDBI 2014) treats the preliminary design as a *code-level evaluation* stage where selected *prescriptive* provisions including minimum base-shear requirement of the San Francisco Building Code are applied while a number of exceptions are allowed, such as removal of force amplification (over-strength) and reliability/redundancy factors, etc. Thus, SFDBI (2014) formally applies a three-stage procedure, while other guidelines (PEER/TBI 2010; LATBSDC 2014) do not formally define the preliminary design as a design

stage and insist on a *non-prescriptive* two-stage scheme by completely eliminating the prescriptive code provisions.

The two-stage *performance evaluation* following the preliminary design includes a *serviceability evaluation* stage under the so-called *service earthquake* and a *collapse level evaluation* stage under the so-called *maximum credible earthquake*, corresponding to 43 and 2,475 year return periods, respectively. The damping is considered 2.5 % in both stages.

The *serviceability evaluation* stage requires the tall building structural system remains essentially elastic (or nearly elastic with almost negligible nonlinear behavior) under frequently occurring small earthquakes.

On the other hand *collapse level evaluation* considers the worst-case scenario, where the structure is evaluated under the *maximum credible earthquake* with a performance objective aiming at a *reasonably low risk of partial or total collapse*, which corresponds to an acceptable level of damage in terms of ductile response quantities while keeping all other brittle response quantities, e.g., internal forces below their strength capacities, thus preserving the gravity load carrying capacity of the structural system.

Preliminary design represents the critical phase of the tall building design where all structural elements need to be preliminarily proportioned and reinforced for the subsequent performance evaluation stages. Here the problem lies with the fact that designer has no reliable analysis tools at this phase other than linear response analysis and application of capacity design principles, which in fact may not provide a guarantee for an acceptable nonlinear response under the *maximum credible earthquake*. It means that the preliminary design may need to be revised according to the results of the nonlinear performance evaluation. In other words, the so-called *performance evaluation stage* should not be considered only as an evaluation stage, but at the same time as a *design improvement stage*.

In this contribution particular emphasis will be given to the preliminary design of *coupled core wall systems*, which are the most commonly used tall building structural systems for seismic resistance. In an attempt to search for alternate preliminary design procedures, attention will be focused on a recently developed simple and novel capacity estimation procedure as well as a ductility demand estimation procedure (Vuran 2014; Vuran and Aydınoglu 2015). In addition, *shear amplification* and *shear migration* effects will be considered during the preliminary design stage, which are relatively lesser-known but very significant effects governing the core wall seismic design.

9.2 Preliminary Design Issues

Preliminary design stage needs to be given a special emphasis for the development of a suitable tall building structural system later to be evaluated/designed on performance basis through nonlinear seismic analysis.

In this respect, LATBSDC (2014) considers the preliminary design stage as merely equivalent to the application of *capacity design rules* while SFDBI (2014) applies the *prescriptive* provision of *minimum base shear* strength requirement. On the other hand TBI (PEER/TBI 2010) treats the preliminary design issue in a more detailed fashion, additionally including recommendations on system configuration, wind effects, limiting building deformations, setbacks and offsets, diaphragm demands, outrigger elements, etc.

Capacity design rules are intended to insure that “*structural system for the building has well defined inelastic behavior where nonlinear actions and members are clearly defined and all other members are stronger than the elements designed to experience nonlinear behavior.*” Detailed lists are provided in both TBI (PEER/TBI 2010) and LATBSDC (2014) to identify the “*zones and actions commonly designated for nonlinear behavior*”.

When applying capacity design principles, it is stated in LATBSDC (2014) that “*linear analysis may be used to determine the required strength of the yielding actions*”. This recommendation is problematic in the sense that linear analysis cannot correctly estimate the internal force redistribution in real response due to nonlinear behavior, in particular for coupled core wall systems. On the other hand *capacity protected actions* such as shears in beams and columns may be estimated by capacity design principles to an acceptable accuracy, but shears in walls could be grossly underestimated. In this respect, a frequently encountered example is the preliminary design of coupled core wall systems.

Core walls with peripheral columns represent the most common structural system of tall buildings. Frames with down stand beams are rarely used and in many cases, even completely eliminated leading to flat plate systems. Thus, the so-called *dual systems* with moment-resisting frames (back-up systems) are practically discarded. A number of engineers who faithfully provided the back-up systems in all their past prescriptive code applications appear to be hesitant in accepting this new situation. However it can be argued that properly designed coupled walls with sufficiently stiff and strong coupling beams effectively provide a similar back-up action expected from the moment resisting frames of dual systems with cantilever walls.

Engineers often experience difficulty in preliminary sizing of coupled core wall systems. Reliable practical analysis tools that would help consider the nonlinear seismic behavior of wall piers and coupling beams as well as their combined effect in seismic response of coupled wall systems are not available. Both coupled walls and coupling beams generally undergo significant nonlinear response and coupling beams experience excessive plastic deformations throughout the height of the building. The nonlinear behavior of wall pieces is significantly influenced by the stiffness and strength of coupling beams.

In the current practice, linear analysis is being employed inevitably in the preliminary design stage to identify the stiffness and strength of coupled wall components and their distribution. Such a procedure would most likely lead to an overdesign of coupling beams with inappropriate and probably heavily congested reinforcement requirements. On the other hand, a preliminary design based on a

linear analysis with reduced seismic loads may result in under-designed wall elements especially in terms of their shear strength (Aydinoğlu 2014).

In an attempt to avoid the inappropriate use of linear analysis in the preliminary design stage, employment of multi-mode pushover analysis has been proposed by Aydinoğlu (2014). Based on Incremental Response Spectrum Analysis – IRSA Method (Aydinoğlu 2003, 2004), multi-mode pushover analysis has proven to be a useful tool in preliminary proportioning of coupled core wall systems. In the following, even simpler but very efficient capacity and demand estimation tools are presented, which were developed only recently (Vuran 2014; Vuran and Aydinoğlu 2015).

9.3 Capacity and Ductility Demand Estimation Tools for Preliminary Design of Coupled Core Wall Systems

A simple, *strength-of-materials approach* is developed to estimate the *base overturning moment capacity* and *total coupling shear capacity* of a typical coupled core wall system starting from *first principles*. Based on estimated overturning moment capacity, the simple approach is further extended to estimate the overall *ductility demand* of the coupled core wall system utilizing a novel modification of the pushover concept (Vuran 2014; Vuran and Aydinoğlu 2015).

9.3.1 A Capacity Estimation Tool for Coupled Core Walls

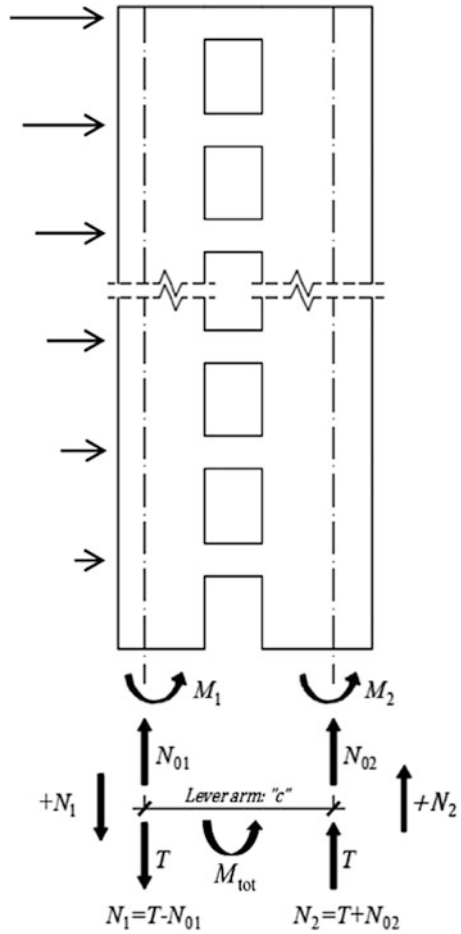
It is assumed that the coupled core wall system shown in Fig. 9.1 responds to earthquake action on its own as the main structural system without stiffness and strength contribution of any other structural element. Actually this is the case in most of tall buildings with core wall at the centre and gravity frames along the periphery.

Using simple equilibrium equations, individual wall axial reaction forces at the base can be expressed as

$$N_1 = -N_{01} + T \quad ; \quad N_2 = N_{02} + T \quad (9.1)$$

where N_1 is considered positive in tension and N_2 positive in compression as indicated in Fig. 9.1, representing the axial force reactions of the so-called *tension wall* and *compression wall*, respectively. N_{01} and N_{02} represent gravity axial loads of walls and T refers to the so-called *total coupling shear* representing the sum of shear forces developed in coupling beams throughout the building. The sense of earthquake direction is assumed from left to right. If opposite, then subscripts 1 and 2 should be interchanged.

Fig. 9.1 Base reactions and coupling shear forces acting on coupled wall system



The base section of the coupled core wall system is the most critical section controlling the nonlinear behaviour of the entire structure. Total base overturning moment reaction of the coupled wall system can be expressed by the following equilibrium equation:

$$M_{tot} = M_1 + M_2 + Tc \tag{9.2}$$

where M_1 and M_2 represent the bending moments of the tension and compression walls, respectively, and c refers to lever arm between the centroids of walls.

The contribution of the force couple, Tc , in total base overturning moment is traditionally represented by *degree of coupling parameter*, A , as follows:

$$A = \frac{Tc}{M_{\text{tot}}} = \frac{Tc}{M_1 + M_2 + Tc} \quad (9.3)$$

The reaction forces and the degree of coupling parameter given above are traditionally evaluated as *demand quantities* obtained from the linear analysis of a given system under a given earthquake action (Paulay and Priestley 1992). However, here they are considered to represent the corresponding *strength capacities*. The ultimate capacity term that would control the coupled wall design is the *total base overturning moment capacity* defined by Eq. (9.2).

It is clear that maximizing the force couple, i.e. the *total coupling shear*, corresponds to maximizing the overturning moment capacity. However, inspection of Eq. (9.1) suggests that *total coupling shear* T should not be increased arbitrarily, as it would lead to increasing tension strains in the tension wall, i.e., spreading of the yielding from the base to the upper parts and hence larger concrete cracking along the wall. At the same time it would lead to increasing compression strains in the compression wall, even it could cause non-ductile compression failure if compressive axial force N_2 exceeds the balance point of axial force-moment interaction. Moreover increased coupling shear would result in reinforcement congestion and construction difficulties in coupling beams.

Thus, it is imperative that a reasonable compromise should be achieved between the strength capacities of individual walls and the coupling beams and such a “*balanced solution*” has to be worked out during the preliminary design stage. This observation has motivated the development of a *capacity estimation procedure* for the initial sizing of the individual walls and the coupling beams in the preliminary design stage.

It has been shown by Vuran and Aydinoglu (2015) that *total coupling shear capacity* and consequently *total base overturning moment capacity* of a coupled core wall system is essentially controlled by three independent parameters:

- (a) Normalized gravity load of the tension wall: $n_{01} = N_{01}/(A_{c1}f_{ce})$
- (b) Mechanical reinforcement ratio of the tension wall: $\rho_{m1} = (A_{s1}/A_{c1})(f_{ye}/f_{ce})$
- (c) Relative yield parameter of the tension wall, β_1 , which represents the ratio of the axial load reaction N_1 to its full yield strength in tension, N_{Y1} :

$$N_1 = \beta_1 N_{Y1}$$

where f_{ce} and f_{ye} denote the “*expected compressive strength*” of concrete and “*expected yield strength*” of reinforcing steel with A_{c1} and A_{s1} representing the corresponding areas in the tension wall and ρ_{m1} is the mechanical reinforcement ratio.

Utilizing the first expression in Eq. (9.1), normalized total coupling shear can be expressed as

$$n_{T1} = \frac{T}{A_{c1}f_{ce}} = n_{01} + \beta_1 \rho_{m1} \quad (9.4)$$

from which application range of the relative yield parameter β_1 can be defined as

$$-\frac{n_{01}}{\rho_{m1}} \leq \beta_1 \leq 1 \quad (9.5)$$

This relationship suggests that the limiting condition $\beta_1 = 1$ corresponds to the largest attainable axial tension force in the tension wall (strain-hardening is neglected for the sake of simplicity) and hence greatest coupling shear according to Eq. (9.1). On the other hand $\beta_1 = -n_{01}/\rho_{m1}$ corresponds to the other limiting condition leading to zero coupling shear, i.e., $n_{T1} = 0$ in Eq. (9.4), which corresponds to the degeneration of the coupled wall system into two individual cantilever walls with axial force reactions equal to their gravity loads only, i.e., $-n_{0i}$.

By appropriate selection of the independent parameters defined above, total *coupling shear capacity* can be readily estimated from Eq. (9.4), and *total base overturning moment capacity* can be calculated from Eq. (9.2) by adding bending moment capacities of individual walls, namely M_1 and M_2 . Implementation details are given in Vuran and Aydinoglu (2015).

Note that although above-described capacity estimation procedure is given for a simple coupled wall system shown in Fig. 9.1, it can be extended to more complex systems by appropriate applications of equilibrium equations.

9.3.2 A Ductility Demand Estimation Tool for Coupled Core Walls

Following the estimation of total base overturning moment capacity of the coupled core wall system, it needs to be checked whether it is sufficient for the purpose of preliminary design. This is achieved by evaluating the *overall ductility demand*, μ , of the system under maximum credible earthquake (MCE) through a novel application of an alternate pushover concept developed, the details of which can also be found in Vuran and Aydinoglu (2015). As an end product, ductility demand, μ , is estimated as

$$\mu = S_{ac}(T_1) \frac{m_{o1}^*}{M_{tot}} \quad (9.6)$$

where $S_{ac}(T_1)$ refers to first-mode spectral pseudo-acceleration of the MCE level earthquake and m_{o1}^* represents the “*participating modal mass for the base overturning moment*” of the first (dominant) mode, which can be calculated as

$$m_{o1}^* = L_{o1}^* \frac{L_{x1}^*}{M_1^*} \tag{9.7}$$

The parameters of the above equation are defined as

$$L_{o1}^* = \mathbf{h}_o^T \mathbf{M} \Phi_1 \quad ; \quad L_{x1}^* = \mathbf{i}_x^T \mathbf{M} \Phi_1 \quad ; \quad M_1^* = \Phi_1^T \mathbf{M} \Phi_1 \tag{9.8}$$

where \mathbf{M} represents the mass matrix and Φ_1 denotes the first (dominant) mode shape vector. \mathbf{i}_x refers to a vector whose elements are unity for degrees of freedom in x earthquake direction while others are zero. \mathbf{h}_o is a similar vector whose nonzero elements are the story elevations each measured from the base level.

If ductility demand calculated from Eq. (9.6) falls below an acceptable value, the preliminary design may be deemed to be successfully completed. For a satisfactory seismic performance under MCE level earthquake, results of the nonlinear response history analyses (Vuran 2014) have suggested that overall ductility demand of a typical coupled core wall system should be approximately bounded by the limits of $2.5 \leq \mu \leq 3.5$.

If the ductility demand is found acceptable, nonlinear performance evaluation stage can be initiated based on reinforcements calculated for the individual walls and the coupling beams, the latter of which is selected on the basis of coupling shear capacity estimated by Eq. (9.4).

A preliminary estimation may also be made for the base shear demands of tension and compression walls by amplifying the first-mode base shear, which can be approximately calculated in terms of M_{tot} . Based on nonlinear response history analysis performed for symmetrical coupled core wall systems (Vuran 2014), base shear demand for each wall individual may be estimated for preliminary design purpose as (Vuran and Aydınoğlu 2015)

$$V_{base} \cong \frac{M_{tot}}{0.7H} \alpha_{vH} \alpha_{vM} \tag{9.9}$$

where H represents the total building height, α_{vH} is the dynamic shear amplification factor accounting for *higher mode effects* and α_{vM} denotes the dynamic shear amplification factor representing *shear migration* from the yielding tension wall to the compression wall at sections near the base. Recommended dynamic shear amplification factors for preliminary design are:

$$\alpha_{vH} \cong 1.5 \quad ; \quad \alpha_{vM} \cong 2 \tag{9.10}$$

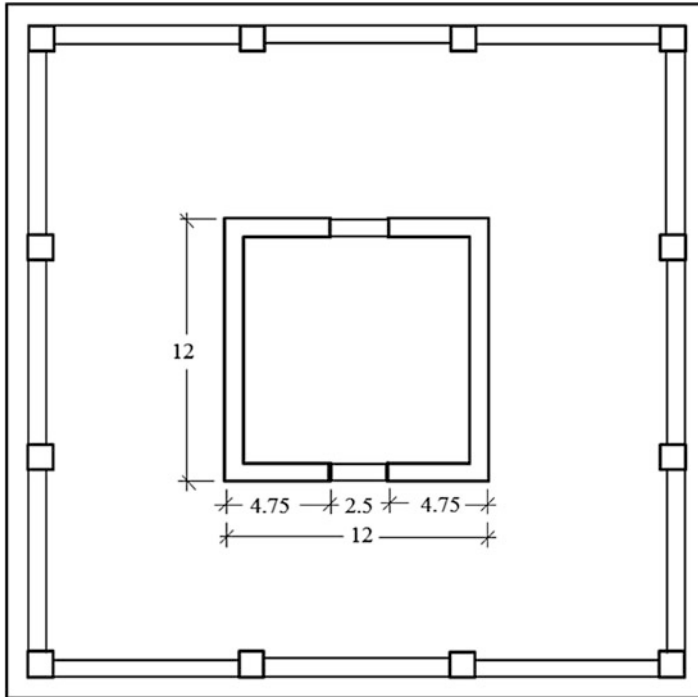


Fig. 9.2 Tall building floor plan with coupled core wall system CW12

9.4 Evaluation of Capacity and Ductility Demand Estimation Tools for Preliminary Design of Coupled Core Wall Systems

In order to evaluate the effects of three independent parameters controlling the capacity of the coupled core wall system, a parametric study is performed (Vuran and Aydinoglu 2015).

Several tall buildings with a central core wall system and gravity columns are designed, ranging from 25 to 50 stories. All cores are of square hollow sections in plan with openings only in one direction spanned by coupling beams with a constant depth/span ratio of $\frac{1}{2}$, thus forming a symmetrical coupled core wall system in that direction. Outer plan dimensions of square cores are selected as 10, 12, 14 and 16 m.

For space limitations, only 12 m^2 symmetrical core wall system, called CW12 is evaluated here, as shown in Fig. 9.2. Details of the dimensions and loading combinations of the other core wall systems can be found in Vuran (2014).

CW12 has two types with 30 and 40 stories. In 30 story building wall thicknesses are 0.75 m at 1st–10th stories, 0.60 m at 11th–20th stories and 0.45 m at 21st–30th stories. Same wall thicknesses are applied to 40 story building at 1st–15th stories, 16–30th stories and 31st–40th stories, respectively.

Table 9.1 Variation of n_T and μ with respect to n_0 , ρ_m and β for CW12

ρ_m	β	30 story building				40 story building			
		$T_1 = 3.3 s$				$T_1 = 5.7 s$			
		$n_0 = 0.075$		$n_0 = 0.125$		$n_0 = 0.175$		$n_0 = 0.225$	
		n_T	μ	n_T	μ	n_T	μ	n_T	μ
ρ_{mI}	- 1.0	0.041	7.1	0.091	4.3	0.141	4.2	0.191	3.3
	- 0.5	0.058	6.0	0.108	3.9	0.158	3.9	0.208	3.1
	0	0.075	5.3	0.125	3.6	0.175	3.7	0.225	3.0
	0.5	0.092	4.7	0.142	3.3	0.192	3.5	0.242	2.8
	1.0	0.110	4.2	0.160	3.1	0.210	3.3	0.260	2.7
$2\rho_{mI}$	- 1.0	0.006	8.9	0.056	4.8	0.106	4.6	0.156	3.5
	- 0.5	0.041	6.1	0.091	3.9	0.141	3.9	0.191	3.1
	0	0.075	4.6	0.125	3.3	0.175	3.5	0.225	2.8
	0.5	0.110	3.8	0.160	2.9	0.210	3.1	0.260	2.6
	1.0	0.144	3.2	0.194	2.5	0.244	2.8	0.294	2.4
$3\rho_{mI}$	- 1.0	-	-	0.022	5.6	0.072	5.1	0.122	3.7
	- 0.5	0.023	6.2	0.073	3.9	0.123	4.0	0.173	3.1
	0	0.075	4.2	0.125	3.0	0.175	3.3	0.225	2.7
	0.5	0.127	3.2	0.177	2.5	0.227	2.9	0.277	2.4
	1.0	0.179	2.6	0.229	2.2	0.279	2.5	0.329	2.2

$$f_{ce} = 65 \text{ Mpa}; f_{ye} = 491.4 \text{ Mpa}; \rho_I = 0.00457; \rho_{mI} = (f_{ye}/f_{ce}) \rho_I = 0.0345$$

For each building type, two sets of wall gravity loading were considered by changing the number and distribution of gravity columns and hence tributary floor areas of cores. Total floor masses were kept unchanged. This has been deliberately arranged such that normalized wall gravity loads are specified as 0.075 and 0.125 at the base level of the 30 story building and, 0.175 and 0.225 for the 40 story building. Thus for each building type, only one linear dynamic model is defined based on the linear stiffness characteristics, while two different nonlinear dynamic models are defined based on different strength characteristics due to different gravity loading applied to the core walls. Masses are the same in both linear and nonlinear models, which are all developed in accordance with rigid diaphragm assumption. First-mode natural vibration periods of 30 story and 40 story buildings are calculated as 3.3 and 5.7 s, respectively.

Walls are reinforced according to the requirements of the Turkish Seismic Design Code. Minimum wall total reinforcement ratio is designated as ρ_I . Table 9.1 summarizes the results in terms of *total normalized coupling shear*, n_T , versus *ductility demand*, μ , calculated for a typical MCE level earthquake (see Fig. 9.3 for pseudo-acceleration spectrum) for four levels of *normalized wall gravity load*, n_0 , three levels of wall reinforcement ratio, ρ , and five levels of relative yield factor, β , of the tension wall (wall numbers as subscripts are dropped due to symmetrical system considered). *Expected material strengths* are used as indicated at the footer of Table 9.1.

The results given in Table 9.1 are also displayed in Figs. 9.4, 9.5, 9.6, and 9.7 where acceptable range for the ductility demand ($2.5 \leq \mu \leq 3.5$) is indicated.

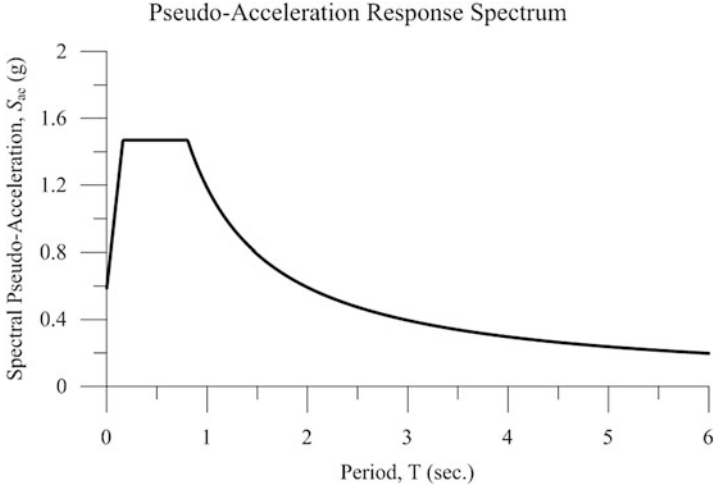


Fig. 9.3 Pseudo-acceleration spectrum for a typical MCE level earthquake

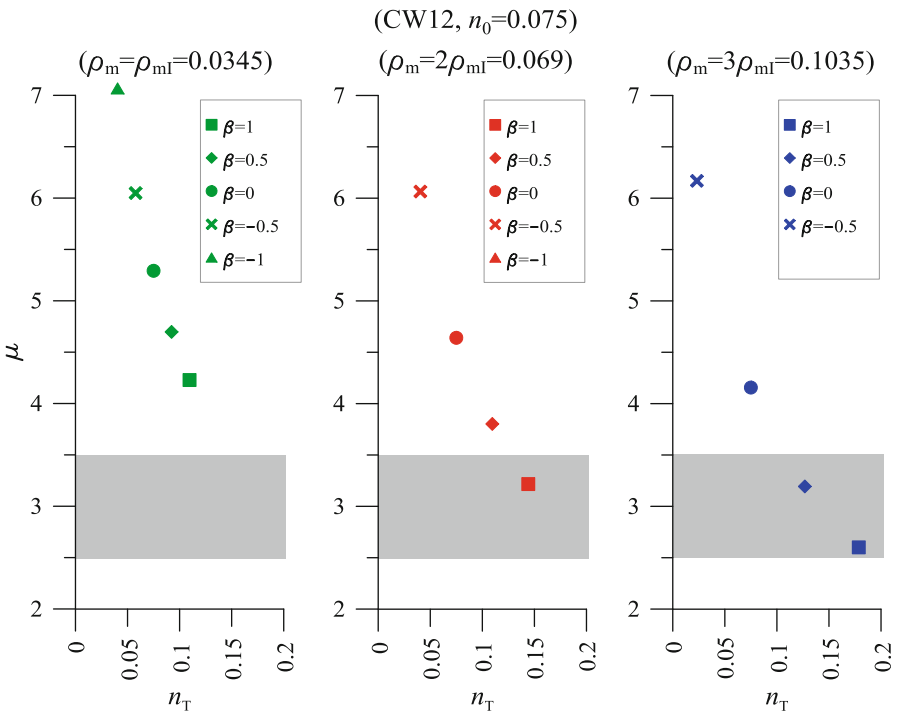


Fig. 9.4 Ductility demand vs total coupling shear for various combinations of wall mechanical reinforcement ratio and relative yield parameter (CW12, $n_0=0.075$)

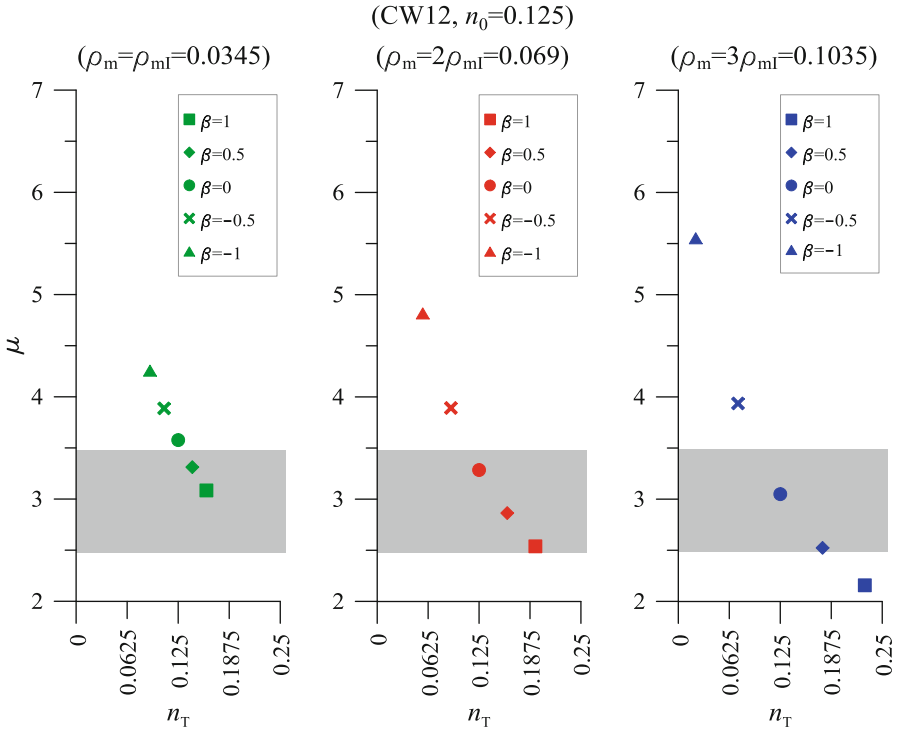


Fig. 9.5 Ductility demand vs total coupling shear for various combinations of wall mechanical reinforcement ratio and relative yield parameter (CW12, $n_0=0.125$)

Total base overturning capacities obtained by the proposed procedure have been confirmed by nonlinear response history analysis performed for a typical parameter set under Chi-chi earthquake (record no: TCU065), whose response spectrum matches well with the typical MCE level spectrum shown in Fig. 9.3. Nonlinear analysis results are shown in Fig. 9.8 in terms of peak base overturning moment normalized with respect to that estimated by the proposed simple procedure versus ductility demand. Acceptable range for the ductility demand ($2.5 \leq \mu \leq 3.5$) is also indicated on the figure.

Following conclusions may be drawn from Table 9.1 and Figs. 9.4, 9.5, 9.6, 9.7, and 9.8.

- (a) As long as concrete crushing is avoided in the compression wall, higher values of wall gravity loads n_0 are beneficial in \supset shaped walls. The outcome would be a direct increase in base overturning moment capacity and decrease in overall ductility demand.
- (b) Contribution of $\beta\rho_m$ to total coupling shear capacity (see Eq. (9.4)) is more pronounced for lower n_0 levels. For higher values of n_0 , contribution of $\beta\rho_m$ remains limited.

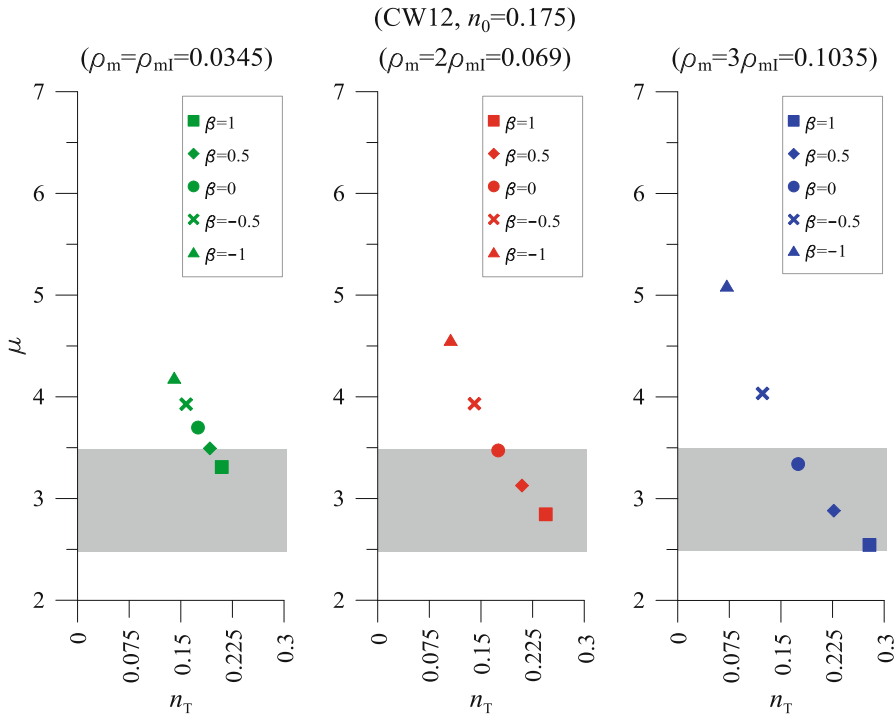


Fig. 9.6 Ductility demand vs total coupling shear for various combinations of wall mechanical reinforcement ratio and relative yield parameter (CW12, $n_0 = 0.175$)

(c) Results show that reinforcement ratio ρ_m as well as relative yield parameter β of the tension wall cannot be selected arbitrarily, as only certain combinations of those parameters would result in acceptable ductility demand levels. Ease of implementation of the proposed simple capacity and ductility demand estimation tools allows the designer to play with the independent parameters to reach an acceptable design configuration with a minimum effort. Implementation details are given in Vuran and Aydınoglu (2015).

9.5 Concluding Remarks

The following remarks can be made to conclude this contribution:

- (a) Preliminary design based on linear analysis may lead to unacceptable sizing and reinforcing of the main structural elements of tall buildings.
- (b) In particular, linear preliminary design procedures applied to coupled core wall systems would most likely lead to an overdesign of coupling beams with inappropriate and heavily congested reinforcement requirements. On the

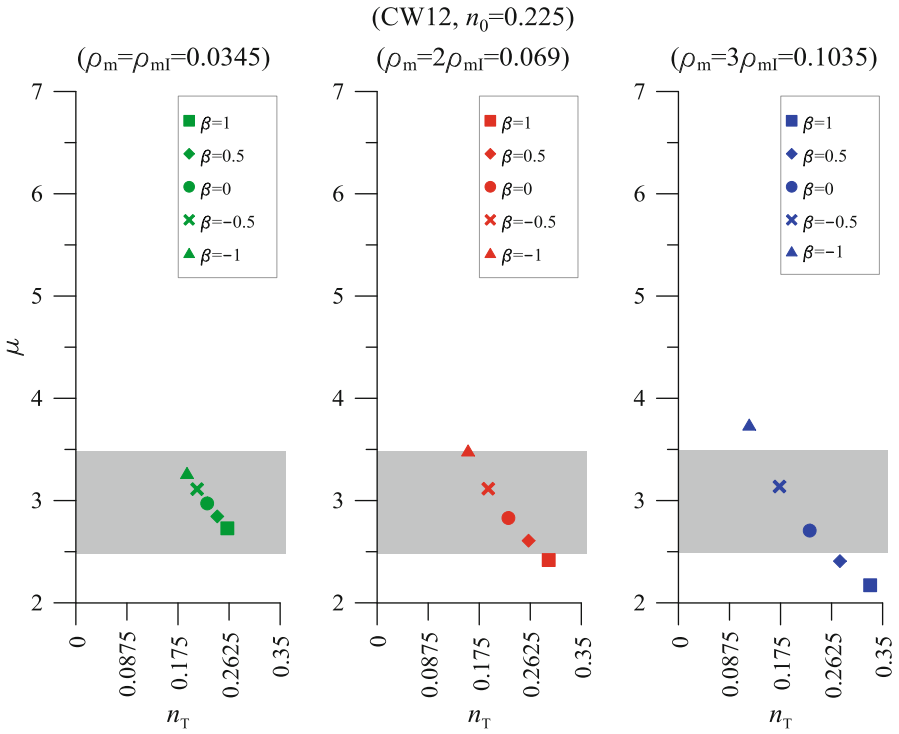


Fig. 9.7 Ductility demand vs total coupling shear for various combinations of wall mechanical reinforcement ratio and relative yield parameter (CW12, $n_0=0.225$)

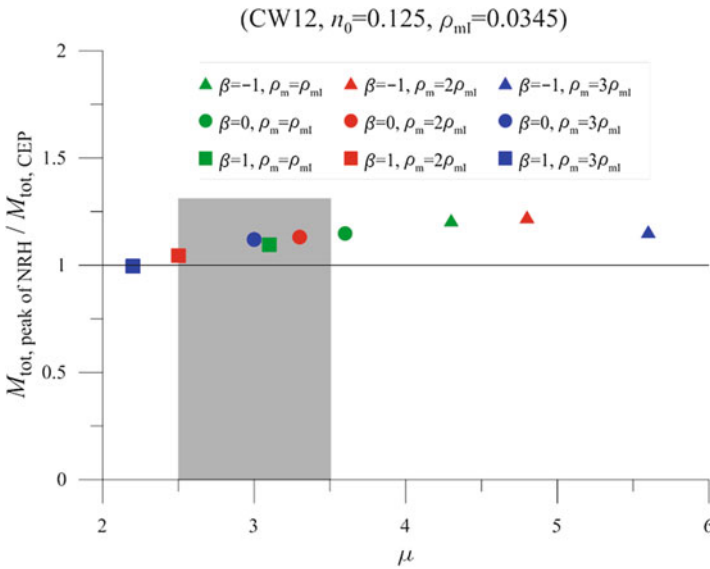


Fig. 9.8 Total base overturning moment capacity obtained from NRHA divided by the same from proposed procedure versus ductility demand (CW12, $n_0=0.125$, Chi-chi earthquake – record no: TCU065)

contrary, linear analysis with reduced seismic loads may result in under-designed wall elements especially in terms of their shear strength.

- (c) Total coupling shear capacity and total base overturning moment capacity of a coupled core wall system can be successfully estimated in the preliminary design stage by a simple procedure, which starts from the “*first principles*” based on limit equilibrium conditions.
- (d) In order to assess the adequacy of total base overturning moment capacity, overall ductility demand of the coupled core wall system can be estimated again by a simple procedure based on an alternate implementation of the pushover concept.
- (e) Since capacity and ductility demand estimation procedures are very easy to implement and not time consuming, several trials can be made during the preliminary design stage by playing with the independent variables to reach an acceptable ductility level.
- (f) A reasonable estimate of the base shear can also be made considering significant amplifications due to higher mode effects and shear migration from the tension wall to the compression wall.

Open Access This chapter is distributed under the terms of the Creative Commons Attribution Noncommercial License, which permits any noncommercial use, distribution, and reproduction in any medium, provided the original author(s) and source are credited.

References

- Aydınoğlu MN (2003) An incremental response spectrum analysis based on inelastic spectral displacement for multi-mode seismic performance evaluation. *Bull Earthq Eng* 1:3–36
- Aydınoğlu MN (2004) An improved pushover procedure for engineering practice: Incremental Response Spectrum Analysis (IRSA). International workshop on “performance-based seismic design: concepts and implementation, Bled, 2004, PEER report 2004/05, pp 345–356
- Aydınoğlu MN (2011) Draft seismic design code for tall buildings in Istanbul Metropolitan area. U.S.-Iran-Turkey seismic workshop on “seismic risk management in urban areas, Dec 14–16, 2010 – Istanbul – PEER report 2011/07, pp 55–63
- Aydınoğlu MN (2014) Challenges and problems in performance-based design of tall buildings: Chapter 20. In: *Performance-based seismic engineering: vision for a earthquake resilient society*, Proceedings of International Workshop in Bled, 2011. Springer, pp 279–300
- CTBUH (2008) Recommendations for the seismic design of high-rise buildings – a consensus document. Council on Tall Buildings and Urban Habitat, Seismic Working Group, Chicago
- IMM (2008) Istanbul seismic design code for tall buildings, draft version IV. Istanbul Metropolitan Municipality, Istanbul
- LATBSDC (2005, 2008, 2011, 2013, 2014) An alternative procedure for seismic analysis and design of tall buildings located in the Los Angeles region – a consensus document. Los Angeles Tall Buildings Structural Design Council, Los Angeles
- Paulay T, Priestley MJN (1992) *Seismic design of reinforced concrete and masonry buildings*. Wiley, New York, 744 p
- PEER/ATC (2010) Modeling and acceptance criteria for seismic design and analysis of tall buildings. PEER/ATC 72-1. Applied Technology Council, Redwood City – Pacific Earthquake Engineering Center, Berkeley

- PEER/TBI (2010) Guidelines for performance-based seismic design of tall buildings, version 1.0. Pacific Earthquake Engineering Research Center, PEER report 2010/05, Nov 2010. Prepared by the Tall Buildings Initiative (TBI) Guidelines Working Group, Berkeley
- SEAONC (2007) AB-083: recommended administrative bulletin on the seismic design & review of tall buildings using non-prescriptive procedures. Prepared for San Francisco Department of Building Inspection by Tall Buildings Task Group, Structural Engineers Association of Northern California, April 2007, San Francisco
- SFDBI (2014) Requirements and guidelines for the seismic design of new tall buildings using non-prescriptive seismic-design procedures. Administrative bulletin no. AB-083, San Francisco Department of Building Inspection, San Francisco
- Vuran E (2014) Development and verification of seismic capacity and ductility demand estimation procedures for coupled core wall systems. PhD dissertation, Boğaziçi University, Kandilli Observatory and Earthquake Research Institute, Department of Earthquake Engineering, June 2014
- Vuran E, Aydınoğlu MN (2015) Capacity and ductility demand estimation procedures for preliminary design of coupled core wall systems of tall buildings. Bull Earth Eng (submitted)

Chapter 10

Seismic Response of Underground Lifeline Systems

Selçuk Toprak, Engin Nacaroğlu, and A. Cem Koç

Abstract This paper presents and discusses the recent developments related to seismic performance and assessment of buried pipelines. The experience from the performance of pipelines during last earthquakes provided invaluable information and lead to new developments in the analysis and technologies. Especially, the pipeline performance during Canterbury earthquake sequence in New Zealand is taken as a case study here. The data collected for the earthquake sequence are unprecedented in size and detail, involving ground motion recordings from scores of seismograph stations, high resolution light detection and ranging (LiDAR) measurements of vertical and lateral movements after each event, and detailed repair records for thousands of km of underground pipelines with coordinates for the location of each repair. One of the important learnings from the recent earthquakes is that some earthquake resistant design and technologies proved to be working. This provides a motivation to increase international exchange and cooperation on earthquake resistant technologies. Another observation is that preventive maintenance is important to reduce the pipeline damage risk from seismic and other hazards. To increase the applicability and sustainability, seismic improvements should be incorporated into the pipe replacement and asset management programs as part of the preventive maintenance concept. However, it is also important to put in the most proper pipeline from the start as replacing or retrofitting the pipelines later requires substantial investment. In this respect, seismic considerations should be taken into account properly in the design phase.

10.1 Introduction

Observations from recent earthquakes provided opportunities to evaluate the pipeline performances with respect to pipeline properties, soil conditions and different levels of loadings. Earthquake damage to buried pipelines can be attributed to

S. Toprak (✉) • E. Nacaroğlu • A.C. Koç
Department of Civil Engineering, Pamukkale University, Denizli, Turkey
e-mail: stoprak@pau.edu.tr; enacaroglu@pau.edu.tr; a_c_koc@pau.edu.tr

© The Author(s) 2015

A. Ansal (ed.), *Perspectives on European Earthquake Engineering and Seismology*, Geotechnical, Geological and Earthquake Engineering 39, DOI 10.1007/978-3-319-16964-4_10

245

transient ground deformation (TGD) or to permanent ground deformation (PGD) or both. TGD occurs as a result of seismic waves and often stated as wave propagation or ground shaking effect. PGD occurs as a result of surface faulting, liquefaction, landslides, and differential settlement from consolidation of cohesionless soil. The effect of earthquake loading on pipelines can be expressed in terms of axial and flexural deformations. At locations where the pipeline is relatively weak because of corrosion, etc., breaks and/or cracks may be observed on the pipelines. If deformations are high, the damages can be in the form of separations of joints, wrinkling, buckling and tearing of pipelines.

There exist many studies which evaluated the effect of earthquakes on buried pipeline systems (Chen et al. 2002; Tromans et al. 2004; Hwang et al. 2004; Scawthorn et al. 2006; Yifan et al. 2008). A comprehensive study for a very large pipeline system can be found in O'Rourke and Toprak (1997) and Toprak (1998) which assess the Los Angeles water supply damage caused by the 1994 Northridge earthquake. A more recent example can be found in Toprak et al. (2014) and O'Rourke et al. (2012, 2014) regarding pipeline performance during Canterbury earthquake sequence in New Zealand. Following the 7.1 Mw Sept. 4, 2010 Darfield earthquake, thousands of aftershocks with Mw as high as 6.2 have been recorded in the area of Christchurch, NZ. These earthquakes, termed the Canterbury earthquake sequence are unprecedented in terms of repeated earthquake shocks with substantial levels of ground motion affecting a major city with modern infrastructure. Furthermore, the earthquakes were accompanied by multiple episodes of widespread and severe liquefaction with large PGD levels imposed on underground lifelines during each event. The data collected for the earthquake sequence are likewise unprecedented in size and detail, involving ground motion recordings from scores of seismograph stations, high resolution light detection and ranging (LiDAR) measurements of vertical and lateral movements after each event, and detailed repair records for thousands of km of underground pipelines with coordinates for the location of each repair.

One of the most critical lessons of the recent earthquakes is the need for seismic planning for lifelines, with appropriate supplies and backup systems for emergency repair and restoration. Seismic planning however requires physical loss estimations before the earthquakes occur. Methodologies for estimating potential pipelines damage use relationships which are often called in different names such as "fragility curves", "damage functions", "vulnerability functions" or "damage relationships". These relationships are primarily empirical and obtained from past earthquakes. Buried pipeline damage correlations are critical part of loss estimation procedures applied to lifelines for future earthquakes. An extensive review of the past pipeline damage relationships primarily for ground shaking (transient ground deformations) can be found in Toprak (1998), Toprak and Taşkın (2007), Pineda-Porras and Najafi (2010). Especially, the Northridge earthquake was an important event for a leap in the development of pipeline damage relationships. The substantial earthquake damage in the City of Los Angeles water supply system and availability of the strong motion instruments throughout the area provided a unique opportunity to develop and improve damage correlations. The extensive database

required use of geographical information systems (GIS) in the assessments. By using this database, Toprak (1998) and O'Rourke et al. (1998) relationships were developed primarily from cast iron (CI) pipeline damage although they made limited comparisons with damage for other pipe types. O'Rourke and Jeon (1999, 2000) went one step ahead and developed separate relationships for CI, ductile iron (DI), asbestos cement (AC), and steel pipelines. They also developed relationships which uses pipe diameter (D_p) and PGV together. Trifunac and Todorovska (1997) developed pipeline damage relationships using the 1994 Northridge earthquake data. Their relationships relate the average number of water pipe breaks per km^2 with the peak strain in the soil or intensity of shaking at the site. American Lifelines Alliance (2001) project combined data from 12 US, Japan, and Mexico earthquakes and developed relationships for wave propagation damage. O'Rourke and Deyoe (2004) investigated why there is significant difference between HAZUS relationship and the other relationships developed after the 1994 Northridge earthquake. They concluded that the most significant difference between the data sets is seismic wave type. When plotted on repair rate versus ground strain, it appears that the scatter of data points from Mexico and other earthquakes reduces substantially. In terms of PGV, they introduce two different relationships, one to use in the case of R waves and the other for S waves. Most recently, O'Rourke et al. (2012, 2014) concluded that the Christchurch data for RR vs. PGV follows the trends for AC and CI pipelines observed in previous earthquakes. The data and linear regressions are shown in Fig. 10.1. It is important to include the new data as they become available after earthquakes in order to develop more robust regressions for future fragility analyses of lifeline earthquake performance.

Continuous service of lifeline systems such as drinking water and natural gas pipeline systems or getting their functionality quickly back right after an earthquake is very important and crucial for urban societies. It was observed in the past earthquakes that pipeline damage density was much higher at locations where permanent ground deformations (PGD) were observed. Hence, this paper deals with especially PGD effect evaluations. PGD occurs as a result of surface faulting, liquefaction, landslides and differential settlement from consolidation of cohesionless soils. It is important for utility companies to evaluate their existing systems against PGD effects as well as to design their new systems resistant to these effects. This paper presents the recent developments in the assessment of PGD effects on pipelines.

10.2 Pipeline Properties and Preventive Maintenance

Performance of pipelines in past earthquakes showed that the pipe material and joint type are important for the response to earthquake loading. Pipe compositions of pipeline systems may differ in cities and countries. The comparisons of water distribution networks in various countries (e.g., Toprak et al. 2007) show that pipe compositions (including joint types) in the water distribution networks differ

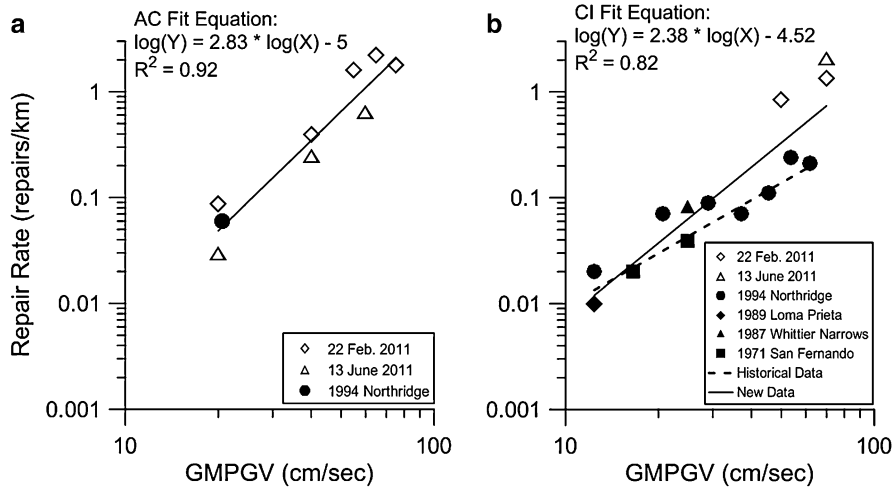


Fig. 10.1 Repair rate vs. GMPGV for (a) AC pipelines and (b) CI pipelines (O’Rourke et al. 2014)

significantly from country to country. The history and development of water supply systems in urban areas of countries affect the existing pipe compositions. For example, the main types of buried water pipes in Japan are ductile cast iron pipes (DIP), grey cast iron pipes (CIP), steel pipes (SP), polyethylene pipes (PE), polyvinyl chloride pipes (PVC), and asbestos cement pipes (ACP). Ductile cast iron pipes account for 60 % of the total length of buried water pipes (Miyajima 2012). Especially, asbestos cement pipes are well known for their high damage rates during earthquakes.

Figure 10.2 shows some typical joint types in Japan water distribution systems. These joints were primarily used in pipelines greater than 300 mm in diameter (Eidinger 1998). Table 10.1 provides properties of the seismic joints. Types “S” and “S-II” joints are special earthquake resistant joints whereas type K is a mechanical joint. Type “S” joints have 2–4 cm of flexibility (500–2,600 mm diameter) and type “S-II” joints have 5–7 cm of flexibility (100–450 mm diameter). Type “S” were used until 1980 and type “S-II” were used since 1980. During the 1995 Kobe earthquake, the performance of type “S” joints was average whereas performance of type “S-II” joints was very well. Type K joints didn’t performed well. A more recent earthquake resistant joint ductile iron pipe (ERDIP) performed very well in recent earthquakes and selected by Los Angeles Department of Water and Power (LADPW) for pilot applications in USA (Davis 2012). Purpose of the pilot project is to allow the LADWP to become acquainted with the ERDIP, to obtain direct observations and experience of the design and installation procedures, to compare the design and installation of ERDIP with pipes normally installed by LADWP, and to make own assessment on suitability for using the ERDIP to improve network reliability (Miyajima 2012; Davis 2012).

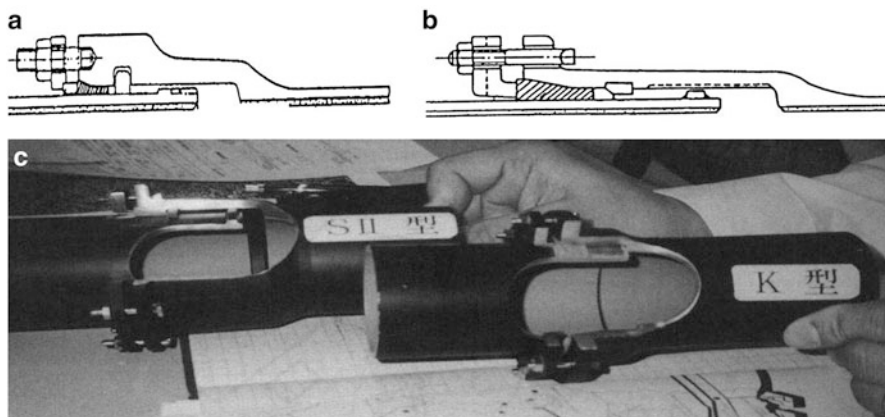


Fig. 10.2 Typical joint types in Japan water distribution systems. (a) S Type Joint. (b) SII Type Joint. (c) SII and K Type Joints (From Eidinger 1998)

Table 10.1 Characteristics of joint types (Miyajima 2012)

Joint	Characteristics
Type A	A rectangular rubber gasket is placed around the socket and the joint bolts are tightened with a gland
Type T	A rubber gasket is placed around the socket and the spigot is inserted into the socket
Type K	A modified version of Type A. This has only a rubber gasket which a rectangular one and a round one are combined
Type S, Type S-II	A rubber gasket and a lock ring are placed around the socket and the spigot is inserted into the socket. The joint has good earthquake resistance with high elasticity and flexibility and a disengagement prevention mechanism
Type NS	Same earthquake resistance as Type S but is easier to use than Type S

It is important to put in the most proper pipeline from the start as replacing or retrofitting the pipelines later requires substantial investment. Sufficient considerations should be given regarding the pipe materials and joints from the life expectancy and hazards points of view. Buried pipes of distribution systems are worn in the length of time because of the temperature, soil moisture, corrosion and other aging effects (Toprak et al. 2012). For example, aging of pipes in a water distribution system may have three main results. First, aging of pipe material causes a decrease in the strength of pipe. Then pipe breaks are increased at the high pressure areas of the system. Second, aging of a pipe increases the friction coefficient of the pipe so the energy loss in that pipe rises. Then more pumping cost occurs and sometimes a gravity working system needs pumping. Finally, aging of pipes affect the water quality in the system and may cause discolored water. Aging of a pipe is unavoidable but this process may be delayed by some precautions. Cathodic protection for steel pipes, lining and coating for steel and ductile iron pipes are some anti-aging techniques. In the design phase of a water distribution

system, analyzing the temperature changes in the area, pressure values of the system, chemical components of the soil and ground water helps for the selection of long life pipe material and suitable burial depth of pipes.

Most public water utilities use the concept of “maintenance only when a breakdown occurs”. However, in recent years “preventive maintenance” and “pro-active management” concept is getting more attraction. The logic behind preventive maintenance (PM) is that it costs far less to regularly schedule downtime and maintenance than it does to operate the network until breakdown at which repair or replacement is imperative. The primary goal of PM is thus to prevent the failure of components of the network before they actually occur by using advanced methods of statistical and risk analysis. The consequences of “maintenance on the run” are unreliable service, customer dissatisfaction, and significant water losses of valuable resources due to leakage or pipe rupture. To take full advantage of this, the utilities must have an accurate topological image of the network, the age and type of materials used in its various branches and past maintenance records.

An interesting project on this topic was presented by Tsakiris et al. (2011) and Toprak et al. (2012). The project is a European project under the Leonardo da Vinci program and entitled “Preventive Maintenance for Water Utility Networks (PM4WAT)”. The project consortium was composed of seven organizations from four European countries, all Mediterranean that face similar problems with water resources and distribution (Toprak and Koç 2013). Some of these countries have old and non-homogeneous networks that are subject to ageing, massive water losses, seismic activity and other natural hazards. The consortium includes universities and research institutions, an ICT organization, VET providers and urban utility networks, selected with a view to their knowledge and experience. In particular the project objectives are: to transfer state of the art on preventive maintenance methodologies and practices from domain experts from the participating countries to personnel working in urban water utilities; to develop a training simulation (TS) platform that will advise trainees to estimate the reliability of a network and to examine various “what-if” scenarios; to provide training on pro-active rehabilitation and on the effects of natural hazards; and to develop courseware for web-based and off-line training on preventive maintenance of urban utility networks, made available in the four languages of the participating countries (English, Greek, Italian and Turkish).

The training simulator of the PM4WAT project is based on a Fifth Framework project SEISLINES (Age-Variant Seismic Structural Reliability of Existing Underground Water Pipelines) which was performed between 2000 and 2002 (Becker et al. 2002; Camarinopoulos et al. 2001). The product of SEISLINES was re-designed and adapted for the purposes of PM4WAT project. The training simulator uses real geographical information on the topology of the water utility networks as well as real data on the properties of the elements in the branches of the network. There are four intermittent (surge pressure, frost, seismic and thermal) and four permanent (earth, water, traffic and working pressure) loads considered by the simulator (Camarinopoulos et al. 2001). The original software SEISLINES has been thoroughly revised with the view to simplify the sequence of steps necessary

to view the water network, select the critical points at which the reliability will be estimated and finally display of the results. The final product was with a user-friendly wizard, which would guide the user and provide functionality and with additional features such as exporting the archived reliability and rehabilitation results in Excel or text files for further investigation and analysis (Fig. 10.3).

A good example of replacement program was applied in Denizli, Turkey. In year 2003, Denizli Municipality evaluated the water balance of Denizli City, Turkey. The water balance was prepared as part of a project supported by the World Bank according to the IWA/AWWA methodology (Denizli City Water Works 2005). The results showed that there existed about 43 % non-revenue water. Physical losses amounted up to 36 %. Because of these relatively high physical losses and water quality issues and also seismicity considerations, Denizli Municipality decided to speed up the pipe replacement efforts. Pipeline repair logs and complaints from the customers pointed to especially the pipelines located in the central part of the city. A comprehensive evaluation of the system following the elements of a distribution integrity management program (DIMP) plan showed that any replacement should have started from the central part of the city. And replacements program started in 2008. Ductile iron was selected as the pipe material. The replacement program is still continuing but in the first few years pipelines primarily in the liquefaction prone areas (e.g., Toprak et al. 2009) were renewed. Contractors obtained ductile iron pipes and their fittings mainly from two sources. One of them is the Samsun Makina Sanayi Inc. from Turkey and the other is the Saint-Gobain Group from France (Fig. 10.4a, b, respectively). Samsun Makina Sanayi Inc. produces special earthquake resistant type connections in order to avoid the deformation of the socket and pipe end. The socket parts of those pipes are manufactured with “long standard-type sockets”, which has a longer design length than the standard manufactured pipes’ sockets and inside the socket standard-type gasket is used together with the rubber backed steel ring, which prevents the pipe displacing from the socket. The groove opened to the end of the pipe prevents the pipe from displacing by attaching the steel ring. According to the Samsun Makina Inc. earthquake resistant type connection conforms the values mentioned in ISO 16134: 2006 (E) (Samsun Makina 2014).

- Expansion/Contraction performance: Class S-1 \pm % 1 of L (L is the length of pipe usually 6 m)
- Slip-out resistance: Class A \geq 3D kN (D is the nominal diameter of pipe),
- Joint deflection angle: M-2 \pm 7.5° to $<$ 15°.

BLUTOP is the patented name of the Saint-Gobain PAM Group ductile iron pipes which are designed to withstand a particularly high angular deviation of 6°. The enhanced jointing depth also decreases the risk of pipe dislocation. As a result, BLUTOP® offers excellent performance in soil subject to ground movements (Saint-Gobain-PAM 2014).

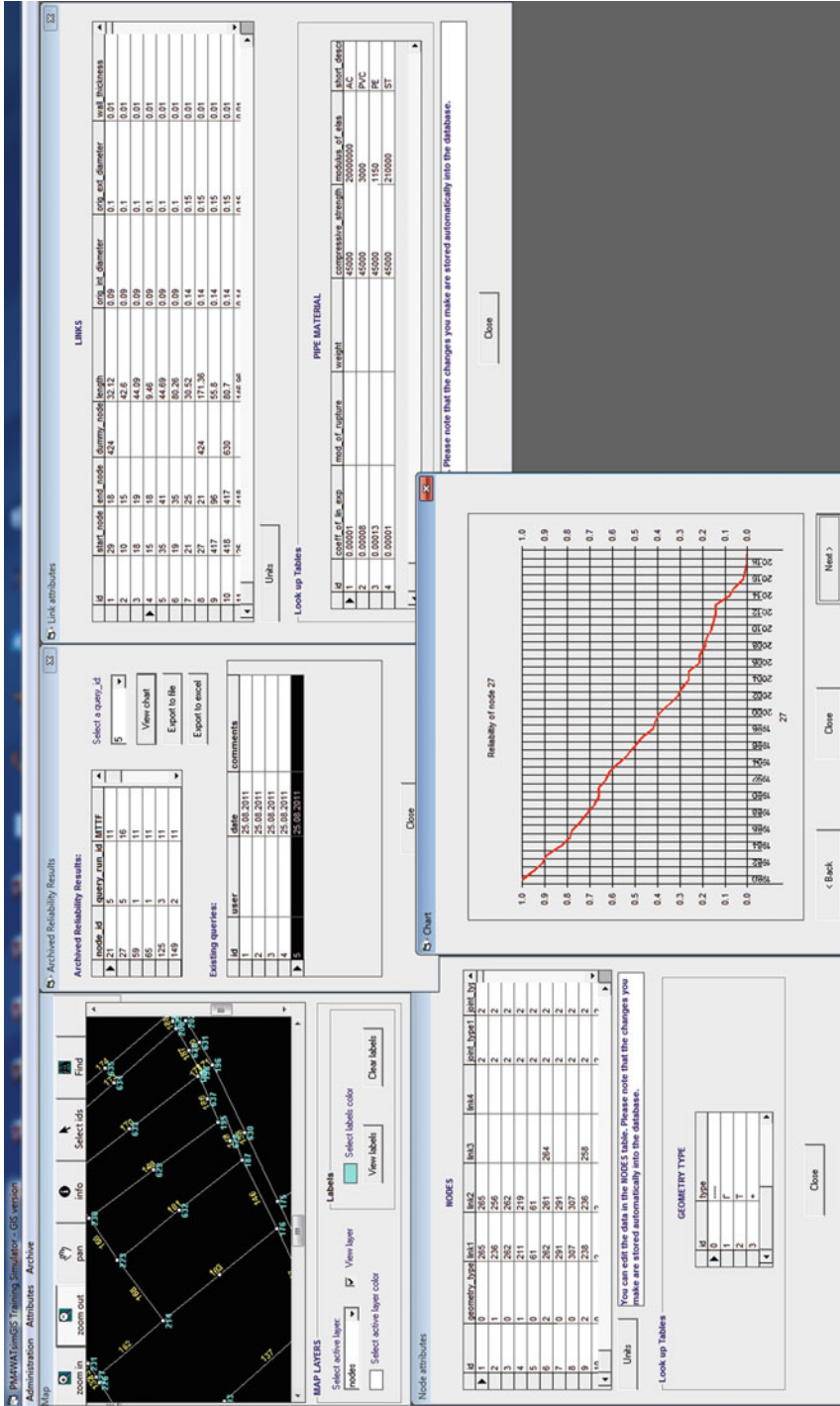


Fig. 10.3 Training simulator – GIS version reliability results (Toprak et al. 2012)

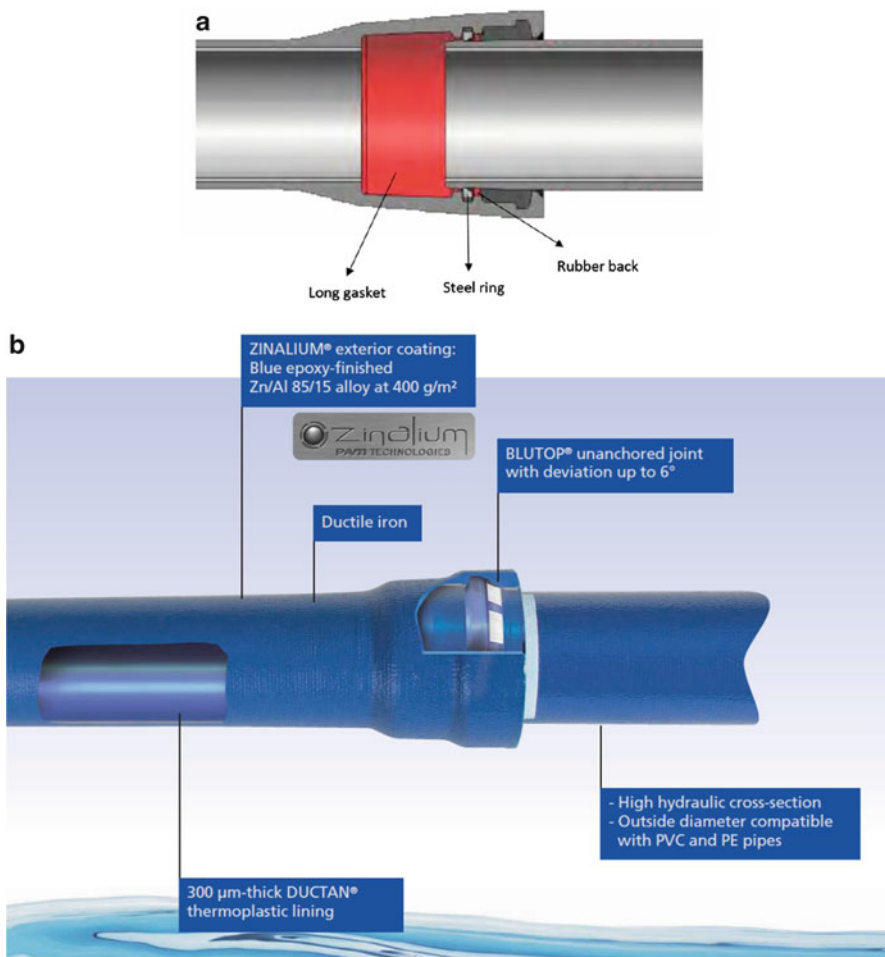


Fig. 10.4 Seismic joints used in Denizli, Turkey water pipelines replacement program. (a) Samsun Makina Sanayi Inc. earthquake resistant type connection. (b) The Saint-Gobain PAM BLUTOP® jointing

10.3 Field Observations of Pipeline Damage and Ground Deformations

Among the most notable research accomplishments in the last quarter of this century is the work of Hamada and coworkers (Hamada, et al. 1986; Hamada and O'Rourke 1992) in the use of stereo-pair air photos before and after an earthquake to perform photogrammetric analysis of large ground deformation. This process has influenced the way engineers evaluate soil displacements by providing a global view of deformation that allows patterns of distortion to be quantified and related to

geologic and topographic characteristics. There are several examples where air photo measurements were used in pipeline damage assessment (e.g., Sano et al. 1999).

In recent years, light detection and ranging (LiDAR) data were being used to detect ground displacement hazards to pipeline systems. Stewart et al. (2009) investigated the use of multiepoch airborne and terrestrial LiDAR to detect and measure ground displacements of sufficient magnitude to damage buried pipelines and other water system facilities that might result, for example, from earthquake or rainfall-induced landslides. They concluded that observed LiDAR bias and standard deviations enable reliable detection of damaging ground displacements for some pipeline types.

Toprak et al. (2014) evaluated pipeline damages by using ground displacements from air photo and LiDAR measurements and made comparisons. High resolution LiDAR data were available through the Canterbury Earthquake Recovery Authority (CERA). Also horizontal and vertical displacements were available from stereopair air photos taken before and after the earthquakes to perform photogrammetric analysis of large ground deformations around Avonside area in Christchurch, NZ. Avonside area was in liquefaction zone.

Geospatial data in the form of GIS maps of the Christchurch water and wastewater distribution systems, locations of pipeline repair, and areas of observed liquefaction effects were integrated into a master GIS file. For the water supply systems, Toprak et al. (2014) study focuses on damage to water mains, which are pipelines with diameters typically between 75 and 600 mm, conveying the largest flows in the system. It does not include repairs to smaller diameter submains and customer service laterals. The database was presented in detail and discussed in O'Rourke et al. (2012).

Figure 10.5 shows the water pipelines and repair locations in Avonside area. Also shown in the figure are air photo and LiDAR horizontal displacements. Measurements of lateral movement derived from the LiDAR surveys are provided as displacement in the east-west (EW) and north-south (NS) directions at 56-m intervals (CERA 2012). Horizontal displacements from air photo measurements are provided at 680 locations. There exist some benchmark displacement measurements in Christchurch area after the Canterbury earthquake sequence. Canterbury Geotechnical Database (CGD) provides about 403 benchmarks and their movement relative to earliest survey values after three big earthquakes. These data consist of information from Land Information New Zealand (LINZ 2014), Christchurch City Council, the Earthquake Commission (EQC) and CERA. There are 25 benchmarks from 403 benchmarks in Avonside area which are used in comparisons with LiDAR and air photos displacements.

For the purpose of horizontal strain calculations, the horizontal displacement data points are considered as corners of square elements. The grid with square elements may be regarded as a finite element mesh with bilinear quadrilateral elements. Knowing the coordinates of each corner and the corresponding displacement, the strains in the EW and NS directions (ϵ_x and ϵ_y , respectively) and shear strains (γ_{xy}) can be calculated by computing the spatial derivatives of displacements

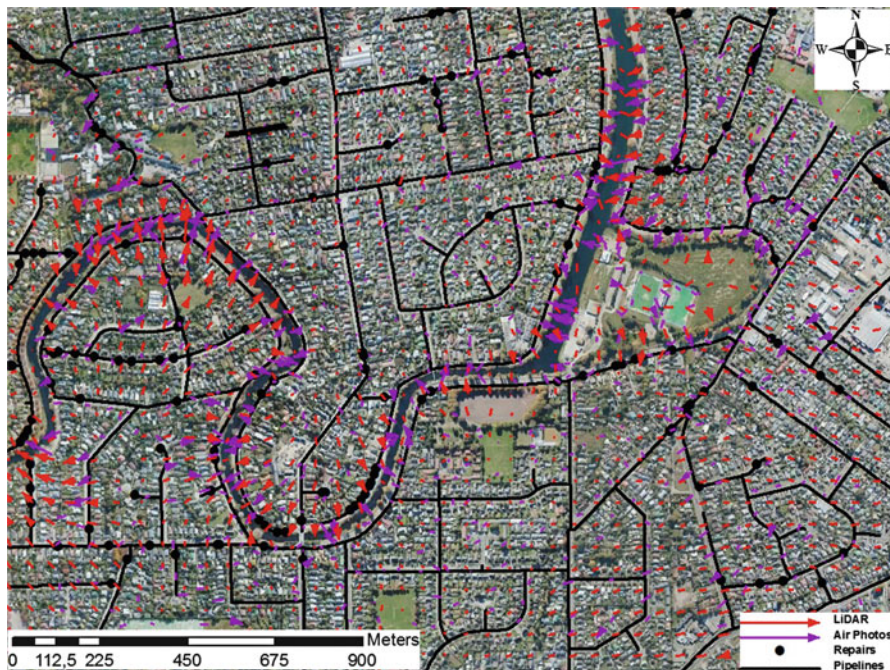


Fig. 10.5 Ground displacement from LiDAR and air photos superimposed on pipelines and pipe repairs in Avonside (Toprak et al. 2014)

using linear interpolation. Accordingly, finite element formulations were used to determine horizontal ground strains in the center of the elements, following the method described by Cook (1995). Pipeline repair rates (RRs), repairs/km, corresponding to different strain levels were calculated from air photo and LiDAR lateral movement measurements. Because RR represents damage normalized by available pipe length, the RRs are a good indicator of relative vulnerability (Toprak et al. 2009, 2011). The r squared values for the correlation between pipeline damage and lateral ground strains from LiDAR are higher than the correlation from air photo, indicating stronger correlation. The difference between the regressions is not so significant for lower strains and almost identical for higher strain values.

One of the most recent development in the pipeline damage correlations is to include the combined effects of horizontal ground strain and angular distortion. O'Rourke et al. (2012, 2014) developed the correlations for the 22 Feb. 2011 earthquake. This concept is used frequently in the evaluation of building damage caused by ground deformation from deep excavations and tunnelling. A figure correlating the severity of building damage with respect to horizontal strain and angular distortion was developed by Boscardin and Cording (1989) from field measurements and observations at actual buildings combined with the results of analytical models of building response to ground movements. This approach is used

extensively to predict and plan for the effects of ground deformation on surface structures.

Angular distortion, β , is defined as the differential vertical movement between two adjacent LiDAR points ($dv_1 - dv_2$) divided by the horizontal distance, l , separating them, such that $\beta = (dv_1 - dv_2)/l$. It is used in this work to evaluate the effects of differential vertical movement on pipeline damage. There are several advantages associated with this parameter. First, it is dimensionless, and thus can be scaled to the dimensions appropriate for future applications. Second, by subtracting the vertical movements of two adjacent points, one eliminates some systematic errors associated with the LiDAR elevation surfaces. Finally, angular distortion is a parameter used widely and successfully in geotechnical engineering to evaluate the effects of ground deformation on buildings (e.g., Boscardin and Cording 1989; Clough and O'Rourke 1990). The angular distortion for each 5-m cell associated with the LiDAR measurements was calculated in the GIS analysis with a third order finite difference method proposed by Horn (1981). Correlations of RR for different pipe types vs. β were shown in Fig. 10.6a.

Horizontal strain calculations (ϵ_{HP}) were performed according to the approach described above for Avonside area. Correlations of RR for different pipe types vs. ϵ_{HP} were shown in Fig. 10.6b. Figure 10.7 provides the framework for predicting RR for AC and CI pipelines under the combined effects of lateral strain and differential vertical ground movement. The correlation was performed by counting repairs and lengths of AC and CI pipelines associated with ϵ_{HP} and β intervals of 1×10^{-3} . This type of chart expands on the correlations generally used for buried pipeline fragility characterization to provide a more comprehensive treatment of ground deformation effects. Moreover, it provides a unified framework for predicting PGD effects on both buildings and underground lifelines.

10.4 Pipelines and Fault Crossings

Many water, natural gas, and oil pipelines must cross active faults. Faults can be strike, reverse, and normal slip. When reverse and normal faulting involve significant components of strike slip, the resulting movement is referred to as oblique slip. Reverse and normal faults tend to promote compression and tension, respectively in underground pipelines. Strike-slip may induce compression or tension, depending on the angle of intersection between the fault and pipeline. The angle of pipeline-fault intersection is a critical factor affecting the pipeline's performance. Two applications of a pipeline crossing fault zone are presented below: one is above ground and the other underground.

Figure 10.8 shows Trans-Alaska Oil Pipeline, built in the 1970s crossing Denali Fault. The pipeline survived the 2002 Denali Fault earthquake without any break, only with some minor support damages. During the design phase it was estimated that the pipeline could be subjected to a magnitude 8.0 earthquake in which the ground might slip 20 ft (6.1 m) horizontally and 5 ft (1.5 m) vertically. To

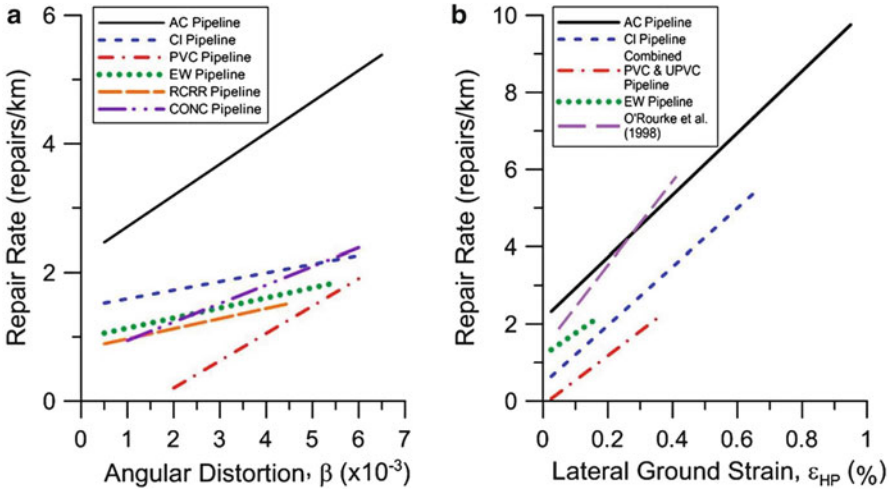


Fig. 10.6 Comparison of repair rate vs. angular distortion and lateral strain for different pipe types (O'Rourke et al. 2014)

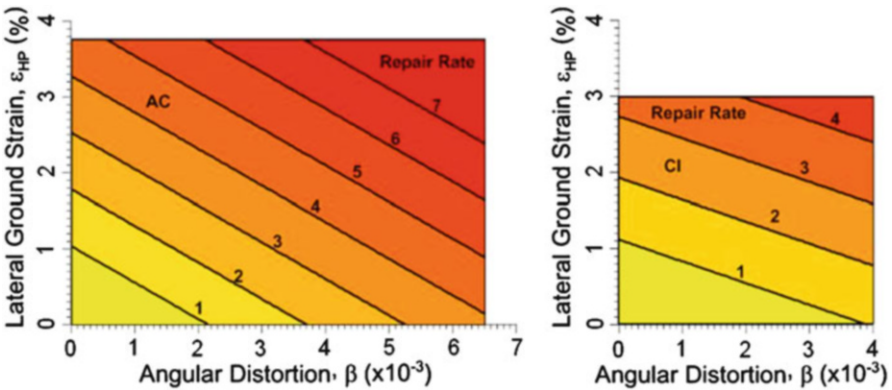


Fig. 10.7 Repair rate vs lateral strain, and angular distortion for AC and CI pipelines (O'Rourke et al. 2014)

accommodate the projected fault movement and intense earthquake shaking from a magnitude 8.0 quake, the zigzagging Trans-Alaska Oil Pipeline, where it crosses the Denali Fault, is supported on Teflon shoes that are free to slide on long horizontal steel beams. The design values proved to be remarkably accurate for the 2002 magnitude 7.9 earthquake and the fault shifted about 14 ft (4.3 m) horizontally and 2.5 ft (0.75 m) vertically. Such a prediction and the response is considered as success story for this vital pipeline which transports about 17 % of the domestic oil supply for the United States (USGS 2003).



Fig. 10.8 Trans-Alaska Oil Pipeline and Denali Fault crossing (USGS 2003)

One of the recent pipeline construction projects which had to take into account seismic considerations is the Sakhalin 2 Pipeline Project. It is one of the largest integrated oil and gas developments in the world. Twin oil (20 and 24 in.) and gas (20 and 48 in.) pipeline systems stretching 800 km were constructed to connect offshore hydrocarbon deposits from the Sakhalin II concession in the North to an LNG plant and oil export terminal in the South of Sakhalin island. The onshore pipeline route follows a regional fault zone and crosses individual active faults at 19 locations (Mattiozzi and Strom 2008; Vitali and Mattiozzi 2014; Vitali 2014). A two-tier approach was adopted in the design: (1) The pipeline shall withstand the “Safe Level Earthquake” (SLE) without or with minimal interruption of normal operation for any extensive repairs. The return period for the SLE event shall be 200 years. (2) The pipeline shall survive the “Design Level Earthquake” (DLE) without rupturing. Extensive damage but no leakage could occur to the pipeline, which would interrupt operation and require repair at one or more locations. The return period for the DLE event shall be 1,000 years. Table 10.2 shows the design requirements for the buried pipelines.

For the fault crossings in the Sakhalin Project, special trenches were considered in order to ensure safety of the pipelines subject to the design earthquake. The trench geometry and the backfilling nature have been adapted to results from the stress analysis. Different trench types and backfill materials were utilized along the

Table 10.2 Seismic design criteria for buried pipelines (API 5 L Grades X52 to X70), (Vitali 2014)

Failure mode	SLE criterion 200-year event	DLE criterion 1,000-year event
Maximum tensile strain (in bending)	$\epsilon_b/\epsilon_{M\ max} \leq 0.90$	$\epsilon_b \leq 0.04$ (4.0 %)
Collapse in compression/wrinkling	$\epsilon_{ac}/\epsilon_w \leq 0.80$	$\epsilon_{ac}/\epsilon_w \leq 1.0$
Weld fracture	$\epsilon_{at} \leq 0.02$ (2.0 %)	$\epsilon_{at} \leq 0.04$
	$\sigma_w/\sigma_y \geq 1.25$	$\sigma_w/\sigma_y \geq 1.25$
Upheaval buckling	$H_f/H_{st} \geq 1.10$	No requirement

ϵ_b bending strain, $\epsilon_{M\ max}$ strain at peak moment in moment vs. strain curve, ϵ_{ac} net compressive strain due to axial load, ϵ_w compressive strain at which wrinkling occurs, ϵ_{at} tensile strain in pipe, σ_w minimum yield strength of weld/heat affected area, σ_y specified minimum yield strength of pipe, H_f actual burial depth, H_{st} burial depth needed for stability

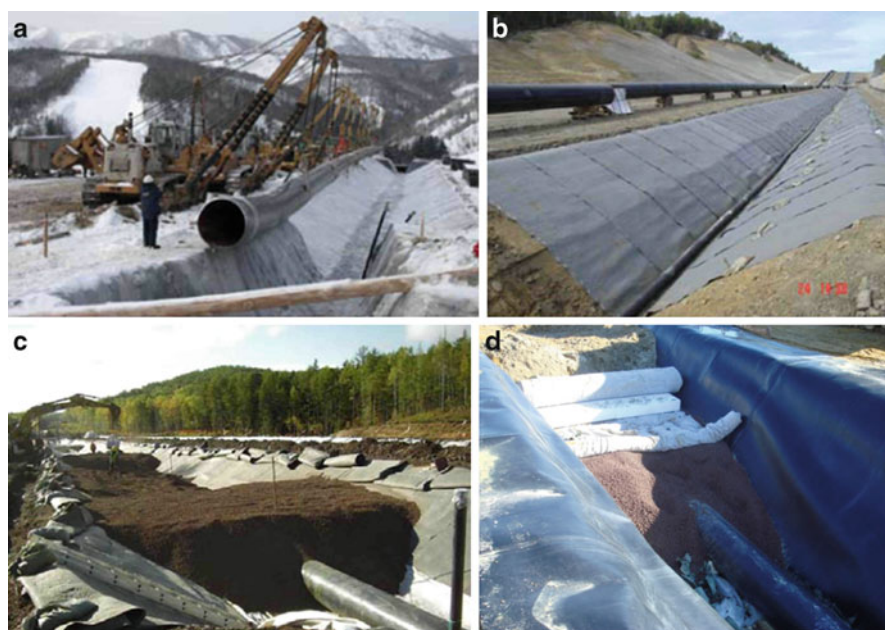


Fig. 10.9 Some pictures during construction of the special trenches. (a) Pipeline lowering in of the special trench. (b) Detail of sub-trench HDPE drainage pipe. (c) Backfilling of wide trenches with LECA (LBM). (d) Backfilling of narrow trenches with LECA (LBM) (Mattiozzi and Strom 2008; Vitali 2014)

pipeline route: “Draining Trenches” at 2 fault crossings, “Waterproof Trench” at 13 fault crossings, and “Waterproof Trench in Embankment” at 4 fault crossings (Fig. 10.9). To avoid freezing, two important factors were controlled inside the trench: (a) Absence of water; (b) Thermal equilibrium. The first aspect is controlled

with the construction of either waterproof or free draining trenches; the second is controlled with the installation of insulating slabs over the pipelines, within the trench. In order to minimize the types and dimensions of special trenches, for each fault crossing, two trench geometries were adopted: (a) Narrow trench; (b) Enlarged trench. Also for the trench backfill material, two solutions were proposed: (a) Clean sand backfill, (b) Light backfill material (LBM).

10.5 Conclusions

In this paper, recent developments related to assessment of seismic performance of buried pipelines are presented. The experience from the performance of pipelines during last earthquakes provided invaluable information and lead to new developments in the analysis. Some earthquake resistant design and technologies proved to be working in those earthquakes. This provides a motivation to increase international exchange and cooperation on earthquake resistant technologies. Another observation is that pipeline monitoring and mitigation studies are important to reduce the pipeline damage risk from seismic and other hazards. To increase the applicability and sustainability, seismic improvements should be incorporated into the pipe replacement and asset management programs. However, it is also important to put in the most proper pipeline from the start as replacing or retrofitting the pipelines later requires substantial investment. In this respect, seismic considerations should be taken into account properly in the design phase. Sufficient considerations should be given regarding the pipe materials, joints and soil-pipe interaction from the life expectancy and hazards points of view.

Acknowledgements This study was partly supported by the European Commission with the Leonardo Da Vinci Project numbered as CZ/13/LLP-LdV-TOI/134014 and by TUBITAK with project no 114M258. This publication reflects the views only of the authors, and the Commission and TUBITAK cannot be held responsible for any use which may be made of the information contained therein. Special thanks go to Luigino Vitali, Manager, Sealines Engineering Department, SAIPEM, Italy for providing information about the Sakhalin 2 Pipeline Project.

Open Access This chapter is distributed under the terms of the Creative Commons Attribution Noncommercial License, which permits any noncommercial use, distribution, and reproduction in any medium, provided the original author(s) and source are credited.

References

- ALA (2001) Seismic fragility formulations for water systems. Part 1 – Guideline. American Lifelines Alliance (ALA), ASCE-FEMA, 104 p.
- Becker G, Camarinopoulos L, Kabranis D (2002) Dynamic reliability under random shocks. *Reliab Eng Syst Safe* 77:239–251

- Boscardin MD, Cording EJ (1989) Building response to excavation-induced settlement. *J Geotech Eng ASCE* 115(1):1–21
- Camarinopoulos L, Frondistou M, Kallidromitis V, Symmakezis C, Sophocleous A (2001) Report on a methodology for the quantitative assessment of the time-dependent seismic structural reliability of deteriorating water-pipes version 2, SEISLINES (Age-Variant Seismic Structural Reliability of Existing Underground Water Pipelines). Commission of the European Communities, DG XII, Contract Reference: EVG1-CT-1999-00005
- Canterbury Earthquake Recovery Authority (CERA) (2012) Geotechnical database for Canterbury earthquake sequence. <https://canterburygeotechnicaldatabase.projectorbit.com>
- Chen WW, Shih BJ, Chen YC, Hung JH, Hwang HH (2002) Seismic response of natural gas and water pipelines in the Ji-Ji earthquake. *Soil Dyn Earthq Eng* 22:1209–1214
- Clough GW, O'Rourke TD (1990) Construction induced movements of in-situ walls. Proceedings, specialty conference on design and performance of earth retaining structures, ASCE, pp 439–470
- Cook RD (1995) Finite element modeling for stress analysis. Wiley, New York
- Davis C (2012) Concepts for distribution pipe network seismic improvements in L.A. and proposed pilot project for Japanese designed earthquake resistant ductile iron pipe. Earthquake and multi-hazard planning and preparedness symposium and workshop, 22 Mar 2012, Los Angeles
- Denizli City Water Works (2005) Denizli Municipality. Denizli. <http://www.denizli.bel.tr/>
- Eidinger J (1998) Water distribution system – The Loma Prieta, California, Earthquake of October 17, 1989 – Lifelines, USGS, Professional Paper 1552-A, Schiff AJ (ed) U.S. Government Printing Office, Washington, A63–A78
- Hamada M, O'Rourke TD (eds) (1992) Case studies of liquefaction and lifeline performance during past earthquakes. Technical Report NCEER-92-0001, National Center for Earthquake Engineering Research, State University of New York at Buffalo
- Hamada M, Yasuda S, Isoyama R, Emoto K (1986) Study on liquefaction induced permanent ground displacement. Association for the Development of Earthquake Prediction, Tokyo
- Horn BKP (1981) Hill shading and the reflectance map. *Proc IEEE* 69(1):14–47
- Hwang H, Chiu YH, Chen W, Shih BJ (2004) Analysis of damage to steel gas pipelines by ground shaking effects during the Chi-Chi, Taiwan Earthquake. *Earthq Spectra* 20(4):1095–1110
- International Standard (ISO) 16134: 2006 Earthquake- and subsidence-resistant design of ductile iron pipelines. Edition: 1, ICS: 23.040.10, TC/SC: ISO/TC 5/SC 2, Published in Switzerland, 32 p.
- Land Information New Zealand (LINZ, 2014) http://apps.linz.govt.nz/gdb/index.aspx?nextform=image&image_id=108377&mode=&sessionid=115555239158881397733794&code=BDVB
- Mattiozzi P, Strom A (2008) Crossing active faults on the Sakhalin II Onshore pipeline route: pipeline design and risk analysis. AIP Conf Proc 1020:1004
- Miyajima M (2012) The 9th international symposium on water supply technology, 20–22 November 2012, Yokohama
- O'Rourke M, Deyoe E (2004) Seismic damage to segmented buried pipe. *Earthq Spectra* 20:1167–1183
- O'Rourke TD, Jeon SS (1999) Factors affecting the earthquake damage of water distribution systems, optimizing post-earthquake lifeline system reliability. In: Elliott WM, McDonough P (eds) Proceedings, fifth U.S. conference on lifeline earthquake engineering. ASCE, Seattle, pp 379–388
- O'Rourke TD, Jeon SS (2000) “Seismic zonation for lifelines and utilities” Invited Keynote Paper on Lifelines. Proceedings sixth international conference on seismic zonation, Palm Springs, EERI CD ROM, 35 p
- O'Rourke TD, Toprak S (1997) GIS assessment of water supply damage from the Northridge Earthquake. In: Frost JD (ed) Geotechnical special publication. ASCE, New York, pp 117–131

- O'Rourke TD, Toprak S, Sano Y (1998) Factors affecting water supply damage caused by the Northridge earthquake. Proceedings of 6th U.S. National conference on earthquake engineering, EERI, Oakland
- O'Rourke TD, Jeon SS, Toprak S, Cubrinovski M, Jung JK (2012) Underground lifeline system performance during the Canterbury Earthquake Sequence. 15th world conference in earthquake engineering, Lisbon, Portugal
- O'Rourke TD, Jeon SS, Toprak S, Cubrinovski M, Hughes M, Ballegooy S, Bouziou D (2014) Earthquake response of underground pipeline networks in Christchurch, NZ. Earthquake Engineering Research Institute, EERI
- Pineda-Porras O, Najafi M (2010) Seismic damage estimation for buried pipelines: challenges after three decades of progress. *J Pipeline Syst Eng Pract* 1(1):19–24
- Saint-Gobain-PAM (2014) <http://www.saint-gobain-pam.co.uk/water-sewer/pipes-and-fittings/water/blutop.htm>
- Samsun Makina (2014) http://www.samsunmakina.com.tr/_tu/_docs/ddb.html
- Sano Y, O'Rourke TD, Hamada M (1999) GIS evaluation of Northridge earthquake ground deformation and water supply damage. Proceedings of fifth U.S. Conference on lifeline earthquake engineering, TCLEE Monograph No. 16, ASCE, pp 832–839
- Scawthorn C, Ono T, Iemura H, Ridha M, Purwanto B (2006) Performance of lifelines in Banda Aceh, Indonesia, during the December 2004 Great Sumatra Earthquake and Tsunami. *Earthq Spectra* 22(S3):S511–S544
- Stewart JP, Hu J, Kayen RE, Lembo AJ Jr, Collins BD, Davis CA, O'Rourke TD (2009) Use of airborne and terrestrial LIDAR to detect ground displacement hazards to water systems. *J Surv Eng* 135(3):113–124
- Toprak S (1998) Earthquake effects on buried lifeline systems, Ph.D. Thesis, Cornell University, Ithaca
- Toprak S, Koç AC (2013) Contribution of Leonardo Projects to Education in Technical Fields, Pamukkale University. *Journal Of Education*, No.33, (January 2013/I), s. 73–91
- Toprak S, Taşkın F (2007) Estimation of earthquake damage to buried pipelines caused by ground shaking. *Nat Hazards (Springer, The Netherlands)* 40:1–24
- Toprak S, Koç AC, Taskin F (2007) Evaluation of water distribution pipeline performance against earthquakes. Paper No: 1748, 4th international conference on earthquake geotechnical engineering, Paper No: 1748, Thessaloniki, 25–28 June 2007
- Toprak S, Taskin F, Koç AC (2009) Prediction of earthquake damage to urban water distribution systems: a case study for Denizli, Turkey. *Bull Eng Geol Environ* 68:499–510
- Toprak S, Nacaroglu E, Koç AC (2011) Seismic damage probabilities for segmented buried pipelines. In: Faber MH, Köhler J, Nishijima K (eds) Applications of statistics and probability in civil engineering. ETH Zurich, Zurich, pp 2199–2203
- Toprak S, Koç AC, Güngör M, Kaya M, Stathaki A (2012) Application of a training project in Turkey on preventive maintenance of water utility networks against earthquakes. Paper No. 5673, 15th world conference on earthquake engineering (15WCEE), Lisbon, 24–28 Sept 2012
- Toprak S, Nacaroglu E, O'Rourke TD, Koç AC, Hamada M, Cubrinovski M, Jeon SS (2014) Pipeline damage assessment using horizontal displacements from air photo and LiDAR measurements Avonside Area, Christchurch, NZ. The second European conference on earthquake engineering and seismology (2ECEES), 24–29 Aug 2014
- Trifunac MD, Todorovska MI (1997) Northridge, California, earthquake of 17 January 1994: density of pipe breaks and surface strains. *Soil Dyn Earthq Eng* 16(3):193–207
- Tromans I, Marlow D, Bommer J (2004) Spatial distribution of pipeline damage in Düzce caused By the 1999 Kocaeli and Düzce Earthquakes. Paper No. 2916, 13th world conference on earthquake engineering, Vancouver, 1–6 Aug
- Tsakiris G, Vangelis H, Tigkas D, Stathaki A, Sofotasios D, Toprak S, Koç AC, Gungor M, Kaya M, DeAngelis E, Iacovou G (2011) Preventive maintenance for water utilities. VI international symposium EWRA 2011, water engineering and management in a changing environment, Catania, June 29–July 2 2011

- USGS (U.S. Geological Survey) (2003) Rupture in South-Central Alaska – the Denali Fault Earthquake of 2002. USGS Fact Sheet 014–03, Menlo Park. <http://geopubs.wr.usgs.gov/factsheet/fs014-03/>
- Vitali L (2014) Pipeline design in harsh environments-geohazards; strainbased design at local features across arctic regions. Geohazards and pipelines, Safety of buried steel pipelines underground-induced actions Delft Technology University, Delft
- Vitali L, Mattiozzi P (2014) Crossing active faults on the Sakhalin II Onshore pipeline route: analysis methodology and basic design. AIP Conf Proc 1020:1014
- Yifan Y, Baitao S, Shanyou L, Mingyu Z, Dezhang S, Guixin Z, Hongfu C, Peilei Y, Xianghua C, Peng Z, Zairong W, Zhihong W (2008) General introduction of engineering damage of Wenchuan Ms8.0 earthquake. J Earthquake Eng Eng Vibration 28(Suppl):1–16

Chapter 11

Seismic Performance of Historical Masonry Structures Through Pushover and Nonlinear Dynamic Analyses

Sergio Lagomarsino and Serena Cattari

Abstract Earthquakes are the main cause of damage for ancient masonry buildings. In order to reduce their vulnerability with compatible and light interventions, it is necessary to have accurate models for the seismic analysis, able to simulate the nonlinear behaviour of masonry, and well defined Performance-Based Assessment (PBA) procedure, aimed to guarantee acceptable levels of risk for the use of the building, the safety of occupants and the conservation of the monument itself. Displacement-based approach is the more appropriate for this type of structures, which cracks even for low intensity earthquakes and can survive to severe ones only if they have a sufficient displacement capacity. Among the wide variety of historical masonry structures, buildings characterized by a box-type behavior are here considered, which can be modeled through the equivalent frame model, considering the assembling of nonlinear piers and spandrels. Thus, the main object of the paper is to establish a strict equivalence between the use of static pushover and incremental dynamic analyses for the PBA. Pros and cons of the two methods are discussed, as well as some critical issues related to their application. A multiscale approach is proposed for the definition of the performance levels, which considers the seismic response at different scales: local damage in single elements, performance of single walls and horizontal diaphragms and global behavior. An original contribution is the use of Proper Orthogonal Decomposition (POD) technique for the correct interpretation of numerical and experimental dynamic results.

S. Lagomarsino (✉) • S. Cattari
Department of Civil, Chemical and Environmental Engineering, University of Genoa, Via
Montallegro 1, Genoa 16145, Italy
e-mail: sergio.lagomarsino@unige.it; serena.cattari@unige.it

11.1 Introduction

Seismic safety evaluations of existing masonry buildings aim to assess whether retrofitting interventions are needed. In the case of historical buildings, conservation principles require that interventions are minimized to protect as much as possible heritage values (beside the ensuring of people safety and durability of original materials). In order to demonstrate that a structural intervention is necessary (in the sense that the building is not safe enough) and effective (in the sense that the intervention is able to achieve a satisfactory safety level), the structural engineer should be able to: (i) minimize the modelling uncertainties of the current structural behaviour and after structural modifications; (ii) adopt accurate and reliable models to predict the seismic response; (iii) adopt reliable criteria for the safety assessment.

Therefore, quantitative and reliable procedures for the evaluation of the seismic safety index of the structure are required. In the last decade, an increasing number of codes for the assessment of existing buildings were published (e.g. EC8-Part 3 2005; ASCE 41–13 2014; CNR DT 212 2013; SIA 269/8 2013). In the case of historical buildings, due to their complex configuration, many recommendations (ICOMOS 2005; ISO 13822 2010; CIB 335 2010) stress the importance of the qualitative approach. However, while a qualitative assessment is usually sufficient for the diagnosis in many critical situations, such as material deterioration or soil settlements, the evaluation of seismic vulnerability without the support of calculations is overambitious; in this case, the qualitative approach and the historical analysis can only suggest which is the expected seismic behaviour, but they are not sufficient to prove the building safety. This is the reason why the Italian Guidelines for the seismic assessment of cultural heritage (P.C.M. 9/2/2011) clearly state that quantitative calculation of the structural safety are necessary and recent research trends (e.g. the PERPETUATE project – Lagomarsino and Cattari 2015; Lagomarsino et al. 2010) are focused on the proposal of proper quantitative procedures also in the case of monumental buildings.

Within this context, the Performance-Based Assessment (PBA) requires the use of nonlinear analyses for the verification through the Displacement-Based Approach (DBA). In fact, due to the high vulnerability of different types of historical structures, which was proved again by the recent earthquakes (Oliveira 2003; Lagomarsino 2012; Cattari et al. 2013; Sorrentino et al. 2013), nonlinear models turn out to be essential for an accurate and reliable assessment, due to the strongly nonlinearity of masonry, despite the complexity of these buildings, both from a geometric and structural point of view.

The mechanical models widely used at present for the analysis of ancient masonry structures consider a verification approach in terms of forces: the consequence is that in the past strengthening techniques were aimed at increasing stiffness and strength. However, earthquake induces deformations and dynamic amplification; therefore, it is better to keep the original flexibility of the structure

and improve the displacement capacity, in terms of ductility or rocking, in order to survive even to rare destructive earthquakes.

This agrees also with the PBA concepts, which consider different Performance Levels (PLs) that must be fulfilled in the occurrence of corresponding earthquake hazard levels (defined by the return period). The need to check the achievement of PLs that are close to structural collapse strongly strengthens the use of static nonlinear models and displacement-based procedures for the assessment, as it is not possible to rely on linear analyses with the behavior factor approach, being existing buildings not capacity designed.

Nonlinear static (pushover) analysis is usually considered as the main tool for the application of the DBA; the vulnerability of the building is described by its capacity curve. Recently, nonlinear dynamic analysis is emerging as a proper alternative tool, which allows to evaluate the capacity, for example, through an Incremental Dynamic Analysis (IDA, Vamvatsikos and Cornell 2002); IDA curves are obtained through the application of a proper number of selected records, by scaling the Intensity Measure (IM) till to reaching the given performance. The two approaches have pros and cons, but an equivalence between them and a clear definition on how to use both in an integrated way is still missing.

The paper focuses on this problem, paying particular attention to the specific issues posed in the case of existing and historical masonry buildings characterized by a box behavior, for which a 3D equivalent frame model of the whole building is appropriate (e.g. Lagomarsino et al. 2013). This modeling approach considers the in-plane behavior of masonry walls, which are discretized by piers and spandrels, connected by rigid nodes, in order to create a plane frame. Piers are vertical panels and are the most important elements since they resist both gravity loads and seismic action; spandrels are the horizontal elements between two vertically-aligned openings and connect two piers, limiting their end rotations. Each element is described by nonlinear constitutive laws, in terms of generalized forces (N , V , M) and displacements (u , v , ϕ), defined by proper failure criteria (e.g. as illustrated in Calderini et al. 2009; Beyer and Mangalathu 2013, for piers and spandrels respectively) and drift limits (e.g. as recently discussed in Petry and Beyer 2014); in addition, in case of nonlinear dynamic analyses, the definition of an accurate cyclic hysteretic behavior is required. Moreover, the possibility of modeling flexible diaphragms (timber floors, masonry vaults), aimed to properly simulate the redistribution of seismic actions among walls, constitutes an essential requisite for a reliable assessment (Lagomarsino et al. 2013).

The equivalent frame modeling approach (explicitly suggested by some codes as the EC8-Part 3) allows the nonlinear analysis (static and dynamic) of complex models with a reasonable computational effort, and its use is widespread not only at research level but also in engineering practice.

However, in the case of complex masonry historical structures, many aspects need to be investigated in terms of equivalence and compatibility of static and dynamic approaches, such as how to consider the contribution of higher modes in static pushover analysis or to define Damage Levels (DL) and related PLs. As regard the first issue, pushover analysis investigates the behavior of the structure

under a predefined mode, induced by a given load pattern, monotonically increased; thus the effects of higher modes, which induce a widespread diffusion of the damage (as it is observed from nonlinear dynamic analyses), are lost. As regard the second issue, the main problem is that the criteria currently adopted in codes, based on the attainment of drift thresholds in structural elements or directly related to the pushover curve through heuristic criteria, are not effective to detect the actual behavior of such complex buildings, irregular in plan and with flexible horizontal diaphragms.

In the following, all the aforementioned issues are deepened and some solutions are proposed. In particular, the use of the Proper Orthogonal Decomposition (POD) technique is suggested to process results of nonlinear dynamic analyses (§11.4) and the multiscale approach is proposed to define the DLs (§11.5).

11.2 Seismic Performance-Based Assessment Through Nonlinear Static and Dynamic Analyses

Seismic PBA of an existing building checks if the construction is able to fulfill some selected Performance Levels (PLs) in case of occurrence of corresponding earthquake hazard levels, defined by the annual rate of exceedance λ (or return period $T_R \approx 1/\lambda$). Once a proper Intensity Measure (IM) has selected as the one better correlated with the building capacity, the maximum IM compatible with the fulfillment of each PL that has to be checked (IM_{PLk} , $k = 1, \dots, 4$ if four PLs are considered) is adopted as relevant outcome of the assessment. In the case of historical buildings, target PLs have to be defined by considering not only the use and safety of people (as usually proposed in codes in the case of new and existing ordinary buildings) but also the conservation of the valuable architectural and artistic assets of the monument: this issue has been recently faced in PERPETU-ATE project (Lagomarsino et al. 2010) by proposing specific PLs that include also requirements related to the *Building Conservation* and *Artistic Asset Conservation* (Lagomarsino and Cattari 2015). According to this proposal, for example in the case of *Building Conservation*, the preservation from building damage is not related, as for ordinary buildings, to the costs of repair or rebuilding but to the possibility of restoration or to the collapse prevention, in order to maintain, at least, the monument as a ruin.

Within this general framework, Fig. 11.1 summarizes the basic principles and steps of the PBA procedure, if nonlinear static or dynamic analyses are adopted.

The first step requires the definition of the seismic input. It is defined by the hazard curve, obtained through a Probabilistic Seismic Hazard Analysis (PSHA), which gives the selected IM as a function of the annual probability of occurrence (or the return period). Peak Ground Acceleration (PGA) is the most frequently adopted IM, due to the large amount of information (strong motion records) and models (Ground Motion Prediction Equations – GMPEs) that are available; it is

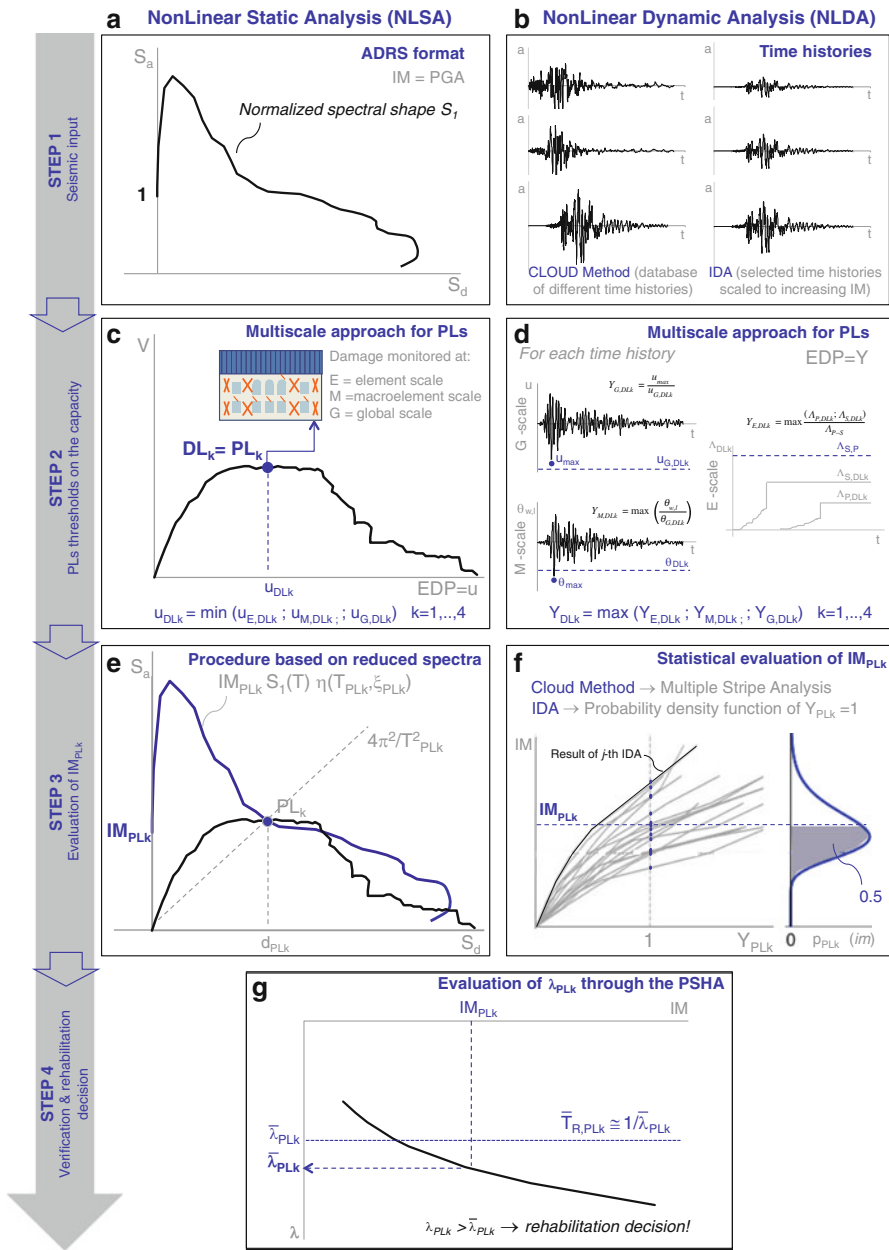


Fig. 11.1 Principles of PBA through nonlinear static and dynamic analyses

usually a good parameter in the case of masonry palaces characterized by a box behavior, due to their relatively short natural period, or of massive structures. Other possible IMs are the spectral acceleration for a significant period of vibration of the

asset, the maximum spectral displacement, Arias intensity and Housner intensity (Douglas et al. 2015). Advices on the proper selection of IM as a function of various architectural assets (towers, obelisks, single or multi-drum columns, ..) are proposed in Lagomarsino and Cattari (2015).

In the case of NonLinear Static Analysis (NLSA), the seismic input (Fig. 11.1a) is described by an Acceleration-Displacement Response Spectrum (ADRS), which must be completely defined, for the specific site of the building under investigation, as a function of the assumed IM. On the contrary, in the case of NonLinear Dynamic Analysis (NLDA) it is represented by a proper set of time histories (Fig. 11.1b). The ADRS may be defined: (1) analytically, as in seismic codes; (2) through a piecewise linear function, by spectral acceleration values $S_a(T_h)$ for a given set of periods T_h ($h = 1, \dots, N$), obtained from GMPEs that already includes the soil amplification effects; (3) as the mean of the time histories selected to be representative of the expected seismic events for the examined area. NLDA may be performed by using a large amount of records (cloud method) or a proper selection of time-histories, scaled in order to perform an IDA. These latter may be selected from real recorded accelerograms (in order to be equivalent, on average, to the target ADRS) or obtained through numerical modeling of the fault mechanism and the propagation towards the site.

Once defined the seismic input, the second step deals with the definition of proper thresholds for PLs correlated to the seismic response of the structure. To this end it is useful to make reference to the empirical definition, adopted in macroseismic post-earthquake assessment (Grunthal 1998), of observational Damage States (DS): (1) slight; (2) moderate; (3) heavy; (4) very heavy; (5) collapse. The behavior of the structure may be described by an Engineering Demand Parameter (EDP), such as the horizontal displacement at the top of the building, which can be evaluated by the static or dynamic nonlinear analyses and is useful, through properly defined thresholds, to identify Damage Levels (DL) on the pushover curve (in case of NLSA) or on the IDA curve (in case of NLDA); DL_k ($k = 1, \dots, 4$) is the point after which the building experiences DS_k . Then, DLs, which are directly related to the structural response, have to be correlated to PLs, which represent the behavior of the building in terms of functionality and consequences (like as the immediate occupancy or the life safety). A first approximation is to establish a direct correspondence between DLs and PLs. For example, Life Safety is usually associated with heavy damage threshold (DL_3), because it is assumed there are very few casualties or injured people with this damage level. From a probabilistic point of view, the attainment of the threshold that corresponds to DL_k means the probability of being in a DS greater of equal to DS_k is 50 %. By using statistical correlations between DSs and losses (in terms of casualties and injured people, homeless, costs of repair), derived from post-earthquake assessment (Coburn and Spence 2002), a refinement of such acceptance criteria is possible (Lagomarsino and Cattari 2015).

As introduced in §11.1, the definition of reliable criteria to correlate DLs with the structural response is a challenging task in the case of complex masonry assets. Herein a multiscale approach (§11.5) is proposed by considering the behavior of

single elements (E), macroelement (M) and of the global building (G). For each scale, proper variables are introduced and their evolution in nonlinear phase is monitored: local damage in piers and spandrels (E); drift in masonry walls and horizontal diaphragms (M); normalized total base shear, from global pushover curve (G). At the end, the EDP associated to the attainment of the given DLk is represented in the case of NLSA by the displacement plotted in the pushover curve (u): the corresponding threshold ($u_{DLk} = u_{PLk}$) derives from the application of such multiscale approach as the minimum value (see Eq. 11.4 in §11.5) coming from the reaching of predefined limit conditions at the aforementioned scales (Fig. 11.1c). In case of NLDA, the results of each single analysis have to be properly processed. To this aim and coherently with the multiscale approach adopted in NLSA, a scalar variable Y_{DLk} ($=Y_{PLk}$) is introduced as EDP (Fig. 11.1d): it derives from the maximum among proper ratios between the maximum value (see Eq. 11.9 in §11.5) of the variables monitored at three different scales, reached through the application of the selected record, and the corresponding threshold. It is assumed that the attainment of $Y_{DLk} = 1$ indicates the reaching of the examined DL. A more thorough description of the multiscale approach is illustrated in §11.5.

Once introduced the EDP and criteria to define the PLs, it is possible to pass to the computation of IM_{PLk} (third step). In the case of NLSA (Fig. 11.1e), IM_{PLk} is obtained by the evaluation of the IM for which the seismic demand, given by a properly reduced (overdamped or inelastic) ADRS, is equal to the displacement capacity, related to the previously defined threshold of the EDP for the specific PL. The capacity curve is obtained by converting the pushover curve (obtained from the MDOF model of the building) into the equivalent nonlinear SDOF system. Herein, the Capacity Spectrum Method (Freeman 1998) with overdamped spectra is adopted as reference with some modifications illustrated at §11.6. In the case of NLDA, numerical results may be represented by plotting the scalar variable Y_{DLk} as function of IM (Fig. 11.1f). Then the procedure is based on a statistical evaluation of IM_{PL} through the Multiple Stripe Analysis (MSA, as described for example in Jalayer e Cornell 2009), in the case of cloud method, or on the IDA curve in correspondence of the attainment of $Y_{DLk} = 1$ condition, in the case of a set of time-histories scaled to increasing values of IM.

Finally, the PBA is completed through the verification step (Fig. 11.1g) by computing, through the hazard curve obtained from the PSHA, the annual rate of exceedance λ_{PLk} of the earthquake correspondent to the given performance (or its return period $T_{R,PLk} \approx 1/\lambda_{PLk}$). Finally, this value is compared with the target earthquake hazard level ($\bar{T}_{R,PLk} \approx 1/\bar{\lambda}_{PLk}$) in order to establish if rehabilitation interventions are necessary or not.

As regards the PBA procedural aspects, first of all it is useful to point out that the application of an acceleration time history at the base of the structure and the evaluation of its nonlinear dynamic response produce a large amount of results: time histories of nodal displacements, element drifts, local and global energy dissipation. These data give a comprehensive picture of the building response and can be properly processed in order to assess if a given PL has been attained or not. However, this is not a simple task and many alternative approaches have been proposed in the past, usually referred to the definition of a global damage index that is well correlated with the DLs. A review of several proposed damage indexes is made in Williams and Sexsmith (1995), being most of them related to reinforced concrete structures, except one proposal for masonry ones (Benedetti et al. 2001) and critical disquisitions by some authors (e.g. Tomazevic 1999). Apart from the definition of damage indexes, recently in Mouyiannou et al. (2014) specific criteria to define PLs from the execution of NLDA have been proposed. However, none of these proposals have been yet implemented in the PBA procedures proposed by codes and recommendations. Indeed, at code level, the common trend is to adopt as reference result of the NLDA the maximum displacement occurred in the structure: thus, to proceed to the verification, it is usually compared with the displacement capacity obtained by the nonlinear static procedure, with the related criteria. It is evident that this use is very simplistic respect to the potentials of such an accurate method. Finally, the proper selection of time history represents a critical issue: on the one hand, the admissibility of scaling records is debated in literature; on the other hand, in the case of cloud method adoption, it is necessary to have a sufficient number of records to apply the MSA, in particular characterized by values of IM which produce a seismic demand very close to the attainment of the given PL (Jalayer and Cornell 2009).

Passing to the NLSA, despite some intrinsic limitations of the static approach, which can be inferred from the first sentence of this section, it represents a quite effective and feasible tool for the PBA of existing masonry buildings, being nowadays widespread not only at research level but also in the engineering practice.

As regard modeling, NLSA requires only the simulation of the monotonic behavior of masonry panels; this makes the formulation and definition of mechanical parameters easier than in case of NLDA. Many nonlinear models have been proposed for the simulation of the in-plane response of masonry panels; the most simple option for the implementation in the equivalent frame approach is the use of a nonlinear beam model, that presents the following main advantages: (i) it is particularly easy to be implemented also in practice-oriented software packages; (ii) it is consistent with the recommendations included in several seismic codes ASCE 41–13 2014; EC8-Part 3 2005); (iii) it is based on few mechanical parameters that may be easily defined and related to in-situ tests. Concerning this, despite the more spread adoption of a simple bilinear law, the increasing requirement to verify also PLs close to the Near Collapse condition makes pressing the adoption of more refined constitutive laws, like as those based on a multilinear backbone curve (Fig. 11.2a).

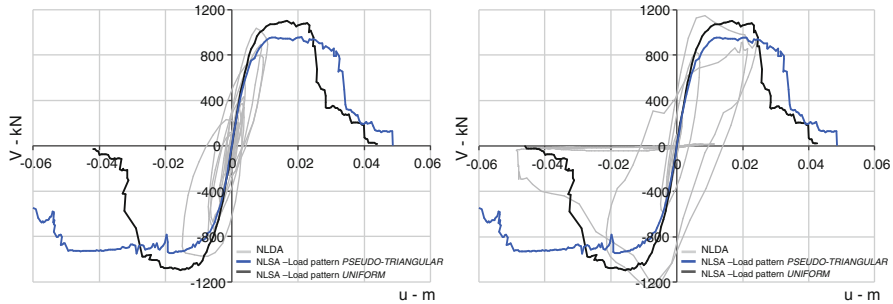


Fig. 11.3 Comparison between backbone obtained by the execution of a NLSA and the results of NLDA achieved by using a seismic input scaled for two different levels of IM

As regards the computational aspects, the execution of pushover analysis requires proper choices concerning: (i) seismic load pattern; (ii) selection of control node (to optimize the numerical convergence); (iii) representative displacement to be considered in the pushover curve. All of them affect the resulting pushover curve, in particular for irregular buildings and in presence of flexible diaphragms.

Regarding load pattern (i), that aims to simulate the seismic action through static incremental horizontal forces, possible options are (Aydinoglu and Onem 2010): (1) proportional to masses (obtained from a *uniform* displacement shape); (2) proportional to the fundamental modal shape (*modal*); (3) given by a proper combination of different modes (SRSS-based); (4) obtained from a triangular displacement shape (*pseudo-triangular*); (5) load pattern adapted to the current displacement shape (*adaptive*). Indeed, the pushover curve aims to represent the backbone achieved by the virtual application of a seismic input with increasing intensity level: to this aim, the comparison with results of NLDA could be very useful to select the most correct load pattern to be adopted (Fig. 11.3).

Usually codes propose to assume at least two patterns, because the inertial force distribution changes, with the occurrence of damage, from an initial *modal* distribution to patterns that are proportional to the deformed shape, which often at collapse is closer to the *uniform* one (in the case of a soft storey mechanism at the base). An alternative is the *adaptive* pushover, in which at each step of the analysis the load pattern is updated as a function of the evolution of the nonlinear response of the structure (Antoniou and Pinho 2004; Chopra et al. 2004; Gupta and Kunnath 2000). However, very few applications to masonry structures can be found in the literature (Galasco et al. 2006), due to their distinctive features, such as the softening response of masonry under shear and the presence of flexible floors.

The *modal* pattern is not reliable in the case of flexible horizontal diaphragms, because each mode mainly involves the local behavior of single walls, having a very low fraction of the participating mass. Thus, in order to reach a significant total mass participation, a SRSS-based load pattern can be defined, in a given direction, by considering the first N_r modes that, in each wall, are characterized by the same sign of displacements at different levels; if the resulting participating mass is still

lower than 75 %, this percentage should be anyhow considered in the conversion to the equivalent SDOF system. If the building is regular in elevation, a simpler alternative is the use of a *pseudo-triangular* load pattern, because it assures that the seismic masses in all parts of the building are involved in the pushover analysis.

An advanced approach, in order to treat the complex configurations (flexible floors, irregularity in plan and in elevation), is the *multi-modal* pushover analysis (Chopra and Goel 2002), which can also combine, if necessary, the effect of both components of the input motion (Reyes and Chopra 2011), instead of considering them as independent.

The choice of control node (ii), both in elevation and plan, is important in order to optimize the convergence of the nonlinear pushover analysis. Regarding the elevation, it is suggested to select the control node above the level in which the collapse occurs. For this reason, codes commonly propose to assume the control node at the top floor. Regarding the in-plan location, the choice represents a very crucial issue in case of existing buildings with timber floors or vaults. In fact, while in the case of rigid floors the results are almost insensitive to the position of the control node, in the case of flexible ones they strongly depend on it, because of the different stiffness and strength of masonry walls. The numerical results are more accurate if the control node is selected in the wall that collapses as the first.

The selection of the representative displacement for the pushover curve (iii) is a crucial point for the conversion into capacity curve when diaphragms are not rigid and/or the building is irregular in plan. In fact, the capacity curve shows very different displacement capacity (ductility) whether the considered displacement is that of a wall that reaches failure or not. Thus, instead of the displacement of the control node, it is preferable to use the average displacement of all nodes at the same level, weighted by the seismic nodal mass. This procedure represents a heuristic approach useful to get an unambiguous outcome, which has also a physical interpretation: indeed, the displacement-based approach considers the capacity of seismic masses to move, in comparison with the earthquake displacement demand.

Once obtained the pushover curve, the PBA requires the adoption of a proper nonlinear static procedure. Various proposals are available in the literature, like as the Capacity Spectrum Method (CSM) and Displacement-Based Method (DBM) (Freeman 1998; Calvi 1999; Priestley et al. 2007), the Coefficient Method (CM) (ASCE 41–13 2014) and the N2 Method (Fajfar 2000). All of them basically require the introduction of some conventional approaches: (i) to convert the original MDOF model into the equivalent SDOF system, to be compared with the seismic input (ADRS); (ii) to reduce the elastic spectra in order to take into account the increasing of dissipation due to the nonlinear structural behavior. As regard the conversion, it is usually based on a transformation factor computed as a function of displacement shape vector, assumed consistent with the fundamental modal shape of the system (Fajfar 2000). As regard the reduction, two approaches are proposed: overdamped spectra (adopted by CSM, DBM, CM methods), in which an equivalent linear model is considered with a properly increased viscous damping, and inelastic spectra (N2 method), which are defined in terms of ductility (only in this

case it is necessary to proceed to a further conversion in a bilinear capacity curve, in order to define the initial equivalent period and the ductility). After a wide set of dynamic parametric analyses on different nonlinear hysteretic SDOF models, some refinements of the CSM have been proposed as Modified ADRS (MADRS) method (FEMA 440 2005), in order to obtain from static nonlinear analysis a displacement demand as much as possible equal to the one obtained from nonlinear dynamic analyses; more recently, further improvements on such direction have been proposed just for masonry buildings (Graziotti et al. 2013). However, an agreement on the most reliable method still represents an open issue.

11.4 Use of Proper Orthogonal Decomposition (POD) for the PBA

One of most critical issue related to the use of NLDA is the availability of effective tools and procedures to properly exploit the large amount of results produced.

To this aim, the use of the Proper Orthogonal Decomposition (POD – Lumley 1970) is proposed for the first time, as far as the Authors know, in the field of seismic assessment; this method is also known as Principal Component Analysis (PCA), in the discrete-space context, or as Karhunen-Loeve Expansion (KLE – Loeve 1945; Karhunen 1946), when used in the context of continuous second-order stochastic processes. Main aim of the POD is to represent, through a non-parametric modal expansion, a random process as a linear combination of deterministic quantities, called modes, modulated by random uncorrelated coefficients called Principal Components (PCs). The modal representation offered by POD is the best in the mean square sense (i.e. energetic), because has the fastest possible convergence among all the possible linear combinations: this means that only some (usually a few) terms of the series are really needed to capture the relevant energetic part of the observed phenomenon. Geometrically, the aim of POD is to find a rotation of the reference system that minimizes the covariance (i.e. the redundancy) of the random variables, maximizing the variance (i.e. the information) of the new variables in the new reference system. The change in basis can be seen as a change of the point of view that improves the “visible” information included in the dataset.

In the past it has been already applied in many other fields, like as economics (Falco et al. 2006) or other engineering applications (Berkooz et al. 1993; Han and Feeny 2003; Solari et al. 2007; Marrè Brunenghi 2014). Herein, the use of the POD is proposed in order to interpret the dynamic structural response to an earthquake excitation, from the results of numerical simulations by NLDA or experimental tests on shaking table, in terms of dominant behaviours. This approach is more effective than referring to single and instantaneous peaks of the response (e.g. the maximum displacement occurred in a point of the structure, like as the top level). Moreover, it could be very useful also to preliminary correct data from

measurements errors or noise, in case of experimental test, or from slight convergence errors, in case of numerical simulations.

The method basically consists in the eigenvalue decomposition of the covariance matrix estimated from the data. Starting from the original dataset, POD aims to find a new set of coordinates in such a way that the first PC has the maximum variance and each succeeding component has the highest variance possible under the constrain that it is orthogonal to the preceding component: in this way the PCs are mutually uncorrelated.

First step to apply this technique consists in arranging the results $\mathbf{q}(t)$ of the NLDA in a data matrix \mathbf{V} , whose columns contain the signal time histories (in such a way that each line displays the variables observed at the same time). Then the matrix \mathbf{V} is decomposed through a basis of orthonormal vectors ($\boldsymbol{\phi}$) in order to obtain a new matrix whose components are uncorrelated:

$$V = \sum_{k=1}^N \phi_k (\phi_k^T V) = \sum_{k=1}^N \phi_k Y_k \quad (11.1)$$

The components Y_k of \mathbf{V} on the basis $\boldsymbol{\phi}$ represent the principal components (PCs). The optimal basis to decompose \mathbf{V} is represented by the covariance matrix \mathbf{C} :

$$\mathbf{C} = E[\mathbf{q}^T \mathbf{q}] = \begin{bmatrix} \sigma_{q_1}^2 & \cdots & C_{q_1 q_N} \\ \vdots & \ddots & \vdots \\ C_{q_1 q_N} & \cdots & \sigma_{q_N}^2 \end{bmatrix} \quad (11.2)$$

The diagonal of \mathbf{C} collects the variances of each signal time history, while the other elements are the covariances of all possible pairs of time histories.

The covariance matrix satisfies some relevant properties, that is to be symmetric and positive definite. Thus the eigenvalues are real and positive, the relative eigenvectors are real and can always be chosen so that they are mutually orthonormal.

Such eigenvalue problem is mathematically formulated as:

$$(\mathbf{C} - \lambda \mathbf{I})\boldsymbol{\phi} = 0 \quad (11.3)$$

where $\boldsymbol{\phi}$ are the eigenvectors and λ the eigenvalues, that is the variances of the \mathbf{Y} rotated components, aimed to quantify the energy associated to each mode. Thus, the principal directions of the process can be obtained by solving such problem.

By sorting the eigenvalues in decreasing order it is possible to identify the dominant modes of the phenomenon.

According to the context in which the POD is herein proposed, the result \mathbf{q} may be represented for example by the displacement or acceleration time histories of all nodes of the equivalent frame model (Fig. 11.4).

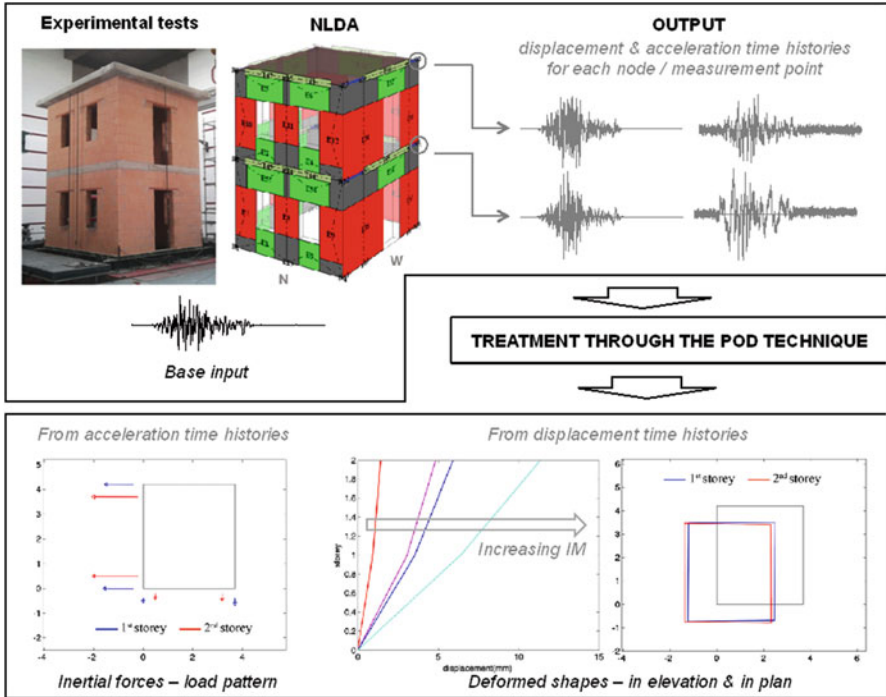


Fig. 11.4 Sketch on the use of POD technique to process data from experimental tests or NLDA results (Data adapted from Cattari et al. (2014))

The application to displacement time histories may support the definition of deformed shapes both in plan and in elevation, while if POD is applied to nodal accelerations the dominant distribution of inertial forces transmitted to the structure can be estimated. This latter application may be very useful to calibrate the load pattern distribution to be adopted in pushover analyses; in particular, if this evaluation is made on the results of IDA analyses, the relevance of considering an adaptive pushover analysis can be assessed. Moreover, in §11.5 the use of POD is also proposed to process data useful to the definition of the PLs according to the multiscale approach, in the case of NLDA.

In Cattari et al. (2014) an application of the POD technique is proposed for the interpretation of shaking-table tests made on two prototypes of two-storey masonry buildings: results include both the analysis of experimental tests measurements and the processing of results from a numerical simulation through NLDA performed by the equivalent frame program Tremuri (Lagomarsino et al. 2013). The POD technique turned out to be very useful and effective.

11.5 Multiscale Approach for the Definition of PLs Thresholds

The definition of DLs thresholds of the EDP (useful to check the fulfillment of corresponding PLs) from NLSA, as well as NLDA, is a complex task.

In the case of existing reinforced concrete buildings, nonlinear elements used for columns and beams are usually elasto-plastic, without strength degradation. Therefore, the pushover curve that is obtained do not present any strength degradation and the verification of PLs is made at the level of single elements, considering: for Damage Limitation PL the occurrence of a given threshold in the first element; while for Near Collapse PL another threshold at element scale which is checked on a combination of elements which give rise to a predefined collapse mechanism (e.g. column sway or beam sway).

In the case of complex historical masonry buildings nonlinear constitutive laws for piers and spandrels take into account strength degradation; this allows to obtain, from the pushover analysis with an equivalent frame model, a capacity curve that shows not only the stiffness degradation and the maximum strength, but also the strength degradation for high values of the displacement demand. For this reason some codes (e.g. EC8 Part 3 2005) define PLs directly on the pushover curve and require a verification directly in terms of displacement demand and capacity, without the a posteriori verification of each masonry element. This approach is not enough accurate in the case of complex masonry buildings with flexible diaphragms and/or big and irregular plan configurations. Indeed in these cases, as far as Near Collapse PL is considered, a significant damage in one single wall may not appear evident in the pushover curve of the whole structure in terms of strength decay. Analogously, for the detection of Damage Limitation PL, it is correct to allow a given damage in some elements, if the global stiffness degradation is still limited and the maximum strength is not reached, but it is not acceptable that damage of structural elements spread too much in the building, even if there is not any tangible effect in the global pushover curve. However, in the case of complex masonry buildings, for Near Collapse PL the a priori selection of predefined failure mechanisms would be quite difficult, due to the possible irregular topology of the equivalent frames, while for Damage Limitation PL the adoption of a structural element approach, based on the checking of the first damaged structural element, would be too conservative.

In Mouyiannou et al. (2014), specific criteria for defining PLs in case of masonry buildings through nonlinear dynamic analyses have been recently proposed. They combine various approaches and variables differentiated as a function of increasing levels of damage severity (until DL3). In case of DL1 (corresponding to Immediate Occupancy PL), the Authors suggest to adopt the displacement associated to the first pier reaching its maximum shear resistance. In case of DL2 (related to Damage Limitation PL) and DL3 (related to Life Safety PL), they tested the use of three different criteria, mainly based on: (i) the global lateral strength evolution (in terms of attainment of the maximum base shear or a 20 % strength degradation); (ii) the

damage diffusion (in terms of percentage of piers area failing); (iii) the degradation of the structural response for increasing levels of the ground motion (monitored through fixed changes in the slope of the IDA curves represented in terms of PGA – drift). Then, after the analysis of results achieved on some prototype buildings (two or three storey buildings, with almost rigid floors and compact plan configurations), the Authors suggested the adoption of criterion i), as that most stable with the record-to-record variability, by expressing the attainment of such DLs in terms of average weighted story drift (DL2) and maximum interstorey drift (DL3). Such criteria are basically coherent also with those suggested in some code (Eurocode 8 – Part 3) in the case of nonlinear static analyses.

However, in particular when horizontal diaphragms are flexible, the adoption of a single criterion seems to be unreliable to detect all possible failure mechanisms. To overcome this problem a multiscale approach for defining DLs in case of historical masonry building was proposed by PERPETUATE project, focused on the assessment of monumental architectural assets (Lagomarsino and Cattari 2015). It aims to combine in an integrated way different criteria and checks at various scales, which are relevant for the seismic response of the building: structural elements scale (local damage, E), architectural elements scale (damage in macroelements, M) and global scale (G). According to this criterion, a coherent approach is applied to define the DLs in case of both NLSA, where the EDP is represented by the displacement u on the pushover curve, and NLDA, where the EPD is constituted by the scalar variable Y introduced in §11.2.

In the case of NLSA, since the final seismic assessment is made through the global pushover curve, the displacement corresponding to attaining DLk ($k = 1, \dots, 4$) is computed as:

$$u_{DLk} = \min(u_{E,DLk}; u_{M,DLk}; u_{G,DLk}) \quad k = 1, \dots, 4 \quad (11.4)$$

where $u_{E,DLk}$, $u_{M,DLk}$, and $u_{G,DLk}$ are the displacements on the pushover curve corresponding to the reaching, respectively, of predefined limit conditions at these scales: element (E, piers or spandrels), macroelement (M, each masonry wall and, eventually, horizontal diaphragms) and global (G, pushover curve).

At global scale, the variable chosen to monitor the attainment of $u_{G,DLk}$ is the rate κ_G of the total base shear over the maximum base shear of the pushover curve ($\kappa_G = V/V_{max}$); proper thresholds (κ_{DLk}) are defined for DL1 and DL2 in the growing branch of the curve while DL3 and DL4 are located on the descending one.

At macroelement scale, the following variables are adopted: in the case of masonry walls, the interstorey drift $\theta_{w,l}$ by any wall and level ($w = 1, \dots, N_w$ – wall number; $l = 1, \dots, N_l$ – level number) must not reach the threshold θ_{DLk} ; in case of diaphragms, the angular strain $\gamma_{q,l}$ ($q = 1, \dots, N_q$ – diaphragm number) must not reach the threshold γ_{DLk} . It is worth noting that usually the interstorey drift is computed referring to the horizontal displacements at floor levels, but this is correct only in the case of strong spandrels (shear-type behaviour). More in general, the interstorey drift of wall $\theta_{w,l}$ has to be evaluated by taking into account the

contribution of both horizontal displacement and rotation of nodes, for example according to:

$$\theta_{w,l} = \frac{\bar{u}_{w,l} - \bar{u}_{w,l-1}}{h_l} + \frac{\bar{\varphi}_{w,l} + \bar{\varphi}_{w,l-1}}{2} \quad (11.5)$$

where: h_l is the interstorey height at level l , while $\bar{u}_{w,l}$ ($\bar{u}_{w,l-1}$) and $\bar{\varphi}_{w,l}$ ($\bar{\varphi}_{w,l-1}$) are the average horizontal displacement and rotation of nodes located at level l (or $l-1$) in wall w (positive if counterclockwise).

Finally, at element scale the cumulative rate of panels that reach a certain DLi (piers – $\Lambda_{P,DLk}$ – and spandrels – $\Lambda_{S,DLk}$) is introduced to check for the attainment of $u_{E,DLk}$. To this aim, proper constitutive laws (e.g. Cattari and Lagomarsino 2013) must be defined for these structural elements (Fig. 11.2a), possibly considering the strength degradation, and able to detect the attainment of progressing DLs, for example by checking the reaching of given drift limits δ_{DLi} (being the damage levels DLi at element scale defined for i from 1 to 5).

The cumulative rate of damage $\Lambda_{S,DLk}$ is defined as the percentage of spandrels that reached or exceeded a given DLi (checked through the given drift thresholds δ_{DLi}):

$$\Lambda_{S,DLk} = \frac{1}{N_S} \sum_s H\left(\frac{\delta_s}{\delta_{DLi}} - 1\right) \quad i = k + 2 \quad (11.6)$$

where the sum is extended to the total number of spandrels ($s = 1, \dots, N_S$) in the building and H is the Heaviside function (equal to 0 until the demand δ_s in the s -th spandrel does not reach the capacity δ_{DLi}).

The cumulative rate of damage $\Lambda_{P,DLk}$ is defined as the percentage of piers that reached or exceeded a given DLi, weighted on the corresponding cross section A_p :

$$\Lambda_{P,DLk} = \frac{\sum_p A_p H\left(\frac{\delta_p}{\delta_{DLi}} - 1\right)}{\sum_p A_p} \quad i = k + 1 \quad (11.7)$$

where the sum is extended to the total number of piers ($p = 1, \dots, N_P$).

It is worth noting that, according to Eqs. (11.6) and (11.7), a higher damage level is accepted in spandrels than in piers. For example, to check the attainment of DL2 ($k = 2$) the reaching of damage levels 3 ($i = k + 1$) and 4 ($i = k + 2$) are checked at the scale of pier and spandrel elements, respectively. In case of DL4, only attainment of damage level 5 in piers is considered. This assumption reflects the different hierarchic role of these elements in the behavior of masonry walls. In fact, piers represent the most important elements, which bear both static loads and seismic action, whereas spandrels are secondary elements, which connect piers by transmitting bending moments.

Table 11.1 proposes ranges of possible values to be used for checks at the different scales; of course these thresholds could be validated or updated by further experimental tests or evidence from observed damage. At local scale, a unique value Λ_{P-S} is proposed as threshold for cumulative rate variables $\Lambda_{P,DLk}$ and $\Lambda_{S,DLk}$ for both piers and spandrels and all DLk; it allows that damage spreads in a limited percentage of elements, but avoids that the DLk is reached due to just one single element. The expression herein proposed has been calibrated through an extensive application of the multiscale approach to several buildings, by considering various irregularities and diaphragms of different stiffness (Cattari and Lagomarsino 2013). In particular, the proposed threshold takes into account the damage induced by the application of the gravity loads ($\Lambda_{P(s),DLk,0}$) and the number of pier and spandrels in the given building. At macroelement scale, interstorey drift limits may be selected within given ranges, which are compatible with values proposed in Calvi (1999). At global scale, range of values for the thresholds of the rate of the maximum overall base shear are compatible with provisions of Eurocode 8, Part 3 (EN 2005); in the case of DL1, a lower bound is defined in order to avoid the occurrence of a slight Damage State in the very beginning of the growing branch of the capacity curve. In some cases, additional checks at macroelement scale (e.g. for horizontal diaphragms) or local scale (e.g. by monitoring the damage in some relevant elements) should be considered for specific performance requirements (e.g. related to the safety of people).

Figure 11.5 illustrates synthetically the steps to be followed in the case of NLSA for the definition of DLk on the pushover curve, by the multiscale approach.

In the case of NLDA, in order to be compatible as much as possible with the multiscale approach defined for NLSA, the scalar variable Y_{DLk} for a given nonlinear dynamic analysis is introduced as:

$$Y_{DLk} = \max(Y_{E,DLk}; Y_{M,DLk}; Y_{G,DLk}) \quad k = 1, \dots, 4 \quad (11.8)$$

where the scalar variables $Y_{E,DLk}$, $Y_{M,DLk}$, and $Y_{G,DLk}$ are computed as the ratio between the maximum value, attained during the time history, of the variables afore introduced at three different scales ($E = \Lambda_P, \Lambda_S$; $M = \theta_{w,l}, \gamma_{q,l}$; $G = u$) and the corresponding thresholds.

More specifically, Y_{DLk} is computed as:

$$Y_{DLk} = \max \left[\frac{\max(\Lambda_{P,DLk}; \Lambda_{S,DLk})}{\Lambda_{P-S}}; \max \left(\frac{\theta_{w,l}}{\theta_{DLk}}; \frac{\gamma_{q,l}}{\gamma_{DLk}} \right); \frac{u_{max}}{u_{G,DLk}} \right] \quad (11.9)$$

where the displacement u is the same representative of the structural response selected in the case of NLSA. It is worth noting that in the case of DL1 the check at global scale could be performed also in terms of strength (with reference to the reaching of the threshold of $0.5V_{max}$) than displacement capacity. Figure 11.6 summarizes the application of the multiscale approach in the case of results from

Table 11.1 Criteria of the multiscale approach proposed for DLk in case of global response of existing masonry buildings

Scale	Variable	Thresholds	DL1	DL2	DL3	DL4
Local	$\Lambda_{P,DLk} - \Lambda_{S,DLk}$	Λ_{P-S}	$0.04 + \Lambda_{P(S),DLk,0} + \frac{2}{N_{P(S)}}$			
Macroelement	$\theta_{w,l}$	θ_{DLk}	$0.0005 - 0.001$	$0.0015 - 0.003$	$0.0035 - 0.005$	$0.0055 - 0.007$
Global	κ_G	κ_{DLk}	≥ 0.5	$0.95 - 1$	$0.8 - 0.9$	$0.6 - 0.7$

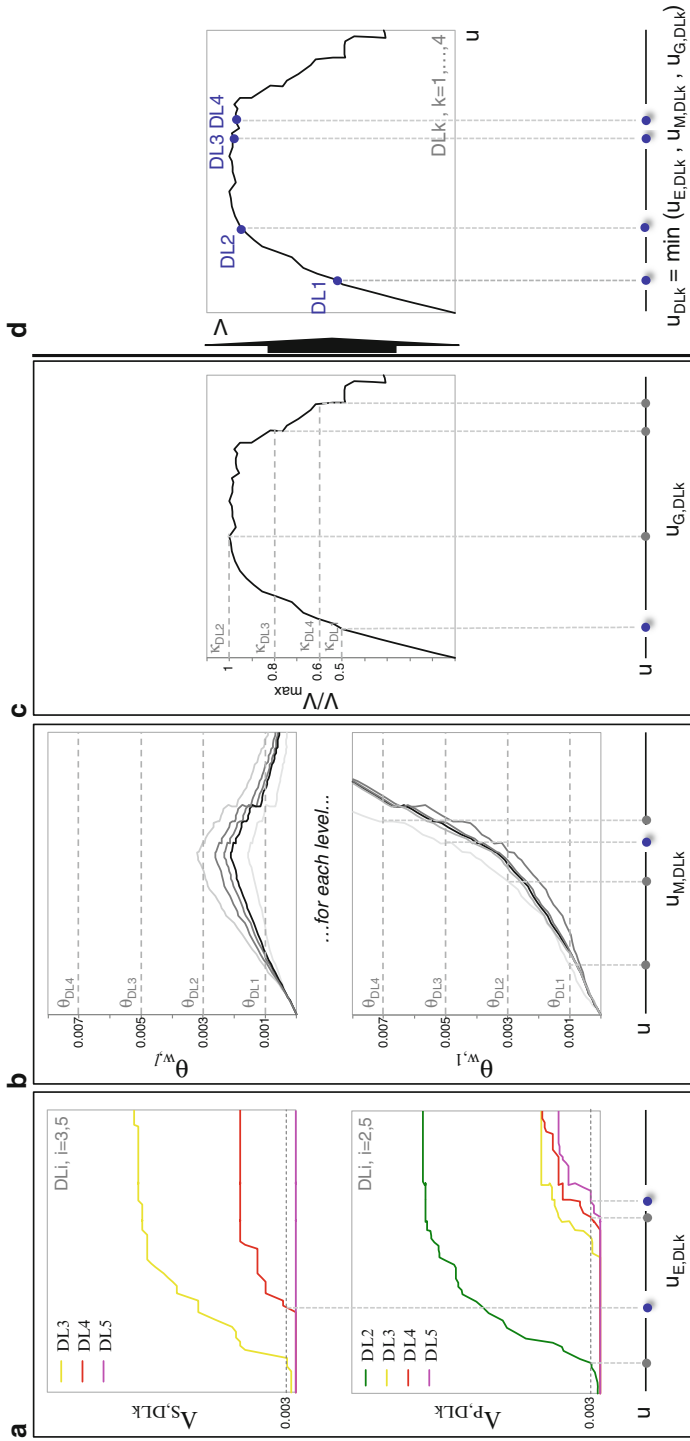


Fig. 11.5 Multiscale approach for the DLs identification in case of NLSA (From Lagomarsino and Cattari 2015): variables monitored at element (a), macroelement (b) and global (c) scales, respectively; (d) final position of DLk on the pushover curve as resulting from the worst condition at different scales examined

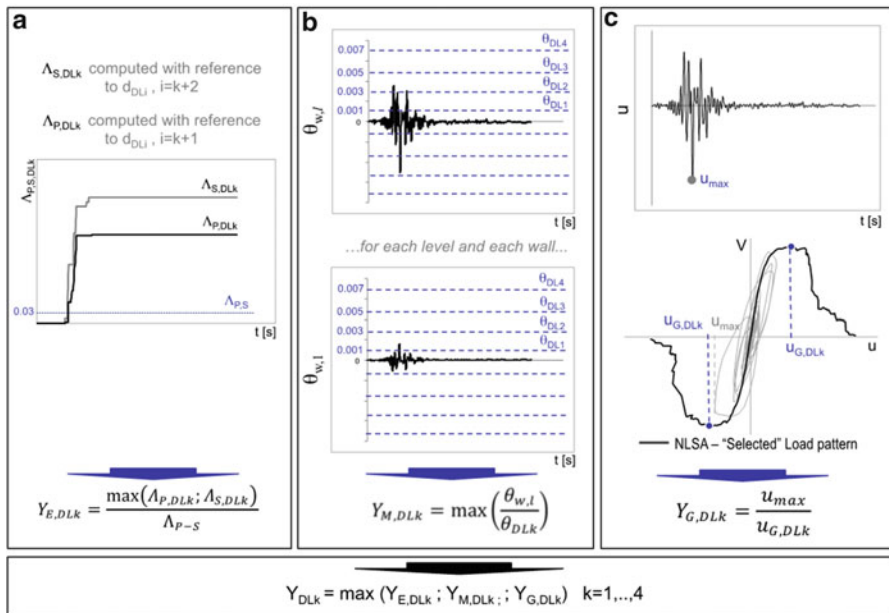


Fig. 11.6 Multiscale approach for the DLs identification in case of NLDA (for a given time history as scaled to a given intensity measure, in the case of IDA method). (a) Element scale. (b) Macroelement scale. (c) Global scale

a single NLDA (that is, for a given time history, scaled to a given intensity measure, in the case of IDA method). Of course results of all analyses have to be properly processed: it is assumed the attainment of $Y_{DLk} = 1$ indicates the reaching of the examined DL. The threshold $u_{G,DLk}$ (computed according to the criteria adopted at global scale in case of NLSA) is obtained for example by considering the pushover curve resulting from the adoption of the most correct load pattern, as selected through a preliminary comparison with the results of NLDA; as introduced in §11.4, to this aim the application of the POD technique to the acceleration time histories turns out to be very useful.

In the case of checks performed at global scale, it is worth to point out that the maximum displacement u_{max} at top level could be affected by single peaks of the response, due to the contribution of higher modes or even to numerical convergence problems. In order to be coherent with the displacement $u_{G,DLk}$, obtained by the NLSA, it is suggested to use the displacement time history (u) preliminary treated by the application of the POD technique by considering as vector q (see Eq. 11.2) the weighted average displacement at all levels of the building (N_l).

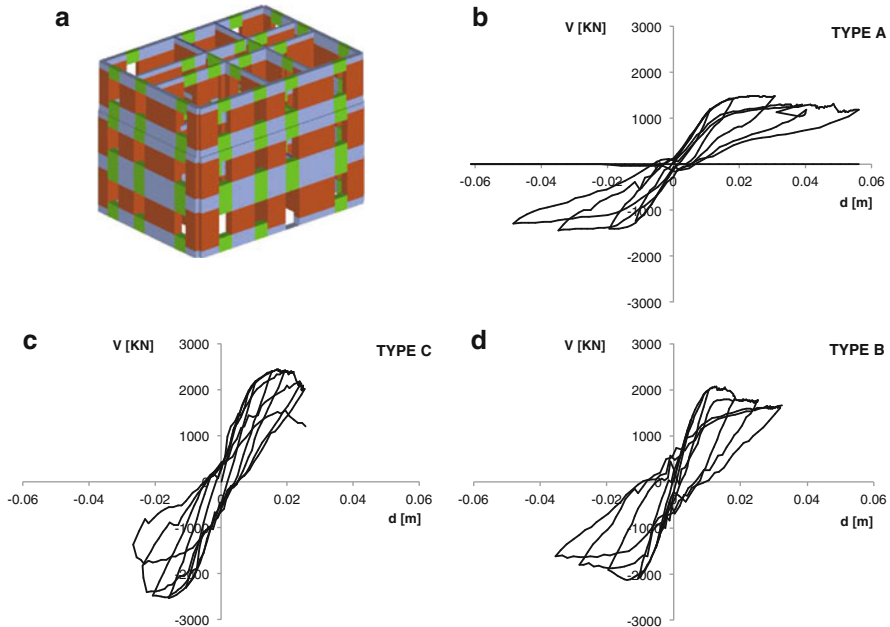


Fig. 11.7 Results of cyclic pushover analyses on a three storey URM masonry building as a function of different structural details (From Cattari and Lagomarsino 2013): (a) 3D view of Equivalent Frame model; (b) Type A – representative of Weak Spandrel-Strong Pier failure mode (with very weak spandrels, without tensile resistant elements coupled and poor interlocking); (c) Type C – representative of Strong Spandrel-Weak Pier (soft storey) failure mode (with reinforced concrete elements coupled to spandrels); (d) Type B – intermediate failure mode (with spandrels characterized by a good interlocking)

11.6 Computation of the Seismic Input Compatible with Each PL

In case of NLSA, the method herein adopted as basic reference is the classical CSM which uses overdamped spectra. If the seismic input is given, the evaluation of the displacement demand requires an iterative procedure. On the contrary, the evaluation of the seismic input that produces a given displacement (that is the adopted outcome of the assessment, IM_{PL}) is straightforward, once the corresponding equivalent viscous damping (ξ_{PL}) is known. This latter may be computed from cyclic pushover analyses or from analytical expressions proposed in literature for similar buildings (Calvi 1999; Priestley et al. 2007; Blandon and Priestley 2005; Sullivan and Calvi 2013). Recently in Cattari and Lagomarsino (2013) some expressions specifically calibrated for existing masonry buildings have been proposed on basis of cyclic pushover analyses on different configurations that exhibited various global failure mechanisms (i.e. soft storey or with damage spreads also in spandrels), directly related to specific structural details (e.g. the presence of reinforced concrete ring beams coupled to spandrels). Figure 11.7

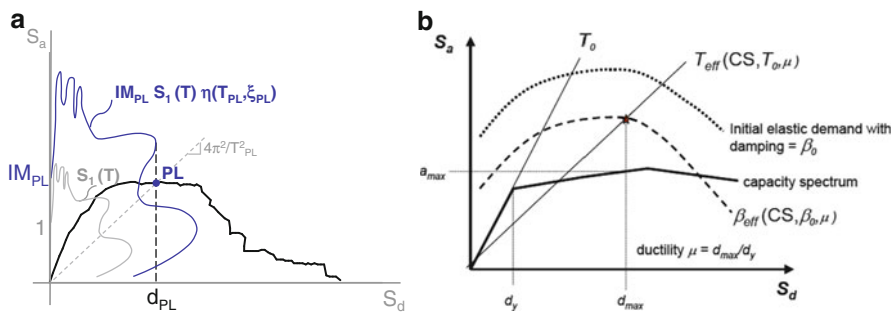


Fig. 11.8 (a) General CSM procedure proposed for the evaluation of IMPL; (b) MADRS procedure proposed in FEMA 440

summarizes some of results discussed more in detail in Cattari and Lagomarsino (2013) in the case of analyses performed on a three storey URM masonry building.

Once defined ξ_{PL} and the corresponding period (T_{PL}), if the ADRS is regular and the spectral displacement increases monotonically with the period T (or remains constant), IM_{PL} can be simply evaluated as the IM for which the spectral displacement demand $S_d(T_{PL}, IM, \xi_{PL})$ is equal to d_{PL} , being d the displacement of the capacity curve (that is the original displacement u of the pushover curve properly converted in the SDOF system).

In order to extend the CSM application to the case of irregular ADRS (Fig. 11.8a), the following expression is proposed for the evaluation of IM_{PL} :

$$IM_{PL} = \frac{d_{PL}}{\max[S_1(T)\eta(T, \xi_{PL}); T_{DL1} < T < T_{PL}]} \quad (11.10)$$

where: $S_1(T)$ is the response spectrum normalized to IM and $\eta(T, \xi_{PL})$ is the reduction factor applied to obtain the overdamped spectra, which may be assumed according to analytical expressions suggested in Eurocode 8 (2004) or in ASCE 41–13 (2014).

With respect to the original CSM, Eq. (11.10) aims to modify the evaluation of displacement demand with respect the classical direct intersection between reduced demand and capacity, taking into account the maximum displacement demand that the structure might have experienced from its elastic dynamic behavior until the reaching of the given T_{PL} . Such proposal has been supported by the results of an extensive set of nonlinear dynamic analyses on single blocks subjected to rocking failure (Lagomarsino 2015). This modification, that does not strictly use the secant period, is consistent also with the modification proposed by the MADRS method (FEMA 440 2005) that highlighted the need, on the basis of evidence from results of nonlinear dynamic analyses, to use for the definition of the equivalent linear SDOF system, values of the period and damping (called “effective”) that are different from those associated to the secant ones in order to obtain more accurate results. (Fig. 11.8b). Then, the value of effective periods and damping are obtained through

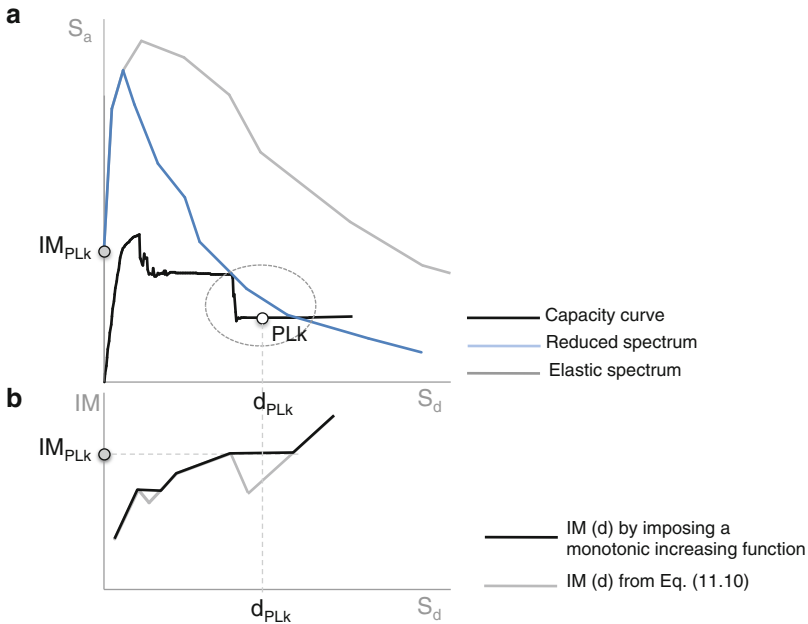


Fig. 11.9 CSM procedure proposed for the evaluation of IM_{PL} in case of capacity curves characterized by sudden base shear decay

analytical expressions differentiated as a function of various possible hysteretic responses.

The proposal introduced by Eq. (11.10) is relevant in the case of irregular spectra, similar to the one of Fig. 11.8a, which are typical when obtained directly from a number of real records or by numerical models that evaluate soil amplification phenomena.

Finally a last comment concerning the use of Eq. (11.10) is related to the case in which the capacity curve presents brittle behaviors with a sudden strength degradation, quite common in case of masonry buildings. The Incremental Static Analysis (ISA) curve can be defined as the IM that causes a given displacement d as a function of d ; the application of Eq. (11.10) without additional restriction could provide a not strictly monotonic ISA curve, which should be inconsistent (because you cannot obtain a displacement demand with a value of IM lower than that which produces a lower displacement). Figure 11.9 shows such specific case, in the case of adoption of an analytical ADRS input (as that proposed in EC8 2004). In this case the IM is represented by the PGA; in Fig. 11.9b the grey line corresponds to the evaluation provided according to Eq. (11.10), the black one that consistent with the assumption of a monotonic increasing function. Moreover, Fig. 11.9a shows the comparison between the capacity curve and the overdamped spectrum, scaled to the IM_{PLK} value; each point of the overdamped reduced spectra refers to the corresponding value of reduction compatible with the equivalent viscous damping

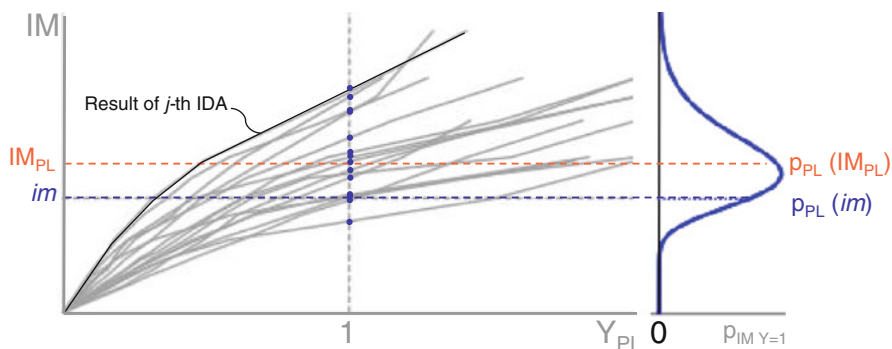


Fig. 11.10 Results of IDA and evaluation of IM_{PL}

on the capacity curve. From this figure it is evident that in the range marked by the dotted circle the adoption only of Eq. (11.10) would lead to inconsistent results.

Finally, in case of NLDA, the procedure is based on a statistical evaluation of IM_{PL} through the Multiple Stripe Analysis (MSA), in the case of cloud method, or the IDA curves in correspondence of the attainment of $Y_{DL} = 1$ condition, in the case of a set of time-histories scaled to increasing IM (Fig. 11.10).

11.7 Conclusions

A discussion on the use of nonlinear static and dynamic analyses for the Performance Based Assessment of masonry existing buildings is presented focusing the attention on structures dominated by a global behavior and reliably modeled through the equivalent frame approach. Some original contributions to strengthen the equivalence of criteria adopted in the two methods are proposed. In particular, such proposals deal with the definition of performance level thresholds for the structural capacity (to be adopted for checking the fulfillment of PLs) and the tools to enhance the use of rich amount of data carried out through nonlinear dynamic analyses.

As regard the first objective, a multiscale approach is introduced aimed to combine in an integrate way different criteria and checks at various scales which are relevant for the seismic response of the building (element, macroelement, global). This approach is needed for complex masonry buildings, in particular when horizontal diaphragms are flexible. PLs are defined through the introduction of proper variables, directly obtained by numerical models, in a consistent way in the case of static and dynamic methods.

As regard the second one, the use of the Proper Orthogonal Decomposition (POD) technique is proposed to detect the dominant behaviors highlighted by the structure when a nonlinear dynamic analysis or shaking table tests are performed, appearing this approach more effective than referring to single and instantaneous

peaks of the response (more affected by random noise, due to numerical convergence problems or measurements errors). Beside interpreting the results in a more effective way, the processing of data through the POD technique is also useful to provide information on the correct deformed shape and load pattern to be adopted in the case of static procedures for verification.

Acknowledgments The research was funded by the national project ReLUIIS-DPC 2014–2018 (www.reluis.it), supported by the Italian Civil Protection Agency, within the research thematic “Masonry buildings”.

Open Access This chapter is distributed under the terms of the Creative Commons Attribution Noncommercial License, which permits any noncommercial use, distribution, and reproduction in any medium, provided the original author(s) and source are credited.

References

- Antoniou S, Pinho R (2004) Development and verification of a displacement-based adaptive pushover procedure. *J Earthq Eng* 8(5):643–661
- ASCE/SEI 41–13 (2014) Seismic evaluation and retrofit of existing buildings. American Society of Civil Engineers, Reston. ISBN 978-0-7844-7791-5
- Aydinoglu MN, Onem G (2010) Evaluation of analysis procedures for seismic assessment and retrofit design. In: Garevsky M, Ansal A (eds) *Earthquake engineering in Europe*. Springer, Dordrecht, Netherlands, pp 171–198
- Benedetti D, Carydis P, Limongelli MP (2001) Evaluation of the seismic response of masonry buildings based on energy functions. *Earthq Eng Struct Dyn* 30:1061–1081
- Berkooz G, Holmes P, Lumley JL (1993) The proper orthogonal decomposition in the analysis of turbulent flows. *Annu Rev Fluid Mech* 25:539–575
- Beyer K, Mangalathu S (2013) Review of existing strength models for spandrels. *Bull Earthq Eng* 11(2):521–542
- Blandon CA, Priestley MJN (2005) Equivalent viscous damping equations for direct displacement based design. *J Earthq Eng* 9(Special Issue 2):257–278
- Calderini C, Cattari S, Lagomarsino S (2009) In-plane strength of unreinforced masonry piers. *Earthq Eng Struct Dyn* 38(2):243–267
- Calvi GM (1999) A displacement-based approach for vulnerability evaluation of classes of buildings. *J Earthq Eng* 3(3):411–438
- Cattari S, Lagomarsino S (2013) Masonry structures, pp 151–200. In: Sullivan T, Calvi GM (eds) *Developments in the field of displacement based seismic assessment*. IUSS Press and EUCENTRE, Pavia, Italy, p 524. ISBN:978-88-6198-090-7
- Cattari S, Degli Abbatì S, Ferretti D, Lagomarsino S, Ottonelli D, Tralli A (2013) Damage assessment of fortresses after the 2012 Emilia earthquake (Italy). *Bull Earthq Eng*. doi:10.1007/s10518-013-9520-x
- Cattari S, Chiocciariello A, Degée H, Doneaux C, Lagomarsino S, Mordant C (2014) Seismic assessment of masonry buildings from shaking table tests and nonlinear dynamic simulations by the Proper Orthogonal Decomposition (POD). In: *Proceedings of the second European conference on earthquake engineering and seismology (ECEES)*, Istanbul, 25–29 Aug 2014
- Chopra AK, Goel RK (2002) A modal pushover analysis procedure for estimating seismic demands for buildings. *Earthq Eng Struct Dyn* 31(3):561–582
- Chopra AK, Goel RK, Chintanapakee C (2004) Evaluation of a modified MPA procedure assuming higher modes as elastic to estimate seismic demands. *Earthq Spectra* 20(3):757–778

- CIB 335 (2010) Guide for the structural rehabilitation of heritage buildings, prepared by CIB commission W023 – Wall Structures, ISBN 978-90-6363-066-9
- CNR-DT212 (2013) Recommendations for the probabilistic seismic assessment of existing buildings. Consiglio Nazionale delle Ricerche, Rome, Italy (in Italian). <http://www.cnr.it/sitocnr/IICNR/Attivita/NormazioneeCertificazione/DT212.html>
- Coburn A, Spence R (2002) Earthquake protection. Wiley, Chichester, West Sussex, England. ISBN:978-0-470-84923-1
- Douglas J, Seyedi DM, Ulrich T, Modaressi H, Foerster E, Pitilakis K, Pitilakis D, Karatzetzou A, Gazetas G, Garini E, Loli M (2015) Evaluation of the seismic hazard for the assessment of historical elements at risk: description of input and selection of intensity measures. *Bull Earthq Eng* 13. doi:10.1007/s10518-014-9606-0
- EN 1998-1 (2004) Eurocode 8: design of structures for earthquake resistance – Part 1: General rules, seismic actions and rules for buildings. CEN (European Committee for Standardization), Brussels
- EN 1998-3 (2005) Eurocode 8: design of structures for earthquake resistance – Part 3: Assessment and retrofitting of buildings. CEN (European Committee for Standardization), Brussels
- Fajfar P (2000) A non linear analysis method for performance-based seismic design. *Earthq Spectra* 16(3):573–591
- Falco A, Chinesta F, Gonzalez M (2006) Model reduction methods in option pricing. Instituto Valenciano de Investigaciones Economicas, Valencia, Spain
- FEMA 440 (2005) Improvement of nonlinear static seismic analysis procedures. ATC, Washington, DC
- Freeman SA (1998) The capacity spectrum method as a tool for seismic design. In: Proceedings of 11th European conference of earthquake engineering, Paris
- Galasco A, Lagomarsino S, Penna A (2006) On the use of pushover analysis for existing masonry buildings. In: Proceedings of the 13th European conference on earthquake engineering, Geneva (CH), 3–8 Sept 2006, ID 1080
- Graziotti F, Penna A, Magenes G (2013) Use of equivalent SDOF systems for the evaluation of the displacement demand for masonry buildings. Proceedings of VEESD, (p. Paper No. 347), Vienna
- Grunthal G (1998) European Macroseismic Scale 1998: EMS-98, vol 15. Chaiers du Centre Européen de Géodynamique et de Séismologie, Luxembourg
- Gupta B, Kunnath SK (2000) Adaptive spectra-based pushover procedure for seismic evaluation of structures. *Earthq Spectra* 16:367–392
- Han S, Feeny B (2003) Application of proper orthogonal decomposition to structural vibration analysis. *Mech Syst Signal Pr* 17(5):989–1001
- ICOMOS (2005) Recommendations for the analysis, conservation and structural restoration of architectural heritage. International Scientific Committee for Analysis and Restoration of Structures and Architectural Heritage (ISCARSAH), Document approved on 15/6/2005 in Barcelona
- ISO 13822 (2010) Bases for design of structures – assessment of existing structures, 2nd edn. 2010-08-01. ISO International Standard, Geneva
- Jalayer F, Cornell CA (2009) Alternative non-linear demand estimation methods for probability-based seismic assessments. *Earthq Eng Struct Dyn* 38:951–972
- Karhunen K (1946) Zur spektraltheorie stochastischer prozess. *Ann Acad Sci Fenn Math* 1:34
- Lagomarsino S (2012) Damage assessment of churches after L'Aquila earthquake (2009). *Bull Earthq Eng* 10(1):73–92
- Lagomarsino S (2015) Seismic assessment of rocking masonry structures. *Bull Earthq Eng* 13:97–128. doi:10.1007/s10518-014-9609-x
- Lagomarsino S, Cattari S (2015) guidelines for seismic performance-based assessment of cultural heritage masonry structures. *Bull Earthq Eng* 13:13–47. doi:10.1007/s10518-014-9674-1

- Lagomarsino S, Modaressi H, Ptilakis K, Bosjlikov V, Calderini C, D'Ayala D, Benouar D, Cattari S (2010) PERPETUATE Project: the proposal of a performance-based approach to earthquake protection of cultural heritage. *Adv Mater Res* 133–134:1119–1124
- Lagomarsino S, Penna A, Galasco A, Cattari S (2013) TREMURI program: an equivalent frame model for the nonlinear seismic analysis of masonry buildings. *Eng Struct* 56:1787–1799. doi: <http://dx.doi.org/10.1016/j.engstruct.2013.08.002>
- Loeve M (1945) Fonctions aléatoire de second ordre. *Comptes Rendus de l'Académie des sciences, Paris*, p 220
- Lumley JL (1970) *Stochastic tools in turbulence*. Academic, New York
- Marrè Brunenghi M (2014) Probabilistic tools for the qualitative analysis of wind actions on structures, PhD Thesis, University of Genoa
- Mouyianou A, Rota M, Penna A, Magenes G (2014) Identification of suitable limit states from nonlinear dynamic analyses of masonry structures. *J Earthq Eng* 18(2):231–267. doi: [10.1080/13632469.2013.842190](https://doi.org/10.1080/13632469.2013.842190)
- Oliveira CS (2003) Seismic vulnerability of historical monuments: a contribution. *Bull Earthq Eng* 1:37–82
- Petry S, Beyer K (2014) Influence of boundary conditions and size effect on the drift capacity of URM walls. *Eng Struct* 65:76–88
- Priestley MJN, Calvi GM, Kowalsky MJ (2007) *Displacement-based seismic design of structures*. IUSS Press, Pavia, 721 pp. ISBN:978-88-6198-000-6
- Recommendations P.C.M. (2011) Assessment and mitigation of seismic risk of cultural heritage with reference to the Technical Code for the design of constructions, issued by D.M. 14/1/2008. Directive of the Prime Minister, 9/02/2011. G.U. no. 47, 26/02/2011 (suppl. ord. no. 54) (in Italian)
- Reyes J, Chopra A (2011) Three dimensional modal pushover analysis of buildings subjected to two components of ground motion, including its evaluation for tall buildings. *Earthq Eng Struct Dyn* 40:789–806
- SIA 269/8 (2013) Existing structures – earthquakes, draft. Swiss Society of Engineers and Architects, Zürich
- Solari G, Carassale L, Tubino F (2007) Proper orthogonal decomposition in wind engineering: Part 1: A state-of-the-art and some prospects. *Wind Struct* 10(2):153–176
- Sorrentino L, Liberatore L, Decanini LD, Liberatore D (2013) The performance of churches in the 2012 Emilia earthquakes. *Bull Earthq Eng* 12. doi: [10.1007/s10518-013-9519-3](https://doi.org/10.1007/s10518-013-9519-3)
- Sullivan T, Calvi GM (2013) Development in the field of displacement based seismic assessment, Ed. IUSS Press (PAVIA) and EUCENTRE, pp 524. ISBN:978-88-6198-090-7
- Tomazevic M (1999) *Earthquake-resistant design of masonry buildings*. Imperial College Press, ISBN 9781860940668
- Vamvatsikos D, Cornell CA (2002) Incremental dynamic analysis. *Earthq Eng Struct Dyn* 31(3):491–514
- Williams M, Sexsmith RG (1995) Seismic damage indices for concrete structures: a state-of-the-art review. *Earthq Spectra* 11(2):319–349

Chapter 12

Developments in Ground Motion Predictive Models and Accelerometric Data Archiving in the Broader European Region

Sinan Akkar and Özkan Kale

Abstract This paper summarizes the evolution of major strong-motion databases and ground-motion prediction equations (GMPEs) for shallow active crustal regions (SACRs) in Europe and surrounding regions. It concludes with some case studies to show the sensitivity of hazard results at different seismicity levels and exceedance rates for local (developed from country-specific databases) and global (based on databases of multiple countries) GMPEs of the same region. The case studies are enriched by considering other global GMPEs of SACRs that are recently developed in the USA. The hazard estimates computed from local and global GMPEs from the broader Europe as well as those obtained from global GMPEs developed in the US differ. These differences are generally significant and their variation depends on the annual exceedance rate and seismicity. Current efforts to improve the accelerometric data archives in the broader Europe as well as more refined GMPEs that will be developed from these databases would help the researchers to understand the above mentioned differences in seismic hazard.

12.1 Introduction

The development of ground-motion prediction equations (GMPEs) for shallow active crustal regions in Europe has initiated with the efforts of Ambraseys (1975), approximately a decade after the first ground-motion model proposed by

S. Akkar (✉)

Kandilli Observatory and Earthquake Research Institute, Boğaziçi University,

İstanbul 34684, Turkey

e-mail: sinan.akkar@boun.edu.tr

Ö. Kale, PhD

Department of Civil Engineering, Middle East Technical University, Ankara 06800, Turkey

e-mail: ozkankale@gmail.com

© The Author(s) 2015

A. Ansal (ed.), *Perspectives on European Earthquake Engineering and Seismology*,

Geotechnical, Geological and Earthquake Engineering 39,

DOI 10.1007/978-3-319-16964-4_12

Esteva and Rosenblueth (1964).¹ In the past 40 years, well over 100 GMPEs are developed in Europe and neighboring countries for estimating the future ground-motion levels in terms of elastic spectral ordinates and peak ground acceleration, PGA (Douglas 2011).² Most of these GMPEs are tailored from datasets specific to a region or country but there are also ground-motion models developed by combining strong motions of many countries in the broader Europe.³ As everywhere else in the world, the quality and quantity of GMPEs in Europe are directly related to the availability of observational datasets. Their level of complexity to explain the physical process of earthquakes has also direct connection with the strong-motion data collection efforts under international or national programs.

As indicated above, there are three common practices in Europe for developing GMPEs. The first approach focuses on the regional datasets to estimate ground motions (e.g., Massa et al. 2008; Bragato and Slejko 2005). The second approach uses country-based datasets (e.g., Akkar and Çağnan 2010; Bindi et al. 2011), whereas the third group of model developers combines data from different countries in and around Europe (e.g., Ambraseys et al. 2005). (In some cases supplementary strong-motion data from USA or Japan are also used by the third group modelers). Researchers from the first two groups aim to capture the region-specific source, path and site effects on the ground-motion amplitudes estimates without contaminating the indigenous data from other regions. The GMPEs developed from regional and country-based datasets are generically called as local GMPEs. Researchers following the last approach accentuate that recordings from countries that are located in similar tectonic regimes are expected to exhibit similar features. This assumption generally yields larger ground-motion datasets with better distribution, for example in magnitude-distance space, with respect to regional or country-based datasets. Therefore, the regressed functional forms of the third group models are generally better constrained in terms of main estimator parameters. However, possible data contamination, for example due to regional attenuation differences, may provoke speculations on their efficient use in some hazard studies. As the third group ground-motion models are developed from datasets of multiple countries, they are called as global GMPEs. Their datasets are also referred to as global databases.

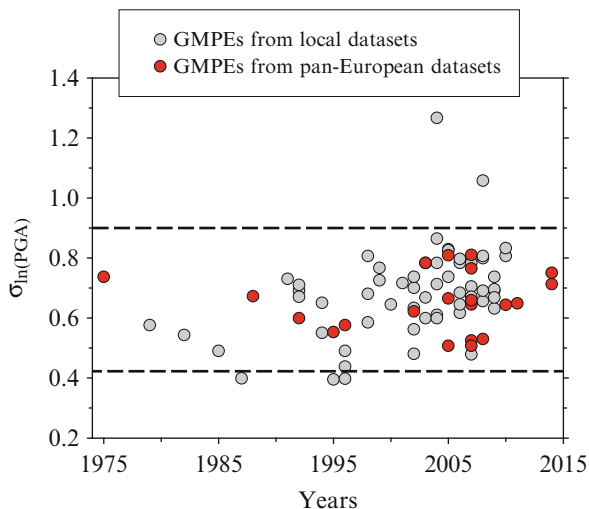
Different perspectives in the above approaches raise questions about the existence of regional dependence among the European GMPEs with emphasis on the epistemic and aleatory uncertainties. The aleatory uncertainty (measured with the standard deviation, σ , of GMPE) that is generally referred to as intrinsic variability of

¹ Predictive model by Esteva and Rosenblueth (1964) was proposed for the Western USA whereas the Ambraseys (1975) GMPE was developed for Europe.

² There are other ground-motion equations estimating peak ground velocity (e.g., Akkar and Bommer 2007; Tromans and Bommer 2002) and ground-motion intensity measures such as vertical-to-horizontal spectral ratios (e.g., Akkar et al. 2014b; Bommer et al. 2011) for Europe and surrounding regions. These predictive models are not considered in this article.

³ Datasets compiled from different European and neighboring countries are generally referred to as pan-European datasets (Bommer et al. 2010). The GMPEs developed from these datasets are called as pan-European GMPEs.

Fig. 12.1 Comparisons between the standard deviations of local and pan-European (global) predictive models that estimate PGA



ground motions may also reflect the uncertainties stemming from dataset quality and its composition (e.g., local vs. global databases), modeling of GMPE and regression technique used in fitting (Strasser et al. 2009). For example, GMPEs for PGA that are developed from local or pan-European (global) datasets do not show a clear difference in sigma distribution as given in Fig. 12.1. Thus, the better constrained pan-European GMPEs do not possess lesser aleatory variability with respect to their local counterparts. The converse of this argument is also defensible: local GMPEs do not show reduced aleatory variability to speculate lesser contamination in their data.

Figure 12.2 compares the period-dependent sigma trends between NGA-West1⁴ (Power et al. 2008), NGA-West2⁴ (Bozorgnia et al. 2014) and the most recent pan-European GMPEs (Akkar et al. 2014c; Bindi et al. 2014; Akkar and Bommer 2010; Ambraseys et al. 2005). NGA-West1 and NGA-West2 GMPEs use wide spread shallow active crustal ground motions mainly from California, Taiwan (NGA-West1) and additionally from Japan, China and New Zealand (NGA-West2). They are also referred to as global GMPEs. The comparisons in Fig. 12.2 are done for M_w 5 and M_w 7 and the shaded areas in each panel represent the upper and lower sigma bounds of the chosen pan-European equations. The NGA-West1 and NGA-West2 GMPEs tend to yield lower sigma with respect to pan-European GMPEs. Note that the NGA-West2 predictive models are developed to bring improvements over NGA-West1 GMPEs in terms of additional data, explanatory variables and extended magnitude and distance ranges but their sigma values are larger with respect to their predecessors. The larger standard deviations in NGA-West2 GMPEs can be the manifestations of aggregated

⁴NGA-West1 and NGA-West2 are two projects to develop shallow active crustal GMPEs for seismic hazard assessment in the Western US. NGA-West2 project is the successor of NGA-West1.

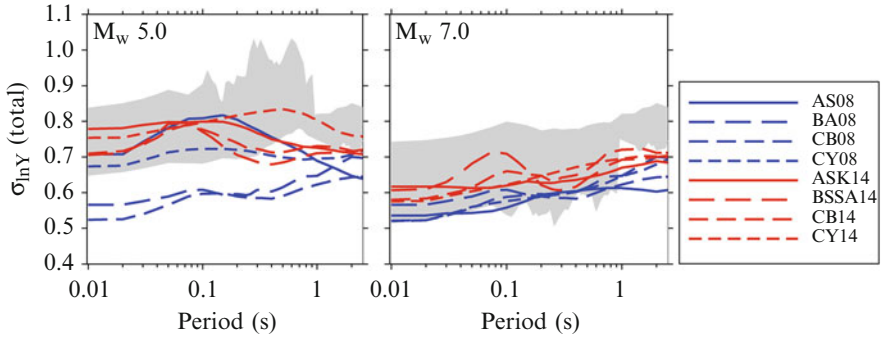


Fig. 12.2 Comparisons of sigma between NGA-West1 (Abrahamson and Silva (2008) – AS08, Boore and Atkinson (2008) – BA08, Campbell and Bozorgnia (2008) – CB08, Chiou and Youngs (2008) – CY08), NGA-West2 (Abrahamson et al. (2014) – ASK14, Boore et al. (2014) – BSSA14, Campbell and Bozorgnia (2014) – CB14, Chiou and Youngs (2014) – CY14) and some representative pan-European GMPEs (Akkar et al. 2014c; Bindi et al. 2014; Akkar and Bommer 2010; Ambraseys et al. 2005). The *gray shaded areas* show the upper and lower sigma bounds of pan-European GMPEs. The *blue and red lines* refer to period-dependent sigma variations of NGA-West1 and NGA-West2 predictive models, respectively. Comparisons are done for a rock site ($V_{S30} = 760$ m/s) located 10 km away from a 90° dipping strike-slip fault. The selected magnitudes for comparisons are M_w 5 (*left panel*) and M_w 7 (*right panel*)

uncertainty due to new data and additional explanatory variables. Interestingly, the core accelerometric data sources of NGA-West1 and NGA-West2 GMPEs do not include large numbers of ground motions from Europe that can, speculatively, be a factor for the observed differences in the sigma variation between NGA and pan-European GMPEs.

The above observations suggest that further systematic studies are required to understand the sources of differences or similarities in the aleatory variability between local and pan-European GMPEs. Such studies should also be performed between European and other well constrained global ground-motion models that are developed outside of Europe. An extensive summary about the factors controlling sigma and worldwide studies to reduce sigma can be found in Strasser et al. (2009).

Douglas (2004, 2007) indicated that there is no strong evidence confirming regional dependence for the GMPEs produced in the broader European region since the empirical observations are still limited. He also emphasized that the level of complexity in the current pan-European GMPEs is insufficient for a clear understanding about the contribution of epistemic uncertainty on the median ground-motion estimates (Douglas 2010). However, complexity in ground-motion models does not necessarily imply a better identification of epistemic uncertainty as complex GMPEs contain superior numbers of estimator parameters that may lead to overfit to empirical observations (Kaklamanos and Baise 2011). Bommer et al. (2010) showed that GMPEs developed from pan-European datasets and ground-motion models derived from NGA-West1 GMPEs would yield similar ground-motion estimates for moderate-to-large magnitude earthquakes. These authors indicated that the regional differences in ground-motion estimates would

be prominent towards smaller magnitude earthquakes, which is a parallel observation with the studies conducted in the other parts of the world (Chiou et al. 2010; Atkinson and Morrison 2009). On the other hand, Scasserra et al. (2009) emphasized that the use of NGA-West1 GMPEs may over predict the hazard in Italy at large distances because Italian data attenuate faster than the trends depicted in NGA-West1 GMPEs. In a separate study, Akkar and Çağnan (2010) who developed a GMPE from an extended Turkish database showed that NGA-West1 GMPEs and ground-motion predictive models from pan-European datasets would yield conservative estimates with respect to their GMPE for different earthquake scenarios at different spectral ordinates. Recently, Kale et al. (2015) showed the existence of distance and magnitude dependent differences between the Iranian and Turkish shallow active crustal ground-motion amplitudes. Yenier and Atkinson (2014) found evidence on the regional dependence of large magnitude earthquakes in New Zealand and western North America. Almost all NGA-West2 GMPEs consider regional differences in their ground-motion estimates (Gregor et al. 2014).

Understanding the driving factors behind the observations highlighted in the above paragraphs requires detailed studies that consider different aspects of several topics related to database quality, GMPEs and their interdependencies. This paper does not intend to conduct such a study but aims at a comprehensive discussion about the current state of accelerometric databases and GMPEs for SACRs in the broader Europe. We believe that this information would provide a strong ground for the aforementioned detailed studies to scrutinize the existence of regional differences within broader Europe for shallow active crustal earthquakes. The paper ends by presenting the results of some probabilistic seismic hazard studies (PSHA) to evaluate the level of differences in the estimated hazard upon the use of most recent local and global European GMPEs as well as those developed in NGA-West1 and NGA-West2 projects. The comparative PSHA results essentially emphasize the impact of using current local and global GMPEs to the estimated ground motions in terms of annual exceedance rates and seismicity level.

12.2 Evolution of Major Strong-Motion Databases in the Broader Europe

Strong-motion data collection in Europe started in the beginning of 1970s in Imperial College under the leadership of Prof. Ambraseys (deceased in 2012). It is continued progressively through multi-national collaborations (Ambraseys 1990; Ambraseys and Bommer 1990, 1991) and a CD-ROM of 1,068 tri-axial accelerometric data was released in 2000 as a solid product of this effort (Ambraseys et al. 2000). The data in the CD-ROM were expanded to a total of 2,213 accelerograms from 856 earthquakes recorded at 691 strong-motion stations (Ambraseys et al. 2004a) and it is disseminated through the Internet Site for European Strong-Motion Data (ISESD) web page (<http://www.isesd.hi.is>).

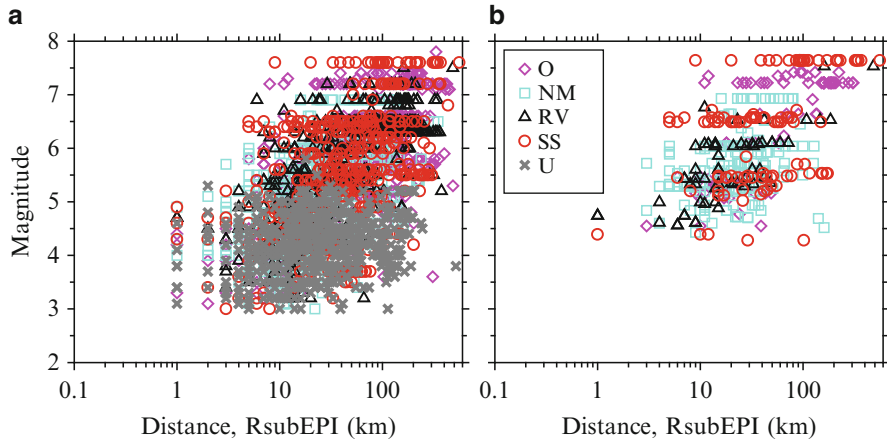


Fig. 12.3 Magnitude vs. distance scatters of (a) IESD, (b) ESMD. Different symbols with different color codes show the distribution of fault mechanisms in these databases (O odd, NM normal, RV reverse, SS strike-slip, U unknown). Almost 50 % of the data in IESD and ESMD are collected from Italy, Greece and Turkey. These countries are followed by Iran (11 % of the whole data)

Figure 12.3a shows the magnitude vs. distance scatter of IESD strong-motion database. It spans accelerograms from broader Europe between 1976 and 2004. The earthquake metadata (e.g., geometry, style-of-faulting, magnitude estimations etc.) in IESD was extracted either from specific earthquake studies (institutional reports and papers published in peer-reviewed journals) or ISC bulletin (International Seismological Center, www.isc.ac.uk). The earthquake location information was taken from local or national seismic networks whenever they were assessed as more reliable than the international networks. The strong-motion station information (site conditions, station coordinates, shelter type) was obtained from the network owners. The soil classification of strong-motion sites in IESD relies on V_{S30} (average shear-wave velocity in the upper 30m soil profile). However, the V_{S30} data were mostly inferred from geological observations in IESD as the measured shear-wave velocity profiles were typically unavailable by the time when it was assembled. The processed strong-motion records in IESD were band-pass filtered using an elliptical filter with constant high-pass and low-pass filter cut-off frequencies (0.25 and 25 Hz, respectively). After the release of IESD, a small subset of this database was re-processed using the phaseless (acausal) Butterworth filter with filter cut-off frequencies adjusted individually for each accelerogram. The individual filter cut-off frequencies were determined from the signal-to-noise ratio of each accelerogram. This subset was published as another CD-ROM that is referred to as European Strong-Motion Data (ESMD; Ambraseys et al. 2004b). The extent of ESMD in terms of magnitude and distance is given in Fig. 12.3b.

The dissemination of IESD and ESMD strong-motion databases was followed by important national and international strong-motion and seismic hazard projects in Europe and surrounding regions. Among these projects, the Italian

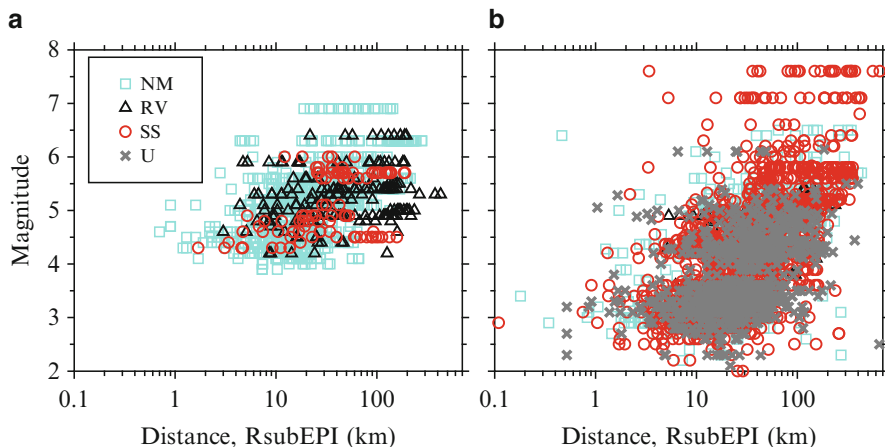


Fig. 12.4 Magnitude vs. distance scatters of (a) ITACA and (b) T-NSMP databases. The ITACA⁵ project compiled a total of 2,182 accelerograms from 1,004 events (Luzi et al. 2008) whereas T-NSMP studied 4,607 strong-motion records from 2,996 earthquakes recorded at 209 stations (Akkar et al. 2010). The symbols on the scatter plots show the distribution of fault mechanism in each database (Refer to the caption of Fig. 12.3 for abbreviations in the legends)

ACcelerometric Archive⁵ project (ITACA; <http://itaca.mi.ingv.it>; Luzi et al. 2008), the Turkish National Strong-Motion Project (T-NSMP; <http://kyh.deprem.gov.tr>; Akkar et al. 2010) and the Hellenic Accelerogram Database Project (HEAD; <http://www.itsak.gr>; Theodulidis et al. 2004) are national efforts to compile, process and archive local (national) accelerometric data using state-of-the-art techniques. Figures 12.4a, b show the magnitude vs. distance scatters of ITACA⁵ and T-NSMP databases as of the day they are released. These national projects improved the site characterization of strong-motion stations either by reassessing the existing shear-wave velocity profiles and soil column lithology information or by utilizing invasive or noninvasive site exploration techniques to compute the unknown V_{S30} and other relevant site parameters (e.g., see Sandikkaya et al. 2010 for site characterization methods of Turkish accelerometric archive). They also uniformly processed the strong-motion records by implementing a reliable and consistent data processing scheme. None of these data processing algorithms implemented constant filter cut-off frequencies to remove the high-frequency and low-frequency noise from the raw accelerograms.

The NERIES (Network of Research Infrastructures for European Seismology; www.neries-eu.org) and SHARE (Seismic Hazard HARMonization in Europe; www.share.eu.org) projects that are funded by European Council also contributed significantly to the integral efforts for collecting and compiling accelerometric data

⁵The ITACA database referenced in this article is now called as “ITACA v1” as a newer version is recently released on the same web site. The new release covers Italian strong-motion records from 1972 to the end of 2013.

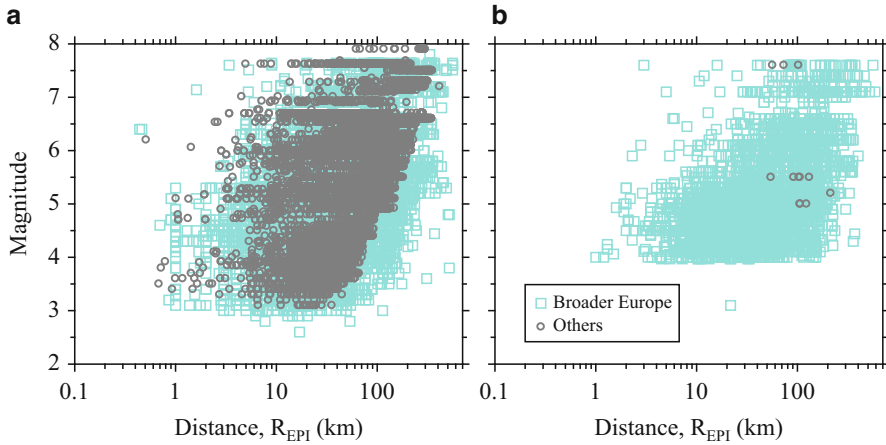


Fig. 12.5 Magnitude and distance distributions of (a) SHARE and (b) EMME strong-motion databases. The SHARE accelerograms from the broader Europe are shown in cyan to give a more clear view on the fraction of recordings from this region in the SHARE database. Same color codes are used in the EMME scatter plot to compare the strong-motion data distribution of broader Europe between these two databases

in the broader Europe. The NERIES project created a new infrastructure to collect, process and distribute near-real time accelerometric data from across Europe (www.seismicportal.eu). The SHARE project compiled a comprehensive strong-motion database (Yenier et al. 2010) by collecting worldwide shallow active crustal accelerometric data that includes recordings from ISESD, ESMD, ITACA and T-NSMP. The SHARE strong-motion database (13,500 records from 2,268 events recoded at 3,708 stations) was mainly used to test the candidate GMPEs for the seismic hazard calculations in SHARE project. The developers of SHARE database neither aimed for updating the metadata information nor developing a uniformly processed accelerometric data archive from the collected strong-motion recordings. The EMME (Earthquake Model of the Middle East Region; www.emme-gem.org) project that is funded by Global Earthquake Model (GEM) organization with objectives parallel to SHARE also established a strong-motion database for SACRs in the Middle East, Iran, Pakistan and Caucasus. The EMME strong-motion database that consists of 4,920 accelerograms from 1803 events is mainly used to identify the most proper GMPEs for hazard computations in the SACRs covered by the project. One of the major differences between the EMME and SHARE strong-motion databases is the uniform data processing implemented to the accelerograms in EMME. Besides, the earthquake and strong-motion station metadata information of the EMME database was reassessed systematically by the project partners (Akkar et al. 2014a). Figures 12.5a, b compare the magnitude and distance distributions of these two databases. Note that the magnitude and distance coverage of EMME strong-motion database is not as uniform as in the case of SHARE database. This is because the latter strong-motion inventory includes shallow

active crustal earthquake accelerograms from the entire world. EMME strong-motion database is particularly rich in Iranian and Turkish recordings. When both databases are compared for accelerograms originating from the pan-European region, one may infer that EMME and SHARE databases can reveal significant amount of information about the characteristics of strong-motion data from this region.

The efforts put forward in the development of ISESD as well as other databases that are compiled from well-organized national and international projects had considerable impact on the improvement of accelerometric data quality in and around Europe. However, they suffer from certain drawbacks at different technical and operational levels. Although ISESD is an integrated database representing the strong-motion data archive of broader Europe, the poor strong-motion site characterization and the use of constant filter cut-offs in data processing are the major shortcomings of this database. The use of fixed filter cut-offs has been proven to be inappropriate as it may result in wrong representation of actual ground-motion frequency content of the recorded events (e.g., Akkar and Bommer 2006). The national strong-motion projects as well as EMME project took their precautions against such drawbacks but they implemented their own methodologies while assembling the databases. Thus, there is a lack of uniformity among these projects for metadata compilation and record processing for their integration under a single strong-motion database. The SHARE project did no attempt to homogenize the data processing of accelerograms. Improvements in earthquake and station metadata were also out of scope of SHARE. The recordings from the most recent pan-European earthquakes of engineering interest (e.g., 2009 L'Aquila Earthquake M_w 6.3; 2011 Van Earthquake M_w 7.1; 2011 Van-Edremit Earthquake M_w 5.6; 2011 Kütahya-Simav Earthquake M_w 5.9; 2010 Elazığ-Kovancilar Earthquake M_w 6.1) were either entirely or mostly discarded in the SHARE strong-motion database. The NERIES attempt was mostly limited to creating an infrastructure for integrated accelerometric data archive within from Europe. However, the proposed infrastructure focuses on the near-real time accelerograms that are hosted by NERIES portal (www.seismicportal.eu). These recordings are from the last decade with limited engineering significance (i.e. mostly small magnitude events). Moreover, the proposed data archiving and dissemination structure by NERIES is not entirely devised for the engineering needs of accelerometric data use.

Currently, the most up-to-date pan-European strong-motion database is RESORCE (Reference Database for Seismic Ground-Motion in Europe; resorce-portal.eu) that is developed under the SIGMA (Seismic Ground Motion Assessment; projet-sigma.com) project. The primary motivation of RESORCE (Traversa et al. 2014) is to update and extend the ISESD accelerometric archive by using the information gathered from recently carried out strong-motion database projects as well as other relevant earthquake-specific studies in the literature. To this end, RESORCE made use of the already compiled metadata and waveform information from ITACA, T-NSMP, HEAD, SHARE, ISESD and ESMD. The information gathered from these databases were extended by considering the French (French Accelerometric Network; RAP; www-rap.obs.ujf-grenoble.fr) and Swiss (Swiss Seismological Service; SED; seismo.ethz.ch) accelerometric data that are from

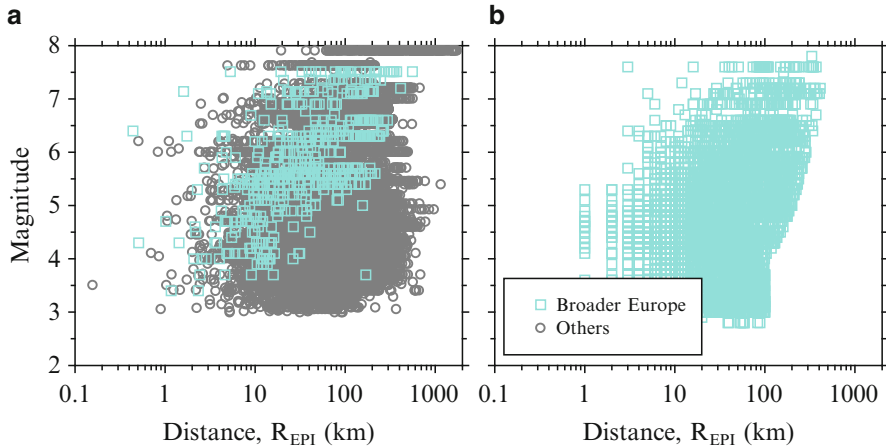


Fig. 12.6 Comparison of (a) NGA-West2 and (b) RESORCE strong-motion databases in terms of magnitude and distance distribution. The NGA-West 2 database contains 21,336 strong-motion recordings and only 2 % of the data is from the pan-European region. The colored data given on the scatter plot of NGA-West2 show the pan-European accelerograms in this database

moderate-to-small magnitude events. The RESORCE developer team also did an extensive literature survey from peer-reviewed journals to improve the earthquake metadata information of earthquakes from the broader Europe. The uniform data processing of accelerograms following the discussions in Boore et al. (2012) as well as improved magnitude and source-to-site distance distributions constitute the other important achievements in RESORCE. The current data size of RESORCE is 5,882 accelerograms recorded from 1,814 events. The number of strong-motion stations included in RESORCE is 1,540. The magnitude and distance range covered by RESORCE is $2.8 \leq M_w \leq 7.8$ and $R_{JB} \leq 370$ km. The strategy followed in the compilation of RESORCE as well as its main features are given in Akkar et al. (2014d) and Sandıkkaya and Akkar (2013). Figure 12.6 compares the magnitude vs. distance distribution of RESORCE and NGA-West2 database (Ancheta et al. 2014) that is used in the development of NGA-West2 GMPEs. The NGA-West2 database covers a small fraction of accelerograms from the broader European region. Thus, the information provided in RESORCE, when used systematically with NGA-West2 database, can be a good basis to understand the significance of regional differences in shallow active crustal earthquakes between Europe and the other parts of the world. Table 12.1 compares the essential features of major strong-motion databases compiled from the recordings of broader Europe. The information presented in Table 12.1 once again confirms that RESORCE contains the most up-to-date data for the broader European region. The main sources of accelerograms are Turkey, Italy and Greece. Yet to be considered in RESORCE, for example, is to extend it by including the strong-motion data of other seismic prone countries in the region (e.g., Iran). To this end, EMME strong-motion database can be a good source but, as indicated previously, differences in database

Table 12.1 Important characteristics of strong-motion databases developed in broader Europe

Database	Years covered	Region	No of Acc	No of Eqs	No of Sta	Data process ^a	Main count ^{s,b}	M range ^c	D range ^c (km)
ISESD	1967	Europe & Middle East	2,213	856	691	Uni EBP	IT, TR & GR	3.0–7.8	0–558
	2004								
ESMD	1973	Europe & Middle East	462	110	261	Ind ABP	IT, TR & GR	4.3–7.6	0–558
	2003								
T-NSMP	1976	Turkey	4,607	2,996	209	Ind ABP	TR	1.6–7.6	0–655
	2007								
ITACA	1972	Italy	2,182	1,004	–	Ind ABP	IT	3.0–6.9	–
	2004								
EMME	1973	Middle East	4,920	1,803	1,260	Ind & Uni ABP	TR & IR	3.1–7.6	0–586
	2011								
RESORCE	1967	Europe & Middle East	5,882	1,814	1,540	Ind ABP	TR & IT	2.8–7.8	0–587
	2012								

^aUni uniform, Ind individual, EBP elliptical bandpass filtering, ABP acausal bandpass filtering

^bGR Greece, IR Iran, IT Italy, TR Turkey

^cM refers to moment magnitude and D refers to epicentral distance

compilation between RESORCE and EMME would create difficulties while integrating these strong-motion archives.

The NERA (Network for European Research Infrastructures for Earthquake Risk Assessment and Mitigation; www.nera-eu.org) project builds a general framework on top of the above summarized efforts by proposing an integral infrastructure for a single, high-quality accelerometric database. The proposed system opts for the adoption of common data and metadata dissemination strategies and standards by forming a well-organized consortium among accelerometric data providers in and around Europe. The efforts to form this consortium have already started under Orfeus (Observatories and Research Facilities for European Seismology; www.orfeus-eu.org) with the contributions of NERA. The consortium will consist of the representatives of accelerometric data networks in the broader Europe for an integrated, sustainable and dynamically growing pan-European strong-motion database. In fact, the prototype of such accelerometric database has already been developed in NERA that is called as Engineering Strong Motion database (ESM_db). If the strong-motion consortium under Orfeus can be firmly established and if this consortium can maintain the so-called ESM_db with high standards, the pan-European endeavor to establish a long-term and reliable accelerometric data archive will make its most future promising progress for the last 40 years. The activities of NERA on accelerometric data networks as well as integrated pan-European accelerometric database are summarized in Akkar et al. (2014e).

12.3 Ground-Motion Prediction Equations (GMPEs) in the Broader European Region

Bommer et al. (2010) and Akkar et al. (2014c) give a detailed review on some of the selected pan-European (global) GMPEs. This paper not only focuses on the evolution of global GMPEs in Europe and surroundings but also discusses the progress in the local European GMPEs by presenting overall statistics on some of the key aspects in these predictive models. We also make comparisons among the local and global GMPEs in Europe and extend these comparisons to NGA-West1 and NGA-West2 GMPEs to emphasize the differences (or similarities) between these ground-motion models. The statistics in this paper are primarily compiled from Douglas (2011). We used the statistics of other reports and papers for GMPEs that are published after Douglas (2011).

Figure 12.7 gives the number of GMPEs developed in the broader Europe as a function of time. The trends given for every decade depict that the number of GMPEs increases significantly after 1990 when strong-motion database compilation and dissemination is accelerated in Europe. (See discussions in the previous section). After 2000, the modelers started to develop GMPEs on elastic spectral ordinates rather than deriving equations only for PGA. This observation may suggest the increased significance of spectral ordinates in engineering design in

Fig. 12.7 Number of GMPEs developed in the broader Europe between 1970 and present. The black vertical bars show the number of GMPEs estimating PGA only. The gray vertical bars display GMPEs estimating pseudo-acceleration spectral ordinates (PSA) and PGA

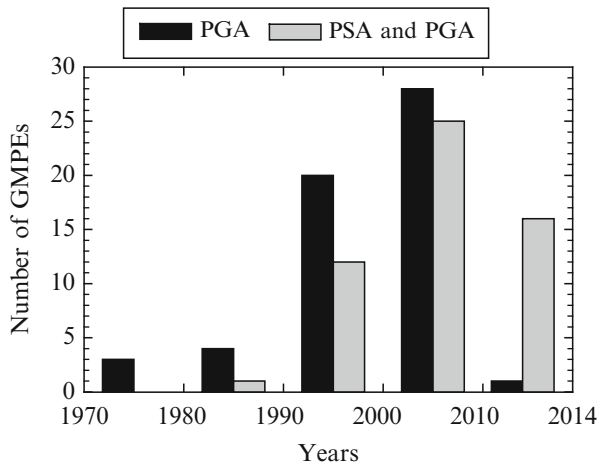
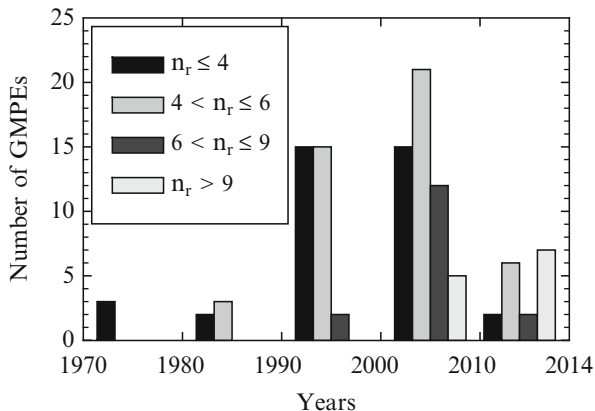


Fig. 12.8 Number of regression coefficients in GMPEs developed in the broader Europe between 1970 and present



Europe after 2000. It may also indicate the improvements in strong-motion databases after mid 90s because computation of spectral ordinates requires implementation of strong-motion data processing on the raw accelerometric data.

Figure 12.8 presents the modeling complexity of GMPEs in the broader Europe. The histogram in this figure shows the change in the number of regression coefficients as a function of time. The majority of functional forms (~80 %) in Europe are relatively simple; consisting of regression coefficients up to 4 ($n_r \leq 4$) or between 5 and 6 ($4 < n_r \leq 6$). GMPEs from the first group ($n_r \leq 4$) are mainly developed before 2000 but their number is still significant in the decade following 2000. The second group GMPEs (i.e., $4 < n_r \leq 6$) has become frequent after 90s that coincides with the commencement of efforts for compiling higher quality databases in Europe. The functional forms with $4 < n_r \leq 6$ generally account for the site effects on ground-motion estimates that constitute the major difference with respect to the GMPEs of $n_r \leq 4$. More complicated GMPEs (i.e., equations having $n_r > 6$) became

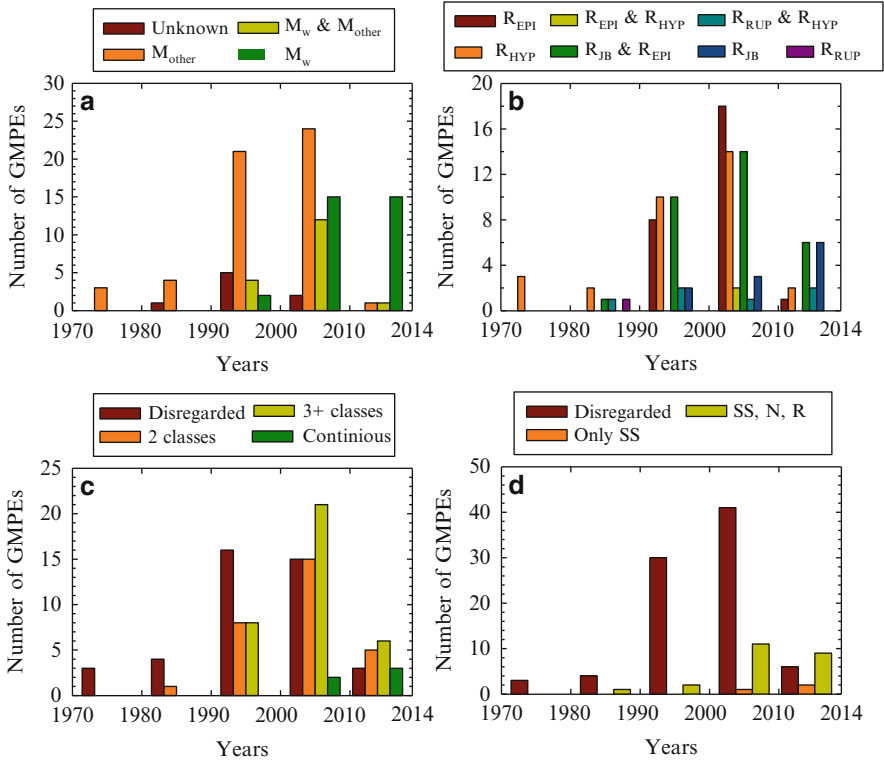


Fig. 12.9 Statistics on (a) preferred magnitude scaling, (b) preferred distance measure, (c) consideration of site conditions and (d) consideration of faulting type in GMPEs developed in the broader Europe. (Explanation of abbreviations in the legends: “Unknown” refers to GMPEs that do not indicate the type of magnitude in their functional forms, “ M_w & M_{other} ” indicates GMPEs combining moment magnitude and other magnitude scales in their functional forms, “ M_{other} ” stands for GMPEs that use magnitude scales other than M_w , GMPEs that combine epicentral and hypocentral distances in their functional forms are abbreviated as “ R_{EPI} & R_{HYP} .” “ R_{JB} & R_{EPI} ” and “ R_{RUP} & R_{HYP} ” are used to indicate GMPEs using epicentral and Joyner-Boore distances and hypocentral and rupture distances, respectively. “Disregarded” stands for functional forms ignoring either site classification or style-of-faulting, “2 classes” and “3+ classes” indicate functional forms considering 2 and 3 or more site classes, respectively. “Only SS” describes GMPEs that treat strike-slip fault mechanism separately in their functional forms and “SS, N, R” is the abbreviation for functional forms that consider the effect of strike-slip, normal and reverse faults on ground-motions)

available after 2000 (more precisely in the last 10 years) because improvements in the database quality in and around Europe have come to a mature level following the dissemination of first pan-European strong-motion database CD-ROM by Ambraseys et al. (2004a). Currently, consideration of site effects and style-of-faulting has almost become standard in the local and global European GMPEs.

Figure 12.9 shows another aspect of modeling complexity in the local and global European GMPEs by giving statistics on the specific features of estimator

parameters. Figure 12.9a presents the time-dependent variation of preferred magnitude scaling in the functional forms. Figure 12.9b displays a similar statistics on the preferred distance measures whereas Figs. 12.9c, d illustrate modeling of soil conditions and faulting type, respectively. The information given in these histograms complements the discussions on Fig. 12.8. The increased quality of strong-motion datasets leads to the utilization of more complicated estimator parameters for developing ground-motion models in the broader Europe. For example, the functional forms of GMPEs developed in the last 15 years generally use moment magnitude (Fig. 12.9a) and consider more rigorous schemes for site effects (Fig. 12.9c). In fact, some of the most recent local and global GMPEs in Europe describe the soil influence on ground motions by using continuous functions of V_{S30} (see Douglas et al. 2014). The use of point-source distance measures⁶ (i.e., epicentral distance, R_{epi} and hypocentral distance, R_{hyp}) that are always appealing among the GMPE developers in Europe reduced after 90s because strong-motion databases started to include extended-source distance measures (i.e., Joyner-Boore distance, R_{JB} and rupture distance, R_{rup}). To this end, GMPEs utilizing only extended-source distance metrics or those that combine extended- and point-source distance metrics have become more frequent in the last 15 years as displayed in Fig. 12.9b. Local and global European GMPEs that use hybrid distance measures (i.e., $R_{\text{RUP}} \& R_{\text{HYP}}$ or $R_{\text{JB}} \& R_{\text{EPI}}$) assume $R_{\text{RUP}} \approx R_{\text{HYP}}$ and $R_{\text{JB}} \approx R_{\text{EPI}}$ for small magnitude events (i.e., $M_w \leq 5.5$).

The discussions in the above paragraphs suggest that the efforts to improve strong-motion databases in the broader Europe result in enhanced local and global European GMPEs. Figure 12.10 shows the country-based distribution of predictive models for shallow active crustal earthquakes in the region of interest. Seismic prone countries that are active in database compilation are also active in developing GMPEs. As we have already emphasized, GMPEs developed from country-based (local) and global (multiple country) datasets are one of the topics of discussion among the seismological research community in Europe. The limitations in local strong-motion datasets due to uneven distribution of main estimator parameters as well as poor quality metadata and waveforms are the arguments augmenting the doubts about the reliability of GMPEs developed from such datasets. However, systematic attempts to improve the national strong-motion databases as well as international projects that make use of these well-studied national databases have brought another insight to such discussions. This point is demonstrated in Figs. 12.11 and 12.12. Figure 12.11 shows the median PGA estimates of local and pan-European GMPEs as a function of distance. The median PGA estimates are computed for a 90° dipping strike-slip earthquake of M_w 6. The selected moment magnitude approximates the central magnitude value of the strong-motion

⁶The point-source distance measures do not consider the source geometry and approximates the ruptured fault segment as a point. The extended-source distance metrics account for the source geometry and can show the variation in ground-motion amplitudes more appropriately for large events at sites closer to the source.

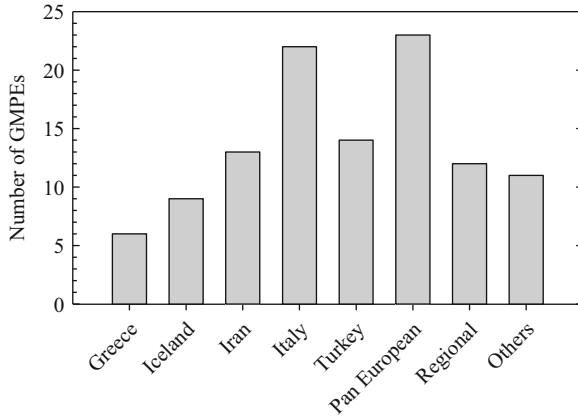


Fig. 12.10 Country-based distribution of GMPEs that are developed in the broader Europe. “Regional” GMPEs are developed from databases of specific regions in and around Europe (e.g., northern Italy, western Balkans, etc.). The label “Others” indicate GMPEs of European countries that are not listed on the horizontal axis of the figure (e.g., France, Switzerland, etc.). The “Pan European” class refers to global GMPEs developed for Europe and surroundings by using strong-motion recordings of multiple countries in and around Europe

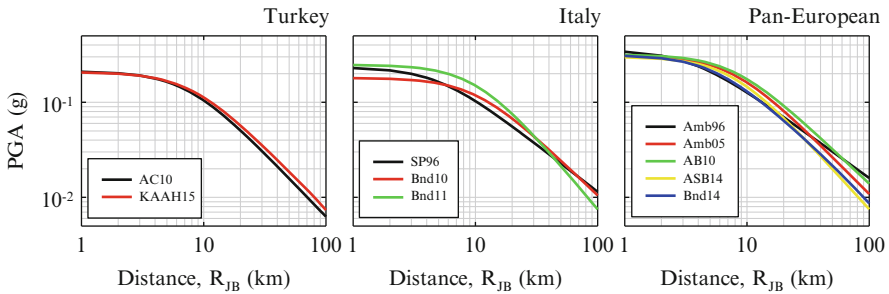


Fig. 12.11 Median PGA trends of some selected Turkish, Italian and pan-European GMPEs for M_w 6 and for a generic rock site

databases used in the development of predictive models compared in these figures. The site considered for the fictitious earthquake scenario is assumed to be rock with $V_{S30} = 760$ m/s. The hypocentral depth is taken as 9.7 km. Note that we try to reduce the likely effects of epistemic uncertainty on the subject discussions by limiting the comparisons to median ground estimations and by using the central magnitude of the databases of compared GMPEs.

The local (country-based) GMPEs are selected from Turkey and Italy as they provide the largest amount of shallow active crustal earthquake recordings to pan-European databases. The ground-motion predictive models from Turkey are Akkar and Çağnan (2010) (AC10) and Kale et al. (2015) (KAAH15). These two recent GMPEs were developed from different versions of strong-motion datasets

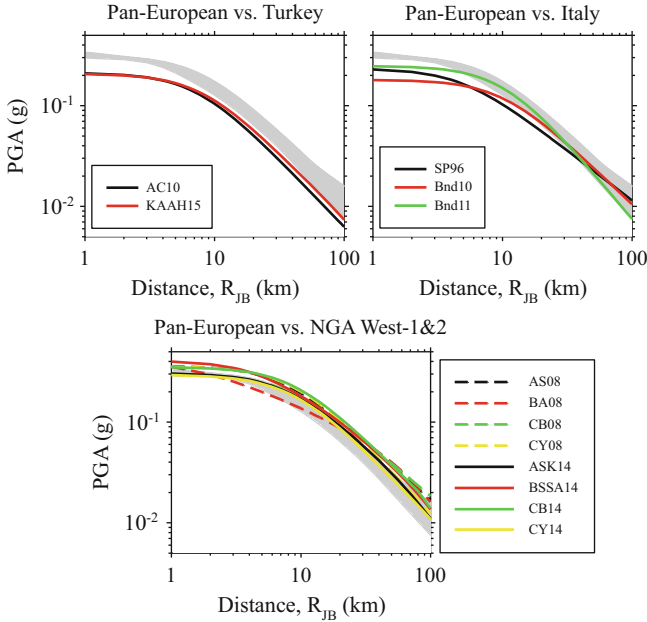


Fig. 12.12 Comparisons of Turkish, Italian as well as NGA-West1 and NGA-West2 GMPEs with pan-European predictive models for the earthquake scenario given in Fig. 12.11. The *gray shaded areas* indicate the lower and upper bound median PGA estimates of pan-European GMPEs

developed from the whole country. In a similar manner, Sabetta and Pugliese (1996) (SP96) and Bindi et al. (2010, 2011) (Bnd10, Bnd11) GMPEs are selected for Italy as their datasets represent the progressive improvements of strong-motion data quality in Italy for the last two decades. The pan-European GMPEs used in the comparative plots [Ambraseys et al. 1996 (Amb96); Ambraseys et al. 2005 (Amb05); Akkar and Bommer 2010 (AB10); Akkar et al. 2014c (ASB14) and Bindi et al. 2014 (Bnd14)] are among the best representatives of global European models at the time when they were developed. The horizontal component definition is geometric mean (GM) in the comparative plots. If any one of the above predictive models is originally developed for a different horizontal component definition, we used the Beyer and Bommer (2006) empirical relationships for its modification for GM. We also used the geometry of fictitious fault to utilize each GMPE with its original distance metric. However, we preferred using Joyner-Boore distance (R_{JB}) in the plots because the distance measure of most of the selected GMPEs for comparison is R_{JB}.

The median PGA curves in Fig. 12.11 depict that the Turkish GMPEs follow each other closely for M_w 6. We observe the similar behaviors within the Italian and pan-European GMPEs. The distance-dependent PGA amplitude estimations of these groups show discrepancies with respect to each other. These observations can indicate the existence of regional differences that is verified by another set of comparisons in Fig. 12.12.

The upper row panels in Fig. 12.12 compare the median PGA estimates from Turkish (left panel) and Italian (right panel) GMPEs with the upper and lower bound median PGA estimates of pan-European GMPEs (represented as the gray shaded area in the panels). Note that the earthquake scenario and the predictive models in Fig. 12.12 are the same ones used in Fig. 12.11. The upper and lower bound median PGA estimates of pan-European GMPEs are compared with those predicted from the NGA-West1 and NGA-West2 GMPEs in the bottom panel of Fig. 12.12. The NGA-West1 GMPEs used in the comparative plots are Abrahamson and Silva (2008) (AS08), Boore and Atkinson (2008) (BA08), Campbell and Bozorgnia (2008) (CB08) and Chiou and Youngs (2008) (CY08). Abrahamson et al. (2014) (ASK14), Boore et al. (2014) (BSSA14), Campbell and Bozorgnia (2014) (CB14) and Chiou and Youngs (2014) (CY14) are the NGA-West2 GMPEs (successors of NGA-West1). The comparisons point differences in the median PGA estimates between the local vs. global European GMPEs. The PGA estimates of global European GMPEs also differ with respect to NGA-West1 and NGA-West2 GMPEs. The level of differences varies as a function of distance. The differences between the local and global GMPE estimates can be interpreted as the significance of regional effects that should be accounted for while developing consistent predictive models in the broader Europe. The discrepancy between the global NGA and pan-European GMPEs advocate the implementation of a similar strategy while estimating the ground-motion amplitudes in the SACRs of broader Europe and the other parts the world. We note that the remarks highlighted from these comparisons should be augmented by further statistical tests to reach more conclusive results about the regional differences in different scales.

12.4 Implications of Using Local and Global GMPEs from Broader Europe in Seismic Hazard

The discussions in the previous section that show the differences between recent local and global GMPEs are deliberately based on a single earthquake scenario (M_w 6; central magnitude) and for median PGA. The selected earthquake scenario and comparisons on median ground-motion estimates would be a first-order approximation to give a clear idea on the level of discrepancies between the considered local and global GMPEs. However, they will fail to give an overall picture to understand how these differences would map onto probabilistic seismic hazard assessment (PSHA). Thus, using the same local and global European GMPEs of the previous case study we present the PSHA results of two specific locations featuring different seismic patterns. We note that running PSHA would show the influence of GMPE sigma and magnitude interval on the estimated ground motions for a given exceedance probability. Moreover, as the local and global European GMPEs discussed in the previous section are frequently used in Europe, the presented PSHA results would be the realistic indicators of how and when the

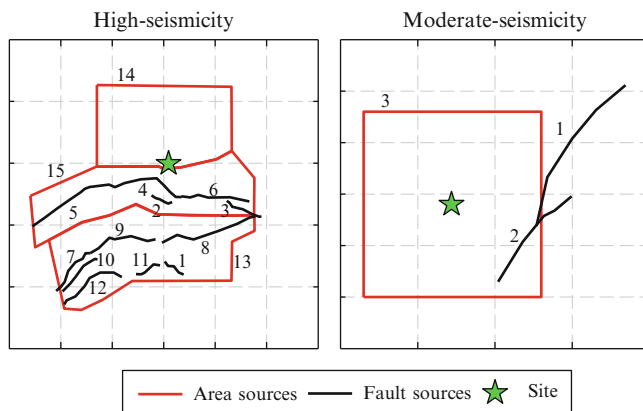


Fig. 12.13 High-seismicity (*left panel*) and moderate-seismicity (*right panel*) sites and corresponding seismic source layouts used in the PSHA case studies

local and pan-European GMPEs would differ from each other as a function of annual exceedance rate and for varying levels of seismicity. We also include the PSHA results of NGA-West2 GMPEs into the comparisons to augment the discussions for the ground-motion estimates between global European and non-European GMPEs. In essence, these case studies will convey a more complete but at the same time more complicated picture about the effects of using local and global European GMPEs on seismic hazard assessment in the broader Europe.

Our PSHA case studies not only focus on PGA but also consider pseudo elastic spectral accelerations (PSA) at $T = 0.2s$, $T = 1.0s$ and $T = 2.0s$ for a broader view about the topic of discussion. PGA is currently the anchor spectral ordinate to describe design ground-motion demand in Eurocode 8 (CEN 2004) whereas the US codes (e.g., ASCE 2010) use spectral accelerations at $T = 0.2s$ and $T = 1.0s$ for design spectrum. PSA at $T = 2.0s$ would show the estimated seismic hazard trends for local and global European GMPEs towards long-period spectral ordinates. Figure 12.13 shows the layouts of two locations used in the PSHA case studies. The location on the left panel is in the vicinity of active faults with significant seismicity. The seismic source pattern is complicated. The activity of seismic sources on the right panel is moderate and the configuration of seismic sources is simpler.

We call these sites (regions) as high seismicity (left panel) and moderate seismicity (right panel). Table 12.2 lists the seismic source parameters and their corresponding values used in PSHA modeling. The seismic source characterization is compiled from different studies in the literature for the locations of interest and they are within the acceptable ranges to reflect the target seismicity level for each study region. Figure 12.14 displays the comparisons of moderate-seismicity hazard curves between Turkish vs. pan-European GMPEs (Fig. 12.14a) and Turkish vs. - NGA-West2 GMPEs (Fig. 12.14b). Figure 12.15 displays the same comparisons for the high-seismicity region. The gray shaded areas in these figures display the upper

Table 12.2 Seismic source parameters used in the PSHA modeling of high-seismicity and moderate-seismicity sites

	Source ID	Type ^a - dip angle	B	\dot{S} (month/year)	v_{Mmin}^b	M_{min}	M_{max}
Moderate Seismicity	1	Strike slip-90°	0.	2.0	–	6.2	6.8
	2	Strike slip-90°	0.	6.0	–	7.0	7.5
	3	Area (strike slip)	2.28	–	1.52	4.0	5.9
High seismicity	1	Strike slip-90°	0.	3.0	–	6.5	7.0
	2	Normal-60°	0.	18.5	–	6.5	7.0
	3	Strike slip-90°	0.	24.0	–	6.5	7.2
	4	Strike slip-90°	0.	24.0	–	6.5	7.5
	5	Strike slip-90°	0.	24.0	–	6.5	7.5
	6	Strike slip-90°	0.	24.0	–	6.5	7.5
	7	Strike slip-90°	0.	3.0	–	6.5	7.2
	8	Strike slip-90°	0.	6.0	–	6.5	7.5
	9	Strike slip-90°	0.	4.5	–	6.5	7.5
	10	Strike slip-90°	0.	3.0	–	6.5	7.5
	11	Strike slip-90°	0.	3.0	–	6.5	7.0
	12	Strike slip-90°	0.	3.0	–	6.5	7.2
	13	Area (strike slip)	2.03	–	2.08	4.0	6.4
	14	Area (strike slip)	1.44	–	0.243	4.0	6.4
	15	Area (strike slip)	1.86	–	2.34	4.0	6.4

^aAnnual slip rate^bMinimum activity

and lower limits of hazard curves computed from the selected Turkish GMPEs (AC10 and KAAH15). The comparative plots for moderate seismicity (Fig. 12.14) depict that both pan-European and NGA-West2 GMPEs tend to give larger values for very short and short periods (i.e., PGA and PSA at $T=0.2s$) with respect to Turkish GMPEs. The NGA-West2 GMPEs estimate lesser ground motions towards longer periods whereas the pan-European models yield similar spectral accelerations as of Turkish GMPEs at longer periods (i.e., $T=1.0s$ and $T=2.0s$). The pan-European GMPEs yield larger spectral values when compared to Turkish GMPEs for the high-seismicity site (Fig. 12.15) for the spectral ordinates considered in the comparisons. The hazard trends between the Turkish and NGA-West2 GMPEs in the high-seismicity region show similarities with those of Fig. 12.14b (i.e., moderate-seismicity case). However, the hazard estimates of these two sets of predictive models (i.e., NGA-West2 and Turkish GMPEs) are closer to each other for the high-seismicity case. The discrepancy between the Turkish and global GMPEs (both European and non-European) increases with decreasing annual exceedance rates in most cases.

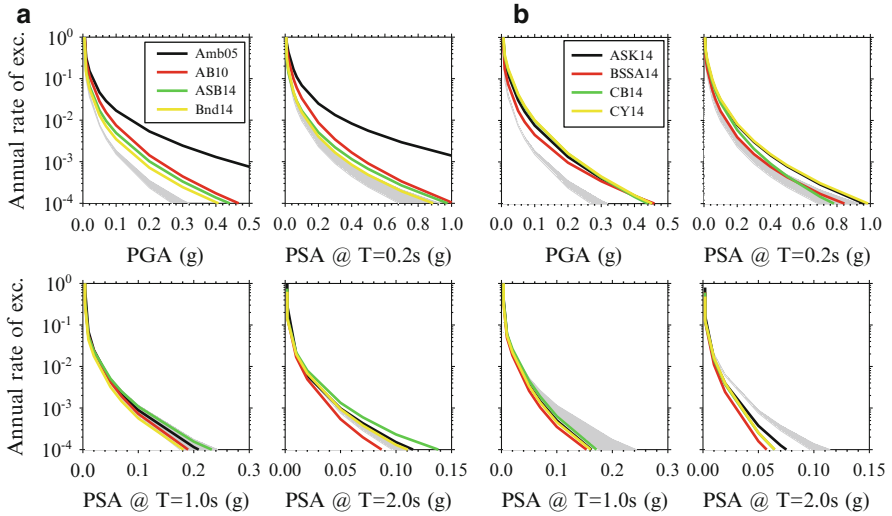


Fig. 12.14 Comparisons of hazard curves for PGA, PSA at T=0.2s, T=1.0s and T=2.0s between (a) Turkish vs. pan-European GMPEs and (b) Turkish vs. NGA-West2 GMPEs for the chosen moderate-seismicity region

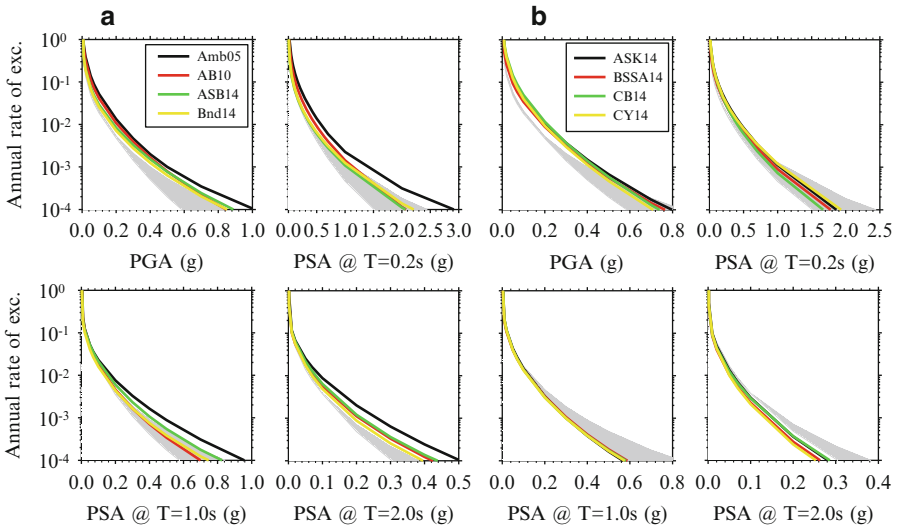


Fig. 12.15 Comparisons of hazard curves for PGA, PSA at T=0.2s, T=1.0s and T=2.0s between (a) Turkish vs. pan-European GMPEs and (b) Turkish vs. NGA-West2 GMPEs for the chosen high-seismicity region

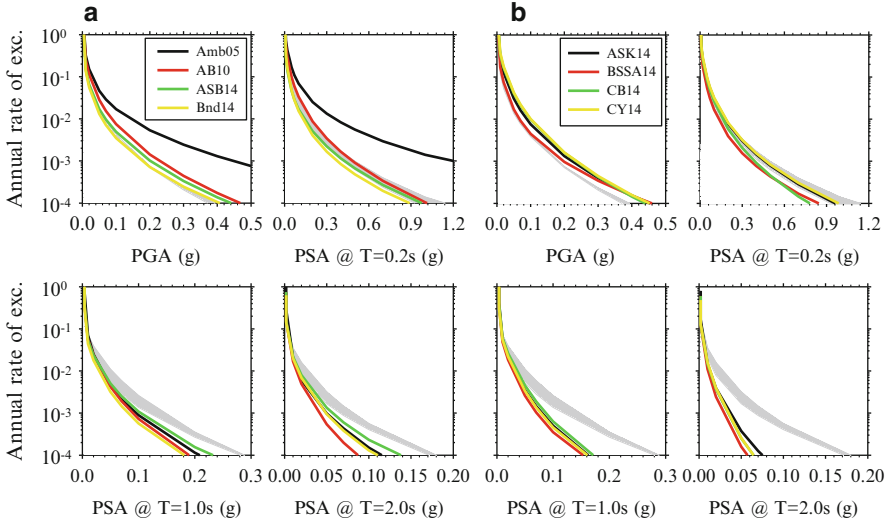


Fig. 12.16 Same as Fig. 12.14 but the comparisons are between (a) Italian vs. pan-European GMPEs and (b) Italian vs. NGA-West2 GMPEs for moderate seismicity

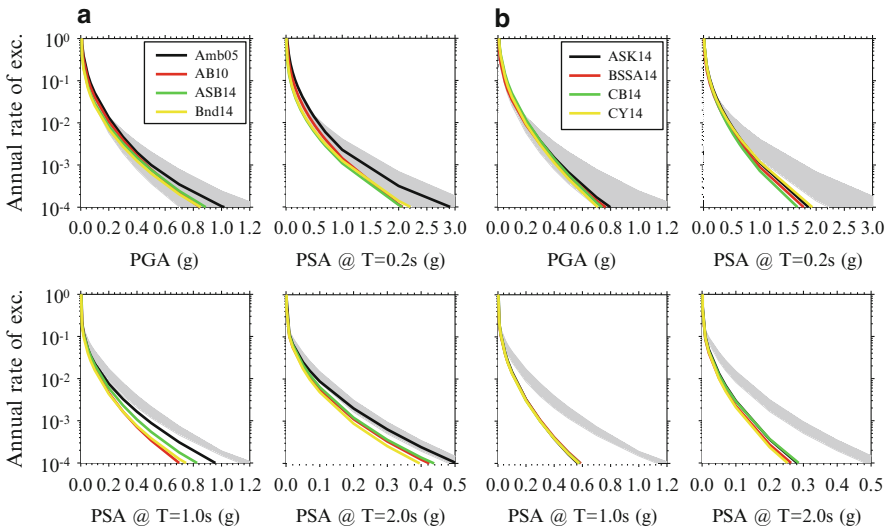


Fig. 12.17 Same as Fig. 12.15 but the comparisons are between (a) Italian vs. pan-European GMPEs and (b) Italian vs. NGA-West2 GMPEs for high-seismicity case

Figures 12.16 and 12.17 make similar comparisons as of Figs. 12.14 and 12.15, respectively, for Italian vs. pan-European and Italian vs. NGA-West2 ground-motion equations. Bnd10 and Bnd11 models are used as the Italian GMPEs because they are developed from the last generation Italian ground-motion datasets. The

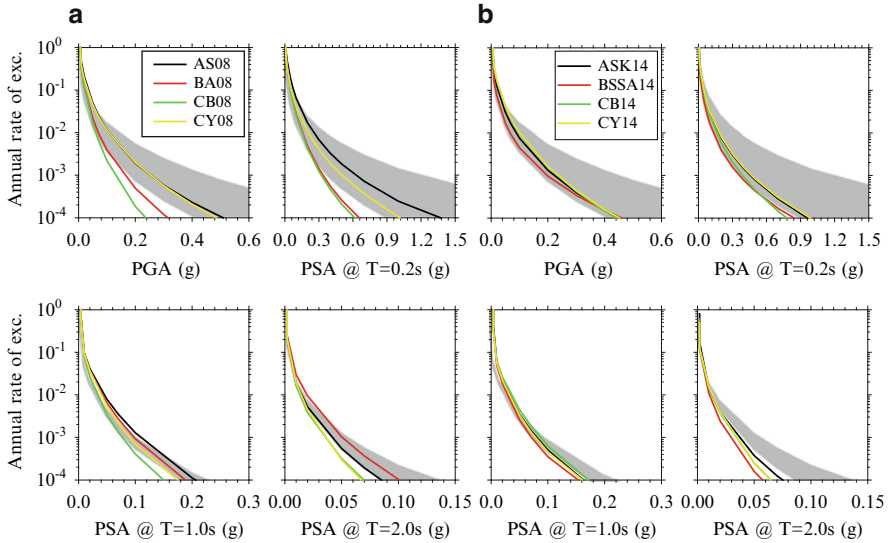


Fig. 12.18 Same as Figs. 12.14 and 12.16 but comparisons are between (a) NGA-West1 vs. pan-European GMPEs and (b) NGA-West2 vs. pan-European GMPEs for moderate-seismicity region

comparisons in Figs. 12.16a, b suggest that the global (i.e., pan-European and NGA-West2 models) and Italian GMPEs yield similar spectral accelerations for PGA and PSA at $T = 0.2\text{s}$. The only exception to this observation is the Amb05 pan-European model that yields significantly different acceleration values with respect to the rest of the GMPEs.⁷ (in fact, Amb05 depicts a significant difference with respect to Turkish GMPEs for short and very-short spectral ordinates as shown in Fig. 12.14). The pan-European and NGA-West2 GMPEs tend to estimate smaller with respect to Italian GMPEs towards longer period spectral acceleration values (i.e., $T = 1.0\text{s}$ and $T = 2.0\text{s}$). The level of underestimation is more significant in NGA-West2 GMPEs. We note that the trends summarized in Fig. 12.16 are fairly valid for Fig. 12.17 as well. In both cases (i.e., moderate- and high-seismicity locations), the decrease in annual exceedance rates triggers larger long-period PSA differences between the Italian and global GMPEs.

The last comparative plots in this section show the differences between the hazard estimates of pan-European, NGA-West1 and NGA-West2 GMPEs. The format and order of the comparative plots follow the previous figures. Figure 12.18 compares the NGA-West1 (Fig. 12.18a) and NGA-West2 (Fig. 12.18b) GMPEs with the pan-European GMPEs for moderate-seismicity case. Figure 12.19 does the same comparison for high seismicity. The shaded areas in these plots represent the

⁷The magnitude-dependent standard deviation of Amb05 attains very large values at small magnitudes that govern the moderate-seismicity case. Although we did not explore the computed hazard results in great detail, we believe that the large sigma of Amb05 at small magnitudes is the major reason behind the inflated short and very-short period PSA by this GMPE.

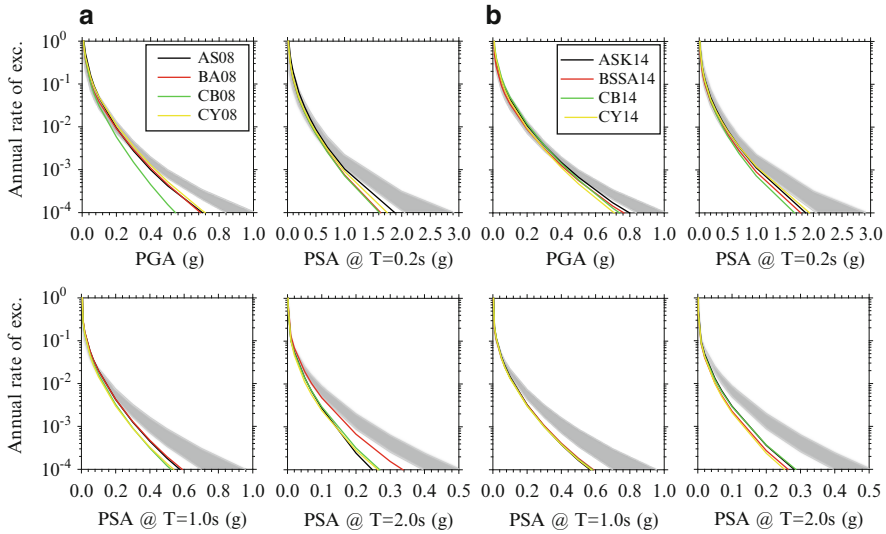


Fig. 12.19 Same as Figs. 12.15 and 12.17 but comparisons are between (a) NGA-West1 vs. pan-European GMPEs and (b) NGA-West2 vs. pan-European GMPEs for high-seismicity region

upper and lower limits of hazard curves computed from the pan-European GMPEs. The comparisons in these figures indicate that NGA models tend to yield smaller spectral accelerations with respect to pan-European GMPEs. The small accelerations are generally more pronounced for NGA-West2 GMPEs. The discrepancy between the European and non-European global GMPEs increases with decreasing annual exceedance rates. This observation is more notable towards longer period spectral accelerations. The underestimations between these two groups of predictive models are also more definite in the high-seismicity case (Fig. 12.19).

The overall discussions in this section indicate that there are differences between the hazard estimates of local and global GMPEs developed from the ground-motion sets of broader Europe. The discrepancies depend on the level of seismicity, annual exceedance rate and spectral period. They are generally significant with decreasing annual exceedance rates (i.e., less frequent but at the same time more critical earthquakes). Note that the local and global GMPEs employed in these case studies are recent and they are developed from reliable local and global databases of Europe. To this end, the highlighted observations from these case studies may partially point the consequential effect of regional differences on seismic hazard.

12.5 Conclusions

The metadata information as well as waveform quality of local and global databases compiled in the broader Europe have shown considerable improvements during the last 15 years due to the grants raised by national and international research programs. This progress has reflected on to the quality and quantity of local and global European GMPEs that are developed in the same period. Our basic analyses indicate that there are differences in the ground-motion estimates of these local and global European GMPEs although their databases are now much more reliable with respect to past. Our comparisons also suggest the existence of similar differences between non-European (NGA) and European global GMPEs. Some part of the observed discrepancies between these ground-motion models can be the attributes of regional differences. Thus, the seismic hazard expert should be aware of such differences among the local and global GMPEs while considering a proper set of GMPEs for the region (site) of interest. Identification of proper GMPEs partly relies on assembling test-bed databases from the strong-motion recordings of the region of interest. Because these specific databases are used for evaluating the candidate GMPEs to establish the most suitable GMPE set for hazard assessment. Such a comprehensive and specific data collection can be done from reliable pan-European strong-motion data archives. Currently, there are ongoing serious efforts among the European research community to establish a good infrastructure for a long-term and integrated accelerometric data archive within the broader Europe. This endeavor is evolving under Orfeus in a systematic manner. The success of this attempt will also lead to the development of more refined GMPEs for the broader Europe for a more proper consideration of regional effects. Such predictive models would certainly increase the accuracy of seismic hazard assessment in Europe and surroundings.

Open Access This chapter is distributed under the terms of the Creative Commons Attribution Noncommercial License, which permits any noncommercial use, distribution, and reproduction in any medium, provided the original author(s) and source are credited.

References

- Abrahamson N, Silva W (2008) Summary of the Abrahamson & Silva NGA ground-motion relations. *Earthq Spectra* 24(1):67–97
- Abrahamson N, Silva W, Kamai R (2014) Summary of the ASK14 ground-motion relation for active crustal regions. *Earthq Spectra* 30(3):1025–1055
- Akkar S, Bommer JJ (2006) Influence of long-period filter cut-off on elastic spectral displacements. *Earthq Eng Struct Dyn* 35:1145–1165
- Akkar S, Bommer JJ (2007) Empirical prediction equations for peak ground velocity derived from strong-motion records from Europe and the Middle East. *Bull Seismol Soc Am* 97(2):511–530

- Akkar S, Bommer JJ (2010) Empirical equations for the prediction of PGA, PGV and spectral accelerations in Europe, the Mediterranean region and the Middle East. *Seismol Res Lett* 81(2):195–206
- Akkar S, Çağnan Z (2010) A local ground-motion predictive model for Turkey and its comparison with other regional and global ground-motion models. *Bull Seismol Soc Am* 100(6):2978–2995
- Akkar S, Çağnan Z, Yenier E, Erdogan Ö, Sandikkaya MA, Gülkan P (2010) The recently compiled Turkish strong-motion database: preliminary investigation for seismological parameters. *J Seismol* 14:457–479
- Akkar S, Kale Ö, Ansari A, Durgaryan R, Askan Gündoğan A, Hamzehloo H, Harmandar E, Tsereteli N, Waseem M, Yazjeen T, Yılmaz MT (2014a) EMME strong-motion database serving for predictive model selection to EMME ground-motion logic-tree applications. Second European conference on earthquake engineering and seismology, İstanbul, Abstract no. 3220
- Akkar S, Sandikkaya MA, Ay BÖ (2014b) Compatible ground-motion prediction equations for damping scaling factors and vertical-to-horizontal spectral amplitude ratios for the broader Europe region. *Bull Earthq Eng* 12(1):517–547
- Akkar S, Sandikkaya MA, Bommer JJ (2014c) Empirical ground-motion models for point- and extended-source crustal earthquake scenarios in Europe and the Middle East. *Bull Earthq Eng* 12(1):359–387
- Akkar S, Sandikkaya MA, Şenyurt M, Azari Sisi A, Ay BÖ, Traversa P, Douglas J, Cotton F, Luzi L, Hernandez B, Godey S (2014d) Reference database for seismic ground-motion in Europe (RESORCE). *Bull Earthq Eng* 12:311–339
- Akkar S, Bossu R, Cauzzi C, Clinton J, D'amico M, Van Eck T, Frobert L, Godey S, Gueguen P, Kästli P, Luzi L, Pacor F, Pequegnat C, Puglia R, Russo E, Sleeman R (2014e) Network of European research infrastructures for earthquake risk assessment and mitigation (NERA) – networking accelerometric networks and Sm Data Users (NA3). Second European conference on earthquake engineering and seismology, İstanbul
- Ambraseys NN (1975) Trends in engineering seismology in Europe. In: *Proceedings of fifth European conference on earthquake engineering*, vol 3. pp 39–52, September 22–25, İstanbul, Turkey
- Ambraseys NN (1990) Uniform magnitude re-evaluation of European earthquake associated with strong-motion records. *Earthq Eng Struct Dynam* 19:1–20
- Ambraseys NN, Bommer JJ (1990) Uniform magnitude re-evaluation for the strong-motion database of Europe and adjacent regions. *Eur Earthq Eng* 4:3–16
- Ambraseys NN, Bommer JJ (1991) Database of European strong-motion records. *Eur Earthq Eng* 5:18–37
- Ambraseys NN, Douglas J, Sigbjörnsson R, Berge-Thierry C, Suhadolc P, Costa G, Smit PM (2004a) Dissemination of European strong-motion data, vol 2. In: *Proceedings of the 13th world conference on earthquake engineering*, Vancouver, British Columbia
- Ambraseys NN, Smit P, Douglas J, Margaris B, Sigbjörnsson R, Olafsson S, Suhadolc P, Costa G (2004b) Internet site for European strong-motion data. *Boll Geofis Teor Appl* 45:113–129
- Ambraseys NN, Douglas J, Sarma SK, Smit PM (2005) Equations for the estimation of strong ground motions from shallow crustal earthquakes using data from Europe and the Middle East: horizontal peak ground acceleration and spectral acceleration. *Bull Earthq Eng* 3(1):1–53
- Ambraseys NN, Simpson KA, Bommer JJ (1996) Prediction of horizontal response spectra in Europe. *Earthq Eng Struct Dynam* 25(4):371–400
- Ambraseys N, Smit P, Berardi R, Rinaldis D, Cotton F, Berge-Thierry C (2000) Dissemination of European strong-motion data, CD-ROM collection. European Commission, Directorate General XII, Science, Research and Development, Environment and Climate Programme, Bruxelles
- ASCE (2010) Minimum design loads for buildings and other structures (7-10). American Society of Civil Engineers, ASCE/SEI7-10

- Ancheta TD, Robert BD, Stewart PS, Seyhan E, Silva WJ, Chiou BSJ, Wooddell KE, Graves RW, Kottke AR, Boore DM, Kishida T, Donahue JL (2014) NGA-West 2 database. *Earthq Spectra* 30(3):989–1005
- Atkinson GM, Morrison M (2009) Observations on regional variability in ground-motion amplitudes for small-to-moderate earthquakes in North America. *Bull Seismol Soc Am* 99(4):2393–2409
- Bindi D, Luzi L, Massa M, Pacor F (2010) Horizontal and vertical ground motion prediction equations derived from the Italian accelerometric archive (ITACA). *Bull Earthq Eng* 8:1209–1230
- Bindi D, Massa M, Luzi L, Ameri G, Pacor F, Puglia R, Augliera P (2014) Pan-European ground-motion prediction equations for the average horizontal component of PGA, PGV, and 5%-damped PSA at spectral periods up to 3.0 s using the RESORCE dataset. *Bull Earthq Eng* 12:391–430
- Bindi D, Pacor F, Luzi L, Puglia R, Massa M, Ameri G, Paolucci R (2011) Ground motion prediction equations derived from the Italian strong motion database. *Bull Earthq Eng* 9:1899–1920
- Beyer B, Bommer JJ (2006) Relationships between median values and between aleatory variabilities for different definitions of the horizontal component of motion. *Bull Seismol Soc Am* 96(4A):1512–1522
- Bommer JJ, Akkar S, Kale Ö (2011) A model for vertical-to-horizontal response spectral ratios for Europe and the Middle East. *Bull Seismol Soc Am* 101(4):1783–1806
- Bommer JJ, Stafford PJ, Akkar S (2010) Current empirical ground-motion prediction equations for Europe and their application to Eurocode 8. *Bull Earthq Eng* 8:5–26
- Boore DM, Atkinson G (2008) Ground-motion prediction equations for the average horizontal component of PGA, PGV, and 5%-damped PSA at spectral periods between 0.01 s and 10.0 s. *Earthq Spectra* 24(1):99–138
- Boore DM, Azari Sisi A, Akkar S (2012) Using pad-stripped acausally filtered strong-motion data. *Bull Seismol Soc Am* 102:751–760
- Boore DM, Stewart JP, Seyhan E, Atkinson GM (2014) NGA-West 2 equations for predicting PGA, PGV, and 5%-damped PSA for shallow crustal earthquakes. *Earthq Spectra* 30(3):1057–1085
- Bozorgnia Y, Abrahamson NA, Al Atik L, Ancheta TD, Atkinson GM, Baker JW, Baltay A, Boore DM, Campbell KW, Chiou BSJ et al (2014) NGA-West2 Research Project. *Earthq Spectra* 30(3):973–987
- Bragato PL, Slejko D (2005) Empirical ground-motion attenuation relations for the eastern Alps in the magnitude range 2.5–6.3. *Bull Seismol Soc Am* 95(1):252–276
- Campbell KW, Bozorgnia Y (2008) NGA ground motion model for the geometric mean horizontal component of PGA, PGV, PGD and 5% damped linear elastic response spectra for periods ranging from 0.01 to 10 s. *Earthq Spectra* 24(1):139–171
- Campbell KW, Bozorgnia Y (2014) NGA-West2 ground motion model for the average horizontal components of PGA, PGV, and 5%-damped linear acceleration response spectra. *Earthq Spectra*. 30(3):1087–1115
- CEN (2004) Eurocode 8: design of structures for earthquake resistance—part 1: General rules, seismic actions, and rules for buildings, EN1998-1:2004. Comité Européen de Normalisation, Brussels
- Chiou BS-J, Youngs RR (2008) An NGA model for the average horizontal component of peak ground motion and response spectra. *Earthq Spectra* 24(1):173–215
- Chiou BS-J, Youngs RR (2014) Update of the Chiou and Youngs NGA model for the average horizontal component of peak ground motion and response spectra. *Earthq Spectra*
- Chiou BS-J, Youngs RR, Abrahamson N, Addo K (2010) Ground-motion attenuation model for small-to-moderate shallow crustal earthquakes in California and its implications on regionalization of ground-motion prediction models. *Earthq Spectra* 26:907–926
- Douglas J (2004) An investigation of analysis of variance as a tool for exploring regional differences in strong ground motions. *J Seismol* 8:485–496

- Douglas J (2007) On the regional dependence of earthquake response spectra. *ISET J Earthq Technol* 44(1):71–99
- Douglas J (2010) Assessing the epistemic uncertainty of ground-motion predictions. In: Proceedings of the ninth US National and 10th Canadian conference on earthquake engineering, July 25–29, Toronto, Ontario, Canada
- Douglas J (2011) Ground-motion prediction equations 1964–2010. *PEER* 2011/102
- Douglas J, Akkar S, Ameri G, Bard P-Y, Bindi D, Bommer JJ, Bora SS, Cotton F, Derras B, Hermkes M, Kuehn NM, Luzi L, Massa M, Pacor F, Riggelsen C, Sandikkaya MA, Scherbaum F, Stafford PJ, Traversa P (2014) Comparisons among the five ground-motion models 1 developed using RESORCE for the prediction of response spectral accelerations due to earthquakes in Europe and the Middle East. *Bull Earthq Eng* 12(1):341–358
- Esteva L, Rosenblueth E (1964) Espectros de temblores a distancias moderadas y grandes. *Boletín Sociedad Mexicana de Ingeniería Sísmica* 2:1–18, In Spanish
- Gregor N, Abrahamson NA, Atkinson GM, Boore DM, Bozorgnia Y, Campbell KW, Chiou BS-J, Idriss IM, Kamaï R, Seyhan E, Silva W, Stewart JP, Youngs R (2014) Comparison of NGA-West2 GMPEs. *Earthq Spectra* 30(3):1179–1197
- Kaklamanos J, Baise LG (2011) Model validations and comparisons of the next generation attenuation of ground motions (NGA-West) project. *Bull Seismol Soc Am* 101:160–175
- Kale Ö, Akkar S, Ansari A, Hamzehloo H (2015) A ground-motion predictive model for Iran and Turkey for horizontal PGA, PGV and 5%-damped response spectrum: investigation of possible regional effects. *Bull Seismol Soc Am* (Submitted)
- Luzi L, Hailemichael S, Bindi D, Pacor F, Mele F, Sabetta F (2008) ITACA (ITalian ACcelerometric Archive): a web portal for the dissemination of the Italian strong motion data. *Seismol Res Lett* 79:716–722
- Massa M, Morasca P, Moratto L, Marzorati S, Costa G, Spallarossa D (2008) Empirical ground-motion prediction equations for northern Italy using weak- and strong-motion amplitudes, frequency content, and duration parameters. *Bull Seismol Soc Am* 98(3):1319–1342
- Power M, Chiou B, Abrahamson N, Bozorgnia Y, Shantz T, Roblee C (2008) An overview of the NGA project. *Earthq Spectra* 24:3–21
- Sabetta F, Pugliese A (1996) Estimation of response spectra and simulation of nonstationary earthquake ground motions. *Bull Seismol Soc Am* 86(2):337–352
- Sandikkaya MA, Akkar S (2013) Reference database for seismic ground-motion in Europe (version 2). EERC-METU, Ankara
- Sandikkaya MA, Yılmaz MT, Bakır BS, Yılmaz Ö (2010) Site classification of Turkish national strong-motion stations. *J Seismol* 14:543–563
- Scasserra G, Stewart JP, Bazzurro P, Lanzo G, Mollaioli F (2009) A comparison of NGA ground-motion prediction equations to Italian data. *Bull Seismol Soc Am* 99:2961–2978
- Strasser FO, Abrahamson NA, Bommer JJ (2009) Sigma: issues, insights, and challenges. *Seismol Res Lett* 80(1):40–56
- Theodulidis N, Kalogeras I, Papazachos C, Karastathis V, Margaritis B, Papaioannou C, Skarlatoudis A (2004) HEAD 1.0: a unified Hellenic accelerogram database. *Seismol Res Lett* 75:36–45
- Traversa P, Akkar S, Ameri G, Cotton F, Douglas J, Frobert L, Godey S, Hernandez B, Luzi L, Sandikkaya MA (2014) REference databaSe fOR seismic groundmotion in Europe. Second European conference on earthquake engineering and seismology, İstanbul
- Tromans JJ, Bommer JJ (2002) The attenuation of strong-motion peaks in Europe. In: Proceedings of twelfth European conference on earthquake engineering, Paper no.394
- Yenier E, Atkinson G (2014) Equivalent point-source modeling of moderate-to-large magnitude earthquakes and associated ground-motion saturation effects. *Bull Seismol Soc Am* 104(3):1458–1478
- Yenier E, Sandikkaya MA, Akkar S (2010) Report on the fundamental features of the extended strong motion databank prepared for the SHARE project. Deliverable 4.1 of seventh framework programme project seismic hazard harmonization in Europe (SHARE), 34 pages, Ankara, p 44

Chapter 13

Towards the “Ultimate Earthquake-Proof” Building: Development of an Integrated Low-Damage System

Stefano Pampanin

Abstract The 2010–2011 Canterbury earthquake sequence has highlighted the severe mismatch between societal expectations over the reality of seismic performance of modern buildings. A paradigm shift in performance-based design criteria and objectives towards damage-control or low-damage design philosophy and technologies is urgently required. The increased awareness by the general public, tenants, building owners, territorial authorities as well as (re)insurers, of the severe socio-economic impacts of moderate-strong earthquakes in terms of damage/dollars/downtime, has indeed stimulated and facilitated the wider acceptance and implementation of cost-efficient damage-control (or low-damage) technologies.

The ‘bar’ has been raised significantly with the request to fast-track the development of what the wider general public would hope, and somehow expect, to live in, i.e. an “earthquake-proof” building system, capable of sustaining the shaking of a severe earthquake basically unscathed.

The paper provides an overview of recent advances through extensive research, carried out at the University of Canterbury in the past decade towards the development of a low-damage building system as a whole, within an integrated performance-based framework, including the skeleton of the superstructure, the non-structural components and the interaction with the soil/foundation system.

Examples of real on site-applications of such technology in New Zealand, using concrete, timber (engineered wood), steel or a combination of these materials, and featuring some of the latest innovative technical solutions developed in the laboratory are presented as examples of successful transfer of performance-based seismic design approach and advanced technology from theory to practice.

S. Pampanin (✉)

Department of Civil and Natural Resources Engineering, University of Canterbury,
Christchurch, New Zealand

e-mail: stefano.pampanin@canterbury.ac.nz

© The Author(s) 2015

A. Ansal (ed.), *Perspectives on European Earthquake Engineering and Seismology*,
Geotechnical, Geological and Earthquake Engineering 39,
DOI 10.1007/978-3-319-16964-4_13

321

13.1 Introduction

The Canterbury earthquakes sequence in 2010–2011 has represented a tough reality check for the international community of seismic engineering, highlighting the severe mismatch between societal expectations over the reality of seismic performance of modern buildings.

In general, albeit with some unfortunate exceptions, modern multi-storey buildings performed as expected from a technical point of view, in particular when considering the intensity of the shaking they were subjected to. As per capacity design principles, plastic hinges formed in discrete predetermined regions, e.g. beam-to-column interface, column-to-foundation and wall-to foundation connections, allowing the buildings to sway and stand and people to evacuate. Nevertheless, in many cases, these buildings were deemed too expensive to be repaired and were consequently demolished leading to the controlled demolition of large portion of the Central Building District of the second largest city in New Zealand and to an economic impact evaluated in the range of 40 Billion NZ\$, corresponding to approximately 20 % of the GDP (Gross Domestic Product).

Targeting life-safety is arguably not enough for our modern society, at least when dealing with new building construction. A paradigm shift in performance-based design criteria and objective towards damage-control design philosophy and technologies is clearly and urgently required.

In general, the next steps in performance-based seismic design should more explicitly focus towards the development of an integrated approach, involving all aspects of design framework, design procedures and tools and technological solutions for engineers and stakeholders to control the performance/damage of the building system as a whole, thus including superstructure, non-structural elements and soil/foundation system.

In the aftermath of the Canterbury Earthquake sequence, the increased public awareness of seismic risk and better understanding on the concept of building performance, has resulted into a renewed appetite for cost-efficient technological solutions to meet the higher public expectations, i.e. sustaining low-level of damage and thus limited business interruption after a design level earthquake.

In additional to more “traditional” damage-control technology as base isolation and supplemental dissipative braces, which are experiencing a resurgence in New Zealand, particular interest is being received by alternative and more recently developed “low-damage” systems, based on post-tensioned rocking mechanisms, combining self-centering and dissipating capabilities, for either concrete, timber and steel.

In such a context, the first and core part of the paper will provide an overview of recent advances and on-going research carried out at the University of Canterbury in the past decade towards the development of a low-damage building system as a whole, within an integrated performance-based framework, including the skeleton of the superstructure, the non-structural components and the interaction with the soil/foundation system.

In the second and conclusive part, examples of real on site-applications of such technology in New Zealand, using concrete, timber (engineered wood), steel or a combination of these materials, and featuring some of the latest innovative technical solutions developed in the laboratory, are presented, as examples of successful transfer of performance-based seismic design approach and advanced technology from theory to practice.

13.2 The Canterbury Earthquake Sequence: A Reality Check for Current Performance-Based Earthquake Engineering

The Mw 6.3 Christchurch (Lyttelton) earthquake occurred at 12.51 pm on Tuesday 22nd Feb 2011, approximately 5 months after the Mw 7.1 Darfield (Canterbury) main shock. Due to the proximity of the epicenter to the Central Building District, CBD, (10 km south-east), its shallow depth (5 km) and peculiar directionality effects (steep slope angle of the fault rupture), significant shaking was experienced in the city centre (Fig. 13.1), the eastern suburbs, Lyttelton-Sumner-Porter Hills areas.

The aftermath counted 185 fatalities, the collapse of several unreinforced masonry buildings and of two reinforced concrete (RC) buildings, extensive damage deemed beyond reparability to several RC buildings, damage to tenths of thousands of (mostly timber) houses. Unprecedented liquefaction effects occurred in whole parts of the city, compromising housing and building foundations as well as causing severe damage and impact on the main infrastructures and lifelines systems of the city including road, water and wastewater networks, and the electricity transmission systems (though quickly restored within 2 weeks). The estimated total losses were in the range of NZ\$ 40 Billion, corresponding to approximately 20 % of the GDP (Gross Domestic Product).

For a more comprehensive information on the overall earthquake impact, the reader is referred to Special Issues dedicated to the Canterbury Earthquake sequence (NZSEE 2010, 2011) and (EERI/NZSEE 2014).

Considering the high level of shaking, as indicated by the acceleration and displacement response spectra of the ground motions recorded in the CBD, shown in Fig. 13.2, the overall behaviour of modern reinforced concrete structures (dominant type of multi-storey building in the CBD) can be classified, in general terms and with some exceptions, as quite satisfactory.

However, the extent of structural damage (Fig. 13.3) was deemed in most cases beyond reparability level, for either technical and/or economical considerations, highlighting the whole controversy of traditional design philosophies, mainly focused on collapse-prevention and life-safety and not yet embracing a damage-control objective.



Fig. 13.1 Skyline of Christchurch CBD before (*Top*) and just after (*bottom*) the 22 Feb 2011 earthquake (Photo taken by Gilly Needham)

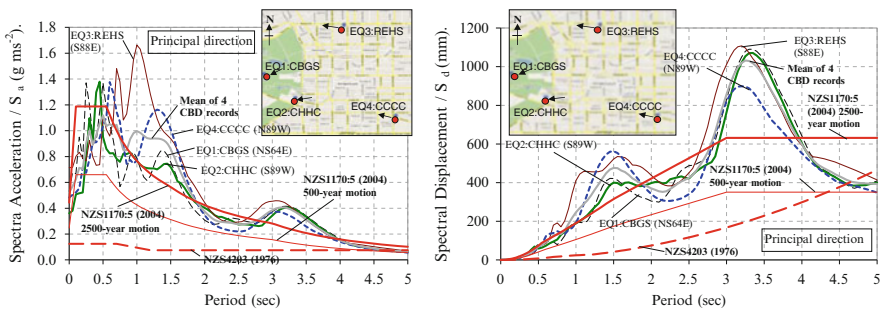


Fig. 13.2 Acceleration and Displacement response spectra from 4 records in the CBD of the 22nd Feb 2011 event, compared with the code design spectra (NZS1170:5 2004) *thick red line* = 1/2,500 years event (MCE); *red line* = 1/500 years event (DBE) (Kam and Pampanin 2011)

As a result, most of relatively modern buildings (mid-1980s and onwards) were demolished. The surprisingly high demolition rate (70 % in the CBD, Fig. 13.4) has been also arguably facilitated by the significant level of insurance coverage for partial or full replacement. In either cases, either demolition or repairing, the level of business interruption and downtime, was very severe and significantly beyond anticipations, also due to the long closure of a widely affected area in the CBD.



Fig. 13.3 Example of damage to RC frames and walls (all these buildings have been demolished) (From Kam et al. 2011; Pampanin 2012)



Fig. 13.4 *Left*: distribution of buildings tagging statistics in the CBD (updated to 12 June 2011, Kam et al. 2011); *Centre*: Aerial view of CBD with entire lots demolished and “cleaned up” (Photo courtesy of Kam Weng and Umut Akguzel); *Right*: CERA Blueprint

A Christchurch Central Recovery Plan (CCRP) has been developed by the Canterbury Earthquake Recovery Authority (CERA)’s Christchurch Central Development Unit (CCDU), outlining the future development of central Christchurch. The Plan incorporated a spatial Blueprint Plan (Fig. 13.4 right), developed by a professional consortium working with CERA/CCDU over a 100 days period and released to the public on 30 July 2012. The Blueprint provides a special framework for the development of the central city, including the locations of ‘anchor’ projects which are expected to stimulate further development.

13.3 Raising the Bar to Meet Societal Expectation: From Life-Safety to Damage Control and Holistic Approach

The excessive socio-economic impacts of the Canterbury earthquakes sequence in 2010–2011 have clearly and critically highlighted the mismatch between the societal expectations over the reality of engineered buildings’ seismic performance.

On one hand, a better communication between technical and non-technical communities could help clarifying and disclosing to the wider public what are the accepted/targeted performance levels built in a design code, itself to be considered a ‘minimum’ (not a maximum) standard. On the other hand, the earthquake engineering community is challenged with the complex task to “raise the bar”, by shifting the targeted performance goals from the typically accepted Life-Safety level (for a design level earthquake or 1/500 years event for an ordinary structure), to a more appropriate and needed Damage-Control level (see performance matrix in Fig. 13.5), all this without increasing (too significantly) the cost of constructions. These increased expectations would require a significant paradigm shift in terms of performance-based design, which can be accomplished by the development and/or further refinement of design methodologies as well as of high seismic-performance, whilst cost-effective, technologies.

More importantly, the next steps in performance-based seismic design should more explicitly focus towards the development of an integrated approach,

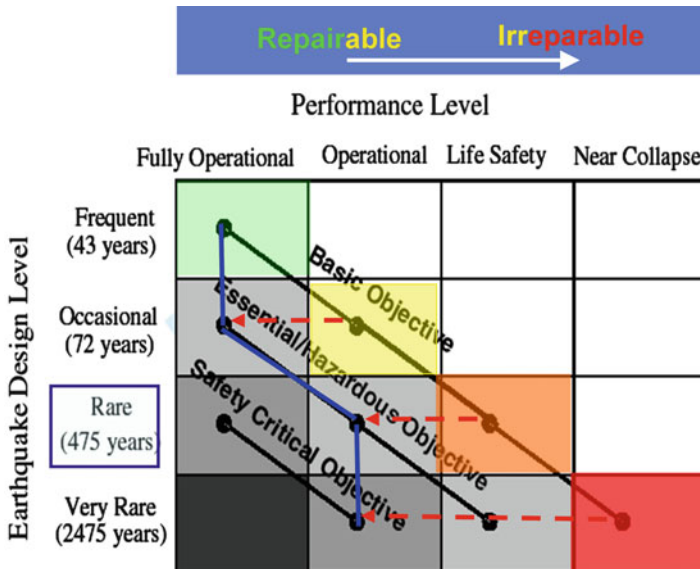


Fig. 13.5 Seismic Performance Design Objective Matrix as defined by SEAOC Vision 2000 PBSE Guidelines, herein rearranged to match building tagging, and proposed/required modification of the Basic-Objective curve towards a damage-control approach (blue line, Modified after Pampanin (2010), Kam et al. (2011))

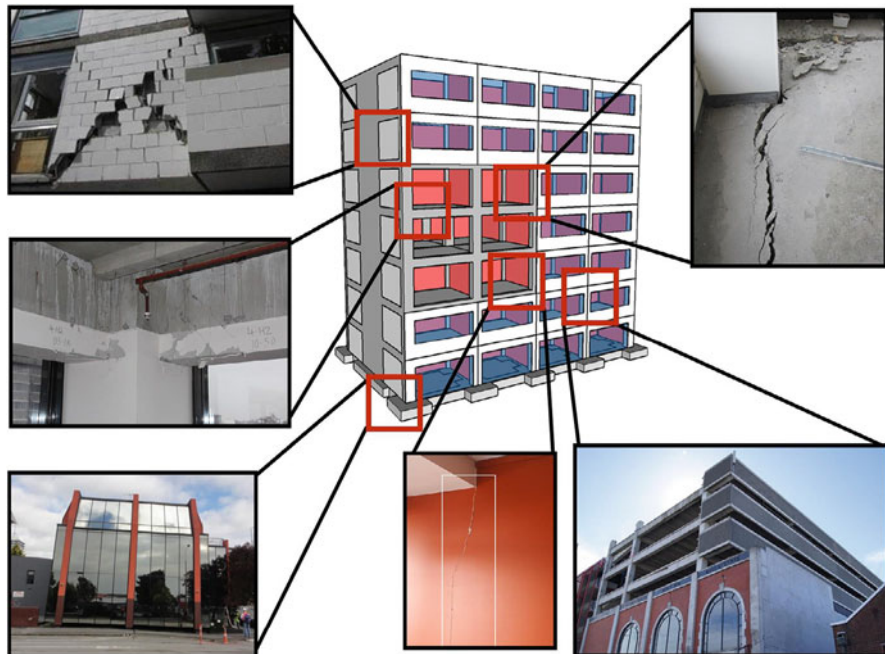


Fig. 13.6 Holistic representation of damage/performance to a modern building, including structural skeleton (frame system, floor diaphragm), non-structural components (lightweight partitions, heavy brick infills and precast concrete facades) and foundation system (significant settlements and residual tilting) (Modified after Johnston et al. (2014))

involving, in a holistic view, all aspects of the design framework, design procedures and tools and technological solutions for engineers and stakeholders to control the performance/damage of the building system as a whole, thus including superstructure, non-structural elements and soil/foundation system (Fig. 13.6).

13.4 The Next Generation of Low-Damage Seismic Resisting Systems

In addition to, or better complementary and integrative of, more “traditional” damage-control technology such as base isolation and dissipative braces, which are experiencing a resurgence in New Zealand after the Canterbury earthquake sequence, particular interest is being received by alternative and more recently developed “low-damage” systems, based on post-tensioned rocking & dissipative mechanisms for either concrete, timber and steel structures.

Such technology, also broadly referred to as PRESSS-technology from its original developments in the 1990s for precast concrete construction under the US PRESSS

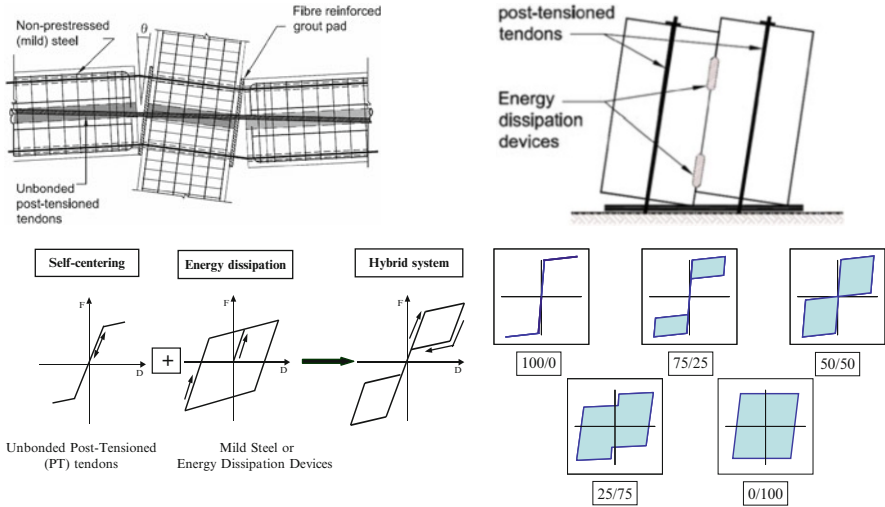


Fig. 13.7 *Top*: Jointed precast “hybrid” frame and wall connections developed in the US PRESSS-Program (*fib* 2003; NZS 3101:2006, NZCS 2010. *Bottom*: flag-shape hysteresis loop for a hybrid system (modified after *fib* (2003)) and effects of varying the ratio between re-centering vs. dissipative contribution (courtesy of Nakaki and Stanton)

Program (Priestley 1991; Priestley et al. 1999), relies upon the use of jointed ductile connections, where structural elements are jointed together through unbonded post-tensioning tendons/strands or bars creating moment-resisting connections. Additional damping and moment contribution can be provided by mild steel rebars either internally located (first generation) or by alternative dissipaters externally located and replaceable (recently developed). The combination of unbonded post-tensioning and additional dissipaters, lead to a so-called hybrid system (Priestley 1996; Stanton et al. 1997). The recentering and dissipative mechanism of a hybrid system, also referred to as controlled rocking, is described by a peculiar “flag-shape” hysteresis behaviour (Fig. 13.6, bottom), whose properties and shape can be modified by the designer by varying the ration between the re-centering and dissipative (moment) contributions, provided by the post-tensioned tendons/bars (and/or axial load) and mild steel/dissipaters, respectively (Fig. 13.7).

During the earthquake shaking, the inelastic demand is accommodated within the connection itself (beam-column, column-to-foundation or wall-to-foundation critical interface), through the opening and closing of an existing gap (rocking motion). The mechanism acts as a fuse or “internal isolation system” with negligible or no damage accumulating in the structural elements, basically maintained in the elastic range. The basic structural skeleton of the building would thus remain undamaged after a major design level earthquake without any need for repairing intervention.

This is a major difference and improvement when compared to cast-in-situ solutions where, as mentioned, damage has to be expected and it is actually

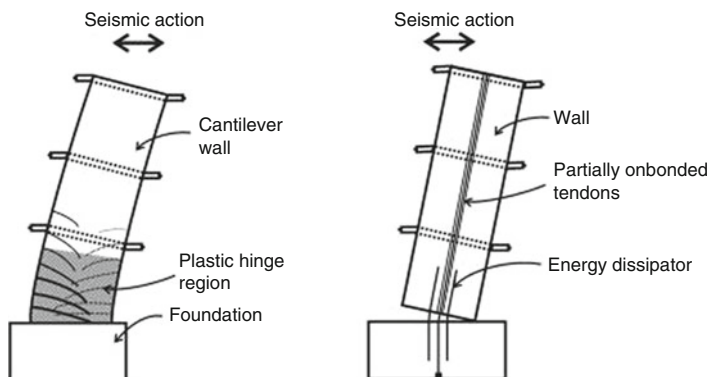


Fig. 13.8 Comparative response of a traditional monolithic system (damage in the plastic hinge and residual deformations) and a jointed precast (hybrid) solution (rocking mechanism with negligible damage and negligible residual deformations *fib* 2003)

accepted to occur in the plastic hinge regions, leading to substantial costs of repairing and business interruption.

The plastic hinge, or sacrificial damage-mechanics, is thus substituted by this “controlled rocking” mechanism (dissipative and re-centering) at the critical interface with no or negligible damage (Figs. 13.8 and 13.18).

13.5 Reparability of the Weakest Link of the Chain: “Plug&Play” Replaceable Dissipaters

In the last decade, extensive research and developments have been carried out at the University of Canterbury in New Zealand on low-damage PRESSS-technology for both concrete and timber structures (buildings and bridges), resulting into the development of a wide range of improvements and new features.

As part of the overall scope, significant effort has been dedicated towards the development of cost-efficient external and replaceable dissipaters, which after an earthquake event could be easily accessed, inspected and, if needed, replaced (Pampanin 2005; Marriott et al. 2008, 2009; NZCS 2010; Sarti et al. 2013). These dissipaters, referred to as “Plug&Play” and consisting for example of axial, tension-compression yielding mild steel short-bar-elements, machined down to the desired “fuse” dimension and inserted and grouted (or epoxied) in a steel tube acting as anti-buckling restrainers, have been developed and extensively tested within several subassemblies configurations, i.e. beam-column joint connections, wall systems, column (or bridge pier)-to-foundation connections (Fig. 13.9).

This option gives the possibility to conceive a modular system with replaceable sacrificial fuses at the rocking connection, acting as the “weakest link of the chain” according to capacity design principles, with the additional feature of being

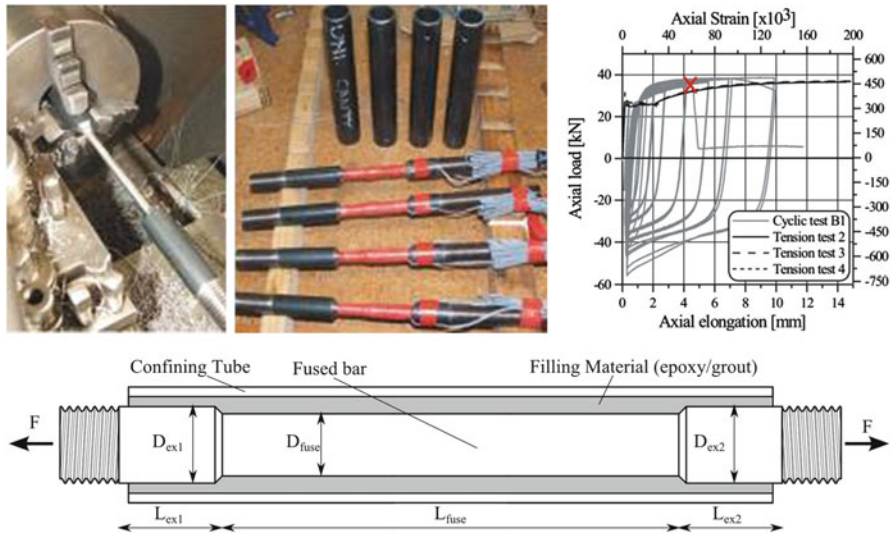


Fig. 13.9 Fused Type “Plug&Play” dissipaters: Manufacturing process and testing (Marriott et al. 2008, 2009); schematic of geometry and element composition (Sarti et al. 2013)

repairable. The traditional assumption “ductility equal to damage” (and consequent repair costs and business downtime) is thus not anymore a necessary compromise of a ductile design (Fig. 13.10).

Either metallic and/or other advanced materials (e.g. shape memory alloys, visco-elastic systems) can be used and implemented to provide alternative type of dissipation mechanisms (elasto-plastic due to axial or flexural yielding, friction, visco-elastic). Examples of application of friction and viscous devices in unbonded post-tensioned systems have been given in Kurama (2001) and Kurama and Shen (2004).

A second generation of self-centering/dissipative high-performance systems, referred to as advanced flag-shape systems (AFS) has been proposed, tested and implemented in real practice (Kam et al. 2006; Marriott et al. 2008; Latham et al. 2013). AFS systems combine alternative forms of displacement-proportional and velocity-proportional energy dissipation (i.e. yielding, friction or viscous damping) in series and/or in parallel with the main source of re-centering capacity (unbonded post-tensioned tendons, mechanical springs or Shape Memory Alloys (SMA) with super-elastic behaviour). As a result, an enhanced and very robust seismic performance, under either far field and near field events (high velocity pulse) can be achieved, as proven by numerical investigations (Kam et al. 2006) and shake table testing (Fig. 13.11) (Marriott et al. 2008).

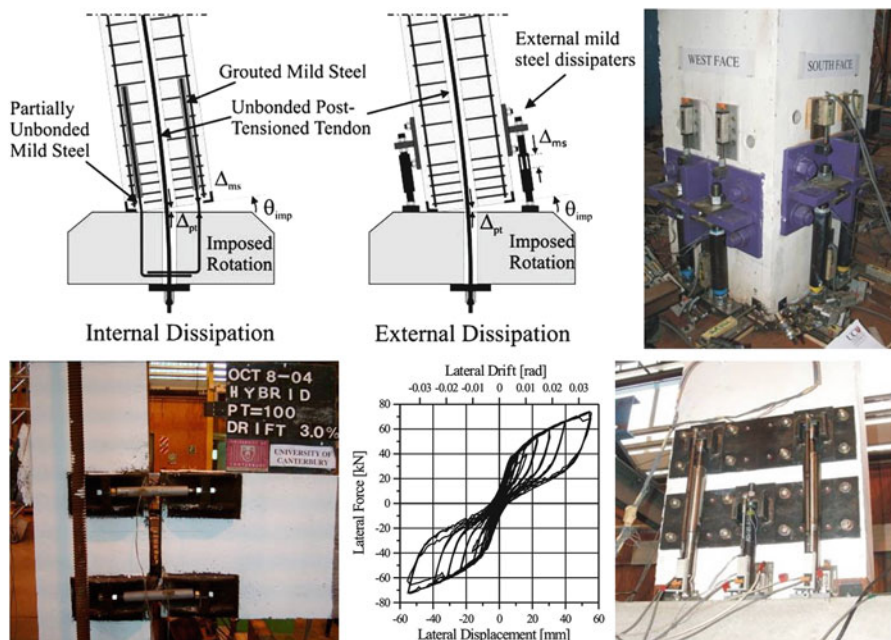


Fig. 13.10 Top: Internal vs. external replaceable dissipaters/fuses in a column/pier. Bottom: Alternative configuration of Plug&Play dissipaters for bc joints or walls (Marriott et al. 2008, 2009, 2010)

13.6 Low-Damage Solution for Multi-storey Timber Buildings: the Pres-Lam System

The concept of post-tensioned hybrid (recentering&dissipating) system has been in the past decade successfully extended from precast concrete to timber (engineered wood) frames and walls (Palermo et al. 2005; Pampanin et al. 2006b). Since 2004, a series of experimental tests, including quasi-static cyclic, pseudodynamic and shake-table, have been carried out on several subassemblies or larger scale structural systems at the University of Canterbury to develop different arrangements of connections for unbonded post-tensioned timber frame and walls (Fig. 13.12).

Due to its high homogeneity and good mechanical properties, laminated veneer lumber (LVL) was initially selected as the preferred engineered wood material for the first phase of the research and development. However, any other engineered wood product as Glulam or Cross-lam (X-lam) can be adopted as shown by recent experimental tests and numerical analyses on both materials (Smith et al. 2014; Dunbar et al. 2014).

The extensive experimental and numerical campaign has provided very satisfactory results and confirmation of the high potential of this new construction

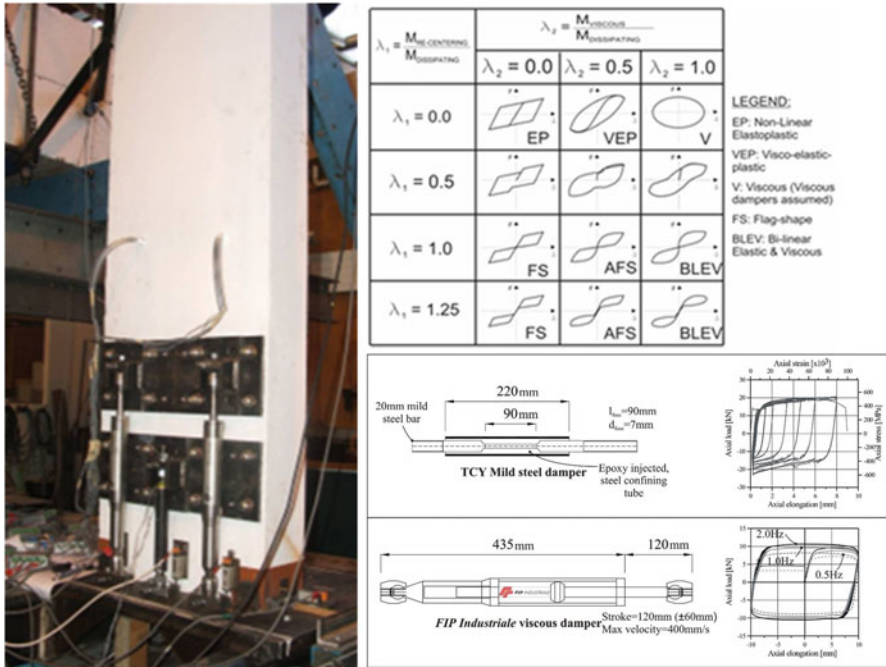


Fig. 13.11 Concept, implementation and experimental validation (*shake-table*) of the concept of Advanced Flag-Shape applied to a post-tensioned wall (Kam et al. 2010; Marriott et al. 2008, 2009). Combination in parallel of hysteretic and viscous dampers

system, referred to as a Pres-Lam system (acronym for Prestressed Laminated timber). The extension of low-damage systems to engineered wood solutions opens new opportunities for much greater use of timber and engineered wood products in multi-storey and large buildings, using innovative technologies for creating high quality buildings with large open spaces, excellent living and working environments, and resistance to hazards such as earthquakes, fires and extreme weather events (Buchanan et al. 2011).

Examples of on-site applications of structural frames, walls, combination of them and hybrid material construction will be given in the later part of this paper.

13.7 Controlling and Reducing the Damage to the Floor-Diaphragm

The peculiarity of a jointed ductile connection, consisting of an “articulated” assembly of precast elements, can be further exploited and extended to the design of floor-to-lateral-load-resisting-system connections in order to minimize and control the damage to the diaphragms, as observed in recent earthquakes.

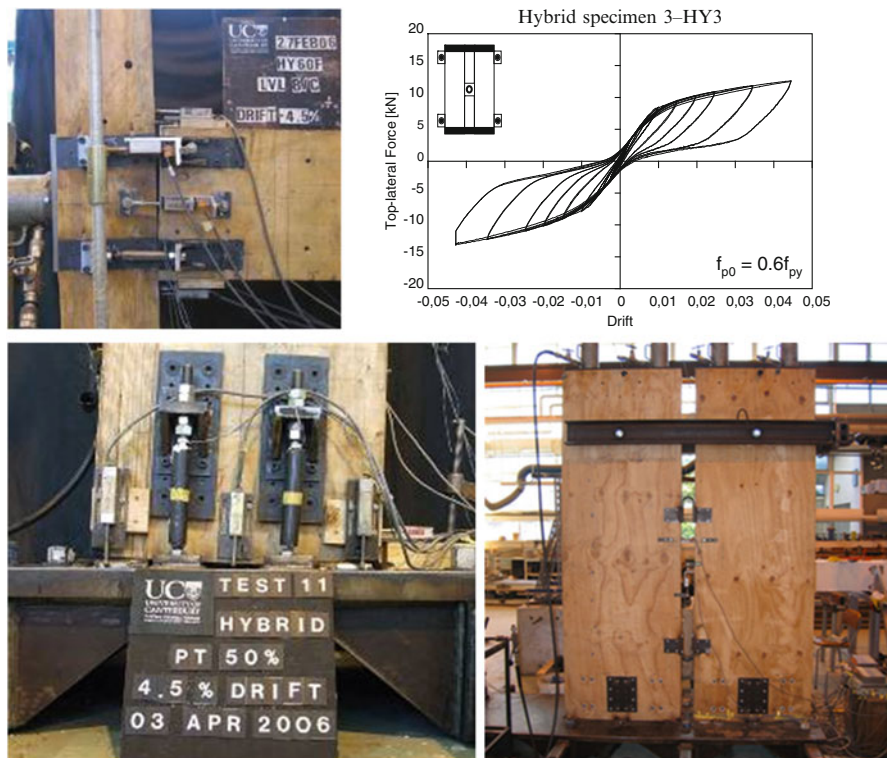


Fig. 13.12 Testing of hybrid post-tensioned timber (Pres-Lam) beam-column joints, column-to-foundation connections and coupled walls with replaceable dissipaters (Palermo et al. 2005, 2006)

The latter topic has been receiving a growing attention in the engineering community in the last decade, following the several examples of poor performance of floor-diaphragm observed in recent earthquakes, including the Canterbury earthquake sequence (Fig. 13.14 right). Damage to the floor diaphragm can compromise the structural performance of the whole building when not leading to collapse of entire floors.

During the seismic response of a building, significant displacement incompatibilities issues can arise between the main lateral resisting systems (frames and walls) and the floor-diaphragm. In general terms they can be classified into vertical incompatibility (primarily associated to the wall response and uplifting, but also incurred into frames) and horizontal incompatibility (more typical of frame system subject to beam elongation effects, Fenwick and Megget 1993).

In the case of walls, regardless of them being based on a rocking mechanism or on a monolithic plastic hinge behaviour, the development of inelastic action at the base (in the form of a concentrated or distributed plastic hinge) result into a geometrical uplifting of the wall. If the axial load (or additional post-tensioning) acting on the wall is not sufficient to re-center the system, at each subsequent cycle

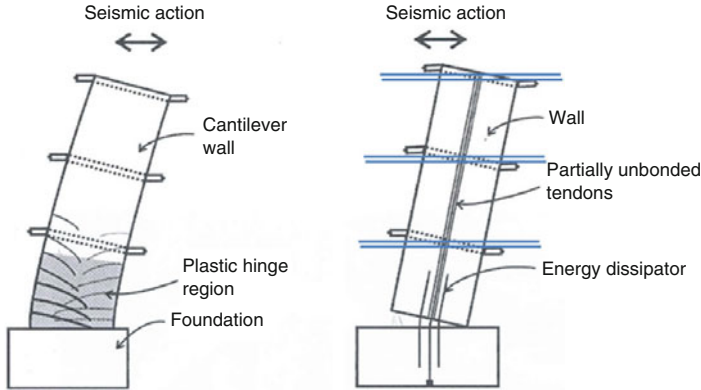


Fig. 13.13 Vertical displacement incompatibility between a ductile shear wall (uplifting) and the floor system. *Right*: slotted shear key solution to accommodate the relative movement (after *fib* 2003)

with larger ductility demand, the wall would tend to vertically elongate (beam elongation effects in the vertical directions). The resulting interaction with the floor-diaphragm can lead either to significant deformation and damage to the floor system itself (see Fig. 13.13b) and/or to an unexpected brittle mechanism in the walls due to the significant increased level of axial and shear forces acting in the wall (see Fig. 13.3). A conceptual solution to limit this effect is to develop connection details between wall and floors able to accommodate the relative vertical movement of the two systems while transferring the shear forces. An example of a practical solution to achieve this scope was proposed of in the PRESSS Five-Storey building tested at UCSD in 1999 at the culmination of the PRESSS Program and later adopted in the *fib* guidelines on seismic design of precast concrete construction (*fib* 2003, see Fig. 13.13 right): the shear connection between walls and floors should resemble the behavior of a shear key in the horizontal direction and be inserted into a vertical slot to accommodate the vertical displacement incompatibility.

Alternative solutions could include the use of a flexible (vertically, while stiff as needed horizontally) transfer/tie beams as well as cast-in-situ (timber infill) units adjacent to the wall, so to spread the localized relative deformation demand to a wider area.

When dealing with frame systems, both vertical and horizontal displacement compatibility issues between the lateral resisting systems and the floor-diaphragm can arise, as highlighted by a series of experimental tests on 3-dimensional performance of precast super-assemblages including frames and hollowcore units (Fig. 13.14) (Matthews et al. 2003; Muir et al. 2012)

Alternative innovative solutions have been recently developed and proposed in literature to minimize the damage to the floor system due to displacement

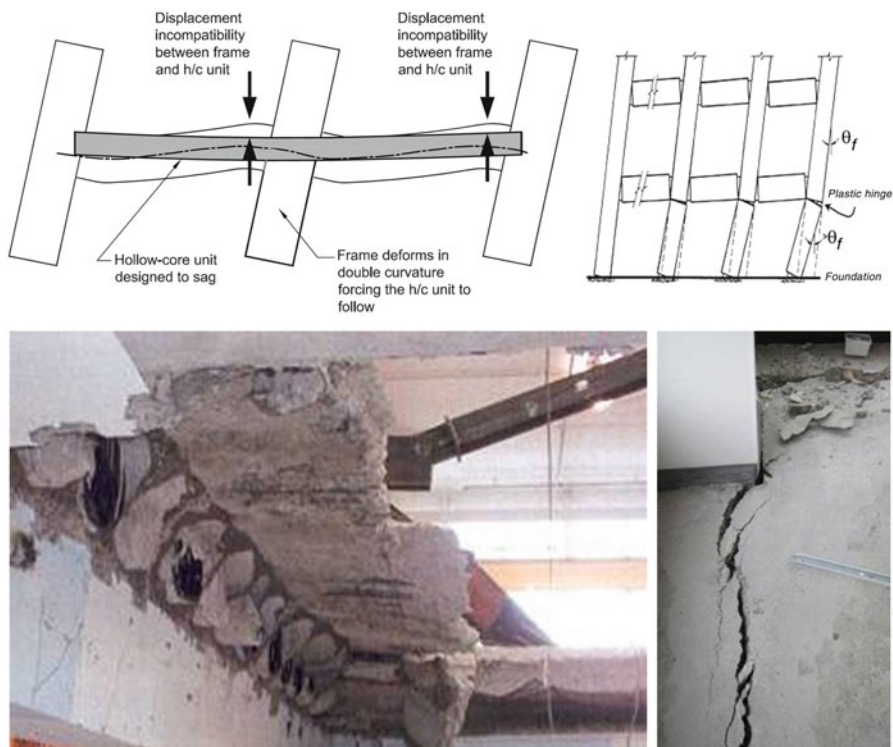


Fig. 13.14 Top: Example of vertical (left: after Matthews et al. 2003) and horizontal (due to beam elongation effects) displacement incompatibility (right: after fib 2003). Bottom: collapse of floor units in an 3-D experimental superassemblage test (left: after Matthews et al. 2003) and extensive damage to the diaphragm topping of precast concrete floors in a multi-storey building following the 22 Feb 2011 Canterbury Earthquake (right: after Kam et al. 2011)

incompatibilities with the response of the seismic resisting frame, while guaranteeing a reliable diaphragm action.

A jointed “articulated” floor system

The first approach is based on the concept of an articulated or “jointed” floor system to be combined with precast rocking/dissipative frames (Amaris et al. 2007, 2008). According to this proposed solution, developed from the original concept of discrete X-plate mechanical connectors implemented in the Five-Storey PRESSS Building tested at UCSD (Priestley et al. 1999, Fig. 13.15), the floor (hollowcore in this case) units are connected to the beams by mechanical connectors, acting as shear keys when the floor moves orthogonal to the beam and as sliders when the floor moves parallel to the beam (Fig. 13.16).

As a result, the system is able to accommodate the displacement compatibilities demand between floor and frame by creating an articulated or jointed mechanism, which is effectively decoupled in the two directions. Also, due to the low flexural stiffness of the shear keys-connectors in the out-of-plane directions, torsion of the



Fig. 13.15 “X-connectors” between precast floor (pre-topped double-tee) units and frames as implemented in the PRESS Five Storey Building (Priestley et al. 1999)

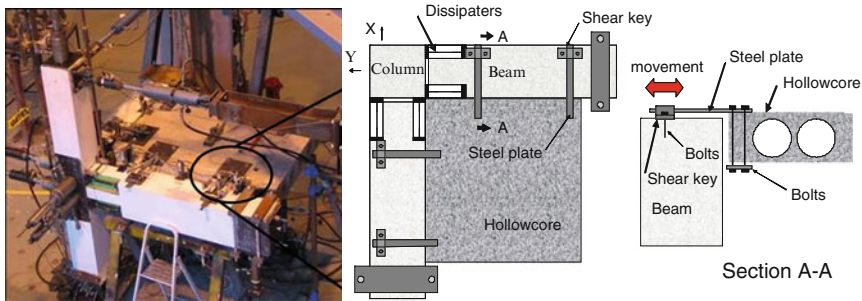


Fig. 13.16 “Articulated floor” system. Concept, connection details and response under uni-directional and bi-directional cyclic tests (Amaris et al. 2007, 2008)

beam elements, due to pull out of the floor or relative rotation of the floor and the edge support, can be limited.

A relatively simple design option which can reduce the extent of floor damage due to beam elongation is to use a combination of walls and frames to resist lateral loads, with walls in one directions and frames in the other. If the precast one-way floors run parallel to the walls and orthogonal to the frame, the elongation effects of the frame to the floor are reduced. This approach can be combined with partial de-bonding of the reinforcing bars (starters) in the concrete topping, and the use of a thin cast-in-situ slab or “timber infill” slab in the critical regions adjacent to the beams, to enhance the capacity to accommodate relative deformations.

Top Hinge “Non-tearing floor” solution

An alternative method to prevent/control damage to the floor-diaphragm due to beam elongation effects can rely upon a newly developed “top-hinge” or “top-hung” system in combination with a standard floor solution (i.e. topping and continuous starter bars). In its general concept, the top hinge allows the relative

rotation between beams and column to occur and the bottom reinforcement to yield in tension and compression. The presence of a slot or gap on the bottom part of the beam prevents direct contact between beams and columns, thus avoiding the beam elongation and the consequent tearing action on the floor. A debonded length is adopted in the bottom steel rebars to prevent premature buckling, as per a typical PRESSS jointed ductile connections.

The development of this concept originates from the evolution of the Tension-Compression Yield-Gap connection (TCY-Gap), developed during the PRESSS-Program, which used internally grouted mild-steel bars on the top, unbonded post-tensioned tendons at the bottom and a slot/gap at the interface between column and beam. Such solution would prevent the beam elongation effect but not the tearing action to the floor due to the opening of the gap at the top of the beam. An intermediate improved version would consist of an “inverted” TCY-Gap solution based on a single top hinge with the gap and the grouted internal mild steel bars placed in the bottom part of the beam. This modification, as per the “slotted beam” connection proposed by Ohkubo and Hamamoto (2004), for cast-in-situ frames (without post-tensioning), would succeed in preventing both elongation and tearing effects in the floor, but would not yet be capable of providing re-centring due to the location and straight profile of the tendons.

A further conceptual evolution and details refinement have led to the development at the University of Canterbury of what is referred to as a “non-tearing floor” beam-column connection which could be combined with any traditional floor system (Amaris et al. 2007, 2008; Au et al. 2010; Muir et al. 2012; Pampanin et al. 2006a). Based on a series of experimental testing on interior, exterior beam column subassemblies and on 2-D and 3D frame building specimens, a number of solutions have been developed, either with or without post-tensioning, and ranging from partially to fully precast connection (Fig. 13.17).

Similar considerations on displacement compatibilities issues apply, in general, to low-damage (controlled rocking) timber connections.

A series of experimental testing have been carried out at University of Canterbury to investigate the extent of displacement incompatibilities and propose technical solutions to reduce or mitigate their effects (Moroder et al. 2013, 2014). In addition to proving the efficiency of a number of different connection detailing, the experimental results showed that the flexibility of the timber elements, combined with proper connection detailing, can provide some additional allowance to mitigate damage to the floor diaphragm at high level of interstorey drift demand.

13.8 Low-Damage Solutions for Non-structural Elements

A rapid and wide implementation of low-damage structural systems, capable of protecting the main “skeleton”, including frames, walls and floor diaphragm from extensive damage at a design level earthquake would already be a major achievement. The next step towards the development of that “ultimate earthquake



Fig. 13.17 “Non tearing floor” or top-hinge solution: *Top left*: schematic (left, Muir et al. 2013) and comparison of damage to plastic hinges (*Top centre and right*) and to the floor (*bottom left and right*) from the testing of a 3-D superassemblage implementing a top-hinge solution (*top centre and bottom left*, Muir et al. 2012) vs. a traditional beam-column connection (*top right* from MacPherson 2005, *bottom right*, Lindsay 2004)

proof” building that the society expects would be to “dress” such structural skeleton with a compatible low-damage envelope and fit-outs, including all non-structural components (infills/partitions, facades, ceilings, services and contents).

Valuable tentative recommendations/suggestions have been proposed in the past in the form of pair of limit states or performance requirements for both structural and non-structural elements (e.g. FEMA 450 2003; FEMA E-74 2011). Yet, practical cost-efficient solutions for low-damage resisting non-structural elements for the daily use of practitioners and contractor need to be specified and developed.

Not unexpectedly, the sequence of strong aftershocks that followed the main event of the Canterbury earthquakes (4 September 2010 Darfield earthquake), caused significant and repetitive damage to the non-structural components requiring continuous and expensive repairing.

In parallel to the refinements of low-damage structural systems, a substantial effort has been dedicated at the University of Canterbury since 2009 (thus well before the main earthquake event) to the development of low-damage

non-structural components (Palermo et al. 2010), with focus on either vertical elements, e.g. infills/partitions (Tasligedik et al. 2012) and façades (Baird et al. 2011), or horizontal, e.g. ceilings (Dhakal et al. 2014).

In the case of infilled walls, either being lightweight partitions (drywalls) or “heavy” concrete or clay brick infills (more typical of the European Construction practice), the conceptual solution for a low-damage system is based once again on the possibility to create an articulated mechanism or jointed system, so to accommodate the interstorey drift demand through a sort of internal rocking mechanism of smaller panels with concentrated inelastic behaviour in few discrete locations, between adjacent panels and between panel and surrounding frame (Fig. 13.19). The low-damage infilled wall solutions were able to sustain 2–2.5 % interstorey drift, under quasi-static cyclic loading, corresponding to the maximum code-allowed demand under a design level earthquake, without evident cracking/damage, thus well beyond the expected performance of traditional infilled walls and in line with the ideal expectation of a more resilient building system.

Full details of the experimental campaign and suggested construction details can be found in Tasligedik (2014) and Tasligedik et al. (2014) (Fig. 13.18).

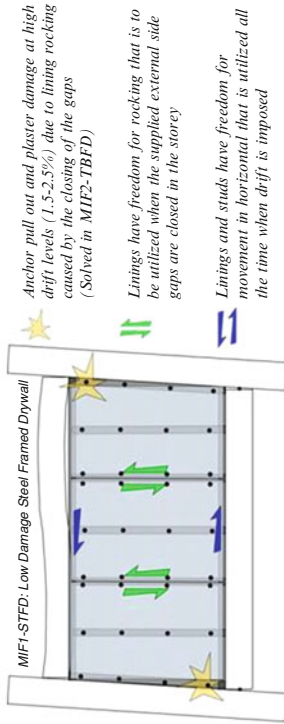
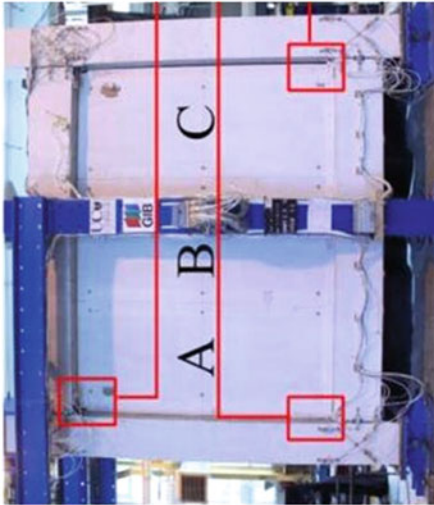
In the case of precast concrete facades/claddings, a number of connection solutions and detailing has been tested, ranging from traditional ones relying upon rods of different length, to slotted-bolted connections, to innovative solution with dissipative U-shape Flexural Plates (Kelly et al. 1972; Priestley et al. 1999), widely adopted in PRESS or Pres-Lam structures as dissipative coupling systems for rocking walls. The target strategy could be either a full disconnection between the façade and the bare structures or a controlled disconnection with additional dissipation capability provided by ad-hoc designed elements (i.e., UFP). For detailed information the reader is referred to Baird et al. (2014) (Fig. 13.19).

13.9 First Prototype Test Building with Integrated Low-Damage Solutions

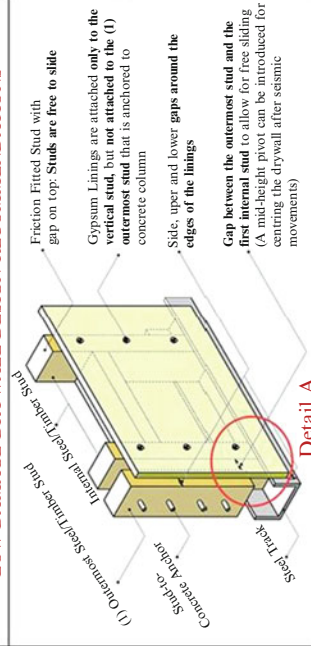
In the previous paragraph, an overview of the recently developed low-damage solutions for both structural and non-structural systems, capable to withstand high levels of drift with negligible damage has been presented, including dry jointed ductile connections for frames and walls, articulated floor solutions, low damage infilled walls (drywall/partitions) and low damage facade/cladding connections.

As inherent part of any research and development such solutions have been developed, refined and tested independently (mostly under quasi-static cyclic testing).

The next challenge towards the development of an integrated low-damage resisting building system would be to assess the feasibility and seismic performance



LOW DAMAGE DRYWALL DESIGN RECOMMENDATIONS



LOW DAMAGE UNREINFORCED CLAY BRICK INFILL WALL DESIGN RECOMMENDATIONS (Shown on a single skin)

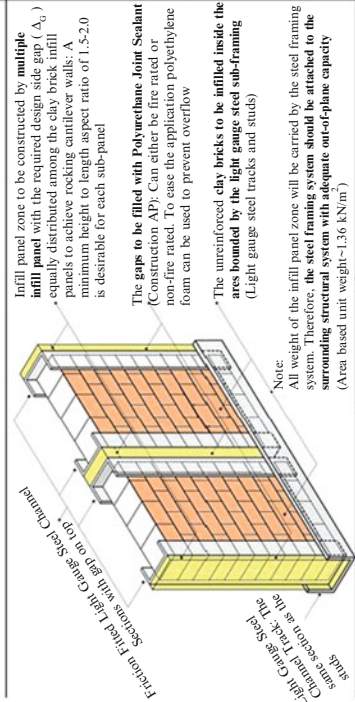


Fig. 13.18 Low-damage solution for infilled walls/partitions (After Tasligedik et al. 2014)

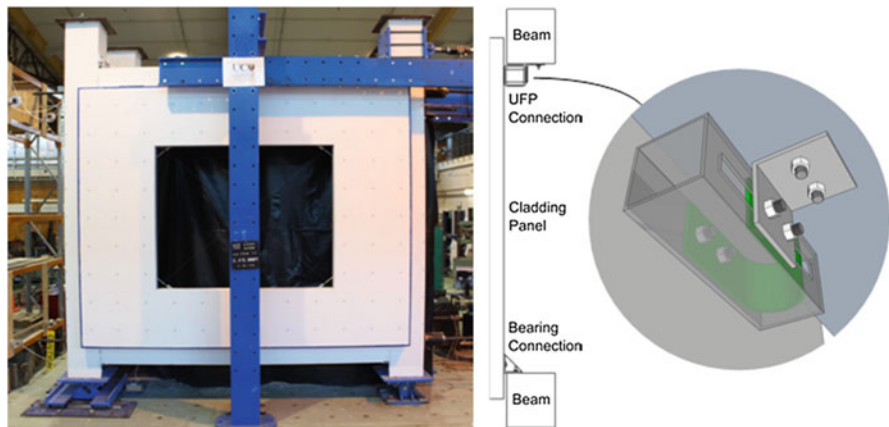


Fig. 13.19 Low-damage solution for precast concrete facades with UFP dissipative connectors (After Baird et al. 2014)

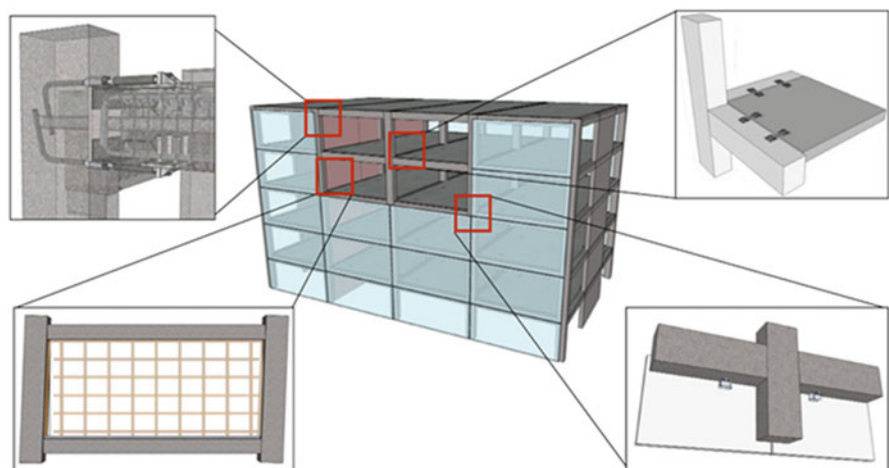


Fig. 13.20 Low-damage building system prototype (After Johnston et al. 2014)

of a building system prototype combining the aforementioned low-damage solutions for both skeleton and envelope (Fig. 13.20).

With this scope, shake table tests of a two storey, 1/2 scale, concrete frame building consisting of a post-tensioned rocking hybrid frame and incorporating an articulated floor solution (with U-shape Flexural Plates), low damage drywall infills and façades were carried out (Johnston et al. 2014). An overview on design, fabrication, set-up and preliminary shake table testing can be found in Johnston et al. (2014). The test building was tested under different configurations and subjected to over 400 earthquakes of different intensity levels, with no evident

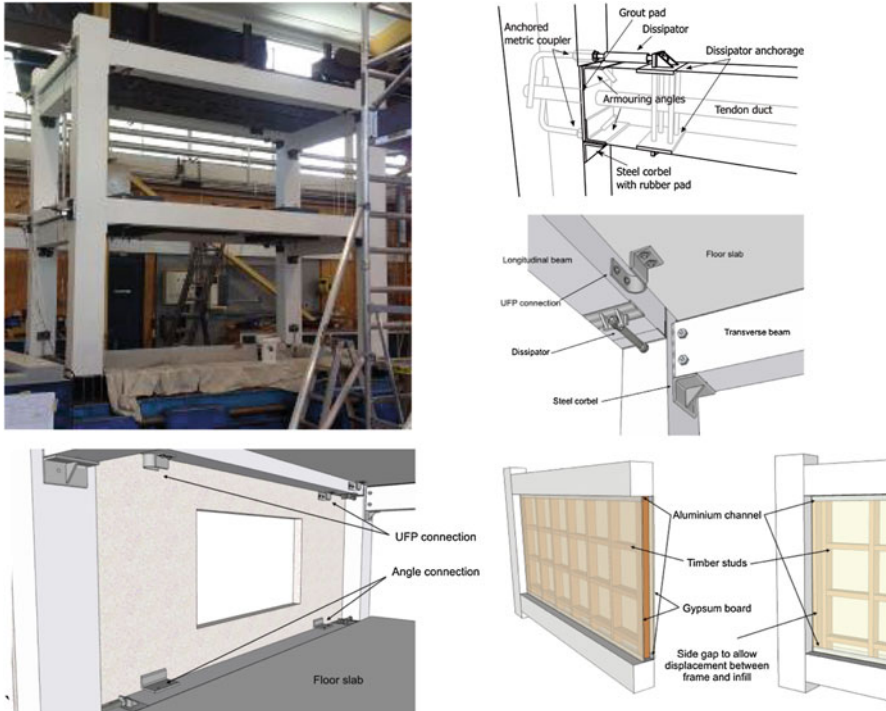


Fig. 13.21 Low-damage test-building (After Johnston et al. 2014)

level of structural and non-structural damage. More information can be found in Johnston et al. (2014) and in future publications under preparation (Fig. 13.21).

13.10 Towards an Integrated Structure-Foundation Performance-Based Design

The Canterbury earthquake has emphasised the actual impact (in terms of final outcome: demolition vs. repair) of combined damage to the superstructures and the foundation-soil system (Fig. 13.22, Giorgini et al. 2012, 2014). The area of Soil-Foundation-Structure Interaction has received in the past decades a substantial attention reaching a significant maturity. Yet, there is strong need to convert the available information into practical guidelines for an integrated structure-soil-foundation performance based design. This would require the definition and setting of specific and jointed limit states for the superstructure and the foundation and suggest the corresponding design parameters to achieve that “integrated” level of performance. In the aftermath of the reconstruction of Christchurch, this issue is

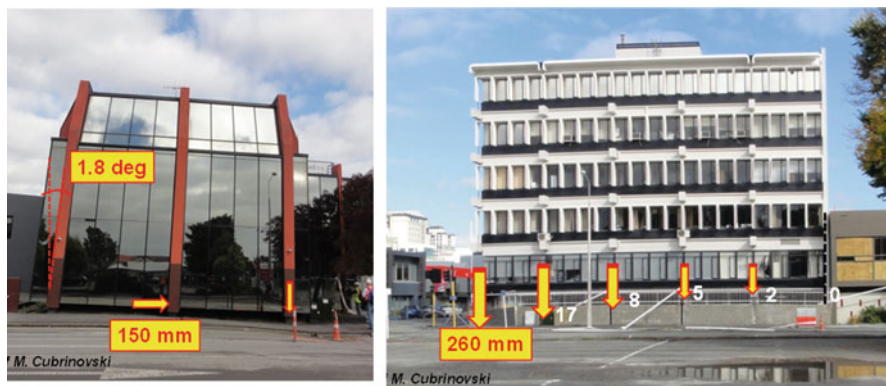


Fig. 13.22 Example of significant tilting and differential settlement in buildings in the CBD after the 22 Feb 2011 Canterbury Earthquake (From Giorgini et al. 2012, 2014)

becoming more apparent, as the designers of new buildings are requested by the clients to be able to specify the targeted overall performance of the building, thus including the superstructure (skeleton and non-structural elements) and foundation-soil system.

An attempt to develop a framework for an integrated structure-foundation performance-based design approach where limit stated and associated damage of superstructure and foundation can be combined into a performance matrix with defined objective and criteria is under-going at the University of Canterbury. More information on the overall integrated framework and on the more specific displacement based design approach can be found in Giorgini et al. (2014) and Millen et al. (2014), respectively (Fig. 13.23).

13.11 On Site Implementation of Low-Damage PRESSS and Pres-Lam Technology

The continuous and rapid developments of jointed ductile connections using PRESSS-technology for seismic resisting systems have resulted in a wide range of alternative arrangements currently available to designers and contractors for practical applications.

On site implementations of PRESSS-technology buildings have happened in different seismic-prone countries around the world, e.g. U.S., Central and South America, Europe and New Zealand. Overviews of research and developments, design criteria and examples of on-site implementations can be found for concrete structures in Pampanin (2005) and in the PRESSS Design Handbook (2010).

In the following sections, focus will be given to some implementations in New Zealand, highlighting the novel features resulting from the more recent experimental and numerical research and developments and presenting some

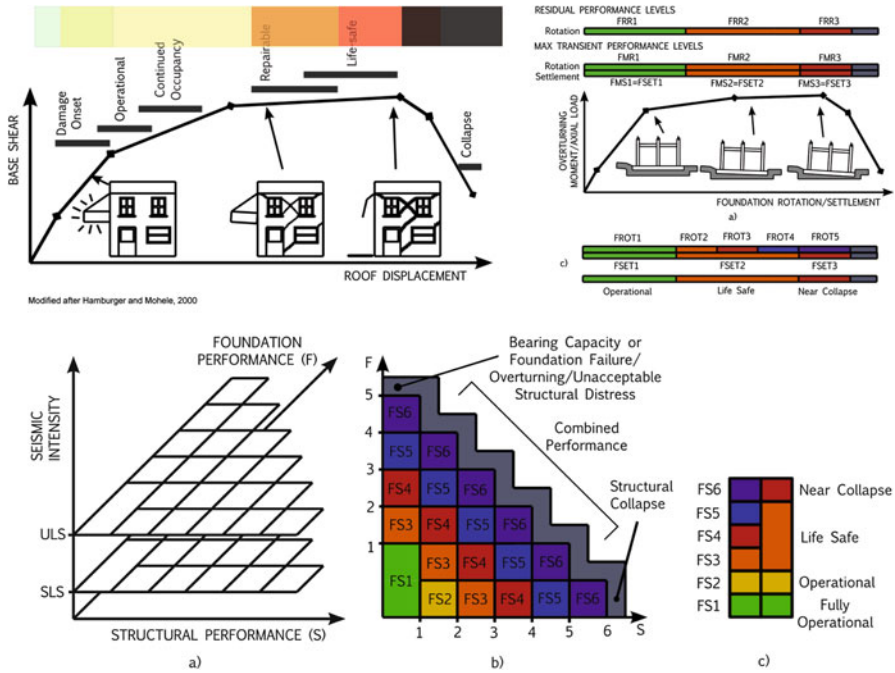


Fig. 13.23 Concept of a performance matrix (*bottom*) for integrated structure-foundation design combining limit states for structure (*top left*) and foundation (*top right*) (Giorgini et al. 2014)

more recent case studies designed and constructed following the Canterbury earthquake sequence in 2010–2011.

PRESSS (concrete) Buildings

The first multi-storey PRESSS-building in New Zealand is the Alan MacDiarmid Building at Victoria University of Wellington (Fig. 13.24), designed by Dunning Thornton Consulting Ltd. The building has post-tensioned seismic frames in one direction and coupled (by slender coupling beam yielding in flexure) post-tensioned walls (precast sandwich panels) in the other direction, with straight unbonded post-tensioned tendons. The seismic-resisting systems feature some of the latest technical solutions previously described, such as the external and replaceable dissipaters in the moment-resisting frame at both the beam-column connections and the base-column connections. Another novelty was the use of a deep cap-beam to guarantee rocking of the walls at both the base and the top sections (Cattanach and Pampanin 2008). This building was awarded the NZ Concrete Society’s Supreme Award in 2009 and several other innovation awards.

The design and construction of the second PRESSS-Building in New Zealand and first in South Island followed at close distance and is represented by the Endoscopy Consultants’ Building in Christchurch, designed for Southern Cross Hospitals (SCH) Ltd by Structex Metro Ltd (Fig. 13.25). Also in this case both

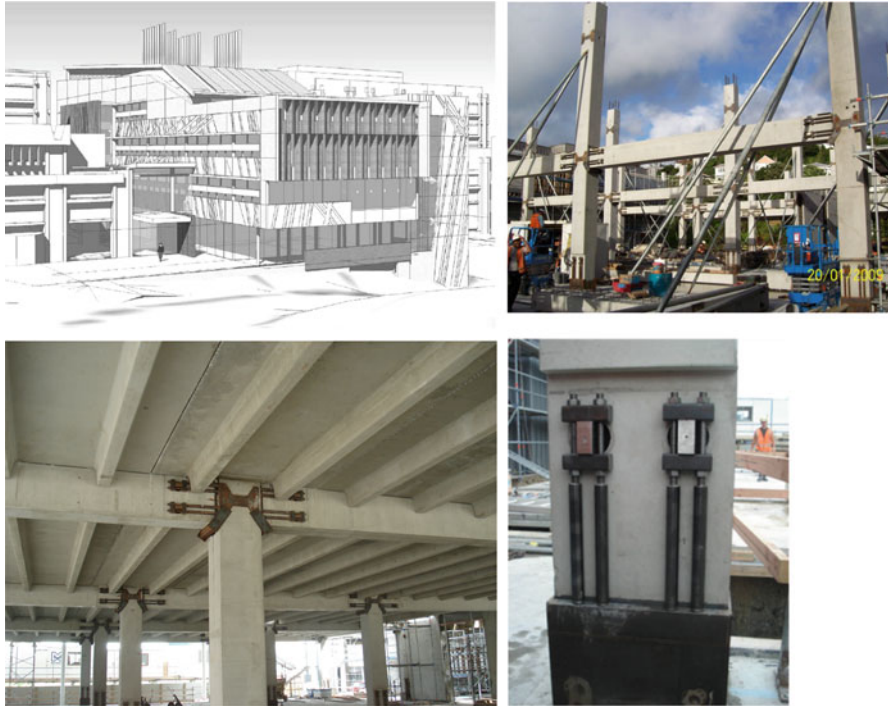


Fig. 13.24 First multi-storey PRESSS-Building in New Zealand (Structural Engineers: Dunning Thornton Consultants; Cattanach and Pampanin 2008)

frames and coupled walls were used in the two orthogonal directions. The post-tensioned frame system relies upon a non-symmetric section reinforcement with internal mild steel located on the top of the beam only and casted on site along with the floor topping. The unbonded post-tensioned walls are coupled with UFPs.

The building passed with high performance the very severe tests of the Canterbury earthquake sequence in 2010–2011. The more devastating 22 February 2011 ground motion was very close to the hospital with a very high level of shaking. Only minor or cosmetic damage was sustained by the structural system. The medical theatres containing very sophisticated and expensive machineries were basically operational the day after the earthquake. One of the main features in the design of a rocking-dissipative solution is in fact the possibility to tune the level of floor accelerations (not only drift) to protect both structural and non-structural elements including content and acceleration-sensitive equipment. More information on the design concept, performance criteria, modelling and analysis, construction and observed seismic behaviour can be found in Pampanin et al. (2011).

The Police Station in Rotorua (North Island, New Zealand) is a three storey building designed as a critical facility (or importance level IL4) with post-tensioned



Fig. 13.25 Southern Cross Hospital Endoscopy Building, Christchurch Rendering, construction of the frame, details of beams, walls and U-shape Flexural Plate dissipaters (Structural Engineers: Structex Metro, Pampanin et al. 2011)

rocking/dissipative concrete (PRESSS) walls in both directions, implementing external and replaceable (Plug & Play) dissipaters (Fig. 13.26)

Pres-Lam (timber) Buildings

Following the research described on post-tensioned timber (Pres-Lam) buildings at the University of Canterbury, several new post-tensioned timber buildings have been constructed in New Zealand incorporating this technology. The world’s first commercial building using a Pres-Lam system is the Nelson Marlborough Institute of Technology (NMIT) building, constructed in Nelson. This building has vertically post-tensioned timber walls resisting all lateral loads as shown in Fig. 13.27 (Devereux et al. 2011). Coupled walls in both direction are post-tensioned to the



Fig. 13.26 Police Station in Rotorua. Post-tensioned concrete (PRESSS) walls with external & replaceable dissipaters in both directions (Structural Engineers: Spiire)



Fig. 13.27 Nelson Marlborough Institute of Technology, (NMIT), Nelson, New Zealand. Post-tensioned timber (Pres-Lam) walls coupled with UFPs (Structural Engineers Aurecon; Architects Irving-Smith-Jack, Devereux et al. 2011)



Fig. 13.28 Carterton Events Centre, New Zealand. Single-storey building with LVL truss roof (Designed by Opus International: Dekker et al. 2012)

foundation through high strength bars with a cavity allocated for the bar couplers. Steel UFP devices link the pairs of structural walls together and provide dissipative capacity to the system. The building was opened in January 2011.

The Carterton Events Centre, located 100 km north of Wellington, is the second building in the World to adopt the Pres-Lam system (Fig. 13.28). Post-tensioned rocking walls were designed as the lateral load resisting system (six walls in one direction and five in the other direction). The post-tensioning details are similar to the NMIT building, while internal epoxied internal bars are used for energy dissipation.

The University of Canterbury EXPAN building (Fig. 13.29) was originally a two-third scaled prototype building tested in the laboratory under severe bi-directional loading conditions (Newcombe et al. 2010) After a successful testing programme, the building was demounted and re-erected as the head office for the Research Consortium STIC (Structural Timber Innovation Company Ltd). Due to the low mass, the connections of the remounted building ended up being post-tensioned only without dissipation devices. The light weight of the structure allowed the main timber frames of the building to be post-tensioned on the ground and lifted into places.

The new College of Creative Arts (CoCa) building for Massey University's Wellington campus (Fig. 13.30) is the first to combine post-tensioned timber (Pres-Lam) frames with innovative draped post-tensioning profiles to reduce deflections under vertical loading. Additional dissipation is added in the frame directions by using UFP devices, placed horizontally and activated by the relative movement between (some of) the first floor beams and the elevated concrete walls/pedestal. This is a mixed material damage-resistant building which relies on post-tensioned rocking precast concrete walls (PRESSS) in one direction and Pres-Lam timber frames in the other direction.



Fig. 13.29 From laboratory specimen to office building: 3D Test Specimen tested in the lab (Newcombe et al. 2010), dismantled and reconstructed (Smith et al. 2011) on UC campus as EXPAN/STIC office



Fig. 13.30 College of Creating Arts – MacDiarmid Building, Massey University, Wellington, New Zealand. Post-tensioned timber (Pres-Lam) frames in the transverse directions with horizontal U-Shape flexural plate dissipaters on the first floor and Post-tensioned concrete (PRESS) walls in the longitudinal direction (Structural Engineers: Dunning Thornton Consultants)



Fig. 13.31 Merritt Building, Victoria Street, Christchurch. Three Storey commercial Building consisting of Post-tensioned timber (Pres-Lam) frames in the transverse direction and cast-in-situ reinforced concrete wall in the longitudinal direction (Structural Engineers: Kirk and Roberts; Architects: Sheppard and Rout)

As part of the Christchurch Rebuild, a number of buildings implementing the aforementioned damage-resisting technologies have been already completed and more are under construction or design (e.g. Figs. 13.31, 13.32, and 13.33). In some cases the structural systems use mixed materials (timber/concrete/steel) and/or a combination of rocking systems with base isolations and other supplemental damping devices. As notable from the pictures shown in the following paragraphs, in most cases the low-damage seismic resisting systems, and in particular the details of the external and replaceable dissipaters, have been partly or fully exposed to the view of the public/tenants as architectural features.

PRESSS-Steel Buildings

The Forté Health Medical Centre in Kilmore Street, Christchurch is the first PRESSS-Steel building in New Zealand and possibly the first in the World using this technology in steel. The three storey building includes over 5,000 m² of specialist medical facilities, including four operating theatres, patient bedrooms and urology, radiology, orthopaedics and fertility clinics. The lateral load resistance, with the high performance requirements of a critical facility (IL4 design level), is provided by post-tensioned steel rocking coupled ‘walls’ (or braced-frames) in both directions, combining hysteretic and viscous dampers (High



Fig. 13.32 Trimble Building , Christchurch. Two storey office building (more than 5,000 m²) consisting of post-tensioned timber (Pres-Lam) frames with external replaceable dissipaters at the beam-column connections and at the column-to-foundation connection and Pres-Lam coupled (with UFP, U-shape Flexural Plates) walls with external dissipaters at the base-connections (Design-build project with Architecture and Structures by Opus International and construction by Mainzeal/City Care, Brown et al. 2012)

Force-to-Volume Lead extrusion devices, developed at University of Canterbury Mechanical Engineering Department, Rodgers 2009) in parallel, for what is referred to as Advanced-Flag Shape System, AFS (Kam et al. 2010).

The internal frames implement another low-damage system, widely adopted in New Zealand as part of the Christchurch Rebuild and referred to as “sliding hinge joint” solution (MacRae et al. 2010) acting as second moment-resisting frame, in order to provide a additional redundancy to the primary lateral resisting systems and stability to the building during erection and after a fire (Fig. 13.34). The beam-column connections, consisting of a “top flange hinge” and a slotted- bolted connection at the bottom flange, are designed to accommodate the lateral displacements required for displacement compatibility with the main seismic resisting system with minimum stresses/strain demand on the floor/slab plate.



Fig. 13.33 Former ‘St Elmo Courts’ Building, Christchurch. Five storey building, combining base-isolation and two-ways post-tensioned frames in the superstructure with timber beams and concrete columns (Architect: Ricky Proko, Structural Engineers: Ruamoko Solutions)

13.12 Conclusions

The increased awareness by the general public/tenants, building owners, territorial authorities as well as insurers/reinsurers, of the severe economic impacts in terms of damage/dollars/downtime of moderate-strong earthquakes has indeed stimulated and facilitated the wider acceptance and implementation of cost-efficient damage-control, also referred to as low-damage, technologies in New Zealand, based on concrete, timber, steel or combination of the above material.

From an earthquake engineering community prospective, the challenge is still significant:

- on one hand, maintaining and supporting this (local and temporary) renewed appetite for seismic protection for both new buildings and existing ones (retrofit);
- on the other hand, pushing towards a wider internationally dissemination and acceptance of damage-resisting technologies according to current best know-how and practice

Somehow the target goal has not changed but the societal expectations (the ‘bar’) are higher and the allowed time frame shorter: to develop, at comparable

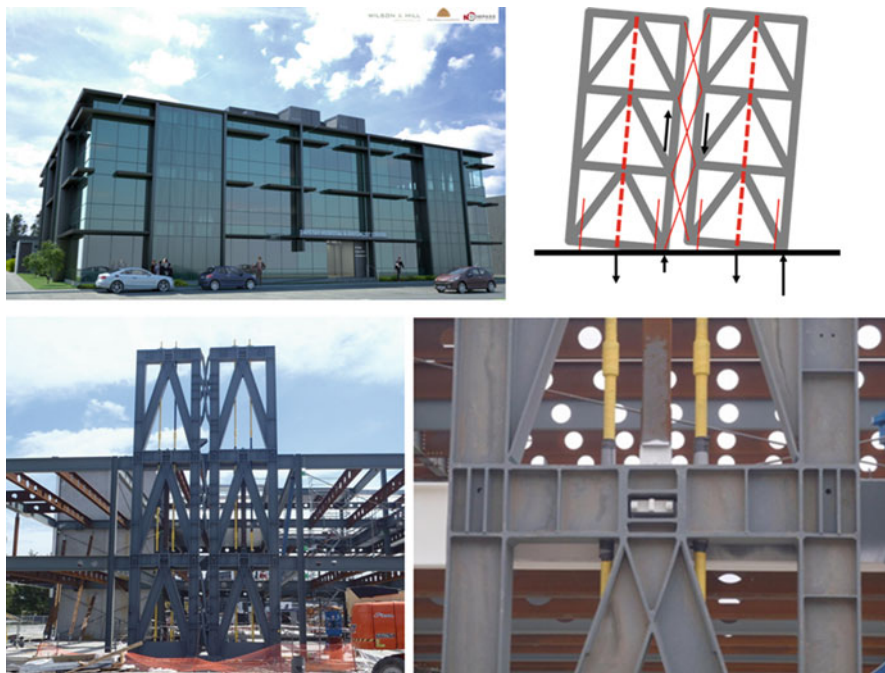


Fig. 13.34 Forté Health Medical Centre, three storey building with over 5,000 m² of specialist medical facilities. Post-tensioned steel rocking coupled ‘walls’ (or braced-frames) in both directions, combining hysteretic and viscous dampers in parallel for “an advanced flag-shape” system. *Bottom right:* secondary interior moment-resisting frames implementing a sliding hinge joint beam-column connection solution

costs, what the general public would referred to as an “ultimate earthquake-proof” building system (including skeleton, non-structural components/contents and foundation systems) capable as a whole of sustaining the shaking of a severe earthquake basically unscathed, thus including structural skeleton, non-structural components/contents and the soil-foundation system.

Acknowledgements The research, development and implementation of low-damage solutions described in this paper are the results of the exceptional support and collaborative effort between a great number of individuals and organizations from academia, the wider industry, governmental and funding agencies, at national and international level, a list of whom would be practically impossible to prepare. Nevertheless, the author wishes to acknowledge and sincerely thank all those involved in this extended and extraordinary “research team”.

Open Access This chapter is distributed under the terms of the Creative Commons Attribution Noncommercial License, which permits any noncommercial use, distribution, and reproduction in any medium, provided the original author(s) and source are credited.

References

- Amaris A, Pampanin S, Bull DK, Carr A (2007) Development of a non-tearing floor solution for jointed precast frame systems. Proceedings NZSEE conference, Palmerston North, paper 14
- Amaris AD, Pampanin S, Bull DK, Carr AJ (2008) Solutions to control and minimize floor damage in precast concrete buildings under severe earthquake loading. NZ Concrete Industry Conference, Rotorua, 2–4 October
- Au EV, Bull D, Pampanin S (2010) Experimental investigation of the seismic behaviour of slotted reinforced concrete beam-column connections. 2010 New Zealand Society of Earthquake Engineering (NZSEE) conference, Wellington, 26–28 Mar 2010
- Baird A, Palermo A, Pampanin S, Riccio P (2011) Focusing on reducing the earthquake damage to Façade systems. Bull N Z Soc Earthq Eng 44(2):108–120, ISSN: 1174–9857
- Baird A, Tasligedik AS, Palermo A, Pampanin S (2014) Seismic performance of vertical non-structural components in the 22nd February 2011 Christchurch earthquake. Earthq Spectra 30:401–425
- Brown A, Lester J, Pampanin S, Pietra D (2012) Rebuilding timber navigation's offices using a damage-limiting seismic system. World Conference on Timber Engineering, Quebec City
- Buchanan AH, Palermo A, Carradine D, Pampanin S (2011) Post-tensioned timber frame buildings. Struct Eng 89(17):24–31, ISSN: 1466–5123
- Cattanach A, Pampanin S (2008) 21st century precast: the detailing and manufacture of NZ's first multi-storey PRESSS-building. NZ Concrete Industry conference, Rotorua
- Christopoulos C, Pampanin S, Priestley MJN (2003) Performance-based seismic response of frame structures including residual deformations. Part I: single-degree-of-freedom systems. J Earthq Eng 7(1):97–118
- CERC (2012) Canterbury Earthquake Royal Commission (CERC) websites. Available at: <http://canterbury.royalcommission.govt.nz>
- DBH (2004) Building Act 2004. Department of Building and Housing (DBH), Wellington
- Dekker D, Chung S, Palermo A (2012) Carterton events centre auditorium pre-lam wall design and construction. New Zealand Society for Earthquake Engineering: 2012 annual technical conference (NZSEE), 13–15 Apr
- Devereux CP, Holden TJ, Buchanan AH, Pampanin S (2011) NMIT arts & media building – damage mitigation using post-tensioned timber walls. Proceedings of the ninth pacific conference on earthquake engineering. Building an Earthquake-Resilient Society, Auckland, 14–16 Apr 2011, paper 90
- Dhakal RP, Pampanin S, Palermo A, MacRae G, Pournali A, Tasligedik S, Yeow T, Baird A (2014) Seismic performance of non-structural components and contents in buildings: an overview of NZ research. International workshop in non-structural element
- Dunbar A, Moroder D, Pampanin S, Buchanan A (2014) Timber core-walls for lateral load resistance of multi-storey timber buildings. World Conference of Timber Engin, Quebec City
- EAG (2011) Engineering Advisory Group, Guidance on detailed engineering evaluation of earthquake affected non-residential buildings in Canterbury. Part 2 – evaluation procedure. Revision 5 19 July 2011. Structural Engineering Society New Zealand (SESOC), Christchurch
- Earthquake Engineering Research Institute (EERI) (2014) 2010–2011 Canterbury earthquake sequence special issue. Earthq Spectra 30(1), pp. fmi–605
- Englerkirk R (2002) Design-construction of the paramount – a 39 story precast prestressed concrete apartment building. PCI J 47(4):56–71
- FEMA E-74 (2011) Reducing the risks of non-structural earthquake damage – a practical guide. Federal Emergency Management Agency, Washington, DC
- FEMA 450 (2003) NEHRP recommended provisions and commentary for seismic regulations for new buildings and other structures. USA Federal Emergency Management Agency, Washington, DC
- Fenwick RC, Megget LM (1993) Elongation and load deflection characteristics of reinforced concrete members containing plastic hinges. Bull N Z Natl Soc Earthq Eng 26(1):28–41

- fib (2003) International Federation for Structural Concrete. Seismic design of precast concrete building structures. Bulletin No. 27, Lausanne, 254 pp
- Garcia JR, Miranda E (2006) Residual displacement ratios for assessment of existing structures. *Earthqu Eng Struct Dyn* 35(3):315–336
- Giorgini S, Taylor M, Cubrinovski M, Pampanin S (2011) Preliminary observations of multi-storey RC building foundation performance in Christchurch following the 22nd February 2011 Earthquake. NZ Concrete Society, Rotorua
- Giorgini S, Cubrinovski M, Pampanin S, Carr AJ, Moghaddasi M (2012) Integrated foundation-structure modelling of a case study from the Christchurch 2011 earthquake. In: Proceedings 15th world conference on earthquake engineering, Lisbon, 24–28 Sept 2012
- Giorgini S, Pampanin S, Cubrinovski M (2014) Towards performance-based seismic design of integrated foundation-structure systems considering soil-foundation interface nonlinearity. NZSEE conference, Auckland, 21–23 Mar 2014, paper no. P016
- Iqbal A, Pampanin S, Buchanan AH, Palermo A (2007) Improved seismic performance of LVL post-tensioned walls coupled with UFP devices. Proceedings of 8th Pacific conference on earthquake engineering, Singapore
- Johnston H, Watson C, Pampanin S, Palermo A (2014) Shake table testing of an integrated low damage building system. 2nd European conference in earthquake engineering and seismology, Istanbul, 25–29 Aug 2014
- Kam WY, Pampanin S (2011) General performance of buildings in Christchurch CDB after the 22 Feb 2011 earthquake: a contextual report (prepared for the Department of Building and Housing). Department of Civil and Natural Resources Engineering, University of Canterbury
- Kam WY, Pampanin S, Palermo A, Carr A (2006) Advanced flag-shaped systems for high seismic performance. *Isr ECEES*, Geneva
- Kam WY, Pampanin S, Palermo A, Carr A (2010a) Self-centering structural systems with combination of hysteretic and viscous energy dissipations. *Earthqu Eng Struct Dyn* 39 (10):1083–1108
- Kam WY, Pampanin S, Dhakal RP, Gavin H, Roeder CW (2010b) Seismic performance of reinforced concrete buildings in the September 2010 Darfield (Canterbury) earthquakes. *Bull N Z Soc Earthq Eng* 43(4):340–350
- Kam WY, Pampanin S, Elwood K (2011) Seismic performance of reinforced concrete buildings in the 22 February Christchurch (Lyttleton) earthquake. *Bull N Z Soc Earthq Eng* 44(4):239–279. ISSN: 1174–9875 (Special Issue)
- Kawashima K (1997) The 1996 Japanese seismic design specifications of highway bridges and the performance based design. In: Fajfar P, Krawinkler H (eds) Proceedings of seismic design methodologies for the next generation of codes. Balkema, Rotterdam, pp 371–382
- Kelly JM, Skinner RI, Heine AJ (1972) Mechanisms of energy absorption in special devices for use in earthquake resistant structures. *Bull N Z Soc Earthq Eng* 5(3):63–88
- Kurama YC (2001) Seismic design of unbonded post-tensioned precast concrete walls with supplementary viscous damping. *ACI Struct J* 97(4):648–658
- Kurama Y, Shen Q (2004) Posttensioned hybrid coupled walls under lateral loads. *J Struct Eng ASCE* 130(2):297–309
- Latham DA, Reay AM, Pampanin S (2013) Kilmore Street Medical Centre: application of an advanced flag-shape steel rocking system. In: Latham DA, Reay AM (eds) New Zealand Society for Earthquake Engineering – NZSEE – conference, Wellington, 26–28 Apr 2013
- Lindsay R (2004) Experiments on the seismic performance of hollow-core floor systems in precast concrete buildings. ME thesis, University of Canterbury
- MacPherson C (2005) Seismic performance and forensic analysis of a precast concrete hollow-core floor superassemblage. ME thesis, University of Canterbury
- MacRae GA, Clifton GC, Mackinven H, Mago N, Butterworth J, Pampanin S (2010) The sliding hinge joint moment connection. *Bull N Z Soc Earthq Eng* 43(3):202–212

- Marriott D, Pampanin S, Bull D, Palermo A (2008) Dynamic testing of precast, post-tensioned rocking wall systems with alternative dissipating solutions. *Bull N Z Soc Earthq Eng* 41 (2):90–103
- Marriott D, Pampanin S, Palermo A (2009) Quasi-static and pseudo-dynamic testing of unbonded post-tensioned rocking bridge piers with external replaceable dissipaters. *Earthq Eng Struct Dyn* 38(3):331–354
- Matthews J, Bull D, Mander J (2003) Hollowcore floor slab performance following a severe earthquake. *Proceeding of fib symposium, Concrete structures in seismic regions, Athens*
- Millen MDL, Pampanin S, Cubrinovski M, Carr A (2014) A design framework for soil-foundation-structure interaction. 2nd European conference in earthquake engineering and seismology, Istanbul, 25–29 Aug 2014
- Moroder D, Buchanan AH, Pampanin S (2013) Preventing seismic damage to floors in post-tensioned timber frame buildings. *New Zealand Society of Earthquake Engineering Conference, Wellington*
- Moroder D, Sarti F, Palermo A, Pampanin S, Buchanan AH (2014) Experimental investigation of wall-to-floor connections in post-tensioned timber buildings. *NZSEE conference, Auckland, 21–23 Mar 2014, paper no. P25*
- Muir C, Bull D, Pampanin S (2012) Preliminary observations from biaxial testing of a two-storey, two-by-one bay, reinforced concrete slotted beam superassembly. *Bull N Z Soc Earthq Eng* 45(3):97–104, ISSN 1174–9875
- Muir CA, Bull DK, Pampanin S (2013) Seismic testing of the slotted beam detail for reinforced concrete structures. In: *Proceedings of the structures congress, Pittsburgh*
- New Zealand Society for Earthquake Engineering (NZSEE) (2010) Special issue on the darfield earthquake 4 Sept 2010. *NZSEE Bulletin* 43(4):215–439
- New Zealand Society for Earthquake Engineering (NZSEE) (2011) Special issue on the Christchurch earthquake 22 February 2011. *NZSEE Bulletin* B44 (4):181–430
- Newcombe MP, Pampanin S, Buchanan AH (2010) Design, fabrication and assembly of a two-storey post-tensioned timber building. *Proceedings of 11th world conference on timber engineering, Riva del Garda*
- NZCS (2010) *PRESSS design handbook* (Editor: S. Pampanin). NZ Concrete Society, Wellington
- NZS1170 (2004) *NZS 1170.5:2004 structural design actions. Part 5: earthquake actions – New Zealand*. Standards New Zealand, Wellington
- NZS 3101 (2006) *Appendix B: special provisions for the seismic design of ductile jointed precast concrete structural systems*. Standards New Zealand, Wellington
- Ohkubo M, Hamamoto T (2004) Developing reinforced concrete slotted beam structures to reduce earthquake damage and enhance seismic structural performance. In: *Proceedings of the 13th annual world conference on earthquake engineering, Vancouver*
- Palermo A, Pampanin S, Buchanan AH, Newcombe MP (2005) Seismic design of multi-storey buildings using Laminated Veneer Lumber (LVL). *Proceedings of New Zealand Society for Earthquake Engineering conference, Wairakei*
- Palermo A, Pampanin S, Buchanan A (2006) Experimental investigations on LVL seismic resistant wall and frame subassemblies. 1st ECEES, Geneva, Sept 3–8, paper n. 983
- Palermo A, Pampanin S, Baird A, Riccio P (2010) Focusing on reducing the earthquake damage to non-structural components in buildings: research needs and future internationally coordinated plans. In: *Proceedings NZSEE conference, Wellington, 26–28 Mar 2010, paper 70*
- Pampanin S (2005) Emerging solutions for high seismic performance of precast -prestressed concrete buildings. *J Adv Concrete Technol* 3(2):202–222, invited paper
- Pampanin S (2010) Chapter 28: Damage-control self-centering structures: from laboratory testing to on-site applications. In: *Fardis M (ed) Advancements in performance-based earthquake*

- engineering, part 3, vol 13, Geotechnical, geological, and earthquake engineering. Springer, Dordrecht, pp 297–308, ISBN: 978-90-481-8745-4 (Print) 978-90-481-8746-1 (Online)
- Pampanin S (2012) Reality-check and renewed challenges in earthquake engineering: implementing low-damage structural systems – from theory to practice. *Bull N Z Soc Earthq Eng* 45(4):137–160, ISSN 1174–9875
- Pampanin S, Christopoulos C, Priestley MJN (2003) Performance-based seismic response of frame structures including residual deformations. Part II: multi-degree-of-freedom systems. *J Earthq Eng* 7(1):119–147
- Pampanin S, Pagani C, Zambelli S (2004) Cable stayed and suspended solution for precast concrete frames: the Brooklyn system. Proceedings of the New Zealand Concrete Industry conference, Queenstown, 16–18 Sept 2004
- Pampanin S, Amaris A, Akguzel U, Palermo A (2006a) Experimental investigations on high-performance jointed ductile connections for precast frames. Proceedings of the 1st European conference on earthquake engineering and seismology, Geneva
- Pampanin S, Palermo A, Buchanan A, Fragiaco M, Deam B (2006b) Code provisions for seismic design of multi-storey post-tensioned timber buildings, CIB Workshop, Florence
- Pampanin S, Kam WY, Tasligedik AS, Quintana-Gallo P, Akguzel U (2010) Considerations on the seismic performance of pre-1970s RC buildings in the Christchurch CBD during the 4th Sept 2010 Canterbury earthquake: was that really a big one? Proceedings of 9th Pacific conference on earthquake engineering. New Zealand Society for Earthquake Engineering (NZSEE), Auckland
- Pampanin S, Kam W, Haverland G, Gardiner S (2011) Expectation meets reality: seismic performance of post-tensioned precast concrete southern cross endoscopy building during the 22nd Feb 2011 Christchurch earthquake. NZ Concrete Industry Conference, Rotorua
- Pampanin S, Kam WY, Akguzel U, Tasligedik AS, Quintana-Gallo P (2012) Report on the observed earthquake damage of reinforced concrete buildings in the Christchurch CBD on the 22 February 2011 earthquake, vol 1 and 2. University of Canterbury, Christchurch
- Park R (2002) Seismic design and construction of precast concrete buildings in New Zealand. *PCI J* 47(5):60–75
- Paulay T, Priestley MJN (1992) Seismic design of reinforced concrete and masonry buildings. Wiley, Chichester
- Priestley MJN (1991) Overview of the PRESSS research programme. *PCI J* 36(4):50–57
- Priestley MJN (1996) The PRESSS program current status and proposed plans for phase III. *PCI J* 41(2):22–40
- Priestley MJN (1998) Displacement-based approaches to rational limit states design of new structures. Keynote Address, 11th European conference on earthquake engineering, Paris
- Priestley MJN, Sritharan S, Conley JR, Pampanin S (1999) Preliminary results and conclusions from the PRESSS five-storey precast concrete test building. *PCI J* 44(6):42–67
- Priestley MJN, Calvi GM, Kowalsky MJ (2007) Displacement-based seismic design of structures. IUSS Press, Pavia
- Restrepo JI (1993) Seismic behaviour of connections between precast concrete elements. Ph.D. dissertation, Department of Civil Engineering, University of Canterbury, Christchurch
- Rodgers GW (2009) Next generation structural technologies: implementing high force-to-volume energy absorbers. Ph.D. thesis, University of Canterbury, Christchurch
- Sarti F, Smith T, Palermo A, Pampanin S, Bonardi D, Carradine DM (2013) Experimental and analytical study of replaceable Buckling-Restrained Fused-type (BRF) mild steel dissipaters. NZSEE Conference, Wellington, 26–28 Apr
- SEAOC (1995) Vision 2000 Committee, performance-based seismic engineering. Structural Engineers Association of California, Sacramento
- SESOC (2011) Preliminary observations from Christchurch earthquakes. Structural Engineering Society New Zealand (SESOC), Auckland
- Smith T, Wong R, Newcombe M, Carradine D, Pampanin S, Buchanan A, Seville R, McGregor E (2011) The demountability, relocation and re-use of a high performance timber building.

- In: Proceedings of the ninth Pacific conference on earthquake engineering. Building an Earthquake-Resilient Society, Auckland, 14–16 Apr 2011, paper 187
- Smith T, Ponzo F, Di Cesare A, Pampanin S, Carradine D, Buchanan A, Nigro D (2014) Post-tensioned glulam beam-column joints with advanced damping systems: testing and numerical analysis. *J Earthq Eng* 18(1):147–167(21)
- Stanton JF, Stone WC, Cheok GS (1997) A hybrid reinforced precast frame for seismic regions. *PCI J* 42(2):20–32
- Tasligedik AS (2014) Damage mitigation strategies for non-structural infill walls. PhD dissertation, Department of Civil and Natural Resources Engineering, University of Canterbury, Christchurch
- Tasligedik AS, Pampanin S, Palermo A (2012) Damage states and cyclic behaviour of drywalls infilled RC frames. *Bull N Z Soc Earthq Eng* 45(2):84–94, ISSN 1174–9875
- Tasligedik AS, Pampanin S, Palermo A (2014) Low-damage seismic solutions for non-structural drywall partitions. *Bull Earthq Eng* 13(4):1029–1050

Chapter 14

Archive of Historical Earthquake Data for the European-Mediterranean Area

Andrea Rovida and Mario Locati

Abstract The importance of historical earthquake data is largely recognized by both seismologists and engineers, who use such data in a wide range of applications.

At the European-Mediterranean scale, several databases dealing with historical earthquake data – mostly intensity data points – exist and are constantly maintained and updated, as well as national earthquake catalogues. In addition, a number of studies on historical earthquakes are published every year. Most of these activities are being performed at a national scale, depending on each country's needs, and according to diverse methodologies. As a result, the earthquake history of Europe is today fragmented in a puzzle of different, only partially overlapping sets of data, which, at the continent scale, are not homogeneously collected and interpreted. This situation is particularly evident in the frontier areas, where historical earthquakes are often interpreted in a conflicting and/or partial way by the catalogues of the bordering countries. In addition, the background information upon which several historical catalogues are built is not published or not easily accessible.

In recent years, a major effort was made to bridge over these gaps, by establishing cooperation among existing national databases, and creating new ones according to common standards. Particular attention was devoted to retrieve the earthquake background information, that is, the results of historical earthquake investigation in terms of a paper, a report, a book chapter, a map, etc. As most of the information on an historical earthquake can be summarized in a set of Macroseismic Data Points (MDPs) – i.e. a list of localities (name and coordinates) with a macroseismic intensity assessment and the related macroseismic scale – a dedicated effort was addressed to make such data publicly available.

The described activities resulted in the European Archive of Historical Earthquake Data (AHEAD). The Archive is conceived as a pan-European common and open platform supporting the research activities in the field of historical seismology by (i) tracing back, preserving and granting access to the sources of data on the earthquake history of Europe (papers, reports, MDPs, and catalogues), and (ii) establishing relations among these data. AHEAD inventories multiple sets of information concerning each European earthquake in the time-window 1000–1899.

A. Rovida (✉) • M. Locati

Istituto Nazionale di Geofisica e Vulcanologia, Milano, Italy

e-mail: andrea.rovida@ingv.it; mario.locati@ingv.it

© The Author(s) 2015

A. Ansal (ed.), *Perspectives on European Earthquake Engineering and Seismology*, Geotechnical, Geological and Earthquake Engineering 39, DOI 10.1007/978-3-319-16964-4_14

359

The AHEAD web portal (<http://www.emidius.eu/AHEAD/>) gives access, as of today, to 4,722 earthquakes and the related background information as provided by 338 data sources. All these data can be queried by earthquake and by study, through a user-friendly web-interface. The distinguishing feature of AHEAD is to grant access not only to one study, but to all the available (published) data sources dealing with each individual earthquake, allowing researchers to take into account the different point of views and interpretations.

14.1 Introduction

The importance of historical earthquake data is broadly recognized by both seismologists and engineers, who use such data in a wide range of applications, including seismotectonic studies, seismic hazard assessments for supporting building codes and critical facilities, and land use planning.

Earthquake catalogues represent the most popular and ready-to-use type of historical earthquake data, since they provide a list of earthquakes complemented with the same parametric information (epicentral coordinates, hypocentral depth, magnitude, etc.) as instrumental earthquake catalogues. They constitute one of the basic ingredients for the mentioned applications, and represent the final result and summary of historical earthquake research.

Over the past decades the compilation of earthquake catalogues in Europe, as well as historical earthquake research, has been performed at national scales, depending on each country's needs, and according to diverse methodologies. Each European country put major efforts in compiling an historical earthquake catalogue for its own territory according to its own procedures; such catalogues are still today maintained and updated according to different time-schedule and criteria. Several databases dealing with historical earthquake data - mostly intensity data points - have also been published in Europe. In addition, a number of studies on historical earthquakes, either on single events or specific historical periods and areas, are published every year in the scientific literature.

As a result, the earthquake history of the European-Mediterranean area is fragmented in a puzzle of different, only partially overlapping sets of data, which, at the continent scale, are not homogeneously collected and interpreted.

In recent years a major effort, started in 2006 in the framework of the European Commission project NERIES ("Network of Research Infrastructures for European Seismology"), was made to establish cooperation among existing national databases, and creating new ones according to common compilation standards. Such an effort resulted in the Archive of Historical Earthquake Data (AHEAD). The Archive is conceived as a pan-European common and open platform supporting the research activities in the field of historical seismology by (i) tracing back, preserving and granting access to the sources of data on the earthquake history of Europe (papers, reports, MDPs, and catalogues), and

(ii) establishing relations among these data. AHEAD covers the time-window 1000–1899 and is available through a dedicated web-portal since May 2010 at <http://www.emidius.eu/AHEAD/>. The AHEAD portal inventories and gives access to multiple sets of information concerning each earthquake, and allows users to get comprehensive information about individual earthquakes.

14.2 Content of the Archive

Primary historical earthquake data are written records of seismic effects, as supplied by historical sources. These primary data are then put together and interpreted in historical earthquake studies, aimed at retrieving a comprehensive description of the earthquake impact, from which the earthquake location and size can be evaluated for the compilation of parametric catalogues. Catalogues usually mention the data supporting each earthquake, being them historical sources, one or more historical earthquake studies, or another parametric catalogue. Historical earthquake data present themselves in a variety of different formats. Some studies simply consist in the transcription of the historical sources, with or without any interpretation of them. On the contrary, other studies just present the interpretation of historical sources, making reference to them or even, in extreme cases, not. Modern in-depth historical studies should provide a comprehensive description of the historical sources, the historical context in which these sources were produced, how and where they were preserved, and how they were retrieved; historical sources should then be critically analysed and interpreted in terms of earthquake effects. The effects distribution is either provided as a mere description or, in modern studies, interpreted in terms of Macroscopic Data Points (MDPs), i.e. a list of places with name and coordinates with a macroseismic intensity assessment and the related macroseismic scale, as a minimum. In some cases the complete earthquake study is not formalized and only MDPs are provided. Although inhomogeneous at the European scale, the results of the mentioned studies and investigations (hereafter referred to as “data sources”), involving and gathering different disciplines and expertise, provide scientific results that altogether constitute the knowledge on a given historical earthquake.

One of the main scopes of AHEAD is tracing back, preserving and granting access to the data sources on historical earthquakes in Europe. The compilation of AHEAD started from the identification, collection and critical organization of the best and most recent data sources in any of the formats briefly analysed above. Following the identification of the data sources dealing with a given earthquake, the full information on such earthquake has been extracted from the data source and a record of the AHEAD database has been compiled. The AHEAD database structure is described in Locati et al. (2014). As an earthquake can be the subject of multiple studies, multiple records from different data sources can relate to the same earthquake. Conversely, one data source may deal with several earthquakes and contribute several records to AHEAD. Records referred to the same earthquake have

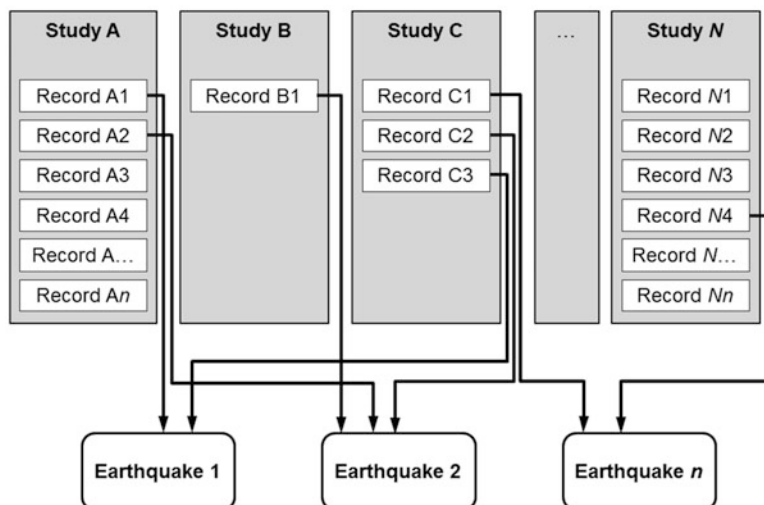


Fig. 14.1 Scheme of the compilation of AHEAD

been then grouped together by means of the same identification number (see Locati et al. 2014). As a result each earthquake is represented in AHEAD by the multiplicity of the data sources related to it, as shown in Fig. 14.1. In this way, the information supporting each earthquake is easily traced back and the state-of-the-art of the research on a specific earthquake is fully represented.

Different data sources may provide conflicting information and grouping records referred to the same earthquake is not always easy, for example if the same earthquake is reported in different studies with different dates (a common situation for historical earthquakes in Europe, where different calendars have been in use through history). For this reason, the grouping of records was manually performed, case by case by expert judgment, examining and comparing the content of each study. Automatic clustering has been avoided, since it may lead to big mistakes when data sources provide for the same earthquake different time and location.

AHEAD today considers 4,722 earthquakes in the Euro-Mediterranean area in the time window 1000–1899 (Fig. 14.2), as described in 338 data sources; the total number of records of the AHEAD database is 11,018.

Two thirds of AHEAD data are contributed by eight regional online databases, run by European institutions involved in historical earthquake research: ASMI (ASMI Working Group), ECOS-09 (Fäh et al. 2011), SisFrance (BRGM-EDF-IRSN/SisFrance 2010), Macroseismic Data of Southern Balkan area (University of Thessaloniki 2003), Base de Datos Macrosísmica (Instituto Geográfico Nacional 2010), UK Historical Earthquake Database (British Geological Survey 2010), Hellenic Macroseismic Database (Kouskouna and Sakkas 2013) and Base de Dades Macrosísmica (Institut Geològic de Catalunya 2010). The remaining one third of the data sources inventoried by AHEAD is constituted by (i) papers, reports, and volumes describing the results of historical earthquake investigations, and

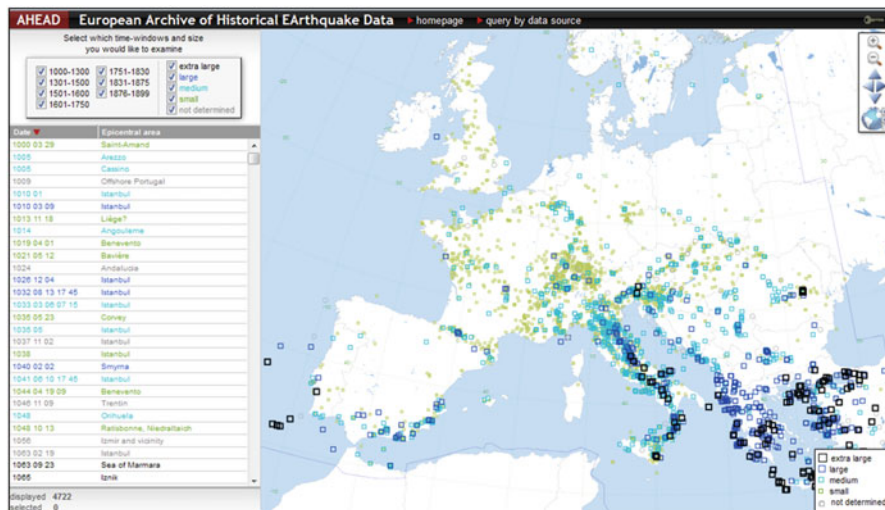


Fig. 14.2 Plot of the 4,722 earthquakes (1000–1899) considered by AHEAD, from the “query by earthquake” section of the AHEAD portal

(ii) parametric catalogues, with or without the references to their sources of information.

In the AHEAD portal each data source is listed in the “Query by data source” section, which give access to the data source full reference, the complete text as a PDF file, if possible, and the link to online data sources (e.g., databases and catalogues) when available. The archive can be queried also by earthquake (Fig. 14.2); once an earthquake is selected either from a list or a map, the user may investigate the available information, subdivided into two sections: (i) “Catalogues”, supplying the parameters extracted from the main catalogues, and (ii) “Studies”, showing the list of the relevant earthquake investigations. When available, the MDP set from each study is shown in a map.

14.3 Use and Potential of AHEAD

All earthquake catalogues and intensity databases provide one set of data per earthquake. AHEAD conversely grants access to multiple data sources per earthquake, each supplying different kinds of data, such as MDPs sets and earthquake parameters.

The number of data sources made available for each of the 4,722 considered earthquakes ranges from 1 to 10; at least two alternative data sources are archived for the 77 % of the earthquakes, and for the 14 % of them at least four data sources are available. Alternative data sources may supply different interpretations of the same earthquake, resulting in alternative data. Figure 14.3 shows the availability of

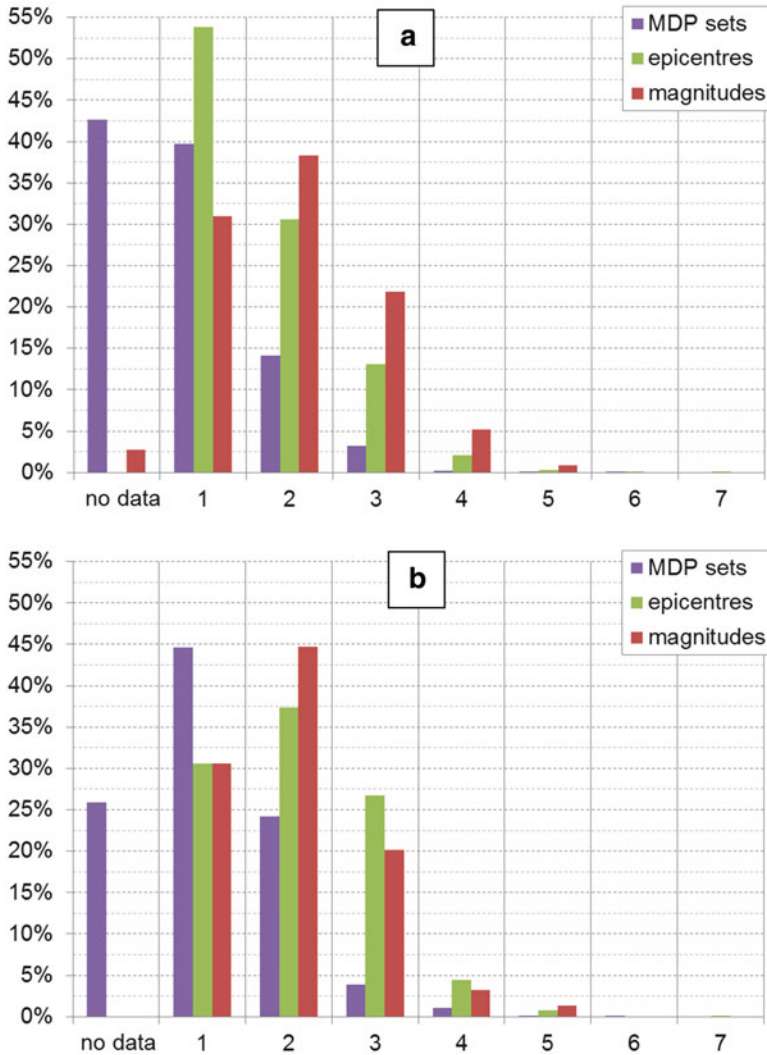


Fig. 14.3 Number of alternatives per earthquake: (a) percentages for all 4,722 earthquakes, (b) percentages only for earthquakes with $M_w \geq 5.6$

alternative solutions in terms of (i) alternative MDP sets; (ii) alternative epicentres, and (iii) alternative magnitude assessments; Fig. 14.3a refers to all the 4,722 considered earthquakes, Fig. 14.3b refers to the most damaging earthquakes (indicatively $M \geq 5.6$).

In the compilation of AHEAD, particular attention was devoted to retrieve data sources providing Macroseismic Data Points (MDPs), since they supply a comprehensive and quantitative image of an earthquake. As a whole, about 5,000 MDPs sets derived from 147 different data sources are archived, for a total of more than

94,500 MDPs. For the 57 % of the 4,722 considered earthquakes, AHEAD archived at least one MDP set; considering the 818 earthquakes with $M \geq 5.6$, MDPs are available for the 74 % of them. For the 39 % of the archived earthquakes only one MDP set is available, while alternative sets exist for the 18 % them, about the 15 % is represented by earthquake with two alternative sets (Fig. 14.3a). For earthquakes with $M \geq 5.6$, the percentages of $M \geq 5.6$ earthquakes with one, two, or more MDP sets are 45, 24, and 5 % respectively (Fig 14.3b). Figure 14.3 also shows the same analysis on alternative epicentres and magnitude values.

AHEAD provides the full representation of the wealth of alternative solutions for each European historical earthquake, granting access to the available knowledge of it and, at the same time, to the uncertainty associated to the interpretation of past earthquakes.

The exploration of alternative solutions is particularly important for the evaluation of earthquakes in frontier areas, where historical earthquakes are often interpreted in a conflicting and/or partial way by the catalogues of the bordering countries. Differences depend, among other factors, on the considered historical sources, and the way they were interpreted by each author. Figure 14.4 shows the diversity of data sources available for the 14 April 1895, Ljubljana earthquake, as represented in the AHEAD portal. The 1895 earthquake is a transfrontier event that affected a large area today split among three bordering countries (Slovenia, Austria, and Italy). Although the available parametric catalogues propose similar epicentral locations and magnitude values around 6 (Fig. 14.4a), the two alternative MDP distributions by Guidoboni et al. (2007) and Cekić (1998), respectively shown in Fig. 14.4b,c, lead to a very different earthquake scenario. AHEAD, providing access to these different scenarios and an easy comparison of different datasources on the same earthquake, stimulated a complete reappraisal of the earthquake (Cekić et al. 2014).

The described situation is common for European cross-border earthquakes, for which MDPs distributions are often limited to one country and the effects in the bordering country have not been investigated. Alternatively, a second MDPs distribution is available for the neighbouring country and is referred to another, supposed local earthquake. Such partial effects distributions reflect on the final location and size of the earthquake, which may either be located in the country where the effects have been recognized or listed in the catalogues of both the bordering countries, each with its own (wrong) location and magnitude. AHEAD lists all the available data sources for the same earthquake and helps sorting out the described situations.

The value of AHEAD is not only limited to emphasize different interpretations by different authors, but also to keep trace of the evolution of the knowledge of an earthquake, as the historical investigation progresses, the understanding of the phenomena grows. The more complete is the overall picture, the more is possible to assess the confidence level of the earthquake parameters proposed by a catalogue.

AHEAD provided the list of earthquakes for the compilation of the European earthquake catalogue SHEEC (SHARE European Earthquake Catalogue; Stucchi

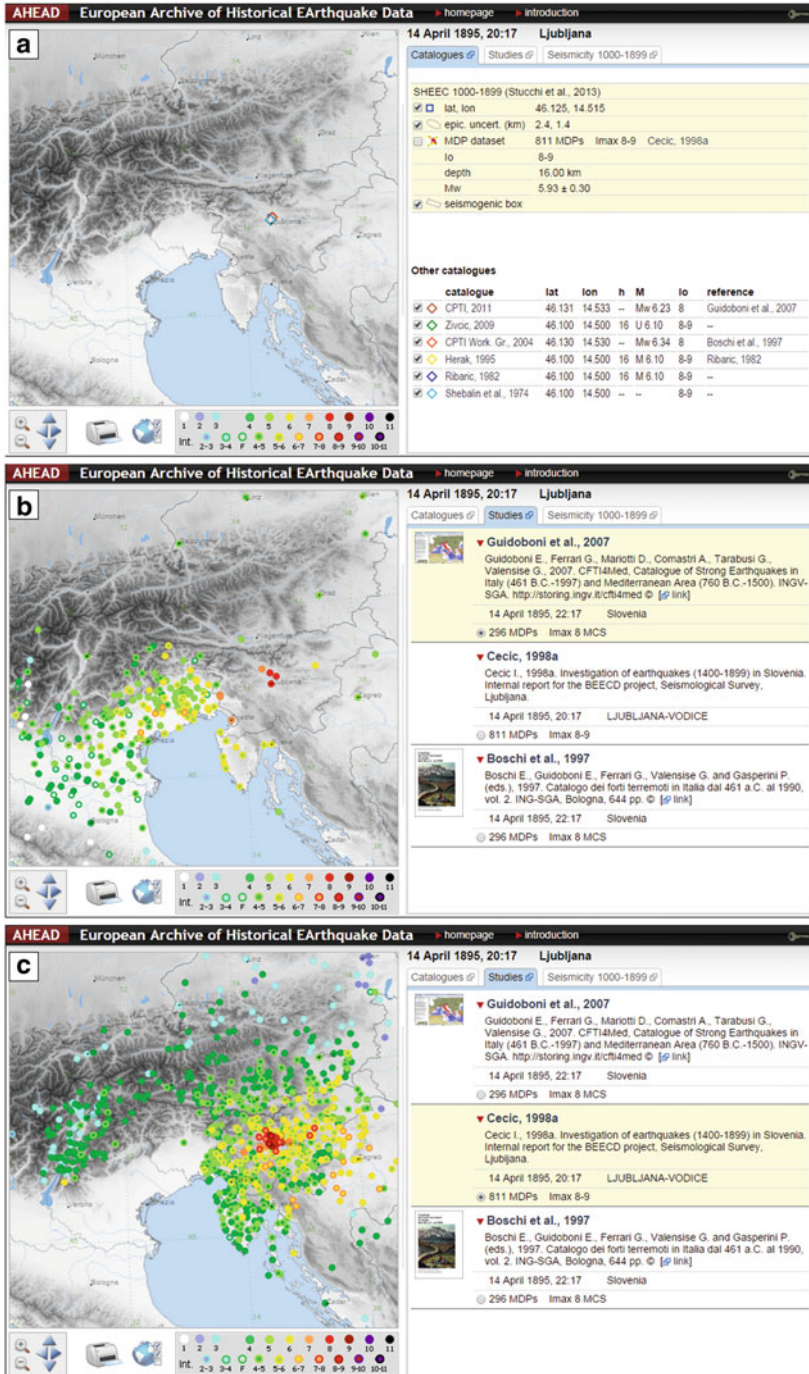


Fig. 14.4 The 14 April 1895, Ljubljana earthquake: (a) parameters according to different catalogues, (b) the MDP set as provided by Guidoboni et al. (2007), and (c) as provided by Cecic (1998)

et al. 2012) 1000–1899, used for the evaluation of the seismic hazard of Europe in the framework of the SHARE (Seismic Hazard Harmonization in Europe) EC Project (Giardini et al. 2014). AHEAD permitted a careful comparison of the available data sources for each earthquake and the selection, among them, of the most reliable, upon which the catalogue entry have been built. AHEAD also permitted to critically deal with the situations described above, in particular to sort out: (i) duplications, (ii) earthquakes missing in one or more catalogues, and (iii) fake events. In particular, AHEAD allowed the compilers of SHEEC to identify 306 earthquakes not mentioned in national catalogues, commonly because investigated for the first time by studies published after the national catalogues.

14.4 Long-Term Plan

AHEAD is proposed as the reference node for providing historical data on European earthquakes for EPOS, the European Plate Observing System (Cocco and the EPOS Consortium 2013). EPOS is a long-term integrated research infrastructure plan of the European Commission aimed at integrating data from existing national and regional research infrastructures in order to increase the accessibility and usability of multidisciplinary data, enhancing worldwide interoperability in Earth science. AHEAD is the “Community Layer” that will interface national and regional research infrastructures with the cross-domain “Integrated Services” of EPOS, allowing researchers from different fields to access historical earthquake data.

The long-term plan of AHEAD foresees its expansion both in time and space, a new section in the portal for fake earthquakes, the promotion of common standards for the compilation of historical earthquake data, and a support for dedicated research activities on cross-border earthquakes. The covered time-window will be extended to the first half of the 20th century, this will lead to an exponential increase of the number of earthquakes and an additional complexity in order to accommodate (early) instrumental earthquake data together with the existing macroseismic ones. The extension in space will start with the integration of Central and Eastern Turkey; the extension to other Mediterranean areas is envisioned in the long term. A section dealing with fake earthquakes will be opened in the portal. During its compilation, AHEAD dedicated particular care in archiving studies that identify earthquakes as fake, for example other natural phenomena that have been wrongly interpreted as earthquakes and included in earthquake catalogues. AHEAD deals with about 350 fake earthquakes and it will help avoiding the inclusion of such earthquakes in future catalogues. The structure of AHEAD will permit to clearly understand why an event is declared as a fake by tracing back the misinterpretation of the historical sources.

AHEAD will continue promoting common compilation standards among the involved research infrastructures. The next milestone in this field will be the finalization of a shared file format for exchanging macroseismic data (Locati

2014), based on the extension of the existing QuakeML format (Schorlemmer et al. 2006), already in use for exchanging event parameters originated from instrumentally recorded data.

Finally, AHEAD will support new research initiatives aimed at investigating cross-border earthquakes which today present conflicting or partial data in different regional databases, and for those earthquakes with a complete lack of background information.

14.5 Conclusions

AHEAD provides a consistent description of the Euro-Mediterranean long-term earthquake history, allowing researchers to better exploit historical earthquake data spanning over a millennium.

AHEAD helps users to easily retrieve and compare the largest amount of available, historical earthquake data and to better understand the origin of different interpretations. This goal is achieved by (i) tracing back, preserving, and granting access to the studies and the parameters for each earthquake and (ii) creating relations among these studies. AHEAD is available on the web with a user interface designed to emphasize its distinctive features.

The cooperation of more than 50 researchers from more than 20 European research institutions and countries, supported by two European initiatives (2006–2013), contributed to the creation and establishing of AHEAD. Now that a consistent description of the Euro-Mediterranean long-term earthquake history does exist, through the increased awareness and cooperative action of the European and national research institutions, AHEAD could become a durable platform continuously fed with new pieces of information on past earthquakes.

Open Access This chapter is distributed under the terms of the Creative Commons Attribution Noncommercial License, which permits any noncommercial use, distribution, and reproduction in any medium, provided the original author(s) and source are credited.

References

- ASMI Working Group ASMI, Archivio Storico Macrosismico Italiano. <http://emidius.mi.ingv.it/ASMI/>
- BRGM-EDF-IRSN/SisFrance (2010) Histoire et caractéristiques des séismes ressentis en France. <http://www.sisfrance.net/>
- British Geological Survey (2010) UK historical earthquake database. <http://quakes.bgs.ac.uk/historical/>
- Cecić I (1998) Investigation of earthquakes (1400-1899) in Slovenia. Internal report for the BEECD project, Seismological Survey, Ljubljana

- Cecić I, Albini P, Hammerl CH (2014) 14 April 1895, Ljubljana earthquake – a cross-border study. Abstract volume of the 2nd European conference on earthquake engineering and seismology, Istanbul, 25–29 Aug 2014
- Cocco M, EPOS Consortium (2013) The EPOS architecture: integrated services for solid earth science. *Geophys Res Abstr* 15:EGU2013–5531
- Fäh D, Giardini D, Kästli P, Deichmann N, Gisler M, Schwarz-Zanetti G, Alvarez-Rubio S, Sellami S, Edwards B, Allmann B, Bethmann F, Wössner J, Gassner-Stamm G, Fritsche S, Eberhard D (2011) ECOS-09 earthquake catalogue of Switzerland release 2011 report and database, public catalogue. Swiss Seismological Service ETH, Zurich, Report SED/RISK/R/001/20110417, 42 pp. + Appendices; <http://hitseddb.ethz.ch:8080/ecos09>
- Giardini D, Wössner J, Danciu L (2014) Mapping Europe’s seismic hazard. *Eos* 95(29):261–262
- Guidoboni E, Ferrari G, Mariotti D, Comastri A, Tarabusi G, Valensise G (2007) CFTI4Med, catalogue of strong earthquakes in Italy (461 B.C.-1997) and Mediterranean Area (760 B.C.-1500). INGV-SGA. <http://storing.ingv.it/cfti4med>
- Institut Geològic de Catalunya (2010) Base de Dades Macro sísmica. http://www.igc.cat/web/ca/sismologia_bdmacrosis.html
- Instituto Geográfico Nacional (2010) Bases de datos macro sísmica. <http://www.ign.es/ign/layoutIn/bdmacrosismica.do>
- Kouskouna V, Sakkas G (2013) The University of Athens Hellenic Macro seismic Database (HMDB.UoA): historical earthquakes. *J Seismol* 17(4):1253–1280. <http://macroseismology.geol.uoa.gr/>
- Locati M (2014) Describing non-instrumental seismological data in Quakeml: the need for a macro seismic extension. Abstract volume of the 2nd European conference on earthquake engineering and seismology, Istanbul, 25–29 Aug 2014
- Locati M, Rovida A, Albini P, Stucchi M (2014) The AHEAD portal: a gateway to European historical earthquake data. *Seismol Res Lett* 85(3):727–734
- Schorlemmer D, Saul J, Euchner F, Becker J, Heinloo A, Kästli P, Maraini S, Weber B, Wyss A (2006) QuakeML, an XML representation of seismological data, part 1: basic event description. Deliverable of the Joint Research Activity 2, NERIES Project, 35 pp
- Stucchi M, Rovida A, Gomez Capera AA, Alexandre P, Camelbeeck T, Demircioglu MB, Gasperini P, Kouskouna V, Musson RMW, Radulian M, Sesetyan K, Vilanova S, Baumont D, Faeh D, Lenhardt W, Makropoulos K, Martinez Solares JM, Scotti O, Zivcic M, Albini P, Batllo J, Papaioannou C, Tatevossian R, Locati M, Meletti C, Viganò D, Giardini D (2012) The SHARE European earthquake catalogue (SHEEC) 1000-1899. *J Seismol* 17:523–524
- University of Thessaloniki (2003) Macro seismic data of Southern Balkan area. http://www.itsak.gr/en/db/data/macro seismic_data/

Chapter 15

A Review and Some New Issues on the Theory of the H/V Technique for Ambient Vibrations

Enrico Lunedei and Peter Malischewsky

Abstract In spite of the Horizontal-to-Vertical Spectral Ratio (HVSR or H/V) technique obtained by the ambient vibrations is a very popular tool, a full theoretical explanation of it has been not reached yet. A short *excursus* is here presented on the theoretical models explaining the H/V spectral ratio that have been development in last decades. It leads to the present two main research lines: one aims at describing the H/V curve by taking in account the whole ambient-vibration wavefield, and another just studies the Rayleigh ellipticity. For the first theoretical branch, a comparison between the most recent two models of the ambient-vibration wavefield is presented, which are the Distributed Surface Sources (DSS) one and the Diffuse Field Approach (DFA). A mention is done of the current developments of these models and of the use of the DSS for comparing the H/V spectral ratio definitions present in literature. For the second research branch, some insights about the connection between the so-called osculation points of the Rayleigh dispersion curves and the behaviour of the H/V curve are discussed.

15.1 Introduction

The Horizontal-to-Vertical Spectral Ratio (HVSR or H/V) technique is a way to retrieve information about the shallow-subsoil seismic properties (which are of engineering interest) by single-station measurements carried out on the Earth's surface. This method is widely used in seismic exploration as a tool for a quick detection and evaluation of seismic-amplification effects in terms of S-wave resonance frequency as well as for constraining the elastic properties of the shallow geological structure (usually under the assumption of horizontally layered

E. Lunedei, PhD (✉)

Dipartimento di Scienze Fisiche, della Terra e dell'Ambiente, Università di Siena, Siena, Italy
e-mail: lunedei@unisi.it

P. Malischewsky

Institute of Geosciences, Friedrich-Schiller University Jena, Jena, Germany
e-mail: p.mali@uni-jena.de

© The Author(s) 2015

A. Ansal (ed.), *Perspectives on European Earthquake Engineering and Seismology*,
Geotechnical, Geological and Earthquake Engineering 39,
DOI 10.1007/978-3-319-16964-4_15

medium). Nevertheless, some controversial aspects about the exact physical interpretation of the outcome provided by this technique (the H/V curve) remain. Most of them are related with the nature of the ambient-vibration wavefield and of its sources. These differences in the H/V curve modelling might have consequences in the results of inversion procedures used to infer the subsoil stratigraphical profile from experimental measurements.

From the experimental point of view, this technique requires a three-component ground-motion acquisition and consists in performing the ratio between its horizontal and vertical Fourier spectrum, properly averaged on an adequate sample. This ratio, which is a function of the frequency, is called the H/V (or HVSR) curve (or function). The ratio is usually computed by using ground-motion velocity spectra, but displacement or acceleration spectra can be used as well. The two horizontal motion components can be combined in different ways (*vide infra*).

In order to fully exploit the H/V curve to constrain subsoil seismic-properties, some theoretical model is necessary to link the H/V pattern to the mechanical properties of geological bodies under the measuring site. As the H/V refers to ambient vibrations, any model of H/V is also a model, explicit or tacit, of the ambient-vibration wavefield, and thus it should be consistent with the other findings about the ambient-vibration wavefield, and not just gives a plausible way to reproduce the H/V curve only.

In next section, a short *excursus* on the history of the H/V theoretical explanations is presented. The most part of the proposed models, which are the sole ones considered in this review, describes the Earth as 1D medium, *i.e.*, a stack of homogeneous and isotropic horizontal layers overlying an half-space with the same characteristics. They are the models widely used, while 2D and 3D ones, which are very cumbersome under many aspects, have been playing, so far, a minor role, being their use limited to specific problems (see, *e.g.*, Bonnefoy-Claudet et al. 2004).

15.2 A Short Review on the H/V Theory

Kanai and Tanaka (1961) use the ambient-vibration horizontal-motion spectra to infer seismic subsoil properties, even if they already recognize that the ambient-vibration features depend on both site mechanical-properties and ambient-vibration sources' characteristics. Other authors, however, note that ambient-vibration spectra often reflect more the sources' characteristics rather than the subsoil ones (cf. Tokimatsu 1997).

15.2.1 The H/V Origins: Body-Wave Based Theories

Nakamura and Ueno (1986), after the Nogoshi and Igarashi's (1971) work, widespread the H/V technique, in which the effects of the source are supposed to be minimized normalizing the horizontal ground-motion spectral component by the vertical one. In the first theoretical explanation proposed by Nakamura (1989), ambient vibrations are supposed to be composed by S and Rayleigh waves, but the effect of these last ones is "eliminated" by considering the H/V spectral ratio

$$HV(\omega) \equiv \frac{A_{H,surface}^{FW}(\omega)}{A_{V,surface}^{FW}(\omega)}, \quad (15.1)$$

where $A_{H,surface}^{FW}$ and $A_{V,surface}^{FW}$ are the total (hereafter, *FW* means full-wavefield) spectral amplitudes of the horizontal and, respectively, vertical ground-motion at the Earth's surface, and ω is the angular frequency. By assuming that the analogous H/V spectral ratio computed at the bedrock is approximately unitary and that the vertical motion does not undergo any stratigraphical amplification, the Author shows that the ratio in Eq. 15.1 equals the horizontal soil transfer-function normalized by the vertical one. In this view, the H/V ratio directly would represent the amplification phenomena affecting the horizontal ground-motion. After some criticisms, Nakamura modified his interpretation of H/V spectral ratio. As expressed in Nakamura (2000), by considering the ambient-vibration wavefield composed by just vertically incident P and S waves along with Rayleigh waves, he separates these components by writing the horizontal and vertical spectral ground-motion amplitudes at the Earth's surface as

$$\begin{aligned} A_{\delta,surface}^{FW}(\omega) &= A_{\delta,surface}^{BW}(\omega) + A_{\delta,surface}^{SW}(\omega) \\ &= T_{\delta}(\omega) \cdot A_{\delta,bedrock}^{BW}(\omega) + A_{\delta,surface}^{SW}(\omega), \end{aligned} \quad (15.2)$$

where $\delta = H, V$ means horizontal and vertical component, *BW* stands for body-waves, *SW* for surface-waves and T_{δ} are the horizontal and vertical transfer functions. Equation (15.1) then gives

$$\begin{aligned} HV(\omega) &= \frac{T_H(\omega) \cdot A_{H,bedrock}^{BW}(\omega) + A_{H,surface}^{SW}(\omega)}{T_V(\omega) \cdot A_{V,bedrock}^{BW}(\omega) + A_{V,surface}^{SW}(\omega)} \\ &= \frac{A_{H,bedrock}^{BW}(\omega)}{A_{V,bedrock}^{BW}(\omega)} \cdot \frac{T_H(\omega) + \frac{A_{H,surface}^{SW}(\omega)}{A_{H,bedrock}^{BW}(\omega)}}{T_V(\omega) + \frac{A_{V,surface}^{SW}(\omega)}{A_{V,bedrock}^{BW}(\omega)}}, \end{aligned} \quad (15.3)$$

which the Author calls "quasi transfer spectrum" (QTS). Based on the hypothesis that the H/V spectral ratio at the bedrock is approximately unitary, *i.e.*,

$$A_{H,bedrock}^{BW}(\omega)/A_{V,bedrock}^{BW}(\omega) \simeq 1, \quad (15.4)$$

Eq. (15.3) shows that, when the surface-wave contribution is negligible, the function HV is close to T_H/T_V . As vertically incident body-waves are taken in account only, the P-wave and S-wave oscillation constitute respectively the vertical and horizontal ground-motion. In this theory, amplification in P-waves is not expected near the S-wave lower proper frequency, since P-wave velocity is supposed to be many times greater than the S-wave one, so the function HV should approximate the S-wave transfer function, around its peak frequency. If instead Rayleigh waves dominate, the function HV approximates the ratio $A_{H,surface}^{SW}/A_{V,surface}^{SW}$, whose peak frequency should, according to Nakamura, approximate the S-wave site resonance-frequency. Relying on other strong controversial assumptions (cf. Bard 1998), the Author concludes that the maximum of the function HV , hereafter called the H/V peak, represents the site S-wave lower resonance-frequency and the relative amplification factor, regardless of the Rayleigh-wave influence degree. The idea that the H/V peak only depend on S-wave resonance is reasserted in Nakamura (2008).

The one described above is, *de facto*, the first theoretical explanation of the H/V curve, whose the most important implication is probably that the peak frequency and amplitude of the function HV correspond to the S-wave resonance frequency and amplification factor of the site, respectively. Although this description is probably inadequate, it marked a turning point and made the fortune of the H/V technique. Indeed, while the statement about the amplitude has been proved to be almost always false, the correspondence between S-wave resonance and H/V-peak frequency has been always confirmed since then, in innumerable field experiments as well as by numerical simulations. This is by far the most useful and the most used feature of the H/V curve, but, surprisingly, it has not find a suitable complete theoretical explanation yet. Just in the particular case that surface waves are considered only (*vide infra*), the analytical formulae of Malischewsky and Scherbaum (2004) for the Rayleigh ellipticity demonstrate that the implication concerning the peak frequency is correct, in so far the impedance contrast is high enough. It is worth noting that Nakamura's theory explains the H/V curve just around its main peak frequency, and any extension to the whole H/V curve requests further assumptions (cf. Bard 1998).

Herak (2008) proposed a way to compute the H/V curve, which only involves vertically incident P and S waves. Like in first version of Nakamura's theory, no role is played by other seismic phases, included surface waves, but, differently from it, no *a priori* hypothesis is made about the P-wave site amplification. As Eq. 15.4 is supposed to hold at the bedrock, the H/V curve is given by

$$HV(\omega) \equiv \frac{A_{H,surface}^{BW}(\omega)}{A_{V,surface}^{BW}(\omega)} = \frac{AMP_S(\omega)}{AMP_P(\omega)}, \quad (15.5)$$

where $A_{H,surface}^{BW}$ is given by the S-wave spectral amplitude and $A_{V,surface}^{BW}$ is given by

the P-wave spectral amplitude, both computed at the Earth's free surface. AMP_P and AMP_S are the P-wave and S-wave amplification functions between the bedrock and the free surface, which are computed by the Herak's method, following Tsai (1970). Equation (15.5) shows that a direct estimation of the S-wave transfer function by the H/V is not always possible, because it is clear that $HV(\omega) \simeq AMP_S(\omega)$ only if $AMP_P(\omega) \simeq 1$ for all frequencies of interest. This approximation is valid only for relatively high Poisson's ratios, *i.e.*, when P-waves propagate through the topmost layers much faster than S-waves do, so that their resonance frequency is very higher than S-wave one (the Nakamura's hypothesis).

15.2.2 The Role of the Surface Waves

The fact that the H/V can be described in term of body waves travelling along particular patterns only is not at all obvious. In fact, the composition of ambient vibrations in term of the different seismic phases is not clearly understood till today, but all authors share the opinion that them are composed by all seismic phases travelling in the subsoil, although in not univocally defined proportions: the key and controversial aspect is the relative contribution of these seismic phases (see, *e.g.*, SESAME 2004). In fact, contrasting results exist both in field experiments and in numerical simulations, and it seems likely that the content in different seismic phases can drastically change in dependence on the subsoil stratigraphy and on sources' characteristics as well as in different frequency ranges.

So, as a sort of "counterparty" of the theories relied on body waves, theories based on surface-wave dominance have been developed. Already Nogoshi and Igarashi (1971) compare H/V curves from ambient vibrations with the ellipticity pattern of Rayleigh fundamental-mode, reckoning from the possibility of this comparison that this seismic phase plays the main role in the ambient vibrations. Subsequently, several other authors (*e.g.*, Lanchet and Bard 1994, 1995; Tokimatsu 1997; Konno and Ohmachi 1998; Wathelet et al. 2004) have been agreeing on the close relation existing between the H/V spectral ratio and the ellipticity of Rayleigh waves, which is reckoned as a consequence of their energetic predominance. In particular, Arai et al. (1996) and Tokimatsu (1997), like Nogoshi and Igarashi (1971), explain the ambient-vibration H/V curve by the ellipticity of the first mode of Rayleigh waves, and consider the feasibility of this explanation a suggestion of the surface-wave dominance. Surface-wave based is also the interpretation given by Konno and Ohmachi (1998), who point out that the H/V peak by ambient vibrations could be explained by the ellipticity of the fundamental Rayleigh mode as well as by the Airy phase of the fundamental Love mode, and also examine the role of the first higher Rayleigh mode. Moreover, in numerical simulations performed by these Authors, the H/V-peak amplitude roughly approximates the S-wave amplification factor, providing that a specific proportion between Rayleigh and Love waves exists; this mimics the Nakamura's statement, but in terms of surface waves instead that of body waves.

15.2.3 The Sources' Role and the Full-Wavefield

The above-mentioned theories give an explanation of the possible origin of the H/V curve, especially around its lower-frequency peak, but do not insert this explanation in a theory of the ambient-vibration wavefield. In other words, they say nothing about the origin of the H/V-curve overall shape, since they are not models for the ambient-vibration wavefield. In order to construct such a model, besides the composition of the ambient-vibration wavefield in terms of different seismic phases, another key element is its dependence on the subsoil properties. Without this piece of information, no possibility exists of using any experimental datum to estimate subsoil characteristics. For the models based on the hypothesis that just vertically incident P and S waves are important to describe the H/V curves, this aspect is simply exhausted by computing the propagation of these phases in a stratified model, as is the case of the above-mentioned Herak's approach. When the characteristics of free Rayleigh waves are needed, classical algorithms to compute them in a stratified medium can be applied. Besides these simple cases, some models have been developed in last couple of decades that manage this aspect by means of more detailed analysis of the ambient-vibration wavefield.

Lanchet and Bard (1994, 1995) consider that the ambient-vibration wavefield cannot be described in a deterministic way, because the greatest number of its sources are randomly located on the Earth's surface. So, they carry out a numerical simulation of the ambient-vibration wavefield by arranging a number of sources of different kinds acting in aleatory ways inside a given horizontal circle surrounding the receiver. For computational reasons, sources are located at depth of 2 m, while the receiver is on the Earth's surface. In this simulation, ambient-vibration displacement is the sum, in the time domain, of the ones produced by these sources in a fixed lapse of time and the H/V curve is the ratio between their horizontal and vertical Fourier amplitude-spectra. This is a purely numerical way to simulate the H/V curve, which has been used many times since then. By means of this model, Lanchet and Bard show the correspondence between the H/V peak-frequency and the S-wave resonance-frequency. Moreover, they also show that the H/V peak-frequency corresponds to the ellipticity peak-frequency of the Rayleigh fundamental mode as well as to the first-peak position of the ratio between horizontal and vertical ground-motion produced by S waves incident from a range of angles. Finally, they suggest that the overall shape of the H/V is determined by all seismic phases, and check that the peak amplitude, depending on many variables, does not correspond to the site amplification factor.

About in the same period, Field and Jacob (1993) propose a theoretical way to connect ambient-vibration displacement power-spectrum to the Green's function of the ground. They assume that the ambient vibrations are generated by an infinitude of uncorrelated point-like sources, uniformly located on the Earth's surface. The H/V curve in a point of the Earth's surface is obtained as the square root of the ratio between the horizontal and the vertical total power, computed, for any subsoil profile, as a finite sum of the contribution, in the frequency domain, given by the sources in a succession of annuli centred on the receiver and with increasing radii.

Differently from the Lanchet and Bard's model, which is purely numerical, this is an analytical model, although the sums have to be computed numerically. A decade later, Arai and Tokimatsu (2000, 2004) specialize this model to surface waves generated by sources with independent phases, which are approximated as continuously distributed on the Earth's surface. In this way, the total average spectral power is given by an integration on the horizontal plain, which can be carried out analytically. A source-free area around the receiver also exists in this model, with a radius equal to one wavelength of each propagation mode, in order to guarantee the surface-wave dominance and the possibility of describing these waves as plane waves. In order to make the power-integrals converging, these Authors insert an exponential damping factor originated by the "scattering" of the considered waves in the subsoil. A slightly modified version of this model was proposed by Lunedei and Albarello (2009), in which the damping originates by the material viscosity and the source-free area dimension does not more depend on each single propagation mode and can be done independent from the frequency too.

Fäh et al. (2001) use two ways to generate H/V synthetic curves. The first one is a numerical simulation made by a finite difference technique: these Authors agree that ambient-vibration sources are superficial, but they also introduce buried sources to describe scattering and wave conversion due to lateral heterogeneities. A large number of sources, with positions, depths and time-dependences chosen randomly, are distributed around a receiver. The second technique is a mode summation (Landisman et al. 1970). They particularly focus on the Rayleigh wave ellipticity of fundamental and higher modes, to explain the H/V-peak frequency, which they regard as the only trustworthy element, in that its amplitude and other features of the H/V curve also depend on other variables besides the S-wave velocity profile. Moreover, they identify stable parts of the H/V ratio, which are independent of the sources' distance and are dominated by the ellipticity of the fundamental Rayleigh mode, in the frequency band between the H/V-peak frequency, which they check to be close to the site S-wave fundamental resonance-frequency, and the first minimum of the H/V curve.

In their very important series of papers, Bonnefoy-Claudet et al. (2004, 2006, 2008) carry out a systematic study of the H/V curve by numerical simulations, in which the ambient vibrations are generated by a multitude of point-like forces, randomly oriented in the space and located relatively near to the observation point. They take advantage by a code developed by Hisada (1994, 1995) to compute the full displacement wavefield produced by these sources at some receivers, which are located on the Earth's surface. The total displacement at each receiver is computed by summing up, in the time domain, the one due to each sources. The H/V curve at each receiver is then computed as ratio between the average horizontal and the vertical Fourier-transform of this total displacement. In Bonnefoy-Claudet et al. (2006) the quasi-independence of the H/V curve from the specific sources' time-dependence has been confirmed. A dependency on the spatial horizontal distribution of near-surface sources as well as on the depth of buried sources has instead been observed, which however only slightly concerns the main-peak frequency. It instead shows relevant effects on H/V-peak amplitude and on the

appearance of secondary peaks. By using surface sources and several simple stratigraphical profiles, Bonnefoy-Claudet et al. (2008) check the good correspondence between the H/V-peak frequency and the S-wave resonance one. They also conclude that the H/V peak-frequency could be explained, depending on the stratigraphical situation, by Rayleigh ellipticity, Love Airy phase, S-wave resonance or a mix of them. In particular, the possibility of explaining the H/V main peak in term of Rayleigh ellipticity seems limited to profile with high impedance contrast (more than 4). An interesting result of this work is the coming out of the significant role of Love waves in the H/V curve and, more in general, in composing the ambient-vibration horizontal ground-motion. Moreover, the importance of taking into account all seismic phases propagating in the subsoil in constructing a suitable H/V model as well as the key role of the impedance contrast in controlling the origin of the H/V peak have been pointed out.

These pieces of work confirm that all seismic phases should be take into account to provide a reliable interpretation of the H/V curves. Then, the best way to reach an exhaustive description of the H/V curve by ambient vibrations seems the one firstly drawn by Field and Jacob (1993). In this line, Lunedei and Albarello (2010) extend their model, later denominated DSS (Distributed Surface Sources), to include all seismic phases. So, this model describes the full wavefield that composes the ambient vibrations, which are described as generated by a surface distribution of random sources. In this frame, the total average spectral-power is obtained by integrating the power given by the full Green's function relative to each sources and carried out by the above-mentioned Hisada's (1994, 1995) computer-program. Consequently, this model requires a double numerical integration: in the wavenumber and in the source/receiver distance. This model closely follows the Field and Jacob's (1993) one, the only relevant differences being in the relative weights between the horizontal and the vertical power, in taking into account the viscosity, and in the numerical code used to compute the Green's function. Both in full-wavefield and in surface-wave version of the DSS model, the H/V spectral ratio is obtained as square root of the ratio between the average spectral powers on the horizontal plane and along the vertical direction. By using these two versions of the DSS model, Albarello and Lunedei (2011) obtain some insights about the ambient-vibration wavefield structure. For a stratigraphical profile-set equal to the group M2* in Table 15.1 (except for the damping values), characterized by a singular impedance contrast (*vide infra*), three frequency ranges are identified:

- Low-frequencies (below the S-wave resonance frequency, f_S), where ambient-vibration spectral-powers are relatively low; in this range, the shallow layer acts as a high-pass filter, with an effect as more pronounced as sharper the impedance contrast is; both near sources and body waves dominate the wavefield; power spectra and H/V curves are significantly affected by source-free area dimension, V_P/V_S ratio and impedance-contrast strength at the bottom of the shallow layer;
- High-frequencies (above $\max\{f_P, 2f_S\}$, where f_P is the P-wave resonance frequency), where surface waves (both Love and Rayleigh, in their fundamental and higher modes) dominate the wavefield; in this range, spectral powers

Table 15.1 Stratigraphical profiles used in the numerical experiments

M2					
h (m)	V_S (m/s)	ν	ρ (g/cm ³)	D_P	D_S
25	200	0.333	1.9	0.001	0.001
5,000	1,000	0.333	2.5	0.001	0.001
∞	2,000	0.257	2.5	0.001	0.001
M2*					
h (m)	V_S (m/s)	ν	ρ (g/cm ³)	D_P	D_S
25	200	0.01–0.49	1.9	0.001	0.001
5,000	228–1,520	0.333	2.5	0.001	0.001
∞	2,000	0.257	2.5	0.001	0.001
M3					
h (m)	V_S (m/s)	V_P (m/s)	ρ/ρ_4	D_P	D_S
5	30	500	1	0.001	0.001
25	100	500	1	0.001	0.001
50	150	500	1	0.001	0.001
∞	500	1,500	1	0.001	0.001

smoothly decrease with frequency as an effect of material damping, which also results in the fact that relatively near sources mostly contribute to ambient vibrations, as more as the frequency increases; H/V curves are almost unaffected by subsoil configuration and source/receiver distances;

- Intermediate frequencies, where the most of the ambient-vibration energy concentrates; in this range, sharp peaks in the horizontal and vertical spectral powers are revealed around its left and right bounds; irrespective of the subsoil structure and source-free area considered, horizontal ground motion is dominated by surface waves, with a varying combination of Love (in the fundamental mode) and Rayleigh waves that depends on the shallow-layer Poisson’s ratio (Love-wave contribution increases with it) and, to a minor extent, on the strength of the impedance contrast; in the vertical component, Rayleigh and other phases play different roles, both depending on the source-free area dimension and of V_P and V_S profiles.

In synthetic H/V curves produced by Albarello and Lunedei (2011), the peak frequency is generally very near to f_S , irrespective of the Poisson’s ratio and of the dimension of the source-free area. A weak sensitivity is revealed with respect to the impedance contrast only, and these findings enforce the common idea that the H/V peak-frequency is a good estimate of f_S . Amplitude and shape of the H/V curve around the peak appear instead more sensitive to subsoil and source configurations, and, in particular, no linear relationship results to exist between the H/V peak-amplitude and the impedance contrast, although, in general, this amplitude increases with the impedance contrast. Moreover, a significant dependence of the H/V-peak amplitude on the dimension of the source-free area (the amplitude tendentially increases with its dimension), on the shallow-layer Poisson’s ratio (the amplitude increases with it) and thickness (the amplitude decreases when the thickness increases) was obtained.

15.2.4 *A Different Point of View: The Diffuse Wavefield*

The model proposed more recently, named DFA (Diffuse Field Approach), significantly differs from the other ones, because it assumes that ambient vibrations constitute a diffuse wavefield. This means that seismic waves propagate in every (three-dimensional) spatial direction in a uniform and isotropic way and that a specific energetic proportion between P and S waves exists, which is the same whenever and wherever. This theory, initially developed in a full-space (Sánchez-Sesma and Campillo 2006), has been afterwards applied to an half-space and to a layered half-space (Sánchez-Sesma et al. 2011; Kawase et al. 2011). The link between the H/V curve and the subsoil configuration is simply given by the Green's function, computed for source and receiver located in the same position: its imaginary part, in the spectral domain, is proportional to the average spectral-power of the ambient-vibration ground-motion. A key element in the DFA theory, which is implied in the diffuse character of the wavefield, is the loss of any trace of the sources' characteristics, so no link between displacement and its sources is involved in this theory, *ergo*, no description of ambient-vibration sources is necessary. The model can describe the ambient-vibration full-wavefield as well as its surface-wave component only, depending on whether the full-wavefield Green's function or its surface-wave component is used.

15.2.5 *Current Research Branches*

In this relatively long history of the H/V spectral-ratio theory two alternative ways of thinking (cf., *e.g.*, Nakamura 2008) can be recognized: one that tries to explain the H/V features (and in particular its peak) as an effect of body-wave resonance and another that explains them by surface waves only. Although cumbersome under many points of view, theories that take in account the entire ambient-vibration wavefield can constitute the "pacifying" solution. Anyway, at present, surface-wave based theories keeps their interest, since relative computing is remarkably faster and surface-wave properties are more open to the analytical study, with respect the full-wavefield. As a consequence, apart from vertically incident models (which do not present news), the ambient-vibration H/V theoretical study has resulted nowadays in two research branches:

- The branch that studies the ambient-vibration wavefield as a whole; in this case, the theory aims to explain the H/V curve as it is measured in field, with all its components in terms of different seismic phases; this theory has to face the problems about the role of body and surface waves as well as about the role of the sources;

- The branch that should be better named “ellipticity theory” or “Rayleigh-wave H/V”; the subject is, in this case, just the Rayleigh ellipticity, both in theory and in experiments; as it chooses, *a priori*, to take into account the Rayleigh ellipticity only, the relative theory does not need to deal neither with body waves nor with the wavefield sources, while experiments are devoted to extract Rayleigh waves from the recorded signal (*e.g.*, Fäh et al. 2001).

In order to avoid misinterpretations, it is important to distinguish the complete H/V curve from the Rayleigh ellipticity curve.

Currently, the first theory is essentially represented by models that consider surface sources, in all possible variants (the purely numerical one or the semi-analytical DSS) and the DFA: in next section a comparison between the DSS and the DFA is summarized, while in the subsequent a mention to new developments in these models is done. Afterwards, a section is devoted to the ellipticity theory.

15.3 Comparison Between the DSS and the DFA Models

In last years, some conference notes (García-Jerez et al. 2011, 2012a, b, c) were presented to compare the most recent two models of the H/V spectral ratio: the Distributed Surface Sources (DSS) and the Diffuse Field Approach (DFA). Each of them is a complete theory of the ambient vibrations and has solid theoretical foundations. Through this section, which summarizes the salient elements of these comparisons, $G_{ij}(\mathbf{x}_A, \mathbf{x}_B, \omega)$ is the frequency-domain displacement Green’s function for the considered Earth’s model at the point \mathbf{x}_A on the free surface along the i -th Cartesian axis due to a point-like force located at the point \mathbf{x}_B and directed along the j -th Cartesian axis. The three Cartesian spatial directions are marked by subscripts 1, 2 (for the horizontal plane) and 3 (for the vertical direction), while r and θ are the polar coordinates on the horizontal plane.

15.3.1 The DSS Model

The DSS model assumes that the ambient vibrations are generated by a *continuum* of aleatory point-like sources distributed on the Earth’s free-surface. The ground motion that they produce propagates to the receiver without significant scattering, except the one due to the stratigraphical interfaces present in the layered subsoil (impedance contrasts). This model has been formulated under the assumption of weakly dissipative medium, for both ambient-vibration full-wavefield (Lunedei and Albarello 2010) and surface-wave component only (Lunedei and Albarello 2009). For the full-wavefield, ambient-vibration powers along the three spatial Cartesian directions are:

$$\begin{aligned}
 P_1(\omega) + P_2(\omega) = \pi\sigma^2 \int_{r_{\min}}^{\infty} & \left[(\sigma_1^2 + \sigma_2^2) \left(|G_{11}(0, 0, 0; r, 0, 0; \omega)|^2 + \right. \right. \\
 & \left. \left. + |G_{22}(0, 0, 0; r, 0, 0; \omega)|^2 \right) + 2\sigma_3^2 |G_{13}(0, 0, 0; r, 0, 0; \omega)|^2 \right] r dr,
 \end{aligned}
 \tag{15.6}$$

$$\begin{aligned}
 P_3(\omega) = \pi\sigma^2 \int_{r_{\min}}^{\infty} & \left[(\sigma_1^2 + \sigma_2^2) |G_{31}(0, 0, 0; r, 0, 0; \omega)|^2 \right. \\
 & \left. + 2\sigma_3^2 |G_{33}(0, 0, 0; r, 0, 0; \omega)|^2 \right] r dr,
 \end{aligned}
 \tag{15.7}$$

where the arguments of the Green’s function are expressed in Cylindrical coordinates (r, θ, x_3) , σ^2 stands for the total surface variance-density of the random sources and σ_j^2 for its relative component along the j -th Cartesian axis. Formulae in Eqs. (15.6) and (15.7) correct the weight given by Field and Jacob (1993) to the vertical-load Green’s functions. $r_{\min} \geq 0$ is the radius of the circular free-source area surrounding the receiver. Finally, the H/V spectral ratio is calculated as

$$HV(\omega) \equiv \sqrt{\frac{P_1(\omega) + P_2(\omega)}{P_3(\omega)}}.
 \tag{15.8}$$

In the case of predominance of surface waves, expressions in Eqs. (15.6) and (15.7) assume a simpler form. Compact formulae were first given by Arai and Tokimatsu (2004) for an elastic stratified medium, under some additional simplifying hypotheses (asymptotic long-distance forms of the Green’s functions, suitable source-free areas, incoherent summation of modal contributions):

$$\begin{aligned}
 P_1(\omega) + P_2(\omega) = \frac{\kappa}{2}\sigma^2 \left\{ \sum_{m \in \text{RAYLEIGH}} [2\sigma_3^2 + \chi_m^2(\sigma_1^2 + \sigma_2^2)] \left(\frac{A_{Rm}}{k_{Rm}}\right)^2 \chi_m^2 \right. \\
 \left. + \sum_{m \in \text{LOVE}} (\sigma_1^2 + \sigma_2^2) \left(\frac{A_{Lm}}{k_{Lm}}\right)^2 \right\},
 \end{aligned}
 \tag{15.9}$$

$$P_3(\omega) = \frac{\kappa}{2}\sigma^2 \sum_{m \in \text{RAYLEIGH}} [2\sigma_3^2 + \chi_m^2(\sigma_1^2 + \sigma_2^2)] \left(\frac{A_{Rm}}{k_{Rm}}\right)^2,
 \tag{15.10}$$

where A_{Rm} and A_{Lm} represent the medium response of Rayleigh and Love waves for the m -th mode (Harkrider 1964) and χ_m is the corresponding Rayleigh wave ellipticity (as a real quantity), while κ is a frequency independent damping parameter, representative of the “scattering” effect. Under the same simplifying hypotheses, Lunedei and Albarello (2009) proposed a different implementation, which includes the effects of material damping (viscosity):

$$P_1(\omega) + P_2(\omega) = \frac{\sigma^2}{4} \sum_{m \in \text{RAYLEIGH}} [2\sigma_3^2 + \chi_m^2(\sigma_1^2 + \sigma_2^2)] \chi_m^2 \frac{(A_{Rm})^2}{k_{Rm} \alpha_{Rm}} \exp(-2\alpha_{Rm} r_{\min}) + \frac{\sigma^2}{4} \sum_{m \in \text{LOVE}} \frac{(A_{Lm})^2}{k_{Lm} \alpha_{Lm}} \exp(-2\alpha_{Lm} r_{\min}) \quad (15.11)$$

$$P_3(\omega) = \frac{\sigma^2}{4} \sum_{m \in \text{RAYLEIGH}} [2\sigma_3^2 + \chi_m^2(\sigma_1^2 + \sigma_2^2)] \frac{(A_{Rm})^2}{k_{Rm} \alpha_{Rm}} \exp(-2\alpha_{Rm} r_{\min}), \quad (15.12)$$

where α_{Lm} and α_{Rm} are the attenuation factors for the m -th Love and Rayleigh mode respectively, which depend on the viscous properties of the medium. These formulae explicitly depend on the source-free area radius $r_{\min} \geq 0$, which can be set either constant or frequency dependent.

15.3.2 The DFA Model

The DFA model assumes that the relative power of each seismic phase is prescribed by the energy equipartition principle. Under this hypothesis, proportionality exists between the Fourier-transformed autocorrelation (power spectrum), at any point of the medium, and the imaginary part of the Green's function computed when source location corresponds to the one of the receiver (Sánchez-Sesma et al. 2011). The assumption of a major role of multiple scattering involving all possible wavelengths is behind this formulation.

In this model, under the assumption of a pure 1D configuration (horizontal layering), where the horizontal directions are indistinguishable, the H/V spectral ratio is given as

$$HV(\omega) \equiv \sqrt{\frac{P_1(\omega) + P_2(\omega)}{P_3(\omega)}} = \sqrt{\frac{2\text{Im}[G_{11}(\mathbf{x}; \mathbf{x}; \omega)]}{\text{Im}[G_{33}(\mathbf{x}; \mathbf{x}; \omega)]}}, \quad (15.13)$$

where $P_j(\omega) \propto \text{Im}[G_{jj}(\mathbf{x}; \mathbf{x}; \omega)]$ for $j = 1, 2, 3$, \mathbf{x} is an arbitrary point on the free surface and “Im” means imaginary part. Equation (15.13) links the function HV with the subsoil mechanical properties, and accounts for the contributions of surface and body waves.

Whenever surface waves can be considered to represent the dominant contribution to the wavefield, the model can be simplified by rewriting the Green's functions in terms of their well-known modal characteristic, so the powers can be expressed as

$$P_1(\omega) = P_2(\omega) \propto -\text{Im}[G_{11}(\mathbf{x}; \mathbf{x}; \omega)] \rightarrow \frac{1}{4} \sum_m \{A_{Rm} \chi_m^2 + A_{Lm}\}, \quad (15.14)$$

$$P_3(\omega) \propto -\text{Im}[G_{33}(\mathbf{x}; \mathbf{x}; \omega)] \rightarrow \frac{1}{2} \sum_m A_{Rm}. \quad (15.15)$$

15.3.3 Comparison

The differences between DSS and DFA model are shown in a more explicit form if their versions for surface waves are compared (Eqs. 15.9, 15.10 or 15.11, 15.12 vs 15.14, 15.15). The formulae have a similar structure, but the contributions of each wave-type and mode to the total power differ. Indeed, they depend on $A_{\bullet m}$ in the DFA formulation and on $\left(\frac{A_{\bullet m}}{k_{\bullet m}}\right)^2$ or $\frac{(A_{\bullet m})^2}{k_{\bullet m} \alpha_{\bullet m}} \cdot \exp(-2\alpha_{\bullet m} x_{\min})$ in the DSS one, where “ \bullet ” indicates Love or Rayleigh waves. The square operator in the last model is a consequence of the power computation; in the DFA model, the correct physical dimension is guaranteed by an appropriate factor that multiplies the imaginary part of the Green’s function. So, while in the DSS the energy repartition among contributing waves depends on the energy of each wave (expressed by its square amplitude), in the DFA this repartition is established by the Green’s function for coincident source and receiver. This is a very important physical difference between the two models. The common inverse wavenumber $1/k_{\bullet m}$ in the DSS formulae represents an effect of the long-range wave propagation from the generic source to the receiver, while the other $1/k_{\bullet m}$ factor or the correspondent $1/\alpha_{\bullet m}$ is the effect of the integration on the horizontal distance to compute the total source distribution effect. Both these elements are obviously absent in the DFA. In both the considered models, the function HV restricted to surface-waves tends to the ellipticity of (non-dispersive) Rayleigh waves over a half-space and depend on the characteristics of the deeper medium, as $\omega \rightarrow 0$.

In order to study the differences and similarities of these two models, a set of synthetic tests was performed (see notes quoted at the beginning of the section): results relative to stratigraphic profiles listed in Table 15.1 are here shown. The group of profiles M2* is generated by varying the profile M2, and all these profiles basically consist of a layer overlying an half-space (although a intermediate thick buffer layer exists, which prevents from sharply unrealistic truncation of surface-wave higher modes in the range of frequency of interest). The profile M3, instead, presents two major and a weak impedance contrasts. For the DSS model, $\sigma_1^2 = \sigma_2^2 = \sigma_3^2 = 1/3$ was set.

Albarelo and Lunedei (2011) find, for the profile M2, significant contributions of body waves for frequencies around and below the S-wave resonance frequency f_s (2 Hz in this case), and a clear surface-wave dominance for frequencies larger than the P-wave one f_p (4 Hz in this case). This fact reflects on the deviation between blue (full wavefield, FW) and green (surface waves, SW) curves in Fig. 15.1a around the peak frequency. When a circular source-free area with a radius of 10 m exists (Fig. 15.1b), the FW produces an H/V peak equal to the one of the SW,

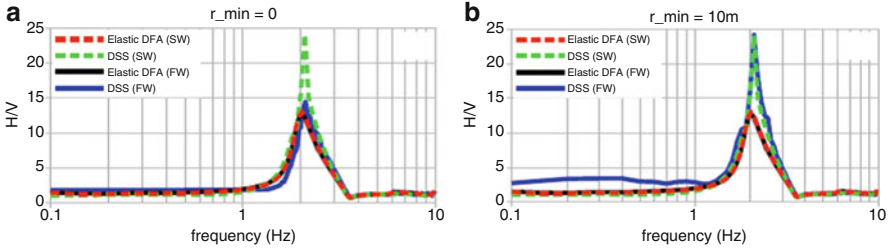


Fig. 15.1 H/V curves for the stratigraphy M2 obtained by the DSS for the full-wavefield (blue) and the surface-wave component (green), as well as by the DFA for the full-wavefield (black) and the surface-wave component (red); (a) no source-free area is considered; (b) a source-free area with radius 10 m is set in the DSS

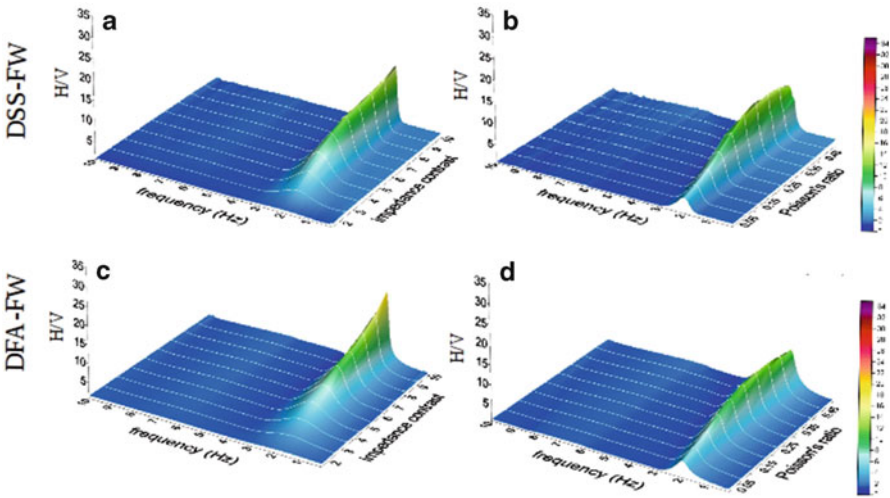


Fig. 15.2 Upper panels: H/V curves computed by the full-wavefield DSS for models in set M2*, with $r_{min}=0$. Lower panels: respective counterparts obtained by using the full-wavefield DFA

probably as a consequence of the more efficient propagation of these last at long distances. The elastic DFA results show no difference between FW and SW H/V-curve, which peak amplitude is less than the DSS one.

Moreover, as said in the previous section, a parametric study of this stratigraphy is realized by considering the profiles' family M2*, which full-wavefield results are shown in Fig. 15.2.

By using the profile M3, which presents two important impedance contrasts at 5 and 80 m and a minor one at 30 m depth, it has been pointed out that, differently from the single-layer case, remarkable differences in the H/V shape deduced from DFA and DSS can occur for more complicated subsurface structures. Rough calculations from the S-wave travel-time lead to expected resonance frequencies of 1.5 and 0.33 Hz respectively for the principal contrasts and 0.6 for the secondary one. Two

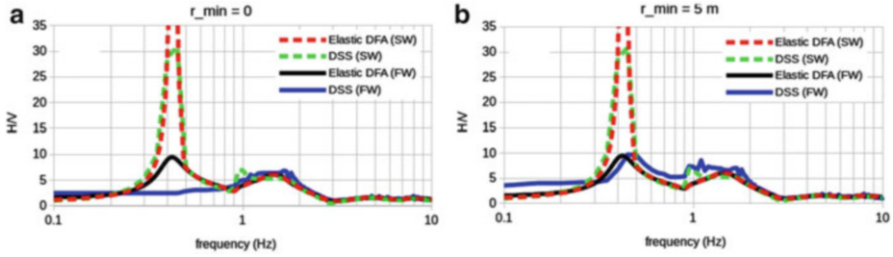


Fig. 15.3 H/V curves from DFA and DSS method for the profile M3; (a) sources are allowed on the whole Earth's surface; (b) near sources are removed from around the receiver up to the distance of 5 m

peaks appear in the elastic DFA computation near to 0.4 and 1.5 Hz (which can be associated with the two subsoil principal interfaces), both for the FW (black lines in Fig. 15.3) and the SW (red lines in Fig. 15.3). The DSS response is more complex. When no source-free area exists, the DSS-FW H/V (blue line in Fig. 15.3a) only shows the peak correspondent to the shallowest impedance contrast, while the other is retrieved by the DSS-SW counterpart (green line in Fig. 15.3a). The main peak is recovered in the DSS-FW H/V curve if close sources are removed from the calculations, as Fig. 15.3b (blue line) shows for $r_{\min} = 5$ m, and in that case the overall shape of the DFA-FW and DSS-FW curves approximately approach. These results suggest that DFA and DSS might lead to closer results whenever a suitable source-free area is used in the DSS-FW computations, letting surface waves play a predominant role. The SW results seem very similar in every case.

The results obtained indicate that both the DSS and the DFA provide reasonable full-wavefield and surface-wave synthetics of H/V spectral ratios. In spite of the rather different underlying hypotheses, DFA and DSS lead to similar H/V curves for stratigraphic profiles with a dominant impedance contrast (M2*). Relative H/V main peaks match the first S-wave resonance frequency (f_S) in a very good way. Nevertheless, peak amplitudes may differ and show non-trivial dependence on impedance contrast and Poisson's ratio. Results relative to DSS also depend on the source distribution around the receiver. For both models, surface waves represent the dominant contribution at high enough frequencies, whereas body waves play an important role around and below f_S . For a stratigraphy with more impedance contrasts, some variability occurs in the overall shape of the H/V curve in the full-wavefield DSS when sources are present or absent near the receiver. Whenever near sources are eliminated from the DSS computation (so surface waves are playing the major role), both DFA and DSS provide very similar results, and this seems suggest that, although physical bases are different, surface-wave behaviour described by DFA and DSS is very similar. In any case, the differences in the overall H/V curve features make clear that further investigations on the relationships between DFA and DSS are still necessary.

15.4 A Mention to the Most Recent Results in H/V Modelling

To overcome some limits of the full-wavefield DSS model, a new version of it has been very recently proposed by Lunedei and Albarello (2014, 2015). This new theory bases on describing the ambient-vibration ground-motion displacement and its generating force fields as three-variate, three-dimensional stochastic processes stationary both in time and space. In this frame, the displacement power can be linked with the source filed power *via* the Green's function, which, in turn, depends on the subsoil configuration.

About the DFA model, very recently García-Jerez et al. (2013) have shown some consequence, at low and high frequencies, of its application to a simple crustal model. The most recent development of this model is its application to a case where a lateral variation exists, by Matsushima et al. (2014).

Finally, the DSS model gives a suitable base to compare the different definitions of the H/V curve appeared in literature. Called H_N and H_E the spectra of the ambient-vibration ground-motion horizontal components along two orthogonal directions, Albarello and Lunedei (2013) compare the following definitions for the merging of these horizontal components:

1. No combination, that is, two H/V curves are computed by considering separately the two directions,
2. Arithmetic mean, $H \equiv (H_N + H_E)/2$,
3. Geometric mean, $H \equiv \sqrt{H_N \cdot H_E}$,
4. Vector summation, $H \equiv \sqrt{H_N^2 + H_E^2}$,
5. Quadratic mean, $H \equiv \sqrt{(H_N^2 + H_E^2)/2}$,
6. Maximum horizontal value, $H \equiv \max\{H_N, H_E\}$,

and, given L elements of the statistical sample (typically, time-windows), the two ways to experimentally define the H/V ratio:

- (a) The square root of the ratio between the arithmetic mean of the spectral powers on the L time-windows,
- (b) The arithmetic mean of the H/V ratios computed in each of the L time-windows.

It results that the H/V estimates are biased of 46 % to more than 100 % and that, while the definition (a) quickly reduces its bias-size (for all cases 1–6) as L increases, this does not happen for the definition (b). Figure 15.4 shows the bias pattern when the number of degree of freedom ($m=2L$) increases. A role of the smoothing procedures in reducing the bias also emerges in the quoted paper.

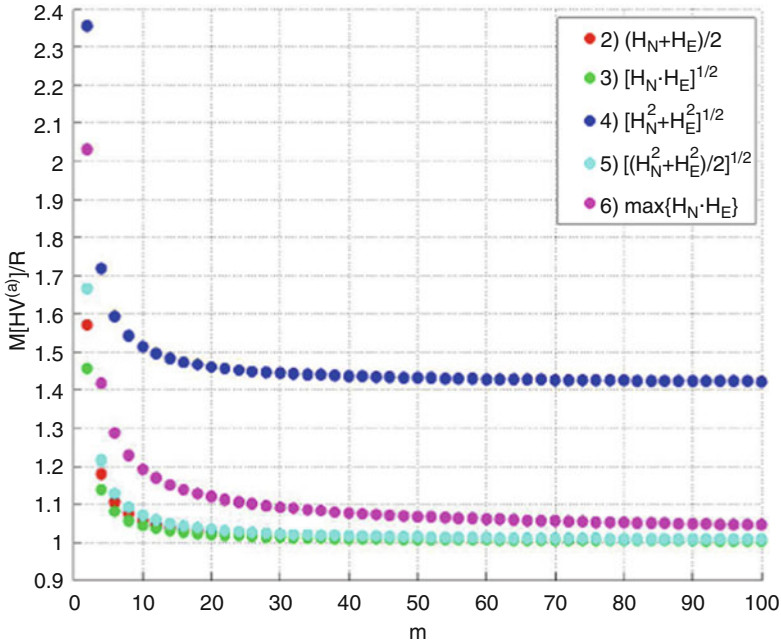


Fig. 15.4 Relative bias of the different H/V definitions with respect the mathematical expectations of H/V (named R)

15.5 Rayleigh Ellipticity Theory

In this research branch, the H/V curve is identified *a priori* and by definition with the ellipticity of Rayleigh waves, which is the subject of the study. A short summary on this topic can be found, *e.g.*, in SESAME (2004). Moreover, a part of the popular Geopsy software (<http://www.geopsy.org/>) is focused on the ellipticity. Fäh et al. (2001) propose a way to extract Rayleigh ellipticity experimentally and to compare it with a theoretical model. Malischewsky and Scherbaum (2004) investigate some important properties of H/V on the basis of Rayleigh waves by re-analysing an old formula of Love, and obtaining essential results to apply the H/V method. Later, the theory for the ellipticity of Rayleigh waves was carefully studied by Tran (2009) and Tran et al. (2011) with particular regard to applications for the H/V method.

15.5.1 Osculation Points

An interesting special and less-known feature of the ellipticity is the role of so-called osculation points, which are those points (see, *e.g.*, Forbriger 2003) where two dispersion curves of surface waves (especially Rayleigh waves) come

very near to each other and eventually even cross under certain circumstances (see Kausel et al. 2015). For sake of simplicity, just a stratigraphic profile constituted by a single horizontal layer over an half-space (LOH) is used to describe the special behaviour of the ellipticity at these points. Named h and V_{S1} the shallow-layer thickness and S-wave velocity respectively, V_{S2} the S-wave velocity of the half-space, r_d the ratio between their densities and $r_S \equiv V_{S1}/V_{S2}$, the only impedance contrast of the profile is $r_S \cdot r_d$. Dimensionless surface-wave phase-velocity $C = c/V_{S1}$ and frequency $\bar{f} \equiv \frac{h}{V_{S1}} \cdot f$ are also defined. The limit case of this model is the model LFB (layer with fixed bottom), defined by the limit $r_S \rightarrow 0$. Some analytical formulae exist for the LFB model, but for the LOH model there are approximate formulae only. Usually it is assumed, for the LOH model, that the Rayleigh-wave H/V (ellipticity) curve has, as a function of the frequency, one peak depending on the subsoil properties, whereas a model with two layers over a half-space may have two peaks (e.g., Wathelet et al. 2004). However, a more careful theoretical analysis shows that also a LOH model exhibits two peaks within a certain parameter range. Tran (2009) establishes that two peaks emerge for the LFB model when the Poisson's ratio ν_1 of the shallow layer is in the interval $\nu_1^{(1)} < \nu_1 < \nu_1^{(2)}$, with $\nu_1^{(2)} = 0.25$ and $\nu_1^{(1)} \approx 0.2026$, which last is a solution of the equation

$$1 - 2\sqrt{\gamma} \sin\left(\frac{\pi}{2}\sqrt{\gamma}\right) = 0, \quad (15.16)$$

with $\gamma \equiv \frac{1-2\nu_1}{2(1-\nu_1)} = \frac{V_{S1}^2}{V_{S2}^2 \rho_1}$. The first peak of the Rayleigh-wave H/V curve (i.e., in this frame, the Rayleigh ellipticity curve) is for $\bar{f}_1 = 0.25$, while the second peak occurs for

$$\bar{f}_2 = \frac{C}{2\pi\sqrt{C^2\gamma - 1}} \cdot \arccos\sqrt{\frac{\gamma(1 - C^2) + C^2/4}{\gamma(1 - C^2) + 1}}, \quad (15.17)$$

and C is the solution of the transcendental equation

$$\begin{aligned} & \sqrt{C^2 - 1} \cdot \arccos\sqrt{\frac{\gamma(1 - C^2) + C^2/4}{\gamma(1 - C^2) + 1}} \\ &= \sqrt{C^2\gamma - 1} \cdot \arccos\left[\frac{2}{2 - C^2} \cdot \sqrt{\frac{\gamma(1 - C^2) + C^2/4}{\gamma(1 - C^2) + 1}}\right]. \end{aligned} \quad (15.18)$$

At the osculation point, which for the LFB occurs at $\nu_1^{(2)}$ and is a degeneration point, the H/V curve changes its properties from having two peaks to having one peak and one zero-point. A similar behaviour is exhibited for the LOH model:

- if $\bar{\nu}_1^{(1)} < \nu_1 < \bar{\nu}_1^{(2)}$ the H/V curve has two peaks,
- if $\bar{\nu}_1^{(2)} < \nu_1 < 0.5$ the H/V curve has one peak and one zero-point,

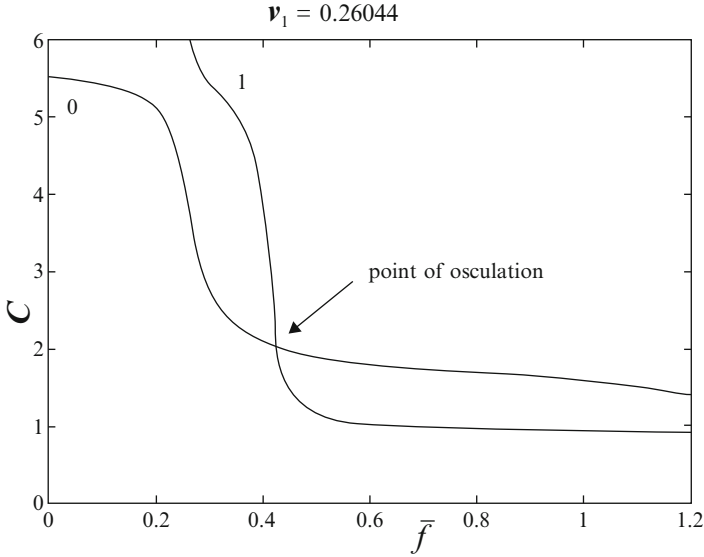


Fig. 15.5 Dimensionless dispersion curves $C(\bar{f})$ for the fundamental (0) and first higher (1) Rayleigh mode for a LOH model with parameters $r_s = 1/6$, $r_d = 2/2.7$, $\nu_1 = 0.26044$, $\nu_2 = 0.2506$, where ν_1 and ν_2 are the Poisson’s ratios of the shallow layer and the half-space, respectively (After Tran 2009)

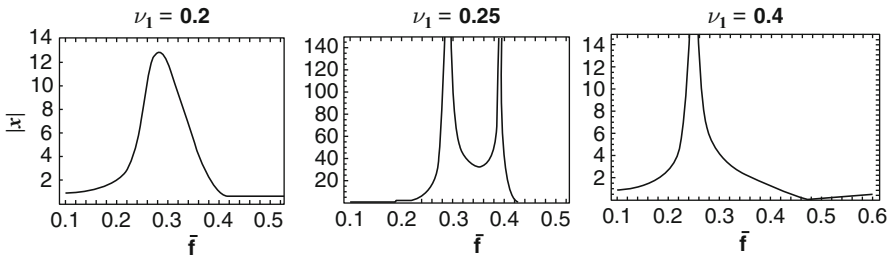


Fig. 15.6 Behaviour of H/V curve for the fundamental mode for different shallow-layer Poisson’s ratios. *Left*: $\nu_1 = 0.2$ (one maximum, *i.e.*, one peak with finite amplitude); *middle*: $\nu_1 = 0.25$ (2 peaks); *right*: $\nu_1 = 0.4$ (one peak and one zero-point)

where $\bar{\nu}_1^{(1)}$ and $\bar{\nu}_1^{(2)}$ are complicated functions of the model parameters; in particular, $\bar{\nu}_1^{(2)}$ is the value at which the osculation point occurs, whose an example is shown in Fig. 15.5. The first peak occurs nearby $\bar{f} = 0.25$ when r_s is small enough (Malischewsky and Scherbaum 2004).

The behaviour of the H/V given by the Rayleigh ellipticity $\bar{\chi}$ in dependence on \bar{f} for the LOH model with parameters of Fig. 15.5 and different ν_1 values is presented in Fig. 15.6. The critical values $\bar{\nu}_1^{(1)}$ and $\bar{\nu}_1^{(2)}$ are, in this case, $\bar{\nu}_1^{(1)} = 0.24319$ and $\bar{\nu}_1^{(2)} = 0.26044$.

It turns out that the osculation point is, for LOH again, the point where the H/V curve changes its behaviour dramatically. The practical consequences of this behaviour are discussed for models in Israel and Mexico in Malischewsky et al. (2010).

15.6 Conclusions

This short *excursus* on the way to construct a theory able to explain the H/V curve features shows that, in spite of the strongly different hypothesis underlying the various proposed theories, the key element of the H/V curve, *i.e.*, the main peak frequency, is reproduced in a more than acceptable way by all of them. Even though, in order to be able to profoundly understand the relative role of the model and of the stratigraphy in affecting the synthetic H/V curves, a big systematic comparative work would be necessary, the capability of different theories of giving realistic features of this quantity reinforces the idea that the H/V curve, and in particular its main peak frequency, express intrinsic properties of the subsoil, *i.e.*, that it is eminently determined by the stratigraphical profile, *ergo* it gives a true piece of information about the subsoil seismic properties. By a phrase, the H/V seems to resist theories!

Acknowledgments Authors are grateful to Prof. Dario Albarello for useful suggestions about the subject of this paper.

Open Access This chapter is distributed under the terms of the Creative Commons Attribution Noncommercial License, which permits any noncommercial use, distribution, and reproduction in any medium, provided the original author(s) and source are credited.

References

- Albarello D, Lunedei E (2011) Structure of an ambient vibration wavefield in the frequency range of engineering interest ([0.5, 20] Hz): insights from numerical modelling. *Near Surface Geophys* 9:543–559. doi:[10.3997/1873-0604.2011017](https://doi.org/10.3997/1873-0604.2011017)
- Albarello D, Lunedei E (2013) Combining horizontal ambient vibration components for H/V spectral ratio estimates. *Geophys J Int* 194:936–951. doi:[10.1093/gji/ggt130](https://doi.org/10.1093/gji/ggt130)
- Arai H, Tokimatsu K, Abe A (1996) Comparison of local amplifications estimated from microtremor f-k spectrum analysis with earthquake records. In: Proceedings of the 11th world conferences on earthquake engineering (WCEE), Acapulco. <http://www.nicee.org/wcee/>
- Arai H, Tokimatsu K (2000) Effect of Rayleigh and Love waves on microtremor H/V spectra. In: Proceedings of the 12th world conferences on earthquake engineering (WCEE), Auckland. <http://www.nicee.org/wcee/>
- Arai H, Tokimatsu K (2004) S-wave velocity profiling by inversion of microtremor H/V spectrum. *Bull Seismol Soc Am* 94(1):53–63

- Bard PY (1998) Microtremor measurements: a tool for site effect estimation? In: Proceedings of the 2nd international symposium on the effects of surface geology on seismic motion, Yokohama, pp 1251–1279
- Bonnefoy-Claudet S, Cornou C, Kristek J, Ohrnberger M, Wathelet M, Bard PY, Moczo P, Fäh D, Cotton F (2004) Simulation of seismic ambient noise: I. Results of H/V and array techniques on canonical models. In: Proceedings of the 13th world conferences on earthquake engineering (WCEE), Vancouver. <http://www.nicee.org/wcee/>
- Bonnefoy-Claudet S, Cornou C, Bard PY, Cotton F, Moczo P, Kristek J, Fäh D (2006) H/V ratio: a tool for site effects evaluation. Results from 1-D noise simulation. *Geophys J Int* 167:827–837. doi:[10.1111/j.1365-246X.2006.03154.x](https://doi.org/10.1111/j.1365-246X.2006.03154.x)
- Bonnefoy-Claudet S, Köhler A, Cornou C, Wathelet M, Bard PY (2008) Effects of Love waves on microtremor H/V ratio. *Bull Seismol Soc Am* 98(1):288–300. doi:[10.1785/0120070063](https://doi.org/10.1785/0120070063)
- Fäh D, Kind F, Giardini D (2001) A theoretical investigation of average H/V ratios. *Geophys J Int* 145:535–549
- Field E, Jacob K (1993) The theoretical response of sedimentary layers to ambient seismic noise. *Geophys Res Lett* 20(24):2925–2928
- Forbriger T (2003) Inversion of shallow-seismic wavefields: I. Wavefield transformation. *Geophys J Int* 153:735–752
- García-Jerez A, Luzón F, Sánchez-Sesma FJ, Santoyo MA, Albarello D, Lunedei E, Campillo M, Iturrarán-Viveros U (2011) Comparison between two methods for forward calculation of ambient noise H/V spectral ratios. AGU Fall Meeting 2011, 5–9 Dec 2011, San Francisco. <http://abstractsearch.agu.org/meetings/2011/FM/sections/S/sessions/S23A/abstracts/S23A-2230.html>
- García-Jerez A, Luzón F, Albarello D, Lunedei E, Sánchez-Sesma FJ, Santoyo MA (2012a) Comparison between ambient vibration H/V synthetics obtained from the Diffuse Field Approach and from the Distributed Surface Load method. In: Proceedings of the XXIII general assembly of the European seismological commission (ESC 2012), 25–30 Aug 2012, Moscow, pp 412–413
- García-Jerez A, Luzón F, Albarello D, Lunedei E, Santoyo MA, Margerin L, Sánchez-Sesma FJ (2012b) Comparison between ambient vibrations H/V obtained from the diffuse field and distributed surface source models. In: Proceedings of the 15th world conferences on earthquake engineering (WCEE), 24–28 Sept 2012, Lisbon. <http://www.nicee.org/wcee/>
- García-Jerez A, Luzón F, Lunedei E, Albarello D, Santoyo MA, Margerin L, Sánchez-Sesma FJ (2012c) Confronto fra le curve H/V da vibrazioni ambientali prodotte dai modelli di distribuzione superficiale di sorgenti e di campo diffuso, Atti del XXXI Convegno Nazionale del Gruppo Nazionale di Geofisica della Terra Solida, 20–22 Nov 2012, Potenza, pp 148–157. <http://www2.ogs.trieste.it/gngts/> (Sessione 2, Tema 2) (in Italian)
- García-Jerez A, Luzón F, Sánchez-Sesma FJ, Lunedei E, Albarello D, Santoyo MA, Almendros J (2013) Diffuse elastic wavefield within a simple crustal model. Some consequences for low and high frequencies. *J Geophys Res* 118:1–19. doi:[10.1002/2013JB010107](https://doi.org/10.1002/2013JB010107)
- Harkrider DG (1964) Surface waves in multilayered elastic media. Part 1. *Bull Seismol Soc Am* 54:627–679
- Herak M (2008) ModelHVSR – a Matlab® tool to model horizontal-to-vertical spectral ratio of ambient noise. *Comput Geosci* 34(11):1514–1526. doi:[10.1016/j.cageo.2007.07.009](https://doi.org/10.1016/j.cageo.2007.07.009)
- Hisada Y (1994) An efficient method for computing Green's functions for a layered half-space with sources and receivers at close depths. *Bull Seismol Soc Am* 84(5):1456–1472
- Hisada Y (1995) An efficient method for computing Green's functions for a layered half-space with sources and receivers at close depths (part 2). *Bull Seismol Soc Am* 85(4):1080–1093
- Kanai K, Tanaka T (1961) On microtremors. VIII. *Bull Earthq Res Inst* 39:97–114
- Kausel E, Malischewsky P, Barbosa J (2015) Osculations of spectral lines in a layered medium. *Wave Motion* (in press). doi:[10.1016/j.wavemoti.2015.01.004](https://doi.org/10.1016/j.wavemoti.2015.01.004), (<http://dx.doi.org/10.1016/j.wavemoti.2015.01.004>)
- Kawase H, Sánchez-Sesma FJ, Matsushima S (2011) The optimal use of horizontal-to-vertical spectral ratios of earthquake motions for velocity inversions based on diffuse-field theory for plane waves. *Bull Seismol Soc Am* 101(5):2001–2014. doi:[10.1785/0120100263](https://doi.org/10.1785/0120100263)

- Konno K, Ohmachi T (1998) Ground-motion characteristics estimated from spectral ratio between horizontal and vertical components of microtremors. *Bull Seismol Soc Am* 88(1):228–241
- Lanchet C, Bard PY (1994) Numerical and theoretical investigations on the possibilities and limitations of Nakamura's technique. *J Phys Earth* 42:377–397
- Lanchet C, Bard PY (1995) Theoretical investigations on the Nakamura's technique. In: Proceedings of the 3rd international conference on recent advanced in geotechnical earthquake engineering and soil dynamics, 2–7 Apr 1995, St. Louis (Missouri), vol II
- Landisman L, Usami T, Sato Y, Massè R (1970) Contributions of theoretical seismograms to the study of modes, rays, and the earth. *Rev Geophys Space Phys* 8(3):533–589
- Lunedei E, Albarello D (2009) On the seismic noise wavefield in a weakly dissipative layered Earth. *Geophys J Int* 177:1001–1014. doi:[10.1111/j.1365-246X.2008.04062.x](https://doi.org/10.1111/j.1365-246X.2008.04062.x) (Erratum: *Geophys J Int* 179:670. doi:[10.1111/j.1365-246X.2009.04344.x](https://doi.org/10.1111/j.1365-246X.2009.04344.x))
- Lunedei E, Albarello D (2010) Theoretical HVSR curves from full wavefield modelling of ambient vibrations in a weakly dissipative layered Earth. *Geophys J Int* 181:1093–1108. doi:[10.1111/j.1365-246X.2010.04560.x](https://doi.org/10.1111/j.1365-246X.2010.04560.x) (Erratum: *Geophys J Int* 192:1342. doi:[10.1093/gji/ggs047](https://doi.org/10.1093/gji/ggs047))
- Lunedei E, Albarello D (2014) Complete wavefield modelling of ambient vibrations from a distribution of correlated aleatory surface sources: computation of HVSR. Special Session “Ambient Noise for soil and building studies” of the Second European Conference on Earthquake Engineering and Seismology (2ECEES), 24–29 Aug 2014, Istanbul
- Lunedei E, Albarello D (2015) Horizontal-to-vertical spectral ratios from a full-wavefield model of ambient vibrations generated by a distribution of spatially correlated surface sources. *Geophys J Int* 201:1140–1153. doi:[10.1093/gji/ggv046](https://doi.org/10.1093/gji/ggv046)
- Malischewsky PG, Scherbaum F (2004) Love's formula and H/V-ratio (ellipticity) of Rayleigh waves. *Wave Motion* 40:57–67
- Malischewsky PG, Zaslavsky Y, Gorstein M, Pinsky V, Tran TT, Scherbaum F, Flores Estrella H (2010) Some new theoretical considerations about the ellipticity of Rayleigh waves in the light of site-effect studies in Israel and Mexico. *Geofisica Int* 49:141–151
- Matsushima S, Hirokawa T, De Martin F, Kawase H, Sánchez-Sesma FJ (2014) The effect of lateral heterogeneity on horizontal-to-vertical spectral ratio of microtremors inferred from observation and synthetics. *Bull Seismol Soc Am* 104(1):381–393. doi:[10.1785/0120120321](https://doi.org/10.1785/0120120321)
- Nakamura Y, Ueno M (1986) A simple estimation method of dynamic characteristics of subsoil. In: Proceedings of the 7th Japan earthquake engineering symposium, Tokyo, pp 265–270 (in Japanese)
- Nakamura Y (1989) A method for dynamic characteristics estimation of subsurface using microtremor on the ground surface. *Q Rep Railw Tech Res Inst* 30(1):25–30
- Nakamura Y (2000) Clear identification of fundamental idea of Nakamura's technique and its applications. In: Proceedings of the 12th world conference on earthquake engineering (WCEE), Auckland. <http://www.nicee.org/wcee/>
- Nakamura Y (2008) On the H/V spectrum. In: Proceedings of the 14th world conference on earthquake engineering (WCEE), Beijing. <http://www.nicee.org/wcee/>
- Nogoshi M, Igarashi T (1971) On the amplitude characteristics of microtremor (part 2). *J Seismol Soc Jpn* 24:26–40 (in Japanese with English abstract)
- Sánchez-Sesma FJ, Campillo M (2006) Retrieval of the Green's function from cross correlation: the canonical elastic problem. *Bull Seismol Soc Am* 96(3):1182–1191. doi:[10.1785/0120050181](https://doi.org/10.1785/0120050181)
- Sánchez-Sesma FJ, Rodríguez M, Iturrarán-Viveros U, Luzón F, Campillo M, Margerin L, García-Jerez A, Suarez M, Santoyo MA, Rodríguez-Castellanos A (2011) A theory for microtremor H/V spectral ratio: application for a layered medium. *Geophys J Int* 186:221–225
- SESAME (2004) European Research Project, WP12–deliverable D23.12. Guidelines for the implementation of the H/V spectral ratio technique on ambient vibrations: measurements, processing and interpretation (see Bard PY et al (2004) The SESAME Project: an overview and main results. In: 13th world conference on earthquake engineering (WCEE), Vancouver, 1–6 Aug 2004, paper no. 2207, <http://www.nicee.org/wcee/>)

- Tokimatsu K (1997) Geotechnical site characterization using surface waves. In: Ishihara K (ed) *Earthquake geotechnical engineering: proceedings of IS-Tokyo '95, the first international conference on earthquake geotechnical engineering*, Tokyo, 14–16 Nov 1995, vol 3. A A Balkema Publishers, Rotterdam, pp 1333–1368
- Tsai NC (1970) A note on the steady-state response of an elastic half-space. *Bull Seismol Soc Am* 60:795–808
- Tran TT (2009) The ellipticity (H/V-ratio) of Rayleigh surface waves. PhD dissertation, Friedrich-Schiller-University, Jena
- Tuan TT, Scherbaum F, Malischewsky PG (2011) On the relationship of peaks and troughs of the ellipticity (H/V) of Rayleigh waves and the transmission response of single layer over half-space models. *Geophys J Int* 184:793–800
- Wathelet M, Jongmans D, Ohrnberger M (2004) Surface-wave inversion using a direct search algorithm and its application to ambient vibration measurements. *Near Surface Geophys* 2:211–221

Chapter 16

Macroseismic Intervention Group: The Necessary Field Observation

Christophe Sira

Abstract French territory is characterized by moderate seismicity, but statistically a strong earthquake strikes mainland France every century. The French Central Seismological Office (BCSF) is in charge of macroseismic enquiries and intensity estimations for each earthquake that effects French territory.

Having used various forms of inquiry since 1921, the BCSF became aware of the limits and biases of macroseismic forms for the collection of the seismic effects, in particular for the estimation of the intensities larger or equal to VI including the damages of buildings. The field observations bring crucial informations for an accurate estimation of the intensities higher or equal to VI.

The last earthquakes in metropolitan France and West Indies islands have motivated the BCSF to create a large professional group dedicated on collecting macroseismic field observations. This group, called the Macroseismic Intervention Group (GIM), includes several earthquake specialists in various specific domains, such as vulnerability, site effects, historical intensity estimates, etc. It contributes to the European macroseismic scale, in its evolution and its future updates. By employing young specialists in this group we allow the continuity of the macroseismic work while improving the use of the acquired field data.

16.1 Introduction

Even if the basic concept of macroseismic intensity has not changed over the last century in terms of evaluating the severity of the shake from observations by currents indicators, macroseismic scales have evolved, and in particular the way macroseismic data are collected has been drastically improved over the last 15 years. This improvement is mainly related to the development of reliable Internet communications. Today, many seismic institutions and international agencies use internet forms to asking people for rapid intensity estimations of shock waves (De Rubeis et al. 2009) and the macroseismic intensity is estimated using

C. Sira (✉)

Bureau Central Sismologique Français (BCSF) UMS830, Université de Strasbourg/EOST
CNRS, 5 rue R. Descartes, Strasbourg Cedex 67084, France
e-mail: sira@unistra.fr; <http://www.franceseisme.fr>

© The Author(s) 2015

A. Ansal (ed.), *Perspectives on European Earthquake Engineering and Seismology*,
Geotechnical, Geological and Earthquake Engineering 39,
DOI 10.1007/978-3-319-16964-4_16

395

different methods of statistic treatment (De Rubeis et al. 1992). This consists on asking inhabitants how they felt the earthquake and what kinds of effects they observe on their nearby environment: objects movements, damages of furniture and buildings. We collect numerous data over a broad region where the earthquake has been felt, but very little within one specific locality. Two kinds of forms exist: one for individual person and one for a whole city. Therefore, analysts at the observatory works on a resulting data set, consisting either on a sum of individual answers or on an statistical answer at the scale of one city. Using fast Internet communications, macroseismic maps can be produced over entire affected zones, either as preliminary maps through an automatic procedure or as consolidated maps after a subsequent analysis.

At the same time, remote sensing techniques have revolutionised data access to damages to buildings. Several services are now able to provide a map of damages in a few hours or days after the earthquake.

It is therefore legitimate to address the following questions: Why do specialists go to the field, spend time and money, sometimes running the risk of injuries from exposure of aftershocks? Could Internet reports and remote sensing observations entirely replace the field observations? Why is the fieldwork essential for improving the quality of macroseismic observations?

16.2 The Necessity of Field Observations

In France, two types of informations have been systematically processed by BCSF to evaluate the EMS-98 intensity (Grünthal 1998). The first one comes from individuals spontaneously reporting to the BCSF web site,¹ within a few minutes after the shock. These individual reports correspond to the answers of 43 questions. In order to estimate in real time the shake levels and the intensity, we use the pictures provided by the person filling in the report (Fig. 16.1). Doing so, we get an individual value of the intensity (Single Query Intensity - SQI). The average of a number of SQI over each locality gives the preliminary Internet Intensity, available few minutes after the shock on our Internet web site. We archived 50,000 testimonies in our database since 2000.

The second source of information comes from official administrative procedures. Communal questionnaires, adapted to the EMS-98, are filled in within each “commune” by municipal authorities, mayor, policeman, or fireman station officers. These are aimed at giving some statistical overall view of the noticed effects within the territory of the municipality. It represents our official data for the final intensity values.

Using inquiry forms since 1921, the BCSF became aware of limits and biases of the macroseismic forms for the collection of the seismic effects, in particular for the

¹ www.franceseisme.fr

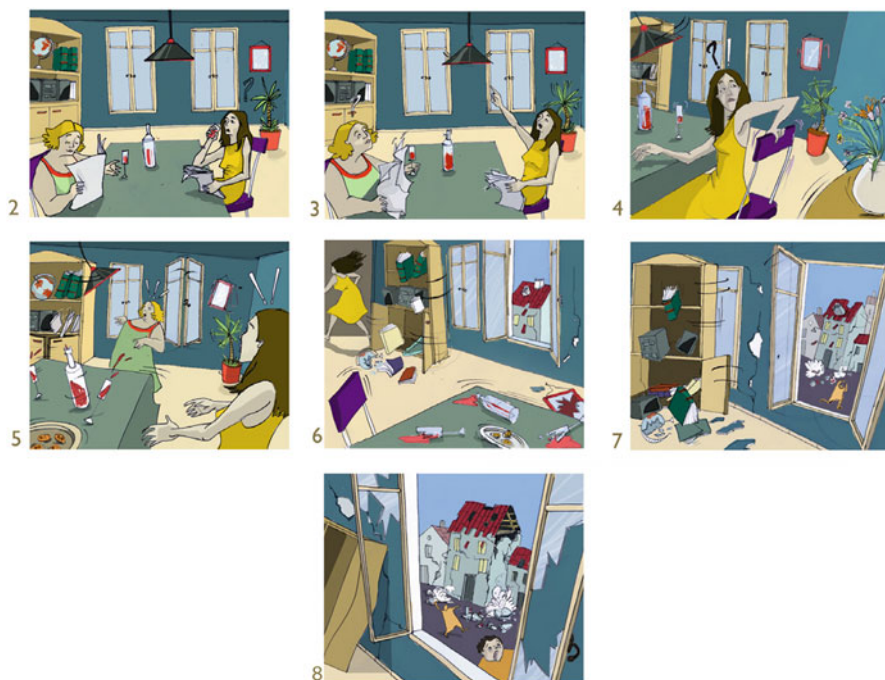


Fig. 16.1 Extract of the selectable images of the individual form representing the various levels of shock (2,3,4,5... indicates intensity level by picture)

estimation of the intensities higher or equal to VI. At this level of intensity, the description of the building vulnerability and the level of damage are important. To estimate intensity, and more exactly to use the last European scale (EMS-98), we have to know the profile of vulnerability of the city to balance the observed effects. We have to know how many building are affected in each vulnerability class (Fig. 16.2) and to what degree of damage they suffer (Fig. 16.3). However, this description is very difficult for municipal officials or inhabitants using collective or individual forms. This work is much more complicated than simply answering the questions: inhabitants may have been worried, frightened or panicked, for instanced, or the objects may have moved or fallen, or many people may have gone out in the street for the first level of intensities. In fact, the vulnerability of the buildings depends on the type of structure, and people do not to know exactly how buildings are constructed. We have observed widely varied estimates for the same municipality in our database since 2000.

In addition, in France intensity is an important criterion for the refund of damages by insurance companies. The inhabitants often exaggerate the damages or incorporate prior damages to the last earthquake in their civic declarations.

The pictures we receive from inhabitants are often too difficult to interpret or to reconcile with the data: lack of basic information such as the scale and frequency of

Fig. 16.2 Differentiation of structures (buildings) into vulnerability classes (Grünthal 1998, EMS-98 scale)

Type of Structure	Vulnerability Class					
	A	B	C	D	E	F
MASONRY	○					
	○—					
	—○					
		—○—				
		—○—				
			—○—			
				—○—		
REINFORCED CONCRETE (RC)			—○—			
				—○—		
					—○—	
			—○—			
				—○—		
					—○—	
STEEL				—○—		
WOOD			—○—			

○ most likely vulnerability class; — probable range; ----range of less probable, exceptional cases

damage, specific photo dates, etc. Our experts in the field can verify the level of the damage and decipher which originate with effects from the earthquake.

By directly interviewing the authorities, an expert in the field can obtain good results (Cecic and Musson 2004). Precision and certitude of effects can be discerned to estimate the profile of vulnerability of the municipality (Fig. 16.4). Experts can examine the list of damages collected by the city hall, visit some damage sites selected from several districts differing in types of vulnerability. They can interpret various reasons for the damage to a building and take this into account in their evaluations (Fig. 16.5).

With individual testimonies, the other biases are due to the nature of spontaneously collection via Internet. In France, the average number of individual forms collected by a city, for earthquakes since 2000, is only 3, corresponding to on average only 0.86 % of the population with a maximum at 3 %. In this case, how can we be sure to find in this individual sample the representative effects for example at the intensities VI where we should find between 2 and 15 % of the building of vulnerability A or B affected by damage degrees of 3 or 4? When we use communal answer, how to be certain that the witness knows all the rare present damages on the municipality? On the other hand, when people suffer high damages

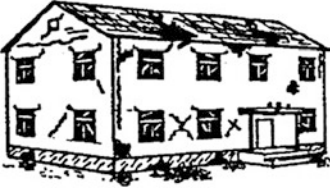
Classification of damage to masonry buildings	
	<p>Grade 1: Negligible to slight damage (no structural damage, slight non-structural damage) Hair-line cracks in very few walls. Fall of small pieces of plaster only. Fall of loose stones from upper parts of buildings in very few cases.</p>
	<p>Grade 2: Moderate damage (slight structural damage, moderate non-structural damage) Cracks in many walls. Fall of fairly large pieces of plaster. Partial collapse of chimneys.</p>
	<p>Grade 3: Substantial to heavy damage (moderate structural damage, heavy non-structural damage) Large and extensive cracks in most walls. Roof tiles detach. Chimneys fracture at the roof line; failure of individual non-structural elements (partitions, gable walls).</p>
	<p>Grade 4: Very heavy damage (heavy structural damage, very heavy non-structural damage) Serious failure of walls; partial structural failure of roofs and floors.</p>
	<p>Grade 5: Destruction (very heavy structural damage) Total or near total collapse.</p>

Fig. 16.3 Classification of damage to masonry building (Grünthal 1998, EMS-98 scale)

due to an earthquake, their concern is not to fill in forms on the Internet, but to clean and to repair their houses.

In small cities, particularly in mountain zones, the most vulnerable houses are old mainly located in the historical centre, and inhabited by elderly people typically with less Internet access. We have very little reliable data for such buildings. Even

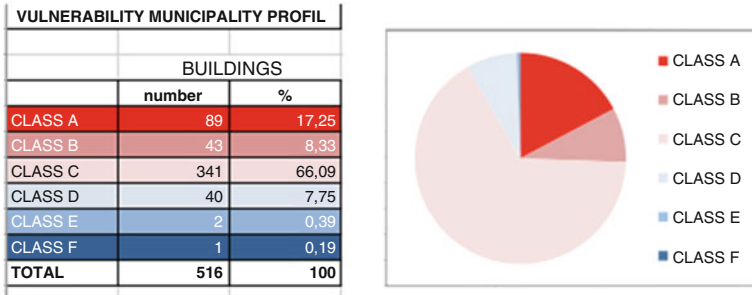


Fig. 16.4 Example of percentage of damage by vulnerability class of a city (BCSF Tool)

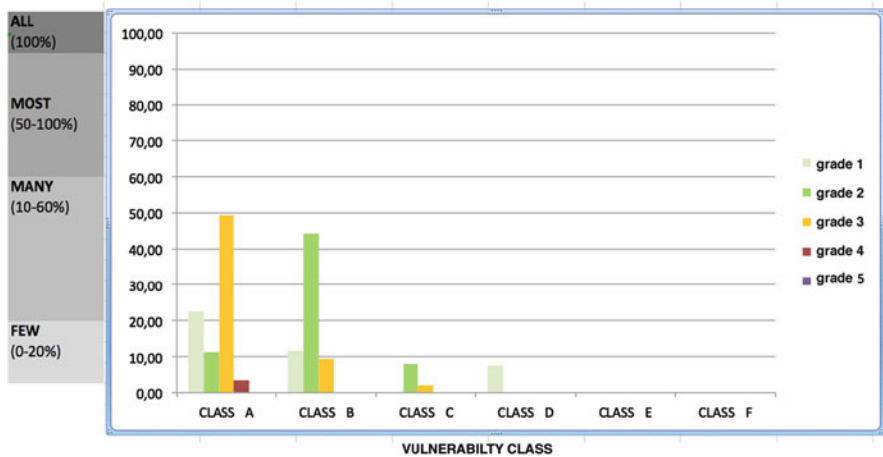


Fig. 16.5 Example of vulnerability city profile (BCSF Tool)



Fig. 16.6 False declaration by the inhabitants of terrace collapse (Les Saintes earthquake 2004). In fact the terrace is not collapse and it's only an increase of existing crack created by an amplification of differential collapse. We can see on the right picture the presence of vegetation in the crack, meaning the age of this damage

Table 16.1 Comparison of internet intensity (individual testimonies) and field intensity (by expertise) on epicentral zone (less than 20 km of epicenter) for Barcelonnette earthquake 7 April 2014 (magnitude 5.2 M_L)

Municipality	Number of inhabitants	Epicentral distance (km)	Intensity (EMS-98) evaluated by:	
			Internet (number of individual testimonies)	Field enquiry
Saint-Paul-sur-Ubaye	230	6	IV (3)	V–VI
La Condamine-Chatelard	175	6	V (6)	VI
Barcelonnette	2,883	11.5	IV (11)	VI
Saint-Pons	791	12	IV (5)	V–VI
Uvernet-Fours	633	15	IV (4)	V
Jausiers	1,163	9	V (21)	VI
Meolans-Revel	348	16.5	VI (2)	V
Faucon-de-Barcelonnette	319	11	IV–V (3)	V

if they are the first ones to be affected by the shock, and it is uncertain whether we collected this information via the ten answers we have received.

By comparison with field estimation, we know that our Internet intensity values issued from individual forms generate lower intensities in the epicentre zone (Table 16.1), as we observed again during the last earthquake in Barcelonnette in April 2014 (Sira et al. 2014).

To use reliable Internet intensities, it is essential to make a comparison with field data.

Similarly, remote sensing data analysis allows the identification with accuracy of damages of degree 5, partially degree 4 (Fig. 16.7), but not degree 3 (Fig. 16.8). This indicate that the assessable level of intensities is a function of vulnerabilities present in the municipality. So we can estimate intensities from VII if vulnerabilities A exist in the municipality, or from VIII if vulnerabilities B exist. In the field, you can observe all the levels of damages affecting buildings even if classes of high vulnerabilities are not present.

The remote sensing have lot of difficulties to give with precision the vulnerability of the building. Without vulnerability profil of commune we cannot provide intensities merely through remote sensing.

The fieldwork certainly cannot be realized on a complete zone affected, but all these observations made over the years made us aware of the necessity of working in the field.



Fig. 16.7 Unreinforced masonry with RC floors, grade of damage 4 (Grünthal 1998, EMS-98 scale)

16.3 The BCSF Decision to Create a Macroseismic Intervention Group (GIM)

Three damage producing earthquakes lead to the BCSF decision to create a large professional macroseismic group trained in field inquiries:

- The earthquake of Rambervillers in 2003 (magnitude 5.4, maximal intensity EMS-98 VI-VII) Cara et al. (2003),
- The West Indies Guadeloupe earthquake in 2004 (magnitude 6.4, maximal intensity EMS-98 VIII) Cara et al. (2005),
- And the west Indies Martinique earthquake in 2007 (magnitude 7.4, maximal intensity EMS-98 VI-VII) Schlupp et al. (2008).

During these events, the BCSF welcomed and benefited from between 4 and 10 voluntary seismologists of various French organizations that were not particularly well prepared in terms of safety procedures. The resulting estimates of the damage degrees and of building vulnerabilities widely confirmed the need for a group of training field experts.



Fig. 16.8 Unreinforced masonry with RC floors, grade of damage 3, in Greece 1995 (Grünthal 1998, EMS-98 scale)

French territory is characterized by moderate seismicity (<http://www.planseisme.fr/Zonage-sismique-de-la-France.html>), but statistically a major earthquake has struck mainland France every century, and France involves a zone of strong seismicity in a subduction context: the French West Indies.

During the last major earthquake occurred in 1909 in Lambesc (Provence), 65 municipalities had known intensities higher than or equal to VI. A small macroseismic survey team is clearly insufficient to covering several thousand square kilometers. The numerous aftershocks that generally follow an event of this size require quick field visits so that the effects of the main shock are well characterized and distinct of the effects of aftershock.

A large and trained team ready to intervene in a short period of time is required quickly in several cities.

During the last missions of BCSF, it appeared that last minute recruitment from the community of seismologists was difficult. All the seismologists know the intensity concept, but few of them know exactly the procedure to collect data and make estimation. The scale of intensity is frequently confused with a scale of damages of the earthquake. If you know that an earthquake produced intensity IX and that you do not know the vulnerability of the city affected by this intensity (Haiti or Tokyo for example), you cannot deduce the likely damages from it. This is partly due to the scale of intensity only being a classification of the severity of the shock on the ground in a determined zone and not a scale of damage. The scale uses the damages like an indicator, balanced by the vulnerability of buildings.

The estimation of the intensities in the field requires some experiences in data collection, through interviews and other methods of enquiry. Such investigations are not merely brief stops in the city, but necessarily careful interviews on specifically what has happened. Consulting city officials and helpful citizens can pinpoint vulnerabilities on the map more precisely.

It is crucial to accurately know the intensity scale and to be able to properly identify the damages in buildings. It is important to note that a person with a good training and practice will be able to do the work faster than a not warned person.

Macroseismic study is a specific type of work that cannot be led by the groups that assess the buildings for safety (tagging data), because their objectives are not the same. Assessment groups give an appreciation of the risk to inhabitants. Some damages represent a threat for inhabitants, but are not directly related to the severity of the shock (plaster decorations, windows cracks, other threatening factors such as nearby construction). Building safety inspectors do not evaluate the initial vulnerability but work on habitability after the first shock. Usually they determine three levels of damage: nothing to light, moderate, severe. Choices are then made between three levels of classification: green for livable, orange for temporary evacuation and restricted access, red for uninhabitable. From gathering such information, five levels of damage of the scale EMS-98 is difficult to obtain.

For this reason, the BCSF created the Intervention Macroseismic Group (GIM) in 2010, having a first training session in April 2011. The group consists of 54 trained experts from 26 institutions, including 6 experts in the West Indies.

Six training experts come from countries bordering France: Switzerland, Spain, and Belgium. The GIM represents one of the biggest groups of experts in the world dedicated to macroseismic research today.

16.4 The GIM and Its Organisation

Our observations of the situation during our missions, or the situation during recent earthquakes (l'Aquila and Haiti), and a simulation of a major earthquake in Alsace (France-Thann, magnitude 6.2 April 2013), helped to consolidate our strategy our organisation (Fig. 16.9). The objectives during the implementation of this group were:

- Share the on average low available human resources within each structure to be able to complete the research for an earthquake impacting a large area with lots of experts. This also allows a more detailed work in large cities, in order to determine the largest local intensity variations (site effects);
- Have experts trained for the EMS-98 scale, using a common and tested survey method. We created specific tools such as data collection forms to evaluate



Fig. 16.9 Two GIM experts with Wickershihr mayor during the training simulation in 2013 (Thann earthquake 6.2 M_L)

building vulnerabilities, to evaluate degrees of damage, and to provide a tool to help make estimations in accordance with the EMS-98 scale. We use a common method to investigate municipalities, to interview people, and to photograph the damage;

- Use security procedures for the work conducted in disaster areas. The members must know INSARAG (Intervention Search and Rescue Advisory Group) conventions to be associated with safety teams (civil security) in the field in case of emergency;
- Set up the essential autonomy of the group for its security and its accommodation in the field (specific materials);
- Organize members in teams of two for better security for experts and better objectivity of results;
- Be identified via indicative clothing by the authorities in the field, to benefit from more cohesive functioning with other groups.

Several points still remain to be improved, in particular some of the administrative aspects. Each member of the GIM is insured and partly financed by its organisation for each mission.

16.5 The GIM and the Border Countries Experts

The GIM is now a French-based cross-organizational group based on the sharing of human and logistic means. It is coordinated for French territory by the BCSF. The GIM is willing for more exchanges with bordering countries in particular to optimize the analysis of cross-border events and the coherence of the results (Michel et al. 2005).

This perspective has triggered fruitful collaborations with our Swiss, Spanish and Belgian colleagues, who have been integrated into the GIM, have followed the training courses, and who can now share in using a common approach for developing their own national group. Several European seismological institutions have organised permanent networks of voluntary observers in the field (Cecic and Musson 2004). As we have done in France, we hope that all the national macroseismic group are clearly recognized and identified by their neighbouring European countries to facilitate the exchanges and cross-border collaborations, before, during and after any major European seismic events.

16.6 Needs for a Future Macroseismic Survey

The fieldwork and intensities estimation training allows the participating scientists to identify the limits of intensity use, but also to consider the macroseismic data for seismic hazard and risk studies. The fieldwork allows a better analysis and interpretation of the data stemming from historical documents.

Few earthquake specialists, such as computer scientists, historians, structural engineers or architects in earthquake-resistance, have joined the GIM and share their skill or confront the gaps in their seismological knowledge. This group contributes to the advancement of each in its specific domain from field experience.

They contribute to the European macroseismic scale, in its evolution and its future development. Through the integration of young experts we allow the continuity of the macroseismic work while improving the use of the acquired field data too as well.

At this time when our working interface is mainly connected to online data via the computer, field work seems essential for the transcription of the severity of a shock. The record of intensity of seismic events must keep its essential quality: to be the reflection of the reality.

It seems crucial not to separate the macroseismic teams, those who work on the intensities stemming from Internet data and those who do the more traditional work of survey in the field. Each of them has to have the opportunity to understand the information of the other ones to be able to translate it into a more qualitative understanding of intensity. According to the distances to the epicenter, according to the levels of damages, according to the size of the city, it is important to shift emphasis (from field to individual forms) in order to obtain good quality of intensity

readings. In any case, the field will remain the reference of macroseismic observation if we want to update intensity scale or to calibrate our prediction models in particular in epicentral zone.

Acknowledgments My thanks are sent to the various institutions, both French and foreign, involved in the GIM and which supported this project of field enquiries, all the members of the group, as well as Michel Cara, Michel Granet, Frédéric Masson, successive directors of the BCSF who have supported the development of the group. Special thanks goes to Antoine Schlupp, who is my first management partner for the GIM.

Open Access This chapter is distributed under the terms of the Creative Commons Attribution Noncommercial License, which permits any noncommercial use, distribution, and reproduction in any medium, provided the original author(s) and source are credited.

References

Journal Article

- Cecic I, Musson R (2004) Macroseismic survey in theory and practice. *Nat Hazards* 31:39–61
- De Rubeis V, Gasparini C, Tosi P (1992) Determination of macroseismic field by means of trend and multivariate analysis of questionnaire data. *Bull Seismol Soc Am* 82(3):1206–1222
- De Rubeis V, Sbarra P, Sorentino D, Tosi P (2009) Web based macroseismic survey: fast information exchange and elaboration of seismic intensity effects in Italy. In: Langren J, Jul S (eds) *Proceeding of the 6th international ISCRAM conference*, Valerio De Rubeis, Gothenburg
- Michel C, Wolfgang B, Gisler M, Kastli P, Sira C, Weihermuller C, Lambert J (2005) Transfrontier macroseismic observation of the $M_l = 5.4$ earthquake of February 22, 2003 at Rambervillers, France. *J Seismol* 9:317–328

Book

- Grünthal G (1998) *European Macroseismic Scale 1998*, Conseil de l'Europe – Cahiers du Centre Européen de Géodynamique et de Séismologie, vol 15. Editor G. Grünthal, Luxembourg (Not edited anymore but available at: <http://www.franceseisme.fr/ems98.html>)

Reports

- Cara M, Sira C, Jacques E, Haessler H, Van Der Woerd J, Lebrun B, Dominique P, Beauval C (2003) *Séisme de Rambervillers (France) du 22 février 2003*, BCSF2003-01, 14 p., 11 figures, 2 tables, EOST – Université de Strasbourg

- Cara M, Sira C, Jacques E, Bertil D, Feuillet N, Taponnier P, Guegen P, Bengougou M, Lebrun B (2005) Séisme des Saintes (Guadeloupe) du 21 novembre 2004, BCSF2005-NP3, 62 p., 101 figures, 28 tables, 5 annexes, EOST – Université de Strasbourg
- Schlupp A, Sira C, Cara M, Bazin S, Michel C, Régnier J, Beauval C, Feuillet N, De Chabalier J-B, Barras A-V, Auclair S, Bouin M-P, Duclos C, Granet M (2008) Séisme de Martinique du 29 novembre 2007, BCSF2008-R1, 132 p., 266 figures, 3 tableaux, 5 annexes, EOST – Université de Strasbourg
- Sira C, Schlupp A, Schaming M, Chesnais C, Cornou C, Dechamp A, Delavaud E, Maufroy E (2014) Séisme de Barcelonnette du 7 avril 2014, BCSF2014-R1b, 76p, 22 figures, 6 annexes, EOST – Université de Strasbourg

Internet Sites

BCSF. <http://www.franceseisme.fr>

French sismique zonation. <http://www.planseisme.fr/Zonage-sismique-de-la-France.html>

GIM. <https://groupes.renater.fr/sympa/info/gim>

Chapter 17

Bridging the Gap Between Nonlinear Seismology as Reality and Earthquake Engineering

Gheorghe Marmureanu, Carmen Ortanza Cioflan,
Alexandru Marmureanu, Constantin Ionescu, and Elena Florinela Manea

Moto: The nonlinear seismology is the rule, The linear seismology is the exception. Paraphrasing Tullio Levi-Civita

Abstract In seismic hazard evaluation and risk mitigation, there are many random and epistemic uncertainties. On the another hand, the researches in this area as part of knowledge are with rest, that is, the results are with interpretable questions with *open answers*. The knowledge cannot be exhausted by results. The authors developed in last time the concept of “*Nonlinear Seismology – The Seismology of the XXI Century*” (Marmureanu et al. Nonlinear seismology-the seismology of XXI century. In: Modern seismology perspectives, vol 105. Springer, New York, pp 49–70, 2005).

The leading question is: how many cities, villages, metropolitan areas, etc., in seismic regions are constructed on rock? Most of them are located on soil deposits. A soil is of basic type sand or gravel (termed coarse soils), silt or clay (termed fine soils), etc. Strong ground accelerations from large earthquakes can produce a nonlinear response in shallow soils. This can be studied by comparing surface and borehole seismic records for earthquakes of different sizes. When a nonlinear site response is present, then the shaking from large earthquakes cannot be predicted by simple scaling of records from small earthquakes (Shearer, Introduction to seismology, 2nd edn. Cambridge University Press, Cambridge, 2009). *Nonlinear amplification at sediments sites appears to be more pervasive than seismologists used to think...Any attempt at seismic zonation must take into account the local site condition and this nonlinear amplification* (Aki, Tectonophysics 218:93–111, 1993).

G. Marmureanu (✉) • C.O. Cioflan • E.F. Manea
Department of Engineering Seismology, National Institute of Earth Physics (NIEP) &
Physics Faculty, Bucharest, Romania
e-mail: marmur@infp.ro; cioflan@infp.ro; manea.elena@infp.ro

A. Marmureanu • C. Ionescu
Department of National Seismic Network, NIEP, Bucharest, Romania
e-mail: marmura@infp.ro; viorel@infp.ro

© The Author(s) 2015

A. Ansal (ed.), *Perspectives on European Earthquake Engineering and Seismology*,
Geotechnical, Geological and Earthquake Engineering 39,
DOI 10.1007/978-3-319-16964-4_17

409

The difficulty for seismologists is to demonstrate the nonlinear site effects, these being overshadowed by the overall patterns of shock generation and propagation. In other words, the seismological detection of the nonlinear site effects requires a simultaneous understanding/knowledge of *earthquake source, propagation path, and local geological* site conditions. To see the actual influence of nonlinearity of the *whole system* (seismic source-path propagation-local geological structure), *the authors used to study the free field response spectra which are the last in this chain and are taken into account in seismic design of all structures.* Soils from the local geological structure at the recording site exhibit a strong nonlinear behavior under cyclic loading conditions and although they have many common mechanical properties, the use of different models to describe their seismic behavior is required.

The studies made by the authors in this chapter show that using real spectral amplification factors (SAF), amplifications showing local effects, have values which differ totally from those of crustal earthquakes. The spectral amplifications highlight strong nonlinear response of soil composed of fractured limestone, limestone with clay, marl, sands, clay, etc., and these amplifications are strongly dependent of earthquake magnitude and nature of soils from site. Finally, these amplifiers are compared to those from Regulatory Guide 1.60 of the U. S. Atomic Energy Commission (Design response spectra for seismic design of nuclear power plants. Regulatory Guide 1.60. Rev. 1, Washington, D.C., 1973) which can be used only for crustal earthquakes and not for deep and strong Vrancea earthquakes from Romania. The study of the nonlinear behavior of soils during strong earthquakes may clarify uncertainties in ground motion prediction equations used by probabilistic and classical deterministic seismic hazard analysis.

17.1 Introduction

The Vrancea seismogenic zone denotes a peculiar source of seismic hazard, which represents a major concern in Europe, especially to neighboring regions from Bulgaria, Serbia, Republic of Moldova, etc. The strong seismic events that can occur in this area can generate the most destructive effects in Romania, and may seriously affect high-risk man-made structures such as nuclear power plants (Cernavoda, Kosloduj, etc.), chemical plants, large dams, and pipelines located within a wide area from Central Europe to Moscow.

Earthquakes in the Carpathian–Pannonian region are confined to the crust, except the Vrancea zone, where earthquakes with focal depth down to 200 km occur. For example, the ruptured area migrated from 140 to 180 km (November 10, 1940 earthquake, $M_w = 7.7$), from 90 to 110 km (March 4, 1977 earthquake, $M_w = 7.4$), from 130 to 150 km (August 30, 1986 earthquake, $M_w = 7.1$), and from 70 to 90 km (May 30, 1990 earthquake, $M_w = 6.9$) depth. The depth interval between 110 and 130 km remains not ruptured since October 26, 1802, when it was the strongest earthquake occurred in this part of Central Europe. The magnitude is assumed to be $M_w = 7.9$ – 8.0 and this depth interval is a natural candidate for the next strong Vrancea event (Fig. 17.1).

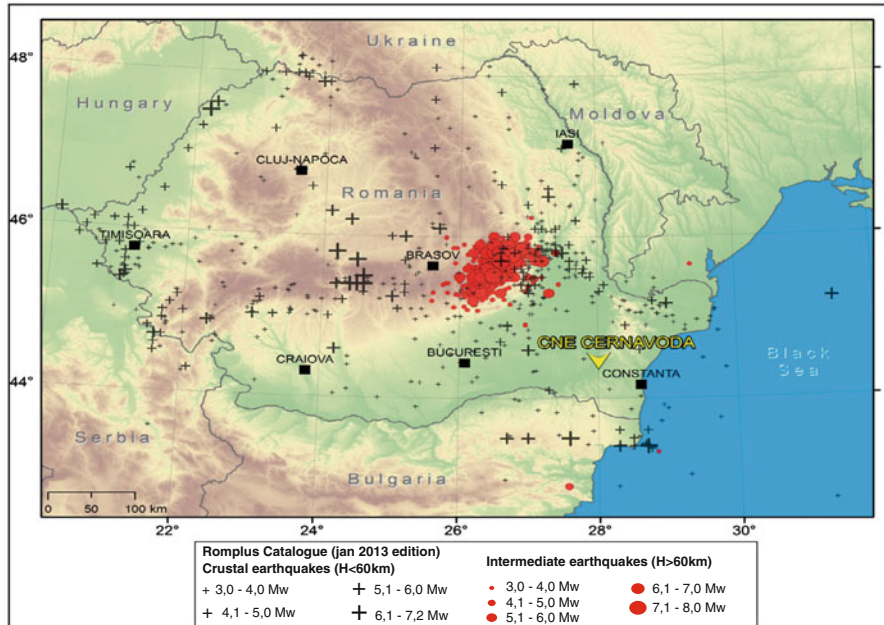


Fig. 17.1 Vrancea seismogenic zone and extra-Carpathian area

Bucharest City is located in Moesian Platform. From geological point of view, above Cretaceous and Miocene deposits (isobaths around 1,400 m depth), a Pliocene shallow water deposit (~700 m thick) was settled. The surface geology consists mainly of Quaternary alluvial deposits, later covered by loess. In the extra-Carpathian area, there are thick soil deposits (Buzau: 4.5 km; Bucharest: 0.55–1.4 km; etc.) (Mandrescu et al. 2008). There are large fundamental periods (T_s) for soils in all extra-Carpathian area. Nonlinear amplification at sediments sites appears to be more pervasive than seismologists used to think... Any attempt at seismic zonation must take into account the local site condition and this nonlinear amplification (Aki, Tectonophysics 218:93–111, 1993).

This basic material characteristic shall be taken into account when we are evaluating the seismic response of soil deposits or earth structures. The model of linear elastic response of the Earth to earthquakes has been almost universally used in seismology to model teleseismic, weak, and also strong earthquakes.

For teleseismic and weak ground motions, there is no reason to doubt that this model is acceptable, but for strong ground motions, particularly when are recorded on soils, the consequences of nonlinear soil behavior have to be seriously considered.

Soils exhibit a strong nonlinear behavior under cyclic loading conditions. In the elastic zone, soil particles do not slide relative to each other under a small stress increment and the stiffness is at its maximum. The stiffness begins to decrease from the linear elastic value as the applied strains or stresses increase, and the deformation moves into the nonlinear elastic zone (Fig. 17.2).

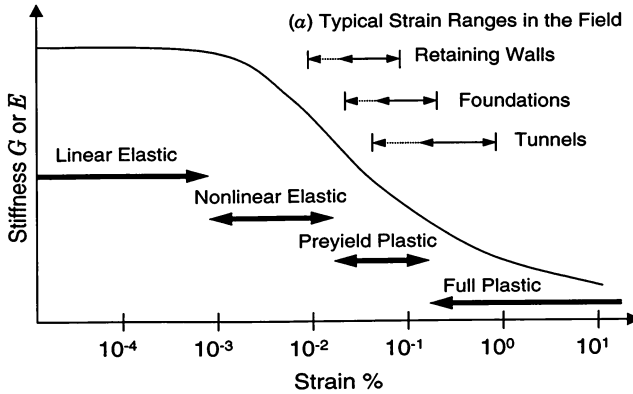


Fig. 17.2 Stiffness degradation curve in terms of shear modulus G and Young's modulus E : stiffness plotted against logarithm of typical strain levels observed during construction of typical geotechnical structures (Marmureanu et al. 2013)

Stress and strain states are not enough to determine the mechanical behavior of soils. It is necessary, in addition, to model the relation between stresses and deformations by using *specific constitutive laws to soils*. Currently, there are no constitutive laws to describe all real mechanical behaviors of deformable materials like soils. From *mechanical behavior* point of view, there are two main groups of essential importance: *sands* and *clays*. Although these soils have many common mechanical properties, they require the use of different models to describe the differences in their seismic behavior. Soils are simple materials with memory: sands are “*rate-independent*” type and clays are “*rate-dependent*” ones, terms used in deformable body mechanics. However, the complexity of these “simple” models exceeds the possibility of solving and requires the use of simplifying assumptions or conditions that are restricting the loading conditions, which makes additional permissible assumptions. Sands typically have low rheological properties and can be shaped with an acceptable *linear elastic model* (Borcherdt 2009) by using Boltzmann's formulation of the constitutive relation between stresses and strains. Clays which frequently present significant changes over time can be shaped by a *nonlinear viscoelastic model*.

17.2 Quantitative Evidence of Nonlinear Behavior of Soils

Laboratory tests made by using Hardin or Drnevich resonant columns consistently show the decreasing of dynamic torsion function (G) and increasing of torsion damping function ($D\%$) with shear strains ($\gamma\%$) induced by strong earthquakes; $G = G(\gamma)$, respectively, $D\% = D\%(\gamma)$; therefore, nonlinear viscoelastic constitutive laws are required (Fig. 17.2). The strong dependence of response on strain amplitude (Figs. 17.3, 17.4, 17.5, 17.6, and 17.7) with earthquake magnitude becomes a standard assumption in evaluation of Vrancea strong earthquake effects on urban environment.

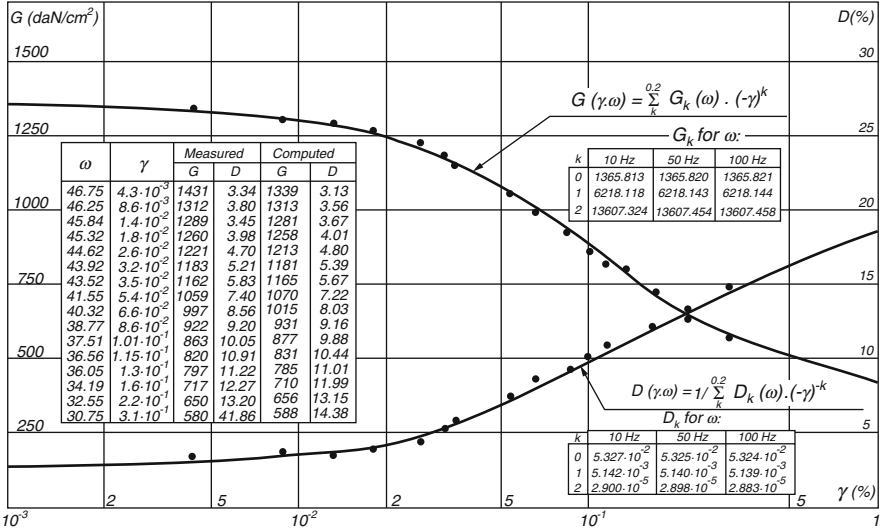


Fig. 17.3 The absolute values of the variation of dynamic torsion modulus function (G , daN/cm²) and torsion damping function (D %) of specific strain (γ %) for marl samples obtained in Hardin and Drnevich resonant columns from NIEP (USA patent), Laboratory of Earthquake Engineering (Marmureanu et al. 2010)

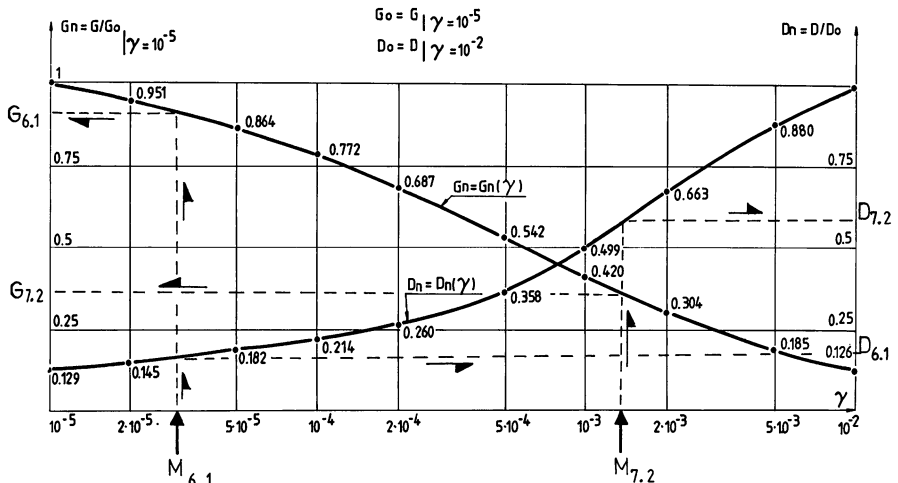


Fig. 17.4 The normalized values of the variation of dynamic torsion modulus function (G , daN/cm²) and torsion damping function (D %) of specific strain (γ %) for sand and gravel samples with normal humidity obtained in Hardin and Drnevich resonant columns from NIEP (USA patent) (Marmureanu et al. 2010)

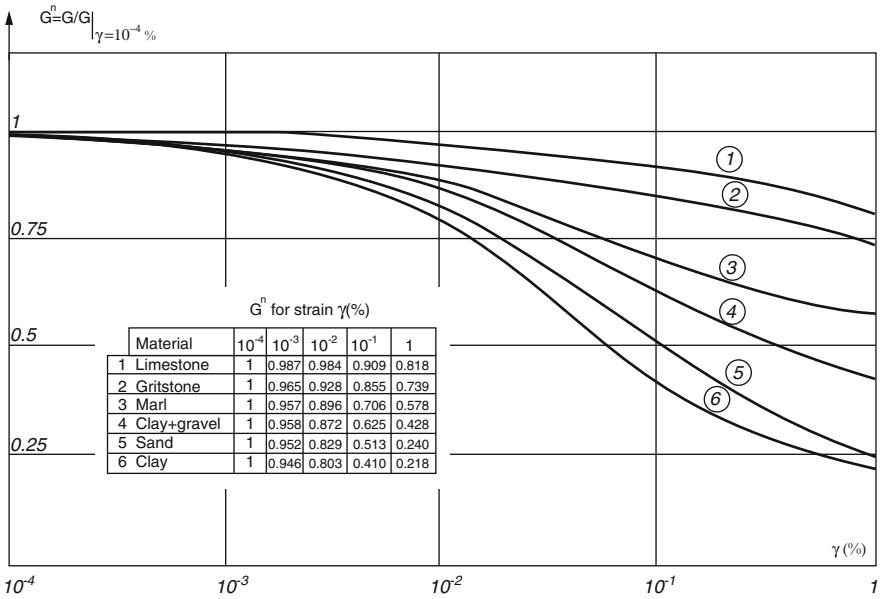


Fig. 17.5 Nonlinear relation between dynamic torsion modulus (G , daN/cm²) and shear-strain ($\gamma\%$) experimental data from Hardin and Drnevich resonant columns from NIEP (USA patent). Normalized values for limestone, gritstone, marl, clay+gravel, sand, and clay (Marmureanu et al. 2010)

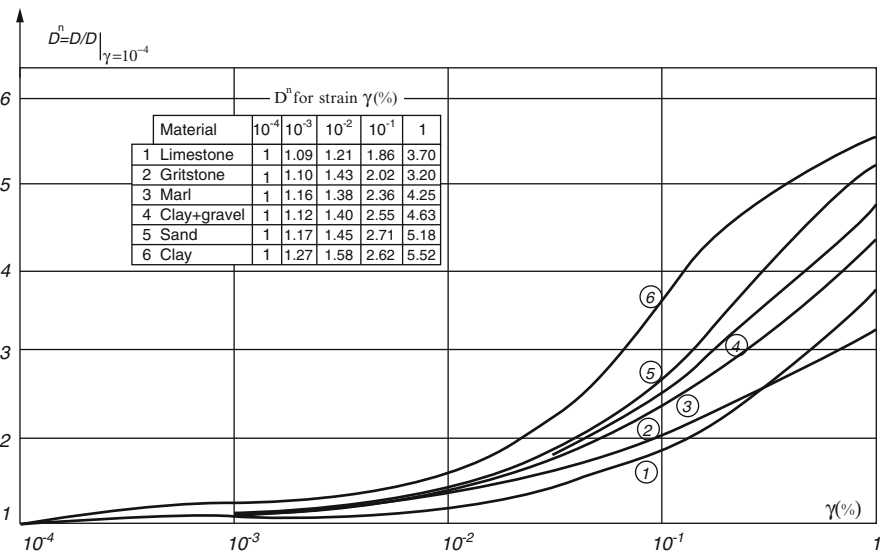


Fig. 17.6 Nonlinear relation between torsion damping function ($D\%$) and shear-strain ($\gamma\%$) experimental data from Hardin and Drnevich resonant columns from NIEP (USA patent). Normalized values for limestone, gritstone, marl, clay+gravel, sand, and clay (Marmureanu et al. 2010)

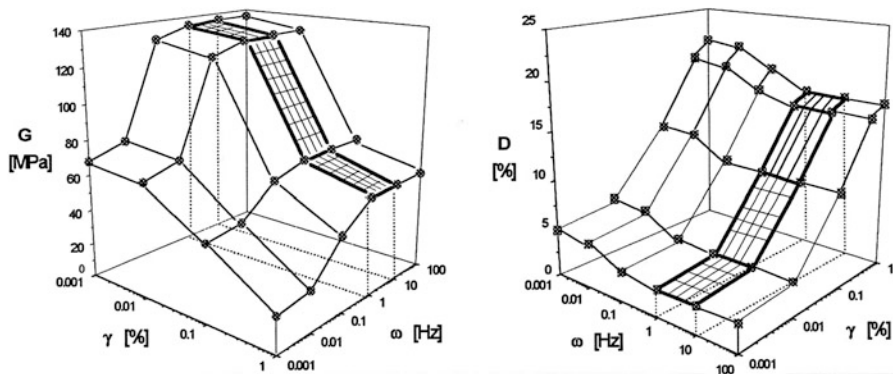


Fig. 17.7 Dependence of dynamic torsion modulus function (G , daN/cm²) and torsion damping function ($D\%$) with shear strains $\gamma\%$ and frequency ω . For frequencies between 1 and 10 Hz, shear modulus (G) and damping ratio are constant in this main field used in engineering (Bratosin 2002; Marmureanu et al. 2005, 2010, 2013)

The dependence of dynamic torsion modulus function (G , daN/cm²) and torsion damping function ($D\%$) with shear strains ($\gamma\%$) and frequency ω are given. In Fig. 17.7 one can observe the constant values of $G(\gamma)$ and $D(\gamma)$ between 1 and 10 Hz, the domain used in civil engineering structures design.

The analysis of several resonant column tests shows a major weight of the strain level on modulus and damping values and a minor influence of the frequency values between 1 and 10 Hz (Marmureanu et al. 2005, 2010). Therefore, for practical purposes, we can consider these functions as constants in terms of frequency ω at least between 1 and 10 Hz. This hypothesis involves only the independence of ω of these soil functions and not of the soil response.

For smaller deep Vrancea earthquakes ($M_W = 6.1$), the strains are smaller and we are in the left-hand side of Fig. 17.4; for strong earthquakes ($M_W = 7.2$), the strains are larger and we are in the right-hand-side of Fig. 17.4 with large damping. Consequently the responses of a system of nonlinear viscoelastic materials (clays, marls, gravel, sands, etc.) subjected, for example, to vertically traveling shear waves are far away from being linear and generating large discrepancies. In this case, the SH wave vertical propagation equation is (Marmureanu et al. 2005, 2010):

$$G \frac{\partial^2 u_2(x_1, t)}{\partial x_1^2} + D \frac{\partial^3 u_2(x_1, t)}{\partial t \partial x_1^2} = \rho \frac{\partial^2 u_2(x_1, t)}{\partial t^2} \quad (17.1)$$

where G (daN/cm²) is the dynamic torsion modulus function and $D(\%)$ is the torsion damping function; both of them are functions of shear strains ($\gamma\%$) induced by strong earthquakes, frequency (ω), confining pressure (σ), depth (h), temperature (t°), void ratio (v), etc., that is:

$G = G(\gamma, \omega, \sigma, h, t, v, \dots)$ and $D = D(\gamma, \omega, \sigma, h, t, v, \dots)$. If we accept a strain-history of forms (harmonic and stationary): $\gamma(t) = \gamma_0 \exp(-i\omega t)$ and from Fig. 17.7, where for frequencies ω between 1 and 10 Hz, shear modulus (G) and damping ratio (D) are constant in this main field used in engineering, then $G(\gamma)$ and $D(\gamma)$ will depend only of shear strain ($\gamma\%$) developed during of strong Vrancea earthquakes (Marmureanu et al. 2013).

17.2.1 Spectral Amplification Factors (SAF) Dependence of Magnitude

Currently, there are no constitutive laws to describe all real mechanical behaviors of deformable materials like soils. In order to make quantitative evidence of large nonlinear effects, the authors introduced and developed after 2005 (Marmureanu et al. 2005) the concept of nonlinear spectral amplification factor (SAF). SAF is the ratio between maximum spectral absolute acceleration S_a^{max} , relative velocity S_v^{max} , relative displacement S_d^{max} from response spectra for a fraction of critical damping (β , %) and peak values of acceleration (a_{max}), velocity (v_{max}), and displacement (d_{max}), respectively. From processed strong motion records, one can compute (SAF)_a = S_a^{max}/a_{max} ; (SAF)_v = S_v^{max}/v_{max} ; (SAF)_d = S_d^{max}/d_{max} .

The analysis was conducted for last strong and deep Vrancea earthquakes (March 04, 1977: $M_W=7.4$ and $h=94$ km; August 30, 1986: $M_W=7.1$ and $h=134.4$ km; May 30 1990: $M_W=6.9$ and $h=90.9$ km; May 31, 1990: $M_W=6.4$ and $h=86.9$ km). The spectral amplification factors decrease with increasing the magnitudes of deep strong Vrancea earthquakes and these values are far of that given by Regulatory Guide 1.60 of the U. S. Atomic Energy Commission and accepted by IAEA Vienna (Cioflan et al. 2011; Marmureanu et al. 2013; U.S. Atomic Energy Commission 1973).

A characteristic of the nonlinearity is a systematic decrease in variability of peak ground accelerations with increasing earthquake magnitude. For example, for the last Vrancea earthquakes, in extra-Carpathian area, spectral amplification factor (SAF) decreases from 5.89 ($M_W=6.4$) to 5.16 ($M_W=6.9$) and to 4.04 ($M_W=7.1$) at Bacau Seismic Station. The amplification factors decrease as the earthquake magnitude increases. This is consistent with our data which confirm that the ground accelerations tend to decrease as earthquake magnitude increases. As the excitation level increases, the response spectrum is larger for the linear case than for the nonlinear one. The analysis for a site indicates that the effect of nonlinearity is large and peak ground acceleration is 45.7 % smaller assuming that response of soil to earthquake with $M_W=6.4$ is still in elastic domain and then the possibility to compare to it (an example is in Table 17.1).

At Bucharest-Panduri Seismic Station (Table 17.2) and Fig. 17.8, close to borehole 172, for horizontal components and $\beta=5$ % damping, the values of the SAF for accelerations are 3.29 for August 30, 1986 Vrancea earthquake ($M_W=7.1$); 4.49 for May 30, 1990 ($M_W=6.9$); and 4.98 for May 31, 1990 ($M_W=6.4$). The effect of nonlinearity is large and peak ground accelerations is 51.3 smaller assuming that the response of soil to Vrancea earthquake on May 31, 1990 ($M_W=6.4$) is still in elastic domain and then we have the possibility to compare to it (Tables 17.3 and 17.4, Figs. 17.9).

On the other hand, from Table 17.5 and Fig. 17.10 we can see that there is a strong nonlinear dependence of the spectral amplification factors on earthquake magnitude (Mar. 1996) for other seismic stations on Romanian territory on extra-

Table 17.1 Bacău-BAC2 Seismic Station (EW component): $\varphi^0 = 46.567$ and $\lambda^0 = 26.900$ (Cioflan et al. 2011; Marmureanu et al. 2005; Marmureanu et al. 2010)

Earthquake	a_{\max} (cm/s ²) (recorded)	S_a^{\max} ($\beta = 5\%$)	S_a^{\max}/a_{\max} (SAF)	S_a^* (elastic)/ S_a^{\max} (record)	S_a^* ($\beta = 5\%$)	S_a^* as elastic	%
August 30, 1986 ($M_w = 7.1$)	72.20	292 cm/s ²	4.0443	1.457	425.44	105.19	45.7 %
May 30, 1990 ($M_w = 6.9$)	132.43	684 cm/s ²	5.1649	1.141	780.44	151.10	24.1 %
May 31, 1990 ($M_w = 6.4$)	63.07	372 cm/s ²	5.8942	1.000	372.00	63.07	–

Table 17.2 Bucharest-Panduri Seismic Station (N131E component): $\varphi^0 = 44,426$ and $\lambda^0 = 26,065$ (Cioflan et al. 2011; Marmureanu et al. 2005, 2010)

Earthquake	a_{\max} (cm/s ²) (recorded)	S_a^{\max} ($\beta = 5$ %)	S_a^{\max}/a_{\max} (SAF)	S_a^* (elastic)/ S_a^{\max} (record)	S_a^* ($\beta = 5$ %)	a*	%
August 30, 1986 ($M_w = 7.1$)	89.4	295 cm/s ²	3.29	1,513	446.33	135.26	51.3 %
May 30, 1990 ($M_w = 6.9$)	131.3	590 cm/s ²	4.49	1.109	654.31	145.61	10.9 %
May 31, 1990 ($M_w = 6.4$)	33.0	160 cm/s ²	4.98	1.000	160.00	33.00	–

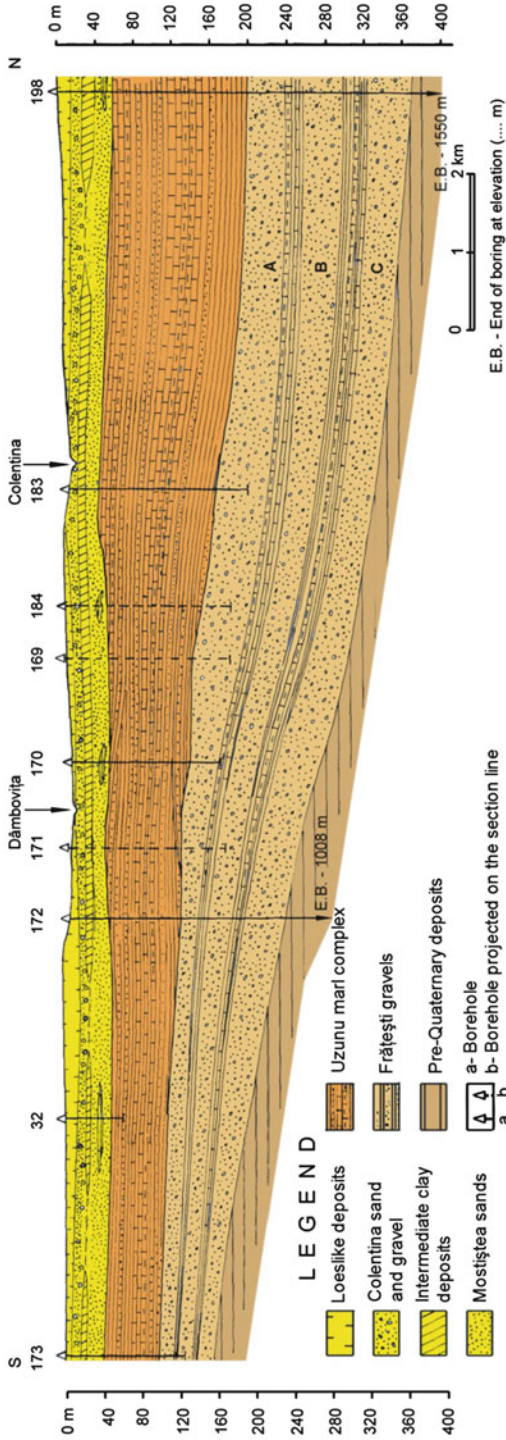


Fig. 17.8 Geological structure under Bucharest. Isobars are generally oriented East to West with slope of 8 % down from South to North. In the same direction, the thickness of layers becomes larger (Mandrescu et al. 2008)

Table 17.3 Bucharest-INCERC Seismic Station (NS component): $\phi^0 = 44.442$ and $\lambda^0 = 26.105$ (Marmureanu et al. 2005)

Earthquake	a_{\max} (cm/s ²) (recorded)	S_a^{\max} ($\beta = 5$ %)	S_a^{\max}/a_{\max} (SAF)	c	S_a^* (g) ($\beta = 5$ %)	a^*	%
April 03, 1977 ($M_W = 7.4$)	206.90	650 cm/s ²	3.14	1.322	859.3	273.5	32.2 %
August 30, 1986 ($M_W = 7.1$)	96.96	255 cm/s ²	2.62	1.583	403.6	153.4	58.3 %
May 30, 1990 ($M_W = 6.9$)	66.21	275 cm/s ²	4.15	1.000	275.0	66.21	–

Table 17.4 Bucharest-Măgurele Seismic Station (EW component): $\phi^0 = 47.347$ and $\lambda^0 = 26.030$ (Fig. 17.10) (Marmureanu et al. 2010)

Earthquake	$a_{\max}(\text{g})$ (recorded)	$S_a^{\max} (\beta = 5 \%)$	$S_a^{\max} / a_{\max} \text{ (SAF)}$	c	$S_a^* (\beta = 5 \%)$	a^*	%
August 30, 1986	0.116 g	0.313 g	2.6892	1.3294	0.4161 g	0.1542 g	32.94
May 30, 1990	0.092 g	0.330 g	3.5869	1.0000	0.330 g	0.092 g	—

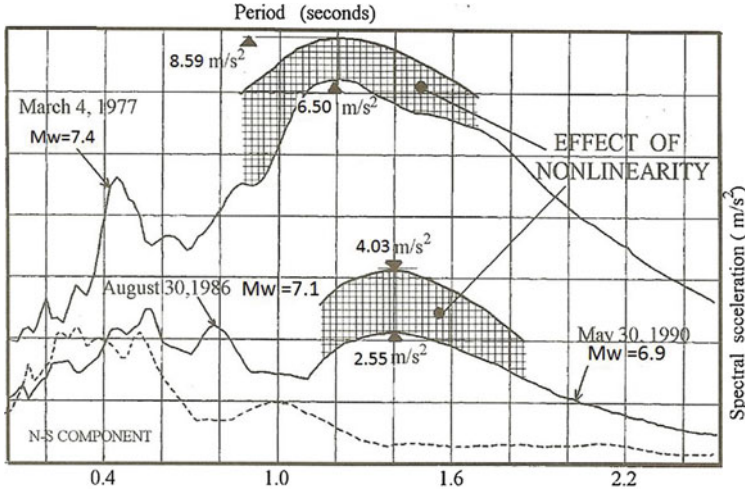


Fig. 17.9 Acceleration response spectra for Bucharest-INCERC Seismic Station, NS components and the effects of nonlinearity of soil (cross-hatched areas) for last strong Vrancea earthquakes: March 04, 1977; August 30, 1986; and May 30, 1990. The fundamental periods (T , s) are not the same for the three earthquakes ($\beta = 5\%$) (Marmureanu et al. 2005)

Table 17.5 Median values of SAF for last three strong Vrancea earthquakes recorded on 26 extra-Carpathian seismic stations (Marmureanu et al. 2010)

Damping (%)	August 30, 1986 ($M_w = 7.1$)		May 30, 1990 ($M_w = 6.9$)		May 31, 1990 ($M_w = 6.2$)	
	S_a^{max}/a_{max}	S_v^{max}/v_{max}	S_a^{max}/a_{max}	S_v^{max}/v_{max}	S_a^{max}/a_{max}	S_v^{max}/v_{max}
2	4.74 (4.25)	3.61 (3.54)	5.58 (4.25)	3.72 (3.54)	6.22 (4.25)	4.84 (3.54)
5	3.26 (3.13)	2.69 (2.61)	3.63 (3.13)	2.95 (2.61)	4.16 (3.13)	3.48 (2.61)
10	2.43 (2.28)	1.99 (1.90)	2.56 (2.28)	2.14 (1.90)	2.92 (2.28)	2.69 (1.90)
20	1.78 (1.63)	1.50 (1.51)	1.82 (1.63)	1.58 (1.51)	2.13 (1.63)	1.86 (1.51)

Carpathian area (Iasi, Focsani, Bucharest-NIEP, Bucharest-INCERC, etc.). In brackets are the values from Regulatory Guide 1.60 of the U. S. Atomic Commission and IAEA Vienna (U.S. Atomic Energy Commission 1973).

The spectral amplification factors (SAF) and, in fact, the nonlinearity, are functions of Vrancea earthquake magnitude. The amplification factors decrease as the magnitude increases (Fig. 17.11) for all the extra-Carpathian area.

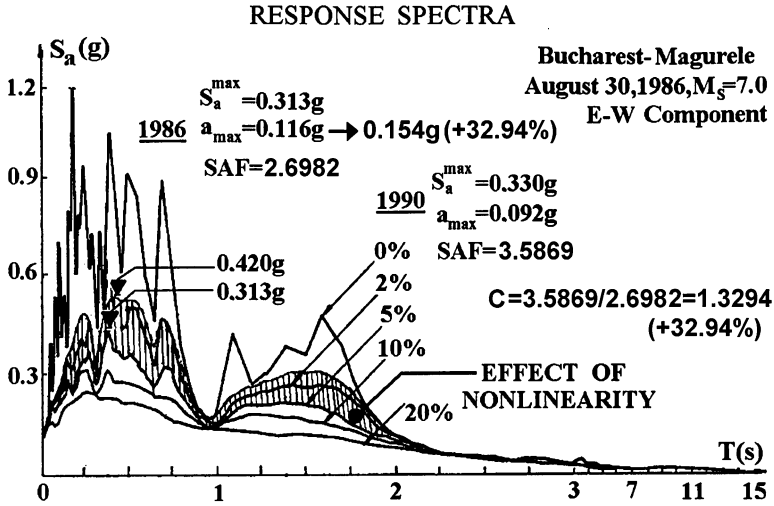


Fig. 17.10 Acceleration response spectra for Bucharest-Măgurele Seismic Station (*EW component*) and the effect of nonlinearity of soil behavior (*shaded area*) for strong Vrancea earthquake on August 30, 1986 ($M_W = 7.1$; $h = 141.4$ km)

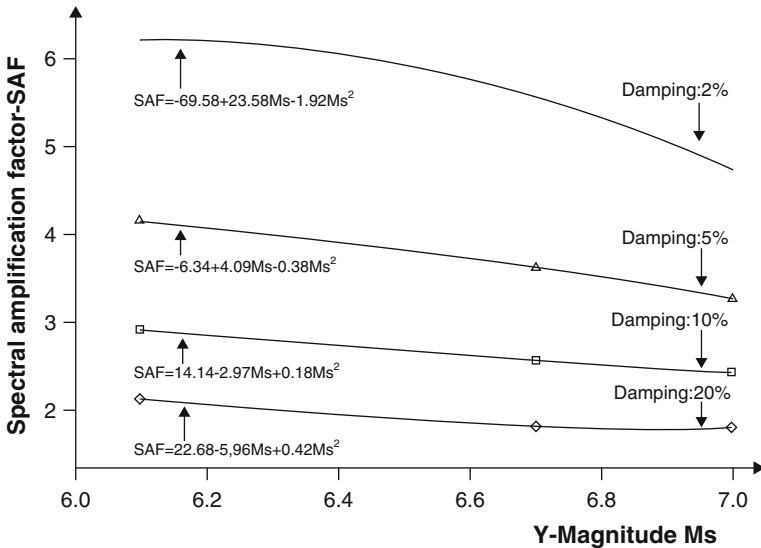


Fig. 17.11 Strong nonlinear dependence of spectral amplification factors (*SAF*) of Vrancea earthquake magnitude on extra-Carpathian area (Marmureanu et al. 2013). Magnitude M_S is on Richter scale (Marmureanu et al. 2010)

17.3 The Implications of Soil Nonlinearity During Strong Earthquakes in PSHA

In seismic hazard evaluation and risk mitigation, there were many random and epistemic uncertainties. The main ones are in step “*ground motion evaluation.*” Probabilistic or deterministic seismic hazard analysis (PSHA/DSHA) are commonly used in engineering, nuclear power plants, bridges, military objectives, dams, etc. (Fig. 17.12). Ground motion characteristics at a site, conditional on a given earthquake, can be estimated in several ways, which depend on the earthquake source characteristics available. If peak motion characteristics have been estimated (depth, magnitude, seismic moment, time, etc.), then the response spectrum can be derived via spectral amplification factors (SAF). Empirical ground motion equation characteristics are the oldest estimates in seismic hazard analysis, dating from the 1960s and they typically have the following type of form:

$$\ln A = c_o + f(m) + f(r) + f(\text{soil}) + \varepsilon \quad (17.2)$$

where A is ground motion amplitude, which can be a peak motion parameter or spectral amplitude; c_o is a constant; $f(m)$, $f(r)$ are functions of magnitude and distance; ε is a random variable taking on a specific value for each observation. As can be observed the nonlinear behaviors of soils are not included in GMPE. It is important to understand the strengths and weaknesses of one equation versus another. One is never sure of having the “*correct*” functional form of a ground motion equation.

Linear stress–strain theory is generally valid at the low strains typical of most seismic waves. Strong ground accelerations from large earthquakes can produce a nonlinear response in shallow soils. This can be studied by using many ways. When a nonlinear site response is present, then the shaking from large earthquakes cannot be predicted by simple scaling of records from small earthquakes (Shearer 2009).

The fundamental understanding about both uncertainties in ground motion comes from the large scatter in observations, even when they are normalized by magnitude, distance, and other parameters.

Seismic hazard $P(A > a)$ as a function of soil level of movement is given in probabilistic seismic hazard analysis by:

$$P(A \geq a) = 1 - \exp(-\lambda(a)) \quad (17.3)$$

$$\lambda(a) = \sum_{i=1}^s \nu_i \iint \Phi' \left(\frac{\ln a - g(m, r)}{\sigma} \right) f_{R_i}(r|m) f_{M_i}(m) dr dm \quad (17.4)$$

where s – number of seismic sources; $\ln(a) - g(m, r)$ – attenuation law; σ – standard deviation; Σ – summation over sources; ν_i – annual average frequency; $f_{R_i}(r|m)$ – probability density function of the distances from the site; $f_{M_i}(m)$ – probability

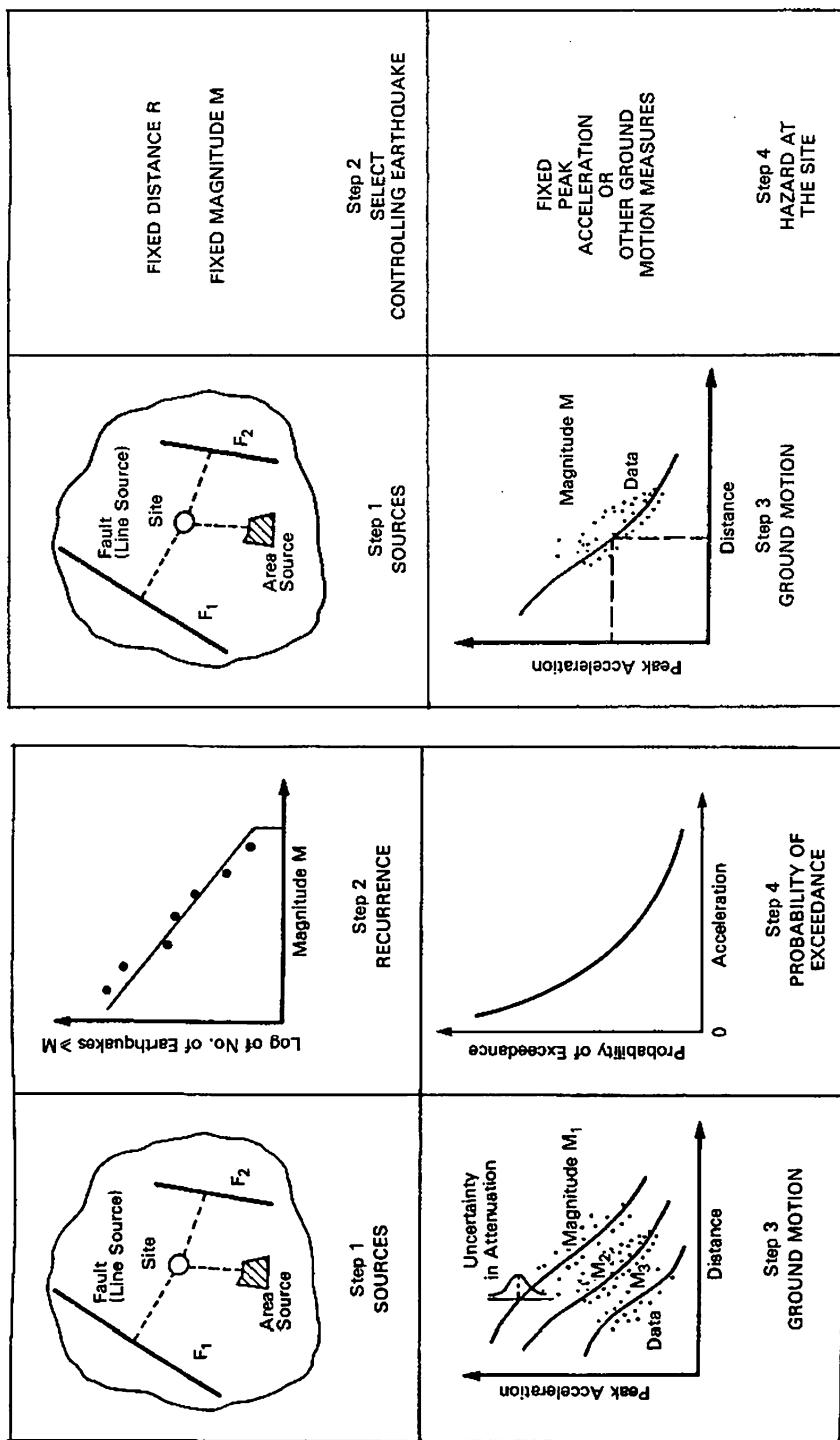


Fig. 17.12 Basic steps in probabilistic (PSHA) – left and deterministic (DSHA) – right seismic hazard analysis (Marmureanu et al. 2010)

density function of magnitude (M); $\lambda(a)$ – the annual probability of exceedance of peak ground acceleration at the site by considering a *Poissonian process*.

It was developed from *mathematical statistics* (Benjamin and Cornell 1970) under *four fundamental assumptions* (Cornell 1968, 1971; Marmureanu et al. 2010, 2013):

1. The constant in time is an average occurrence rate of earthquakes.
2. Equal likelihood of earthquake occurrence along a line or over an areal source: in fact a single point source.
3. Variability of ground motion at a site is independent.
4. Poisson (or “*memory-less*”) behavior of earthquake occurrences.

In the case of Fukushima Nuclear Power Plant, deterministic hazard assessment methods were used for the original design, but Japanese authorities recently moved to probabilistic assessment methods and the resulted probability of exceedance of the design basis acceleration was expected to be 10⁻⁴-10⁻⁶ (Klügel 2014). The design basis seismic data were exceeded during the March 11, 2011, earthquake ($M=9.0$) at Fukushima NPP as shown in (Klügel 2014). Ignoring their own information from historical events caused a violation of the deterministic hazard analysis principles!

What is wrong with traditional PSHA or DSHA?

- (a) A Poisson process is a *stochastic process*. This *Poissonian process* implies that the occurrence of events/earthquakes is independent of time and space. The nature of earthquake occurrence is not Poissonian! Earthquake occurrence is characterized by a self-exciting behavior and a self-correcting behavior
- (b) *Ground motion prediction equations*. The empirical equations represent far field approximations (symmetric isotropic wave propagation). The so-called *aleatory variability* (ϵ) is just the error of this assumption – source of diffusivity making the Khinchine (Хинчин) (Хинчин 1926) theorem valid (superposition of stochastic processes with none of them dominating converges asymptotically to a resulting Poissonian process):

$$\ln Y = f(m, r, X) + \epsilon\sigma \quad (17.5)$$

Also, ergodic assumption(s) – pooling of world wide data → supports the *log-normal* assumption because of the *central limit theorem*. There are ground motion uncertainties: *aleatory uncertainties in random effects and epistemic uncertainties in knowledge*.

The fundamental understanding about both uncertainties in ground motion comes from the large scatter in observations, even when they are normalized by magnitude, distance, and other parameters. One is never sure of having the “*correct*” functional form of a ground motion equation and the nonlinear behavior of soil to strong earthquakes is still unknown to many structural designers.

17.4 Conclusions

The authors developed in last time the concept of “*Nonlinear Seismology – The Seismology of the XXI Century*”(Marmureanu et al. 2005). The difficulty for seismologists and structural engineers to demonstrate the nonlinear effects of the site lies in the difficulty of *separating* the effects of the source from the effects of the path between sources to free field of site (Greco et al. 2007). To see the actual influence of nonlinearity of the whole system (seismic source – path propagation – local geological structure) *the authors used to study the spectral amplification factors (SAF) from response spectra because they are the last in this chain and, of course, that they are the ones who are taken into account in seismic design of structures.*

There is a strong dependence of the spectral amplification factors (SAF) with earthquake magnitude. At the same seismic station, for example at Bacau NIEP Seismic Station, horizontal components and 5 % damping, the values of the SAF for accelerations are 4.0443 for August 30,1986 Vrancea earthquake ($M_W=7.1$); 5.1649 for May 30, 1990 ($M_W=7.9$); and 5.8942 for May 31, 1990 ($M_W=6.4$). Also, for Bucharest-Panduri Seismic Station the values are 3.29, 4.49, and 4.98 (Tables 17.1 and 17.2) by considering linear behavior of soils during Vrancea earthquake on May 31, 1990 with magnitude $M_W=6.4$. A characteristic of the nonlinearity is a systematic decrease in variability of peak ground acceleration with increasing earthquake magnitude.

The spectral amplification factors for last three strong and deep Vrancea earthquakes for NPP Cernavoda site are larger than the values given by Regulatory Guide 1.60 of the U. S. Atomic Energy Commission, IAEA Vienna-through Safety Series No. 5-SG-S1, and the values used by AECL-Canada in 1978 (U.S. Atomic Energy Commission 1973).

It is essential for seismologists and engineers to understand seismic hazard and risk, as well as the science behind them. PSHA emphasizes the probability, which depends on the statistical models, whereas NDSHA emphasizes the ground motion, which depends on the *physical models*.

This knowledge can be very fruitfully used by civil engineers in the design of new seismic resistant constructions and in the reinforcement of the existing built environment, and, therefore, supply a particularly powerful tool for the prevention aspects of Civil Protection.

Acknowledgments This work is performed in the frame of the National Romanian Plan for Research, Development and Innovation, NII, Partnership Program; Project “*Bridging the gap between seismology and earthquake engineering. From the seismicity of Romania towards refined implementation of seismic action of European Norm EN 1998-1 in earthquake resistant design of buildings*” (BIGSEES), Contract nr. 72/2012–2016.

This work was supported partially by a grant of the Romanian National Authority for Scientific Research, CNCS – UEFISCDI, project number PN-II-RU-TE-2012-3-0215.

Open Access This chapter is distributed under the terms of the Creative Commons Attribution Noncommercial License, which permits any noncommercial use, distribution, and reproduction in any medium, provided the original author(s) and source are credited.

References

- Aki A (1993) Local site effects on weak and strong ground motion. *Tectonophysics* 218:93–111
- Benjamin JR, Cornell CA (1970) *Probability, statistics and decision for civil engineers*. McGraw-Hill, New York
- Borcherdt RD (2009) *Viscoelastic waves in layered media*. Cambridge University Press, Cambridge/New York, 350 pp. ISBN 978-0521898539
- Bratosin D (2002) *Soil dynamics elements*. Romanian Academy Publishing House, Bucharest, p 136
- Cioflan CO, Marmureanu A, Marmureanu G (2011) The quantitative evidence of the soil nonlinear behavior during of strong Vrancea earthquakes in real/nonlinear seismology. *Rom Rep Phys* 63:839–851
- Cornell CA (1968) Engineering seismic risk analysis. *Bull Seismol Soc Am* 58(5):1583–1606
- Cornell CA (1971) Probabilistic analysis of damage to structures under seismic loads. In: Howells Greu B, Radulian M, Mandrescu N, Panza GF (2007) H/V spectral ratios technique application in the city of Bucharest: can we get rid of source effect? *J Seismol Earthq Eng* 9(1–2):1–4
- Klügel JU (2014) Lessons not yet learned from the Fukushima disaster. *EGU*, 27 April 2014, ISSO, Vienna
- Mandrescu N, Radulian M, Marmureanu GH, Ionescu C (2008) Integrate research of the geological, geophysical and seismological data for local response evaluation in bucharest urban area. Romanian Academy Publishing House, Bucuresti, p 134
- Mărmureanu GH, Mișicu M, Cioflan CO, Balan FS, Apostol BF (2005) *Nonlinear seismology-the Seismology of the XXI century*. Lecture notes of earth sciences, perspective in modern seismology, vol 105. Springer, Heidelberg, pp 47–68
- Marmureanu GH, Cioflan CO, Marmureanu A (2010) *Researches on local seismic hazard (microzonation) of Bucharest metropolitan area*. Microzoning maps accelerations, fundamental periods and intensities for maximum Vrancea earthquake magnitude of 7.5 on Richter scale. Tehnopress Publishing, Iasi, p 472 (in Romanian). ISBN 978-974-702-809-9
- Marmureanu G, Cioflan CO, Marmureanu A (2013) *Nonlinear seismology a reality*. The quantitative data. *EGU*, 22–27 Apr 2012, Section NH4, vol 65. Published in *Romanian Reports in Physics*, Vienna, pp 512–523
- Shearer PM (2009) *Introduction to seismology*, 2nd edn. Cambridge University Press, Cambridge. ISBN 978-0-521-70842-5
- U.S. Atomic Energy Commission (1973) *Design response spectra for seismic design of nuclear power plants*. Regulatory Guide 1.60. Rev. 1, Washington, D.C.
- Хинчин (1926) Иден интуиционизма и борба за предмет в современной математике. *Вестник Коммунистическая Академ* 16:184–192

Chapter 18

The Influence of Earthquake Magnitude on Hazard Related to Induced Seismicity

Benjamin Edwards

Abstract An increased focus on seismic hazard related to induced seismicity means that state-of-the-art approaches for earthquake monitoring and hazard estimation associated to tectonic earthquakes are now being applied at smaller and smaller scales. This chapter focuses on a specific issue related to this shift of focus to relatively small earthquakes in close proximity to urban areas. In tectonic earthquake hazard analyses we typically rely on a simple power-law scaling relating earthquake magnitude and recurrence. It is known, however, that for smaller earthquakes, the scaling between different magnitude types is not necessarily linear – meaning that a power law cannot be maintained over all magnitude types. Extrapolation to estimate the recurrence of earthquakes not yet recorded at the study site is therefore non-trivial. For earthquake hazard, the moment magnitude is typically used as input as it is easy to relate to ground motion through empirical equations or simulation approaches. However, for earthquake monitoring, maintaining a complete catalogue including moment magnitude of small events is technically difficult. Instead, a point-measure based magnitude, such as the local magnitude is usually determined. In the following the impact of the non-linear scaling between the magnitude of choice for local monitoring – the local magnitude – and that used for hazard analysis – the moment magnitude – is explored.

18.1 Introduction

Ground shaking from induced seismicity associated with stimulation and exploitation of the near-surface, for example, related to geothermal reservoirs, shale oil or gas extraction and CO₂ storage increases the risk exposure of the local population. For instance, an enhanced deep-geothermal project in Basel, Switzerland, triggered

B. Edwards (✉)

Swiss Seismological Service, ETH Zürich, Switzerland

Department of Earth, Ocean and Ecological Sciences, University of Liverpool, UK

e-mail: edwards@sed.ethz.ch

© The Author(s) 2015

A. Ansal (ed.), *Perspectives on European Earthquake Engineering and Seismology*, Geotechnical, Geological and Earthquake Engineering 39,

DOI 10.1007/978-3-319-16964-4_18

an $M_L 3.4$ ($M_w 3.2$) earthquake at a depth of less than 5 km below the city (Baer et al. 2007). Along with thousands of aftershocks (Deichmann and Giardini 2009), the event led to insurance claims relating to non-structural damage (e.g., hairline cracks) of more than \$7.5 M with total costs of \$9 M (pers. Comm. Geo Explorers Ltd., 2012; Giardini 2009).

A growing body of evidence, while still inconclusive, suggests that seismicity related to injection induced earthquakes is increasing. For example, Ellsworth (2013) showed that “within the central and eastern United States, the earthquake count has increased dramatically over the past few years”. This, in turn, means that “regions where the rate increased may be more hazardous than forecast by the 2008 version of the U.S. National Seismic Hazard Map” (Ellsworth 2013). Although direct causality between increasing seismicity and projects related to the exploitation of the shallow crust is not clear in all cases, what is important is that the potential for increased hazard related to induced seismicity (and consequently risk) should be assessed prior to, and during, such operations. Two primary components drive estimates of seismic hazard (and its uncertainty): seismicity rates and ground-motion prediction. In the following chapter, the issues surrounding the determination of seismicity rates are discussed with a focus on the influence of earthquake magnitude assessment, as routinely carried out during seismic monitoring.

Seismicity is typically modelled in probabilistic seismic hazard analyses (PSHAs) using the Gutenberg-Richter (1944, hereafter G-R) relation, with the cumulative number of events (with magnitude greater than M), N , given by:

$$\begin{aligned} \log_{10}(N) &= a - bM & M \leq M_{Max} \\ N &= 0 & M > M_{Max} \end{aligned} \quad (18.1)$$

with a maximum magnitude M_{Max} (Smith 1976) defined by a probability density function. In practice the truncated exponential G-R relation is used (Cornell and Vanmarcke 1969). This relation is used to characterize faults or source zones based on observed seismicity in terms of overall activity rate (a) and the proportion of large to small events (b) (e.g., Wiemer and Wyss 2002). While the a -value can be thought of as a measure of the overall seismicity, the b -value has been previously linked to factors such as changes in differential-stress, for example, due to: asperities (Wiemer and Wyss 1997), different faulting regimes (Schorlemmer et al. 2005) or due to source depth (Spada et al. 2013). a - and b -values can be directly estimated for a given source zone or fault based on observed (and historical) seismicity above a time-dependent completeness threshold M_c . Maximum-likelihood approaches (Aki 1965; Utsu 1965; Bender 1983) are normally used to determine a - and b -values, along with their confidence intervals. While based on simple observational statistics, the estimation of G-R parameters is subject to uncertainties due to determined magnitudes (Kijko 1985; Tinti and Mulargia 1985) and due to catalogue completeness (Lee and Brillinger 1979; Weichert 1980).

Given a source model, PSHAs estimate the probability of exceedance for a given ground-motion using a Ground Motion Prediction Equation (GMPE) (Cornell 1968). Moment magnitude (M_w) is the magnitude of choice for seismic hazard

based on tectonic seismicity: it does not saturate and is compatible with palaeoseismological and geological estimates of ancient earthquakes and maximum earthquake magnitude. This is because it is based on the seismic moment (M_0), of which the contributing factors are fault area and slip (assuming constant rigidity). In addition, and of importance to GMPEs developed for induced seismicity is the possibility to base time-series simulations directly on M_w . For instance, Douglas et al. (2013) presented GMPEs using 36 simulation models based on various source (M_w , stress-drop), path (regional Q) and local site conditions (local attenuation κ_0). As a result of these advantages, GMPEs in the literature are predominantly developed using M_w and I will use it as the ‘reference’ magnitude for this discussion.

Clearly, in order to maintain consistency in PSHA, magnitudes used in the source model and the GMPE should be the same. If a G-R based source model was developed using, for example, local magnitude (Richter 1935) – typically routinely determined at seismological observatories – then a magnitude conversion would be required between estimating the rate (based on M_L) and computing the associated ground-motion (based on M_w). In the ideal case, a G-R source model can be developed entirely using M_w (i.e., for tectonic activity in seismically active areas). However, M_w cannot always be calculated for small events due to ambient noise. Furthermore, depending on the frequency content analysed, estimation of M_w for small events may introduce systematic bias due to high frequency effects such as site-amplification and attenuation (Stork et al. 2014). In order to obtain complete earthquake catalogues (critical for measuring the cumulative number of events in Eq. 18.1) local monitoring network operators therefore typically estimate magnitudes based on simple-to-measure parameters such as peak-amplitude (M_L) or signal duration (M_d). These catalogues are then supplemented with M_w in the case that it is available (e.g., Fäh et al. 2011) and conversion equations (e.g., $M_w = f(M_L)$) are used to estimate M_w of small events.

It is logical to reason that an earthquake has a single ‘magnitude’, and that while some scatter may be apparent, each measure (M_w , M_d , M_L ...) should lead to the same broadly consistent value for properly calibrated scales. However, this is not the case: independent estimates of different earthquake properties can lead to systematic differences between different scales, particularly at extremes of magnitudes (either very small or very large) relative to where the initial magnitude scale calibration was made. For instance, Hanks and Boore (1984) showed that the observed curvature of M_L versus M_w data over an extended magnitude range of Californian earthquakes ($0 \leq M_L \leq 7$) could be explained by a frequency-dependent interaction of the earthquake source, attenuation and instrument response of the Wood-Anderson Seismometer. In this case, determination of a linear scaling between M_L and M_w would lead to a systematic underestimation of M_w (Hanks and Boore 1984). Edwards et al. (2010) used the same simulation method to model and explain, in terms of source, path, site, and instrument-effects, the observed curvilinear scaling of Swiss earthquake magnitudes over a range $1.4 \leq M_L \leq 5.5$. Subsequently, Goertz-Allmann et al. (2011) developed a M_L to M_w scaling relation for Switzerland by collecting independent estimates of M_w and M_L over a range of $0.2 \leq M_L \leq 5.5$ and found similar scaling to a model developed based on a Europe-

wide dataset (Grünthal et al. 2009). In the range $3 \leq M_L \leq 6$ the models tend to show that $M_w \approx M_L - 0.3$. However, below M_L 3 the models deviate from 1:1 scaling systematically: with a decrease of 1 unit in M_L corresponding to only a ~ 0.6 – 0.7 unit decrease in M_w .

There is no guarantee that different magnitudes scale 1:1. Indeed, such comparisons extend to many different magnitude scales (e.g., Bormann et al. 2009). Careful initial calibrations nevertheless ensure that over a broad region of interest, earthquake magnitudes using different scales are consistent. For instance, Choy and Boatwright (1995) defined the energy magnitude M_E to be consistent to the surface wave magnitude (M_S) in the range $5.5 < M_S \leq 8.2$. In the past, earthquakes of ‘interest’ have focussed on those easily recordable on national networks (e.g., $M \gtrsim 3$) or teleseismic networks (e.g., $M \gtrsim 5$). This then corresponds to where magnitude scales tend to be broadly consistent (i.e., $M \gtrsim 3$ – 5). In terms of monitoring induced seismicity, and the estimation of seismic hazard based on these observations, we must therefore fully consider not only the influence of measured earthquake magnitude, but also the magnitude scale itself.

18.2 Influence of M_L on G-R a - and b -Values

In the following the focus is placed on M_L as it is the most commonly routinely determined magnitude at seismological observatories or local monitoring networks. The computation of M_L at small scale monitoring networks can be usually considered complete down to even $M_L \approx 1$ or even lower. For example, a small scale monitoring network (consisting of seven stations with inter-station spacing on the order of a few km) related to a deep geothermal project in St. Gallen, Switzerland, had a magnitude of completeness $M_L \approx -1$. Catalogue completeness levels at such low magnitude levels was achieved by implementing cross-correlation techniques and single borehole-station magnitude determination (Edwards et al. 2015). While the G-R relation was initially determined based on the analysis of M_L data in California, common usage tends to make the assumption that it is M_w (and consequently $\log(M_0)$ and its constituents: fault area and slip) that scales as a power law with the cumulative number of events. As an example of the impact of curvilinear scaling between M_L and M_w on seismic hazard estimation I therefore show in the following section its impact on Gutenberg-Richter (G-R) a – and b -values using simulated earthquake catalogues.

18.2.1 Simulation Method

I generate a synthetic earthquake catalogue consisting of events with seven different moment magnitudes (M_w 1–7), with each event recorded at seven locations (10, 20, 30, 50, 70, 100 and 200 km). The occurrence of events follows an arbitrary G-R relation with $a = 3.0$ and $b = 1.0$. For each recording a stochastic seismogram

is generated (Hanks and Boore 1984; Boore 2003), which can in turn be used to determine M_L of the event by measuring the peak amplitude on a synthesized Wood-Anderson Seismometer.

The synthetic stochastic seismograms are generated from a simple model of the Fourier acceleration spectrum (FAS), comprising of the far-field representation of the displacement source (Brune 1970, 1971):

$$E(f) = \frac{M_0 C}{R \left[1 + \left(\frac{f}{f_c} \right)^2 \right]} \tag{18.2}$$

with M_0 the seismic moment (in SI units), and C a constant which accounts for the free-surface, average radiation pattern, slip velocity and density. Geometrical spreading is accounted for using the hypocentral distance, R . The moment magnitude scale is defined by M_0 :

$$M_w = \frac{2}{3} \log_{10} M_0 - 6.03 \tag{18.3}$$

(Hanks and Kanamori 1979). Assuming a circular crack model (Eshelby 1957) the source corner-frequency (f_c) can be calculated using:

$$f_c = 0.4906 \beta \left(\frac{\Delta \sigma}{M_0} \right)^{\frac{1}{3}}, \tag{18.4}$$

where $\Delta \sigma$ is the stress drop of the earthquake (SI units) and β is the shear-wave velocity ($\beta = 3,500 \text{ m/s}$). In order to account for anelastic attenuation along the source-receiver path an exponential decay function is used:

$$B(f) = e^{-\pi f \frac{R}{Q}}, \tag{18.5}$$

(Knopoff 1964) with Q the quality factor and R the hypocentral distance (in m). The full synthetic stochastic acceleration time-series can be calculated based on the FAS ($E(f)B(f)$) and a given duration model. For the duration model we adopt a simple model based on source magnitude and distance from the source:

$$T = \frac{1}{f_c} + 0.05R, \tag{18.6}$$

(Herrmann 1985). The Local Magnitude is calculated using an adapted from of the original relation used by the Swiss Seismological Service:

$$\begin{aligned} M_L &= \log_{10} A + 0.0180R + 1.87 \text{ for } R \leq 60 \text{ km} \\ M_L &= \log_{10} A + 0.0038R + 2.72 \text{ for } R > 60 \text{ km} \end{aligned} \tag{18.7}$$

with R in km and A the peak displacement (in mm) of the ground-motion convolved with the response of a Wood-Anderson Seismograph. In practice, since M_L is based on a peak measure (A) of the Wood-Anderson seismogram with natural period 0.8 s and damping of 0.69, random-vibration theory [RVT, (Cartwright and Longuet-Higgins 1956)] can be used to directly calculate A using the duration model adapted to account for the Wood-Anderson oscillator response (Liu and Pezeshk 1999) and the FAS (Hanks and Boore 1984).

18.3 Results: G-R a - and b -Values from M_L

Across the various simulation models with different source ($\Delta\sigma$, M_w) and attenuation terms (Q) it is apparent, as expected, that the a - and b -values obtained using M_L are different from those obtained using M_w . This fact is of course, consistent with the fact that the M_L to M_w scaling relation is curvilinear. The exact difference is driven by the source properties ($\Delta\sigma$), the attenuation (Q), and the interaction of the earthquake spectrum and the Wood-Anderson Seismometer used to compute M_L . This was originally shown by Hanks and Boore (1984) to be the driving force behind the M_L to M_w scaling behaviour and therefore directly propagates into the G-R relation. As a result of the curvilinear scaling, the magnitude range over which the G-R relation is calculated also has a significant impact on the differences found by using different magnitude scales.

18.3.1 Influence of Stress-Drop

The reference G-R relation using M_w with $b = 1.0$ is shown in Fig. 18.1 along with four simulated catalogues for which M_L is used instead of M_w . In this case only geometrical (not anelastic) attenuation was applied. For each of the four catalogues a different stress drop is used: 0.1, 1, 5 and 10 MPa. The resulting differences show the influence of the stress-drop on M_L and consequently a - and b -values. In Fig. 18.1a it can be immediately seen that the largest deviation from the G-R relation is apparent at higher magnitudes. This is due to the saturation of the M_L scale: at some point, despite increasing the moment of the earthquake in equal steps, the increase in M_L slows (and eventually stops). This is a well-known phenomenon typically considered to occur around $M6-7$, however, an interesting aspect to consider is that the point at which saturation begins is controlled by the stress-drop. For low values (e.g., $\Delta\sigma = 0.1$ MPa to 1 MPa), even $M_L > 4$ events show the beginning of saturation: an effect that artificially increases the b -value. As a general observation, systematically low stress-drop events tend to increase the apparent b -value when using M_L in the high magnitude range. This effect should not be particularly problematic since we can observe a departure from the linear G-R law, and consequently limit the fitting range to below where the effect starts.

Furthermore, for the larger events susceptible to saturation, it is likely that direct computations of M_w will be available.

Avoiding the saturation effect, which is not particularly relevant for induced seismicity, and instead focusing on the lower magnitudes (Fig. 18.1b) we nevertheless still see a systematic variation of the b-value depending on the stress-drop used in the simulations. Generally (apart from the lowest stress-drop catalogue), the b-value is artificially decreased. For the $\Delta\sigma = 10$ MPa catalogue, the b-value is

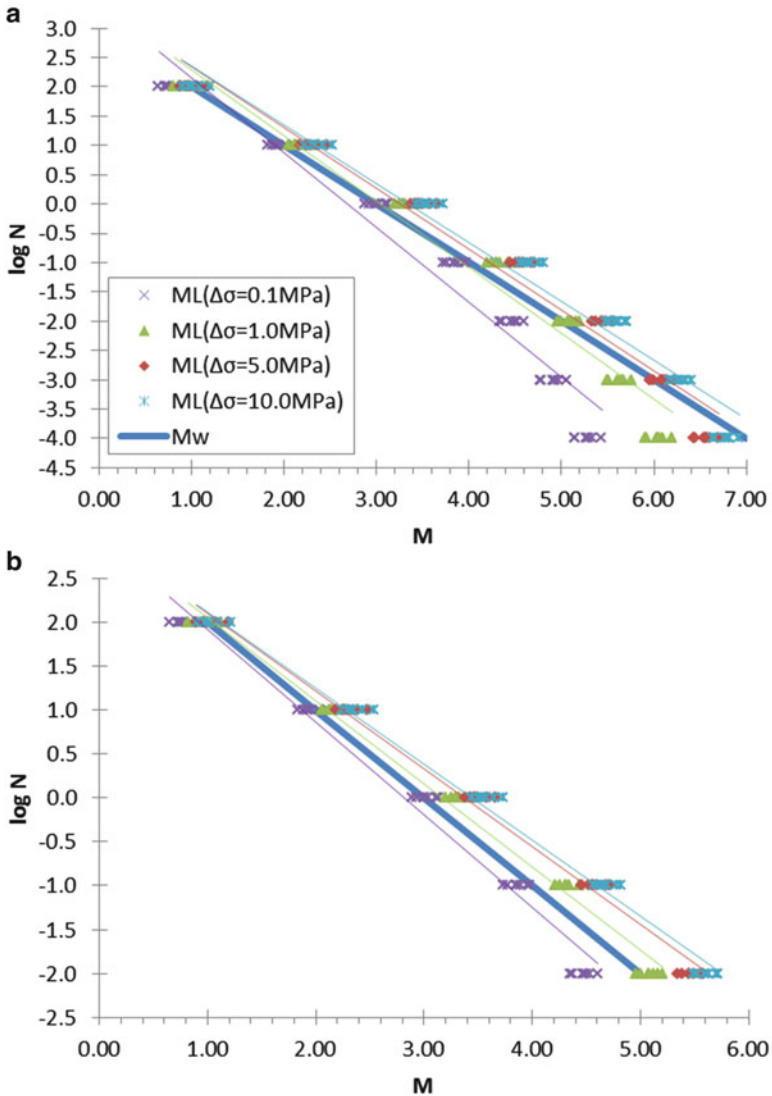


Fig. 18.1 G-R relation using M_w and M_L for the synthetic catalogues. (a) For all events; (b) for events with $M_w \leq 5$

0.86; for $\Delta\sigma = 5$ MPa, $b = 0.89$; for $\Delta\sigma = 1$ MPa, $b = 0.94$ and for $\Delta\sigma = 0.1$ MPa $b = 1.05$. These values are computed over the range $1 \leq M_w \leq 5$, limiting the upper magnitude to 4 may slightly decrease the values further.

18.3.2 Influence of Attenuation

In the previous analysis the influence of the stress-drop was isolated by neglecting anelastic attenuation. However, in reality a complex interaction between the stress-drop, attenuation and the instrument response all play a role in the M_L assigned to a particular event (Hanks and Boore 1984). A further reason that anelastic attenuation is important is apparent if we consider that the M_L relation (Eq. 18.7) only accounts for frequency independent attenuation (i.e., the $+\alpha R$ term).

Taking the catalogue with $\Delta\sigma = 5$ MPa I now apply anelastic attenuation (Fig. 18.2). For $Q = 1,000$ the b -value is further reduced from $b = 0.89$ without attenuation to $b = 0.82$, and using $Q = 500$ I obtain $b = 0.79$. Such variations in the b -value seem quite strong, however, if we look only in the range $3 \leq M_w \leq 5$, where such statistics are often calculated (e.g., for seismic hazard), the smallest effect on the b -value is observed (Fig. 18.3). Interestingly, the a -value is increased in this example, consistent with the aforementioned difference between M_w and M_L of 0.3 in this range (Goertz-Allmann et al. 2011; Grünthal et al. 2009). As a result, if using magnitudes of interest for tectonic seismic hazard ($3 \leq M_w \leq 5$), and applying a simple linear conversion (e.g., $M_w = M_L - 0.3$), one would observe *similar* a - and b -values to if one had been able to use M_w directly. The effects discussed here may also be further pronounced if considering the influence of site-amplification on M_L values. Whilst site amplification tends not to affect M_w due to its long-period basis, M_L is computed over a period range where it is common for strong amplification effects to be present.

18.4 Regional Variability Between M_L Values

So far this chapter has focused on the impact of using M_L in the standard G-R relation without accounting for the curvilinear scaling between M_w and M_L . However, a major problem to address in the prediction of ground motion for induced seismicity is the significant variability of reported earthquake magnitude from agency to agency (Fäh et al. 2011). Edwards and Douglas (2014) homogeneously computed earthquake moment- and local-magnitude for events related to Enhanced Geothermal Systems (EGSs) in Basel (Switzerland), Soultz (France) and Cooper Basin (Australia); natural geothermal fields in Geysers (California) and Hengill (Iceland), and a gas-field in Roswinkel (Netherlands). As shown in previous studies, published catalogue (M_L) magnitudes differed widely with respect to a common M_L - M_w scaling relation, with up to a unit of magnitude difference. Using non-specific conversions from catalogue magnitudes (e.g., M_L) to M_w for use in

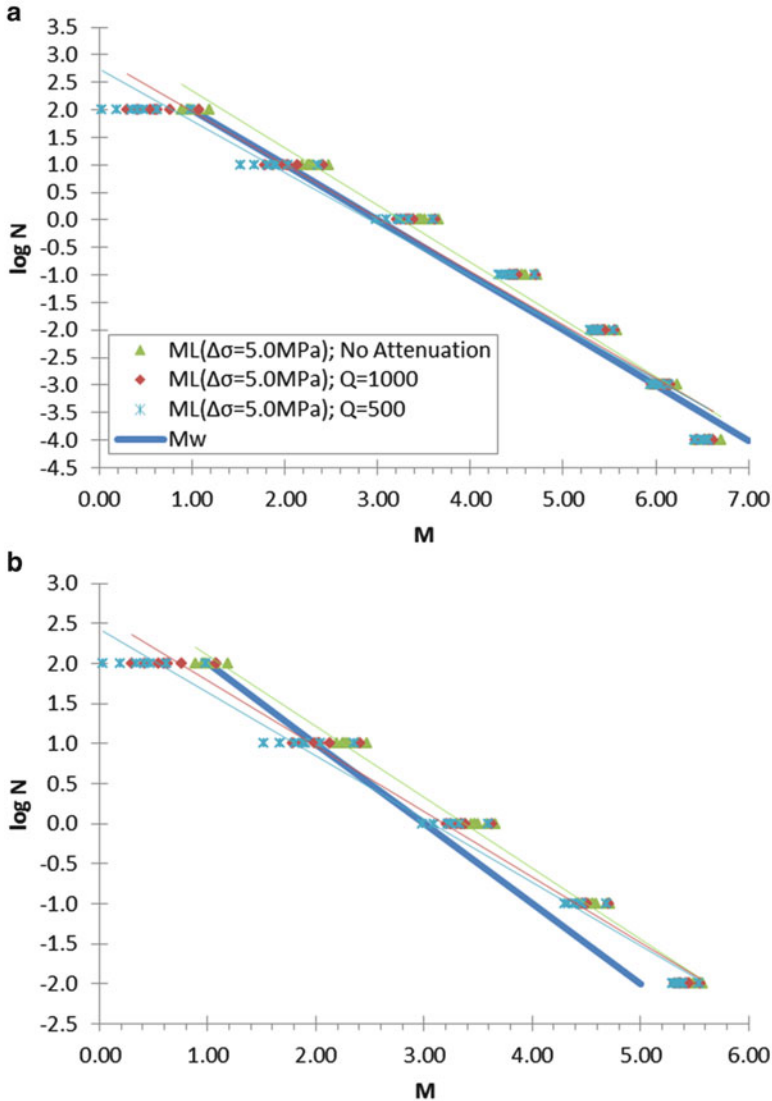


Fig. 18.2 G-R relation using M_w and M_L for synthetic catalogues using $\Delta\sigma = 5$ MPa and different attenuation. (a) For all events; (b) for events with $M_w \leq 5$

GMPEs would subsequently lead to significant bias. On the other hand, Edwards and Douglas (2014) showed that given a common magnitude definition (and corresponding attenuation corrections), the scaling between moment- and local-magnitude of small induced earthquakes follows a second-order polynomial (Fig. 18.4) consistent with previous studies of natural seismicity (Goertz-Allmann et al. 2011; Grünthal et al. 2009). Using both the Southern-California M_L scale and

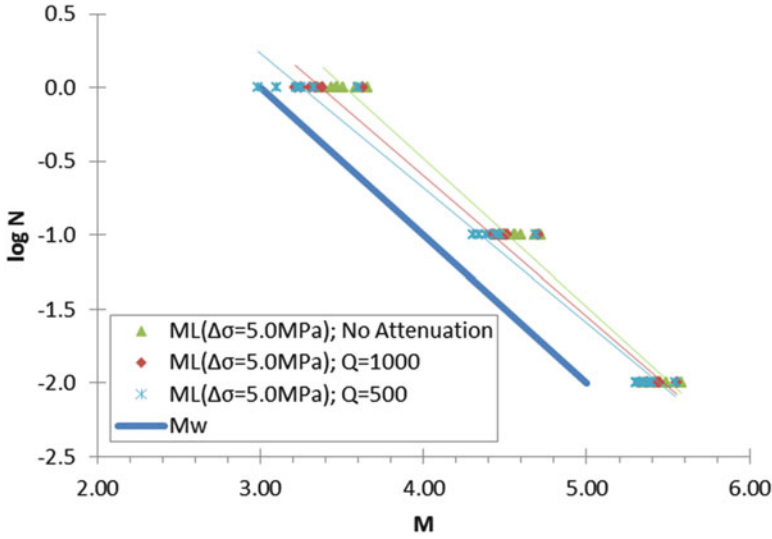


Fig. 18.3 G-R relation using M_w and M_L for synthetic catalogues using $\Delta\sigma = 5$ MPa and different attenuation for events with $3 \leq M_w \leq 5$. Note that, for this magnitude range, after accounting for a generic linear conversion (e.g., $M_w = M_L - 0.3$), one would obtain similar a- and b-values to those for M_w

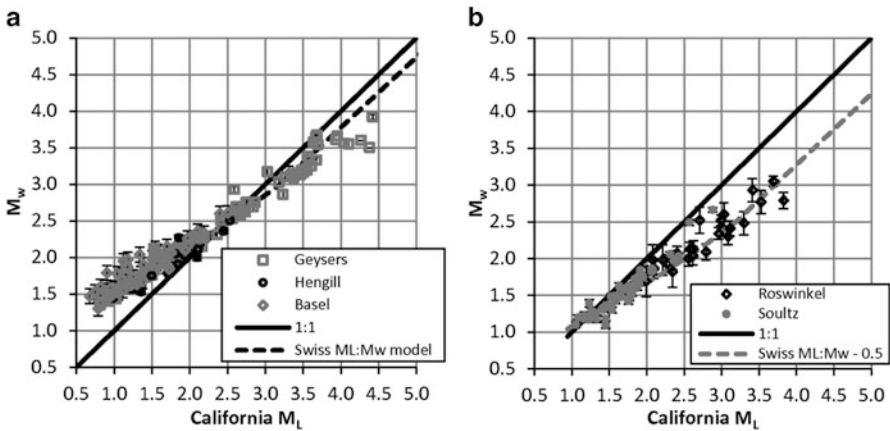


Fig. 18.4 Comparison of common M_L scale versus inverted M_w for all datasets in the study. (a) Geysers, Hengill and Basel events, along with the Swiss $M_L:M_w$ model of (Goertz-Allmann et al. 2011). (b) Roswinkel and Soultz events plotted along with the Swiss $M_L:M_w$ model offset by 0.5 units. From Edwards and Douglas (2014)

M_{equiv} (Bommer et al. 2006) Edwards and Douglas (2014) found that the analysed datasets fell into two subsets offset by 0.5 magnitude units, with well-defined relation to M_w (Fig. 18.4a, b). M_{equiv} was shown to correlate 1:1 with M_L , albeit with region-specific offsets.

18.5 Discussion

From the analysis presented here it is clearly important for consistent and transparent magnitude determination at various stages of seismic hazard analysis. A key conclusion is that if one assumes that the moment magnitude M_w follows the G-R relationship, then the M_L scale does not. The most significant deviation is for $M_L > 5$, where we begin to see the effect of magnitude scale saturation, which leads to locally increased b -values. The magnitude at which this saturation effect occurs depends on the stress-drop. Very low stress-drop events (e.g., 0.1 MPa) led to magnitude saturation effects impacting the b -value estimation at $M \approx 4$ –5. However, since this effect is most significant in the magnitude range where direct computation of M_w is typically available, it is not an issue in PSHA. More importantly for induced seismicity is the fact that at lower magnitudes we noticed that the b -value is typically reduced (for all but the lowest stress-drop catalogue). This is related to the fact that for $M_w \approx 3$ –5, M_L values tend to be greater than M_w for the simulated catalogues (and empirical catalogues), while at lower magnitudes, the difference reverses (M_w tends to be greater than M_L). Attenuation tends to systematically decrease the b -value computed with M_L because it affects increasingly smaller events (with proportionally more high frequency energy) more strongly. For instance, attenuation can be considered as a low-pass filter: for large events with little high frequency energy (relative to the low-frequency energy), this filter has little effect, whereas for smaller events a significant portion of the energy is cut from the signal. Nevertheless, it is evident that these effects offset one another, or are minimised to a certain degree when choosing particular magnitude ranges (e.g., when using $3 \leq M_w \leq 5$, as often the case in hazard studies related to tectonic seismicity).

Routine computation of M_L is often a requirement in order to have a complete data catalogue for computing the G-R relation at small magnitudes. Best practice for recovering b -values should be to convert M_L using a quadratic polynomial (Grünthal et al. 2009) or curvilinear function (Goertz-Allmann et al. 2011) (Fig. 18.5). The form of this polynomial will depend on:

- (a) the local conditions – including source properties (e.g., stress drop or slip velocity), path attenuation (Q and geometrical spreading) and site effects (amplification and attenuation) (Edwards et al. 2010);
- (b) the form of the M_L equation used (Edwards and Douglas 2014).

Since data $M_w - M_L$ pairs are rarely available down to small enough magnitudes; one option to consider is the creation of synthetic catalogues, as used in this chapter. Different source, path and site modelling terms can then also be used to cover the epistemic uncertainty of the M_L to M_w conversion.

Finally, even when we have a homogenous moment magnitude scale and consistent G-R source models, analysis by Douglas et al. (2013) highlighted

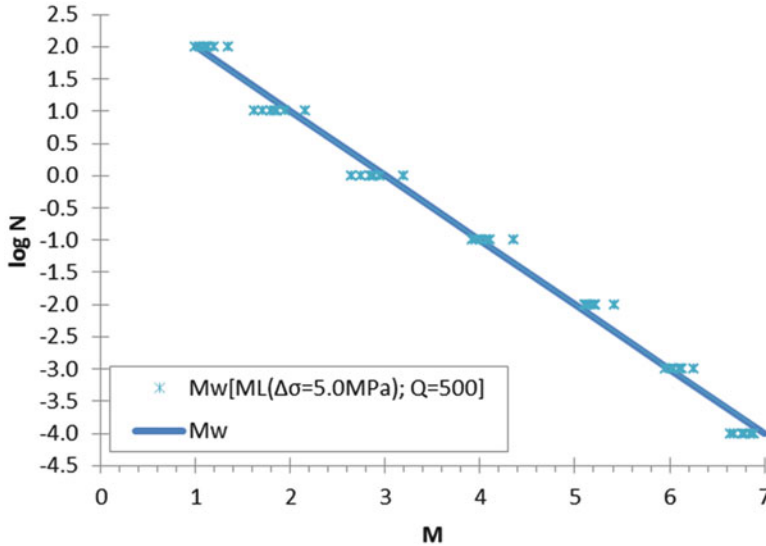


Fig. 18.5 G-R determined from M_L converted to M_w using a second order polynomial equation. Note that the G-R fit to the $M_w(M_L)$ data points exactly coincides with the reference G-R for the M_w

considerable variation in source and path parameters (e.g., stress-drops, local attenuation) among different regions and sites. Both M_L to M_w conversions and ground motion prediction may therefore be region dependent. While the focus here has been on the computation of magnitude for defining G-R models, consistency should be ensured between the conversion used for $M_w(M_L)$ and the model terms used for ground motion prediction in PSHA (or deterministic/scenario based hazard). Clearly, when conducting seismic hazard assessment for a given geothermal project it is not known *a priori* which source, path and site terms (or equivalent GMPEs) are most applicable. However, Edwards and Douglas (2013) showed that as seismograms are recorded at a site, the applicability of particular models becomes quickly evident using either spectral or residual analysis approaches. It is therefore important to establish and maintain an optimised and effective monitoring network, with broad-band (and if possible, borehole) instrumentation. While region specific wave-propagation behaviour is initially difficult to define, it has the advantage that significantly lower values of uncertainty can be observed compared to previous studies combining small earthquakes from different regions.

Open Access This chapter is distributed under the terms of the Creative Commons Attribution Noncommercial License, which permits any noncommercial use, distribution, and reproduction in any medium, provided the original author(s) and source are credited.

References

- Aki K (1965) Maximum likelihood estimate of b in the formula $\log N = a - bM$ and its confidence limits. *Bull Earthquake Res Inst* 43:237–239
- Baer M, Deichmann N, Braunmiller J, Clinton J, Husen S, Fäh D, Giardini D, Kästli P, Kradolfer U, Wienier S (2007) Earthquakes in Switzerland and surrounding regions during 2006. *Swiss J Geosci* 100:517–528. doi:[10.1007/s00015-007-1242-0](https://doi.org/10.1007/s00015-007-1242-0)
- Bender B (1983) Maximum-likelihood estimation of b -values for magnitude grouped data. *Bull Seismol Soc Am* 73:831–851
- Bommer JJ, Oates S, Cepeda JM, Lindholm C, Bird J, Torres R, Marroquin G, Rivas J (2006) Control of hazard due to seismicity induced by a hot fractured rock geothermal project. *Eng Geol* 83:287–306. doi:[10.1016/j.enggeo.2005.11.002](https://doi.org/10.1016/j.enggeo.2005.11.002)
- Boore DM (2003) Simulation of ground motion using the stochastic method. *Pure Appl Geophys* 160:635–676
- Bormann P, Liu R, Xu Z, Ren K, Zhang L, Wendt S (2009) First application of the new IASPEI teleseismic magnitude standards to data of the china national seismographic network. *Bull Seismol Soc Am* 99:1868–1891. doi:[10.1785/0120080010](https://doi.org/10.1785/0120080010)
- Brune JN (1970) Tectonic stress and spectra of seismic shear waves from earthquakes. *J Geophys Res* 75:4997–5009
- Brune JN (1971) Correction. *J Geophys Res* 76:5002
- Cartwright DE, Longuet-Higgins MS (1956) The statistical distribution of the maxima of a random function. *Proc Roy Soc Lond A Math Phys Sci* 237:212–232
- Choy GL, Boatwright JL (1995) Global patterns of radiated seismic energy and apparent stress. *J Geophysical Res Solid Earth* 100:18205–18228
- Cornell CA (1968) Engineering seismic risk analysis. *Bull Seismol Soc Am* 58:1583–&
- Cornell CA, Vanmarcke EH (1969) The major influences on seismic risk. In: *Proceedings of the fourth world conference on earthquake engineering*, vol 1, Chile, pp 69–83
- Deichmann N, Giardini D (2009) Earthquakes induced by the stimulation of an enhanced geothermal system below Basel (Switzerland). *Seismol Res Lett* 80:784–798. doi:[10.1785/gssrl.80.5.784](https://doi.org/10.1785/gssrl.80.5.784)
- Douglas J, Edwards B, Convertito V, Sharma N, Tramelli A, Kraaijpoel D, Cabrera BM, Maercklin N, Troise C (2013) Predicting ground motion from induced earthquakes in geothermal areas. *Bull Seismol Soc Am* 103:1875–1897. doi:[10.1785/0120120197](https://doi.org/10.1785/0120120197)
- Edwards B, Douglas J (2013) Selecting ground-motion models developed for induced seismicity in geothermal areas. *Geophys J Int* 195:1314–1322. doi:[10.1093/gji/ggt310](https://doi.org/10.1093/gji/ggt310)
- Edwards B, Douglas J (2014) Magnitude scaling of induced earthquakes. *Geothermics* 52:132–139. doi: <http://dx.doi.org/10.1016/j.geothermics.2013.09.012>
- Edwards B, Allmann B, Fäh D, Clinton J (2010) Automatic computation of moment magnitudes for small earthquakes and the scaling of local to moment magnitude. *Geophys J Int* 183:407–420. doi:[10.1111/j.1365-246X.2010.04743.x](https://doi.org/10.1111/j.1365-246X.2010.04743.x)
- Edwards B, Kraft T, Cauzzi C, Kästli P, Wiemer S (2015) Seismic monitoring and analysis of deep geothermal projects in St Gallen and Basel, Switzerland. *Geophys J Int* 201:1020–1037. doi:[10.1093/gji/ggv059](https://doi.org/10.1093/gji/ggv059)
- Ellsworth WL (2013) Injection-induced earthquakes. *Science* 341:142–+. doi:[10.1126/Science.1225942](https://doi.org/10.1126/Science.1225942)
- Eshelby JD (1957) The determination of the elastic field of an ellipsoidal inclusion, and related problems. *Proc Roy Soc Lond A Math Phys Sci* 241:376–396
- Fäh D, Giardini D, Kästli P, Deichmann N, Gisler M, Schwarz-Zanetti G, Alvarez-Rubio S, Sellami S, Edwards B, Allmann B (2011) Ecos-09 earthquake catalogue of Switzerland release 2011 report and database. Public catalogue, 17. 4. 2011. Swiss seismological service eth Zurich, p 42
- Giardini D (2009) Geothermal quake risks must be faced. *Nature* 462:848–849. doi:[10.1038/462848a](https://doi.org/10.1038/462848a)

- Goertz-Allmann BP, Edwards B, Bethmann F, Deichmann N, Clinton J, Fäh D, Giardini D (2011) A new empirical magnitude scaling relation for Switzerland. *Bull Seismol Soc Am* 101:3088–3095. doi:[10.1785/0120100291](https://doi.org/10.1785/0120100291)
- Grünthal G, Wahlstrom R, Stromeyer D (2009) The unified catalogue of earthquakes in central, northern, and northwestern Europe (CENEC)-updated and expanded to the last millennium. *J Seismol* 13:517–541. doi:[10.1007/s10950-008-9144-9](https://doi.org/10.1007/s10950-008-9144-9)
- Gutenberg B, Richter CF (1944) Frequency of earthquakes in California. *Bull Seismol Soc Am* 34:185–188
- Hanks TC, Boore DM (1984) Moment-magnitude relations in theory and practice. *J Geophys Res* 89:6229–6235. doi:[10.1029/Jb089ib07p06229](https://doi.org/10.1029/Jb089ib07p06229)
- Hanks TC, Kanamori H (1979) Moment magnitude scale. *J Geophys Res* 84:2348–2350
- Herrmann RB (1985) An extension of random vibration theory estimates of strong ground motion to large distances. *Bull Seismol Soc Am* 75:1447–1453
- Kijko A (1985) A modified form of the Gutenberg-Richter magnitude frequency relation – maximum-likelihood estimation of its parameters. *Bull Seismol Soc Am* 75:319–322
- Knopoff L (1964) *Q. Rev Geophys* 2:625–660
- Lee WHK, Brillinger DR (1979) Chinese earthquake history – attempt to model an incomplete data set by point process analysis. *Pure Appl Geophys* 117:1229–1257. doi:[10.1007/Bf00876217](https://doi.org/10.1007/Bf00876217)
- Liu L, Pezeshk S (1999) An improvement on the estimation of pseudoresponse spectral velocity using RVT method. *Bull Seismol Soc Am* 89:1384–1389
- Richter CF (1935) An instrumental earthquake magnitude scale. *Bull Seismol Soc Am* 25:1–32
- Schorlemmer D, Wiemer S, Wyss M (2005) Variations in earthquake-size distribution across different stress regimes. *Nature* 437:539–542. doi:[10.1038/Nature04094](https://doi.org/10.1038/Nature04094)
- Smith SW (1976) Determination of maximum earthquake magnitude. *Geophysical Research Letters* 3:351–354. doi:[10.1029/G1003i006p00351](https://doi.org/10.1029/G1003i006p00351)
- Spada M, Tormann T, Wiemer S, Enescu B (2013) Generic dependence of the frequency-size distribution of earthquakes on depth and its relation to the strength profile of the crust. *Geophys Res Lett* 40:709–714. doi:[10.1029/2012gl054198](https://doi.org/10.1029/2012gl054198)
- Stork AL, Verdon JP, Kendall J-M (2014) The robustness of seismic moment and magnitudes estimated using spectral analysis. *Geophys Prospect* 62:862–878. doi:[10.1111/1365-2478.12134](https://doi.org/10.1111/1365-2478.12134)
- Tinti S, Mulargia F (1985) Effects of magnitude uncertainties on estimating the parameters in the Gutenberg-Richter frequency-magnitude law. *Bull Seismol Soc Am* 75:1681–1697
- Utsu T (1965) A method for determining the value of b in a formula $\log n = a - bm$ showing the magnitude-frequency relation for earthquakes. *Geophys Bull Hokkaido Univ* 13:103
- Weichert DH (1980) Estimation of the earthquake recurrence parameters for unequal observation periods for different magnitudes. *Bull Seismol Soc Am* 70:1337–1346
- Wiemer S, Wyss M (1997) Mapping the frequency-magnitude distribution in asperities: An improved technique to calculate recurrence times? *J Geophys Res Solid Earth* 102:15115–15128. doi:[10.1029/97jb00726](https://doi.org/10.1029/97jb00726)
- Wiemer S, Wyss M (2002) Mapping spatial variability of the frequency-magnitude distribution of earthquakes. *Adv Geophys* 45(45):259–302

Chapter 19

On the Origin of Mega-thrust Earthquakes

Kuvvet Atakan

Abstract Out of 17 largest earthquakes in the world since 1900 with magnitudes larger than 8.5, 15 of them occurred along convergent plate boundaries as mega-thrust events. Four of these catastrophic earthquakes have occurred during the last decade. The wealth of observational data from these events offer a unique opportunity for Earth Scientists to understand the underlying processes leading to the deformation in subductions zones, not only along the plate interface, but also in plate interiors in both the subducting slab and the overriding plate.

19.1 Introduction

Since the beginning of the twentieth century (i.e. 1900) there have been 17 earthquakes with magnitudes equal to or larger than 8.5 (Fig. 19.1). All of these earthquakes, except two, occurred due to rupture along the plate interface in different subduction zones around the Pacific and Indian oceans. Six of these occurred during the last decade, some of which with catastrophic consequences. Especially the largest of these, 2004 and 2005 Sumatra, Indonesia, 2010 Maule, Chile and the 2011 Tohoku-Oki, Japan earthquakes have provided new insights to the understanding of mega-thrust earthquakes and subduction zone deformation. There is now an unprecedented observational data from these events showing the details of the deformational processes in the convergent plate boundaries, not only along the plate interface of two colliding plates, but also within the plate interiors both on the overriding plate as well as the subducting slab (Table 19.1).

Mega-thrust earthquakes have some common characteristics. However, the wealth of data available for the latest events have highlighted the details of the rupture process and revealed significant differences. It became now clear that the physical properties of the plate interface in subduction zones are critical in the generation of the mega-thrust earthquakes. Understanding these processes in detail

K. Atakan (✉)

Department of Earth Science, University of Bergen, Allégt. 41, Bergen N-5007, Norway
e-mail: Kuvvet.Atakan@geo.uib.no

© The Author(s) 2015

A. Ansal (ed.), *Perspectives on European Earthquake Engineering and Seismology*,
Geotechnical, Geological and Earthquake Engineering 39,
DOI 10.1007/978-3-319-16964-4_19

443

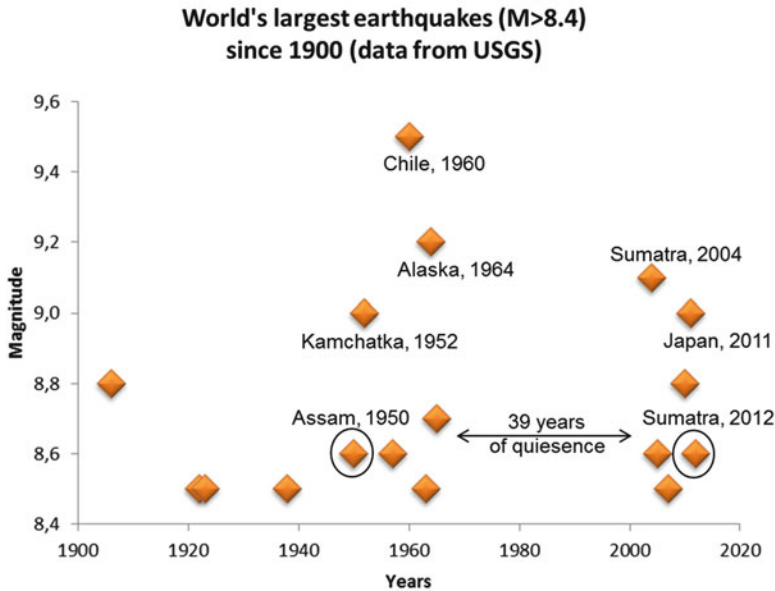


Fig. 19.1 World's largest earthquakes ($M \geq 8.5$) since 1900 (data from USGS). Please note that the largest earthquakes have occurred in two clusters in time separated by 39 years. The two earthquakes, Assam 1950 and Sumatra 2012 earthquakes are not considered in this study as mega-thrust events. The 1950 Assam earthquake have occurred in a different tectonic setting with continent-continent collision, and the 2012 Sumatra earthquake was the largest ever recorded strike-slip faulting event which occurred along one of the fractures zones offshore northern Sumatra

requires multidisciplinary approaches synthesizing a variety of observational data combined with numerical and analogue modeling. Recent studies of the mega-thrust earthquakes have shown that there are methodological issues which may require revisiting some earlier wisdom, but they have also shown the capability of new promising techniques. In the following, we illustrate these challenging issues through various studies conducted on the latest earthquakes with a special emphasis on the 2011 Tohoku-Oki, Japan mega-thrust earthquake ($M = 9.0$).

19.2 Mega-thrust Earthquakes

Although there are far more very large earthquakes ($M \geq 8.0$) that have occurred along the plate interface of various subduction zones which can be considered as mega-thrust events, in this study, we have restricted our definition of mega-thrust earthquakes to those that have magnitudes equal to or larger than 8.5. Among the 17 earthquakes since 1900 (Fig. 19.1), based on the data from USGS (USGS 2014), we consider 15 of them as mega-thrust events since the 1950 Assam earthquake

Table 19.1 List of world's largest earthquakes with $M \geq 8.5$ in the period 1900–2014 (from USGS)

Date and time	Latitude	Longitude	Magnitude	Casualties	Region
1906/01/31 15:36	1.0	-81.5	8.8	1,000	Colombia-Ecuador
1922/11/11 04:32	-28.553	-70.755	8.5		Chile-Argentina Border
1923/02/03 16:01	54.0	161.0	8.5		Kamchatka
1938/02/01 19:04	-5.05	131.62	8.5		Banda Sea
1950/08/15 14:09	28.5	96.5	8.6	1,526	Assam-Tibet
1952/11/04 16:58	52.76	160.06	9.0		Kamchatka, Russia
1957/03/09 14:22	51.56	-175.39	8.6		Andreanof Islands, Alaska
1960/05/22 19:11	-38.29	-73.05	9.5	1,655	Chile
1963/10/13 05:17	44.9	149.6	8.5		Kuril Islands
1964/03/28 03:36	61.02	-147.65	9.2	125	Prince William Sound, Alaska
1965/02/04 05:01	51.21	-178.50	8.7		Rat Islands, Alaska
2004/12/26 00:58	3.295	95.982	9.1	227,898	off the west coast of northern Sumatra
2005/03/28 16:09	2.074	97.013	8.6	1313	Northern Sumatra, Indonesia
2007/09/12 11:10:26	-4.438	101.367	8.5	25	Southern Sumatra, Indonesia
2010/02/27 06:34:14	-35.846	-72.719	8.8	577	Offshore Maule, Chile
2011/03/11 05:46:23	38.322	142.369	9.0	28,050	Near the East Coast of Honshu, Japan
2012/04/11 08:38:37	2.311	93.063	8.6		off the west coast of northern Sumatra

All above earthquakes, except the 2012/04/11 event off the west coast of northern Sumatra, are mega-thrust earthquakes associated with the plate interface of a subduction process. 2012/04/11 event is the largest strike-slip earthquake ever recorded

have occurred in a different tectonic setting with continent-continent collision, and the 2012 Sumatra earthquake was the largest ever recorded strike-slip faulting event which occurred along one of the fractures zones offshore northern Sumatra. The remaining 15 events have all occurred along the various subduction zones in the Pacific and Indian Oceans. Their space/time correlations indicate that the largest of these earthquakes cluster in time. This is clearly shown in Fig. 19.1, with the two

clusters in the time-periods 1950–1964 and 2004–present, separated by a quiescence period of 39 years. The most striking feature of these two clusters is that in the first cluster there were three mega-thrust events with $M \geq 9$ and there were two $M \geq 9.0$ in the second. Although it is tempting to suggest duration of approximately 10–15 years for these clusters with a rough repeat time of 40 years, statistically such conclusions are not warranted. This is mainly due to the fact that the total time of observation during the instrumental period is far too small and the two temporal clusters within 114 years cannot be generalized unless we have longer time series available. In spite of increasing evidence for mega-thrust events in the pre-historic period, assessing the occurrence of mega-thrust events during the historic and pre-historic period has some obvious limitations. In general the uncertainties of the source parameters increase significantly backwards in time. This however, should not undermine the importance of paleoseismological data which has proven useful in cases such as the subduction zone mega-thrust paleo-earthquakes of NW-US (1700, Cascadia earthquake; Satake et al. 1996) and in NE-Japan (869, Jogan earthquake; Minoura et al. 2001).

It is clear that the occurrence of these mega-thrust earthquakes is governed by global tectonics and the total seismic moment-budget associated with the plate convergence rates in the subduction zones (e.g. Pacheco and Sykes 1992; McCaffrey 2007). Nevertheless, their occurrence in time and space is highly dependent on the history of deformation in individual subduction zones and their internal segmentation within the arc. Despite this, there are some common characteristic that can be attributed to the mega-thrust earthquakes. These can be summarized as follows:

- All occur on subduction zones along the plate interface and cluster in time.
- All related to strong coupling along the plate interface, where the location and physical properties of the asperities are critical.
- Total slip is controlled by the size and the location of the strongest asperity (s) and if shallow, also controls the resulting tsunami size.
- Along-dip segmentation of the interface is observed and rupture may include the shallow trench-ward section.
- Along-strike segment boundaries are associated with large structural controls on the subducting plate (earlier sea-floor heterogeneities such as sea mount chains, ridges, fracture zones, etc.).
- All cause significant stress changes in the neighboring segments (including the outer-rise) and hence increase the likelihood of other mega-thrust events.
- All have clear signs of fore-shock activity and significant aftershock activity outside the main asperities.

Based on some of these common features there have been recent attempts to classify the different subduction zones and the associated mega-thrust earthquakes (e.g. Koyama et al. 2013). A simple classification based on three criteria, along-strike segment boundary, along-dip segmentation and the direction of collision (orthogonal or oblique), although useful to sort out some basic differences, still lacks the necessary details and hence forces one to think in terms of these end

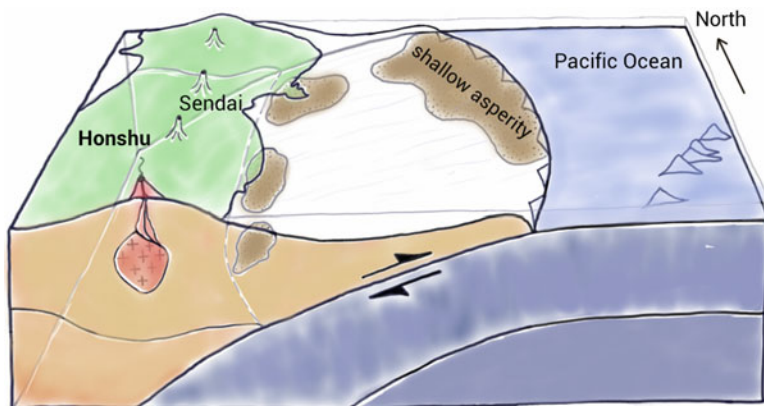


Fig. 19.2 Simplified sketch showing the cross-section along the Honshu, NE-Japan subduction zone. The approximate location of the asperities along the plate interface are shown with brown shaded areas. Note the sea-mount chain in the Pacific Ocean floor. See text for discussion

members only. However, understanding the subduction zone deformation requires a holistic approach to all controlling factors (Fig. 19.2).

A complete deformation cycle in a subduction zone starts with the inter-seismic period of strain accumulation due to the plate convergence, which in cases where there is strong coupling along the plate interface, results in internal deformation both in the overriding and subducting plates. In the overriding plate uplift occurs along the coastal areas of the island arc and inland regions whereas subsidence is seen towards the trench in the ocean-ward side. Both of these effects are the consequence of compressional forces due to locking of the plate interface. Observation of the sea-level changes in Sumatra and the response of the coral micro-atoll growth have demonstrated these long-term effects of overriding plate deformation (e.g. Zachariassen et al. 2000; Sieh et al. 2008). Similarly, in the subducting plate in the outer-rise region, compressional deformation occurs during the inter-seismic period, coupled with the down dip extension at depth giving rise to normal faulting deep intraplate events. Once the plate interface is ruptured through a mega-thrust earthquake (co-seismic deformation) the relaxation period following this favors the reversal of the forces acting in the same regions both in the overriding and subducting plates. Subsidence along the shore and inland regions accompanied by the uplift along the trench are typical for the overriding plate deformation. In the subducting plate the same structures that were reactivated as reverse faults now act as normal faults due to extension in the relaxation period (post-seismic deformation). There is of course processes both prior to the rupture of the plate interface (foreshock activity) and immediately after the mega-thrust earthquakes (aftershocks) which is part of the total deformation cycle. There are few examples that captures this total deformation cycle such as the triple earthquakes that have occurred along the central Kurile subduction zone in 1963 ($M = 7.7$), 2006 ($M = 8.3$) and 2007 ($M = 8.1$) (Raeesi and Atakan 2009).

19.3 Deformation Cycle in Subduction Zones

Understanding the total deformation cycle in subduction zones and the processes associated with it requires multidisciplinary approaches including a variety of observational data combined with analog and numerical modelling (Funiciello et al. 2013). In recent years indeed a wealth of observational data became available. These include,

- Structural data (conventional geology/geophysics)
- Petrophysical data (conventional petrology/geochemistry)
- Seismological data (conventional source parameters)
- Slip inversions based on seismological data for a broad-band of frequencies (backprojection methods for remote arrays etc.)
- Seismic tomography at a regional and detailed scales
- Seismic anisotropy
- Reflection/refraction profiles
- Potential field measurements (gravity, magnetics)
- Sattelite geodesy (GPS, InSAR, TEC)
- Borehole data
- Statistical data
- Paleoseismological data
- Tsunami data (run-up, modeling)
- Bathymetric surveys+DEM (digital elevation models at local scales)

Synthesizing such a variety of data brings along some methodological challenges as well. In the first place, it is necessary to realize the importance as well as the limitations of each data set before applying an appropriate method. Detailed studies of co-seismic slip-inversions through various data sets for the 2011 Tohoku-Oki, Japan mega-thrust earthquake, illustrate this problem very clearly. Following the earthquake of March 11, 2011 in Japan, there has been a number of co-seismic slip inversions published using tele-seismic data (e.g. Ammon et al. 2011; Ishii 2011; Lay et al. 2011; Koper et al. 2011; Wang and Mori 2011), strong-motion data (e.g. Ide et al. 2011; Suzuki et al. 2011), GPS data (e.g. Linuma 2011; Miyazaki et al. 2011; Ozawa et al. 2011; Pollitz et al. 2011) as well as tsunami data (e.g. Fujii et al. 2011; Saito et al. 2011). In addition to these there has also been joint inversions of seismological (teleseismic and strong-motion) and geodetic data (e.g. Koketsu et al. 2011; Yokoto et al. 2011; Yoshida et al. 2011; Kubo and Kakehi 2013). Common for all these inversion results is the shallow asperity with a large slip. In general there is a good agreement on the location of the shallow asperity among the various studies (seismological, GPS and tsunami wave data), where the maximum slip exceeds 40 m. When it comes to the details of the rupture there are significant differences in these inversion results. The main conclusion here is that slip inversions are non-unique and there is strong need for independent data which may help calibrating these. In other words, identifying the location of the strong asperities by multidisciplinary data sets seems critical. Independent evidence for

the shallow asperity and the observed large slip came from the sea-bottom GPS measurements (Sato et al. 2011) and shallow seismic data (Kodaira et al. 2012) combined with cores from the borehole drilled at the tip of the sedimentary wedge (Chester et al. 2013).

The down-dip extent of the fault rupture is on the other hand, debated and some of the studies conclude that rupture propagated to the bottom of the contact zone. A number of inversions based on teleseismic data from large and dens arrays (US-array and the Stations from Europe) have revealed a strong short period radiation at deeper part of the rupture plane (e.g. Ide et al. 2011; Ishii 2011; Koper et al. 2011; Meng et al. 2011; Wang and Mori 2011). It is now understood that the slip associated with the shallow asperity was slow and lacking short-period radiation, whereas the deeper asperities produced strong short-period energy (Koper et al. 2011).

Apart from that, arguably, it can be said that the joint inversions smear out the slip distribution and a lot of details such as the short-period radiation at depth is not resolved (Meng et al. 2011). As such the common understanding that the joint inversions are better than individual data sets is questionable. The rupture complexity with a dynamic variation at various frequencies is better resolved by individual analysis of different data sets that are sensitive to these frequencies. The results from these individual studies, when combined together in a synthesis, seem to be a far better tool than the joint inversion results.

19.4 Rupture Preparation and Post-seismic Slip

Mega-thrust earthquakes along subduction zones are mainly controlled by the plate coupling along the interface. Some critical issues related to the degree of coupling are, the location of the strong and weakly coupled zones (asperities and their origin), role of sediments and fluids in coupling, down-dip limit of the coupled zone as well as coupling in the shallow zone close to trench. Regarding the latter the 2011 Tohoku-Oki earthquake has surprised many. Contrary to the common belief that the shallow part of the coupling along the trench is usually weak controlled by the loose sediments of the accretionary prism accompanied by the fluid interaction reducing the friction, more than 40 m of slip is observed along the trench. This very high slip along the trench was also crucial in the development of the following large tsunami wave.

The strongly coupled shallow asperity along the trench was manifested by the various co-seismic slip inversions as discussed earlier. It is also firmly confirmed by the offshore GPS measurements where significant slip was observed (Sato et al. 2011). The maximum horizontal slip measured was as high as 24 m almost 100 km away from the trench. The vertical uplift was as high as 3 m in the same area. The slip was also observed at the very tip of the trench through high resolution seismic data (Kodaira et al. 2012). Later, Chester et al. (2013) have shown the actual plate interface cutting through the contact between the pelagic sediments of

the subducting plate and the sediments of the accretionary prism representing the overriding plate.

The rupture process had however started already with the onset of increased earthquake activity just at the periphery of this strong asperity at depth some weeks before the main rupture which culminated in a magnitude 7.5 earthquake at the deeper end of the shallow asperity on March 9, 2011. The static stress transfer from this event was probably the triggering mechanism for the main rupture on March 11, 2011. Such foreshock activity is not unique for the Tohoku-Oki earthquake, similar significant foreshock activity was previously documented in other plate interface thrust events (e.g. Raeesi and Atakan 2009) and more recently during the 2014 Iquique earthquake in northern Chile (Hayes et al. 2014).

Post-seismic slip is usually associated with extensive aftershock activity following the mega-thrust events. This was the case for the Tohoku-Oki earthquake where hundreds of aftershocks were registered in the following weeks after the main shock (Nishimura et al. 2011). The most striking feature of the aftershock sequences was their spatial concentration in areas outside the main asperities that had ruptured during the co-seismic slip. The largest of these aftershocks had a magnitude of 7.9 at the southernmost part of the plate interface off Boso, close to the Sagami trough in the south. In addition to the intensive aftershock activity along the plate interface, there has been also triggered seismic activity both in the overriding plate (Kato et al. 2011) and the subducting slab in the outer rise area such as the $M = 7.7$ earthquake (Lay et al. 2011). Such outer rise normal faulting events can be very large as was the case for the 1933 ($M = 8.4$) event further to the north. These events are the manifestation of the total deformation associated with the stress transfer from the main shock (Toda et al. 2011)

19.5 Segmentation of the Plate Interface

Physical conditions leading to the deformation in subduction zones depend on a variety of factors including:

- Direction and speed of the plate convergence.
- Differences in the rheology/composition of the two colliding plates.
- Age and density difference between and density variations within colliding plates.
- Physical/morphological/geological irregularities along the plate interface.
- The degree of coupling along the plate interface between the overriding plate and the subducting slab.
- Accumulated stress/strain.
- Fluid flow along the plate interface.
- Heat gradient and heat-flow.
- Melting process at the magma wedge. Mantle flow and circulations in the subduction system.

Although the total deformation is controlled by these factors, the physical and the morphological irregularities of the oceanic plate converging to the trench will in time have long term consequences in terms of the segmentation of the plate interface. Iquique ridge entering into the subduction zone in the border area between northern Chile and southern Peru is a good example for this (e.g. Pritchard and Simons 2006; Contreras-Reyes and Carrizo 2011; Métois et al. 2013). The strong coupling along this zone has previously been modelled (e.g. Métois et al. 2013; Chlieh et al. 2014) and is expected to produce large mega-thrust earthquakes probably larger than the recent Iquique event of 2014 ($M = 8.2$). Other sea-floor irregularities such as sea-mounts, fracture zones and ridges play thus an important role in the overall segmentation of the plate interface in various subduction zones.

19.6 Mapping Asperities

Once the segmentation of the interface is understood, the next critical issue is to find the location of the asperities. Inevitably, slip inversion of earthquakes constitutes an important contribution in this sense. However, there is a need for additional independent data to calibrate and verify the slip inversions as well as to find out more about the location of asperities in subduction zones where there are no recent large mega-thrust events in the latest instrumental period. One promising recent development is the use of satellite gravity data, GRACE in resolving the co-seismic gravity changes due to mega-thrust events (e.g. Tanaka and Heki 2014; Han et al. 2014). These new data opens new possibilities for detecting the location of asperities, because the repetitive slip along the same asperities of the plate interface causes mass dislocations. In the long-term, cumulative mass dislocations in the same part of the overriding plate will lead to permanent density changes. The accumulated density changes then leave an imprint on the overriding plate due to gravity (buoyancy forces) that change the degree of coupling along the plate interface. Cumulative effect of these variations should therefore be detectable as subtle deviatoric gravity changes parallel to the trench. These strongly coupled areas constitute the asperities that will slip in future large mega-thrust earthquakes. Mapping asperities by gravity data was first introduced by Song and Simons (2003), where trench parallel topography and gravity anomalies in the circum-Pacific region have revealed the strongly coupled areas along the plate interface. This was later modified (Raeesi and Atakan 2009; Raeesi 2009) to include also trench parallel Bouger anomaly.

Mapping asperities along the plate interface using these new techniques, if combined with detailed monitoring of seismological as well as geodetic changes in time with the recent observations regarding the short-term precursory phenomena such as total electron content (TEC) in the ionosphere (e.g. Liu et al. 2011; Tsugawa et al. 2011), may provide important opportunities to understand the deformation processes before the occurrence of the mega-thrust earthquakes.

19.7 Future Perspectives

In order to understand better the complex processes leading to mega-thrust earthquakes and the total deformation in subduction zones, future studies should focus on identifying the gaps for mega-thrust earthquakes as well as identifying the precursory phenomena in both long- and short-term. Following is a short list of research areas that may be helpful in this sense:

Identifying Gaps for Megathrust-Earthquakes

- Mapping the location of strongly coupled plate interface along subduction zones (GPS and stress modeling, stress transfer)
- Mapping the location and size of the largest asperities (Gravity, TPBA, seismic tomography)
- Mapping rupture areas of previous historical and instrumental mega-thrust earthquakes (historical accounts, slip distribution of previous instrumental mega-thrust earthquakes)
- Developing segmentation models for the subduction zones (mapping heterogeneities in the ocean-floor)

Identifying Precursory Phenomena

In the long-term:

- Monitoring overriding plate deformation (geodetic measurements of interseismic period through GPS, InSAR)
- Monitoring space/time variations of seismicity in the interseismic period (dense BB-station networks)

In the short-term:

- Identifying foreshock activity (detailed seismic monitoring)
- Identifying ionospheric disturbances (TEC measurements)

Open Access This chapter is distributed under the terms of the Creative Commons Attribution Noncommercial License, which permits any noncommercial use, distribution, and reproduction in any medium, provided the original author(s) and source are credited.

References

- Ammon CJ, Lay T, Kanamori H, Cleveland M (2011) The rupture model for the great 2011 Tohoku earthquake. *Earth Planets Space* 63:693–696
- Chester FM, Rowe C, Ujiie K, Kirkpatrick J, Regalla C, Remitti F, Moore JC, Toy V, Wolfson-Schwehr M, Bose S, Kameda J, Mori JJ, Brodsky EE, Eguchi N, Toczko S, Expedition 343 and 343 T Scientists, (2013) Structure and composition of the plate-boundary slip zone for the 2011 Tohoku-oki earthquake. *Science* 342:1208. doi:[10.1126/science.1243719](https://doi.org/10.1126/science.1243719)

- Chlieh M, Mothes PA, Nocquet JM, Jarrin P, Charvisa P, Cisneros D, Fonta Y, Collot JY, Villegas-Lanzad JC, Rolandone F, Vallée M, Regnier M, Segovia M, Martin X, Yepes H (2014) Earth Planet Sci Lett 400:292–301. <http://dx.doi.org/10.1016/j.epsl.2014.05.027>
- Contreras-Reyesa E, Carrizo D (2011) Control of high oceanic features and subduction channel on earthquake ruptures along the Chile–Peru subduction zone. Phys Earth Planet In 186:49–58. doi:[10.1016/j.pepi.2011.03.002](https://doi.org/10.1016/j.pepi.2011.03.002)
- Fujii Y, Satake K, Sakai S, Shinohara M, Kanazawa T (2011) Tsunami source of the 2011 off the Pacific coast of Tohoku, Japan earthquake. Earth Planets Space 63:815–820
- Funiciello F, Corbi F, van Dinther Y, Heuret A (2013) Unraveling megathrust seismicity. EOS, Transactions. Am Geophys Union 94(51):497–498, 17 December 2013
- Han SC, Sauber J, Pollitz F (2014) Broad-scale postseismic gravity change following the 2011 Tohoku-oki earthquake and implication for deformation by viscoelastic relaxation and afterslip. Geophys Res Lett. doi:[10.1002/2014GL060905](https://doi.org/10.1002/2014GL060905)
- Hayes GP, Herman MW, Barnhart WD, Furlong KP, Riquelme S, Benz HM, Bergman E, Barrientos S, Earle PS, Samsonov S (2014) Continuing megathrust earthquake potential in Chile after the 2014 Iquique earthquake. Nature 512:295–298. doi:[10.1038/nature13677](https://doi.org/10.1038/nature13677)
- Ide S, Baltay A, Beroza GC (2011) Shallow dynamic overshoot and energetic deep rupture in the 2011 Mw 9.0 Tohoku-oki earthquake. Science 332:1426. doi:[10.1126/science.1207020](https://doi.org/10.1126/science.1207020)
- Ishii M (2011) High-frequency rupture properties of the Mw 9.0 off the Pacific coast of Tohoku earthquake. Earth Planets Space 63:609–614
- Kato A, Sakai S, Obara K (2011) A normal-faulting seismic sequence triggered by the 2011 off the Pacific coast of Tohoku earthquake: wholesale stress regime changes in the upper plate. Earth Planets Space 63:745–748
- Kodaira S, No T, Nakamura Y, Fujiwara T, Kaiho Y, Miura S, Takahashi N, Kaneda Y, Taira A (2012) Coseismic fault rupture at the trench axis during the 2011 Tohoku-oki earthquake. Nat Geosci 5:646–650. doi:[10.1038/NGEO1547](https://doi.org/10.1038/NGEO1547)
- Koketsu K, Yusuke Yokota Y, Nishimura N, Yagi Y, Miyazaki S, Satake K, Fujii Y, Miyake H, Sakai S, Yamanaka Y, Okada T (2011) A unified source model for the 2011 Tohoku earthquake. Earth Planet Sci Lett 310:480–487. doi:[10.1016/j.epsl.2011.09.009](https://doi.org/10.1016/j.epsl.2011.09.009)
- Koper KD, Hutko AR, Lay T, Ammon CJ, Kanamori H (2011) Frequency-dependent rupture process of the 2011 Mw 9.0 Tohoku earthquake: comparison of short-period P wave backprojection images and broadband seismic rupture models. Earth Planets Space 63:599–602
- Koyama J, Yoshizawa K, Yomogida K, Tsuzuki M (2013) Variability of megathrust earthquakes in the world revealed by the 2011 Tohoku-oki earthquake. Earth Planets Space 64:1189–1198
- Kubo H, Kakehi H (2013) Source process of the 2011 Tohoku earthquake estimated from the joint inversion of teleseismic body waves and geodetic data including seafloor observation data: source model with enhanced reliability by using objectively determined inversion settings. Bull Seismol Soc Am 103(2B):1195–1220. doi:[10.1785/0120120113](https://doi.org/10.1785/0120120113)
- Lay T, Ammon CJ, Kanamori H, Xue L, Kim MJ (2011) Possible large near-trench slip during the 2011 Mw 9.0 off the Pacific coast of Tohoku earthquake. Earth Planets Space 63:687–692
- Linuma T (2011) Coseismic slip distribution of the 2011 off the Pacific coast of Tohoku earthquake (M 9.0) estimated based on GPS data—was the asperity in Miyagi-oki ruptured? Earth Planets Space 63:643–648
- Liu JY, Chen CH, Lin CH, Tsai HF, Chen CH, Kamogawa M (2011) Ionospheric disturbances triggered by the 11 March 2011 M9.0 Tohoku earthquake. J Geophys Res. 116:A06319. doi:[10.1029/2011JA016761](https://doi.org/10.1029/2011JA016761)
- McCaffrey R (2007) The next great earthquake. Science 315:1675–1676
- Meng L, Inbal A, Ampuero JP (2011) A window into the complexity of the dynamic rupture of the 2011 Mw 9 Tohoku-Oki earthquake. Geophys Res Lett. 38:L00G07. doi:[10.1029/2011GL048118](https://doi.org/10.1029/2011GL048118)

- Métois M, Socquet A, Vigny C, Carrizo D, Peyrat S, Delorme A, Maureira E, Valderas-Bermejo MC, Ortega I (2013) Revisiting the North Chile seismic gap segmentation using GPS-derived interseismic coupling. *Geophys J Int* 194(3):1283–1294. doi:[10.1093/gji/ggt183](https://doi.org/10.1093/gji/ggt183)
- Minoura K, Imamura F, Sugawara D, Kono Y, Iwashita T (2001) The 869 Jogan tsunami deposit and recurrence interval of large-scale tsunamis on the Pacific coast of northeast Japan. *J Nat Disaster Sci* 23(2):83–88
- Miyazaki S, McGuire JJ, Segall P (2011) Seismic and aseismic fault slip before and during the 2011 off the Pacific coast of Tohoku earthquake. *Earth Planets Space* 63:637–642
- Nishimura T, Munekane H, Yurai H (2011) The 2011 off the Pacific coast of Tohoku earthquake and its aftershocks observed by GEONET. *Earth Planets Space* 63:631–636
- Ozawa S, Nishimura T, Suito H, Kobayashi T, Tobita M, Imakiire T (2011) Coseismic and postseismic slip of the 2011 magnitude-9 Tohoku-Oki earthquake. *Nature* 475:373–376. doi:[10.1038/nature10227](https://doi.org/10.1038/nature10227)
- Pacheco JF, Sykes LR (1992) Seismic moment catalogue of large shallow earthquakes. *Bull Seismol Soc Am* 82(3):1309–1349
- Pollitz FF, Bürgmann R, Banerjee P (2011) Geodetic slip model of the 2011 M9.0 Tohoku earthquake. *Geophys Res Lett.* 38:L00G08. doi:[10.1029/2011GL048632](https://doi.org/10.1029/2011GL048632)
- Pritchard ME, Simons M (2006) An aseismic slip pulse in northern Chile and along-strike variations in seismogenic behavior, *J Geophys Res.* 111:B08405. doi:[10.1029/2006JB004258](https://doi.org/10.1029/2006JB004258)
- Raeesi M (2009) Asperity detection along subduction zones. Unpublished PhD-thesis, University of Bergen, Department of Earth Science
- Raeesi M, Atakan K (2009) On the deformation cycle of a strongly coupled plate interface: the triple earthquakes of 16 March 1963, 15 November 2006, and 13 January 2007 along the Kurile subduction zone. *J Geophys Res.* 114:B10301, 30. doi:[10.1029/2008JB006184](https://doi.org/10.1029/2008JB006184)
- Saito T, Ito Y, Inazu D, Hino R (2011) Tsunami source of the 2011 Tohoku-Oki earthquake, Japan: inversion analysis based on dispersive tsunami simulations. *Geophys Res Lett.* 38:L00G19. doi:[10.1029/2011GL049089](https://doi.org/10.1029/2011GL049089)
- Satake K, Shimazaki K, Tsuji Y, Ueda K (1996) Time and size of a giant earthquake in Cascadia inferred from Japanese tsunami records of January 1700. *Nature* 379:246–249
- Sato M, Ishikawa T, Ujihara N, Yoshida S, Fujita M, Mochizuki M, Asada A (2011) Displacement above the hypocenter of the 2011 Tohoku-oki earthquake. *Science* 332:1395. doi:[10.1126/science.1207401](https://doi.org/10.1126/science.1207401)
- Sieh K, Natawidjaja DH, Meltzner AJ, Shen CC, Cheng H, Li KS, Suwargadi BW, Galetzka J, Philibosian B, Edwards RL (2008) Earthquake supercycles inferred from sea-level changes recorded in the corals of West Sumatra. *Science* 322(5908):1674–1678. doi:[10.1126/science.1163589](https://doi.org/10.1126/science.1163589)
- Suzuki W, Aoi S, Sekiguchi H, Kunugi T (2011) Rupture process of the 2011 Tohoku-Oki megathrust earthquake (M9.0) inverted from strongmotion data. *Geophys Res Lett.* 38:L00G16. doi:[10.1029/2011GL049136](https://doi.org/10.1029/2011GL049136)
- Tanaka Y, Heki K (2014) Long- and short-term postseismic gravity changes of megathrust earthquakes from satellite gravimetry. *Geophys Res Lett* 41:5451–5456. doi:[10.1002/2014GL060559](https://doi.org/10.1002/2014GL060559)
- Toda S, Lin J, Stein RS (2011) Using the 2011 M=9.0 Tohoku earthquake to test the Coulomb stress triggering hypothesis and to calculate faults brought closer to failure. *Earth Planets Space* 63:1–6. doi:[10.5047/eps.2011.05.010](https://doi.org/10.5047/eps.2011.05.010)
- Tsugawa T, Saito A, Otsuka Y, Nishioka M, Maruyama T, Kato H, Nagatsuma T, Murata KT (2011) Ionospheric disturbances detected by GPS total electron content observation after the 2011 off the Pacific coast of Tohoku earthquake. *Earth Planets Space* 63:875–879
- USGS (2014) Largest earthquakes in the world since 1900. United States Geological Survey web-site: http://earthquake.usgs.gov/earthquakes/world/10_largest_world.php. Last accessed 6 Sept 2014

- Wang D, Mori J (2011) Rupture process of the 2011 off the Pacific coast of Tohoku earthquake (Mw 9.0) as imaged with back-projection of teleseismic P-waves. *Earth Planets Space* 63:603–607
- Yokota Y, Koketsu K, Fujii Y, Satake K, Sakai S, Shinohara M, Kanazawa T (2011) Joint inversion of strong motion, teleseismic, geodetic, and tsunami datasets for the rupture process of the 2011 Tohoku earthquake. *Geophys Res Lett*, 38:L00G21. doi:[10.1029/2011GL050098](https://doi.org/10.1029/2011GL050098)
- Yoshida Y, Ueno H, Muto D, Aoki S (2011) Source process of the 2011 off the Pacific coast of Tohoku earthquake with the combination of teleseismic and strong motion data. *Earth Planets Space* 63:565–569
- Zachariasen J, Sieh K, Taylor FW, Hantoro WS (2000) Modern vertical deformation above the Sumatran subduction zone: paleogeodetic insights from coral microatolls. *Bull Seismol Soc Am* 90:897–913